



2019

Approaches to the Search of Platinum Anticancer Agents: Derivatizing Current Drugs and Incorporating HDAC Inhibition

Chao Feng

University of the Pacific, fengchaopacific@gmail.com

Follow this and additional works at: https://scholarlycommons.pacific.edu/uop_etds

 Part of the [Chemistry Commons](#)

Recommended Citation

Feng, Chao. (2019). *Approaches to the Search of Platinum Anticancer Agents: Derivatizing Current Drugs and Incorporating HDAC Inhibition*. University of the Pacific, Dissertation.

https://scholarlycommons.pacific.edu/uop_etds/3637

This Dissertation is brought to you for free and open access by the Graduate School at Scholarly Commons. It has been accepted for inclusion in University of the Pacific Theses and Dissertations by an authorized administrator of Scholarly Commons. For more information, please contact mgibney@pacific.edu.

APPROACHES TO THE SEARCH OF PLATINUM ANTICANCER AGENTS:
DERIVATIZING CURRENT DRUGS AND INCORPORATING HDAC INHIBITION

by

Chao Feng

A Dissertation Submitted to the

Graduate School

In Partial Fulfillment of the

Requirements for the Degree of

DOCTOR OF PHILOSOPHY

Thomas J. Long School of Pharmacy and Health Sciences
Pharmaceutical and Chemical Sciences

University of the Pacific
Stockton, CA

2019

APPROACHES TO THE SEARCH OF PLATINUM ANTICANCER AGENTS:
DERIVATIZING CURRENT DRUGS AND INCORPORATING HDAC INHIBITION

by

Chao Feng

APPROVED BY:

Dissertation Advisor: Qinliang Zhao, Ph.D.

Committee Member: Yi Chen, Ph.D.

Committee Member: Liang Xue, Ph.D.

Committee Member: Jianhua Ren, Ph.D.

Committee Member: Jerry Tsai, Ph.D.

Department Chairs: Jianhua Ren, Ph.D.; Jerry Tsai, Ph.D.

Dean of Graduate School: Thomas Naehr, Ph.D.

APPROACHES TO THE SEARCH OF PLATINUM ANTICANCER AGENTS:
DERIVATIZING CURRENT DRUGS AND INCORPORATING HDAC INHIBITION

Copyright 2019

by

Chao Feng

ACKNOWLEDGMENTS

First, and most of all, I would like to thank my Ph.D. advisor Dr. Qinliang Zhao for her endless support during the past five years. Thank her for accepting me as an engineering background student and for giving me the freedom to explore different projects. She is a strong woman, mother, professor, and scientist, and always inspire me of solving problems, not only in research but also in life.

I would like to thank my Ph.D. committee members. Dr. Yi Chen (Newave Pharmaceuticals Inc.) has been guiding me through my whole project. Some of the chemicals were purchased and all the HDAC inhibition screening were conducted with his generous support. Without his help, I could not have learned this much and might not have been able to pursue my career in the pharmaceutical industry. I would like to thank Dr. Liang Xue for his great help with the DNA binding assay and suggestions on biostudies. I would like to thank Dr. Jianhua Ren for allowing me to use mass spectrometers in her lab. I would like to thank Dr. Jerry Tsai for chairing my qualifying exam and aiding me in the course work. I would like to thank all the committee members for being flexible with my defense schedules.

I would also like to thank Prof. O. David Sparkman for teaching me all the knowledge about mass spectrometry and giving me the opportunity to work at pacific mass spectrometry facility. I would like to thank Dr. Andy Franz for his great help in all the NMR, especially the long-hour platinum NMR measurements. I would like to thank Dr.Xin Guo for his help and discussion in cell culture study. I would like to thank Dr. Dingben Chen for helping me with the organic molecule synthesis and purification. I would also like to thank Dr. Brett William and Ms.Susan McCann for taking care of all the paper works and chemical supplies.

I would also like to thank all my colleagues at the University of the Pacific. My labmate, Dr. Michael B. Pastor for being with me in the lab for the first four years and always helping me with my research, English and my life in the United States. Yuntao Zhang for tons of help in mass spectrometry analysis and daily life. Yingbo Huang for all the work and great help in cell culture studies. I would also like to thank Dan Shao. She has been with me and participated in all my projects. I appreciate all her help as a great partner. I would like to thank Ethan Liu for editing my dissertation. I would also like to thank all other members of Dr. Qinliang Zhao's research group.

Lastly, I would like to thank my parents. Without their support and encouragement, I could not be here to finish my Ph.D.

APPROACHES TO THE SEARCH OF PLATINUM ANTICANCER AGENTS:
DERIVATIZING CURRENT DRUGS AND INCORPORATING HDAC INHIBITION

Abstract

by Chao Feng

University of the Pacific
2019

Platinum-based anticancer drugs, such as cisplatin, carboplatin, and oxaliplatin, have been approved for clinical use worldwide for decades. Despite their enormous success, their widespread application is hindered by either cross-resistance or toxic side effects, including nephrotoxicity and neurotoxicity. The need to overcome these drawbacks has stimulated the search for new platinum-based drugs.

This dissertation will start with the accidental discovery of cisplatin, followed by an introduction of other platinum-based anticancer agents, including the action mechanism, general structures, and development history. Picoplatin is a newer generation of platinum-based anticancer agent. The bulky 2-methylpyridine as a non-leaving group on picoplatin could reduce the detoxification effect caused by thiol-containing species, such as glutathione and metallothionein, thus may grant picoplatin the ability to overcome cisplatin resistance. A convenient synthesis route for picoplatin derivatives has been developed. 11 new picoplatin derivatives have been designed by varying the bulkiness of the non-leaving amine group. All complexes have been characterized by different instrumentations, including MS, ^1H NMR, ^{13}C NMR, ^{195}Pt NMR, HMQC, X-ray crystallography, and elemental analysis. Different bioassays, such as DNA binding, cell viability, and cellular accumulation, have been applied to evaluate their efficacy on cisplatin-sensitive ovarian cancer cell line A2780 and cisplatin-resistant ovarian

cancer cell line A2780cis. The newly designed picoplatin derivatives show comparable efficacy with that of picoplatin and less resistance compared with cisplatin. The study of picoplatin derivatives laid the foundation toward the research of bifunctional platinum-based anticancer agents by incorporating histone deacetylase (HDAC) inhibition.

Histone acetyltransferase (HAT) and histone deacetylase (HDAC) are a pair of important enzymes in epigenetic regulation. They work in harmony to acetylate and deacetylate histone lysine residues, resulting in a more relaxed or more condensed chromatin structure, respectively. HDAC has been found to be overexpressed in some cancer cells. Since 2006, 5 HDAC inhibitors (HDACi) have entered clinical use for cancer treatment. 19 new HDACi with additional coordination sites on the phenyl cap have been designed, synthesized, and evaluated. A few of the new HDACi show comparable or even better HDAC inhibition than that of Vorinostat (SAHA, the first FDA approved HDACi).

A logical design would involve the installation of HDACi on the platinum center as a non-leaving group ligand. When the bifunctional drug reaches the cancer cell, the synergistic effect could be maintained as the relaxed chromatin structure makes DNA more susceptible to be attacked by the platinum centers, thus increase the anticancer activity and possibly selectivity toward cancer cells. 6 Pt-HADCi conjugates have been designed and synthesized. Dual functions of the new Pt-HADCi have been confirmed by DNA electrophoresis assay and HDAC inhibition assay. One of the Pt-HADCi (CF-101) shows comparable cytotoxicity with cisplatin and less resistance, which could be used as the lead compound for further structural modification and *in vivo* studies.

TABLE OF CONTENTS

LIST OF TABLES	10
LIST OF FIGURES	11
LIST OF ABBREVIATIONS.....	13
Chapter 1: Platinum Anticancer Agents	15
1.1 The Discovery of Cisplatin.....	15
1.2 Action Mechanism of Cisplatin.....	17
1.3 General Structure of Platinum Anticancer Agents	19
1.4 Clinically Approved Platinum Anticancer Agents	21
Chapter 2: Picoplatin Derivatives	24
2.1 Introduction	24
2.2 Preparation of Picoplatin Derivatives.....	26
2.3 Bioassay Protocols.....	35
2.4 Results and Discussion	37
2.5 Conclusions	45
Chapter 3: HDAC Inhibitors.....	47
3.1 Introduction	47
3.2 Preparation of HDAC Inhibitors.....	51
3.3 HDAC Inhibition and Cell Viability Study	80
3.4 Conclusions	83

Chapter 4: Pt-HDACi Conjugates.....	84
4.1 Introduction	84
4.2 Design of Pt-HDACi Conjugates	86
4.3 Preparation of Pt-HDACi Conjugates	91
4.4 Results and Discussion	96
4.5 Conclusions	105
References.....	107
APPENDIX A: SYNTHESIS SCHEME.....	129
APPENDIX B: NMR SPECTRA DATA	138
APPENDIX C: MASS SPECTRA DATA	300
APPENDIX D: X-RAY DATA.....	369
APPENDIX E: BIOSTUDY DATA.....	372

LIST OF TABLES

Table

2.1 Cytotoxic activities of cisplatin, Pt-1 , Pt-3 , and Pt-4 in cell lines A2780 and A2780cis.....	43
2.2 Cellular accumulation of platinum from cisplatin, Pt-1 , Pt-3 , and Pt-4 in A2780 and A2780cis.*	44
3.1 HDAC1 inhibition and cell viability for compound CF-L01 to CF-L12 .*	81
3.2 HDAC1 inhibition of CF-L13 to CF-L19	83
4.1 ¹⁹⁵ Pt NMR shifts of monodentate Pt-HDACi and its corresponding picoplatin derivatives. .	97
4.2 HDAC1 inhibition of Pt-HDACi conjugates and their corresponding free ligands.	99
4.3 Cell viability IC ₅₀ values of Pt-HDACi in four different cancer cell lines.	101
4.4 Cellular accumulation of platinum from cisplatin, Pt-HDACi in four different cancer cell lines. (treated at 10μM for 24 h).	102

LIST OF FIGURES

Figure

1.1 NIH-registered clinical trials involving cisplatin as of 2019. The numbers only reflect those trials that are recruiting and active, not recruiting. ⁶	16
1.2 Action mechanism of cisplatin. ¹³	18
1.3 General structure of platinum anticancer agents. ⁸	20
1.4 The family tree of platinum anticancer agents.....	22
2.1 Crystal structure of picoplatin.....	24
2.2 Summary of picoplatin derivatives.	28
2.3 DNA gel electrophoresis of picoplatin derivatives.	38
2.4 The DNA binding yield of picoplatin derivatives. (confidence interval: 95%, p<0.01)	39
2.5 DMF % by volume effect on cell viability study of A2780 and A2780cis.	40
2.6 Preliminary cell viability screening of picoplatin derivatives in two ovarian cell lines at two concentrations. (a) A2780 with 5 μ M, (b) A2780 with 20 μ M, (c) A2780cis with 5 μ M, (d) A2780cis with 20 μ M.	41
2.7 IC ₅₀ curve of cisplatin, Pt-1 , Pt-3 , and Pt-4 in (a) A2780 and (b) A2780cis cell lines.	42
2.8 Cellular accumulation of platinum from cisplatin, Pt-1 , Pt-3 , and Pt-4 in A2780 and A2780cis cell lines. (treated at 10 μ M for 24 h) **** p \leq 0.0001, *** p \leq 0.001.	45
3.1 Roles of histone acetyltransferases (HATs) and histone deacetylases (HDACs) in regulating histone proteins (right), and HDACs in deacetylation mechanism (left). ^{82,83}	48
3.2 (a) X-ray crystal structure of SAHA bound to an HDAC-like protein. ¹⁰⁷ (b) Molecular structure of SAHA. ⁸³	49
3.3 Clinically approved HDAC inhibitors with approving agency, year of approval, therapeutic indication, and administration route. ¹⁰⁸	50
3.4 Structures of HDAC inhibitors (CF-L01 to CF-L12).	51
3.5 Structures of HDAC inhibitors (CF-L13 to CF-L17).	53

3.6 Structures of HDAC inhibitors CF-L18 and CF-L19	54
4.1 HDACi-based hybrid agents in clinical trials. ^{6,150,146}	86
4.2 Pt-HDACi hybrid molecule reported by Marmion's team. ^{113,151}	87
4.3 The design logic of Pt-HDACi conjugates.	88
4.4 Pt-HDACi hybrid molecules (bidentate binding) designed in current research.	90
4.5 Pt-HDACi hybrid molecules (bidentate binding) designed in current research.	90
4.6 The stacked ¹ H NMR spectra of CF-L13 (top, blue trace) and CF-102 (bottom, red trace) .	98
4.7 DNA gel electrophoresis of CF-101 , CF-102 , CF-103 and CF-104 , reference to cisplatin and SAHA.....	98
4.8 The DNA binding yields of Pt-HDACi conjugates. (confidence interval: 95%, p<0.1)	99
4.9 IC ₅₀ curve of SAHA, cisplatin, and Pt-HDACi in (a) HCT-116, (b)A549, (c)A2780 and (d) A2780cis cell lines.....	100
4.10 Cellular accumulation of platinum from cisplatin, Pt-HDACi in four different cancer cell lines. (treated at 10μM for 24 h) **** p≤0.0001, *** p≤0.001, * p≤0.1, ns p >0.1.....	102
4.11 Preliminary cell viability screening of Pt-13 , Pt-14 , and Pt-15 in two different ovarian cell lines at two different concentrations. (a) A2780 with 5 μM, (b) A2780 with 20 μM, (c) A2780cis with 5 μM, (d) A2780cis with 20 μM.....	104

LIST OF ABBREVIATIONS

ACN	<u>A</u> cet <u>n</u> itrile
CID	<u>C</u> ollision- <u>i</u> nduced <u>d</u> issociation
CHCl ₃	Chloroform
COSY	Homonuclear <u>C</u> orrelation <u>S</u> pectroscopy
DART	<u>D</u> irect <u>A</u> nalysis in <u>R</u> eal <u>T</u> ime
DCM	<u>D</u> ichloro <u>m</u> ethane
DMF	<u>D</u> imethyl <u>f</u> ormamide
DIEA	<i>N,N</i> - <u>D</u> iisopropylethyl <u>a</u> mine
DI	Deionized
Equiv	<u>E</u> quivalent
Et ₂ O	Diethyl Ether
ESI	<u>E</u> lectrospray <u>I</u> onization
EtOH	Ethanol
EtOAc	Ethyl Acetate
HMBC	<u>H</u> eteronuclear <u>M</u> ultiple- <u>B</u> ond <u>C</u> orrelation spectroscopy
HATU	1-[Bis(dimethylamino)methylene]-1H-1,2,3- triazolo[4,5- b]pyridinium 3-oxid hexafluorophosphate
MS	<u>M</u> ass <u>S</u> pectrometry
m-CPBA	<u>m</u> eta- <u>C</u> hloro <u>p</u> eroxy <u>b</u> enzoic <u>a</u> cid
MeOH	Methanol
NMP	<i>N</i> - <u>M</u> ethyl-2-pyrrolidone

NMR	<u>N</u> uclear <u>M</u> agnetic <u>R</u> esonance
PE	<u>P</u> etroleum <u>E</u> ther
rt	<u>R</u> oom <u>T</u> emperature, 25 °C (also RT)

Chapter 1: Platinum Anticancer Agents

1.1 The Discovery of Cisplatin

Over 50 years ago, Dr. Barnett Rosenberg, a biophysicist at Michigan State University, was applying an electrical field to bacteria in order to investigate whether it could affect the cell division. Because platinum is inert and was thought to have no biological effect in the study, Dr. Rosenberg and his group added platinum electrodes in the growth chamber containing *E. coli*. Once the current was on, the *E. coli* stopped dividing and kept growing as very long filaments (up to 300 times long as normal length), which was quite abnormal. When the power/current was off, the *E. coli* began to divide again. They spent two years trying to understand why the electrical field had such a powerful effect on *E. coli* division. It turned out that this effect was not due to the electrical field but rather the compound formed with platinum that was released from the electrode that blocked cell division. Dr. Rosenberg and his team spent another two years to identify the active complex and later named it cisplatin.¹ It turns out that cisplatin was originally synthesized by the Italian chemist Michele Peyrone in 1845 and named as Peyrone's chloride.^{2,3} Later, cisplatin was approved by the US Food and Drug Administration (FDA) for cancer treatment in 1978. It is the first metal-based anticancer reagent for worldwide clinical use. Before that time, all the chemicals for cancer treatment were either natural products or synthetic organic compounds. Since then, cisplatin became the gold standard for new metal-containing drug design.^{4,5} As of 2019, there are still close to 1,000 clinical trials involving cisplatin all over the world (Figure 1.1).⁶

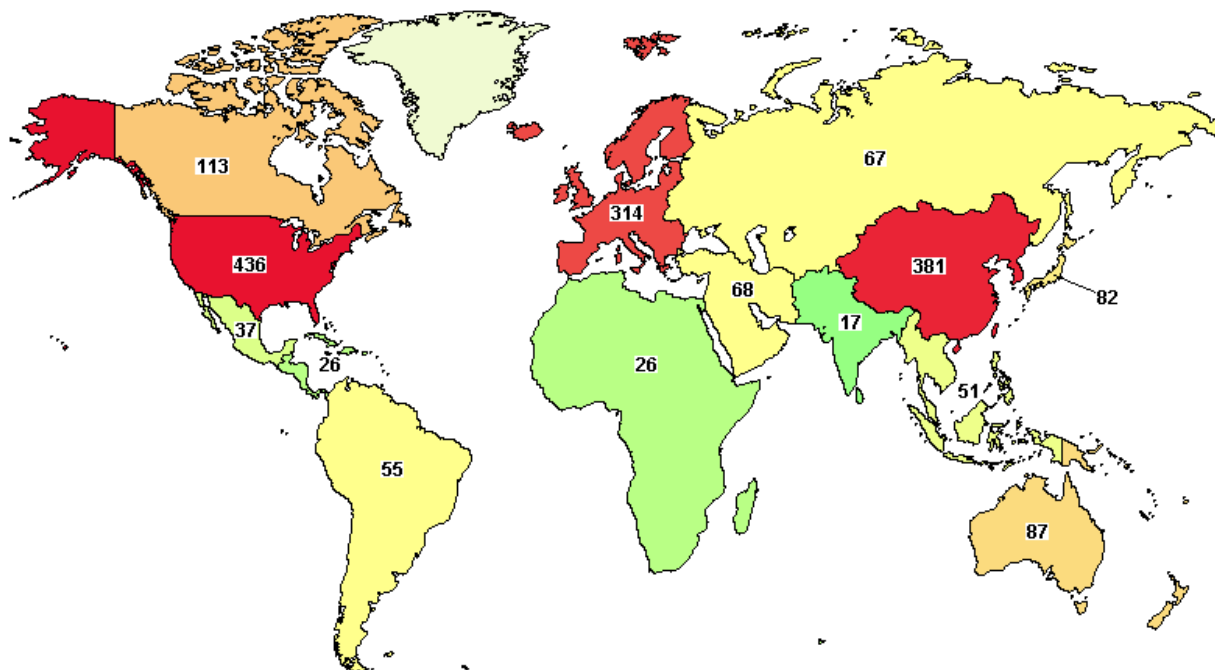
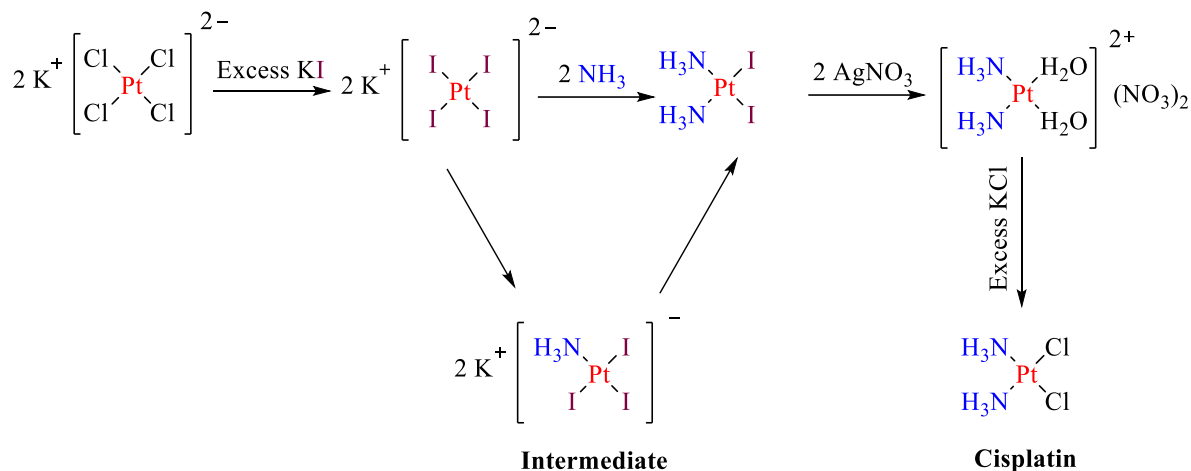


Figure 1.1 NIH-registered clinical trials involving cisplatin as of 2019. The numbers only reflect those trials that are recruiting and active, not recruiting.⁶

The first rapid way to synthesize cisplatin was developed by S. C. Dhara in 1970 (Scheme 1).^{7,8,9} K_2PtCl_4 was first converted to K_2PtI_4 in aqueous solution with an excess of KI. Two equivalents of ammonium hydroxide were added to the dark brown solution of K_2PtI_4 and yielded a yellow precipitate $cis-[Pt(NH_3)_2I_2]$. Iodide ligands were then removed by 2 equiv $AgNO_3$, yielding $cis-[Pt(NH_3)_2(H_2O)_2]^{2+}$. Finally, isometrically pure cisplatin was made by adding excess KCl. The key intermediate during the Dhara synthesis was $K[Pt(NH_3)_3I]$. The stronger *trans* effect of iodide with respect to chloride ensures that the next NH_3 ligand would substitute the position *trans* to an iodide, which affords the *cis* isomer. Cisplatin can be purified by recrystallization in hot water containing either 0.1 M HCl or 0.9 % NaCl solution.^{10,11} The high chloride concentration helps to stabilize the cisplatin during the recrystallization process.



Scheme 1.1 Synthesis of cisplatin (Dhara method).

1.2 Action Mechanism of Cisplatin

Cisplatin has been widely used for different types of cancer treatment, including testicular, ovarian, cervical, breast, bladder, head and neck, esophageal, lung cancer, mesothelioma brain tumors, and neuroblastoma.¹² It is administered intravenously to the patients as a short-term infusion in saline solution. Numerous experiments have been designed and conducted by scientists to study the cisplatin action mechanism. The general mechanism involves four key steps (Figure 1.2), including (i) cellular uptake, (ii) aquation/activation, (iii) DNA binding, and (iv) apoptosis.¹³ Once the cisplatin is administered to the bloodstream, it remains unchanged and neutral due to the high concentration of chloride (~ 100 mM).⁹ However, cisplatin is still susceptible to be attacked by plasma proteins, particularly those containing thiol groups, such as albumin, which lead to the deactivation of cisplatin, causing side effects including nephrotoxicity and neurotoxicity.^{4,9,14} There are two main pathways in the cellular uptake process, either by passive diffusion due to the concentration difference or active transport by membrane proteins, such as copper transporter proteins.^{15,16,17} The relative importance of

these two pathways remains to be determined. Once cisplatin enters the cell, intracellular chloride concentration is decreased (below 20 mM) and chlorine ligands on cisplatin can be easily substituted by water molecules.¹⁸ This process is called aquation/activation. However, such activation is suppressed in the bloodstream due to the high chloride concentration. The positively charged Pt-water complex ion could be attracted to the negatively charged DNA, where the water molecules coordinated to the Pt center could be substituted by the most nucleophilic N7 position on guanine and adenine.¹⁹ The major DNA binding product is the 1,2-d(GpG) intrastrand cross-link adduct (65%), which causes the distortion of DNA.^{20,21} If the cell cannot repair the damage, it will go apoptosis. One of the main mechanisms during the cell apoptosis from platinum treatment is the inhibition of RNA polymerases transcription past platinum lesions.²²

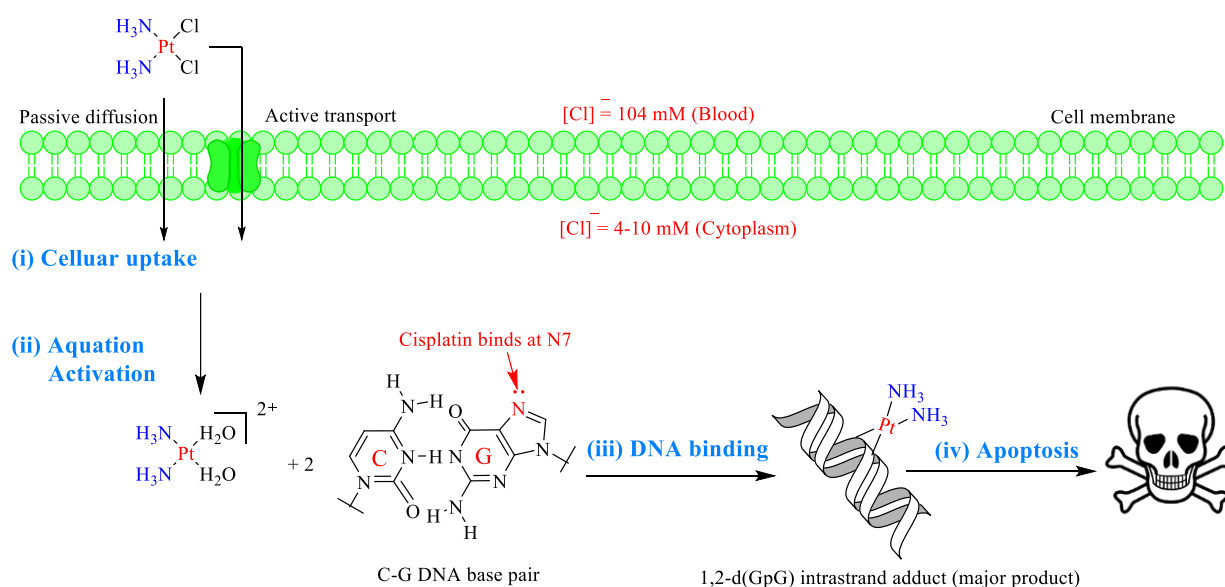


Figure 1.2 Action mechanism of cisplatin.¹³

However, some cancers are intrinsically resistant to cisplatin or acquire resistance during the treatment, either by the lowered uptake efficiency, increased detoxification in the cytoplasm, or resistance mediated after DNA binding.^{1,13} As cisplatin is a highly polar compound compared with other small molecule drugs, the uptake process is relatively slow and influenced by many other factors, like Na⁺ and K⁺ concentrations, and transporter expression. The resistance of cisplatin during the uptake process is mainly due to the low uptake efficiency rather than increased cisplatin efflux, which is a common resistance mechanism for most natural product-based drugs.¹⁵ It has been reported that downregulation of membrane transporters is one of the reasons.¹ However, the detailed molecular mechanism involved in the cisplatin uptake is still poorly understood. Another reason for cisplatin resistance is the increased detoxification caused by the raised concentration of thiol-containing species in the cytoplasm of cancer cells, such as glutathione and metallothioneins. Because cisplatin is easier to bind to sulfur-containing species, the resulting conjugation is more readily exported from the cancer cells.²³⁻²⁵ After the platinum-DNA adducts are formed, cells can survive by either through increased DNA repair or tolerance mechanism. Many cisplatin-resistant cancer cell lines have shown increased DNA repair capacity compared to the sensitive cell lines, like testicular cancer. The major DNA repair pathway involved in the removal of platinum-DNA lesions is nucleotide excision repair.²⁶ The increased tolerance could also come from the loss of DNA mismatch repair,^{27,28} bypass of DNA adducts,^{29,30} or decreased apoptosis.³¹

1.3 General Structure of Platinum Anticancer Agents

Although cisplatin is a very effective anticancer drug, it is highly toxic to kidneys (nephrotoxicity),^{1,32} which have driven chemists and biologists to make safer platinum agents to overcome the toxicity and the cisplatin resistance. In designing new platinum-based anticancer

agents, there are a few moieties that could be modified (Figure 1.3).⁸ Typically, there are three different types of ligands (L, R, and X) that could be incorporated onto the coordination environment of the Pt core. Ligands L, the “non-leaving group” ligands which typically contain nitrogen donors, bind to platinum tightly and stay unchanged in the final platinum-DNA adducts.

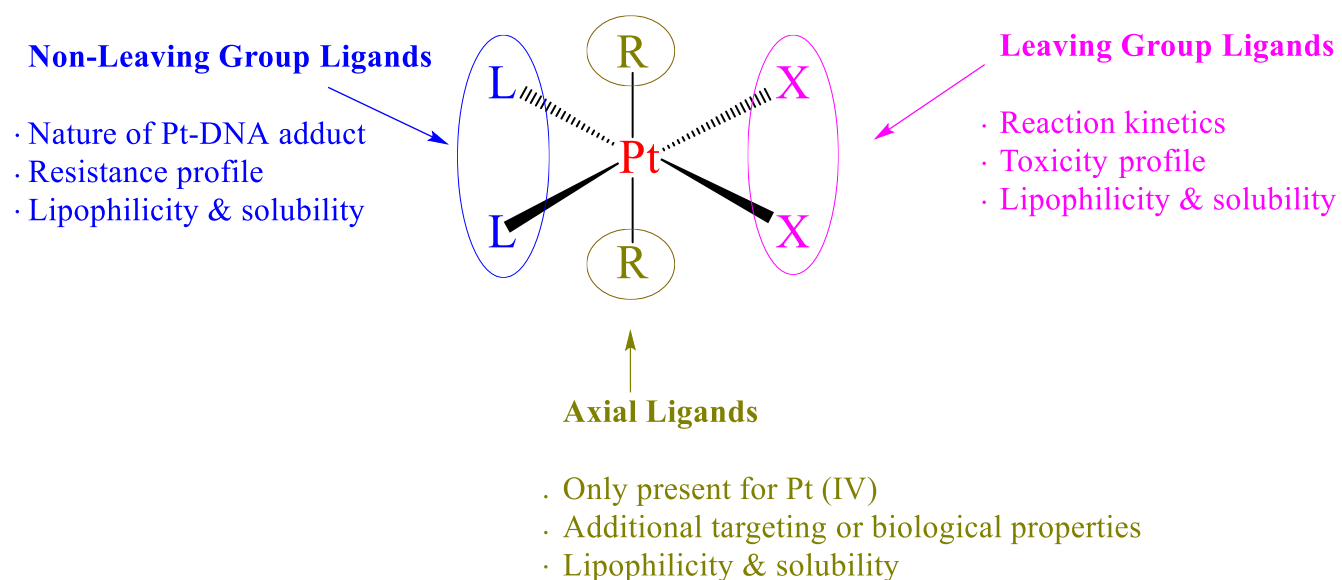


Figure 1.3 General structure of platinum anticancer agents.⁸

Modification of the L ligands would affect the nature of the platinum-DNA adducts, therefore changing the resistance profile.³³⁻³⁵ The leaving group ligands X, commonly halides and carboxylates, are labile and could be replaced through ligand substitution. Modification of ligands X can change the aquation/activation kinetics and therefore changing toxicity profile.³⁶ The axial ligands R only present in tetravalent platinum complexes and will dissociate after biological reduction. They could be used for tumor targeting by incorporating a functional R group aiming for specific cancer cells. Any modification of these three types of ligands will cause the change of lipophilicity and solubility, and both of these properties are very important in

terms of drug design. Ongoing research mainly focuses on reducing the toxic side effects of cisplatin, combating the drug resistance by modifying the ligands or improving the delivery technique.

1.4 Clinically Approved Platinum Anticancer Agents

Since the discovery of the first platinum drug cisplatin, another six platinum drugs (Figure 1.4) have been approved for clinical use in the USA and other countries. Carboplatin, as the second-generation Pt-based drug, was approved by FDA in 1989 and primarily used to treat ovarian cancer.^{12,37} It contains the same non-leaving group as cisplatin, but a different leaving group. The bidentate 1,1-cyclobutanedicarboxylate ligand that binds to Pt is tighter due to the chelation effect, resulted in a much slower aquation/activation rate compared with cisplatin.^{38,39} Because of the slower activation rate, carboplatin is much more gentle to off-target biological nucleophiles and thus has a lower toxicity profile.^{40,41} Therefore, carboplatin can be administered at a higher dosage than cisplatin. Although carboplatin is less toxic than cisplatin, it exhibits the same cross-resistance to cisplatin since they share the same non-leaving group, which results in the same platinum DNA-adducts as cisplatin.^{42,43}

Oxaliplatin mainly used for colorectal cancer treatment, is the third generation of platinum-based anticancer drugs and gained FDA approval in 2002.^{12,37} Like carboplatin, oxaliplatin has a chelating ligand (oxalate) as the leaving group, which are less susceptible to aquation. However, it has a different non-leaving group (1R,2R-diaminocyclohexane), which shows different sensitivity to cancer cell lines compared to cisplatin and carboplatin.⁴² The accumulation of oxaliplatin seems to be less dependent on copper transporters, but more on organic cation transporters, which are normally overexpressed in colon cancer.^{44,45} Oxaliplatin is the first clinically approved platinum drug that can overcome cisplatin resistance.

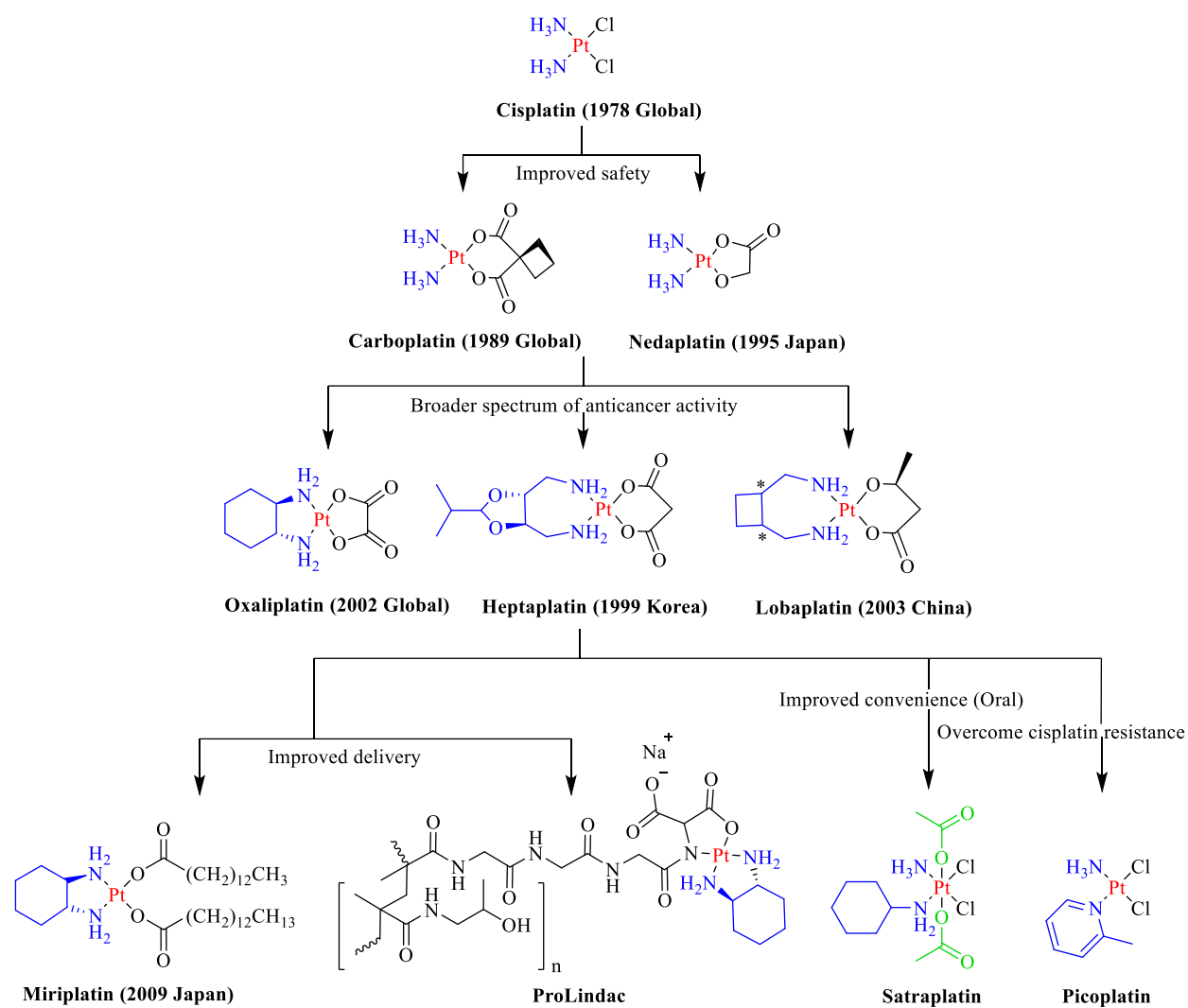


Figure 1.4 The family tree of platinum anticancer agents.

Nedaplatin is a second-generation analog that shares the same non-leaving group as cisplatin and carboplatin, but has a different chelating leaving group (glycolate) compared to carboplatin. The glycolate contributes to nedaplatin's higher water solubility than cisplatin and lower nephrotoxicity than cisplatin and carboplatin.⁴⁶ Nedaplatin was approved in Japan in 1995 and was primarily used for small cell lung cancer and non-small cell lung cancer.^{12,37}

Heptaplatin, approved by South Korea in 1999, is used for gastric cancer treatment.^{12,37} It possesses malonate as a chelating leaving group and bidentate 2-(1-methylethyl)-1,3-dioxolane-4,5-dimethanamine as the non-leaving group. The advantage of heptaplatin is the lower toxic side effects.⁴⁷

Lobaplatin, approved by China in 2003, is used for chronic myelogenous leukemia, breast cancer, and small cell lung cancer.^{12,13,37} It has an S-lactate as the leaving group and a R, R and S, S racemic mixture as the non-leaving group ligand. Therefore, lobaplatin is a mixture of diastereomers.⁴⁸

Miriaplatin, approved by Japan in 2009, is used for hepatocellular carcinoma. It has the same non-leaving group as oxaliplatin and contains myristates as the leaving group, which makes miriaplatin a lipophilic complex. It can be easily suspended in ethyl esters of iodized fatty acids. The advantage of miriaplatin suspension is the reduced toxicities in normal liver and the whole body.⁴⁹

There are a few platinum anticancer agents that have entered clinical trials but not approved yet, such as satraplatin (an orally active prodrug),⁵⁰ picoplatin (overcome cisplatin resistance),⁵¹ prolindac (AP5346, water-soluble biocompatible polymer for advanced delivery),⁵² and et al. Detailed discussion about picoplatin will be included in Chapter 2.

Chapter 2: Picoplatin Derivatives

2.1 Introduction

Numerous studies have indicated that the platinum detoxification by thiol-containing species, such as glutathione and metallothionein, is one of the main reasons for cisplatin resistance.^{23–25} The rationality of the design for a platinum drug containing a bulky ligand is that the bulky ligand could reduce the possibility of platinum binding to thiols which led to the invention of picoplatin (*cis*-aminodichloro(2-methylpyridine) platinum (II)).^{51,53–55}

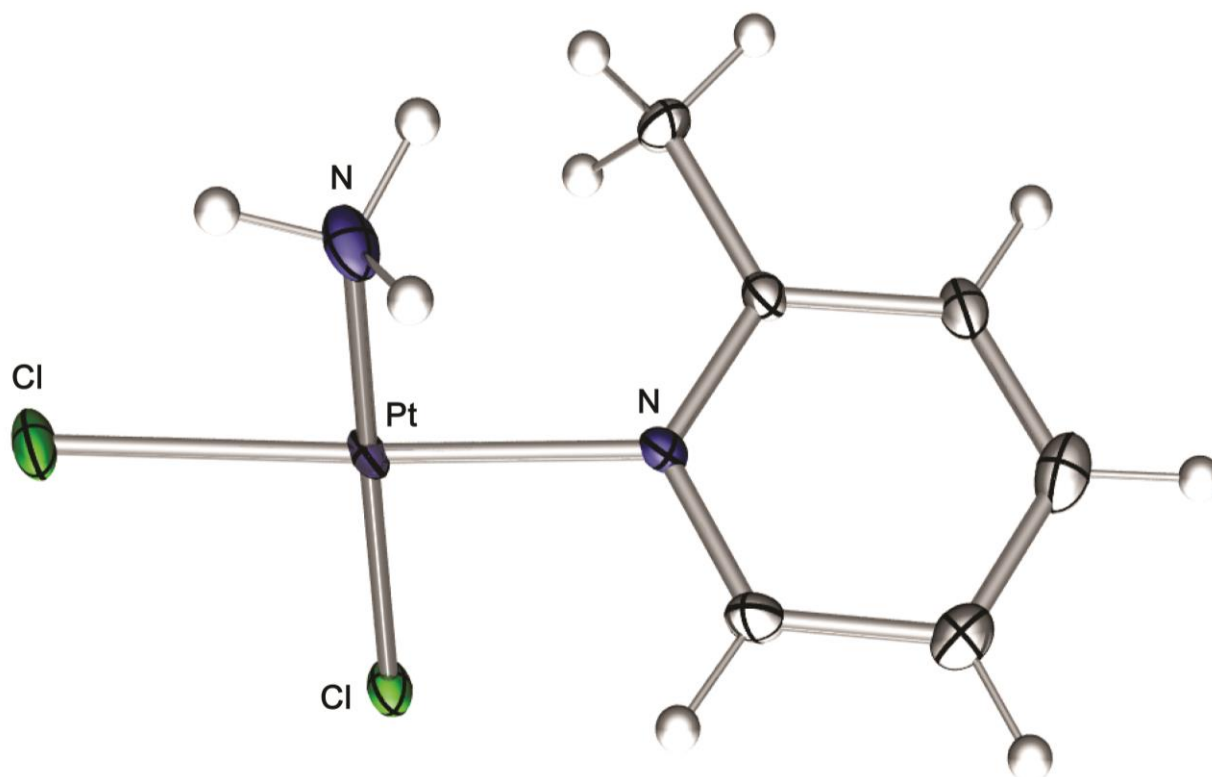


Figure 2.1 Crystal structure of picoplatin.

As shown in Figure 2.1, picoplatin contains a 2-methylpyridine (2-picoline) as one of the non-leaving groups. The pyridine ring is approximately perpendicular to the square planar coordination plane of platinum, leaving the methyl group on 2-picoline pointing to the axial position of the platinum. This provides the steric hindrance that prevents the thiols from attacking the platinum, therefore reducing the drug detoxification. Picoplatin was shown to be less reactive to thiol-containing species than cisplatin and also exhibited a slower aquation rate than cisplatin.^{56,57} The steric methyl group on the pyridine ring significantly affects the substitution kinetics of the picoplatin complex.

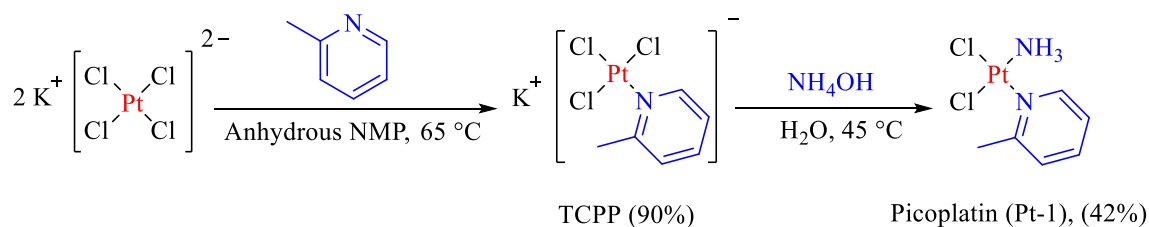
Picoplatin initially came from the collaboration between the Institute of Cancer and Johnson Matthey/AnorMed.⁵³ Preclinical studies have shown that picoplatin has antitumor properties in cisplatin-resistant ovarian cancer cells and lung cancer cell lines.⁵⁸ Studies have shown that cisplatin sensitive ovarian cancer cells (A2780) that were transfected to overexpress metallothionein has around 7-fold higher resistance to cisplatin, whereas there is no appreciable resistance to picoplatin.⁵⁹ Picoplatin also retains anticancer activity in cells with overexpressed drug resistance proteins and cell lines possessing acquired resistance to oxaliplatin.⁶⁰⁻⁶² A phase I clinical trial study of picoplatin started in 1997 and the drug was well tolerated with neutropenia as the common side effect.³⁷ In a phase II clinical trial study, picoplatin was evaluated against platinum pretreated ovarian cancers and small cell lung cancers.⁶³⁻⁶⁵ In a phase III trial study launched in 2007 with 399 participants, picoplatin was used as a second-line treatment for small cell lung cancer, sponsored by Poniard Pharmaceuticals.⁵⁵ There are also other clinical trial studies involving picoplatin as a treatment for different types of cancer.

Picoplatin with potent activity toward cancer cells and advantage over cisplatin-resistance cancer cells due to its steric feature presented us great potential to further fine-tune its structural

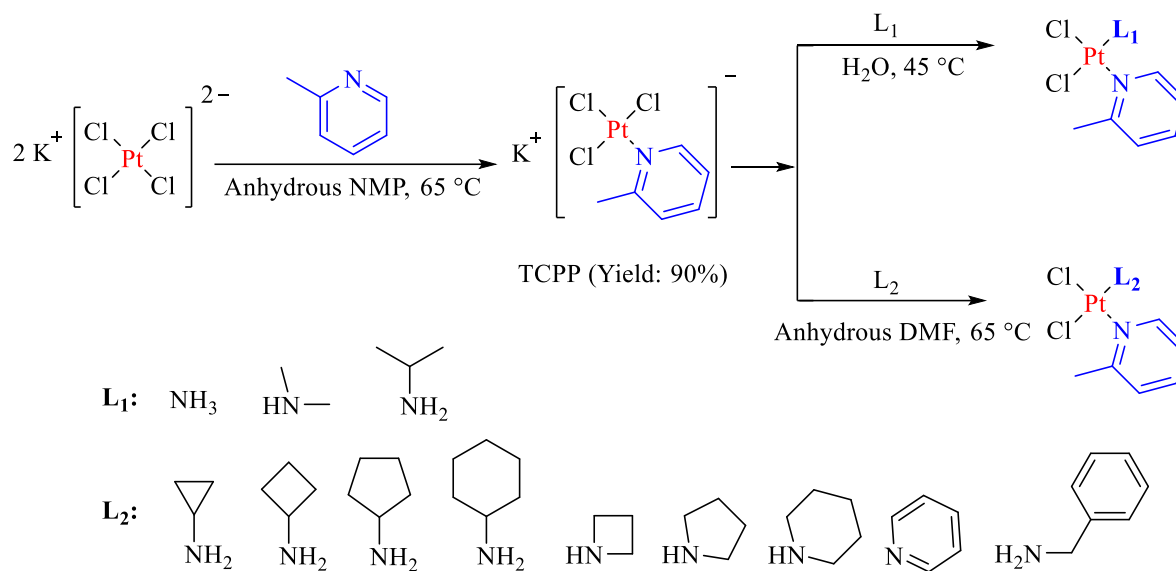
properties. Thus, we set our goal to synthesize families of picoplatin derivatives by varying the bulkiness of the non-leaving amine group. In this chapter, synthesis, characterization and various bioassay studies of picoplatin derivatives will be described in detail, followed by results and discussion.

2.2 Preparation of Picoplatin Derivatives

General procedures. The synthesis was conducted in a regular wet-lab setting in the Chemistry Department, University of the Pacific. All reagents were purchased from commercial vendors and used without further purification. NMR spectra were recorded using a JEOL 600 MHz spectrometer. ^1H NMR data are reported as follows: chemical shift in ppm relative to the residual solvent peaks, multiplicity (s = singlet, d = doublet, t = triplet, q = quartet, quint = quintet, m = multiplet, dd = doublet of doublets, dt = doublet of triplets, td = triplet of doublets, br = broad signal). MS spectra were recorded using JEOL DART/ESI-AccuTOF spectrometer, Varian 320 ESI-MS spectrometer or Thermal ESI-LTQ MS spectrometer. Elemental analysis was performed by Atlantic Microlab, Inc. X-ray structures were collected on Beamline 11.3.1 at the Advanced Light Source, Lawrence Berkeley National Lab using monochromatic radiation ($\lambda = 0.7749 \text{ \AA}$)



Scheme 2.1 Synthesis of Picoplatin.



Scheme 2.2 Synthesis of picoplatin derivatives.

A rapid way to synthesize picoplatin was developed in our lab by modifying the methods in literature⁶⁶ and patent.^{67,68} The synthesis scheme was shown in Scheme 2.1. The key intermediate $\text{K}[\text{PtCl}_3(\text{2-picoline})]$ (TCPP) was synthesized in anhydrous N-methyl-2-pyrrolidone (NMP) and further purified from anhydrous dimethylformamide (DMF). The yield of TCPP could reach 90%. The crystal structure is given in Appendix D. The bulky methyl group on the pyridine ring is crucial to the formation of the monosubstituted Pt intermediate. Picoplatin was then directly synthesized from TCPP in water by adding ammonium hydroxide without adding any other buffer. The purification process is quite straightforward without any use of chromatography. Using TCPP as the key intermediate, more than 10 picoplatin derivatives have been successfully synthesized and isolated (Scheme 2.2). They all secured 2-picoline as one non-leaving group and another non-leaving group, including primary amines, secondary amines, cycloalkyl amines, cyclic amines, pyridine, and benzylamine (Figure 2.2). According to the *trans*

effect theory, all derivatives should have a *cis* configuration, which was confirmed in most of the derivatives by X-ray crystallography (Appendix D).

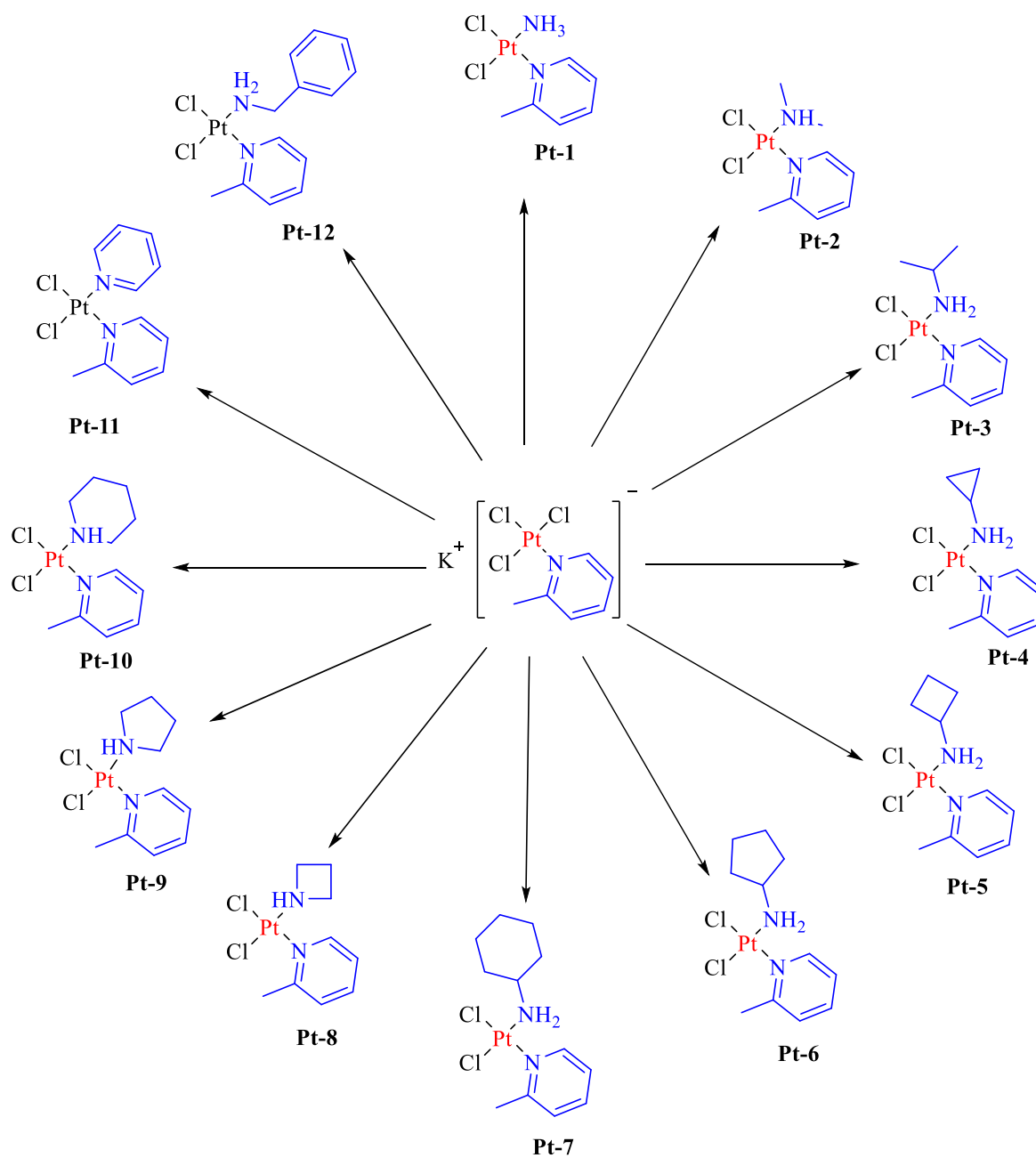


Figure 2.2 Summary of picoplatin derivatives.

K[PtCl₃(2-picoline)] (TCPP). To a mixture of potassium tetrachloroplatinate (II) fine powder, K₂PtCl₄ (1.0 g, 2.41 mmol, 1.0 equiv) in anhydrous NMP (6 mL) was added a solution of 2-picoline (261 μL, 0.464 mmol, 1.1 equiv) in 1 mL NMP at a rate of 20% every 20 min. The reaction was stirred at 65 °C for around 2 h after the complete addition of 2-picoline and stopped after all K₂PtCl₄ has dissolved. Byproduct KCl and a trace amount of unreacted K₂PtCl₄ are removed by vacuum filtration. Dichloromethane (DCM) was added to the filtrate to precipitate/crush out the product as a yellow solid. After the solids settled down, the supernatant was decanted, and the process was repeated three times to help to remove most NMP solvent. The solid was collected via vacuum filtration and washed with DCM, which was then dried overnight. The crude product was further purified by dissolving it in anhydrous DMF (~3-5 mL) and insoluble salts were removed by filtration. DCM was then added to the filtrate to induce product formation. After the solids settled down, the supernatant was decanted, and the process was repeated three times to help to remove most DMF solvent. The solid was collected via vacuum filtration and washed with DCM, which was then dried overnight to afford a yellow solid (0.94g, yield: 90%). ¹H NMR (600 MHz, D₂O): δ 8.82 (dd, J = 6.0, 1.1 Hz, 1H), 7.72 (td, J = 7.8, 1.6 Hz, 1H), 7.43 (d, J = 7.8 Hz, 1H), 7.26 (t, J = 6.7 Hz, 1H), 3.18 (s, 3H). ¹³C NMR (151 MHz, D₂O): δ 161.41, 153.56, 139.00, 126.97, 123.55, 26.02. ¹⁹⁵Pt NMR (129 MHz, D₂O): δ 1781.63. ESI-MS: m/z value of the most abundant isotope peak of C₆H₇Cl₃NPt, [M]⁻ calcd 393.9267, found 393.9. Crystals were obtained by vapor diffusion crystallization set-up with ether diffusing into a methanol solution.

PtCl₂(2-picoline)(NH₃) (Pt-1, picoplatin). To a solution of TCPP (120 mg, 0.277 mmol, 1.0 equiv) in H₂O (1 mL) was added 6 M NH₄OH (231 μL, 1.38 mmol, 5.0 equiv) and stirred at 45 °C in dark. A light-yellow solid started to precipitate out after 10 min. The light-yellow solid was collected via vacuum filtration after 1 h of stirring and washed with cold water and acetone. The

final product was dried under vacuum overnight (43.6 mg, yield: 42%). ^1H NMR (600 MHz, DMF- d_7) δ 9.05 (d, J = 5.7 Hz, 1H), 7.88 (t, J = 7.7 Hz, 1H), 7.56 (d, J = 7.8 Hz, 1H), 7.35 (t, J = 6.6 Hz, 1H), 4.41 (s, 2H), 3.18 (s, 3H). ^{13}C NMR (151 MHz, DMF- d_7): δ 162.84, 155.27, 139.13, 127.31, 123.91, 26.82. ^{195}Pt NMR (129 MHz, DMF- d_7): δ -2042.86. ESI-AccuTOF MS: m/z value of the most abundant isotope peak of $\text{C}_6\text{H}_{10}\text{Cl}_2\text{N}_2\text{PtNa}$, $[\text{M}+\text{Na}]^+$ calcd 398.9747, found 398.9662. Crystals were obtained by vapor diffusion crystallization set-up using MeOH and ether.

PtCl₂(2-picoline)(CH₃)₂NH (Pt-2). To a solution of **TCPP** (100 mg, 0.23 mmol, 1.0 equiv) in H₂O (1 mL) was added dimethylamine with a mass percentage of 40% in water (87.6 μL , 0.69 mmol, 3.0 equiv) and stirred at 45 °C in dark for 1 h. A light-yellow solid that formed was collected via vacuum filtration and washed with cold water, acetone and DCM. The product was dried under vacuum overnight (37 mg, yield: 40 %). ^1H NMR (600 MHz, DMF- d_7) δ 9.16 (d, J = 5.6 Hz, 1H), 7.93 (t, J = 7.5 Hz, 1H), 7.63 (d, J = 7.7 Hz, 1H), 7.42 (t, J = 6.5 Hz, 1H), 5.89 (s, 1H), 3.21 (s, 3H), 2.60 (d, J = 5.7 Hz, 3H), 2.54 (d, J = 5.7 Hz, 3H). ^{13}C NMR (151 MHz, DMF- d_7): δ 162.71, 154.97, 139.48, 127.79, 124.44, 44.29, 44.19, 26.91. ^{195}Pt NMR (129 MHz, DMF- d_7): δ -2088.57. ESI-AccuTOF MS: m/z value of the most abundant isotope peak of $\text{C}_8\text{H}_{14}\text{Cl}_2\text{N}_2\text{PtNa}$, $[\text{M}+\text{Na}]^+$ calcd 427.0061, found 427.0079. Anal. calcd for $\text{C}_8\text{H}_{14}\text{Cl}_2\text{N}_2\text{Pt}$: C, 23.77; H, 3.49; N, 6.93%. Found: C, 23.92; H, 3.45; N, 6.69%. Crystals were obtained by slow evaporation of a saturated DMF solution.

PtCl₂(2-picoline)(CH₃)₂CHNH₂ (Pt-3). Following the same synthesis procedure as **Pt-2**, the reaction afforded a light-yellow solid (yield: 20 %). ^1H NMR (600 MHz, DMF- d_7) δ 9.05 (d, J = 5.8 Hz, 1H), 7.89 (td, J = 7.7, 1.2 Hz, 1H), 7.57 (d, J = 7.8 Hz, 1H), 7.38 (t, J = 6.7 Hz, 1H), 3.18 (s, 3H), 3.12 (m, 1H), 1.33 (d, J = 6.5 Hz, 3H), 1.26 (d, J = 6.5 Hz, 3H). ^{13}C NMR (151 MHz, DMF- d_7): δ 162.87, 155.21, 139.24, 127.54, 124.16, 48.65, 26.84, 23.65, 23.45. ^{195}Pt NMR (129

MHz, DMF-d₇): δ -2101.25. ESI-AccuTOF MS: *m/z* value of the most abundant isotope peak of C₉H₁₆Cl₂N₂PtNa, [M+Na]⁺ calcd 427.0218, found 441.0277. Anal. calcd for C₉H₁₆Cl₂N₂Pt: C, 25.85; H, 3.86; N, 6.70%. Found: C, 26.08; H, 3.72; N, 6.64%. Crystals were obtained by vapor diffusion crystallization set-up using MeOH and ether.

PtCl₂(2-picoline)(cyclopropylamine) (Pt-4). To a solution of **TCPP** (125 mg, 0.288 mmol, 1.0 equiv) in anhydrous DMF (3 mL) was added cyclopropylamine (16.5 mg, 20.0 μ L, 0.288 mmol, 1.0 equiv). The resulting mixture was stirred at 65 °C for 20 h. An insoluble byproduct was removed by filtration and DMF in the filtrate was removed under reduced pressure (40-45 °C, 125 rpm). The residual was then dissolved in acetone (0.5mL), filtered and purified by preparative alumina TLC (DCM/Acetone =3/1). The gel band containing the product was scratched off, dissolved in acetone, filtered, concentrated to dryness, and triturated twice with Et₂O. A light-yellow product was collected via centrifugation, and dried under vacuum overnight (23 mg, yield: 19 %). ¹H NMR (600 MHz, DMF-d₇) δ 9.14 (d, *J* = 5.8 Hz, 1H), 7.90 (td, *J* = 7.8, 1.4 Hz, 1H), 7.59 (d, *J* = 7.9 Hz, 1H), 7.39 (t, *J* = 6.6 Hz, 1H), 5.17 (s, 2H), 3.23 (s, 3H), 2.37 – 2.31 (m, 1H), 0.50 – 0.46 (m, 2H), 0.45 – 0.41 (m, 2H). ¹³C NMR (151 MHz, DMF-d₇): δ 162.87, 155.42, 139.28, 127.41, 123.98, 30.76, 26.94, 6.80, 6.78. ¹⁹⁵Pt NMR (129 MHz, DMF-d₇): δ -2084.60. ESI-AccuTOF MS: *m/z* value of the most abundant isotope peak of C₉H₁₄Cl₂N₂PtNa, [M+Na]⁺ calcd 439.0061, found 439.0069. Anal. calcd for C₉H₁₄Cl₂N₂Pt: C, 25.97; H, 3.39; N, 6.73%. Found: C, 26.17; H, 3.27; N, 6.75%. Crystals of the final product were obtained by slow evaporation of a saturated DMF solution.

PtCl₂(2-picoline)(cyclobutylamine) (Pt-5). Following the same synthesis procedure as **Pt-4**, the reaction led to a light-yellow solid as the final product (yield: 20 %). ¹H NMR (600 MHz, DMF-d₇) δ 9.05 (d, *J* = 5.3 Hz, 1H), 7.90 (t, *J* = 7.7 Hz, 1H), 7.59 (d, *J* = 7.5 Hz, 1H), 7.39 (t, *J* =

6.6 Hz, 1H), 5.32 (d, $J = 49.5$ Hz, 2H), 3.46 – 3.38 (m, 1H), 3.19 (s, 3H), 2.16 (m, 2H), 1.97 (m, 2H), 1.55 (m, 2H). ^{13}C NMR (151 MHz, DMF- d_7): δ 162.86, 155.34, 139.26, 127.49, 124.11, 52.74, 30.88, 30.81, 26.94, 14.38. ^{195}Pt NMR (129 MHz, DMF- d_7): δ -2104.26. ESI-AccuTOF MS: m/z value of the most abundant isotope peak of $\text{C}_{10}\text{H}_{16}\text{Cl}_2\text{N}_2\text{PtNa}$, $[\text{M}+\text{Na}]^+$ calcd 453.0218, found 453.0271. Anal. calcd for $\text{C}_{10}\text{H}_{16}\text{Cl}_2\text{N}_2\text{Pt}$: C, 27.92; H, 3.75; N, 6.51%. Found: C, 28.05; H, 3.78; N, 6.30%. Crystals were obtained by vapor diffusion crystallization set-up using DCM and ether.

PtCl₂(2-picoline)(cyclopentylamine) (Pt-6). A light-yellow solid (yield: 14 %) as the product was obtained by following the same synthesis procedure as **Pt-4**. ^1H NMR (600 MHz, DMF- d_7) δ 9.07 (d, $J = 5.1$ Hz, 1H), 7.89 (t, $J = 7.4$ Hz, 1H), 7.58 (d, $J = 7.5$ Hz, 1H), 7.39 (t, $J = 6.1$ Hz, 1H), 5.12 (s, 2H), 3.26 (m, 1H), 3.20 (s, 3H), 2.08 (m, 1H), 1.98 (m, 1H), 1.65 (m, 4H), 1.49 (m, 2H). ^{13}C NMR (151 MHz, DMF- d_7): δ 162.86, 155.21, 139.22, 127.50, 124.10, 58.64, 34.03, 33.99, 26.87, 24.70, 24.62. ^{195}Pt NMR (129 MHz, DMF- d_7): δ -2099.05. ESI-AccuTOF MS: m/z value of the most abundant isotope peak of $\text{C}_{11}\text{H}_{18}\text{Cl}_2\text{N}_2\text{PtNa}$, $[\text{M}+\text{Na}]^+$ calcd 467.0375, found 467.0442. Anal. calcd for $\text{C}_{11}\text{H}_{18}\text{Cl}_2\text{N}_2\text{Pt}$: C, 29.74; H, 4.08; N, 6.31%. Found: C, 29.85; H, 3.93; N, 6.31%. Crystals were obtained by vapor diffusion crystallization set-up using DCM and ether.

PtCl₂(2-picoline)(cyclohexylamine) (Pt-7). The same synthesis procedure as **Pt-4** was applied, led to the formation of a light-yellow solid, which was further purified by preparative alumina TLC (DCM/EtOAc =1/1). (yield: 23 %). ^1H NMR (600 MHz, DMF- d_7) δ 9.05 (d, $J = 5.2$ Hz, 1H), 7.88 (t, $J = 7.4$ Hz, 1H), 7.57 (d, $J = 7.7$ Hz, 1H), 7.38 (t, $J = 6.3$ Hz, 1H), 5.07 (s, 2H), 3.18 (s, 3H), 2.72 (m, 1H), 2.52 m, 1H), 2.26 (d, $J = 11.2$ Hz, 1H), 1.72 (m, 1H), 1.67 (d, $J = 12.8$ Hz, 1H), 1.54 (d, $J = 12.3$ Hz, 1H), 1.30 – 1.16 (m, 4H), 1.03 (m, 1H). ^{13}C NMR (151

MHz, DMF-d₇): δ 162.85, 155.27, 139.18, 127.49, 124.11, 55.74, 34.53, 34.32, 26.82, 26.31, 25.91, 25.84. ¹⁹⁵Pt NMR (129 MHz, DMF-d₇): δ -2093.93. ESI-AccuTOF MS: m/z value of the most abundant isotope peak of C₁₂H₂₀Cl₂N₂PtNa, [M+Na]⁺ calcd 481.0532, found 481.0679. Anal. calcd for C₁₂H₂₀Cl₂N₂Pt (0.5 H₂O): C, 30.82; H, 4.53; N, 6.00%. Found: C, 31.02; H, 4.60; N, 5.89%. Crystals were obtained by vapor diffusion crystallization set-up using DCM and ether.

PtCl₂(2-picoline)(azetidine) (Pt-8). To a solution of **TCPP** (150 mg, 0.346 mmol, 1.0 equiv) in anhydrous DMF (3 mL) was added azetidine (19.7 mg, 23.3 μ L, 0.346 mmol, 1.0 equiv), and the resulting solution was stirred at 65 °C for 20 h. The insoluble byproducts were removed by filtration. DMF in the filtrate was concentrated under reduced pressure (40-45 °C, 125 rpm) until only ~0.5 mL was left. The residual was triturated twice with H₂O (2.0 mL), decanted, and lyophilized to remove water. The crude product was washed with EtOAc (~1 mL) and Et₂O (5 mL) twice, collected via centrifugation, and dried under vacuum overnight to afford a light-yellow solid (26 mg, yield: 18 %). ¹H NMR (600 MHz, DMF-d₇) δ 9.08 (d, J = 5.4 Hz, 1H), 7.93 (t, J = 7.6 Hz, 1H), 7.61 (d, J = 7.6 Hz, 1H), 7.41 (t, J = 6.6 Hz, 1H), 6.84 (br, 1H), 3.93 (m, 1H), 3.78 (m, 1H), 3.56 – 3.47 (m, 2H), 3.14 (s, 3H), 2.52 (m, 1H), 2.08 (m, 1H). ¹³C NMR (151 MHz, DMF-d₇): δ 162.43, 155.02, 139.45, 127.65, 124.38, 53.93, 53.65, 26.84, 22.56. ¹⁹⁵Pt NMR (129 MHz, DMF-d₇): δ -2139.23. ESI-AccuTOF MS: m/z value of the most abundant isotope peak of C₉H₁₄Cl₂N₂PtNa, [M+Na]⁺ calcd 439.0061, found 438.9988. Anal. calcd for C₉H₁₄Cl₂N₂Pt: C, 25.97; H, 3.39; N, 6.73%. Found: C, 26.13; H, 3.40; N, 6.51%. Crystals were obtained by vapor diffusion crystallization set-up using DCM and ether.

PtCl₂(2-picoline)(pyrrolidine) (Pt-9). Following the same synthesis procedure as **Pt-8**, the reaction led to the formation of a light-yellow crude product, which was purified by preparative

silica TLC (DCM/MeOH =20/1). The gel band containing the product was scratched off, dissolved in anhydrous DMF, filtered, and concentrated to ~0.5 mL. EtOAc was added to precipitate/crush out the final light-yellow product, which was then collected via centrifugation, washed with Et₂O, and dried under vacuum overnight (yield: 31 %). ¹H NMR (600 MHz, DMF-d₇) δ 9.13 (d, J = 5.5 Hz, 1H), 7.91 (t, J = 7.6 Hz, 1H), 7.61 (d, J = 7.7 Hz, 1H), 7.40 (t, J = 6.4 Hz, 1H), 5.89 (br, 1H), 3.21 (s, 3H), 3.18 (m, 2H), 3.04 (m, 1H), 2.83 (m, 1H), 1.66 (m, 4H). ¹³C NMR (151 MHz, DMF-d₇): δ 162.64, 155.05, 139.35, 127.63, 124.36, 52.94, 52.85, 27.02, 24.22, 24.17 (shown in HMQC spectrum). ¹⁹⁵Pt NMR (129 MHz, DMF-d₇): δ -2095.61. ESI-AccuTOF MS: m/z value of the most abundant isotope peak of C₁₀H₁₆Cl₂N₂PtNa, [M+Na]⁺ calcd 453.0218, found 453.0123. Anal. calcd for C₁₀H₁₆Cl₂N₂Pt: C, 27.92; H, 3.75; N, 6.51%. Found: C, 28.00; H, 3.57; N, 6.46%. Crystals were obtained by vapor diffusion crystallization set-up (DCM/Ether).

PtCl₂(2-picoline)(piperidine) (Pt-10). Following the same synthesis procedure as **Pt-8**, **Pt-10** was obtained as a light-yellow solid (yield: 35%). ¹H NMR (600 MHz, DMF-d₇) δ 9.12 (d, J = 5.3 Hz, 1H), 7.91 (t, J = 7.5 Hz, 1H), 7.60 (d, J = 7.6 Hz, 1H), 7.41 (t, J = 6.3 Hz, 1H), 5.60 (br, 1H), 3.41 – 3.31 (m, 2H), 3.20 (s, 3H), 3.02 (m, 1H), 2.82 (m, 1H), 1.65 (m, 2H), 1.56 (m, 1H), 1.47 (m, 2H), 1.33 (m, 1H). ¹³C NMR (151 MHz, DMF-d₇): δ 162.73, 154.91, 139.32, 127.67, 124.37, 54.17, 54.06, 26.98, 26.94, 26.81, 24.33. ¹⁹⁵Pt NMR (129 MHz, DMF-d₇): δ -2122.03. ESI-AccuTOF MS: m/z value of the most abundant isotope peak of C₁₁H₁₈Cl₂N₂PtNa, [M+Na]⁺ calcd 467.0375, found 467.0235. Anal. calcd for C₁₁H₁₈Cl₂N₂Pt: C, 29.74; H, 4.08; N, 6.31%. Found: C, 30.16; H, 4.19; N, 6.13%. Crystals were obtained by vapor diffusion crystallization set-up using MeOH and ether.

PtCl₂(2-picoline)(pyridine) (Pt-11). Using the same synthesis procedure as **Pt-9**, a light-yellow solid was obtained (yield: 18%). ¹H NMR (600 MHz, DMF-d₇) δ 9.22 (d, *J* = 5.4 Hz, 1H), 8.92 (d, *J* = 5.4 Hz, 2H), 8.04 (t, *J* = 7.7 Hz, 1H), 7.93 (t, *J* = 7.4 Hz, 1H), 7.60 (d, *J* = 7.8 Hz, 1H), 7.57-7.53 (m, 2H), 7.43 (t, *J* = 6.6 Hz, 1H), 3.19 (s, 3H). ¹³C NMR (151 MHz, DMF-d₇): δ 162.32, 154.46, 153.96 (2), 140.14, 139.95, 128.03, 127.53 (2), 124.76, 26.46. ¹⁹⁵Pt NMR (129 MHz, DMF-d₇): δ -1979.29. ESI-AccuTOF MS: *m/z* value of the most abundant isotope peak of C₁₁H₁₂Cl₂N₂PtNa, [M+Na]⁺ calcd 460.9905, found 460.9798. Anal. calcd for C₁₁H₁₂Cl₂N₂Pt: C, 30.15; H, 2.76; N, 6.39%. Found: C, 29.88; H, 2.63; N, 6.10%. Crystals were obtained by vapor diffusion crystallization set-up using MeOH and hexanes.

PtCl₂(2-picoline)(benzylamine) (Pt-12). The same synthesis procedure as **Pt-8** was applied to afford a light-yellow crude product (yield: 26%). ¹H NMR (600 MHz, DMF-d₇) δ 8.59 (d, *J* = 5.7 Hz, 1H), 7.83 (t, *J* = 7.6 Hz, 1H), 7.50 (m, 3H), 7.37 (m, 3H), 7.23 (t, *J* = 6.5 Hz, 1H), 5.57 (d, *J* = 41.6 Hz, 2H), 3.97 (m, 1H), 3.90 (m, 1H), 3.05 (s, 3H). ¹³C NMR (151 MHz, DMF-d₇): δ 162.76, 154.81, 139.29, 139.05, 130.15, 129.39, 128.67, 127.30, 123.82, 50.80, 26.70. (The ¹³C peak signals between 127.30 and 130.15 ppm represent 6 aromatic ¹³C, shown in HMQC NMR spectrum) ¹⁹⁵Pt NMR (129 MHz, DMF-d₇): δ -2095.60. ESI-AccuTOF MS: *m/z* value of the most abundant isotope peak of C₁₃H₁₆Cl₂N₂PtNa, [M+Na]⁺ calcd 489.0219, found 489.0150. Anal. calcd for C₁₃H₁₆Cl₂N₂Pt: C, 33.49; H, 3.46; N, 6.01%. Found: C, 33.76; H, 3.52; N, 5.83%. Crystals were obtained by vapor diffusion crystallization set-up using a solvent pair of EtOH and cyclohexane.

2.3 Bioassay Protocols

2.3.1 DNA binding assay. DNA binding study was performed at Dr. Liang Xue's lab in the Chemistry Department, University of the Pacific. The complex was dissolved in DI water

(200 μM) and stirred for 2 h at rt in a darkroom. The complex (20 μM) was then incubated with phosphate buffer (10 μM , pH = 6) and single-strand DNA (5' TCTCCTTCTGGTCTCTTCTC 3', 10 μM) at 37 °C for 5 hrs. Water was removed by lyophilization. The resulting sample was then dissolved in 30% glycerol (20 μL volume, 20 mM concentration) and loaded (5 μL) on a 22.5% of polyacrylamide gel (200 V for 25 h). SYBR green II was used as a stain solution. The staining time was 30-40 min. The gel was destained in deionized water (DI) for 1 min and scanned at 450 nm.

2.3.2 Cell viability assay. Cell viability study was performed in the School of Pharmacy, University of the Pacific in collaboration with Dr. Xin Guo's lab. Two cell lines, ovarian cancer cell line A2780 (cisplatin sensitive) and A2780cis (cisplatin-resistant), were purchased from Sigma Aldrich and used as the screening cell lines. They have shown different morphologies, with round shape morphology for A2780 and fibroblastic morphology for A2780cis (Appendix E). The cells were seeded (10,000) and cultured for 12 h on 96-well plates (UltraCruz® Tissue Culture Plate, catalog: sc-204447). The cell medium is RPMI-1640 with 2 mM Glutamine and 10% Foetal Bovine Serum (FBS). After the test compounds were dosed, the incubation (5% CO₂, 95% humidity, 37°C) of cells was continued for 72 h. Blank and solvent controls were incubated under the same conditions. MTS assay purchased from Promega was used to quantify viable cells which are capable to reduce the tetrazolium compounds into a colored formazan product.⁶⁹ The incubation time is 3 h and then the absorbance at 490 nm was recorded using a 96-well plate reader. The data was processed using GraphPad Prism 7. To maintain the cisplatin resistance of A2780cis, cisplatin as a 1 μM solution in the same medium was added every 2 passages.^{70,71}

2.3.3 Cellular accumulation assay. The cellular uptake study of platinum complexes was conducted using a Thermal ICP-OES instrument (iCAP 6000 series) in our lab at the Chemistry Department, University of the Pacific. Standard calibration curve of Pt in the same nitric acid matrix as the sample, measured at 214.4 nm using a series of dilutions from 1000 ppm stock solution in 5% nitric acid was obtained before the sample measurement. A2780 and A2780cis were cultured at the School of Pharmacy and 10^6 cells were seeded in 6-wells tissue culture plates (UltraCruz[®] Tissue Culture Plate, catalog: sc-204443) with 2 mL cell culture (5% CO₂, 95% humidity, 37°C). The culture was removed after 24 h and replaced by new cell culture with a 10 μ M platinum compound and continue to incubate for 24 h. The cell culture was removed using a pipette and washed three times with phosphate-buffered saline (PBS buffer, 2 mL each wash). Parallel experiments under the same condition except adding platinum compounds were used for cell counting. Concentrated HNO₃ (70%, 1 mL/well) was used to digest the samples. After 2 h, the digested sample was diluted 10 times using DI (0.6 mL to 5.4 mL DI), which was then injected to ICP-OES directly. Wells without cell seeding was used as the blank control. Three independent replicates were conducted for every experiment. After subtracting the values from the blank control, the platinum content was quantified to nanogram Pt per 10^6 cells.^{72,73}

2.4 Results and Discussion

2.4.1 DNA binding study. Since DNA is the biological target of platinum-based anticancer agents and 1,2-d(GpG) intrastrand cross-link adduct is the main product. A single strand 20mer DNA with two adjacent guanines in the middle (5' TCTCCTTCTGGTCTCTTCTC 3')⁷⁴ as the binding site was selected and prepared by Dr. Liang Xue's lab for initial screening.

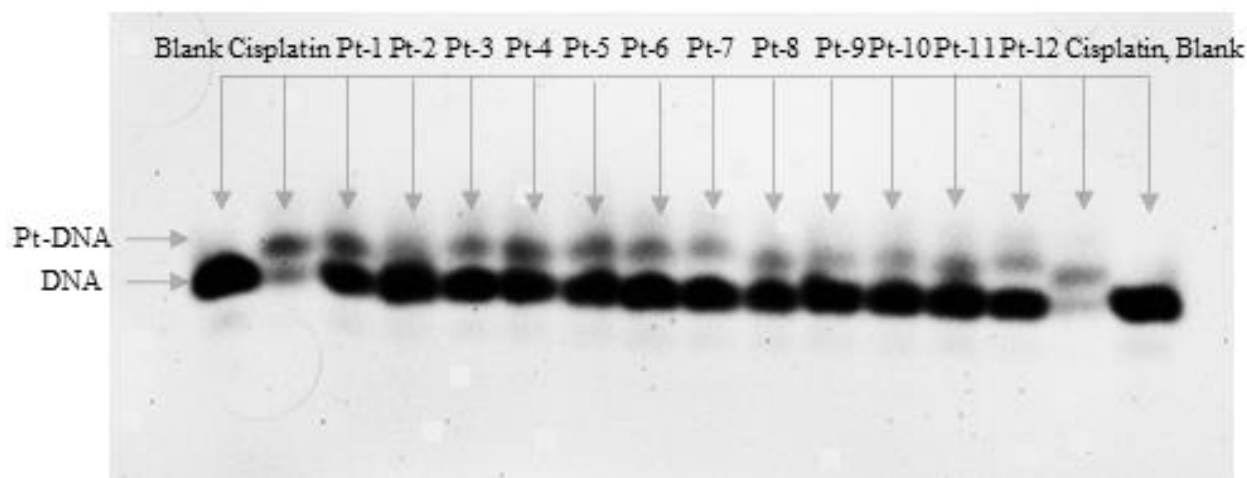


Figure 2.3 DNA gel electrophoresis of picoplatin derivatives.

In the DNA gel electrophoresis graph of Figure 2.3, the bottom darker spot is the pure DNA and the top spot is the Pt-DNA adduct, which has been confirmed by mass spectrometry (Appendix E). Since the molecular weight of Pt-DNA adduct formed with each picoplatin derivative is quite close to that of cisplatin, the separation difference of all Pt-DNA adducts is negligibly small like cisplatin, thus all the Pt-DNA adducts were aligned in the gel electrophoresis. Quantitative study with three runs for each complex has been conducted (Appendix E) and the summary is shown in Figure 2.4. Not surprisingly, cisplatin is still the most efficient one in terms of binding yield. Complexes **Pt-4**, **Pt-5**, and **Pt-6** showed comparable binding efficiency with **Pt-1** (picoplatin). In order to further exam these complexes, a cell viability study was performed.

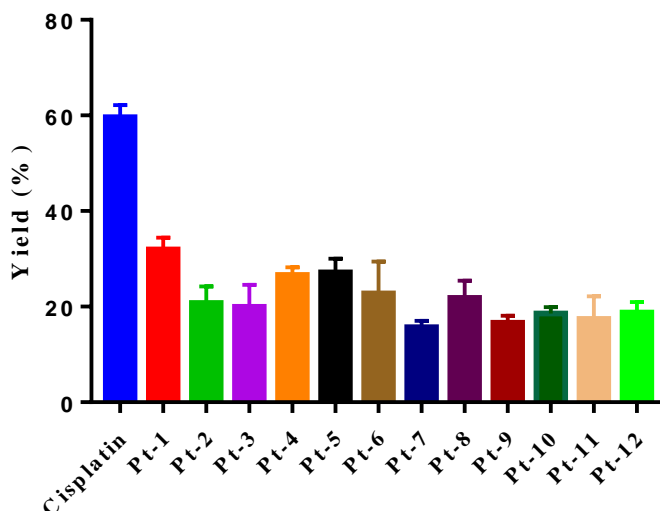


Figure 2.4 The DNA binding yield of picoplatin derivatives. (confidence interval: 95%, $p < 0.01$)

2.4.2 Cell viability study. Before performing the cell viability study, the toxicity of the formulation solvent needed to be evaluated. Dimethyl sulfoxide (DMSO) is the most commonly used formulation solvent in cell viability studies. However, it does not work for platinum-containing agents as the nucleophilic sulfur atom on the DMSO will bind to platinum and deactivate the complex.⁷⁵ As initiated by other researchers, DMF was applied to formulate our platinum compound. Different amount of DMF have been used in the literature, ranging from 0.1% to 1.0% by volume.^{70,71, 76–78} Initially, 1% DMF was chosen, however, most of the cells died before adding any of the platinum complexes. A detailed study was performed to evaluate the percentage of DMF by volume toxicity effect on cell viability, shown in Figure 2.5. The figure demonstrated that DMF at higher concentration does possess higher toxicity toward cells. In order to reduce solvent toxicity but at the same time formulate/dissolve the platinum complex, 0.25 % DMF was chosen in the following studies.

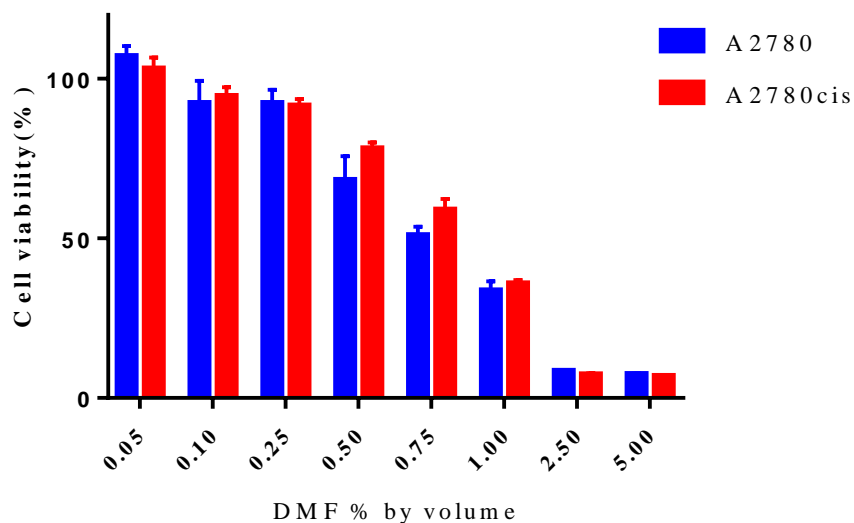


Figure 2.5 DMF % by volume effect on cell viability study of A2780 and A2780cis.

Preliminary cell viability screening of picoplatin derivatives in A2780 and A2780cis cell lines was performed at two different concentrations of 5 μ M, and 20 μ M (Figure 2.6). It is very clear that the A2780 cell line is more sensitive to all complexes. In A2780 cell line, **Pt-4**, **Pt-5**, **Pt-6**, **Pt-11**, and **Pt-12** shows comparable cell viability to cisplatin and picoplatin (**Pt-1**), while the rest are less toxic. In A2780cis cell line, **Pt-4**, **Pt-5**, **Pt-6**, **Pt-11**, and **Pt-12** have comparable cell viability to picoplatin and even better than that of cisplatin. Overall, the picoplatin derivatives bearing a cycloalkyl amine as the non-leaving group showed promising activity, while cyclic amines as the non-leaving group have less efficacy. Pyridine ring (**Pt-11**) and benzylamine (**Pt-12**) as non-leaving groups also showed better efficacy. The study demonstrated that the steric feature and ring constraints of the ligands on the platinum agents played an important role in its efficacy toward cancer cells. **Pt-1**, **Pt-3**, and **Pt-4**, representing a reference and samples with potent efficacy, were used for more detailed study.

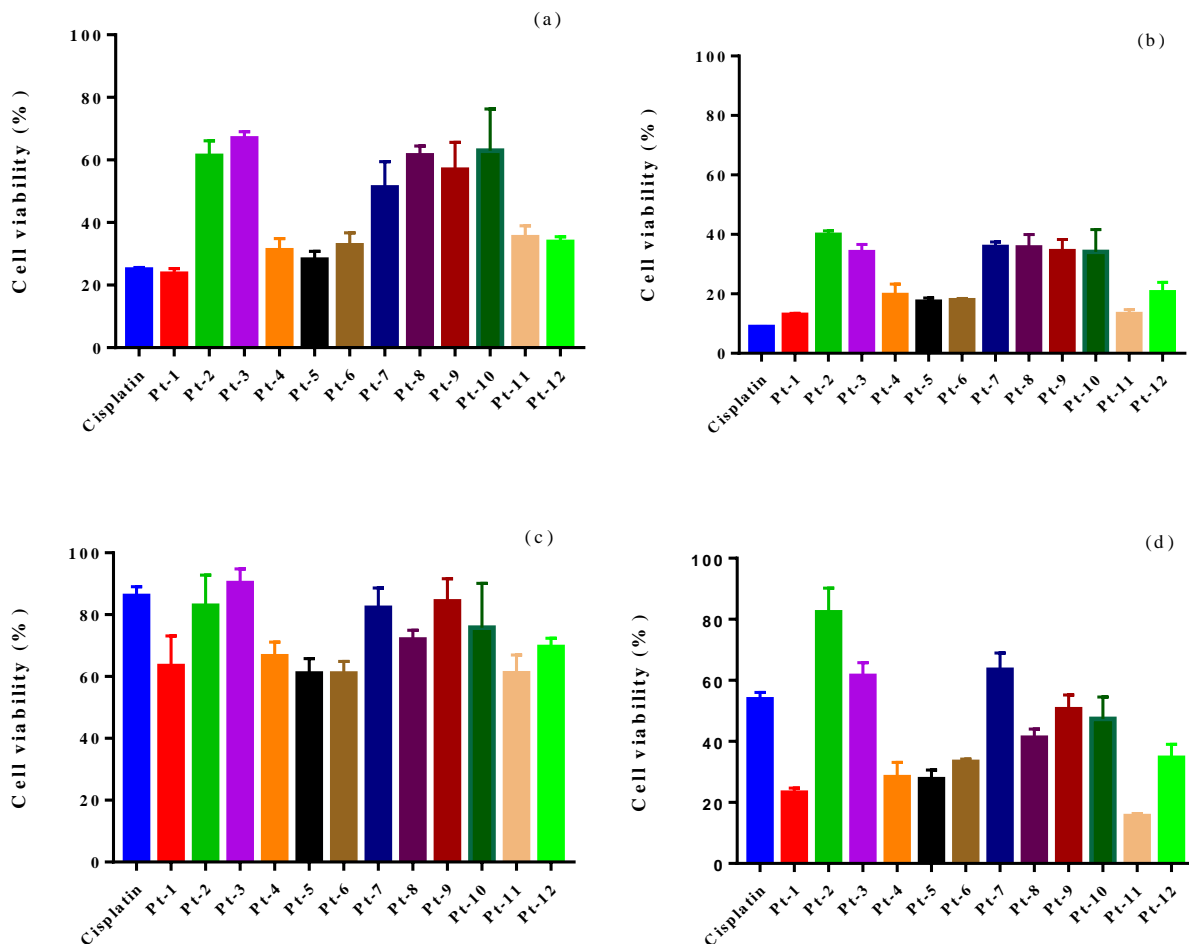


Figure 2.6 Preliminary cell viability screening of picoplantin derivatives in two ovarian cell lines at two concentrations. (a) A2780 with 5 μ M, (b) A2780 with 20 μ M, (c) A2780cis with 5 μ M, (d) A2780cis with 20 μ M.

The IC₅₀ values of **Pt-1**, **Pt-3**, and **Pt-4** against A2780 and A2780cis were reported in Figure 2.7 and summarized in Table 2.1. Cisplatin is used as the reference compound. Directly dissolving the compound in 0.25% or 25% DMF did not work. The pre-formulation strategy was applied in the study. A test compound is first dissolved in pure DMF and then diluted with 3 \times volume of the cell culture media to reach 25% DMF by volume. A series of dilution was done using cell culture media containing 25% DMF by volume to obtain the stock solution. The stock

solution was further diluted 100× using pure cell culture media to obtain the working solution (0.25% DMF by volume), which was directly added to the 96-well plates (200 μ L).

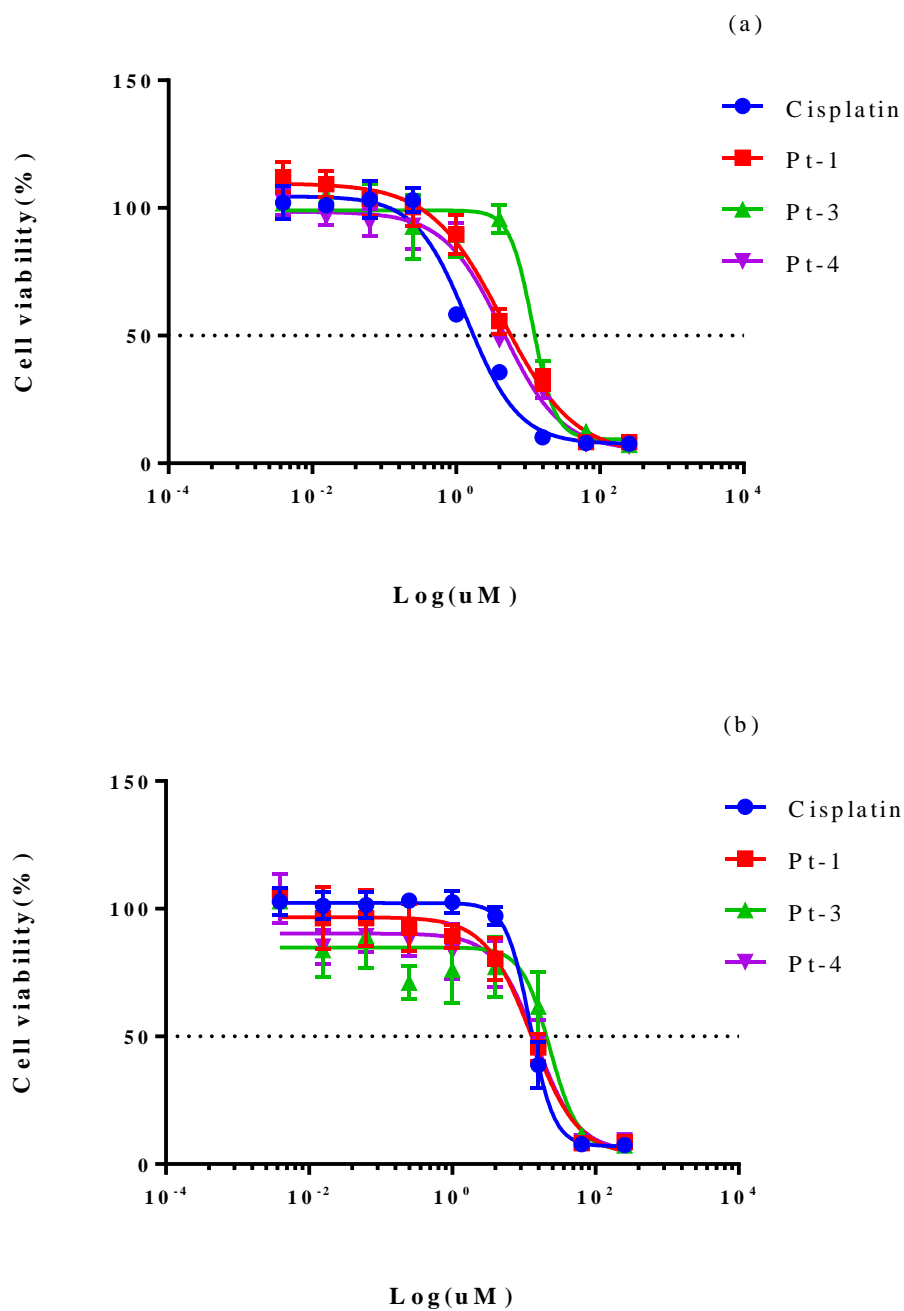


Figure 2.7 IC₅₀ curve of cisplatin, **Pt-1**, **Pt-3**, and **Pt-4** in (a) A2780 and (b) A2780cis cell lines.

Table 2.1 Cytotoxic activities of cisplatin, **Pt-1**, **Pt-3**, and **Pt-4** in cell lines A2780 and A2780cis.

IC ₅₀ (μM)	A2780	A2780cis	Resistance factor (R _f)*
Cisplatin	1.42 ± 0.13	12.26 ± 0.59	8.63
Pt-1	4.40 ± 0.50	12.85 ± 1.59	2.92
Pt-3	11.59 ± 1.05	23.13 ± 4.35	2.00
Pt-4	4.43 ± 0.48	14.81 ± 2.08	3.34

*Resistance factor (R_f) is defined as IC₅₀(A2780cis)/IC₅₀(A2780)

Although **Pt-1** (picoplatin) and **Pt-4** are less toxic than cisplatin in cisplatin sensitive cell line A2780, they show comparable IC₅₀ value with cisplatin in A2780cis. As expected, cisplatin shows a high resistance factor (R_f) of 8.63, which is consistent with the literature data.^{70,71} Both **Pt-1** (picoplatin) and **Pt-4** have a much smaller resistance factor, indicating a low cross-resistance to cisplatin. **Pt-3** has a very similar formula and structure as those of **Pt-4** but less cytotoxic in both A2780 and A2780cis cell lines. In order to further understand the nuance of biological action among these complexes, a cellular accumulation study was conducted.

2.4.3 Cellular accumulation study. Intracellular accumulation is one of the key factors affecting the cytotoxicity of platinum-based anticancer agents. To examine the accumulation level of platinum in A2780 and A2780cis cell lines, cisplatin, **Pt-1**, **Pt-3**, and **Pt-4** were chosen for the study. The test compounds, each at 10 μM, were incubated with the cancer cell lines for 24 h and the platinum level was measured by ICP-OES. Data from Figure 2.8 and Table 2.2 demonstrated that significant difference was observed among the four compounds, with cisplatin being the simplest and smallest platinum agent but having low cellular accumulation. Picoplatin derivatives with more organic components and higher molecular weight, especially **Pt-1** and **Pt-4**, were easier to accumulate in both cell lines than cisplatin. Therefore, the structural feature of the platinum agents played a significant role in the platinum accumulation levels in cells.

However, there is no linear relationship between the bulkiness of the complex and the level of cellular accumulation. Even a minor change in the structure could lead to huge difference in cellular uptake, such as Pt-3 and Pt-4. The only difference between **Pt-3** and **Pt-4** is on one of the non-leaving groups, being isopropylamine on **Pt-3** and cyclopropylamine with ring strain on **Pt-4**. However, the cellular accumulation levels of **Pt-4** in both cell lines are nearly doubled in comparison to those of **Pt-3**. Therefore, a trivial structural variation, such as with or without ring strain, could significantly alter its activity toward cancer cells.

The accumulation levels of platinum in A2780cis are significantly lower than that in A2780 for all four compounds, which explains the decreasing cytotoxicity of these compounds in A2780cis. The research provided strong support for the proposed hypothesis where cancer cells could grow resistance to platinum drugs possibly by downregulation of membrane transporter,^{1,45,79,80,81} or more readily exportation of detoxified conjugation from cells.^{23,24,25} **Pt-1** and **Pt-4** are much easier to accumulate in both A2780 and A2780cis cell lines, however, the IC₅₀ values (Table 2.1) are not smaller than that of cisplatin in A2780, indicating the enhanced cytotoxicity of cisplatin in A2780 is not due to the significantly low cellular accumulation of cisplatin. The higher cellular accumulation of Pt-1 and Pt-4 in A2780cis may contribute to their low IC₅₀ values (Table 2.1), which are comparable to that of cisplatin.

Table 2.2 Cellular accumulation of platinum from cisplatin, **Pt-1**, **Pt-3**, and **Pt-4** in A2780 and A2780cis.*

Mean (ng Pt/10 ⁶ cell)	A2780	A2780cis
Cisplatin	59.59 ± 1.62	10.28 ± 0.41
Pt-1	121.80 ± 0.94	29.89 ± 1.35
Pt-3	55.35 ± 2.64	21.77 ± 2.49
Pt-4	103.50 ± 3.18	51.82 ± 5.17

*treated at 10μM for 24 h

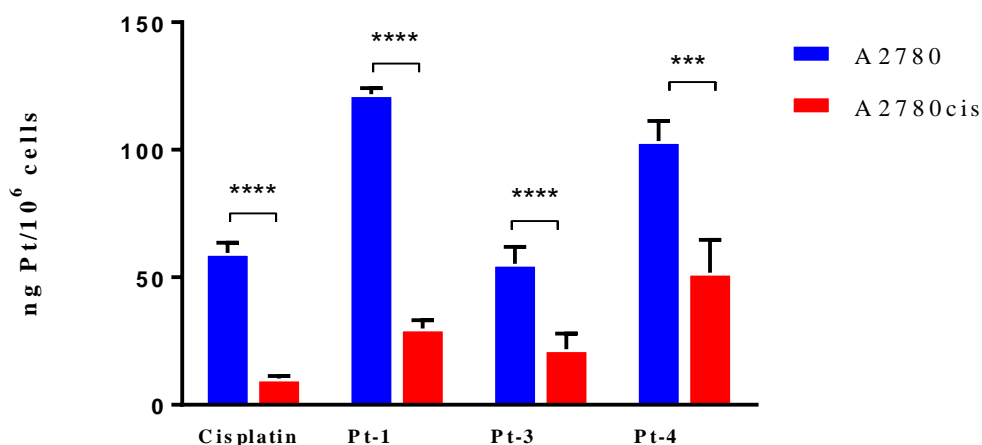


Figure 2.8 Cellular accumulation of platinum from cisplatin, **Pt-1**, **Pt-3**, and **Pt-4** in A2780 and A2780cis cell lines. (treated at 10 μ M for 24 h) **** $p \leq 0.0001$, *** $p \leq 0.001$.

2.5 Conclusions

A convenient synthesis route for picoplatin derivatives have been established and 11 picoplatin derivatives have been synthesized and characterized. The bulky methyl group on 2-picoline is crucial for the formation of monosubstituted product **TCPP**, while **TCPP** is the key intermediate leading to the success of all picoplatin derivatives. The solvent involved in the last step of the synthesis is either protic solvent H₂O or anhydrous aprotic solvent DMF. If the non-leaving group is a small amine and the product formation is quick, H₂O with mild reaction temperature (~45 °C) would be applied, otherwise, anhydrous DMF with moderate reaction temperature (~65 °C) is the first choice. The stronger trans effect of the chloride than that of the pyridine on **TCPP** led to the successful synthesis of the picoplatin derivatives, all in *cis* configuration confirmed by solid-state structural analysis.

Three bioassays were used to evaluate the efficacy of picoplatin derivatives, including DNA binding assay, cell viability assay, and cellular accumulation assay. The DNA gel electrophoresis shows that the picoplatin derivatives have comparable binding efficiency with picoplatin. Cell viability studies show that derivatives with cycloalkyl amines with ring strain as non-leaving group exhibits better efficacy, while that with cyclic amines as non-leaving group shows less efficacy. **Pt-11** with pyridine ring and **Pt-12** with benzylamine as non-leaving groups also show better efficacy. Cellular accumulation study shows a higher level of platinum content in the A2780 cell line than that of A2780cis, which may be one of the explanations for the cisplatin resistance in A2780cis cell line.

The study of picoplatin derivatives laid the foundation for the search of platinum-based anticancer agents through structural attenuation.

Chapter 3: HDAC Inhibitors

3.1 Introduction

It is well known that DNA is wrapped around histone proteins to form chromatin. As shown in Figure 3.1, the positively charged lysine residue of histone protein has strong ionic interaction with the negatively charged DNA, resulting in a more condensed chromatin structure.^{82,83} Histone acetylase (HAT) is an enzyme that can add an acetyl group on the lysine residue, thereby neutralizing the positive charge and forming a relaxed chromatin structure. The more open structure allows transcription factors to access the gene, thereby promoting the gene expression. On the other hand, histone deacetylase (HDAC) is an enzyme that can remove the acetyl group from the acetylated lysine residue and restore the positive charge, therefore returning to the condensed chromatin structure. Deacetylation of the histone proteins will cause gene silencing. The acetylation status is controlled by HAT and HDAC enzyme families and is one of the most extensively studied epigenetic process.^{83,84,85}

There are eighteen HDACs that have been identified in humans and are subdivided into four classes, including class I HDACs (HDAC 1, 2, 3 and 8), class II HDACs (HDAC 4, 5, 6, 7, 9 and 10), class III HDACs (SIRT 1, 2, 3, 4, 5, 6 and 7) and class IV HDACs (HDAC 11).^{86,87} It has been reported that many HDACs are overexpressed in different types of cancers, including HDAC1 in the prostate,⁸⁸ gastric,⁸⁹ colon⁹⁰ and breast cancers⁹¹, HDAC2 in colorectal,^{90,92} cervical⁹³ and gastric cancer,⁹⁴ HDAC3 in colon cancer⁹⁰ and HDAC6 in breast cancer.⁹⁵ On the other hand, knockdown of individual HDACs overexpressed in cancers could suppress cell growth.^{90,92,93,96} It also has been shown that overexpressed HDAC suppress the expression of cancer suppressor genes in many tumors, and HDAC inhibitors (HDACi) could restore the

expression of cancer-suppressive genes and induce apoptosis.^{86,97–103} Therefore, HDAC has become a promising biological target for cancer treatment.^{83,86,104,105}

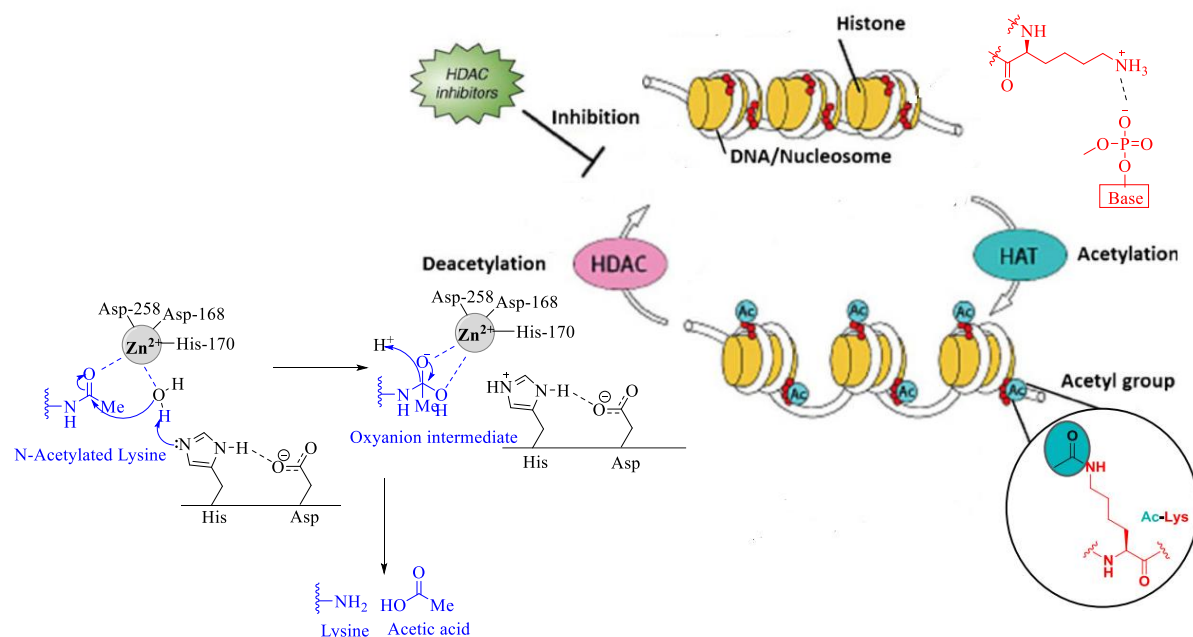


Figure 3.1 Roles of histone acetyltransferases (HATs) and histone deacetylases (HDACs) in regulating histone proteins (right), and HDACs in deacetylation mechanism (left).^{82,83}

Most HDACs have a catalytic zinc domain, as shown in the left part of Figure 3.1.^{82,83} The zinc cofactor acts as a Lewis acid, which interacts with the oxygen atom of the acetyl group and catalyzes its hydrolysis. If there is a stronger chelator that could bind to the catalytic zinc center, the deacetylation would be inhibited, resulting in a more relaxed chromatin structure.

The design of HDACi was originally derived from the understanding of the co-crystal structure between a bacterial homolog of histone deacetylase-like protein and hydroxamic acid Trichostatin A.¹⁰⁶ The scaffold was also based on mimics of acetylated lysine. The first FDA approved HDACi is Vorinostat (SAHA). As shown in Figure 3.2 b, it consists of three main

domains: a surface binding domain (cap), a hydrocarbon linker motif, and a zinc-binding group (ZBG).⁸³ All components are necessary for a new HDAC inhibitor to function effectively. A recent study on the X-ray crystal structure of SAHA bound to an HDAC-like protein discovered an internal cavity adjacent to the zinc-binding domain (Figure 3.2 a), which hinted for additional hydrophobic moiety in the newer HDACi design.¹⁰⁷

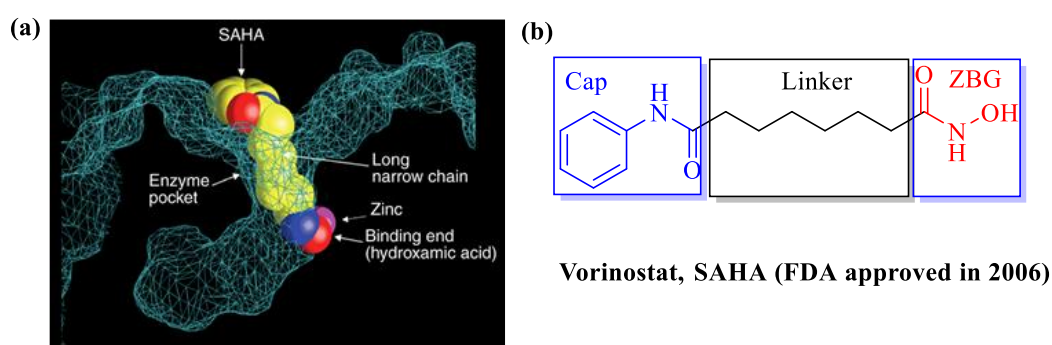
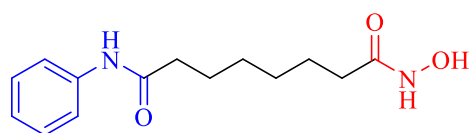


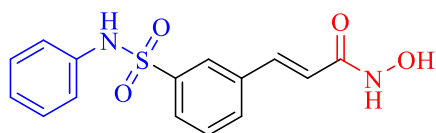
Figure 3.2 (a) X-ray crystal structure of SAHA bound to an HDAC-like protein.¹⁰⁷ (b) Molecular structure of SAHA.⁸³

To date, five HDAC inhibitors shown in Figure 3.3 have entered clinical use, with four approved by US FDA and one approved by the China Food and Drug Administration (CFDA).¹⁰⁸ Vorinostat, belinostat, and panobinostat all have hydroxamic acids as the zinc-binding group. The depsipeptides romidepsin is more like a prodrug and the disulfide bond in romidepsin would be reduced and release the active thiol group acting as the zinc-binding group. Chidamide has *ortho*-aminoanilide as the zinc-binding group. There are many kinds of HDAC inhibitors, including short-chain alkanolic acids, hydroxamic acids, cyclic peptides, and other macrocycles, *ortho*-aminoanilides, et al.^{83,109} As most clinically studied and approved HDAC inhibitors are hydroxamic acids and *ortho*-aminoanilides derivatives, and their synthesis is more

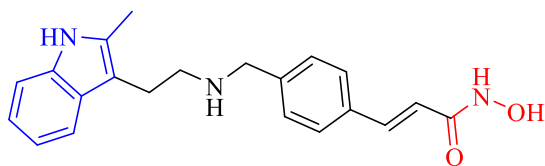
straightforward while compared to cyclic peptides, we will focus on HDAC inhibitors with hydroxamic acids and *ortho*-aminoamides in the following study.



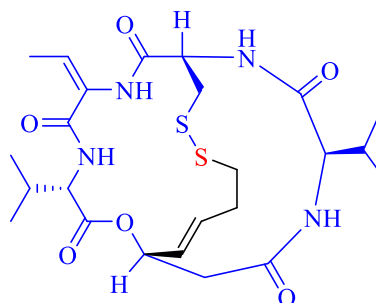
Vorinostat, SAHA (FDA, 2006)
Cutaneous T-cell lymphoma (Oral)



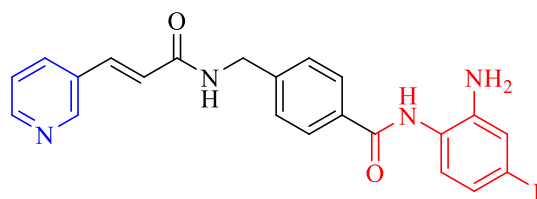
Belinostat (FDA, 2014)
Peripheral T-cell lymphoma (IV)



Panobinostat (FDA, 2015)
Multiple myeloma (Oral)



Romidepsin (FDA, 2009)
Cutaneous T-cell lymphoma (IV)



Chidamide (CFDA, 2014)
Peripheral T-cell lymphoma (Oral)

Figure 3.3 Clinically approved HDAC inhibitors with approving agency, year of approval, therapeutic indication, and administration route.¹⁰⁸

3.2 Preparation of HDAC Inhibitors

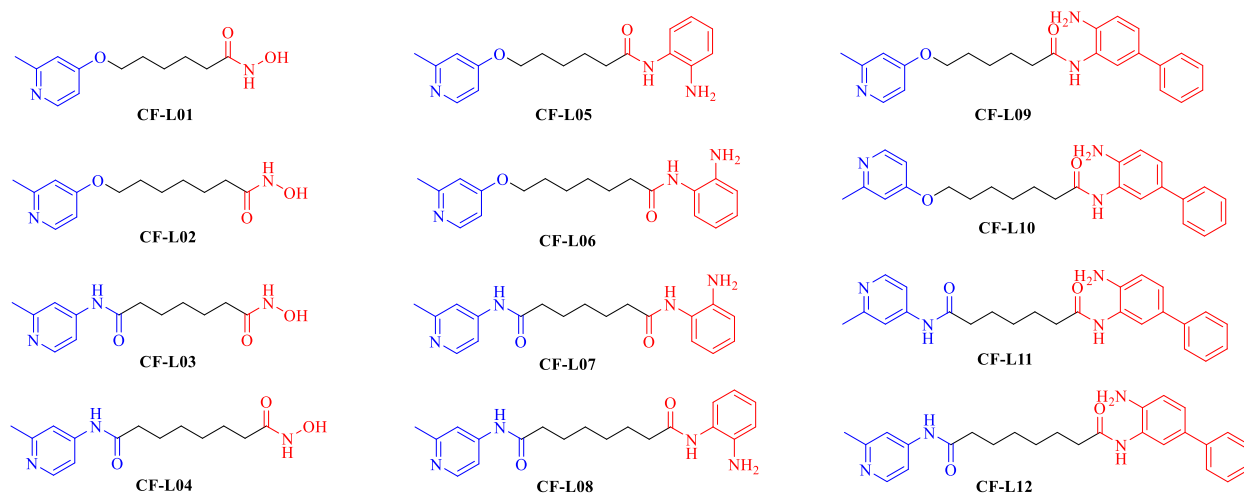
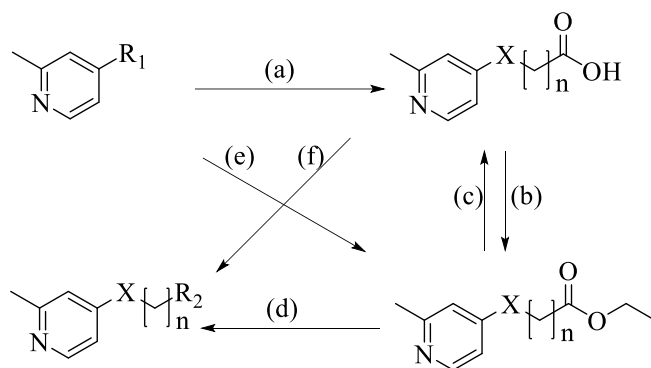


Figure 3.4 Structures of HDAC inhibitors (**CF-L01** to **CF-L12**).

As shown in Figure 3.4, 12 HDAC inhibitors have been synthesized and characterized in our lab. They shared the same cap domain, 2-methyl pyridine, but have variations on the linkage between the cap domain and linker, the linker length, and the zinc-binding group. The linkage between the cap domain and linker could be an ether bond or a reversed amide bond.

Convenience in their synthesis is the main reason in choosing these linkages. The second variation is the linker length, with 5 or 6 carbons, which is the appropriate length approved by various bioassays.^{110–112} The third variation is the zinc-binding group, including hydroxamic acid, *ortho*-aminoamide and *ortho*-aminoamide possessing a C-5 phenyl group that could occupy the internal cavity illustrated in Figure 3.2 a.^{83,106} The general synthesis scheme is shown in Scheme 3.1. Structures of HDAC inhibitors **CF-L13** to **CF-L19** are shown in Figure 3.5 and Figure 3.6. **CF-L13** to **CF-L17** were designed based on the results of structural activity relationship study of **CF-L01** to **CF-L12**. **CF-L18** and **CF-L19** were designed by modifying

Panobinostat. The detailed synthesis scheme of each individual HDAC inhibitor is included Appendix A.



Reagents and conditions: $R_1 = \text{Br}$ (a) oxepan-2-one ($n=5$) or oxocan-2-one ($n=6$), KOH, DMSO, $75\text{ }^\circ\text{C}$
 $X = \text{O}$ (b) concentrated H_2SO_4 , EtOH, reflux
 $X = \text{O}$ or $\text{NH}(\text{C}=\text{O})$ (c) NaOH, THF/ H_2O (1/1), rt
 $R_2 = \text{hydroxamic acid}$ (d) NH_2OH (50 wt% in water), NaOH, DCM/MeOH (1/2), rt
 $R_1 = \text{NH}_2$ (e) ethyl hydrogen pimelate ($n=5$) or 8-Methoxy-8-oxooctanoic acid ($n=6$), HATU, DIEA, DMF rt
 $X = \text{NH}(\text{C}=\text{O})$ (f) o-Phenylenediamine derivatives, HATU, DIEA, DMF rt

Scheme 3.1 Synthesis routes of HDAC inhibitors (**CF-L01** to **CF-L12**).

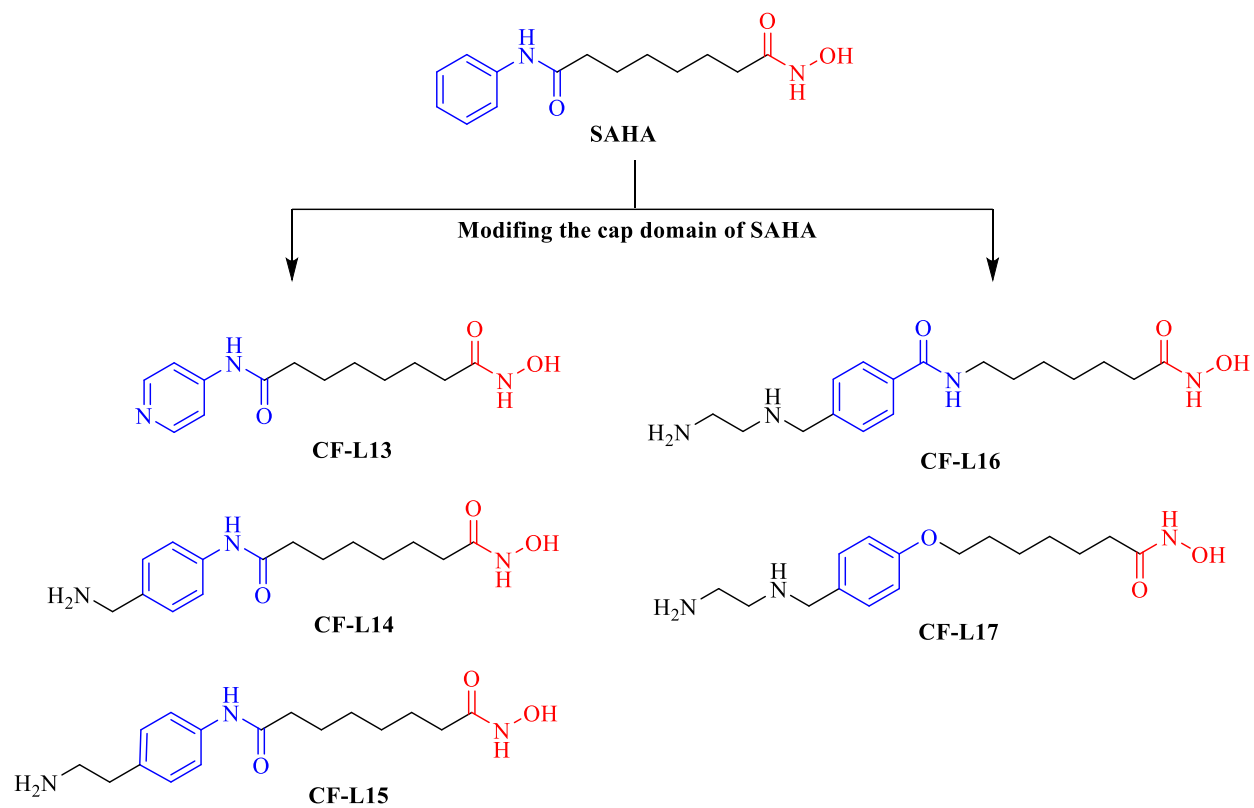


Figure 3.5 Structures of HDAC inhibitors (CF-L13 to CF-L17).

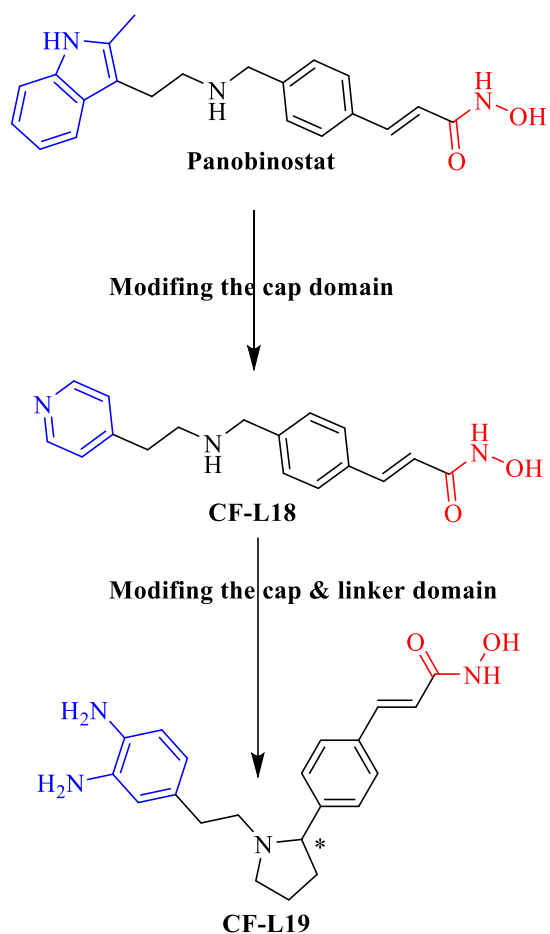


Figure 3.6 Structures of HDAC inhibitors **CF-L18** and **CF-L19**.

General procedures. Refer to part 2.2 in Chapter 2.

Synthesis of *N*-hydroxy-6-((2-methylpyridin-4-yl)oxy)hexanamide (CF-L01)

6-((2-methylpyridin-4-yl)oxy)hexanoic acid (CF-L01-1). Oxepan-2-one (414.0 mg, 3.63 mmol, 1.25 equiv) in DMSO (1 mL) was added dropwise to a stirred suspension of fine KOH powder (570.8 mg, 10.2 mmol, 3.5 equiv) in DMSO (5 mL) at 75 °C. After 30 min, 4-bromo-2-methylpyridine (500 mg, 2.91 mmol, 1.0 equiv) in DMSO (1 mL) was added to the reaction mixture which was stirred for 2 days at 75 °C. After the reaction mixture cooled down, anhydrous EtOH was added and concentrated H₂SO₄ was used to adjust the pH to 1-2. The

compound CF-L01-1 was detected by DART-AccuTOF MS and directly used for the following step without further purification.

Ethyl-6-((2-methylpyridin-4-yl)oxy)hexanoate (CF-L01-2). The mixture from previous step was refluxed overnight. EtOH was removed under reduced pressure. The reaction mixture was extracted with EtOAc and water three times. NaHCO₃ solution was used to neutralize the mixture. The organic layers were combined, washed with brine twice and then dried over anhydrous Na₂SO₄. After filtration, EtOAc was removed under reduced pressure and the crude product was purified by silica gel chromatography (DCM/MeOH=50/1) to afford colorless oil (533 mg, yield: 73%). ¹H NMR (600 MHz, CDCl₃): δ 8.27 (d, J = 5.9 Hz, 1H), 6.65 (d, J = 2.5 Hz, 1H), 6.62 (dd, J = 5.9, 2.5 Hz, 1H), 4.10 (q, J = 7.1 Hz, 2H), 3.98 (t, J = 6.4 Hz, 2H), 2.50 (s, 3H), 2.31 (t, J = 7.5 Hz, 3H), 1.79 (m, 2H), 1.68 (m, 2H), 1.48 (m, 2H), 1.23 (t, J = 7.1 Hz, 3H). ¹³C NMR (151 MHz, CDCl₃): δ 173.62, 165.96, 159.56, 149.56, 109.70, 107.93, 67.75, 60.38, 34.24, 28.67, 25.59, 24.67, 24.19, 14.33. DART-AccuTOF MS: m/z calcd C₁₄H₂₂NO₃ [M+H]⁺ 252.1600, found 252.1517.

N-hydroxy-6-((2-methylpyridin-4-yl)oxy)hexanamide (CF-L01). To a solution of **CF-L01-2** (340.0 mg, 1.35 mmol, 1.0 equiv) in DCM and MeOH (1:2 ratio, 12 mL) at 0 °C, hydroxylamine (50 wt% in water, 1.2 mL, 20.29 mmol, 15.0 equiv) was added, following by fine NaOH powder (541.0 mg, 13.5 mmol, 10.0 equiv). The solution was stirred at 0 °C for 30 min, and then allowed to warm to rt and stirred overnight. The solvent was removed under reduced pressure. Minimum H₂O was added to the residual and insoluble particles were removed by filtration. HCl (conc. 1-2 M) was used to adjust the pH of the aqueous filtrate until a white solid precipitated out from the mixture which was cooled in a cold water bath. The product was collected through filtration, washed by cold water and dried overnight to afford a white solid

(257 mg, yield: 80%). ^1H NMR (600 MHz, CD_3OD): δ 8.19 (d, $J = 6.0$ Hz, 1H), 6.85 (d, $J = 2.3$ Hz, 1H), 6.80 (dd, $J = 6.0, 2.5$ Hz, 1H), 4.07 (t, $J = 6.4$ Hz, 2H), 2.47 (s, 3H), 2.13 (t, $J = 7.4$ Hz, 2H), 1.82 (m, 2H), 1.69 (m, 2H), 1.50 (m, 2H). ^{13}C NMR (151 MHz, CD_3OD): δ 172.77, 167.98, 160.58, 150.08, 111.05, 109.47, 69.13, 33.62, 29.61, 26.51, 26.38, 23.56. DART-AccuTOF MS: m/z calcd $\text{C}_{12}\text{H}_{19}\text{N}_2\text{O}_3$ $[\text{M}+\text{H}]^+$ 239.1396, found 239.1376. HPLC: 99.5%.

Synthesis of *N*-hydroxy-7-((2-methylpyridin-4-yl)oxy)heptanamide (CF-L02)

Oxocan-2-one (CF-L02-1). To a solution of *m*-CPBA (14.98g, 66.86 mmol, <77% purity, 1.50 equiv) in DCM (150mL) was added cycloheptanone (5.0 g, 44.58 mmol, 1.0 equiv) under 0 °C and the resulting reaction was stirred for 10 minutes. The reaction mixture was allowed to warm to rt and stirred for 5-6 days. The reaction mixture was cooled to 0 °C for ~30 min and white precipitates were removed by vacuum filtration. The filtrate was washed with saturated NaHCO_3 , followed by brine twice. The organic layer was dried over anhydrous Na_2SO_4 , filtered and concentrated under reduced pressure to yield a light-yellow liquid, which was confirmed by ^1H NMR (crude yield: 89%), and used for the next step without further purification.

7-((2-methylpyridin-4-yl)oxy)heptanoic acid (CF-L02-2). CF-L02-1 (761.9 mg, 5.94 mmol, 1.0 equiv) in DMSO (1 mL) was added dropwise to a stirred suspension of fine KOH powder (1167.3 mg, 20.8 mmol, 3.5 equiv) in DMSO (7 mL) at 75 °C. After 30 min of stirring, 4-bromo-2-methylpyridine (1.07 g, 6.24 mmol, 1.0 equiv) in DMSO (1 mL) was added to the reaction mixture, which was stirred for 2 days at 75 °C. After the reaction mixture cooled down, anhydrous EtOH was added and concentrated H_2SO_4 was added to adjust the pH to 1 to 2. The

compound **CF-L02-2** was detected by DART-AccuTOF MS and used for the following step without further purification.

Ethyl-7-((2-methylpyridin-4-yl)oxy)heptanoate (CF-L02-3). Following the same synthesis procedure as **CF-L01-2**, a colorless oil was obtained as the product (yield: 54%). ¹H NMR (600 MHz, CDCl₃): δ 8.27 (d, J = 5.9 Hz, 1H), 6.65 (d, J = 2.4 Hz, 1H), 6.62 (dd, J = 5.9, 2.5 Hz, 1H), 4.10 (q, J = 7.1 Hz, 2H), 3.97 (t, J = 6.5 Hz, 2H), 2.50 (s, 3H), 2.29 (t, J = 7.5 Hz, 2H), 1.77 (m, 2H), 1.64 (m, 2H), 1.45 (m, 2H), 1.37 (m, 2H), 1.23 (t, J = 7.1 Hz, 3H). ¹³C NMR (151 MHz, CDCl₃): δ 173.77, 165.96, 159.59, 149.64, 109.68, 107.91, 67.89, 60.32, 34.29, 28.85, 28.78, 25.70, 24.88, 24.26, 14.34. DART-AccuTOF MS: m/z calcd C₁₅H₂₃NO₃ [M+H]⁺ 266.1756, found 266.1662.

N-hydroxy-7-((2-methylpyridin-4-yl)oxy)heptanamide (CF-L02). A white solid product was obtained following the same synthesis procedure as **CF-L01** (yield: 80%). ¹H NMR (600 MHz, CDCl₃): δ 8.17 (d, J = 5.9 Hz, 1H), 6.82 (d, J = 2.3 Hz, 1H), 6.77 (dd, J = 5.9, 2.5 Hz, 1H), 4.05 (t, J = 6.4 Hz, 2H), 2.46 (s, 3H), 2.10 (t, J = 7.4 Hz, 2H), 1.79 (m, 2H), 1.65 (m, 2H), 1.49 (m, 2H), 1.40 (m, 2H). ¹³C NMR (151 MHz, CD₃OD): δ 172.90, 167.74, 160.78, 150.44, 110.92, 109.31, 69.09, 33.67, 29.81, 29.78, 26.67, 26.63, 23.77. DART-AccuTOF MS: m/z calcd C₁₃H₂₁N₂O₃ [M+H]⁺ 253.1552, found 253.1449. HPLC: 99.5%.

Synthesis of *N*¹-hydroxy-*N*⁷-(2-methylpyridin-4-yl)heptanediamide (CF-L03)

Ethyl-7-((2-methylpyridin-4-yl)amino)-7-oxoheptanoate (CF-L03-1). To a solution of ethyl hydrogen pimelate (870.3 mg, 4.62 mmol, 1.0 equiv) in anhydrous DMF (15 mL) was added DIEA (2.4 mL, 13.87 mmol, 3.0 equiv) and HATU (2.2 g, 5.78 mmol, 1.25 equiv). The resulting mixture was stirred for 30 min, followed by the addition of 4-amino-2-picoline (500

mg, 4.62 mmol, 1.0 equiv) and stirring for another 24 h. H₂O (~30 mL) was then added and the mixture was extracted with EtOAc twice. The combined organic layers were washed with brine three times, dried over anhydrous Na₂SO₄, filtered and concentrated under reduced pressure. The crude product was purified by silica gel chromatography (DCM; DCM/MeOH=50/1 to 20/1) to afford a white powder (720 mg, yield: 56%). ¹H NMR (600 MHz, CDCl₃): δ 8.94 (br, 1H), 8.25 (d, J = 5.9 Hz, 1H), 7.61 (d, J = 1.9 Hz, 1H), 7.40 (dd, J = 5.9, 1.9 Hz, 1H), 4.08 (q, J = 7.1 Hz, 2H), 2.48 (s, 3H), 2.38 (t, J = 7.4 Hz, 2H), 2.27 (t, J = 7.4 Hz, 2H), 1.68 (m, 2H), 1.61 (m, 2H), 1.35 (m, 2H), 1.21 (t, J = 7.1 Hz, 3H). ¹³C NMR (151 MHz, CDCl₃): δ 173.99, 173.05, 157.99, 147.82, 147.39, 113.62, 111.73, 77.37, 77.16, 76.95, 60.45, 37.19, 34.09, 28.53, 24.83, 24.51, 23.21, 14.26. DART-AccuTOF MS: m/z calcd C₁₅H₂₃N₂O₃ [M+H]⁺ 279.1709, found 279.1889.

***N*¹-hydroxy-*N*⁷-(2-methylpyridin-4-yl)heptanediamide (CF-L03).** The same synthesis procedure as **CF-L01** was applied, resulting a white solid as the product (yield: 72%). ¹H NMR (600 MHz, DMSO-*d*₆): δ 10.33 (s, 1H), 10.15 (s, 1H), 8.67 (br, 1H), 8.25 (d, J = 5.6 Hz, 1H), 7.44 (d, J = 1.7 Hz, 1H), 7.34 (dd, J = 5.6, 2.0 Hz, 1H), 2.39 (s, 3H), 2.32 (t, J = 7.4 Hz, 2H), 1.94 (t, J = 7.4 Hz, 2H), 1.56 (m, 2H), 1.50 (m, 2H), 1.26 (m, 2H). ¹³C NMR (151 MHz, DMSO-*d*₆): δ 172.36, 169.03, 158.51, 149.55, 146.05, 111.91, 110.52, 36.35, 32.13, 28.17, 24.89, 24.55, 24.28, 24.27. DART-AccuTOF MS: m/z calcd C₁₃H₂₀N₃O₃ [M+H]⁺ 266.1505, found 266.1407. HPLC: 98.7%

Synthesis of ***N*¹-hydroxy-*N*⁸-(2-methylpyridin-4-yl)octanediamide (CF-L04)**

Methyl-8-((2-methylpyridin-4-yl)amino)-8-oxooctanoate (CF-L04-1). To a solution of 8-methoxy-8-oxooctanoic acid (870.3 mg, 4.62 mmol, 1.0 equiv) in anhydrous DMF (15 mL) was added DIEA (2.4 mL, 13.87 mmol, 3.0 equiv) and HATU (2.2 g, 5.78 mmol, 1.25 equiv).

The resulting mixture was stirred for 30 min, 4-amino-2-picoline (500 mg, 4.62 mmol, 1.0 equiv) was then added and the resulting mixture was stirred for 24 h. H₂O (~30 mL) was added and the mixture was extracted with EtOAc twice. The combined organic layers were washed with brine three times, dried over anhydrous Na₂SO₄, filtered and concentrated under reduced pressure. The crude product was purified by silica gel chromatography (DCM; DCM/MeOH=50/1 to 20/1) to afford a white powder (550 mg, yield: 43%). ¹H NMR (600 MHz, CDCl₃): δ 8.68 (s, 1H), 8.26 (d, J = 5.9 Hz, 1H), 7.62 (d, J = 1.9 Hz, 1H), 7.42 (dd, J = 5.9, 2.1 Hz, 1H), 3.64 (s, 3H), 2.50 (s, 3H), 2.39 (t, J = 7.5 Hz, 2H), 2.29 (t, J = 7.4 Hz, 2H), 1.68 (m, 2H), 1.60 (m, 2H), 1.37 – 1.29 (m, 4H). ¹³C NMR (151 MHz, CDCl₃): δ 174.51, 173.10, 158.18, 147.74, 147.62, 113.62, 111.74, 77.37, 77.16, 76.95, 51.65, 37.45, 34.03, 28.74, 28.73, 25.01, 24.72, 23.44. DART-AccuTOF MS: m/z calcd C₁₅H₂₃N₂O₃ [M+H]⁺ 279.1709, found 279.1669.

***N*¹-hydroxy-*N*⁸-(2-methylpyridin-4-yl)octanediamide (CF-L04).** Following the same synthesis procedure as **CF-L01**, a white solid was obtained as the final product (yield: 69%). ¹H NMR (600 MHz, DMSO-*d*₆): δ 10.34 (s, 1H), 10.17 (s, 1H), 8.67 (br, 1H), 8.25 (d, J = 5.6 Hz, 1H), 7.44 (d, J = 1.9 Hz, 1H), 7.34 (dd, J = 5.6, 2.0 Hz, 1H), 2.38 (s, 3H), 2.32 (t, J = 7.4 Hz, 2H), 1.93 (t, J = 7.4 Hz, 2H), 1.56 (m, 2H), 1.48 (m, 2H), 1.30 – 1.21 (m, 4H). ¹³C NMR (151 MHz, DMSO-*d*₆): δ 172.42, 169.10, 158.50, 149.55, 146.07, 111.92, 110.53, 36.46, 32.23, 28.37, 28.34, 25.01, 24.73, 24.29. DART-AccuTOF MS: m/z calcd C₁₄H₂₂N₃O₃ [M+H]⁺ 280.1661, found 280.1621. HPLC: 98.2%

Synthesis of *N*-(2-aminophenyl)-6-((2-methylpyridin-4-yl)oxy)hexanamide (CF-L05)

6-((2-methylpyridin-4-yl)oxy)hexanoic acid (CF-L05-1). Following the same synthesis procedure as **CF-L01-1**, **CF-L05-1** could be synthesized and used for the next step without

further purification. Alternatively, **CF-L05-1** can be synthesized and purified via basic hydrolysis of **CF-L01-2**. More specifically, **CF-L01-2** (798 mg, 3.18 mmol, 1.0 equiv) was dissolved in a 30 mL mixed solution of THF and MeOH (1:1 ratio), followed by the addition of NaOH (1.27 g, 31.8, mmol, 10.0 equiv) in H₂O (7.5 mL). The mixture was stirred at rt overnight, concentrated under reduced pressure, and extracted with EtOAc twice. The organic layer was discarded and the insoluble particles in aqueous phase were removed by filtration. HCl solution (conc 1-2 M) was used to adjust the pH of the aqueous filtrate until a white solid precipitated out under cold water bath. Liquid nitrogen could also be applied to induce the precipitate formation if there are no precipitates formed while using cold water bath alone. The product was collected through filtration, washed by cold water and dried overnight to afford a white powder (384 mg, yield: 35%). ¹H NMR (600 MHz, DMSO-d₆): δ 8.21 (d, J = 5.8 Hz, 1H), 6.80 (d, J = 2.4 Hz, 1H), 6.74 (dd, J = 5.8, 2.5 Hz, 1H), 4.00 (t, J = 6.5 Hz, 2H), 2.38 (s, 3H), 2.22 (t, J = 7.4 Hz, 2H), 1.70 (m, 2H), 1.55 (m, 2H), 1.40 (m, 2H). ¹³C NMR (600 MHz, DMSO-d₆): δ 174.43, 164.83, 159.40, 150.02, 109.15, 107.80, 67.28, 33.62, 28.12, 25.03, 24.21, 24.08. DART-AccuTOF MS: m/z calcd C₁₂H₁₈NO₃ [M+H]⁺ 224.1287, found 224.1238.

***N*-(2-aminophenyl)-6-((2-methylpyridin-4-yl)oxy)hexanamide (CF-L05)**. To a solution of **CF-L05-1** (907 mg, 4.06 mmol, 1.0 equiv) in anhydrous DMF (15 mL) was added DIEA (2.11 mL, 12.19 mmol, 3.0 equiv) and HATU (1.93 g, 5.08 mmol, 1.25 equiv). The solution was stirred for 30 min, followed by the addition of *o*-phenylenediamine (461 mg, 4.26 mmol, 1.05 equiv). The resulting mixture was stirred for another 24 h. H₂O (~30 mL) was added and the mixture was extracted with EtOAc twice. The combined organic layers were washed with brine three times, dried over anhydrous Na₂SO₄, filtered and concentrated under reduced pressure. The crude product was purified by basic alumina gel chromatography

(DCM/MeOH=30/1) to afford a white powder (535 mg, yield: 42%). ^1H NMR (600 MHz, CD_3OD): δ 8.17 (d, $J = 5.9$ Hz, 1H), 7.07 (dd, $J = 7.8, 1.5$ Hz, 1H), 7.02 (td, $J = 7.7, 1.5$ Hz, 1H), 6.85 (dd, $J = 8.0, 1.4$ Hz, 1H), 6.83 (d, $J = 2.3$ Hz, 1H), 6.78 (dd, $J = 5.9, 2.5$ Hz, 1H), 6.71 (td, $J = 7.6, 1.3$ Hz, 1H), 4.08 (t, $J = 6.4$ Hz, 2H), 2.49 – 2.42 (m, 5H), 1.86 (m, 2H), 1.80 (m, 2H), 1.59 (m, 2H). ^{13}C NMR (151 MHz, CD_3OD): δ 174.86, 167.72, 160.79, 150.46, 143.30, 128.24, 127.08, 125.16, 119.50, 118.55, 110.94, 109.33, 69.00, 37.06, 29.71, 26.66, 26.65, 23.78. DART-AccuTOF MS: m/z calcd $\text{C}_{18}\text{H}_{24}\text{N}_3\text{O}_2$ $[\text{M}+\text{H}]^+$ 314.1869, found 314.1916. HPLC: 98.5%.

Synthesis of *N*-(2-aminophenyl)-7-((2-methylpyridin-4-yl)oxy)heptanamide (CF-L06)

7-((2-methylpyridin-4-yl)oxy)heptanoic acid (CF-L06-1). Following the same synthesis procedure as **CF-L02-2**, **CF-L06-1** was synthesized and used for the next step without further purification. Alternatively, **CF-L06-1** could be synthesized and purified via basic hydrolysis of **CF-L02-2**, following a similar synthesis procedure as **CF-L05-1**, yielding a white powder (yield: 48%). ^1H NMR (600 MHz, CD_3OD): δ 8.21 (d, $J = 6.1$ Hz, 1H), 6.90 (d, $J = 2.4$ Hz, 1H), 6.85 (dd, $J = 6.1, 2.5$ Hz, 1H), 4.09 (t, $J = 6.4$ Hz, 2H), 2.49 (s, 3H), 2.29 (t, $J = 7.4$ Hz, 2H), 1.81 (m, 2H), 1.64 (m, 2H), 1.50 (m, 2H), 1.42 (m, 2H). ^{13}C NMR (151 MHz, CD_3OD): δ 178.27, 168.46, 160.21, 149.46, 111.29, 109.73, 69.50, 35.37, 29.91, 29.77, 26.69, 26.16, 23.20. DART-AccuTOF MS: m/z calcd $\text{C}_{13}\text{H}_{20}\text{NO}_3$ $[\text{M}+\text{H}]^+$ 238.1443, found 238.1369.

***N*-(2-aminophenyl)-7-((2-methylpyridin-4-yl)oxy)heptanamide (CF-L06).** The same synthesis procedure as **CF-L05** was applied to afford a white solid (yield: 43%). ^1H NMR (600 MHz, CD_3OD): δ 8.17 (d, $J = 5.9$ Hz, 1H), 7.07 (dd, $J = 7.8, 1.5$ Hz, 1H), 7.02 (td, $J = 7.6, 1.5$ Hz, 1H), 6.84 (dd, $J = 8.0, 1.4$ Hz, 1H), 6.82 (d, $J = 2.3$ Hz, 1H), 6.77 (dd, $J = 5.9, 2.5$ Hz, 1H), 6.70 (td, $J = 7.5, 1.3$ Hz, 1H), 4.07 (t, $J = 6.4$ Hz, 2H), 2.45 – 2.42 (m, 5H), 1.83 (m, 2H), 1.76

(m, 2H), 1.52 (m, 4H). ^{13}C NMR (151 MHz, CD_3OD): δ 175.00, 167.75, 160.77, 150.45, 143.29, 128.23, 127.06, 125.18, 119.51, 118.56, 110.94, 109.32, 69.12, 37.12, 29.95, 29.82, 26.91, 26.76, 23.78. DART-AccuTOF MS: m/z calcd $\text{C}_{19}\text{H}_{26}\text{N}_3\text{O}_2$ $[\text{M}+\text{H}]^+$ 328.2025, found 328.1901. HPLC: 98.8%.

Synthesis of N^1 -(2-aminophenyl)- N^7 -(2-methylpyridin-4-yl)heptanediamide (CF-L07).

7-((2-methylpyridin-4-yl)amino)-7-oxoheptanoic acid (CF-L07-1). A similar synthesis procedure as **CF-L05-1** was applied to afford a white solid (yield: 58%). ^1H NMR (600 MHz, DMSO-d_6): δ 12.03 (br, 1H), 10.16 (s, 1H), 8.25 (d, $J = 5.6$ Hz, 1H), 7.44 (d, $J = 1.8$ Hz, 1H), 7.34 (dd, $J = 5.6, 1.9$ Hz, 1H), 2.39 (s, 3H), 2.32 (t, $J = 7.4$ Hz, 2H), 2.20 (t, $J = 7.4$ Hz, 2H), 1.57 (m, 2H), 1.51 (m, 2H), 1.29 (m, 2H). ^{13}C NMR (151MHz, DMSO-d_6): δ 174.44, 172.35, 158.50, 149.53, 146.06, 111.92, 110.52, 36.35, 33.55, 28.13, 24.56, 24.27, 24.26. DART-AccuTOF MS: m/z calcd $\text{C}_{13}\text{H}_{19}\text{N}_2\text{O}_3$ $[\text{M}+\text{H}]^+$ 251.1396, found 251.1322.

N^1 -(2-aminophenyl)- N^7 -(2-methylpyridin-4-yl)heptanediamide (CF-L07). A similar synthesis procedure as **CF-L05** was used to afford a white solid (yield: 48%). ^1H NMR (600 MHz, CD_3OD): δ 8.23 (d, $J = 5.8$ Hz, 1H), 7.51 (d, $J = 2.0$ Hz, 1H), 7.45 (dd, $J = 5.8, 2.0$ Hz, 1H), 7.06 (dd, $J = 7.9, 1.5$ Hz, 1H), 7.01 (ddd, $J = 8.0, 7.4, 1.5$ Hz, 1H), 6.84 (dd, $J = 8.0, 1.3$ Hz, 1H), 6.69 (td, $J = 7.4, 1.5$ Hz 1H), 2.46 (s, 3H), 2.43 (td, $J = 7.4, 3.2$ Hz, 4H), 1.76 (m, 4H), 1.49 (m 2H). ^{13}C NMR (151 MHz, CD_3OD): δ 175.26, 174.93, 160.04, 149.95, 148.42, 143.30, 128.25, 127.12, 125.11, 119.48, 118.52, 114.19, 112.44, 37.83, 36.95, 29.72, 26.62, 26.13, 23.89. DART-AccuTOF MS: m/z calcd $\text{C}_{19}\text{H}_{25}\text{N}_4\text{O}_2$ $[\text{M}+\text{H}]^+$ 341.1978, found 341.1893. HPLC: 99.3%

Synthesis of N^1 -(2-aminophenyl)- N^8 -(2-methylpyridin-4-yl)octanediamide (CF-L08).

8-((2-methylpyridin-4-yl)amino)-8-oxooctanoic acid (CF-L08-1). The same synthesis procedure as **CF-L05-1** was applied to afford a white solid (yield: 65%). ¹H NMR (600 MHz, DMSO-d₆): δ 12.03 (br, 1H), 10.14 (s, 1H), 8.25 (d, J = 5.6 Hz, 1H), 7.44 (s, 1H), 7.34 (dd, J = 5.6, 0.5 Hz, 1H), 2.39 (s, 3H), 2.32 (t, J = 7.4 Hz, 2H), 2.19 (td, J = 7.4, 1.0 Hz, 2H), 1.57 (m, 2H), 1.49 (m, 2H), 1.28 (m, 4H). ¹³C NMR (151 MHz, DMSO-d₆): δ 174.47, 172.40, 158.48, 149.50, 146.09, 111.93, 110.53, 36.45, 33.62, 28.32, 28.31, 24.69, 24.36, 24.25. DART-AccuTOF MS: m/z calcd C₁₄H₂₁N₂O₃ [M+H]⁺ 265.1552, found 265.1545.

N¹-(2-aminophenyl)-N⁸-(2-methylpyridin-4-yl)octanediamide (CF-L08). Similar synthesis procedure as **CF-L05** was applied to synthesize **CF-L08**. A white solid was obtained as the final product (yield: 51%). ¹H NMR (600 MHz, CD₃OD): δ 8.23 (d, J = 5.8 Hz, 1H), 7.51 (d, J = 1.7 Hz, 1H), 7.45 (dd, J = 5.8, 2.1 Hz, 1H), 7.07 (dd, J = 7.8, 1.5 Hz, 1H), 7.01 (m, 1H), 6.84 (dd, J = 8.0, 1.4 Hz, 1H), 6.70 (td, J = 7.6, 1.4 Hz, 1H), 2.46 (s, 3H), 2.41 (m, 4H), 1.81 – 1.64 (m, 4H), 1.51 – 1.39 (m, 4H). ¹³C NMR (151 MHz, CD₃OD): δ 175.37, 175.04, 159.95, 149.81, 148.54, 143.28, 128.24, 127.10, 125.15, 119.51, 118.54, 114.20, 112.45, 37.96, 37.11, 29.96, 29.92, 26.82, 26.28, 23.81. DART-AccuTOF MS: m/z calcd C₂₀H₂₇N₄O₂ [M+H]⁺ 355.2134, found 355.2068. HPLC: 98.7%

Synthesis of N-(4-amino-[1,1'-biphenyl]-3-yl)-6-((2-methylpyridin-4-yl)oxy)hexanamide (CF-L09).

N-(4-amino-[1,1'-biphenyl]-3-yl)-6-((2-methylpyridin-4-yl)oxy)hexanamide (CF-L09-1). The same synthesis procedure as **CF-L05** was used to afford **CF-L09-1**, which then underwent boc deprotection using 4M HCl in dioxane and EtOH (1:1 ratio) and purified by silica gel chromatography (DCM/MeOH=20/1, 10/1) to afford a white powder (yield: 63%). ¹H NMR

(600 MHz, CD₃OD): δ 8.14 (d, J = 5.9 Hz, 1H), 7.50 (dd, J = 8.3, 1.1 Hz, 2H), 7.40 (d, J = 2.1 Hz, 1H), 7.34 (t, J = 7.8 Hz, 2H), 7.30 (dd, J = 8.3, 2.1 Hz, 1H), 7.22 (m, 1H), 6.91 (d, J = 8.3 Hz, 1H), 6.79 (d, J = 2.4 Hz, 1H), 6.73 (dd, J = 5.9, 2.5 Hz, 1H), 4.04 (t, J = 6.4 Hz, 2H), 2.47 (t, J = 7.4 Hz, 2H), 2.42 (s, 3H), 1.86 – 1.77 (m, 4H), 1.58 (m, 2H). ¹³C NMR (151 MHz, CD₃OD): δ 174.98, 167.68, 160.73, 150.40, 142.76, 142.01, 132.66, 129.73, 127.39, 127.19, 126.66, 125.46, 125.29, 118.78, 110.94, 109.31, 69.00, 37.11, 29.69, 26.67, 26.63, 23.77. DART-AccuTOF MS: m/z calcd C₂₄H₂₈N₃O₂ [M+H]⁺ 390.2182, found 390.2188. HPLC: 96.4%. Crystals were obtained by vapor diffusion crystallization set-up using DCM and ether (Appendix D).

Synthesis of *N*-(4-amino-[1,1'-biphenyl]-3-yl)-7-((2-methylpyridin-4-yl)oxy)heptanamide (CF-L10).

***N*-(4-amino-[1,1'-biphenyl]-3-yl)-7-((2-methylpyridin-4-yl)oxy)heptanamide (CF-L10).** Similar synthesis procedure as **CF-L09** was applied to afford a white powder (yield: 60%). ¹H NMR (600 MHz, CD₃OD): δ 8.14 (d, J = 5.9 Hz, 1H), 7.51 (dd, J = 8.3, 1.1 Hz, 2H), 7.40 (d, J = 2.1 Hz, 1H), 7.34 (t, J = 7.8 Hz, 2H), 7.30 (dd, J = 8.3, 2.2 Hz, 1H), 7.22 (t, J = 7.4 Hz, 1H), 6.91 (d, J = 8.3 Hz, 1H), 6.78 (d, J = 2.3 Hz, 1H), 6.73 (dd, J = 5.9, 2.5 Hz, 1H), 4.02 (t, J = 6.4 Hz, 2H), 2.45 (t, J = 7.4 Hz, 2H), 2.42 (s, 3H), 1.84 – 1.71 (m, 4H), 1.56 – 1.44 (m, 4H). ¹³C NMR (151 MHz, CD₃OD): δ 175.10, 167.69, 160.72, 150.42, 142.72, 142.01, 132.67, 129.72, 127.39, 127.19, 126.62, 125.41, 125.32, 118.79, 110.93, 109.27, 69.10, 37.18, 29.97, 29.80, 26.86, 26.74, 23.78. DART-AccuTOF MS: m/z calcd C₂₅H₃₀N₃O₂ [M+H]⁺ 404.2338, found 404.2333. HPLC: 97.4%. Crystals were obtained by vapor diffusion crystallization set-up using DCM and ether (Appendix D).

Synthesis of *N*¹-(4-amino-[1,1'-biphenyl]-3-yl)-*N*⁷-(2-methylpyridin-4-yl)heptanediamide (CF-L11).

*N*¹-(4-amino-[1,1'-biphenyl]-3-yl)-*N*⁷-(2-methylpyridin-4-yl)heptanediamide (CF-L11). The same synthesis procedure as CF-L07 was used to afford CF-L11-1, which then underwent boc deprotection using 4M HCl in dioxane and MeOH (1:1 ratio) and purified by silica gel chromatography (DCM/MeOH=20/1, 10/1) to afford a white powder (yield: 64%). ¹H NMR (600 MHz, CD₃OD): δ 8.19 (d, J = 5.8 Hz, 1H), 7.52 – 7.49 (m, 3H), 7.45 (dd, J = 5.8, 2.1 Hz, 1H), 7.39 (d, J = 2.2 Hz, 1H), 7.34 (t, J = 7.8 Hz, 2H), 7.30 (dd, J = 8.3, 2.2 Hz, 1H), 7.22 (m, 1H), 6.90 (d, J = 8.3 Hz, 1H), 2.48 – 2.42 (m, 7H), 1.77 (m 4H), 1.50 (m, 2H). ¹³C NMR (151 MHz, CD₃OD): δ 175.26, 175.07, 159.71, 149.47, 148.77, 142.78, 142.00, 132.65, 129.72, 127.38, 127.18, 126.67, 125.51, 125.23, 118.73, 114.25, 112.50, 37.82, 36.99, 29.72, 26.56, 26.06, 23.63. DART-AccuTOF MS: m/z calcd C₂₅H₂₉N₄O₂ [M+H]⁺ 417.2291, found 417.2231. HPLC: 98.0%

Synthesis of *N*¹-(4-amino-[1,1'-biphenyl]-3-yl)-*N*⁸-(2-methylpyridin-4-yl)octanediamide (CF-L12).

*N*¹-(4-amino-[1,1'-biphenyl]-3-yl)-*N*⁸-(2-methylpyridin-4-yl)octanediamide (CF-L12). The same synthesis procedure as CF-L11 was applied to afford a white powder (yield: 51%). ¹H NMR (600 MHz, CD₃OD): δ 8.21 (d, J = 5.8 Hz, 1H), 7.52 – 7.48 (m, 3H), 7.43 (dd, J = 5.8, 2.1 Hz, 1H), 7.38 (d, J = 2.2 Hz, 1H), 7.34 (t, J = 7.8 Hz, 2H), 7.30 (dd, J = 8.3, 2.1 Hz, 1H), 7.22 (m, 1H), 6.91 (d, J = 8.3 Hz, 1H), 2.45 (m, 5H), 2.40 (t, J = 7.5 Hz, 2H), 1.78 – 1.69 (m, 4H), 1.49 – 1.41 (m, 4H). ¹³C NMR (151 MHz, CD₃OD): δ 175.35, 175.16, 159.98, 149.87, 148.45, 142.75, 142.00, 132.70, 129.72, 127.38, 127.19, 126.66, 125.48, 125.29, 118.77, 114.19,

112.43, 37.96, 37.17, 29.97, 29.91, 26.79, 26.28, 23.85. DART-AccuTOF MS: m/z calcd $C_{26}H_{31}N_4O_2$ $[M+H]^+$ 431.2447, found 431.2401. HPLC: 97.7%

Synthesis of *N*¹-hydroxy-*N*⁸-(pyridin-4-yl)octanediamide (CF-L13).

Methyl 8-oxo-8-(pyridin-4-ylamino)octanoate (CF-L13-1). The same synthesis procedure as **CF-L04-1** was used to afford a white solid (yield: 46%). ¹H NMR (600 MHz, CD₃Cl): δ 8.73 (s, 1H), 8.44 (d, J = 5.9 Hz, 2H), 7.56 (d, J = 6.2 Hz, 2H), 3.65 (s, 3H), 2.37 (t, J = 7.5 Hz, 2H), 2.29 (t, J = 7.4 Hz, 2H), 1.70 (m, 2H), 1.60 (m, 2H), 1.37 – 1.29 (m, 4H). ¹³C NMR (151 MHz, CD₃Cl): δ 174.45, 172.66, 150.26, 145.99, 113.81, 51.66, 37.56, 34.01, 28.77, 28.73, 25.12, 24.71. DART-AccuTOF MS: m/z calcd $C_{14}H_{21}N_2O_3$ $[M+H]^+$ 265.1552, found 265.1523.

***N*¹-hydroxy-*N*⁸-(pyridin-4-yl)octanediamide (CF-L13).** A similar synthesis procedure as **CF-L04** afforded a white solid (yield: 39%). ¹H NMR (600 MHz, DMSO-*d*₆): δ 10.33 (s, 1H), 10.24 (s, 1H), 8.67 (s, 1H), 8.39 (dd, J = 4.8, 1.5 Hz, 2H), 7.55 (dd, J = 4.8, 1.6 Hz, 2H), 2.33 (t, J = 7.5 Hz, 2H), 1.93 (t, J = 7.4 Hz, 2H), 1.60 – 1.54 (m, 2H), 1.51 – 1.45 (m, 2H), 1.31 – 1.22 (m, 4H). ¹³C NMR (151 MHz, DMSO-*d*₆): δ 172.49, 169.09, 150.30, 145.76, 113.04, 36.46, 32.23, 28.36, 28.34, 25.00, 24.68. DART-AccuTOF MS: m/z calcd $C_{13}H_{20}N_3O_3$ $[M+H]^+$ 266.1505, found 266.1467. HPLC: 99.0%

Synthesis of *N*¹-(4-(aminomethyl)phenyl)-*N*⁸-hydroxyoctanediamide hydrogen chloride (CF-L14).

Methyl-8-((4-(((tert-butoxycarbonyl)amino)methyl)phenyl)amino)-8-oxooctanoate (CF-L14-1). The same synthesis procedure as **CF-L04-1** afforded the crude product, which was further purified by recrystallization using EtOAc and hexanes and yielded a white powder (82%).

^1H NMR (600 MHz, DMSO- d_6): δ 9.81 (s, 1H), 7.50 (d, J = 8.4 Hz, 2H), 7.31 (t, J = 6.0 Hz, 1H), 7.13 (d, J = 8.4 Hz, 2H), 4.05 (d, J = 6.1 Hz, 2H), 3.57 (s, 3H), 2.28 (m, 4H), 1.54 (m, 4H), 1.39 (s, 9H), 1.30 – 1.24 (m, 4H). ^{13}C NMR (151 MHz, DMSO- d_6): δ 173.33, 171.05, 155.74, 137.93, 134.65, 127.28, 118.94, 77.68, 51.15, 43.00, 36.27, 33.22, 28.31, 28.25, 28.22, 24.94, 24.31. DART-AccuTOF MS: m/z calcd $\text{C}_{21}\text{H}_{33}\text{N}_2\text{O}_5$ $[\text{M}+\text{H}]^+$ 393.2390, found 393.2334. McLafferty rearrangement and decarboxylation occurred during the DART-AccuTOF mass spectrometry measurement.

***tert*-butyl (4-(8-(hydroxyamino)-8-oxooctanamido)benzyl)carbamate (CF-L14-2).** To a solution of **CF-L14-1** (1.35 g, 3.4 mmol, 1.0 equiv) in DCM and MeOH (1:2 ratio, 24 mL) at 0 °C, hydroxylamine (50 wt% in water, 3.04 mL, 51.6 mmol, 15.0 equiv) was added, followed by addition of a fine NaOH powder (1.38 g, 34.4 mmol, 10.0 equiv). The solution was stirred at 0 °C for 30 min, and then allowed to warm to rt and stirred overnight. Solvent was removed under reduced pressure to yield a white solid. H_2O (10 mL) was added to the residual and the solid product was insoluble. HCl (conc 1-2 M) was added to adjust the pH to ~9 while stirring. The product was collected through vacuum filtration, washed by cold water and dried overnight. The aqueous filtrate was washed with EtOAc three times, dried over Na_2SO_4 , filtered and concentrated under reduced pressure to yield a white solid. All white solids were combined and recrystallized from EtOAc (~30-50 mL, not completely soluble) to afford a white powder (1.35 g, yield: quantitative). ^1H NMR (600 MHz, DMSO- d_6): δ 10.19 (br, 1H), 7.54 (d, J = 8.3 Hz, 2H), 7.34 (t, J = 5.8 Hz, 1H), 7.12 (d, J = 8.4 Hz, 2H), 4.04 (d, J = 5.8 Hz, 2H), 2.27 (t, J = 7.4 Hz, 2H), 1.85 (t, J = 7.4 Hz, 2H), 1.55 (m, 2H), 1.44 (m, 2H), 1.38 (s, 9H), 1.30 – 1.18 (m, 4H). ^{13}C NMR (151 MHz, DMSO- d_6): δ 171.29, 167.62, 155.77, 138.13, 134.54, 127.23, 118.98, 77.68, 43.03, 36.27, 32.95, 28.52, 28.43, 28.27, 25.72, 25.18. DART-AccuTOF MS: m/z calcd

$C_{19}H_{32}N_3O_3$ $[M-CO_2+H]^+$ 350.2444, found 350.2405. McLafferty rearrangement and decarboxylation occurred during the DART-AccuTOF mass spectrometry measurement. ESI-AccuTOF MS: m/z calcd $C_{20}H_{31}N_3O_5Na$ $[M+Na]^+$ 416.2161, found 416.2060.

***N*¹-(4-(aminomethyl)phenyl)-*N*⁸-hydroxyoctanediamide hydrogen chloride (CF-L14).** To a mixture of insoluble **CF-L14-2** (700 mg, 1.78 mmol, 1.0 equiv) in anhydrous DCM (3 mL), 1 M HCl in anhydrous EtOAc (9 mL) was added. The mixture was stirred overnight. The organic liquid was removed using centrifuge and the product was washed with dry Et₂O three times and dried overnight to afford a white powder (yield: quantitative). ¹H NMR (600 MHz, DMSO-*d*₆): δ 10.43 (s, 1H), 10.20 (s, 1H), 8.68 (br, 1H), 8.49 (s, 3H), 7.64 (d, *J* = 8.6 Hz, 2H), 7.40 (d, *J* = 8.6 Hz, 2H), 3.91 (q, *J* = 5.4 Hz, 2H), 2.31 (t, *J* = 7.5 Hz, 2H), 1.94 (t, *J* = 7.4 Hz, 2H), 1.56 (m, 2H), 1.47 (m, 2H), 1.32 – 1.20 (m, 4H). ¹³C NMR (151 MHz, DMSO-*d*₆): δ 171.53, 169.22, 139.61, 129.48, 128.27, 118.88, 41.78, 36.31, 32.24, 28.40, 28.38, 25.05, 25.01. ESI-AccuTOF MS: m/z calcd $C_{15}H_{24}N_3O_3$ $[M+H]^+$ 294.1818, found 294.1769. HPLC: 95.1%

Synthesis of *N*¹-(4-(2-aminoethyl)phenyl)-*N*⁸-hydroxyoctanediamide hydrogen chloride (CF-L15).

Methyl-8-((4-(2-((tert-butoxycarbonyl)amino)ethyl)phenyl)amino)-8-oxooctanoate (CF-L15-1). The same synthesis procedure as **CF-L14-1** afforded a white powder (83%). ¹H NMR (600 MHz, DMSO-*d*₆): δ 9.77 (s, 1H), 7.48 (d, *J* = 8.5 Hz, 2H), 7.08 (d, *J* = 8.5 Hz, 2H), 6.84 (t, *J* = 5.6 Hz, 1H), 3.57 (s, 3H), 3.09 (m, 2H), 2.62 (m, 2H), 2.31 – 2.23 (m, 4H), 1.62 – 1.47 (m, 4H), 1.36 (s, 9H), 1.31 – 1.25 (m, 4H). ¹³C NMR (151 MHz, DMSO-*d*₆): δ 173.34, 170.99, 155.50, 137.43, 133.91, 128.71, 119.05, 77.46, 51.15, 41.61, 36.29, 34.92, 33.23, 28.31, 28.26, 28.23, 24.98, 24.32. DART-AccuTOF MS: m/z calcd $C_{22}H_{35}N_2O_5$ $[M+H]^+$ 407.2546,

found 407.2519. McLafferty rearrangement and decarboxylation occurred during the DART-AccuTOF mass spectrometry measurement.

***tert*-butyl (4-(8-(hydroxyamino)-8-oxooctanamido)phenethyl)carbamate (CF-L15-2).**

Similar synthesis procedure as **CF-L14-2** was applied and afforded a white powder (96%). ¹H NMR (600 MHz, DMSO-d₆): δ 10.25 (br, 1H), 7.52 (d, J = 8.4 Hz, 2H), 7.07 (d, J = 8.5 Hz, 2H), 6.87 (t, J = 5.5 Hz, 1H), 3.08 (m, 2H), 2.61 (m, 2H), 2.26 (t, J = 7.4 Hz, 2H), 1.80 (t, J = 7.4 Hz, 2H), 1.59 – 1.49 (m, 2H), 1.47 – 1.39 (m, 2H), 1.36 (s, 9H), 1.27 – 1.20 (m, 4H). ¹³C NMR (151 MHz, DMSO-d₆): δ 171.27, 167.24, 155.52, 137.66, 133.76, 128.66, 119.12, 77.45, 41.63, 36.24, 34.92, 33.35, 28.55, 28.33, 28.28, 26.08, 25.28. DART-AccuTOF MS: m/z calcd C₂₀H₃₄N₃O₃ [M-CO₂+H]⁺ 364.2600, found 364.2589. McLafferty rearrangement and decarboxylation occurred during the DART-AccuTOF mass spectrometry measurement. ESI-AccuTOF MS: m/z calcd C₂₁H₃₃N₃O₅Na [M+Na]⁺ 430.2318, found 430.2265.

***N*¹-(4-(2-aminoethyl)phenyl)-*N*⁸-hydroxyoctanediamide hydrogen chloride (CF-**

L15). The same synthesis procedure as **CF-L14** produced a white powder (yield: quantitative). ¹H NMR (600 MHz, DMSO-d₆): δ 10.49 (s, 1H), 10.12 (s, 1H), 8.27 (s, 3H), 7.57 (d, J = 8.5 Hz, 2H), 7.14 (d, J = 8.5 Hz, 2H), 2.94 (m, 2H), 2.85 (m, 2H), 2.29 (t, J = 7.4 Hz, 2H), 1.94 (t, J = 7.4 Hz, 2H), 1.54(m, 2H), 1.47 (m, 2H), 1.33 – 1.17 (m, 4H). ¹³C NMR (151 MHz, DMSO-d₆): δ 171.26, 169.19, 138.13, 131.75, 128.74, 119.28, 39.99, 36.30, 32.33, 32.23, 28.40, 28.39, 25.08, 25.05. DART-AccuTOF MS: m/z calcd C₁₆H₂₆N₃O₃ [M+H]⁺ 308.1974, found 308.1907. ESI-AccuTOF MS: m/z calcd C₁₆H₂₆N₃O₃ [M+H]⁺ 308.1974, found 308.1961. HPLC: 95.4%

Synthesis of 4-(((2-aminoethyl)amino)methyl)-*N*-(7-(hydroxyamino)-7-oxoheptyl)benzamide hydrogen chloride (CF-L16).

Methyl-7-(4-formylbenzamido)heptanoate (CF-L16-1). Similar synthesis procedure as **CF-L03-1** led to a crude product, which was purified by silica gel chromatography (DCM/EtOAc=1/1) to afford a white powder (yield: 88%). ¹H NMR (600 MHz, CDCl₃): δ 10.05 (s, 1H), 7.91 (s, 4H), 6.44 (s, 1H), 3.64 (s, 3H), 3.44 (dt, J = 7.2, 6.1 Hz, 2H), 2.30 (t, J = 7.4 Hz, 2H), 1.68 – 1.52 (m, 4H), 1.42 – 1.31 (m, 4H). ¹³C NMR (151 MHz, CDCl₃): δ 191.69, 174.29, 166.53, 140.09, 138.19, 129.92, 127.73, 51.61, 40.27, 34.00, 29.44, 28.79, 26.66, 24.82. DART-AccuTOF MS: m/z calcd C₁₆H₂₂NO₄ [M+H]⁺ 292.1549, found 292.1541.

Methyl-7-(4-(((2-((tert-butoxycarbonyl)amino)ethyl)amino)methyl)benzamido)heptanoate (CF-L16-2). To a solution of **CF-L16-1** (635 mg, 2.18 mmol, 1.0 equiv) in MeOH (15 mL) was added *tert*-butyl (2-aminoethyl)carbamate (366.7 mg, 1.05 mmol, 1.05 equiv) and stirred at rt overnight. Fine NaBH₄ powder (123.7 mg, 3.27 mmol, 1.5 equiv) was added in portions at 0 °C. After complete addition, the reaction mixture was stirred for 1 h at rt. MeOH was removed under reduced pressure. The residual was extracted with EtOAc and H₂O twice. The combined organic layers were washed with brine three times, dried over anhydrous Na₂SO₄, filtered and concentrated under reduced pressure. The crude product was purified by silica gel chromatography (DCM; DCM/MeOH=10/1) to afford a white powder (500 mg, yield: 53%). ¹H NMR (600 MHz, DMSO-d₆): δ 8.36 (t, J = 5.6 Hz, 1H), 7.77 (d, J = 8.2 Hz, 2H), 7.38 (d, J = 8.2 Hz, 2H), 6.74 (t, J = 5.4 Hz, 1H), 3.71 (s, 2H), 3.57 (s, 3H), 3.23 (q, J = 6.7 Hz, 2H), 3.02 (q, J = 6.0 Hz, 2H), 2.51 (t, J = 6.5 Hz, 2H), 2.29 (t, J = 7.4 Hz, 2H), 1.51 (m, 4H), 1.36 (s, 9H), 1.32 – 1.25 (m, 4H). ¹³C NMR (151 MHz, DMSO-d₆): δ 173.33, 165.94, 155.62, 144.10, 132.98, 127.54, 126.95, 77.44, 52.23, 51.13, 48.38, 39.95 (shown in HMQC spectrum), 39.06, 33.22, 28.96, 28.23, 28.20, 26.13, 24.38. DART-AccuTOF MS: m/z calcd C₂₃H₃₈N₃O₅ [M+H]⁺ 436.2812, found 436.2709.

***tert*-butyl (2-((4-((7-(hydroxyamino)-7-**

oxoheptyl)carbamoyl)benzyl)amino)ethyl)carbamate (CF-L16-3). To a solution of **CF-L16-2** (150 mg, 0.34 mmol, 1.0 equiv) in DCM and MeOH (1:2 ratio, 12 mL) at 0 °C, hydroxylamine (50 wt% in water, 0.30 mL, 5.17 mmol, 15.0 equiv) was added, following by fine NaOH powder (138 mg, 3.44 mmol, 10.0 equiv). The solution was stirred at 0 °C for 30 min, and then allowed to warm to rt and stirred overnight. Solvent was removed under reduced pressure to yield a white solid. H₂O (2.5 mL) was added to the residual and the insoluble solid was removed by filtration. HCl solution (conc 1-2 M) was added to adjust the pH and no precipitates formed. The mixture was extracted with EtOAc three times, dried over Na₂SO₄, filtered and concentrated under reduced pressure to yield a white solid. The crude product was recrystallized from EtOAc to afford a white powder (100 mg, yield: 67%). ¹H NMR (600 MHz, DMSO-d₆): δ 10.33 (br, 1H), 8.66 (br, 1H), 8.36 (t, J = 5.6 Hz, 1H), 7.77 (d, J = 8.2 Hz, 2H), 7.38 (d, J = 8.2 Hz, 2H), 6.74 (t, J = 5.4 Hz, 1H), 3.71 (s, 2H), 3.34 (br, 1H), 3.23 (q, J = 6.6 Hz, 2H), 3.02 (q, J = 6.2 Hz, 2H), 2.52 (t, J = 6.5 Hz, 2H), 1.94 (t, J = 7.4 Hz, 2H), 1.49 (m, 4H), 1.37 (s, 9H), 1.31 – 1.24 (m, 4H). ¹³C NMR (151 MHz, DMSO-d₆): δ 169.09, 165.96, 155.64, 144.15, 132.98, 127.55, 126.97, 77.46, 52.24, 48.40, 39.97 (shown in HMQC spectrum), 39.12 (shown in HMQC spectrum), 32.24, 29.06, 28.36, 28.25, 26.23, 25.10. DART-AccuTOF MS: m/z calcd C₂₂H₃₇N₄O₅ [M+H]⁺ 437.2764, found 437.2727

4-(((2-aminoethyl)amino)methyl)-N-(7-(hydroxyamino)-7-oxoheptyl)benzamide

hydrogen chloride (CF-L16). Similar synthesis procedure as **CF-L14** was applied in this synthesis, which afforded a white powder (yield: 92%). ¹H NMR (600 MHz, DMSO-d₆): δ 7.87 (d, J = 7.8 Hz, 2H), 7.64 (d, J = 7.5 Hz, 2H), 4.24 (s, 2H), 3.30 – 3.14 (m, 6H), 1.93 (t, J = 7.3 Hz, 2H), 1.52 – 1.43 (m, 4H), 1.30 – 1.21 (m, 4H). ¹³C NMR (151 MHz, DMSO-d₆): δ 169.62,

165.76, 135.18, 134.65, 130.06, 127.62, 49.76, 43.91, 39.30 (shown in HMQC spectrum), 35.23, 32.37, 29.09, 28.47, 26.36, 25.25. DART-AccuTOF MS: m/z calcd $C_{17}H_{29}N_4O_3$ $[M+H]^+$ 337.2240, found 337.2204. HPLC: 96.4%

Synthesis of 7-(4-(((2-aminoethyl)amino)methyl)phenoxy)-*N*-hydroxyheptanamide hydrogen chloride (CF-L17)

Ethyl-7-(4-formylphenoxy)heptanoate (CF-L17-1). To a solution of 4-hydroxybenzaldehyde (1.22 g, 10.0 mmol, 1.0 equiv) in ACN (50 mL) was added ethyl-7-bromoheptanoate (2.37 g, 10.0 mmol, 1.0 equiv) and K_2CO_3 (5.52 g, 40 mmol, 3.0 equiv). The mixture was refluxed overnight. Partial ACN was removed under reduced pressure and the resulting mixture was extracted with EtOAc and H_2O three times. The organic layers were combined, washed with brine, dried over anhydrous Na_2SO_4 , and concentrated under reduced pressure to give a yellow crude product. The crude product was dissolved in Et_2O and hexane and left in freezer overnight, which afforded a light-yellow product (1.5 g, 54%). 1H NMR (600 MHz, $CDCl_3$): δ 9.87 (s, 1H), 7.82 (d, $J = 8.8$ Hz, 2H), 6.97 (d, $J = 8.7$ Hz, 2H), 4.12 (q, $J = 7.1$ Hz, 2H), 4.03 (t, $J = 6.5$ Hz, 2H), 2.31 (t, $J = 7.5$ Hz, 2H), 1.81 (m, 2H), 1.66 (m, 2H), 1.52 – 1.46 (m, 2H), 1.41 (m, 2H), 1.24 (t, $J = 7.1$ Hz, 3H). ^{13}C NMR (151 MHz, $CDCl_3$): δ 190.93, 173.82, 164.31, 132.11, 129.91, 114.86, 68.35, 60.35, 34.34, 28.98, 28.92, 25.79, 24.94, 14.38. DART-AccuTOF MS: m/z calcd $C_{16}H_{23}O_4$ $[M+H]^+$ 279.1596, found 279.1572.

Ethyl-7-(4-(((2-((tert-butoxycarbonyl)amino)ethyl)amino)methyl)phenoxy)heptanoate (CF-L17-2). Similar synthesis procedure as **CF-L16-2** was applied to yield crude product, which was further purified by silica gel chromatography (DCM/MeOH=20/1) to afford a white powder (yield: 92%). 1H

NMR (600 MHz, DMSO- d_6): δ 7.19 (d, J = 8.6 Hz, 2H), 6.83 (d, J = 8.6 Hz, 2H), 6.72 (t, J = 5.4 Hz, 1H), 4.04 (q, J = 7.1 Hz, 2H), 3.91 (t, J = 6.5 Hz, 2H), 3.58 (s, 2H), 3.00 (q, J = 6.3 Hz, 2H), 2.49 (m, 2H), 2.28 (t, J = 7.4 Hz, 2H), 2.00 (s, 1H), 1.72 – 1.63 (m, 2H), 1.57 – 1.50 (m, 2H), 1.42 – 1.30 (m, 13H), 1.17 (t, J = 7.1 Hz, 3H). ^{13}C NMR (151 MHz, DMSO- d_6): δ 172.85, 157.39, 155.61, 132.71, 129.00, 113.98, 77.41, 67.22, 59.62, 52.08, 48.28, 39.93 (shown in HMQC spectrum), 33.43, 28.54, 28.23, 28.17, 25.20, 24.39, 14.11. DART-AccuTOF MS: m/z calcd $\text{C}_{23}\text{H}_{39}\text{N}_2\text{O}_5$ $[\text{M}+\text{H}]^+$ 423.2859, found 279.1572.

***tert*-butyl (2-((4-((7-(hydroxyamino)-7-oxoheptyl)oxy)benzyl)amino)ethyl)carbamate (CF-L17-3).** Similar synthesis procedure as **CF-L16-3** yielded a white wax solid (yield: 75%). ^1H NMR (600 MHz, DMSO- d_6): δ 10.34 (br, 1H), 7.19 (d, J = 8.6 Hz, 2H), 6.83 (d, J = 8.6 Hz, 2H), 6.72 (t, J = 5.7 Hz, 1H), 3.91 (t, J = 6.5 Hz, 2H), 3.58 (s, 2H), 3.00 (q, J = 6.3 Hz, 2H), 2.48 (t, J = 6.5 Hz, 1H), 1.94 (t, J = 7.4 Hz, 2H), 1.69 – 1.65 (m, 2H), 1.53 – 1.46 (m, 2H), 1.42 – 1.34 (m, 11H), 1.31 – 1.25 (m, 2H). ^{13}C NMR (151 MHz, DMSO- d_6): δ 169.05, 157.40, 155.62, 132.71, 129.02, 114.00, 77.43, 67.28, 52.09, 48.29, 39.95 (shown in HMQC spectrum), 32.20, 28.62, 28.34, 28.25, 25.27, 25.07. DART-AccuTOF MS: m/z calcd $\text{C}_{21}\text{H}_{36}\text{N}_3\text{O}_5$ $[\text{M}+\text{H}]^+$ 410.2655, found 410.2661.

7-(4-(((2-aminoethyl)amino)methyl)phenoxy)-*N*-hydroxyheptanamide hydrogen chloride (CF-L17). Similar synthesis procedure as **CF-L16** afforded a white solid (yield: 92%). ^1H NMR (600 MHz, D_2O): δ 7.46 (d, J = 6.0 Hz, 2H), 7.06 (d, J = 6.5 Hz, 2H), 4.28 (s, 2H), 4.08 (t, J = 5.5 Hz, 2H), 3.44 (m, 4H), 2.16 (t, J = 6.8 Hz, 2H), 1.76 (m, 2H), 1.59 (m, 2H), 1.44 (m, 2H), 1.35 (m, 2H). ^{13}C NMR (151 MHz, D_2O): δ 159.40, 131.71, 122.68, 115.53, 100.00, 68.69, 51.21, 43.48, 35.57, 35.55, ESI-AccuTOF MS: m/z calcd $\text{C}_{16}\text{H}_{28}\text{N}_3\text{O}_3$ $[\text{M}+\text{H}]^+$ 310.2131, found 310.2125 HPLC: 95.2%.

Synthesis of (*E*)-*N*-hydroxy-3-(4-(((2-(pyridin-4-yl)ethyl)amino)methyl)phenyl)acrylamide (CF-L18). Similar synthesis procedure as **CF-L16-2** produced a crude product **CF-L18-1**, which was used directly for the following step. Similar synthesis procedure as **CF-L01** was applied to afford a light yellow solid (overall yield: 28%). ¹H NMR (600 MHz, CD₃OD): δ 8.44 (d, J = 6.1 Hz, 2H), 7.56 (m, 3H), 7.41 (d, J = 8.1 Hz, 2H), 7.32 (d, J = 6.1 Hz, 2H), 6.47 (d, J = 15.8 Hz, 1H), 3.93 (s, 2H), 3.00 (m, 2H), 2.93 (dd, J = 8.4, 6.4 Hz, 2H).

Synthesis of (*E*)-3-(4-(1-(3,4-diaminophenethyl)pyrrolidin-2-yl)phenyl)-*N*-hydroxyacrylamide (CF-L19).

4-acetamidophenethyl acetate (CF-L19-1). To a solution of 2-(4-aminophenyl)ethan-1-ol (2.74 g, 19.97 mmol, 1.0 equiv) in DCM (50 mL) was added TEA (8.09 g, 11.1 mL, 79.9 mmol, 4.0 equiv) and Ac₂O (6.12 g, 59.92 mmol, 3.0 equiv). The reaction mixture was stirred under 0 °C for 45 min and then rt for overnight. The reaction was monitored by silica gel TLC (DCM/MeOH=10/1). The mixture was washed by water and brine twice, dried over anhydrous Na₂SO₄, concentrated under reduced pressure to afford a light-yellow solid as a crude product, which was further purified by recrystallization (EtOAc/Cyclohexane) to afford a white solid (3.55 g, yield: 80%). ¹H NMR (600 MHz, CDCl₃): δ 7.76 (s, 1H), 7.43 (d, J = 8.4 Hz, 2H), 7.13 (d, J = 8.4 Hz, 2H), 4.23 (t, J = 7.1 Hz, 2H), 2.88 (t, J = 7.1 Hz, 2H), 2.14 (s, 3H), 2.02 (s, 3H). ¹³C NMR (151 MHz, CDCl₃): δ 171.23, 168.69, 136.67, 133.76, 129.42, 120.23, 65.02, 34.56, 24.54, 21.07. DART-AccuTOF MS: m/z calcd C₁₂H₁₆NO₃ [M+H]⁺ 222.1130, found 222.0921.

4-acetamido-3-nitrophenethyl acetate (CF-L19-2). To a solution of **CF-L19-1** (2.0 g, 9.04 mmol, 1.0 equiv) in DCM (25 mL) was added Ac₂O (1.85 g, 1.71 mL, 18.08 mmol, 2.0 equiv) and cooled at 0 °C. Fuming HNO₃ (0.9 mL, 18.08 mmol, 2.0 equiv) was added to the

mixture and stirred for 1 h. The reaction was monitored by silica TLC (PE/EtOAc=1/1) and another portion of fuming HNO₃ was added if there was still starting material left. The mixture was poured into water and stirred for 30 min, after which the mixture was extracted with DCM three times. The combined organic layers were washed with water twice, dried over anhydrous Na₂SO₄, concentrated under reduced pressure to yield a yellow solid. The crude product was dissolved in minimum Et₂O and left in the freezer for recrystallization. The recrystallized product was collected through vacuum filtration and washed with hexane to afford a bright-yellow solid (2.03 g, yield: 84%). ¹H NMR (600 MHz, CDCl₃): δ 10.24 (s, 1H), 8.69 (d, J = 8.7 Hz, 1H), 8.06 (d, J = 2.1 Hz, 1H), 7.50 (dd, J = 8.7, 2.2 Hz, 1H), 4.28 (t, J = 6.7 Hz, 2H), 2.96 (t, J = 6.6 Hz, 2H), 2.28 (s, 3H), 2.03 (s, 3H). ¹³C NMR (151 MHz, CDCl₃): δ 170.95, 169.09, 136.66, 136.37, 133.73, 133.55, 125.74, 122.51, 64.09, 34.13, 25.70, 20.98. DART-AccuTOF MS: m/z calcd C₁₂H₁₅N₂O₅ [M+H]⁺ 267.0981, found 267.0953.

2-(4-amino-3-nitrophenyl)ethan-1-ol (CF-L19-3). To a solution of **CF-L19-2** (1.8 g, 6.76 mmol, 1.0 equiv) in MeOH (20 mL) was added 10 M NaOH (1.35 mL, 13.52 mmol, 2.0 equiv) and stirred for 15 min. The reaction was monitored by silica gel TLC (PE/EtOAc=1/1) and another portion of NaOH was added if there was still starting material left. MeOH was removed under reduced pressure and the residue was extracted by DCM/H₂O three times. The combined organic layers were washed with water twice, dried over anhydrous Na₂SO₄, concentrated under reduced pressure to afford bright red crystals (1.03 g, yield: 84%). ¹H NMR (600 MHz, DMSO-d₆): δ 7.79 (d, J = 1.9 Hz, 1H), 7.34 – 7.23 (m, 3H), 6.94 (d, J = 8.7 Hz, 1H), 4.60 (t, J = 5.2 Hz, 1H), 3.55 (dt, J = 6.7, 5.3 Hz, 2H), 2.61 (t, J = 6.7 Hz, 2H). ¹³C NMR (151 MHz, DMSO-d₆): δ 144.74, 137.15, 129.93, 126.96, 124.43, 119.06, 61.72, 37.36. DART-AccuTOF MS: m/z calcd C₈H₁₁N₂O₃ [M+H]⁺ 183.0770, found 183.0764.

4-(2-bromoethyl)-2-nitroaniline (CF-L19-4). CF-L19-3 (1.0 g, 5.49 mmol, 1.0 equiv) was dissolved in 48% HBr solution (30 mL) and refluxed for 6 h. The reaction was monitored by silica gel TLC (PE/EtOAc=1/1). After the reaction mixture cooled down, it was poured into a beaker with 30 mL H₂O, neutralized with saturated NaHCO₃, extracted with DCM three times. The combined organic layers were washed with water twice, dried over anhydrous Na₂SO₄, concentrated under reduced pressure to afford an orange oil. The crude product was further purified by silica gel chromatography (EtOAc/PE=1/10-1/5) to afford a yellow oil, from which orange crystals formed after being left in the freezer overnight (1.0 g, yield: 74%). ¹H NMR (600 MHz, CDCl₃): δ 7.97 (d, J = 2.1 Hz, 1H), 7.23 (dd, J = 8.5, 2.1 Hz, 1H), 6.78 (d, J = 8.5 Hz, 1H), 6.04 (s, 2H), 3.53 (t, J = 7.2 Hz, 2H), 3.08 (t, J = 7.2 Hz, 2H). ¹³C NMR (151 MHz, CDCl₃): δ 143.75, 136.51, 132.07, 127.76, 125.77, 119.19, 37.81, 32.93. DART-AccuTOF MS: m/z calcd C₈H₁₀BrN₂O₂ [M+H]⁺ 244.9926, found 244.9903.

tert-butyl 2-(4-bromophenyl)pyrrolidine-1-carboxylate (CF-L19-5). To a solution of 2-(4-bromophenyl)pyrrolidine (2.0 g, 8.84 mmol, 1.0 equiv) in THF (30 mL), 1 M NaOH (9.73 mL, 9.73 mmol, 1.1 equiv) and 1 M Boc₂O in THF (9.29 mL, 9.29 mmol, 1.05 equiv) was added. NMR spectra of the precursors were shown in Appendix B and couldn't differentiate enantiomers. The mixture was stirred at rt overnight. THF was removed under reduced pressure and the residual was extracted with EtOAc three times. The combined organic layers were washed with brine twice, dried over anhydrous Na₂SO₄, concentrated under reduced pressure to yield an oily crude product, which was further purified by silica gel chromatography (DCM) to afford a white solid (2.5 g, 87%). ¹H NMR (600 MHz, DMSO-d₆): δ 7.49 (d, J = 7.3 Hz, 2H), 7.13 (d, J = 7.4 Hz, 2H), 4.80 - 4.63 (m, 1H), 3.57 - 3.38 (m, 2H), 2.36 - 2.14 (m, 1H), 1.79 (m, 2H), 1.70 - 1.60 (m, 1H), 1.38 - 1.11 (s, 9Hs). (two sets of signals indicate two diastereomers).

^{13}C NMR (151 MHz, DMSO- d_6): δ 153.44, 153.30, 144.70, 143.86, 130.96, 130.88, 127.75, 127.66, 119.24, 119.19, 78.48, 78.15, 60.24, 59.69, 46.99, 46.81, 35.48, 34.27, 28.11, 27.79, 23.02, 22.72 (two sets of signals indicate two diastereomers). DART-AccuTOF MS: m/z calcd $\text{C}_{15}\text{H}_{21}\text{BrNO}_2$ $[\text{M}+\text{H}]^+$ 326.0756, found 326.0659. McLafferty rearrangement and decarboxylation occur during the DART-AccuTOF mass spectrometry measurement.

***tert*-butyl (E)-2-(4-(3-methoxy-3-oxoprop-1-en-1-yl)phenyl)pyrrolidine-1-carboxylate (CF-L19-6).** To a solution of **CF-L19-5** (1.63 g, 5.0 mmol, 1.0 equiv) in anhydrous ACN (20 mL) was added $\text{Pd}(\text{OAc})_2$ (56 mg, 0.25 mmol, 0.05 equiv), TEA (2.1 mL, 15 mmol, 3.0 equiv) and methyl acrylate (1.29 g, 15 mmol, 3.0 equiv) under argon. The mixture was stirred at 90 °C for 20 h. All solvent was removed under reduced pressure and the residual was extracted with EtOAc three times. The combined organic layers were washed with brine twice, dried over anhydrous Na_2SO_4 , concentrated under reduced pressure to yield an oily crude product, which was further purified by silica gel chromatography (DCM; DCM/EtOAc=20/1) to afford a white solid (850 mg, yield: 51%). ^1H NMR (600 MHz, CDCl_3): δ 7.67 (d, J = 15.8 Hz, 1H), 7.45 (d, J = 7.7 Hz, 2H), 7.18 (s, 2H), 6.41 (d, J = 15.8 Hz, 1H), 4.93 – 4.75 (m, 1H), 3.78 (s, 3H), 3.61 (m, 2H), 2.32 (m, 1H), 1.97 – 1.74 (m, 3H), 1.44 – 1.16 (s, 9H). ^{13}C NMR (151 MHz, CDCl_3): δ 167.61, 154.54, 144.88, 144.70, 132.86, 128.38, 128.11, 126.17, 126.03, 117.27, 117.16, 79.47, 61.23, 60.65, 51.74, 47.48, 47.19, 36.02, 34.86, 28.59, 28.23, 23.71, 23.33. (two sets of signals indicate two diastereomers). DART-AccuTOF MS: m/z calcd $\text{C}_{19}\text{H}_{26}\text{NO}_4$ $[\text{M}+\text{H}]^+$ 332.1862, found 332.1769.

Methyl (E)-3-(4-(pyrrolidin-2-yl)phenyl)acrylate hydrogen chloride (CF-L19-7).

Following the same synthesis procedure as **CF-L14** afforded a white powder (yield: 86%). ^1H NMR (600 MHz, D_2O): δ 7.57 (m, 3H), 7.45 (d, J = 8.2 Hz, 2H), 6.44 (d, J = 16.1 Hz, 1H), 4.64

(m, 1H), 3.74 (s, 3H), 3.51 – 3.42 (m, 2H), 2.48 – 2.41 (m, 1H), 2.28 – 2.22 (m, 1H), 2.21 – 2.12 (m, 2H). ¹³C NMR (151 MHz, D₂O): δ 169.55, 144.69, 136.71, 134.89, 128.94, 128.03, 118.11, 62.80, 52.30, 45.50, 30.18, 23.48. DART-AccuTOF MS: m/z calcd C₁₄H₁₈NO₂ [M+H]⁺ 232.1338, found 232.1262.

Methyl (*E*)-3-(4-(1-(4-amino-3-nitrophenethyl)pyrrolidin-2-yl)phenyl)acrylate (CF-L19-8). To a solution of CF-L19-4 (450 mg, 1.84 mmol, 1.0 equiv) in ACN (25 mL) was added CF-L19-7 (761 mg, 1.84 mmol, 1.0 equiv) and K₂CO₃ (761 mg, 5.5 mmol, 3.0 equiv). The resulting mixture was refluxed overnight. Partial ACN was removed under reduced pressure and the resulting mixture was extracted with EtOAc and H₂O three times. The organic layers were combined, washed with brine, dried over anhydrous Na₂SO₄, and concentrated under reduced pressure to give a yellow crude product. The crude product was further purified by silica gel chromatography (DCM, DCM/EtOAc=10/1), which afforded a yellow product (500 mg, 69%). ¹H NMR (600 MHz, DMSO-*d*₆): δ 7.67 (d, *J* = 2.0 Hz, 1H), 7.61 (d, *J* = 16.0 Hz, 1H), 7.56 (d, *J* = 8.2 Hz, 2H), 7.29 (s, 2H), 7.24 (d, *J* = 8.2 Hz, 2H), 7.15 (dd, *J* = 8.7, 2.1 Hz, 1H), 6.90 (d, *J* = 8.6 Hz, 1H), 6.55 (d, *J* = 16.0 Hz, 1H), 3.71 (s, 3H), 3.33 – 3.27 (m, 2H), 2.61 – 2.51 (m, 3H), 2.29 – 2.21 (m, 2H), 2.12 – 2.05 (m, 1H), 1.84 – 1.73 (m, 2H), 1.49 – 1.41 (m, 1H). ¹³C NMR (151 MHz, DMSO-*d*₆): δ 166.72, 146.94, 144.69, 144.44, 136.82, 132.60, 129.85, 128.30, 127.69, 127.62, 123.93, 119.00, 117.03, 68.77, 55.04, 52.86, 51.41, 34.91, 32.89, 22.32. DART-AccuTOF MS: m/z calcd C₂₂H₂₆N₃O₄ [M+H]⁺ 396.1923, found 396.1859.

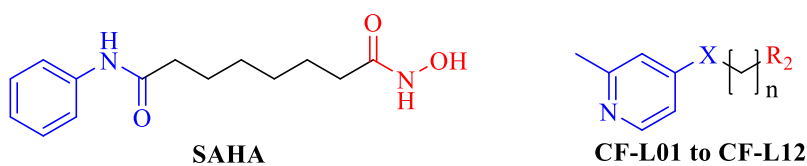
Methyl (*E*)-3-(4-(1-(3,4-diaminophenethyl)pyrrolidin-2-yl)phenyl)acrylate (CF-L19-9). To a solution of CF-L19-8 (450 mg, 1.14 mmol, 1.0 equiv) in EtOH/H₂O (2/1; 20 mL) was added an iron powder (638 mg, 11.4 mmol, 10.0 equiv) and NH₄Cl (305 mg, 5.7 mmol, 5.0 equiv). The reaction mixture was refluxed for 1-2 h and monitored by silica gel TLC

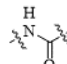
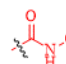
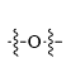
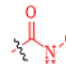
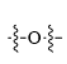
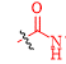
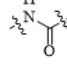
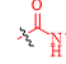
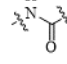
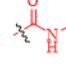
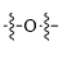
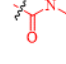
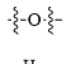
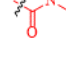
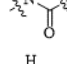
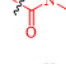
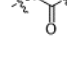
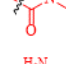
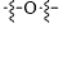
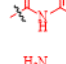
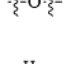
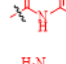
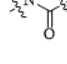
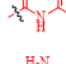
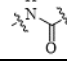
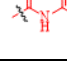
(DCM/MeOH=20/1). All iron powder was removed via gravity filtration and EtOH was removed under reduced pressure. The residual was extracted with DCM three times. The organic layers were combined, washed with brine, dried over anhydrous Na₂SO₄, and concentrated under reduced pressure to give a brown solid (225 mg yield: 54%), which was confirmed by DART-AccuTOF MS and used for the following step without further purification. DART-AccuTOF MS: m/z calcd C₂₂H₂₈N₃O₂ [M+H]⁺ 366.2180, found 366.2117.

(E)-3-(4-(1-(3,4-diaminophenethyl)pyrrolidin-2-yl)phenyl)-N-hydroxyacrylamide (CF-L19). To a solution of **CF-L19-9** (200 mg, 0.547 mmol, 1.0 equiv) in DCM/MeOH (1/2, 12 mL) at 0 °C, hydroxylamine (50 wt% in water, 0.484mL, 8.21 mmol, 15.0 equiv) was added, followed by fine NaOH powder (219 mg, 5.47 mmol, 10.0 equiv). The solution was stirred at 0 °C for 30 min and then allowed to warm to rt and stirred overnight. The solvent was removed under reduced pressure. H₂O (2.5 mL) was added to the residual and the insoluble solid was removed by filtration. HCl (conc. 1-2 M) was added to adjust the pH (~9) and the mixture was extracted with EtOAc three times, dried over Na₂SO₄ and filtered. The EtOAc volume was reduced under reduced pressure and hexanes were added to induce the formation of the product. The organic solvent was removed using a centrifuge and the product was washed with dry Et₂O three times and dried overnight to afford a brown powder (50 mg, yield: 25%). ¹H NMR (600 MHz, DMSO-d₆): δ 10.73 (s, 1H), 9.03 (s, 1H), 7.48 (d, J = 8.1 Hz, 2H), 7.43 (d, J = 15.7 Hz, 1H), 7.33 (d, J = 8.1 Hz, 2H), 6.42 (d, J = 15.8 Hz, 1H), 6.35 (d, J = 7.7 Hz, 1H), 6.23 (d, J = 1.9 Hz, 1H), 6.10 (dd, J = 7.8, 1.9 Hz, 1H), 4.27 (s, 4H), 3.33 – 3.31 (m, 1H), 3.31 – 3.24 (m, 1H), 2.55 (m, 1H), 2.48 (m, 1H), 2.38 – 2.32 (m, 1H), 2.25 (m, 1H), 2.19 – 2.06 (m, 2H), 1.87 – 1.73 (m, 2H), 1.51 (m, 1H). ESI-AccuTOF MS: m/z calcd C₂₁H₂₇N₄O₂ [M+H]⁺ 367.2134, found 367.2010.

3.3 HDAC Inhibition and Cell Viability Study

Two bioassays have been used to evaluate the HDAC inhibitors synthesized in our lab. The HDAC1 inhibition study was conducted by contract research organization Nanosyn, Inc, at Santa Clara, CA with the support from Newave Pharmaceutical. Inc. The cell viability study was performed at the School of Pharmacy in collaboration with Dr. Xin Guo's lab, University of the Pacific. Colon cancer cell line HCT-116 (ATCC) and lung cancer cell line A549 (ATCC) were used for cytotoxicity evaluation. IC₅₀ curves can be found in Appendix E. As all of the compounds synthesized in this project are organic molecules, the formulation solvent is DMSO. Please refer to section 2.3 for more experimental details.

Table 3.1 HDAC1 inhibition and cell viability for compound **CF-L01** to **CF-L12**.*

Compd	X	n	R ₂	HDAC1 inhibition IC ₅₀ (μM)	HCT-116 viability IC ₅₀ (μM)	A549 viability IC ₅₀ (μM)
SAHA		6		0.04	1.05	4.42
CF-L01		5		1.74	17.46	N/A
CF-L02		6		0.17	2.67	9.56
CF-L03		5		0.11	>50	N/A
CF-L04		6		0.04	3.59	13.30
CF-L05		5		>10	>50	N/A
CF-L06		6		4.34	30.16	37.05
CF-L07		5		0.45	4.45	5.93
CF-L08		6		1.79	17.45	>50
CF-L09		5		0.07	6.20	20.09
CF-L10		6		0.03	1.98	43.99
CF-L11		5		0.04	1.13	>50
CF-L12		6		0.04	2.30	>50

* IC₅₀ values are means of at least three replicates

HDAC1 inhibition and cell viability data are summarized in Table 3.1. Compound **CF-L04**, **CF-L10**, **CF-L11**, and **CF-L12** exhibited comparable HDAC1 inhibition activity with reference compound SAHA. When hydroxamic acid was used as the zinc-binding group (**CF-L01** to **CF-L04**), the linker with 6 carbons has significantly smaller IC_{50} values than those with 5 carbons. The linkage being either ether or reversed amide bond does not significantly alter its inhibition. When *ortho*-aminoamide was used as the zinc-binding group (**CF-L05** to **CF-L08**), the linker with 6 carbons has significantly smaller IC_{50} if an ether bond was used as the linkage while the IC_{50} in an opposite trend was observed when a reversed amide bond was used as the linkage. When *ortho*-aminoamide possessing a C-5 phenyl group was used as the zinc-binding group (**CF-L09** to **CF-L12**), the linker with 6 carbons has smaller IC_{50} if an ether bond was used as the linkage while there is no significant difference when a reversed amide bond was used. It might be due to the additional binding of a C-5 phenyl group to the internal cavity, which weakened the effects of linker length. This also explained the high inhibition potency of **CF-L09** to **CF-L12**.

A similar trend was observed in the HCT-116 colon cancer cell viability study, with **CF-L02**, **CF-L04**, **CF-L07**, and **CF-L09** to **CF-L12** showing promising IC_{50} value. The inhibition efficiency of **CF-L09** to **CF-L12** in A549 was low as shown by high IC_{50} values. The overall IC_{50} values are higher in the A549 cell line compared with those in HCT-116, indicating that these compounds might be less effective in treating A549 lung cancer. **CF-L02**, **CF-L04**, and **CF-L07** are promising HDAC inhibitors for future development. Considering the complexity of synthesis and purification, hydroxamic acid with 6 carbon as linker was used for the design and synthesis of following HDAC inhibitors.

CF-L13 to **CF-L17** were synthesized by modifying the cap domain of SAHA while keeping the 6-carbon linker and hydroxamic acid as the zinc-binding group. **CF-L18** and **CF-L19** were synthesized by modifying Panobinostat. Table 3.2 summarized HDAC1 inhibition. **CF-L13** to **CF-L17** have comparable efficacy with SAHA, indicating the modification of the cap domain does not affect the HDAC1 inhibition too much. By changing the cap of Panobinostat to pyridine, **CF-L18** showed comparable inhibition with SAHA. **CF-19** was designed by further increasing the bulkiness and rigidity of the linker. Its HDAC1 inhibition was significantly changed and the IC₅₀ value reached to nM molar level (1.1 nM).

Table 3.2 HDAC1 inhibition of **CF-L13** to **CF-L19**.

Compd	SAHA	CF-L13	CF-L14	CF-L15	CF-L16	CF-L17	CF-L18	CF-L19
HDAC1 IC ₅₀ (nM)	44.8±5.4	52.3±12.1	51.4±6.9	42.2±3.4	28.3±3.4	15.7±1.2	24.7±7.6	1.1±0.1

3.4 Conclusions

19 new HDAC inhibitors have been synthesized, characterized and evaluated by HDAC inhibition assay and cell viability assay. The linker length and zinc-binding group of each inhibitor indeed affected the bioactivity. Modification of the inhibitors directly influences its HDAC inhibition and thus cell viability. The HCT-116 cell line is relative decent model for HDAC1 inhibition screening as the trend is the same as that of HDAC1 enzyme inhibition assay. A549 cell line is less sensitive to the HDAC inhibitors (**CF-L01** to **CF-L12**). The 6-carbon linker demonstrating high efficacy in HDAC inhibition and hydroxamic acid ZBG from convenient synthesis were chosen for further HDAC inhibitor design. Thanks to the bulkiness and higher rigidity of the linker, **CF-19** shows the most promising efficacy in HDAC1 inhibition.

Chapter 4: Pt-HDACi Conjugates

4.1 Introduction

As mentioned in Chapter 1, platinum-based anticancer drugs, such as cisplatin, carboplatin, and oxaliplatin, have been approved for worldwide clinical use for decades. Nearly 50% of all cancer therapies involve the use of them as stand-alone treatments or in combination with other drugs.^{1,113,114} However, their widespread application is hindered by either cross-resistance or toxic side effects.¹ One of the strategies to overcome those drawbacks is to make a newer generation of platinum-based anticancer drugs with multiple functions.¹³ For example, carbohydrates have been conjugated to platinum(II) to achieve targeting glucose receptors since glucose could enhance the uptake by cancer cells.^{115–123} Steroid, such as estrogen, testosterone, and bile acids, have been incorporated with platinum(II), acting as targeting unit that directs the platinum drug to receptors overexpressed with respective tissues.^{123–132} Since the solid-phase peptide synthesis was developed, the research of platinum(II)-peptide conjugates arose, which utilized either the targeting properties of specific peptide sequences^{133,134} or the enhanced cellular uptake properties.^{135–138} Other bioactive agents, such as dichloroacetate,¹³⁹ diclofenac,¹⁴⁰ curcumin,¹⁴¹ and vorinostat¹¹³ have also been installed onto platinum(II) centers through the leaving group carboxylate to achieve dual functions. Triple and even quadruple action of Pt (IV) prodrugs have been extensively explored by encompassing cyclooxygenases (COX) inhibitors, phosphoinositide-dependent protein kinase (PDK) inhibitor, and HDAC inhibitors.^{12,123}

Since histone deacetylase plays a vital role in the epigenetic pathways and is a clinically approved and validated cancer target, HDAC inhibitors have been extensively involved in many designs of hybrid molecules, aiming to simultaneously target two or more biological targets to achieve the synergistic anticancer activity. There are a few HDACi-based hybrid molecules

currently investigated in clinical trial studies. HDACi can synergize with kinase inhibitors by improving the sensitivity of kinase drugs and inducing apoptosis. CUDC-101 depicted in Figure 4.1 was prepared with a receptor tyrosine kinases (RTK) binding domain as the cap. It is derived from erlotinib, an approved drug for epidermal growth factor receptor (HER) inhibition.¹⁴²

CUDC-907, with a phosphatidylinositol-4,5-bisphosphate (PI3K) binding domain as the cap, has dual PI3K and HDAC inhibition and has entered phase II clinical trial studies.^{6,143}

Tinostamustine (EDO-S101) is a **first-in-class** alkylating deacetylase inhibitor, with the bendamustine pharmacophore as the cap domain.¹⁴⁴ As a DNA/HDAC bifunctional agent, it shows enhanced anticancer activities, compared with its parent drugs, namely bendamustine and vorinostat.¹⁴⁵ Domatinostat (4SC-202) is a lysine-specific demethylase 1 (LSD1) and HDAC bifunctional agent while both are crucial in the Wnt and Hedgehog (Hh) pathway. It is mainly employed to target resistant cancer stem cells.¹⁴⁶ Many different HDAC hybrid molecules have been reported in the literature and for more details, the reader could refer to some nice review papers of this research area.^{146,147-149}

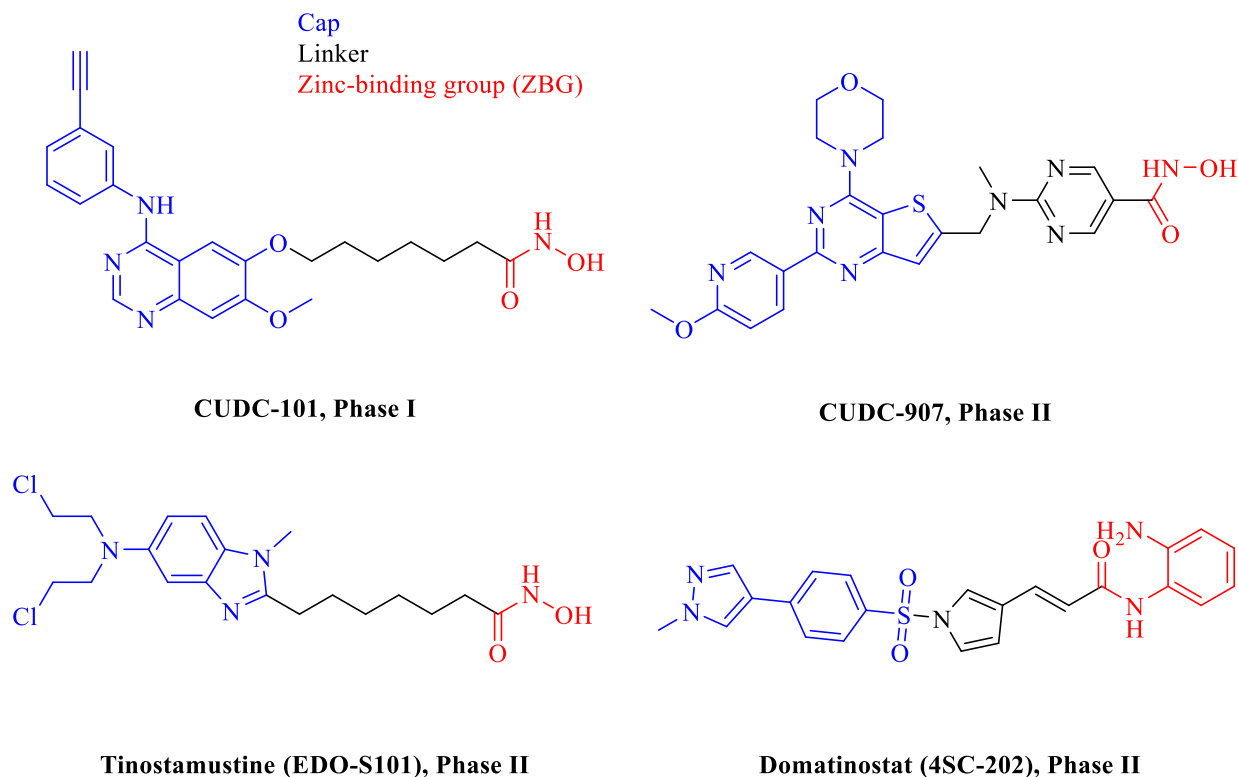


Figure 4.1 HDACi-based hybrid agents in clinical trials. ^{6,150,146}

4.2 Design of Pt-HDACi Conjugates

Since both the multifunctional platinum agents and hybrid HDAC inhibitors have DNA and HDAC as their shared biological targets, several Pt-HDACi conjugates have been reported in the literature.^{113,151,152} The first Pt-HDACi conjugate, shown in Figure 4.2, was reported by Dr. Celine J. Marmion and her research team.¹¹³ The complex is a hybrid molecule of two FDA-approved drugs, cisplatin, and SAHA (vorinostat). Their gel electrophoresis proved the DNA binding function of the hybrid molecule and HDAC1 inhibition assay provided an IC₅₀ value of 1143 nM, which is around **eightfold** less active than the malonic acid precursor. When HDACi is incorporated into the platinum core as the leaving group, the hybrid molecule will eventually

dissociate into two different drugs, which might decrease the efficacy as they have a different pharmacokinetic profile and thus could not achieve enough synergistic effect.

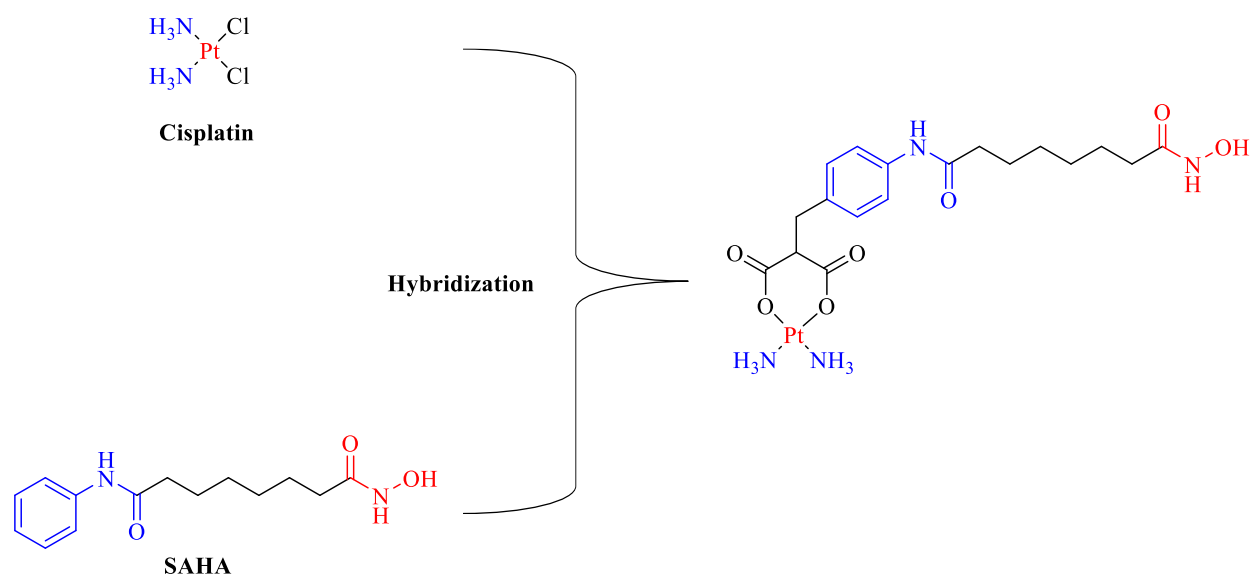


Figure 4.2 Pt-HDACi hybrid molecule reported by Marmion's team.^{113,151}

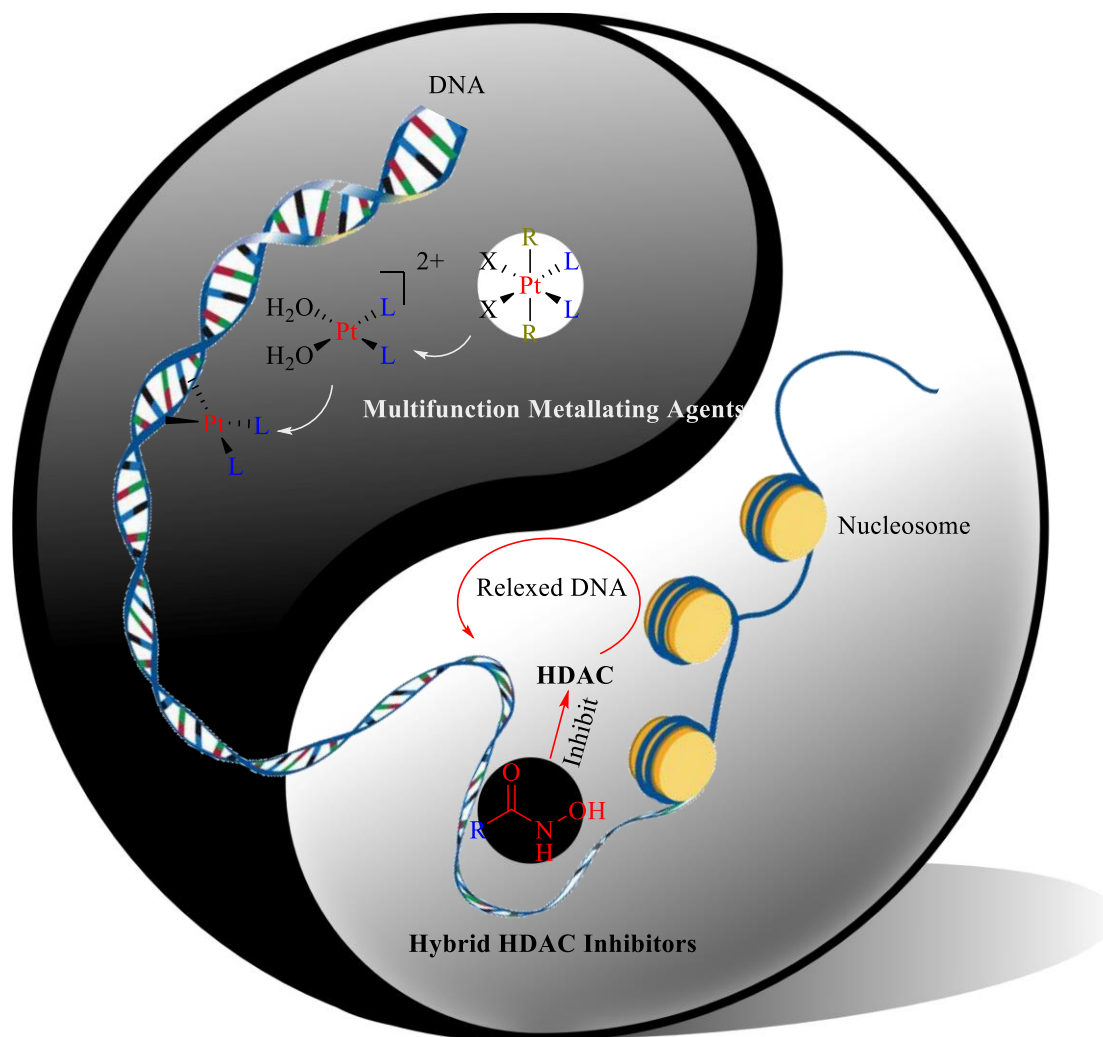


Figure 4.3 The design logic of Pt-HDACi conjugates.

A logical design strategy to incorporate the dual function could involve the installation of HDACi on the platinum center as a non-leaving group ligand. When the hybrid molecule reaches the cancer cells, the synergistic effect could be maintained as the relaxed chromatin structure makes DNA more susceptible to attack by the Pt drug. Picoplatin and SAHA derivatives are hybridized to form Pt-HDACi complexes, shown in Figure 4.3. According to the biostudies of HDACi in Chapter 3, **CF-L02**, **CF-L04**, and **CF-L07** exhibited promising HDAC inhibition and cytotoxicity among the first 12 HDACi (Table 3.1). Only **CF-L02** was used to incorporate with

platinum to form Pt-HDACi, **CF-101**, as it was feasible to obtain the pure product for further evaluation. The 2-methyl pyridine cap is crucial to form the desired monodentate product. According to the biostudies of picoplatin derivatives in Chapter 2, **Pt-11** and **Pt-12** showed comparable cell viability to cisplatin and picoplatin in ovarian cancer cell lines A2780 and A2780cis (Figure 2.8). The crystal structural analysis confirmed the *cis* configuration of **Pt-11** and **Pt-12**. HDAC inhibitors, **CF-L13**, **CF-14**, and **CF-15**, have comparable HDACi inhibition with SAHA (Table 3.2). Therefore, **CF-102**, **CF-103**, and **CF-104** were also designed and synthesized by merging **Pt-11** and **Pt-12** with **CF-L13**, **CF-L14**, and **CF-L15**.

Ethylenediamine has been extensively used as the non-leaving group linker for bifunctional platinum agent's synthesis.¹³ It also showed decent cytotoxicity against A2780 and A2780cis cell lines (Figure 4.10). HDAC inhibitors, **CF-L16** and **CF-17**, have better HDACi inhibition than SAHA (Table 3.2). Therefore, the bidentate Pt-HDACi hybrids (**CF-201**, and **CF-202**) were also synthesized (Figure 4.5) by combining **Pt-13** with **CF-L16** and **CF-L17**.

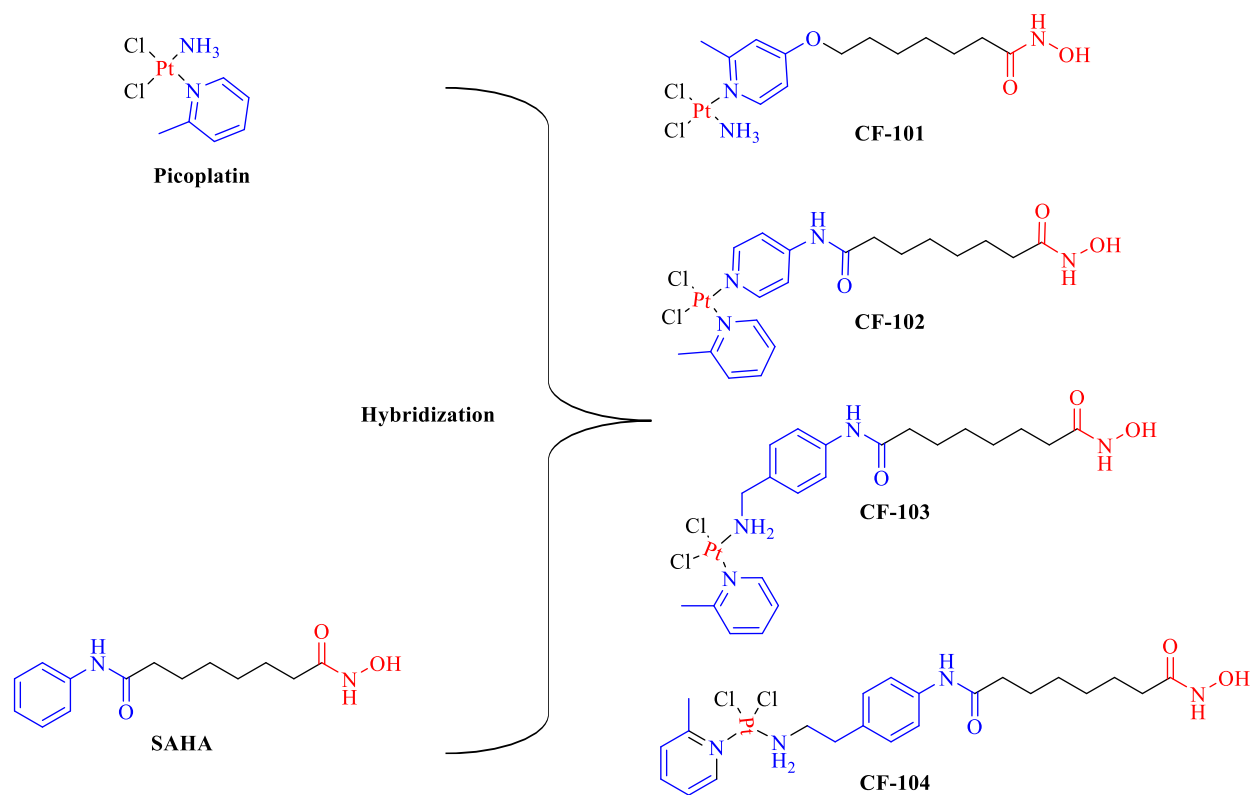


Figure 4.4 Pt-HDACi hybrid molecules (bidentate binding) designed in current research.

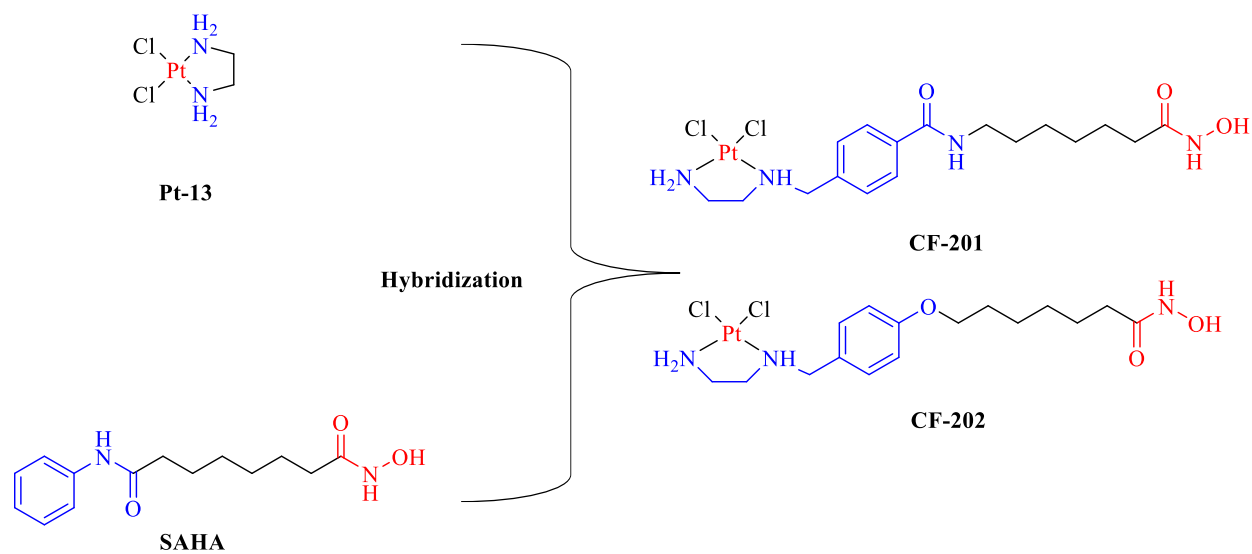
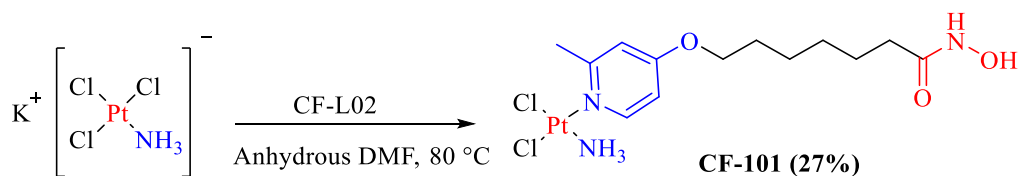


Figure 4.5 Pt-HDACi hybrid molecules (bidentate binding) designed in current research.

4.3 Preparation of Pt-HDACi Conjugates

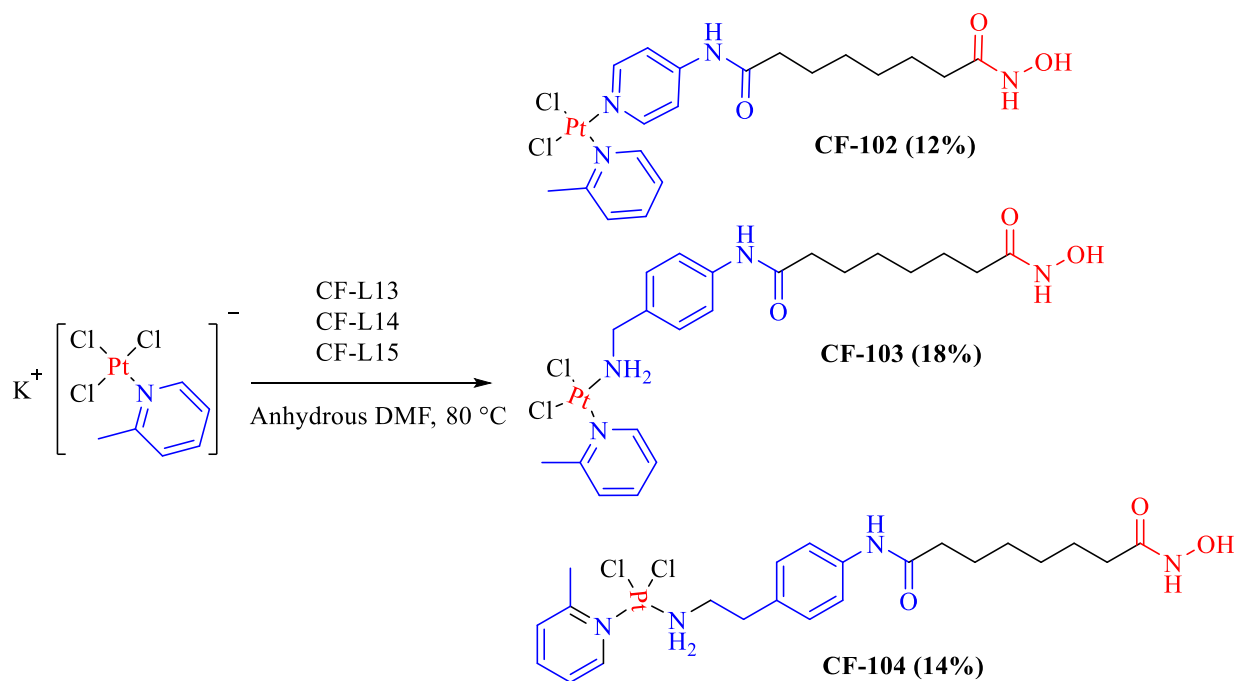
General procedures. Refer to part 2.2 in Chapter 2



Scheme 4.1 Synthesis of CF-101.

CF-101. **CF-L02** (53 mg, 0.21 mmol, 1.0 equiv) dissolved in anhydrous DMF (3.0 mL) was slowly added to a solution of $\text{K}[\text{PtCl}_3(\text{NH}_3)]$ (75 mg, 0.21 mmol, 1.0 equiv) in anhydrous DMF (3.0 mL). The mixture was stirred at 80 °C for 20 h. The byproducts were removed by filtration and the filtrate was concentrated under reduced pressure (40-45 °C, 125 rpm), which was then purified by preparative silica TLC (DCM/MeOH = 5/1). The gel band containing the product was scratched off, dissolved in anhydrous DMF, filtered, and concentrated to ~0.5 mL. The product was crushed out with the addition of EtOAc. The off-white product was collected via centrifugation, washed with EtOAc (twice), Et_2O (three times), and dried under vacuum overnight (30 mg, yield: 23 %). ^1H NMR (600 MHz, DMF-d_7): δ 10.59 (s, 1H), 8.99 (br, 1H), 8.78 (d, $J = 5.3$ Hz, 1H), 7.16 (s, 1H), 6.95 (s, 1H), 4.36 (s, 3H), 4.17 (t, $J = 6.2$ Hz, 2H), 3.10 (s, 3H), 2.09 (t, $J = 6.7$ Hz, 2H), 1.77 (m, 2H), 1.59 (m, 2H), 1.45 (m, 2H), 1.36 (m, 2H). ^{13}C NMR (151 MHz, DMF-d_7): δ 170.53, 166.98, 163.45, 155.73, 112.82, 110.91, 69.77, 33.35, 29.45, 29.29, 26.60, 26.24, 26.21. ^{195}Pt NMR (129 MHz, DMF-d_7): δ -2021.08. ESI-AccuTOF MS: m/z value of the most abundant isotope peak of $\text{C}_{13}\text{H}_{23}\text{Cl}_2\text{N}_3\text{O}_3\text{PtNa}$, $[\text{M}+\text{Na}]^+$ calcd 558.0646, found

558.0630. Anal. calcd for $C_{13}H_{23}Cl_2N_3O_3Pt \cdot (0.5 H_2O)$: C, 28.67; H, 4.44; N, 7.72%. Found: C, 28.77; H, 4.29; N, 7.45%.



Scheme 4.2 Synthesis of CF-102, CF-103 and CF-104.

CF-102. **CF-L13** (46 mg, 0.173 mmol, 1.0 equiv) dissolved in anhydrous DMF (3.0 mL) was slowly added to a solution of $K[PtCl_3(2\text{-picoline})]$ (**TCPP**) (75 mg, 0.173 mmol, 1.0 equiv) in anhydrous DMF (3.0 mL). The mixture was stirred at 80 °C for 20 h. Following the same procedure as **CF-101**, an off-white solid was produced (13 mg, yield: 12%). 1H NMR (600 MHz, DMF- d_7): δ 10.95 (br, 1H), 10.51 (br, 1H), 9.18 (d, $J = 4.9$ Hz, 1H), 8.92 (br, 1H), 8.62 (d, $J = 5.7$ Hz, 2H), 7.91 (t, $J = 7.4$ Hz, 1H), 7.72 (s, 2H), 7.59 (d, $J = 7.7$ Hz, 1H), 7.41 (t, $J = 6.2$ Hz, 1H), 3.17 (s, 3H), 2.44 (m, 2H), 2.05 (t, $J = 7.2$ Hz, 2H), 1.61 (m, 2H), 1.57 – 1.51 (m, 2H), 1.29 (m, 4H). ^{13}C NMR (151 MHz, DMF- d_7): δ 174.34, 170.60, 162.22, 154.49, 153.75 (2), 148.92,

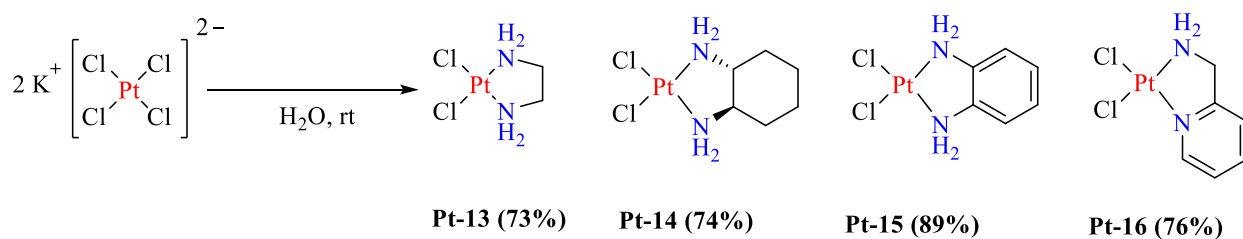
139.80, 127.93, 124.69, 115.74 (2), 37.72, 33.40, 29.53, 29.49, 26.47, 26.23, 25.63. ^{195}Pt NMR (129 MHz, DMF- d_7): δ -1973.65. AccuTOF MS: m/z value of the most abundant isotope peak of $\text{C}_{19}\text{H}_{26}\text{Cl}_2\text{N}_4\text{O}_3\text{PtNa}$, $[\text{M}+\text{Na}]^+$ calcd 647.0913, found 647.0849. Anal. calcd for $\text{C}_{19}\text{H}_{26}\text{Cl}_2\text{N}_4\text{O}_3\text{Pt}$ (0.5 H_2O): C, 36.01; H, 4.30; N, 8.85%. Found: C, 35.66; H, 3.90; N, 8.64%.

CF-103. CF-L14 (57 mg, 0.173 mmol, 1.0 equiv) dissolved in anhydrous DMF (3.0 mL) with DIEA (22.4 mg, 30 μL , 1.0 equiv) was slowly added to a solution of $\text{K}[\text{PtCl}_3(2\text{-picoline})]$ (TCPP) (75 mg, 0.173 mmol, 1.0 equiv) in anhydrous DMF (3.0 mL). The mixture was stirred at 80 $^\circ\text{C}$ for 20 h. An off-white solid was obtained by following the same procedure as **CF-101** (20 mg, yield: 18%). ^1H NMR (600 MHz, DMF- d_7): δ 10.61 (s, 1H), 10.13 (s, 1H), 8.99 (br, 1H), 8.62 (d, $J = 5.1$ Hz, 1H), 7.83 (t, $J = 7.4$ Hz, 1H), 7.69 (d, $J = 8.0$ Hz, 2H), 7.51 (d, $J = 7.6$ Hz, 1H), 7.41 (d, $J = 8.2$ Hz, 2H), 7.24 (t, $J = 6.3$ Hz, 1H), 5.48 (d, $J = 51.9$ Hz, 2H), 3.87 (m, 2H), 3.08 (s, 3H), 2.40 (t, $J = 7.1$ Hz, 2H), 2.08 (t, $J = 7.2$ Hz, 2H), 1.71 – 1.62 (m, 2H), 1.61 – 1.51 (m, 2H), 1.40 – 1.27 (m, 4H). ^{13}C NMR (151 MHz, DMF- d_7): δ 172.66, 170.64, 162.57, 154.70, 140.16, 138.95, 133.66, 130.43, 127.19, 123.71, 119.98, 50.29, 37.49, 33.31, 29.52, 29.46, 26.62, 26.17(2). ^{195}Pt NMR (129 MHz, DMF- d_7): δ -2096.14. AccuTOF MS: m/z value of the most abundant isotope peak of $\text{C}_{21}\text{H}_{30}\text{Cl}_2\text{N}_4\text{O}_3\text{PtNa}$, $[\text{M}+\text{Na}]^+$ calcd 675.1227, found 675.1182. Anal. calcd for $\text{C}_{21}\text{H}_{30}\text{Cl}_2\text{N}_4\text{O}_3\text{Pt}$ (H_2O): C, 37.60; H, 4.81; N, 8.36%. Found: C, 37.21; H, 4.41; N, 8.13%.

CF-104. CF-L15 was used as the starting material and the reaction followed the same procedure as CF-103 to afford an off-white solid (yield: 18%). ^1H NMR (600 MHz, DMF- d_7): δ 10.59 (s, 1H), 9.98 (s, 1H), 9.11 (d, $J = 5.2$ Hz, 1H), 7.89 (t, $J = 7.4$ Hz, 1H), 7.63 (d, $J = 8.1$ Hz, 2H), 7.58 (d, $J = 7.8$ Hz, 1H), 7.39 (t, $J = 6.4$ Hz, 1H), 7.14 (d, $J = 8.2$ Hz, 2H), 5.19 (d, $J = 61.0$ Hz, 2H), 3.20 (s, 3H), 3.02 – 2.94 (m, 2H), 2.90 – 2.79 (m, 2H), 2.37 (t, $J = 7.0$ Hz, 2H), 2.08 (t,

$J = 7.3$ Hz, 2H), 1.68 – 1.61 (m, 2H), 1.60 – 1.53 (m, 2H), 1.39 – 1.28 (m, 4H). δ ^{13}C NMR (151 MHz, DMF- d_7): δ 172.45, 170.64, 162.57, 154.96, 139.18, 139.04, 133.96, 129.65, 127.42, 124.09, 120.14, 48.70, 37.52, 36.62, 33.35, 29.57, 29.51, 26.75, 26.22(2). ^{195}Pt NMR (129 MHz, DMF- d_7): δ -2102.74. AccuTOF MS: m/z value of the most abundant isotope peak of $\text{C}_{22}\text{H}_{32}\text{Cl}_2\text{N}_4\text{O}_3\text{PtNa}$, $[\text{M}+\text{Na}]^+$ calcd 689.1384, found 689.1258. Anal. calcd for $\text{C}_{22}\text{H}_{32}\text{Cl}_2\text{N}_4\text{O}_3\text{Pt}$ (H_2O): C, 38.58; H, 5.01; N, 8.19%. Found: C, 38.35; H, 4.80; N, 7.88%.

Scheme 4.3 Pt-13, Pt-14, Pt-15 and Pt-16 synthesis



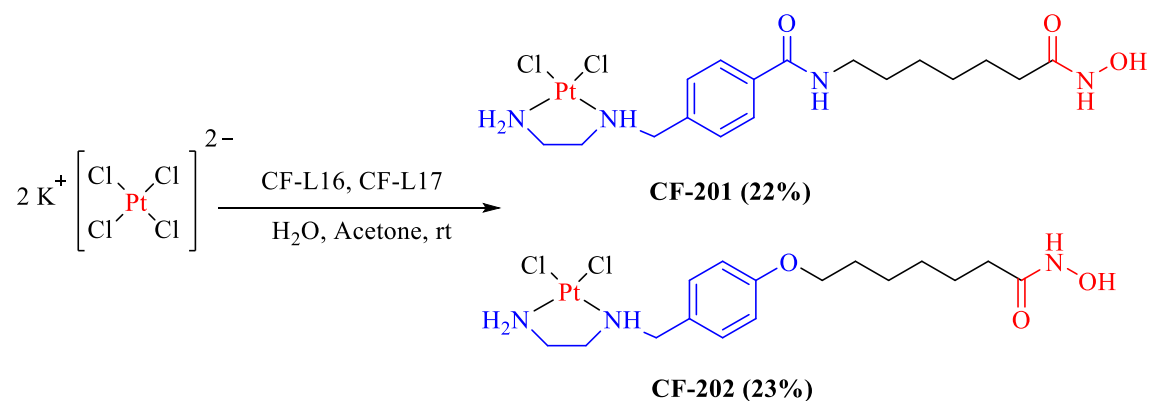
Scheme 4.3 Synthesis of Pt-13, Pt-14, Pt-15 and Pt-16.

PtCl₂(ethylenediamine) (Pt-13). To a solution of ethylenediamine (18.01 mg, 20.13 μL , 0.30 mmol, 1.25 equiv) in 2 mL of H_2O was added a solution of potassium tetrachloroplatinate(II), K_2PtCl_4 (100 mg, 0.241 mmol, 1.0 eq) in 1 mL of H_2O dropwise. A yellow solid precipitated out after 10-20 min of stirring. The solution continued to stir for additional 5-6 h at rt. The yellow solids were collected via vacuum filtration, washed with cold water, acetone, and ether, and dried under vacuum overnight (yield: 73%). ^1H NMR (600 MHz, DMSO- d_6) δ 5.29 (s, 4H), 2.23 (s, 4H).

PtCl₂((±)-trans-1,2-cyclohexanediamine) (Pt-14). The same synthesis procedure as **Pt-13** was applied to afford a light-yellow crude product (yield: 74%). ¹H NMR (600 MHz, DMSO-d₆) δ 6.35 (m, 1H), 6.24 (m, 2H), 5.83 (t, J = 10.2 Hz, 1H), 2.34 (m, 2H), 1.95 (d, J = 12.8 Hz, 1H), 1.89 (d, J = 13.8 Hz, 1H), 1.51 (m, 2H), 1.37 – 1.23 (m, 2H), 1.07 – 0.96 (m, 2H). ESI-AccuTOF MS: m/z value of the most abundant isotope peak of C₆H₁₄Cl₂N₂PtNa, [M+Na]⁺ calcd 403.0060, found 403.0047.

PtCl₂(phenylenediamine) (Pt-15). Following the same synthesis procedure as Pt-13 afforded a light-yellow crude product (yield: 89%). ¹H NMR (600 MHz, DMSO-d₆) δ 7.62 (s, 4H), 7.16 (s, 4H). ESI-AccuTOF MS: m/z value of the most abundant isotope peak of C₆H₈Cl₂N₂PtNa, [M+Na]⁺ calcd 396.9590, found 403.0047.

PtCl₂(2-(aminomethyl)pyridine) (Pt-16). Following the same synthesis procedure as Pt-13 afforded light-yellow crude product (yield: 76%). ¹H NMR (600 MHz, DMSO-d₆) (one set) δ 9.07 (ddd, J = 5.9, 1.5, 0.7 Hz, 1H), 8.12 (td, J = 7.7, 1.6 Hz, 1H), 7.64 (ddd, J = 7.9, 1.5, 0.8 Hz, 1H), 7.48 (m, 1H), 6.20 (m, 2H), 4.08 (t, J = 5.9 Hz, 2H).



Scheme 4.4 Synthesis of CF-201 and CF-202.

CF-201. To solution of **CF-L16** (50 mg, 0.122 mmol, 1.0 equiv) in H₂O (0.8 mL) and acetone (1 mL) was added 1 M NaOH (183 μ L, 0.183 mmol, 1.5 equiv). The total volume is around 2 mL. The solution was stirred for 5 min and then added a solution of K₂PtCl₄ (50.7 mg, 0.122 mmol, 1.0 equiv) in H₂O (0.3 mL) dropwise. The solution was stirred for 3.5 h. The light-yellow solid was collected via vacuum filtration, washed with cold water and acetone, dried under vacuum overnight (16 mg, yield: 22%). ¹H NMR (600 MHz, DMF-d₇): δ 10.53 (s, 1H), 8.51 (s, 1H), 7.99 (d, J = 6.6 Hz, 2H), 7.78 (d, J = 6.8 Hz, 2H), 6.63 (s, 1H), 5.47 (s, 2H), 4.50 (d, J = 12.2 Hz, 1H), 4.23 (m, 1H), 3.36 (m, 2H), 2.74 – 2.50 (m, 3H), 2.50 – 2.38 (m, 1H), 2.07 (t, J = 6.9 Hz, 2H), 1.58 (m, 4H), 1.41 – 1.26 (m, 4H).

CF-202. Following the same procedure as **CF-201** afforded a light-yellow solid (yield: 23%) ¹H NMR (600 MHz, DMF-d₇): δ 7.57 (d, J = 8.3 Hz, 2H), 6.97 (d, J = 8.3 Hz, 2H), 6.41 (s, 1H), 5.43 (s, 2H), 4.39 (d, J = 13.2 Hz, 1H), 4.07 (dd, J = 13.5, 8.7 Hz, 1H), 4.01 (t, J = 6.3 Hz, 2H), 2.64 (m, 2H), 2.58 (m, 1H), 2.44 (m, 1H), 2.09 (t, J = 7.5 Hz, 2H), 1.82 – 1.69 (m, 2H), 1.60 (m, 2H), 1.52 – 1.42 (m, 2H), 1.37 (m, 2H).

4.4 Results and Discussion

Four bioassays have been used to evaluate the Pt-HDACi complexes. The DNA binding study was performed at Dr. Liang Xue's lab in the Chemistry Department, University of the Pacific. The HDAC1 inhibition study was conducted by contract research organization Nanosyn, Inc, at Santa Clara, CA with the support from Newave Phamarceutical Inc. The cell viability study was performed at the pharmacy school with collaboration with Dr. Xin Guo's lab, University of the Pacific. Colon cancer cell line HCT-116 and lung cancer cell line A549, ovarian cancer cell lines A2780 and A2780cis were used for cytotoxicity evaluation. The cellular uptake study was conducted in our lab at the chemistry department, University of the Pacific.

Since the complexes contain platinum, the formulation solvent is DMF. Please refer to section 2.3 for more experimental details.

4.4.1 Monodentate Pt-HDACi conjugate. **CF-101**, **CF-102**, **CF-103**, and **CF-104** were synthesized as hybrid molecules between picoplatin and SAHA derivatives. Mass spectrometry and NMR have been used to confirm the mass and structures of the desired products. For example, the stacked ^1H NMR spectra of **CF-L13** and **CF-102** confirmed the binding of the HDACi to the platinum core (Figure 4.6). Although there is no X-ray data to confirm the *cis* configuration of the Pt-HDACi conjugates, their ^{195}Pt NMR shifts are very close to their corresponding picoplatin derivatives in a *cis* configuration under the same deuterated NMR solvent (Table 4.1). For example, the ^{195}Pt NMR shift of **CF-101** (-2021.08 ppm) is close to that of **Pt-1** (-2042.86 ppm). The ^{195}Pt NMR shift of **CF-102** (-1973.65 ppm) is close to that of **Pt-11** (-1979.29 ppm). The ^{195}Pt NMR shifts of **CF-103** (-2096.14 ppm) and **CF-104** (-2102.74 ppm) are close to that of **Pt-12** (-2095.60 ppm).

Table 4.1 ^{195}Pt NMR shifts of monodentate Pt-HDACi and its corresponding picoplatin derivatives.

Compd	CF-101	CF-102	CF-103	CF-104	Pt-1	Pt-11	Pt-12
^{195}Pt (ppm)	-2021.08	-1973.65	-2096.14	-2102.74	-2042.86	-1979.29	-2095.60

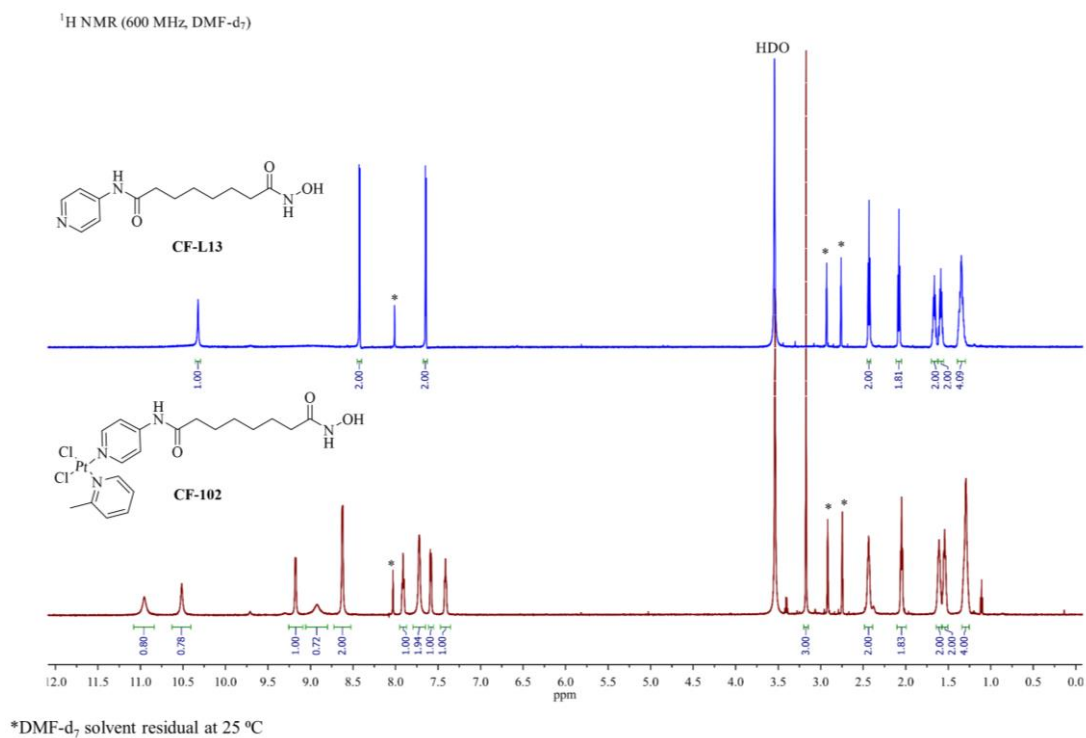


Figure 4.6 The stacked ¹H NMR spectra of **CF-L13** (top, blue trace) and **CF-102** (bottom, red trace)

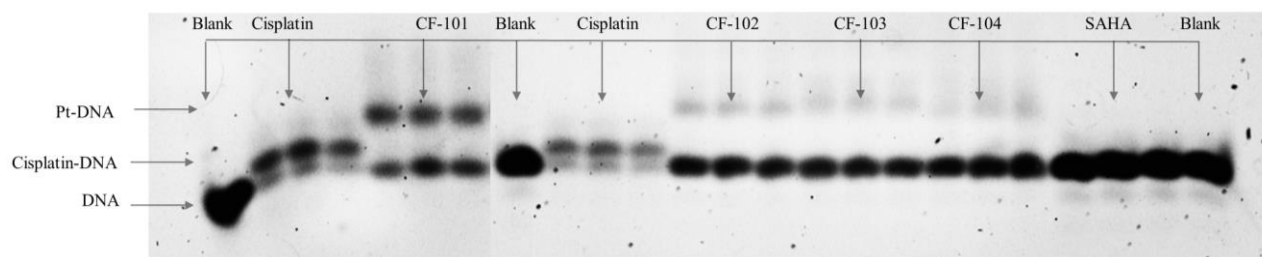


Figure 4.7 DNA gel electrophoresis of **CF-101**, **CF-102**, **CF-103** and **CF-104**, reference to cisplatin and SAHA.

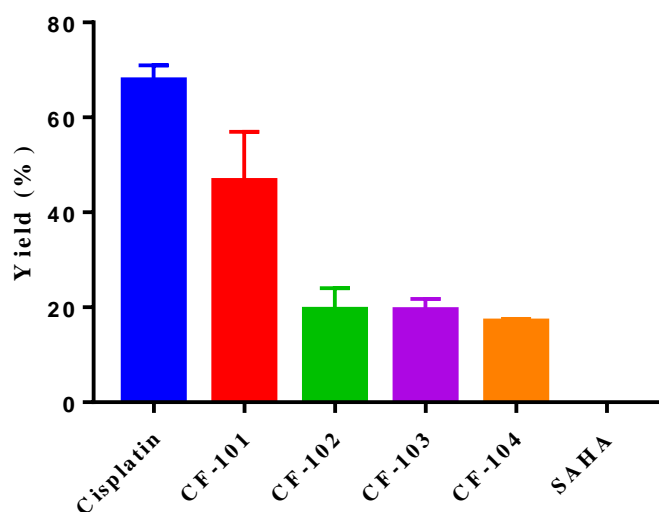


Figure 4.8 The DNA binding yields of Pt-HDACi conjugates. (confidence interval: 95%, $p < 0.1$)

The DNA binding study was conducted following the protocol described in section 2.3. As the molecular weight of Pt-DNA adducts formed with Pt-HDACi conjugates is significantly larger than that of cisplatin adduct, the separation difference of Pt-HDACi is bigger than that of cisplatin (Figure 4.7). SAHA was used as the negative control and it showed no binding between DNA and SAHA. Quantitative study with three runs for each complex has also been conducted (Figure 4.8), which demonstrated that **CF-101** has a better binding efficacy than other conjugates. The DNA binding studies confirm the function of platinum in the Pt-HDACi conjugates.

Table 4.2 HDAC1 inhibition of Pt-HDACi conjugates and their corresponding free ligands.

Pt-HDACi	SAHA	CF-101	CF-102	CF-103	CF-104
HDAC1 IC ₅₀ (nM)	44.8±5.4	148±35.7	25±4.2	22.5±2.4	32.8±5.5
Free ligand	SAHA	CF-L02	CF-L13	CF-L14	CF-L15
HDAC1 IC ₅₀ (nM)	44.8±5.4	165±31.1	52.3±12.1	51.4±6.9	42.2±3.4

Results from HDAC1 inhibition assay were summarized in Table 4.2. **CF-102**, **CF-103**, and **CF-104** showed comparable or even better inhibition efficacy than SAHA. However, **CF-101** exhibited significantly less efficacy than other conjugates. It might be due to the less efficacy of its corresponding free ligand, **CF-L02**. All Pt conjugates showed slightly better HDAC1 inhibition than that of corresponding free ligands. Computational studies could have been applied to further explore the structure-activity relationship.

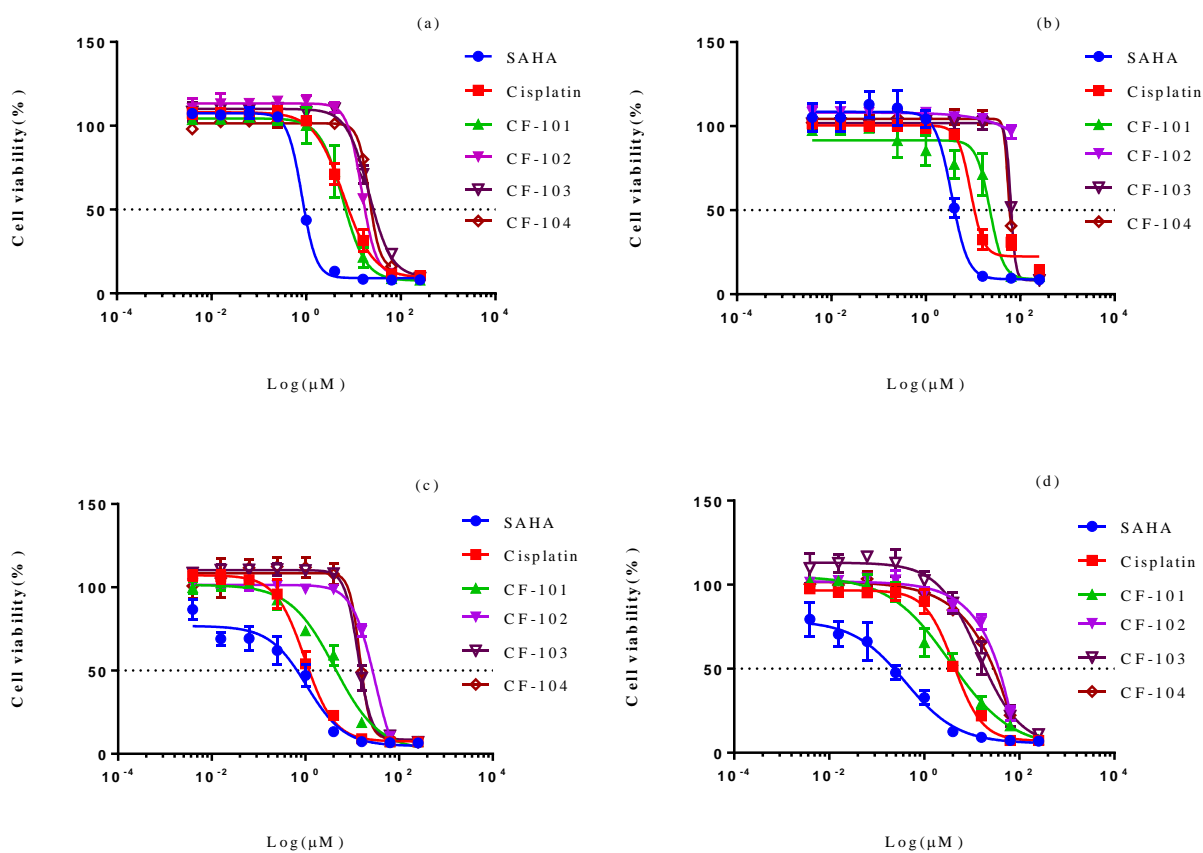


Figure 4.9 IC₅₀ curve of SAHA, cisplatin, and Pt-HDACi in (a) HCT-116, (b) A549, (c) A2780 and (d) A2780cis cell lines.

Table 4.3 Cell viability IC₅₀ values of Pt-HDACi in four different cancer cell lines.

IC ₅₀ (μM)	HCT-116	A549	A2780	A2780cis	Resistance factor*
SAHA	0.81 ± 0.02	3.55 ± 0.18	1.07 ± 0.16	0.40 ± 0.07	N/A
Cisplatin	6.13 ± 0.31	8.88 ± 0.70	0.97 ± 0.06	4.22 ± 0.21	4.35
CF-101	5.95 ± 0.44	22.80 ± 3.66	4.22 ± 0.46	3.53 ± 0.58	0.84
CF-102	14.84 ± 0.39	N/A	30.92 ± 6.64	N/A	N/A
CF-103	21.28 ± 0.96	>50	13.37 ± 0.41	13.39 ± 1.84	1.00
CF-104	21.46 ± 9.69	>50	14.49 ± 1.44	N/A	N/A

*Resistance factor (R_f) is defined as $IC_{50}(A2780cis)/IC_{50}(A2780)$

Four solid tumor cancer cell lines, including colon cancer HCT-116, lung cancer A549 and ovarian cancer A2780 and A2780cis, have been used to evaluate the cytotoxicity of the Pt-HDACi conjugates (Figure 4.9). The IC₅₀ values are summarized in Table 4.3. Although SAHA showed the best efficacy in terms of cytotoxicity in all four cell lines, it has not been approved for colon, lung and ovarian solid tumors treatment and one of the reasons may be its short elimination half-life ($t_{1/2}$: 1-2 h).^{153,154} Our project focuses on Pt-HDACi conjugates and used for solid tumor treatment. Cisplatin is our reference drug with a much longer elimination half-life and less frequent administration depending on the cancer type. Our complex is more effective on HCT-116 and A2780 cell lines while A549 and A2780cis cell lines are less sensitive to our Pt-HDACi conjugates. Among all the Pt-HDACi conjugates, **CF-101** shows the best efficacy, which is comparable with cisplatin in HCT-116 and A2780cis. **CF-101** also has the lowest resistance factor (0.84) whereas cisplatin has a R_f value of 4.35. Further extending the HDACi away from the platinum core (**CF-102**, **CF-103**, and **CF-104**) will decrease the cytotoxicity.

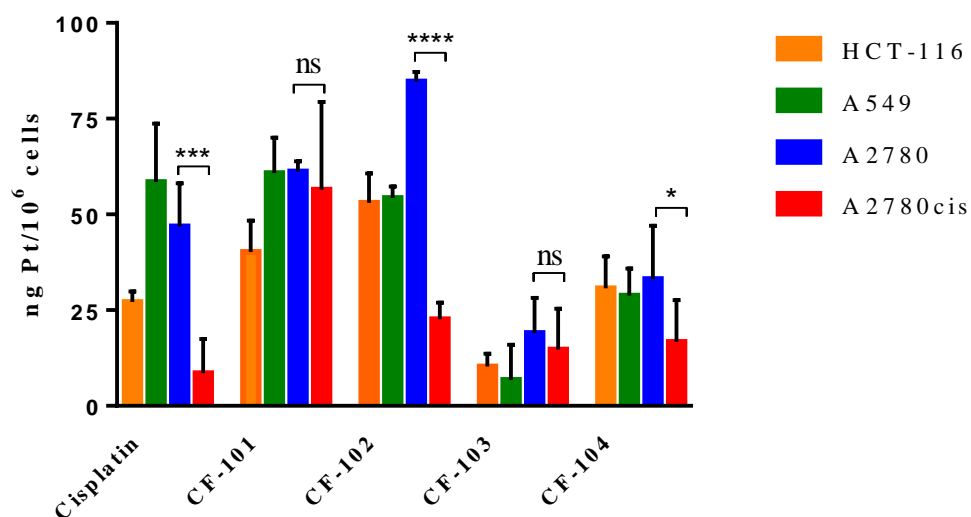


Figure 4.10 Cellular accumulation of platinum from cisplatin, Pt-HDACi in four different cancer cell lines. (treated at 10 μ M for 24 h) **** p \leq 0.0001, *** p \leq 0.001, * p \leq 0.1, ns p $>$ 0.1.

Table 4.4 Cellular accumulation of platinum from cisplatin, Pt-HDACi in four different cancer cell lines. (treated at 10 μ M for 24 h).

Mean (ng Pt/10 ⁶ cell)	HCT-116	A549	A2780	A2780cis
Cisplatin	27.14 \pm 1.10	58.42 \pm 6.17	46.84 \pm 4.54	8.58 \pm 3.58
CF-101	40.22 \pm 3.29	60.77 \pm 3.72	61.19 \pm 1.07	56.44 \pm 9.23
CF-102	53.06 \pm 3.07	54.29 \pm 1.22	84.68 \pm 1.00	22.65 \pm 1.74
CF-103	10.33 \pm 1.32	6.77 \pm 3.70	19.05 \pm 3.69	14.69 \pm 4.30
CF-104	30.69 \pm 3.35	28.77 \pm 2.86	33.1 \pm 5.61	16.67 \pm 4.40

In order to gain more insight, cellular accumulation study was conducted according to the protocol described in section 2.3.3. The test compounds (10 μ M) were incubated with the cancer cell lines for 24 h and the platinum level was measured by ICP-OES (Figure 4.10 and Table 4.4). The higher platinum cellular accumulation of **CF-101** than that of cisplatin (***) p \leq 0.001) in HCT-116 and A2780cis may contribute to the comparable cytotoxicity with cisplatin. The platinum accumulation levels of **CF-103** and **CF-104** in A549 are significantly lower than that of

cisplatin and **CF-101** (**** $p \leq 0.0001$), which explains the decreasing cytotoxicity of these compounds in A549. The platinum accumulation level of **CF-102** in A549 is not significantly different from that of cisplatin and **CF-101** (ns $p > 0.1$), which indicates the low cytotoxicity of **CF-102** is not due to the accumulation. The higher platinum cellular accumulation of **CF-101** in A2780 compared to cisplatin (** $p \leq 0.01$) does not result in higher cytotoxicity. Although the platinum accumulation level of **CF-102** in A2780 is significantly higher than all other test compounds (*** $p \leq 0.001$), it shows the lowest cytotoxicity with highest IC_{50} . The higher platinum cellular accumulation of **CF-103** and **CF-104** in A2780 than that of cisplatin (** $p \leq 0.01$) may contribute to the decent cytotoxicity. The lowest IC_{50} of **CF-101** in A2780cis cell line may derive from the highest platinum cellular level (*** $p \leq 0.001$). The platinum accumulation level of **CF-101** (and **CF-103**) in A2780 and A2780cis cell lines are not significantly different (ns $p > 0.1$), which may contribute to the low resistance factor. Overall, **CF-101** shows promising efficacy as a lead compound and further studies should be performed in the future.

4.4.2 Bidentate Pt-HDACi conjugate. The monodentate Pt-HDACi complex synthesis involves multiple steps and the purification process is time consuming due to running

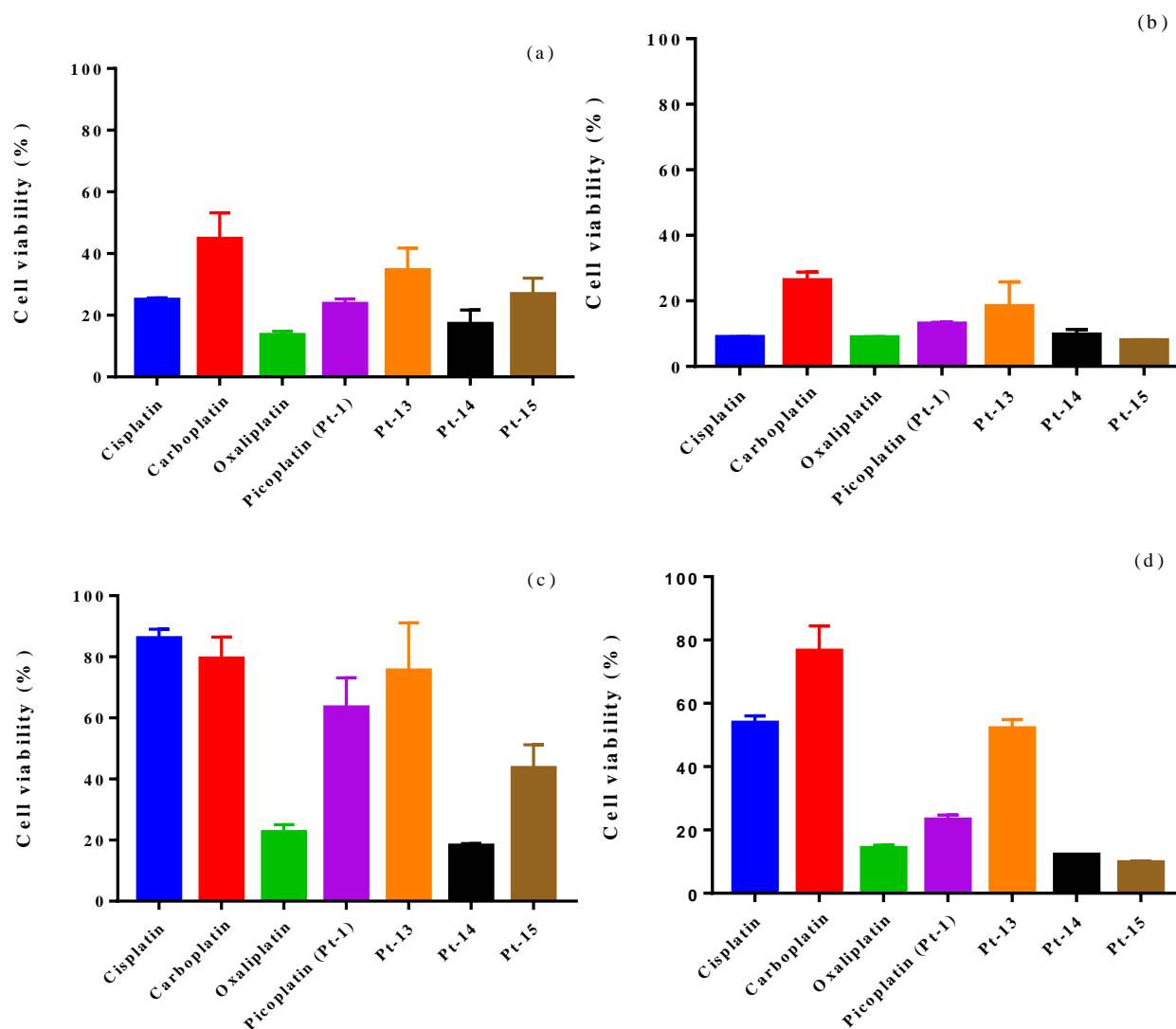


Figure 4.11 Preliminary cell viability screening of **Pt-13**, **Pt-14**, and **Pt-15** in two different ovarian cell lines at two different concentrations. (a) A2780 with 5 μM, (b) A2780 with 20 μM, (c) A2780cis with 5 μM, (d) A2780cis with 20 μM.

chromatography. Therefore, four small bidentate platinum complexes (**Pt-13**, **Pt-14**, **Pt-15**, and **Pt-16**) have been synthesized (Scheme 4.3) and evaluated on A2780 and A2780cis cell lines

(Figure 4.11) (**Pt-16** was eliminated due to the low solubility). All of them show promising efficacy. Although **Pt-14** ($\text{PtCl}_2((\pm)\text{-trans-1,2-cyclohexanediamine})$) shows the best efficacy, it is hard to synthesize the enantiomerically pure ligand with HDAC inhibition. Therefore, only **Pt-13** ($\text{PtCl}_2(\text{ethylenediamine})$) and **Pt-15** ($\text{PtCl}_2(\text{phenylenediamine})$) were further explored.

CF-L16 with ethylenediamine as the binding site was designed and shown even better HDAC1 inhibition (28.3 nM) than SAHA (44.8 nM) (Table 3.2). Therefore, the first bidentate Pt-HDACi was synthesized by combining **CF-L16** and **Pt-13** together. However, the resulting complex **CF-201** (Scheme 4.4) has bad solubility in both aqueous and organic solvents. In order to improve the solubility for biostudies, **CF-202** was designed and synthesized by changing the amide bond to an ether bond (Scheme 4.4). However, there is no big change in solubility.

CF-L19 with a phenylenediamine cap was designed (Figure 3.6) from structure modification of Panobinostat. The tertiary amine will improve the water solubility while sterically hinder the binding with platinum. Although it is a racemic mixture, the HDAC1 IC_{50} has reached nM level (1.1 nM). The enantiomerically pure compound will be obtained and conjugated with platinum soon.

4.5 Conclusions

Four new Pt-HDACi conjugates have been synthesized, characterized and evaluated by DNA electrophoresis, HDAC inhibition assay, cell viability assay, and cellular accumulation assay. All the conjugates could bind to DNA and have HDAC inhibition as bifunctional molecules. **CF-101** shows promising bioactivity data as the lead compound in HCT-116, A549, A2780, and A2780cis. The lowest IC_{50} of **CF-101** in A2780cis cell line may derive from the highest platinum cellular level. The low resistance factor of **CF-101** might be due to the similar

platinum accumulation level in A2780 and A2780cis cell. Two bidentate Pt-HDACi conjugates have been synthesized, but biostudies were not conducted due to the low solubility.

In order to further understand how these Pt-HDACi works, more intracellular experiments need to be conducted to confirm the DNA damage and HDAC inhibition. **CF-101** could be used as the lead compound for further structural modification and *in vivo* studies.

References

- (1) Kelland, L. The Resurgence of Platinum-Based Cancer Chemotherapy. *Nat. Rev. Cancer* **2007**, *7* (8), 573–584.
- (2) Peyrone, M. Ueber Die Einwirkung Des Ammoniaks Auf Platinchlorür. *Justus Liebigs Ann. Chem.* **1844**, *51* (1), 1–29.
- (3) Kauffman, G. B.; Pentimalli, R.; Doldi, S.; Hall, M. D. Michele Peyrone (1813-1883), Discoverer of Cisplatin. *Platin. Met. Rev.* **2010**, *54* (4), 250–256.
- (4) Ghosh, S. Cisplatin: The First Metal Based Anticancer Drug. *Bioorg. Chem.* **2019**, *88*, 102952.
- (5) Rosenberg, B. Platinum Complexes for the Treatment of Cancer: Why the Search Goes On. In *Verlag Helvetica Chimica Acta: Zürich*; 1999.
- (6) National Institutes of Health. Clinical Trials Database. Accessed: 2019
www.clinicaltrials.gov.
- (7) Dhara, S. C. A Rapid Method for the Synthesis of Cis-[Pt(NH₃)₂Cl₂]. *Indian J. Chem.* **1970**, *8*, 193–194.
- (8) Wilson, J. J.; Lippard, S. J. Synthetic Methods for the Preparation of Platinum Anticancer Complexes. *Chem. Rev.* **2014**, *114* (8), 4470–4495.
- (9) Alderden, R. A.; Hall, M. D.; Hambley, T. W. The Discovery and Development of Cisplatin. *J. Chem. Educ.* **2006**, *83* (5), 728–734.
- (10) Hoeschele, J. D.; Butler, T. A.; Roberts, J. A.; Guyer, C. E. Analysis and Refinement of

- the Microscale Synthesis of the ^{195}mPt -Labeled Antitumor Drug, Cys-Dichlorodiammineplatinum(II), Cis-DDP. *Radiochim. Acta* **1982**, *31* (1–2), 27–36.
- (11) Davies, M. S.; Hall, M. D.; Berners-Price, S. J.; Hambley, T. W. [^1H , ^{15}N] Heteronuclear Single Quantum Coherence NMR Study of the Mechanism of Aquation of Platinum(IV) Ammine Complexes. *Inorg. Chem.* **2008**, *47* (17), 7673–7680.
- (12) Deo, K. M.; Ang, D. L.; McGhie, B.; Rajamanickam, A.; Dhiman, A.; Khoury, A.; Holland, J.; Bjelosevic, A.; Pages, B.; Gordon, C.; et al. Platinum Coordination Compounds with Potent Anticancer Activity. *Coord. Chem. Rev.* **2018**, *375*, 148–163.
- (13) Johnstone, T. C.; Suntharalingam, K.; Lippard, S. J. The Next Generation of Platinum Drugs: Targeted Pt(II) Agents, Nanoparticle Delivery, and Pt(IV) Prodrugs. *Chem. Rev.* **2016**, *116* (5), 3436–3486.
- (14) Ivanov, A. I.; Parkinson, J. A.; Sadler, P. J.; Christodoulou, J.; Barnham, K. J.; Tucker, A.; Woodrow, J. Cisplatin Binding Sites on Human Albumin. *J. Biol. Chem.* **1998**, *273* (24), 14721–14730.
- (15) Gately, D. P.; Howell, S. B. Cellular Accumulation of the Anticancer Agent Cisplatin: A Review. *Br. J. Cancer* **1993**, *67* (6), 1171–1176.
- (16) Howell, S. B.; Abada, P. Regulation of Cisplatin Cytotoxicity by Cu Influx Transporters. *Met. Based. Drugs* **2010**, *2010*.
- (17) Stephen B. Howell, Roohangiz Safaei, C. A. L. and M. J. S. Copper Transporters and the Cellular Pharmacology of the Platinum Containing Cancer Drugs. *Mol. Pharmacol.* **2010**, *77* (6), 887–894.

- (18) Reishus, J. W.; Martin Jr, D. S. Cis-Dichlorodiammineplatinum(II). Acid Hydrolysis and Isotopic Exchange of the Chloride Ligands. *J. Am. Chem. Soc.* **1961**, *83* (11), 2457–2462.
- (19) Bancroft, D. P.; Lepre, C. A.; Lippard, S. J. ¹⁹⁵Pt NMR Kinetic and Mechanistic Studies of Cis- and Trans-Diamminedichloroplatinum(II) Bindin to DNA. *J. Am. Chem. Soc.* **1990**, *112* (19), 6860–6871.
- (20) Fichtinger-Schepman, A. M. J.; Lohman, P. H. M.; van der Veer, J. L.; den Hartog, J. H. J.; Reedijk, J. Adducts of the Antitumor Drug Cis-Diamminedichloroplatinum(II) with DNA: Formation, Identification, and Quantitation. *Biochemistry* **1985**, *24* (3), 707–713.
- (21) MEssigmann, M. Recognition of Cisplatin Adducts by Cellular Proteins. *Mutat. Res., Fundam. Mol. Mech. Mutagen.* **2001**, *478* (1–2), 1–21.
- (22) Todd, R. C.; Lippard, S. J. Inhibition of Transcription by Platinum Antitumor Compounds. *Metallomics* **2009**, *1* (4), 280–291.
- (23) Lewis, A. D.; Hayes, J. D.; Wolf, C. R. Glutathione and Glutathione-Dependent Enzymes in Ovarian Adenocarcinoma Cell Lines Derived from a Patient before and after the Onset of Drug Resistance: Intrinsic Differences and Cell Cycle Effects. *Carcinogenesis* **1988**, *9* (7), 1283–1287.
- (24) Mistry, P.; Kelland, L. R.; Abel, G.; Sidhar, S.; Harrap, K. R. The Relationships between Glutathione, Glutathione-S-Transferase and Cytotoxicity of Platinum Drugs and Melphalan in Eight Human Ovarian Carcinoma Cell Lines. *Br. J. Cancer* **1991**, *64* (2), 215–220.
- (25) Ishikawa, T. The ATP-Dependent Glutathione S-Conjugate Export Pump. *Trends*

- Biochem. Sci.* **1992**, *17*, 463–468.
- (26) Johnson, S. W.; Swiggard, P. A.; Handel, L. M.; Brennan, J. M.; Godwin, A. K.; Ozols, R. F.; Hamilton, T. C. Relationship between Platinum-DNA Adduct Formation and Removal and Cisplatin Cytotoxicity in Cisplatin-Sensitive and -Resistant Human Ovarian Cancer Cells. *Cancer Res.* **1994**, *54* (22), 5911–5916.
- (27) Zdraveski, Z. Z.; Mello, J. A.; Farinelli, C. K.; Essigmann, J. M.; Marinus, M. G. MutS Preferentially Recognizes Cisplatin-over Oxaliplatin-Modified DNA. *J. Biol. Chem.* **2002**, *277* (2), 1255–1260.
- (28) Gifford, G.; Paul, J.; Vasey, P. A.; Kaye, S. B.; Brown, R. The Acquisition of HMLH1 Methylation in Plasma DNA after Chemotherapy Predicts Poor Survival for Ovarian Cancer Patients. *Clin. Cancer Res.* **2004**, *10* (13), 4420–4426.
- (29) Ekaterina Bassett, Alexandra Vaisman, Kristen A. Tropea, Chad M. McCall, Chikahide Masutani, Fumio Hanaoka, S. G. C. Frameshifts and Deletions during in Vitro Translesion Synthesis Past Pt-DNA Adducts by DNA Polymerase. *DNA Repair (Amst)*. **2002**, *1*, 1003–1016.
- (30) Albertella, M. R.; Green, C. M.; Lehmann, A. R.; O'Connor, M. J. A Role for Polymerase η in the Cellular Tolerance to Cisplatin-Induced Damage. *Cancer Res.* **2005**, *65* (21), 9799–9806.
- (31) Gadducci A, Cosio S, Muraca S, G. A. Molecular Mechanisms of Apoptosis and Chemosensitivity to Platinum and Paclitaxel in Ovarian Cancer: Biological Data and Clinical Implications. *Eur. J. Gynaecol. Oncol.* **2002**, *23* (5), 390–396.

- (32) Cvitkovic, E.; Spaulding, J.; Bethune, V.; Martin, J.; Whitmore, W. F. Improvement of Cis-dichlorodiammineplatinum (NSC 119875): Therapeutic Index in an Animal Model. *Cancer* **1977**, *39* (4), 1357–1361.
- (33) Spingler, B.; Whittington, D. A.; Lippard, S. J. 2.4 Å Crystal Structure of an Oxaliplatin 1,2-d(GpG) Intrastrand Cross-Link in a DNA Dodecamer Duplex. *Inorg. Chem.* **2001**, *40* (22), 5596–5602.
- (34) Silverman, A. P.; Bu, W.; Cohen, S. M.; Lippard, S. J. 2.4-Å Crystal Structure of the Asymmetric Platinum Complex {Pt(Ammine) (Cyclohexylamine)}₂⁺ Bound to a Dodecamer DNA Duplex. *J. Biol. Chem.* **2002**, *277* (51), 49743–49749.
- (35) Lovejoy, K. S.; Todd, R. C.; Zhang, S.; McCormick, M. S.; D'Aquino, J. A.; Reardon, J. T.; Sancar, A.; Giacomini, K. M.; Lippard, S. J. Cis - Diammine(Pyridine)Chloroplatinum(II), a Monofunctional Platinum(II) Antitumor Agent: Uptake, Structure, Function, and Prospects. *Proc. Natl. Acad. Sci.* **2008**, *105* (26), 8902–8907.
- (36) Cleare, M. J.; Hoeschele, J. D. Anti-Tumour Platinum Compounds: Relationship between Structure and Activity. *Platin. Met. Rev.* **1973**, *17* (1), 2–13.
- (37) Wheate, N. J.; Walker, S.; Craig, G. E.; Oun, R. The Status of Platinum Anticancer Drugs in the Clinic and in Clinical Trials. *Dalt. Trans.* **2010**, *39* (35), 8113–8127.
- (38) Neidle, S.; Ismail, I. M.; Sadler, P. J. The Structure of the Antitumor Complex Cis-(Diammino) (1,1-Cyclobutanedicarboxylato)-Pt(II): X Ray and Nmr Studies. *J. Inorg. Biochem.* **1980**, *13* (3), 205–212.

- (39) Frey, U.; Ranford, J. D.; Sadler, P. J. Ring-Opening Reactions of the Anticancer Drug Carboplatin: NMR Characterization of Cis-[Pt(NH₃)₂(CBDCA-O)(5'-GMP-N7)] in Solution. *Inorg. Chem.* **1993**, *32* (8), 1333–1340.
- (40) Vijgh, W. van der. Clinical Pharmacokinetics of Carboplatin. *Clin. Pharmacokinet.* **1991**, *28* (3), 208–215.
- (41) Chu, G.; Mantin, R.; Shen, Y. -M; Baskett, G.; Sussman, H. Massive Cisplatin Overdose by Accidental Substitution for Carboplatin. Toxicity and Management. *Cancer* **1993**, *72* (12), 3707–3714.
- (42) Olivier Rixe, Waldo Ortuzar, Manuel Alvarez, Ricardo Parker, Eddie Reed, K. P. and T. F. Oxaliplatin, Tetraplatin, Cisplatin, and Carboplatin: Spectrum of Activity in Drug-Resistant Cell Lines and in the Cell Lines of the National Cancer Institutes's Anticancer Drug Screen Panel. *Biochem. Pharmacol.* **1996**, *52*, 1855–1865.
- (43) Knox, R. J.; Friedlos, F.; Lydall, D. A.; Roberts, J. J. Mechanism of Cytotoxicity of Anticancer Platinum Drugs : Evidence and Cis-Diammine Differ Only in the Kinetics of Their Interaction with DNA '. *Cancer Res.* **1986**, *46* (ii), 1972–1979.
- (44) Zhang, S.; Lovejoy, K. S.; Shima, J. E.; Lagpacan, L. L.; Shu, Y.; Lapuk, A.; Chen, Y.; Komori, T.; Gray, J. W.; Chen, X.; et al. Organic Cation Transporters Are Determinants of Oxaliplatin Cytotoxicity. *Cancer Res.* **2006**, *66* (17), 8847–8857.
<https://doi.org/10.1158/0008-5472.CAN-06-0769>.
- (45) Alison K. Holzer, Gerald H. Manorek, and S. B. H. Contribution of the Major Copper Influx Transporter CTR1 to the Cellular Accumulation of Cisplatin, Carboplatin, and

- Oxaliplatin. *Mol. Pharmacol.* **2006**, *70*, 1390–1394.
- (46) Kuwahara, A.; Yamamori, M.; Nishiguchi, K.; Okuno, T.; Chayahara, N.; Miki, I.; Tamura, T.; Inokuma, T.; Takemoto, Y.; Nakamura, T.; et al. Replacement of Cisplatin with Nedaplatin in a Definitive 5-Fluorouracil/Cisplatin-Based Chemoradiotherapy in Japanese Patients with Esophageal Squamous Cell Carcinoma. *Int. J. Med. Sci.* **2009**, *6* (6), 305–311.
- (47) Lee, K. H.; Hyun, M. S.; Kim, H.-K.; Jin, H. M.; Yang, J.; Song, H. S.; Do, Y. R.; Ryoo, H. M.; Chung, J. S.; Zang, D. Y.; et al. Randomized, Multicenter, Phase III Trial of Heptaplatin 1-Hour Infusion and 5-Fluorouracil Combination Chemotherapy Comparing with Cisplatin and 5-Fluorouracil Combination Chemotherapy in Patients with Advanced Gastric Cancer. *Cancer Res. Treat.* **2009**, *41* (1), 12.
- (48) Welink, J.; Boven, E.; Vermorcken, J. B.; Gall, H. E.; Van Der Vijgh, W. J. F. Pharmacokinetics and Pharmacodynamics of Lobaplatin (D-19466) in Patients with Advanced Solid Tumors, Including Patients with Impaired Renal or Liver Function. *Clin. Cancer Res.* **1999**, *5* (9), 2349–2358.
- (49) Tanaka, K.; Kunimatzu, T.; Shimakura, J.; Hanada, M. Development of Miriplatin , a Novel Antitumor Platinum for Hepatocellular Carcinoma. *Sumitomo Kagaku* **2011**, 1–12.
- (50) Bhargava, A.; Vaishampayan, U. N. Satraplatin: Leading the New Generation of Oral Platinum Agents. *Expert Opin. Investig. Drugs* **2009**, *18* (11), 1787–1797.
- (51) Tang, C. H.; Parham, C.; Shocron, E.; McMahon, G.; Patel, N. Picoplatin Overcomes Resistance to Cell Toxicity in Small-Cell Lung Cancer Cells Previously Treated with

- Cisplatin and Carboplatin. *Cancer Chemother. Pharmacol.* **2011**, *67* (6), 1389–1400.
- (52) David P Nowotnik, E. C. ProLindac™(AP5346): A Review of the Development of an HPMA DACH PlatinumPolymer Therapeutic. *Adv. Drug Deliv. Rev.* **2009**, *61*, 1214–1219.
- (53) Kelland, L. Broadening the Clinical Use of Platinum Drug-Based Chemotherapy with New Analogues: Satraplatin and Picoplatin. *Expert Opin. Investig. Drugs* **2007**, *16* (7), 1009–1021. <https://doi.org/10.1517/13543784.16.7.1009>.
- (54) Lloyd R.Kelland, Swee Y.Sharp, Ciaran F.O’Neill, Florence I.Raynaud, Philip J.Beale, I. R. J. Mini-Review: Discovery and Development of Platinum Complexes Designed to Circumvent Cisplatin Resistance. *J. Inorg. Biochem.* **1999**, *77*, 111–115.
- (55) Amin, A.; Buratovich, M. New Platinum and Ruthenium Complexes - the Latest Class of Potential Chemotherapeutic Drugs - a Review of Recent Developments in the Field. *Mini-Reviews Med. Chem.* **2009**, *9* (13), 1489–1503.
- (56) McGowan, G.; Parsons, S.; Sadler, P. J. Contrasting Chemistry of Cis- and Trans-Platinum(II) Diamine Anticancer Compounds: Hydrolysis Studies of Picoline Complexes. *Inorg. Chem.* **2005**, *44* (21), 7459–7467. <https://doi.org/10.1021/ic050763t>.
- (57) Chen, Y.; Guo, Z.; Parsons, S.; Sadler, P. J. Stereospecific and Kinetic Control over the Hydrolysis of a Sterically Hindered Platinum Picoline Anticancer Complex. *Chem. - A Eur. J.* **1998**, *4* (4), 672–676.
- (58) Yoshiko Kawamura-Akiyama, Hitoshi Kusaba, Fumihiko Kanzawa, Tomohide Tamura, Nagahiro Saijo, K. N. Non-Cross Resistance of ZD0473 in Acquired Cisplatin-Resistant

- Lung Cancer Cell Lines. *Lung Cancer* **2002**, 38, 43–50.
- (59) J. Holford, P.J. Beale, F.E. Boxall, S.Y. Sharp, L. R. K. Mechanisms of Drug Resistance to the Platinum Complex ZD0473 in Ovarian Cancer Cell Lines. *Eur. J. Cancer* **2000**, 36 (15), 1984–1990.
- (60) Sharp, S. Y.; Smith, V.; Hobbs, S.; Kelland, L. R. Lack of a Role for MRP1 in Platinum Drug Resistance in Human Ovarian Cancer Cell Lines. *Br. J. Cancer* **1998**, 78 (2), 175–180.
- (61) Holford, J.; Sharp, S. Y.; Murrer, B. A.; Abrams, M.; Kelland, L. R. In Vitro Circumvention of Cisplatin Resistance by the Novel Sterically Hindered Platinum Complex AMD473. *Br. J. Cancer* **1998**, 77 (3), 366–373.
- (62) S.Y. Sharp, C. F. O’Neill, P. Rogers, F.E. Boxall, L. R. K. Retention of Activity by New Generation Platinum Agent AMD0473 in Four Human Tumor Cell Lines Possessing Acquired Resistance to Oxaliplatin. *Eur. J. Cancer* **2002**, 38, 2309–2315.
- (63) M.E. Gore, R.J. Atkinson, H. cure, D. Rischin, P. Beale, P. Bognoux, L. D. and W. M. S. Results of ZD0473 in Platinum-Pretreated Ovarian Cancer: Analysis According to Platinum Free Interval. *Eur. J. Cancer* **2002**, 38 (SUPPL. 8), S7–S12.
- (64) M.E. Gore, R.J. Atkinson, H. cure, D. Rischin, P. Beale, P. Bognoux, L. D. and W. M. S. A Phase II Trial of ZD0473 in Platinum-Pretreated Ovarian Cancer. *Eur. J. Cancer* **2002**, 38, 2416–2420.
- (65) J. Treat, J. Schiller, E. Quoix, A. Mauer, M. Edelman, M. Modiano, P. Bonomi, R. R. and E. L. ZD0473 Treatment in Lung Cancer: An Overview of the Clinical Trial Results. *Eur.*

- J. Cancer* **2002**, 38 (SUPPL. 8), S13–S18.
- (66) Kong, P.-C.; Rochon, F. D. Reactions of K_2PtCl_4 with Pyridine Derivatives in Dimethylformamide and Synthesis of Potassium Trichloro(Pyridine)Platinum(II). *Can. J. Chem.* **1978**, 56 (4), 441–445.
- (67) Ernest S. Y. Wong, C. M. G. Process for Preparing Amine Platinum Complexes. US 6,518,428 B1, 2003.
- (68) Leigh, Alistair, J. Jost, S. Improved Synthesis of Picoplatin. WO 2010/144827 A1, 2010.
- (69) Promega. *CellTiter 96® Aqueous One Solution Cell Proliferation Assay Protocol, Instruction for Use of Products G3580, G3581 and G3582.*; 2012.
- (70) Parker, J. P.; Nimir, H.; Griffith, D. M.; Duff, B.; Chubb, A. J.; Brennan, M. P.; Morgan, M. P.; Egan, D. A.; Marmion, C. J. A Novel Platinum Complex of the Histone Deacetylase Inhibitor Belinostat: Rational Design, Development and in Vitro Cytotoxicity. *J. Inorg. Biochem.* **2013**, 124, 70–77.
- (71) Würtenberger, I.; Angermaier, B.; Kircher, B.; Gust, R. Synthesis and in Vitro Pharmacological Behavior of Platinum(II) Complexes Containing 1,2-Diamino-1-(4-Fluorophenyl)-2-Alkanol Ligands. *J. Med. Chem.* **2013**, 56 (20), 7951–7964.
- (72) Egger, A. E.; Rappel, C.; Jakupec, M. A.; Hartinger, C. G.; Heffeter, P.; Keppler, B. K. Development of an Experimental Protocol for Uptake Studies of Metal Compounds in Adherent Tumor Cells. *J. Anal. At. Spectrom.* **2009**, 24 (1), 51–61.
- (73) J. Gilmour Morrison, Peter White, Sophie McDougall, John W. Firth, Steve G. Woolfrey, Martin A. Graham, D. G. Validation of a Highly Sensitive ICP-MS Method for the

- Determination of Platinum in Biofluids, Application to Clinical Pharmacokinetic Studies with Oxaliplatin. *J. Pharm. Biomed. Anal.* **2000**, *24*, 1–10.
- (74) Poklar, N.; Pilch, D. S.; Lippard, S. J.; Redding, E. A.; Dunham, S. U.; Breslauer, K. J. Influence of Cisplatin Intrastrand Crosslinking on the Conformation, Thermal Stability, and Energetics of a 20-Mer DNA Duplex. *Proc. Natl. Acad. Sci.* **1996**, *93* (15), 7606–7611.
- (75) Hall, M. D.; Telma, K. A.; Chang, K. E.; Lee, T. D.; Madigan, J. P.; Lloyd, J. R.; Goldlust, I. S.; Hoeschele, J. D.; Gottesman, M. M. Say No to DMSO: Dimethylsulfoxide Inactivates Cisplatin, Carboplatin, and Other Platinum Complexes. *Cancer Res.* **2014**, *74* (14), 3913–3922.
- (76) Gu, F.; Ac, L.; C, A.; O, F.; Gu, S.; O, A.; Elmal, A.; Elerman, Y. Synthesis , Cytotoxicity , and DNA Interactions of New Cisplatin Analogues Containing Substituted Benzimidazole Ligands Synthesis , Cytotoxicity , and DNA Interactions of New Cisplatin Analogues Containing. *J. Med. Chem.* **2009**, 1345–1357.
- (77) Margiotta, N.; Denora, N.; Ostuni, R.; Laquintana, V.; Anderson, A.; Johnson, S. W.; Trapani, G.; Natile, G. Platinum(II) Complexes with Bioactive Carrier Ligands Having High Affinity for the Translocator Protein. *J. Med. Chem.* **2010**, *53* (14), 5144–5154.
- (78) Dietrich, A.; Mueller, T.; Paschke, R.; Kalinowski, B.; Behlendorf, T.; Reipsch, F.; Fruehauf, A.; Schmoll, H.; Kloft, C.; Voigt, W. Novel Platinum Compound That Overcomes Cisplatin Resistance and Induces Apoptosis by Mechanisms Different from That of Cisplatin. *J. Med. Chem.* **2008**, *51* (Ii), 5413–5422.

- (79) Ishida, S.; Lee, J.; Thiele, D. J.; Herskowitz, I. Uptake of the Anticancer Drug Cisplatin Mediated by the Copper Transporter Ctr1 in Yeast and Mammals. *Proc. Natl. Acad. Sci.* **2002**, *99* (22), 14298–14302.
- (80) Holzer, A. K.; Howell, S. B. The Internalization and Degradation of Human Copper Transporter 1 Following Cisplatin Exposure. *Cancer Res.* **2006**, *66* (22), 10944–10952.
- (81) Copper, P.; Katano, K.; Kondo, A.; Safaei, R.; Holzer, A.; Samimi, G.; Mishima, M.; Kuo, Y.; Rochdi, M.; Howell, S. B. Acquisition of Resistance to Cisplatin Is Accompanied by Changes in the Cellular. *Gene* **2008**, No. 858, 6559–6565.
- (82) Patrick, G. *An Introduction to Medicinal Chemistry*, sixth edit.; Oxford, 2017.
- (83) Wagner, F. F.; Weiwer, M.; Lewis, M. C.; Holson, E. B. Small Molecule Inhibitors of Zinc-Dependent Histone Deacetylases. *Neurotherapeutics* **2013**, *10* (4), 589–604.
- (84) De-Maw Chuang, Yan Leng, Zoya Marinova, H.-J. K. and C.-T. C. Multiple Roles of HDAC Inhibition in Neurodegenerative Conditions. *Trends Neurosci.* **2009**, *32*, 591–601.
- (85) Haberland, M.; Montgomery, R. L.; Olson, E. N. The Many Roles of Histone Deacetylases in Development and Physiology: Implications for Disease and Therapy. *Nat. Rev. Genet.* **2009**, *10* (1), 32–42.
- (86) Bolden, J. E.; Peart, M. J.; Johnstone, R. W. Anticancer Activities of Histone Deacetylase Inhibitors. *Nat. Rev. Drug Discov.* **2006**, *5* (9), 769–784.
- (87) Sam Thiagalingam, Kuang-Hung Cheng, Hyunjoo J.Lee, Nora Mineva, Arunthathi Thiagalingam, and J. F. P. Histone Deacetylase: Unique Players in Shaping the Epigenetic Histone Code. *Ann. NY Acad. Sci.* **2003**, *983*, 84–100.

- (88) Halkidou, K.; Gaughan, L.; Cook, S.; Leung, H. Y.; Neal, D. E.; Robson, C. N. Upregulation and Nuclear Recruitment of HDAC1 in Hormone Refractory Prostate Cancer. *Prostate* **2004**, *59* (2), 177–189.
- (89) Choi, J. H.; Kwon, H. J.; Yoon, B. I.; Kim, J. H.; Han, S. U.; Joo, H. J.; Kim, D. Y. Expression Profile of Histone Deacetylase 1 in Gastric Cancer Tissues. *Japanese J. Cancer Res.* **2001**, *92* (12), 1300–1304.
- (90) Wilson, A. J.; Byun, D. S.; Popova, N.; Murray, L. B.; L'Italien, K.; Sowa, Y.; Arango, D.; Velcich, A.; Augenlicht, L. H.; Mariadason, J. M. Histone Deacetylase 3 (HDAC3) and Other Class I HDACs Regulate Colon Cell Maturation and P21 Expression and Are Deregulated in Human Colon Cancer. *J. Biol. Chem.* **2006**, *281* (19), 13548–13558.
- (91) Zhang, Z.; Yamashita, H.; Toyama, T.; Sugiura, H.; Ando, Y.; Mita, K.; Hamaguchi, M.; Hara, Y.; Kobayashi, S.; Iwase, H. Quantitation of HDAC1 MRNA Expression in Invasive Carcinoma of the Breast. *Breast Cancer Res. Treat.* **2005**, *94* (1), 11–16.
- (92) Ping Zhu, Elke Martin, Jorg Mengwasser, Peter Schlag, Klaus-Peter Janssen, and M. G. Induction of HDAC2 Expression upon Loss of APC in Colorectal Tumorigenesis. *Cancer Cell* **2004**, *5*, 455–463.
- (93) Huang, B. H.; Laban, M.; Leung, C. H. W.; Lee, L.; Lee, C. K.; Salto-Tellez, M.; Raju, G. C.; Hooi, S. C. Inhibition of Histone Deacetylase 2 Increases Apoptosis and P21 Cip1/WAF1 Expression, Independent of Histone Deacetylase 1. *Cell Death Differ.* **2005**, *12* (4), 395–404.
- (94) NAM, S. W.; EUN, J. W.; SONG, J.; LEE, S. H.; LEE, J. Y.; YOO, N. J.; PARK, W. S.;

- KIM, S. Y.; NOH, J. H.; AHN, Y. M.; et al. Increased Expression of Histone Deacetylase 2 Is Found in Human Gastric Cancer. *APMIS* **2005**, *113* (4), 264–268.
- (95) Zhang, Z.; Yamashita, H.; Toyama, T.; Sugiura, H.; Omoto, Y.; Ando, Y.; Mita, K.; Hamaguchi, M.; Hayashi, S. I.; Iwase, H. HDAC6 Expression Is Correlated with Better Survival in Breast Cancer. *Clin. Cancer Res.* **2004**, *10* (20), 6962–6968.
- (96) Keith B. Glaser, Junling Li, Michael J. Staver, Ru-Qi Wei, Daniel H. Albert, and S. K. D. Role of Class I and Class II Histone Deacetylases in Carcinoma Cells Using SiRNA. *Biochem. Biophys. Res. Commun.* **2003**, *310*, 529–536.
- (97) Ma, Y.; Yue, Y.; Pan, M.; Sun, J.; Chu, J.; Lin, X.; Xu, W.; Feng, L.; Chen, Y.; Chen, D.; et al. Histone Deacetylase 3 Inhibits New Tumor Suppressor Gene DTWD1 in Gastric Cancer. *Am. J. Cancer Res.* **2015**, *5* (2), 663–66373.
- (98) Lee, S. H.; Kim, J.; Kim, W. H.; Lee, Y. M. Hypoxic Silencing of Tumor Suppressor RUNX3 by Histone Modification in Gastric Cancer Cells. *Oncogene* **2009**, *28* (2), 184–194.
- (99) Catalano, M. G.; Fortunati, N.; Pugliese, M.; Marano, F.; Ortoleva, L.; Poli, R.; Asioli, S.; Bandino, A.; Palestini, N.; Grange, C.; et al. Histone Deacetylase Inhibition Modulates E-Cadherin Expression and Suppresses Migration and Invasion of Anaplastic Thyroid Cancer Cells. *J. Clin. Endocrinol. Metab.* **2012**, *97* (7), 1150–1159.
- (100) Li, Y.; Seto, E. HDACs and HDAC Inhibitors in Cancer. *Cold Spring Harb Perspect Med* **2016**, *3* (6), 1–10.
- (101) Osada, H.; Tatematsu, Y.; Saito, H.; Yatabe, Y.; Mitsudomi, T.; Takahashi, T. Reduced

- Expression of Class II Histone Deacetylase Genes Is Associated with Poor Prognosis in Lung Cancer Patients. *Int. J. Cancer* **2004**, *112* (1), 26–32.
- (102) Jin, Z.; Jiang, W.; Jiao, F.; Guo, Z.; Hu, H.; Wang, L.; Wang, L. Decreased Expression of Histone Deacetylase 10 Predicts Poor Prognosis of Gastric Cancer Patients. *Int. J. Clin. Exp. Pathol.* **2014**, *7* (9), 5872–5879.
- (103) West, A. C.; Johnstone, R. W.; West, A. C.; Johnstone, R. W. New and Emerging HDAC Inhibitors for Cancer Treatment Find the Latest Version : Review Series New and Emerging HDAC Inhibitors for Cancer Treatment. *J Clin Invest.* **2014**, *124* (1), 30–39.
- (104) MA Glozak, E. S. Histone Deacetylases and Cancer. *Oncogene* **2007**, *26*, 5420–5432.
- (105) Mohammed Manal, M.J.N. Chandrasekar, Jeyapal Gomathi Priya, M. J. N. Inhibitors of Histone Deacetylase as Antitumor Agents, a Critical Review. *Bioorg. Chem.* **2016**, *67*, 18–42.
- (106) Donigian, J. R.; Cohen, A.; Finnin, M. S.; Pavletich, N. P.; Richon, V. M.; Rifkind, R. A.; Marks, P. A.; Breslow, R. Structures of a Histone Deacetylase Homologue Bound to the TSA and SAHA Inhibitors. *Nature* **1999**, *401* (6749), 188–193.
- (107) Marks, P. A.; Breslow, R. Dimethyl Sulfoxide to Vorinostat: Development of This Histone Deacetylase Inhibitor as an Anticancer Drug. *Nat. Biotechnol.* **2007**, *25* (1), 84–90.
- (108) János Fischer, W. E. C. *Successful Drug Discovery*; 2017; Vol. 2.
- (109) Mottamal, M.; Zheng, S.; Huang, T. L.; Wang, G. Histone Deacetylase Inhibitors in Clinical Studies as Templates for New Anticancer Agents. *Molecules* **2015**, *20* (3), 3898–

- 3941.
- (110) Tashima, T.; Murata, H.; Kodama, H. Design and Synthesis of Novel and Highly-Active Pan-Histone Deacetylase (Pan-HDAC) Inhibitors. *Bioorganic Med. Chem.* **2014**, *22* (14), 3720–3731.
- (111) Maurizio Taddei, Elena Cini, Luca Giannotti, Giuseppe Giannini, Gianfranco Battistuzzi, Davide Vignola, Loredana Vesci, W. C. Lactam Based 7-Amino Suberoylamide Hydroxamic Acids as Potent HDAC Inhibitors. *Bioorg. Med. Chem. Lett.* **2014**, *24*, 61–64.
- (112) Suzuki, T.; Nagano, Y.; Kouketsu, A.; Matsuura, A.; Maruyama, S.; Kurotaki, M.; Nakagawa, H.; Miyata, N. Novel Inhibitors of Human Histone Deacetylases: Design, Synthesis, Enzyme Inhibition, and Cancer Cell Growth Inhibition of SAHA-Based Non-Hydroxamates. *J. Med. Chem.* **2005**, *48* (4), 1019–1032.
- (113) Griffith, D.; Morgan, M. P.; Marmion, C. J. A Novel Anti-Cancer Bifunctional Platinum Drug Candidate with Dual DNA Binding and Histone Deacetylase Inhibitory Activity. *Chem. Commun.* **2009**, No. 44, 6735–6737.
- (114) Galanski, M.; Jakupec, M.; Keppler, B. Update of the Preclinical Situation of Anticancer Platinum Complexes: Novel Design Strategies and Innovative Analytical Approaches. *Curr. Med. Chem.* **2005**, *12* (18), 2075–2094.
- (115) Storr, T.; Thompson, K. H.; Orvig, C. Design of Targeting Ligands in Medicinal Inorganic Chemistry. *Chem. Soc. Rev.* **2006**, *35* (6), 534–544.
- (116) Shaw, R. J. Glucose Metabolism and Cancer. *Curr. Opin. Cell Biol.* **2006**, *18*, 598–608.

- (117) Berger, I.; Nazarov, A. A.; Hartinger, C. G.; Groessl, M.; Valiahdi, S. M.; Jakupec, M. A.; Keppler, B. K. A Glucose Derivative as Natural Alternative to the Cyclohexane-1,2-Diamine Ligand in the Anticancer Drug Oxaliplatin? *ChemMedChem* **2007**, *2* (4), 505–514.
- (118) Stephen Hanessian, J. W. Synthesis and Biological Evaluation of Novel Chiral Non-Racemic Diaminoplatinum Analogs Based on a Tetrahydropyran Motif. *Can. J. Chem.* **1993**, *71*, 886–895.
- (119) Chen, Y.; Heeg, M. J.; Braunschweiler, P. G.; Xie, W.; Wang, P. G. A Carbohydrate-Linked Cisplatin Analogue Having Antitumor Activity. *Angew. Chemie - Int. Ed.* **1999**, *38* (12), 1768–1769.
- (120) Mikata, Y.; Shinohara, Y.; Yoneda, K.; Nakamura, Y. .; Brudzińska, I.; Tanase, T.; Kitayama, T.; Takagi, R.; Okamoto, T. .; Kinoshita, I.; Doe, M.; Orvig, C.; Yano, S. Unprecedented Sugar-Dependent in Vivo Antitumor Activity of Carbohydrate-Pendant Cis-Diaminedichloroplatinum(II) Complexes. *Bioorg. Med. Chem. Lett.* **2001**, *11*, 3045–3047.
- (121) Liu, P.; Lu, Y.; Gao, X.; Liu, R.; Zhang-Negrerie, D.; Shi, Y.; Wang, Y.; Wang, S.; Gao, Q. Highly Water-Soluble Platinum(II) Complexes as GLUT Substrates for Targeted Therapy: Improved Anticancer Efficacy and Transporter-Mediated Cytotoxic Properties. *Chem. Commun.* **2013**, *49* (24), 2421–2423.
- (122) Patra, M.; Johnstone, T. C.; Suntharalingam, K.; Lippard, S. J. A Potent Glucose-Platinum Conjugate Exploits Glucose Transporters and Preferentially Accumulates in Cancer Cells. *Angew. Chemie - Int. Ed.* **2016**, *55* (7), 2550–2554.

- (123) Deo, K. M.; Ang, D. L.; McGhie, B.; Rajamanickam, A.; Dhiman, A.; Khoury, A.; Holland, J.; Bjelosevic, A.; Pages, B.; Gordon, C.; et al. Platinum Coordination Compounds with Potent Anticancer Activity. *Coord. Chem. Rev.* **2018**, *375*, 148–163.
- (124) Knight, W. A.; Livingston, R. B.; Gregory, E. J.; McGuire, W. L. Estrogen Receptor as an Independent Prognostic Factor for Early Recurrence in Breast Cancer. *Cancer Res.* **1977**, *37* (12), 4669–4671.
- (125) Slamon, D. J.; Godolphin, W.; Jones, L. A.; Holt, J. A.; Wong, S. G.; Keith, D. E.; Levin, W. J.; Stuart, S. G.; Udove, J.; Ullrich, A.; et al. Studies of the HER-2/Neu Proto-Oncogene in Human Breast and Ovarian Cancer. *Science (80-.)*. **1989**, *244* (4905), 707–712.
- (126) Levin, M. L.; Unio, A.; Contra, I.; Biotechnol, T.; Wang, J. M.; Lloyd, P.; McNally, M.; Malasky, M.; Topper, E.; Weedon, M.; et al. AIB1 , a Steroid Receptor Coactivator Amplified in Breast and Ovarian Cancer. *Science (80-.)*. **1997**, *277* (August), 965–969.
- (127) Carlsson, J.; Nordgren, H.; Sjöström, J.; Wester, K.; Villman, K.; Bengtsson, N. O.; Ostenstad, B.; Lundqvist, H.; Blomqvist, C. HER2 Expression in Breast Cancer Primary Tumours and Corresponding Metastases. Original Data and Literature Review. *Br. J. Cancer* **2004**, *90* (12), 2344–2348.
- (128) Gust, R.; Beck, W.; Jaouen, G.; Schönenberger, H. Optimization of Cisplatin for Treatment of Hormone Dependent Tumoral Diseases. Part 1: Use of Steroidal Ligands. *Coord. Chem. Rev.* **2009**, *253*, 2742–2759.
- (129) Gabano, E.; Ravera, M.; Osella, D. The Drug Targeting and Delivery Approach Applied

- to Pt-Antitumour Complexes. A Coordination Point of View. *Curr. Med. Chem.* **2009**, *16* (34), 4544–4580.
- (130) Criado, J. J.; Domínguez, M. F.; Medarde, M.; Fernández, E. R.; Macías, R. I. R.; Marín, J. J. G. Structural Characterization, Kinetic Studies, and in Vitro Biological Activity of New Cis-Diamminebis-Cholyglycinate(O,O') Pt(II) and Cis-Diamminebis-Ursodeoxycholate(O,O') Pt(II) Complexes. *Bioconjug. Chem.* **2000**, *11* (2), 167–174.
- (131) Briz, O.; Serrano, M. A.; Macias, R. I. R.; Marin, J. J. G. Overcoming Cisplatin Resistance in Vitro by a Free and Liposome-Encapsulated Bile Acid Derivative: Bamet-R2. *Int. J. Cancer* **2000**, *88* (2), 287–292.
- (132) Criado, J. J.; Macias, R. I. R.; Medarde, M.; Monte, M. J.; Serrano, M. A.; Marin, J. J. G. Synthesis and Characterization of the New Cytostatic Complex Cis-Diammineplatinum(II)-Chlorocholyglycinate. *Bioconjug. Chem.* **1997**, *8* (4), 453–458.
- (133) Colombo, G.; Curnis, F.; De Mori, G. M. S.; Gasparri, A.; Longoni, C.; Sacchi, A.; Longhi, R.; Corti, A. Structure-Activity Relationships of Linear and Cyclic Peptides Containing the NGR Tumor-Homing Motif. *J. Biol. Chem.* **2002**, *277* (49), 47891–47897.
- (134) Ndinguri, M. W.; Solipuram, R.; Gambrell, R. P.; Aggarwal, S.; Hammer, R. P. Peptide Targeting of Platinum Anti-Cancer Drugs. *Bioconjug. Chem.* **2009**, *20* (10), 1869–1878.
- (135) Keld Fosgerau, T. H. Peptide Therapeutics: Current Status and Future Directions. *Drug Discov. Today* **2015**, *20* (1), 122–128.
- (136) Simon P. Wisnovsky, Justin J. Wilson, Robert J. Radford, Mark P. Pereira, Maria R. Chan, Rebecca R. Lapos, Stephen J. Lippard, S. O. K. Targeting Mitochondrial DNA

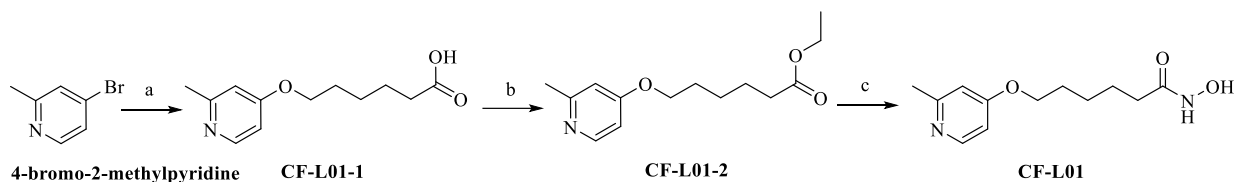
- with a Platinum-Based Anticancer Agent. *Chem Biol.* **2013**, *20* (11), 1323–1328.
- (137) Fonseca SB, Pereira MP, Mourtada R, Gronda M, Horton KL, Hurren R, Minden MD, Schimmer AD, K. S. Rerouting Chlorambucil to Mitochondria Combats Drug Deactivation and Resistance in Cancer Cells. *Chem Biol.* **2011**, *18* (4), 445–453.
- (138) Horton, K. L.; Pereira, M. P.; Stewart, K. M.; Fonseca, S. B.; Kelley, S. O. Tuning the Activity of Mitochondria-Penetrating Peptides for Delivery or Disruption. *ChemBioChem* **2012**, *13* (3), 476–485. <https://doi.org/10.1002/cbic.201100415>.
- (139) Valeria Ferretti, Paola Bergamini, Lorenza Marvelli, Yekatsiaryna Hushcha, Chiara Gemmo, Roberto Gambari, I. L. Synthesis and Characterization of Pt Complexes Containing Dichloroacetate (DCA), Design for Dual Anticancer Action. *Inorganica Chim. Acta* **2018**, *470*, 119–127.
- (140) Intini, F. P.; Zajac, J.; Novohradsky, V.; Saltarella, T.; Pacifico, C.; Brabec, V.; Natile, G.; Kasparkova, J. Novel Antitumor Platinum(II) Conjugates Containing the Nonsteroidal Anti-Inflammatory Agent Diclofenac: Synthesis and Dual Mechanisms of Antiproliferative Effects. *Inorg. Chem.* **2017**, *56* (3), 1483–1497.
- (141) Mitra, K.; Gautam, S.; Kondaiah, P.; Chakravarty, A. R. The Cis-Diammineplatinum(II) Complex of Curcumin: A Dual Action DNA Crosslinking and Photochemotherapeutic Agent. *Angew. Chemie - Int. Ed.* **2015**, *54* (47), 13989–13993.
- (142) Lai, C. J.; Bao, R.; Tao, X.; Wang, J.; Atoyian, R.; Qu, H.; Wang, D. G.; Yin, L.; Samson, M.; Forrester, J.; et al. CUDC-101, a Multitargeted Inhibitor of Histone Deacetylase, Epidermal Growth Factor Receptor, and Human Epidermal Growth Factor Receptor 2,

- Exerts Potent Anticancer Activity. *Cancer Res.* **2010**, *70* (9), 3647–3656.
- (143) Qian, C.; Lai, C. J.; Bao, R.; Wang, D. G.; Wang, J.; Xu, G. X.; Atoyan, R.; Qu, H.; Yin, L.; Samson, M.; et al. Cancer Network Disruption by a Single Molecule Inhibitor Targeting Both Histone Deacetylase Activity and Phosphatidylinositol 3-Kinase Signaling. *Clin. Cancer Res.* **2012**, *18* (15), 4104–4113. <https://doi.org/10.1158/1078-0432.CCR-12-0055>.
- (144) Mehrling, T.; Chen, Y. The Alkylating-HDAC Inhibition Fusion Principle: Taking Chemotherapy to the Next Level with the First in Class Molecule EDO-S101. *Anticancer Agents Med. Chem.* **2015**, *16* (1), 20–28.
- (145) Liu, C.; Ding, H.; Li, X.; Pallasch, C. P.; Hong, L.; Guo, D.; Chen, Y.; Wang, D.; Wang, W.; Wang, Y.; et al. A DNA/HDAC Dual-Targeting Drug CY190602 with Significantly Enhanced Anticancer Potency. *EMBO Mol. Med.* **2015**, *7* (4), 438–449.
- (146) Schobert, R.; Biersack, B. Multimodal HDAC Inhibitors with Improved Anticancer Activity. *Curr. Cancer Drug Targets* **2017**, No. 1, 1–18.
- (147) Ganesan, A. Multitarget Drugs: An Epigenetic Epiphany. *ChemMedChem* **2016**, 1227–1241.
- (148) de Lera, A. R.; Ganesan, A. Epigenetic Polypharmacology: From Combination Therapy to Multitargeted Drugs. *Clin. Epigenetics* **2016**, *8* (1), 1–21.
- (149) Giulia Stazi, Rossella Fioravanti, Antonello Mai, Andrea Mattevi, S. V. Histone Deacetylases as an Epigenetic Pillar for the Development of Hybrid Inhibitors in Cancer. *Curr. Opin. Chem. Biol.* **2019**, *50*, 89–100.

- (150) Bhatia, S.; Krieger, V.; Groll, M.; Osko, J. D.; Reßing, N.; Ahlert, H.; Borkhardt, A.; Kurz, T.; Christianson, D. W.; Hauer, J.; et al. Discovery of the First-in-Class Dual Histone Deacetylase-Proteasome Inhibitor. *J. Med. Chem.* **2018**, *61* (22), 10299–10309.
- (151) Brabec, V.; Griffith, D. M.; Kisova, A.; Kostrhunova, H.; Zerzankova, L.; Marmion, C. J.; Kasparkova, J. Valuable Insight into the Anticancer Activity of the Platinum-Histone Deacetylase Inhibitor Conjugate, Cis-[Pt(NH₃)₂MalSAHA-2H₂O]. *Mol. Pharm.* **2012**, *9* (7), 1990–1999.
- (152) James P. Parker, Hassan Nimir, Darren M. Griffith, Brian Duff, Anthony J. Chubb, Marian P. Brennan, Maria P. Morgan, Denise A. Egan, C. J. M. A Novel Platinum Complex of the Histone Deacetylase Inhibitorbelinostat: Rational Design, Development and in Vitro Cytotoxicity. *J. Inorg. Biochem.* **2013**, *124*, 70–77.
- (153) Ramalingam, S. S.; Parise, R. A.; Ramanathan, R. K.; Lagattuta, T. F.; Musguire, L. A.; Stoller, R. G.; Potter, D. M.; Argiris, A. E.; Zwiebel, J. A.; Egorin, M. J.; et al. Phase I and Pharmacokinetic Study of Vorinostat, a Histone Deacetylase Inhibitor, in Combination with Carboplatin and Paclitaxel for Advanced Solid Malignancies. *Clin. Cancer Res.* **2007**, *13* (12), 3605–3610.
- (154) Fujiwara, Y.; Yamamoto, N.; Yamada, Y.; Yamada, K.; Otsuki, T.; Kanazu, S.; Iwasa, T.; Hardwick, J. S.; Tamura, T. Phase I and Pharmacokinetic Study of Vorinostat (Suberoylanilide Hydroxamic Acid) in Japanese Patients with Solid Tumors. *Cancer Sci.* **2009**, *100* (9), 1728–1734.

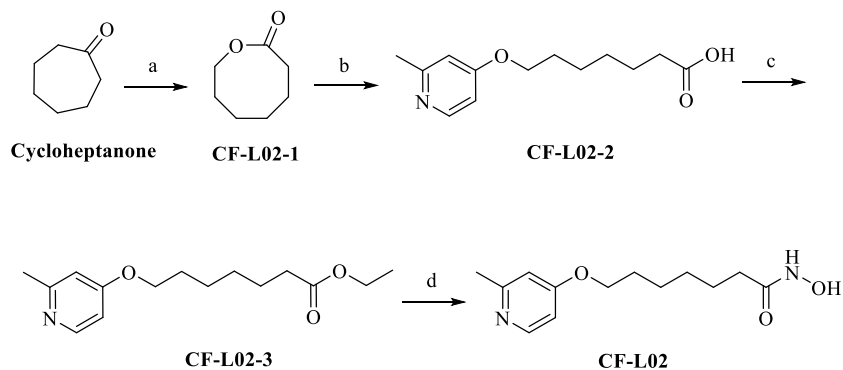
APPENDIX A: SYNTHESIS SCHEME

Scheme 1. Synthesis of HDAC Inhibitor **CF-L01**

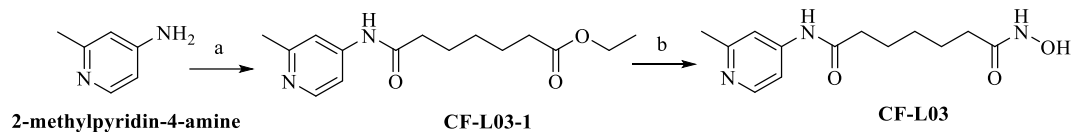


Reagents and conditions: (a) oxepan-2-one, KOH, DMSO, 75 °C; (b) Concentrated H₂SO₄, EtOH, reflux, 73%; (c) NH₂OH (50 wt% in water), NaOH, DCM/MeOH (1/2), rt, 80%.

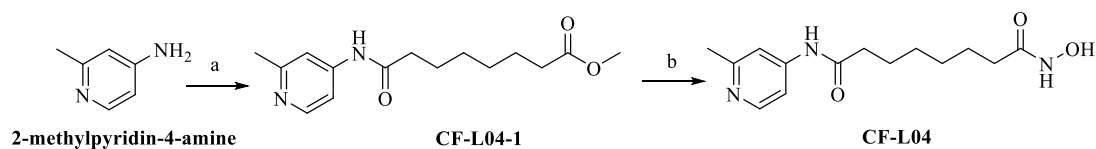
Scheme 2. Synthesis of HDAC Inhibitor **CF-L02**



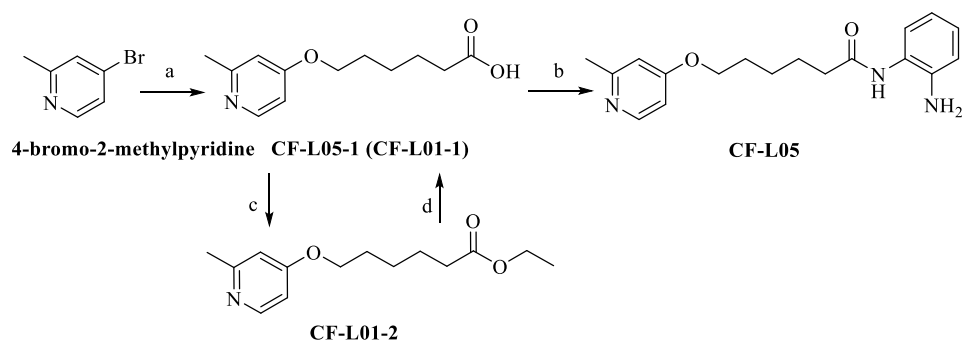
Reagents and conditions: (a) m-CPBA, DCM, rt, 89%; (b) 4-bromo-2-methylpyridine, KOH, DMSO, 75 °C; (c) Concentrated H₂SO₄, EtOH, reflux, 54%; (d) NH₂OH (50 wt% in water), NaOH, DCM/MeOH (1/2), rt, 82%.

Scheme 3. Synthesis of HDAC Inhibitor **CF-L03**

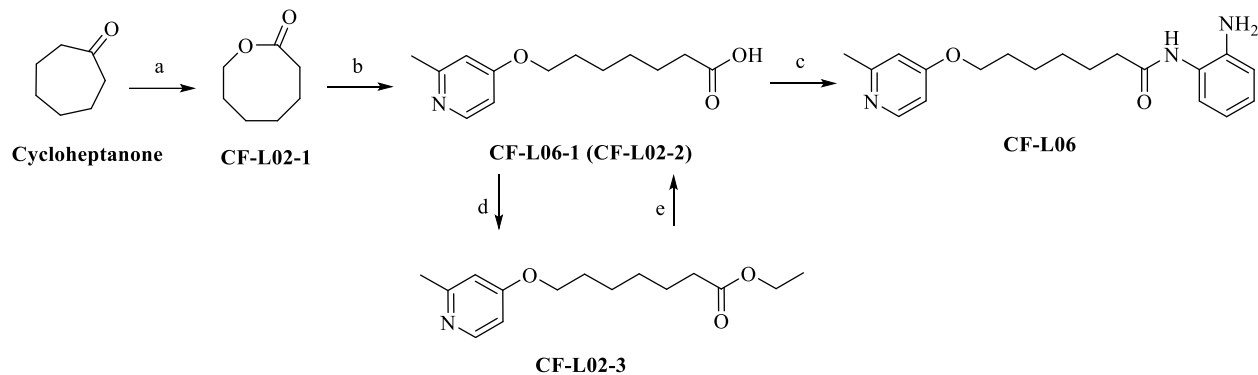
Reagents and conditions: (a) ethyl hydrogen pimelate, HATU, DIEA, DMF rt, 56%; (b) NH_2OH (50 wt% in water), NaOH, DCM/MeOH (1/2), rt, 72%.

Scheme 4. Synthesis of HDAC Inhibitor **CF-L04**

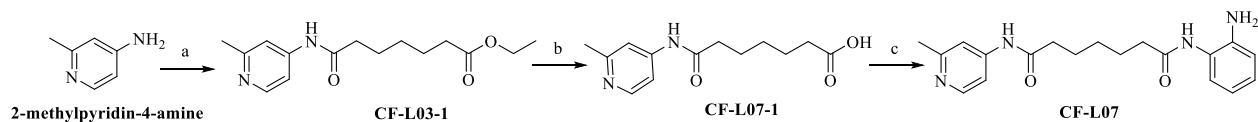
Reagents and conditions: (a) 8-Methoxy-8-oxooctanoic acid, HATU, DIEA, DMF rt, 43%; (b) NH_2OH (50 wt% in water), NaOH, DCM/MeOH (1/2), rt, 69%.

Scheme 5. Synthesis of HDAC Inhibitor **CF-L05**

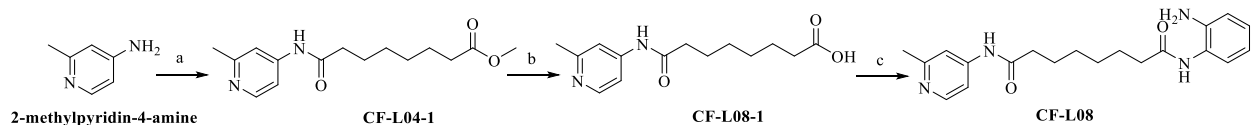
Reagents and conditions: (a) Oxepan-2-one, KOH, DMSO, 75 °C; (b) o-Phenylenediamine, HATU, DIEA, DMF rt, 41%; (c) Concentrated H_2SO_4 , EtOH, reflux, 73%; (d) NaOH, THF/ H_2O (1/1), rt, 35%.

Scheme 6. Synthesis of HDAC Inhibitor **CF-L06**

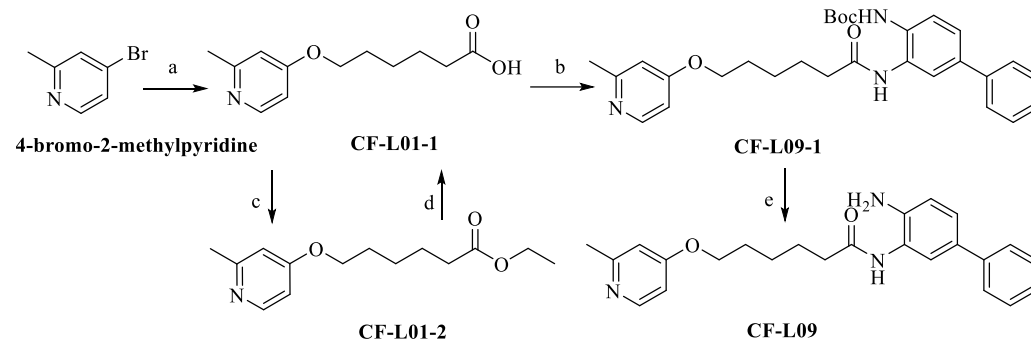
Reagents and conditions: (a) m-CPBA, DCM, rt, 89%; (b) 4-bromo-2-methylpyridine, KOH, DMSO, 75 °C; (c) o-Phenylenediamine, HATU, DIEA, DMF rt, 43%; (d) Concentrated H₂SO₄, EtOH, reflux, 54%; (e) NaOH, THF/H₂O (1/1), rt, 48%.

Scheme 7. Synthesis of HDAC Inhibitor **CF-L07**

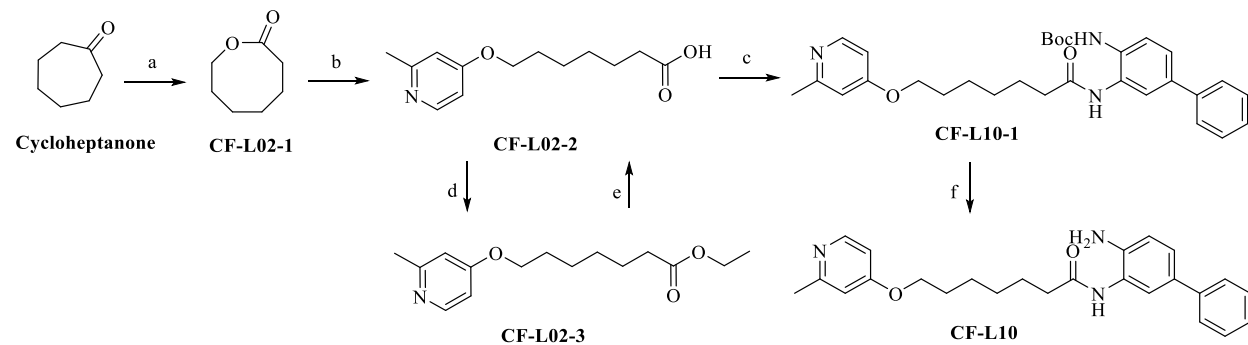
Reagents and conditions: (a) ethyl hydrogen pimelate, HATU, DIEA, DMF rt, 56%; (b) NaOH, THF/H₂O (1/1), rt, 58%; (c) o-Phenylenediamine, HATU, DIEA, DMF rt, 48%.

Scheme 8. Synthesis of HDAC Inhibitor **CF-L08**

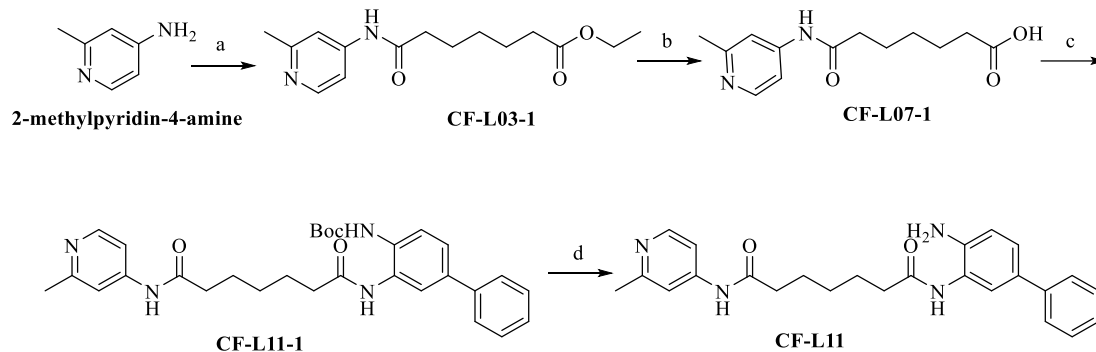
Reagents and conditions: (a) 8-Methoxy-8-oxooctanoic acid, HATU, DIEA, DMF rt, 43%; (b) NaOH, THF/H₂O (1/1), rt, 65%; (c) o-Phenylenediamine, HATU, DIEA, DMF rt, 51%.

Scheme 9. Synthesis of HDAC Inhibitor **CF-L09**

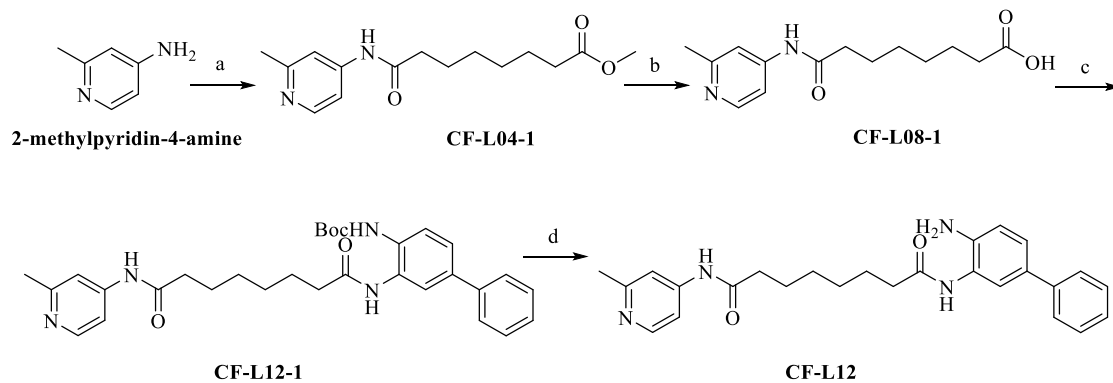
Reagents and conditions: (a) Oxepan-2-one, KOH, DMSO, 75 °C; (b) *tert*-butyl (3-amino-[1,1'-biphenyl]-4-yl)carbamate, HATU, DIEA, DMF rt, 80%; (c) Concentrated H₂SO₄, EtOH, reflux, 73%; (d) NaOH, THF/H₂O (1/1), rt, 35%. (e) 4M HCl in dioxane, rt, 63%.

Scheme 10. Synthesis of HDAC Inhibitor **CF-L10**

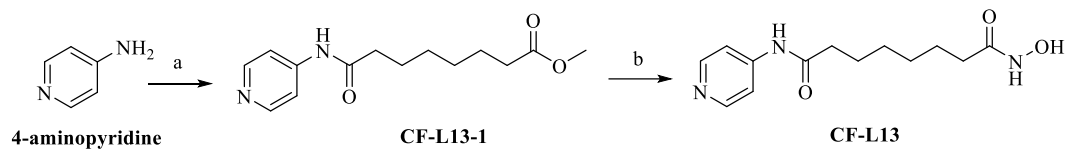
Reagents and conditions: (a) *m*-CPBA, DCM, rt, 89%; (b) 4-bromo-2-methylpyridine, KOH, DMSO, 75 °C; (c) *tert*-butyl (3-amino-[1,1'-biphenyl]-4-yl)carbamate, HATU, DIEA, DMF rt, 75%; (d) Concentrated H₂SO₄, EtOH, reflux, 54%; (e) NaOH, THF/H₂O (1/1), rt, 48%. (f) 4M HCl in dioxane, rt, 60%.

Scheme 11. Synthesis of HDAC Inhibitor **CF-L11**

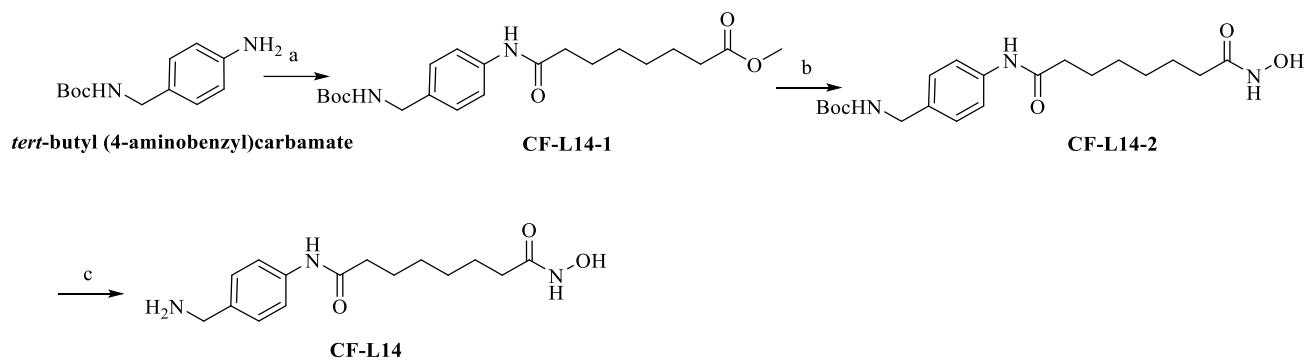
Reagents and conditions: (a) ethyl hydrogen pimelate, HATU, DIEA, DMF rt, 56%; (b) NaOH, THF/H₂O (1/1), rt, 58%; (c) *tert*-butyl (3-amino-[1,1'-biphenyl]-4-yl)carbamate, HATU, DIEA, DMF rt, 93%; (d) 4M HCl in dioxane, rt, 64%.

Scheme 12. Synthesis of HDAC Inhibitor **CF-L12**

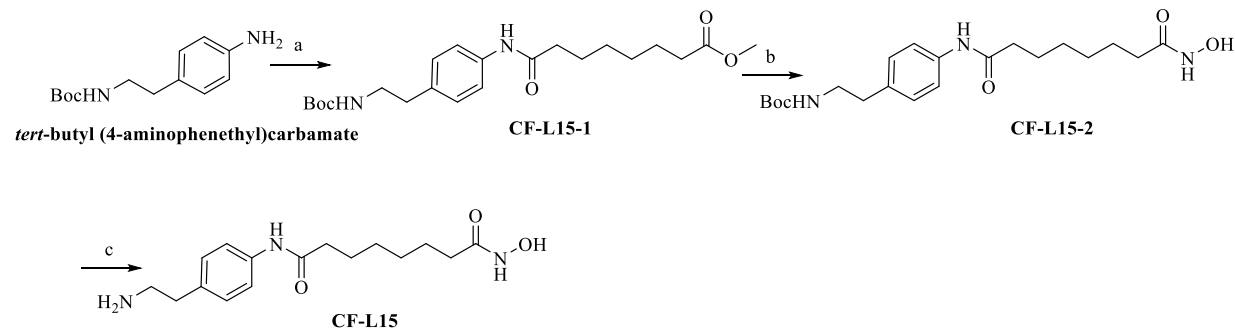
Reagents and conditions: (a) 8-Methoxy-8-oxooctanoic acid, HATU, DIEA, DMF rt, 43%; (b) NaOH, THF/H₂O (1/1), rt, 65%; (c) *tert*-butyl (3-amino-[1,1'-biphenyl]-4-yl)carbamate, HATU, DIEA, DMF rt, 86%; (d) 4M HCl in dioxane, rt, 51%.

Scheme 13. Synthesis of HDAC Inhibitor **CF-L13**

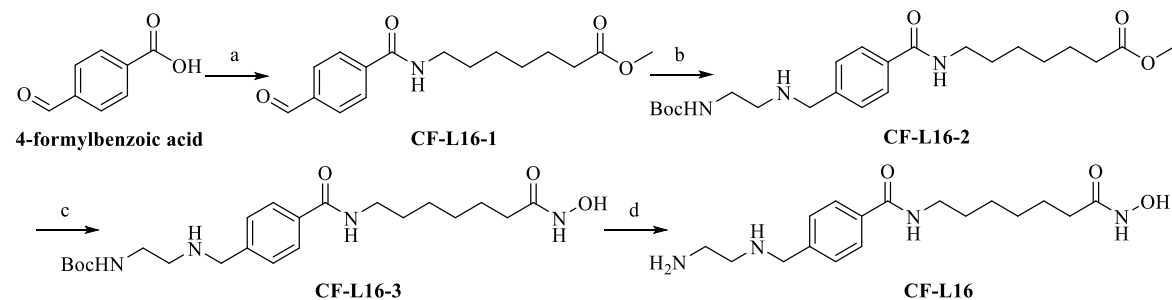
Reagents and conditions: (a) 8-Methoxy-8-oxooctanoic acid, HATU, DIEA, DMF rt, 46%; (b) NH_2OH (50 wt% in water), NaOH, DCM/MeOH (1/2), rt, 39%.

Scheme 14. Synthesis of HDAC Inhibitor **CF-L14**

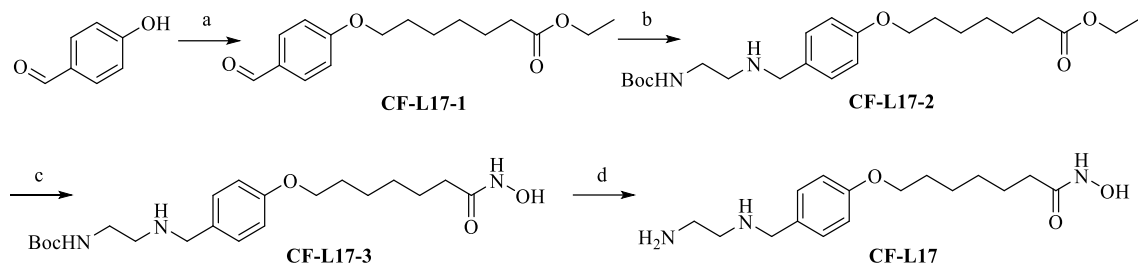
Reagents and conditions: (a) 8-Methoxy-8-oxooctanoic acid, HATU, DIEA, DMF rt, 82%; (b) NH_2OH (50 wt% in water), NaOH, DCM/MeOH (1/2), rt, quantitative yield; (c) 1M HCl in EtOAc, rt, quantitative yield.

Scheme 15. Synthesis of HDAC Inhibitor **CF-L15**

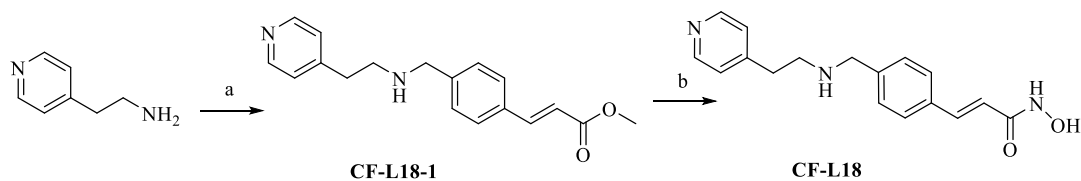
Reagents and conditions: (a) 8-Methoxy-8-oxooctanoic acid, HATU, DIEA, DMF rt, 83%; (b) NH_2OH (50 wt% in water), NaOH, DCM/MeOH (1/2), rt, 96%; (c) 1M HCl in EtOAc, rt, quantitative yield.

Scheme 16. Synthesis of HDAC Inhibitor **CF-L16**

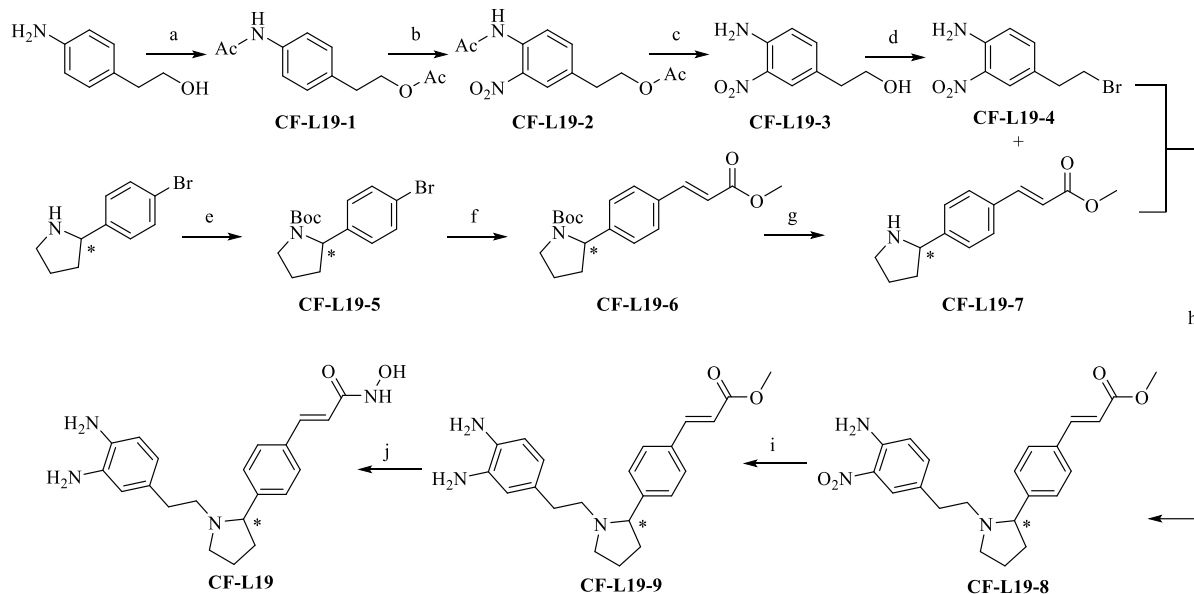
Reagents and conditions: (a) Methyl 7-aminoheptanoate hydrochloride, HATU, DIEA, DMF rt, 88%; (b) *tert*-butyl (2-aminoethyl)carbamate, NaBH_4 , MeOH, rt, 89%; (c) NH_2OH (50 wt% in water), NaOH, DCM/MeOH (1/2), rt, 67%; (d) 1M HCl in EtOAc, rt, 92%.

Scheme 17. Synthesis of HDAC Inhibitor **CF-L17**

Reagents and conditions: (a) Ethyl 7-bromoheptanoate, K_2CO_3 , ACN, reflux, 54%; (b) *tert*-butyl (2-aminoethyl)carbamate, $NaBH_4$, MeOH, rt, 91%; (c) NH_2OH (50 wt% in water), NaOH, DCM/MeOH (1/2), rt, 75%; (d) 1M HCl in EtOAc, rt, 92%.

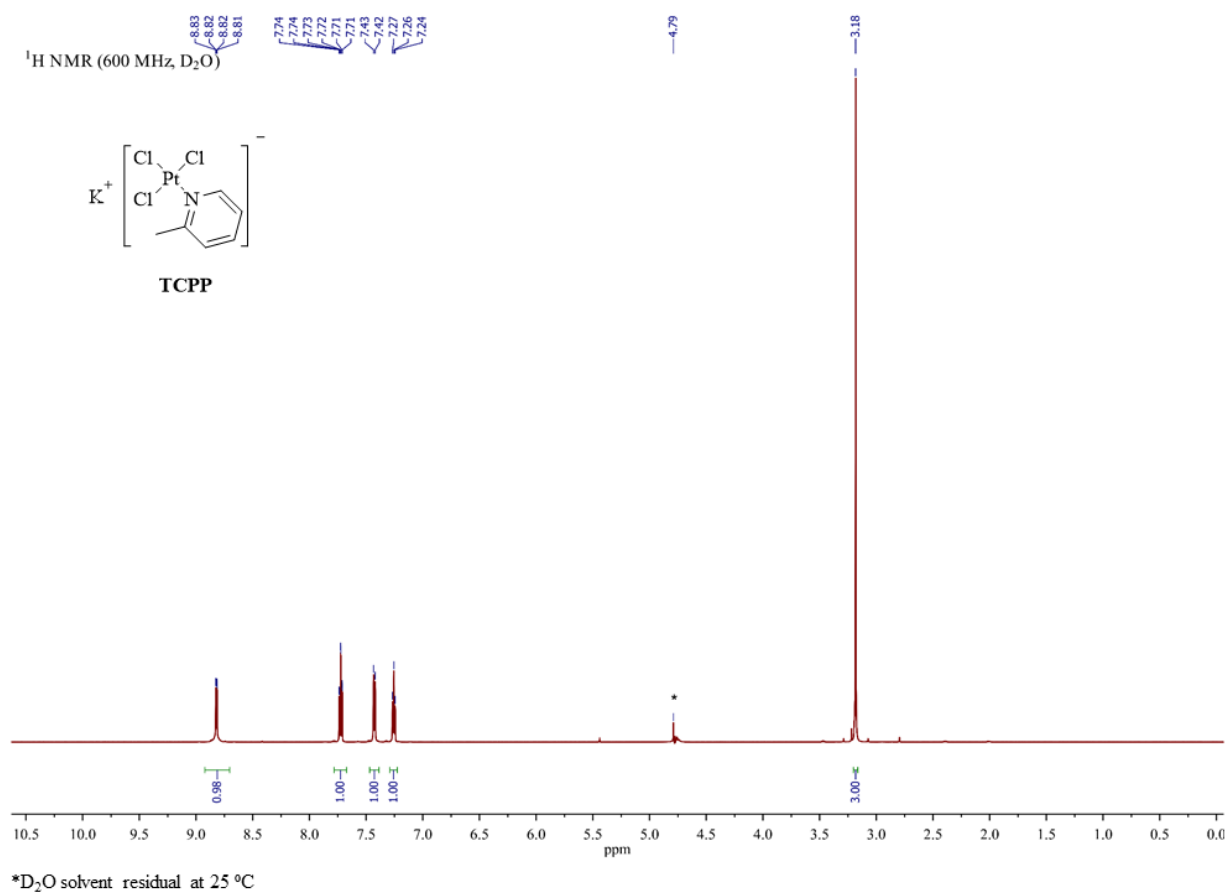
Scheme 18. Synthesis of HDAC Inhibitor **CF-L18**

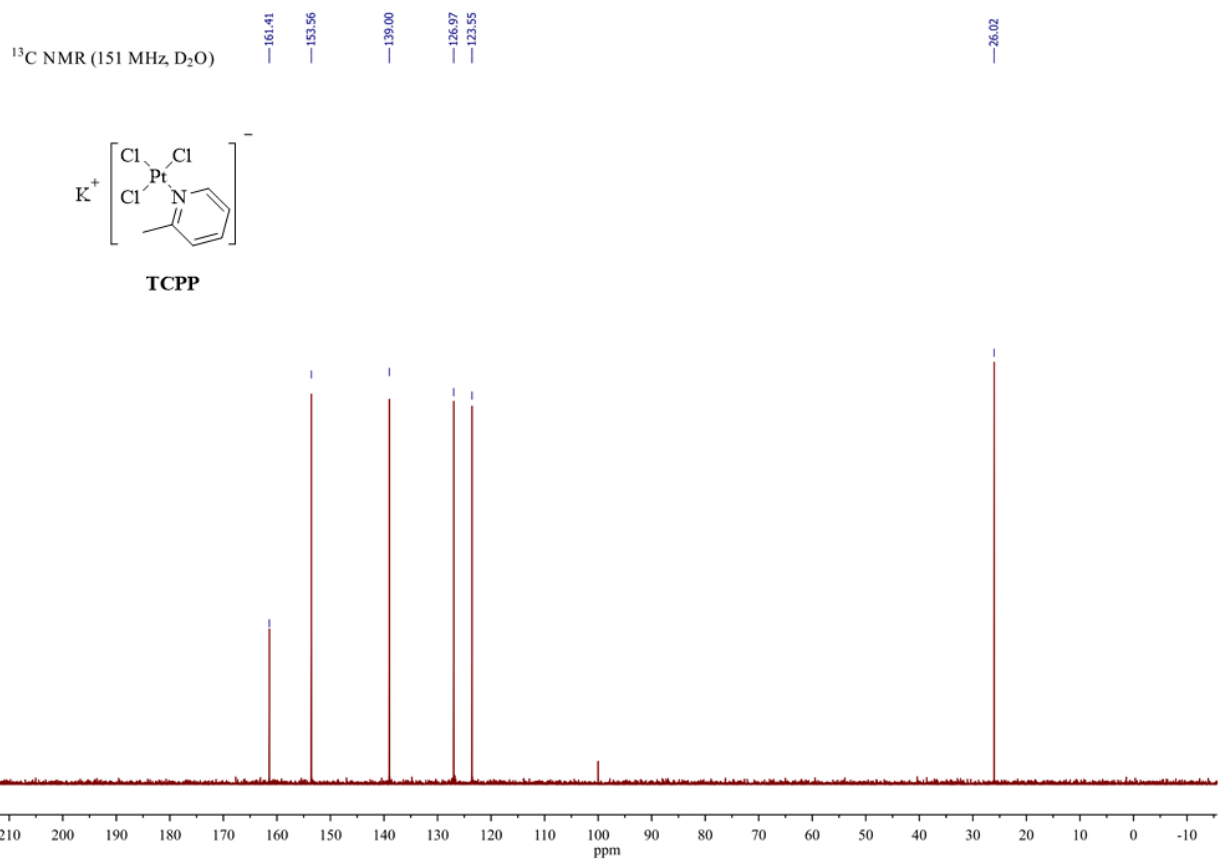
Reagents and conditions: (a) Methyl (*E*)-3-(4-formylphenyl)acrylate, $NaBH_4$, MeOH, rt; (b) NH_2OH (50 wt% in water), NaOH, DCM/MeOH (1/2), rt, 28% overall yield

Scheme 19. Synthesis of HDAC Inhibitor **CF-L19**

Reagents and conditions: (a) Ac_2O , TEA, DCM, rt, overnight, 80%; (b) Fuming HNO_3 , Ac_2O , DCM, 0 °C, 1 h, 84%; (c) NaOH, MeOH, rt, 84%; (d) 48% HBr, reflux, 6 h, 74%; (e) Boc_2O , NaOH, THF, rt, overnight, 87%; (f) methyl acrylate, $\text{Pd}(\text{OAc})_2$, Ph_3P , TEA, anhydrous ACN, 90 °C, 20 hr, 51%; (g) 1M HCl in EtOAc, rt. overnight, 86%; (h) ACN, K_2CO_3 , reflux, overnight, 69%; (i) Fe powder, NH_4Cl , EtOH/ H_2O (2/1), reflux, 54% (j) NH_2OH (50 wt% in water), NaOH, DCM/MeOH (1/2), rt, 25%

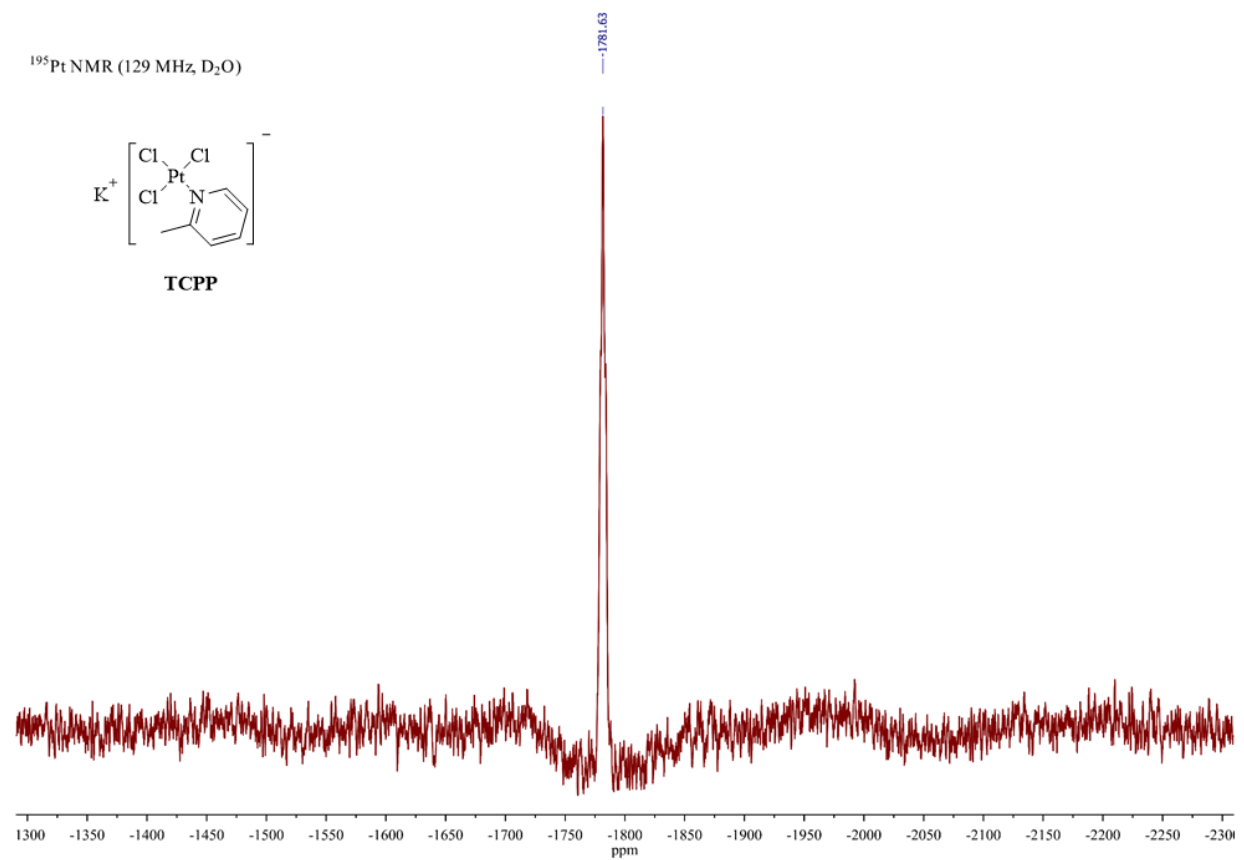
APPENDIX B: NMR SPECTRA DATA

 ^1H NMR spectrum of **TCPP** in D_2O

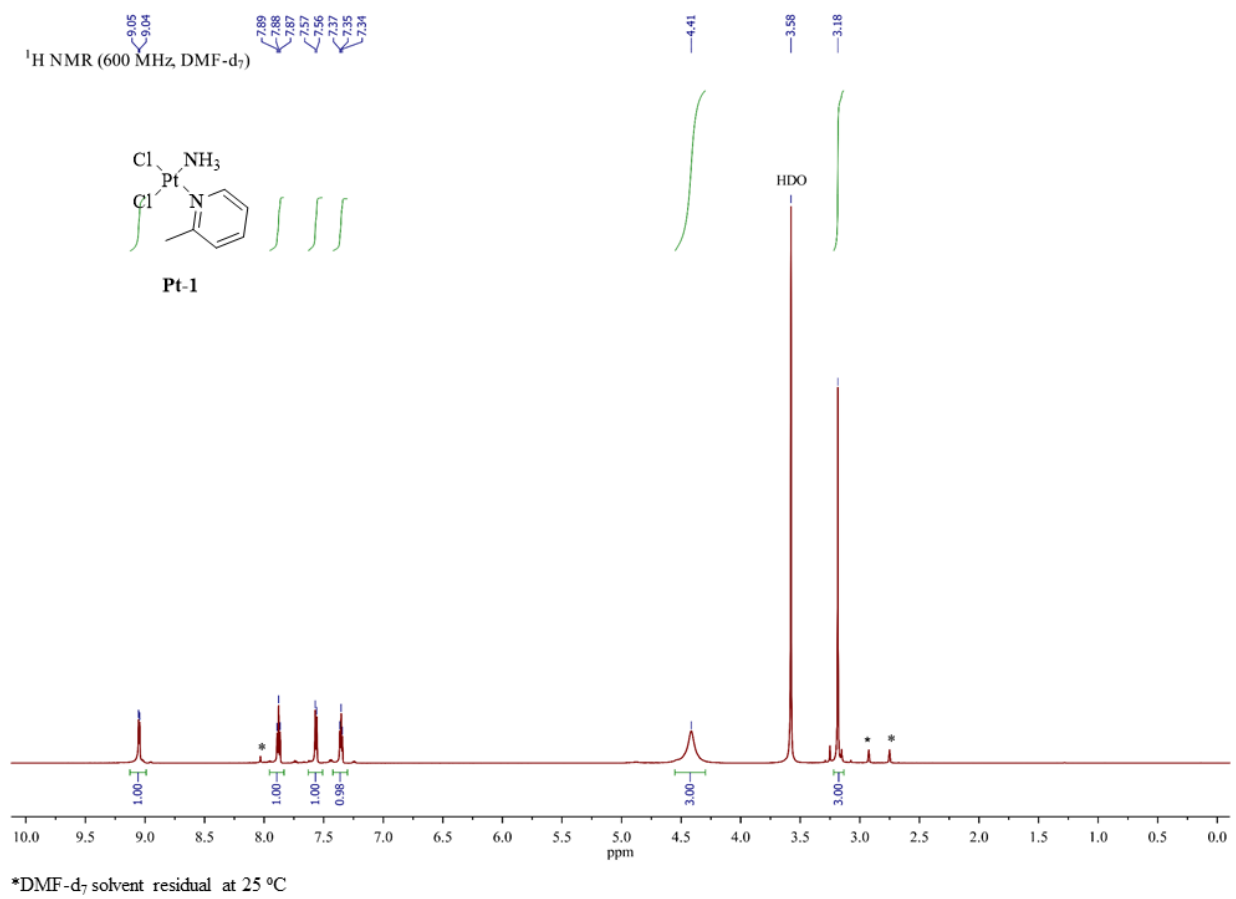


* D_2O solvent residual at 25 °C

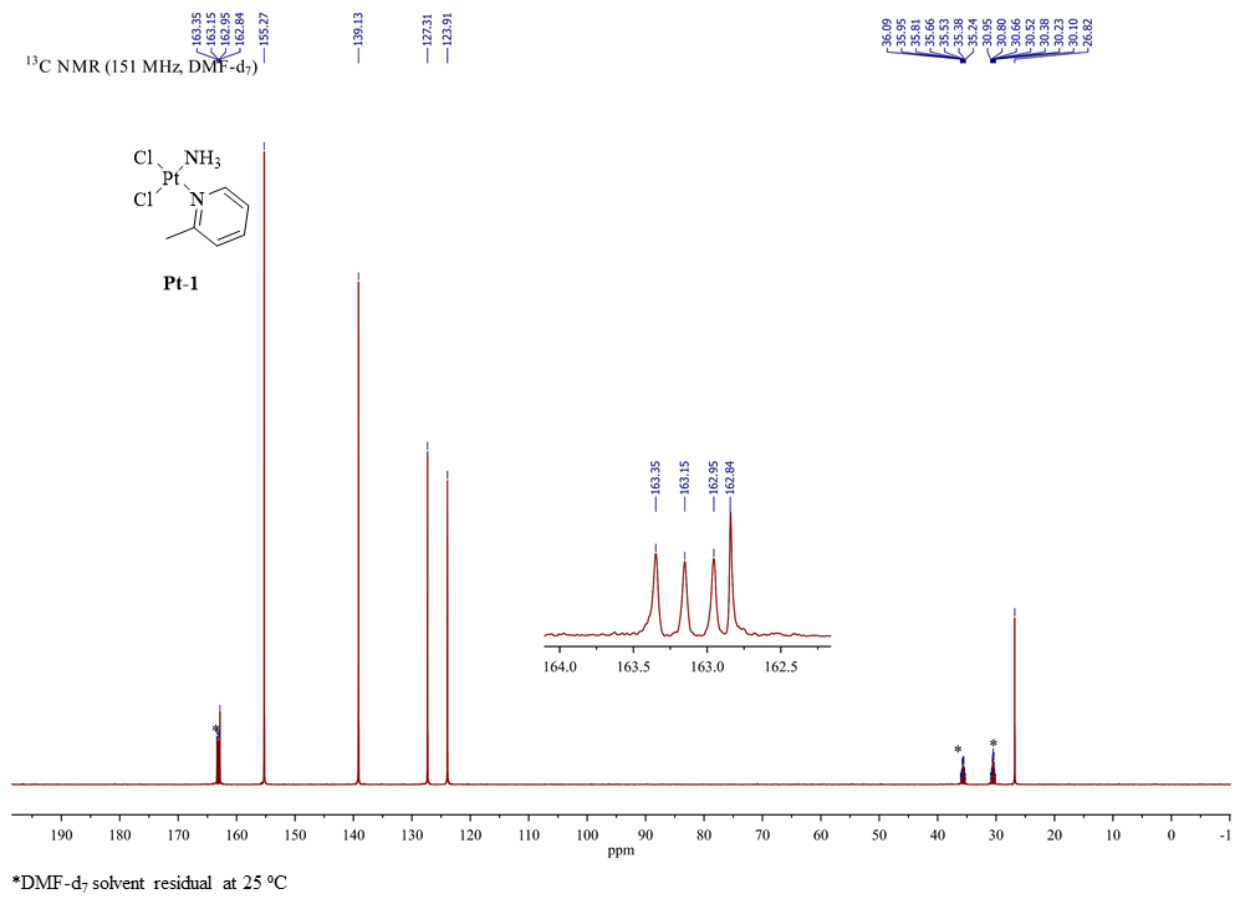
^{13}C NMR spectrum of **TCPP** in D_2O



^{195}Pt NMR spectrum of **TCPP** in D_2O

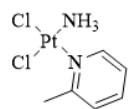


^1H NMR spectrum of **Pt-1** in DMF-d_7

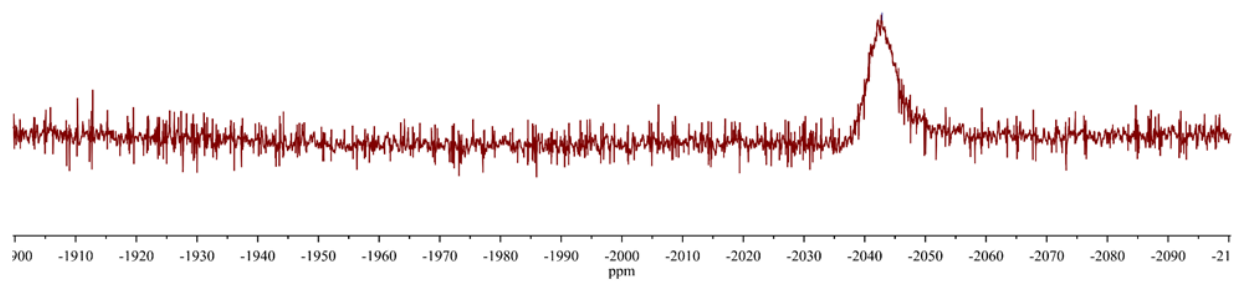


¹³C NMR spectrum of **Pt-1** in DMF-d₇

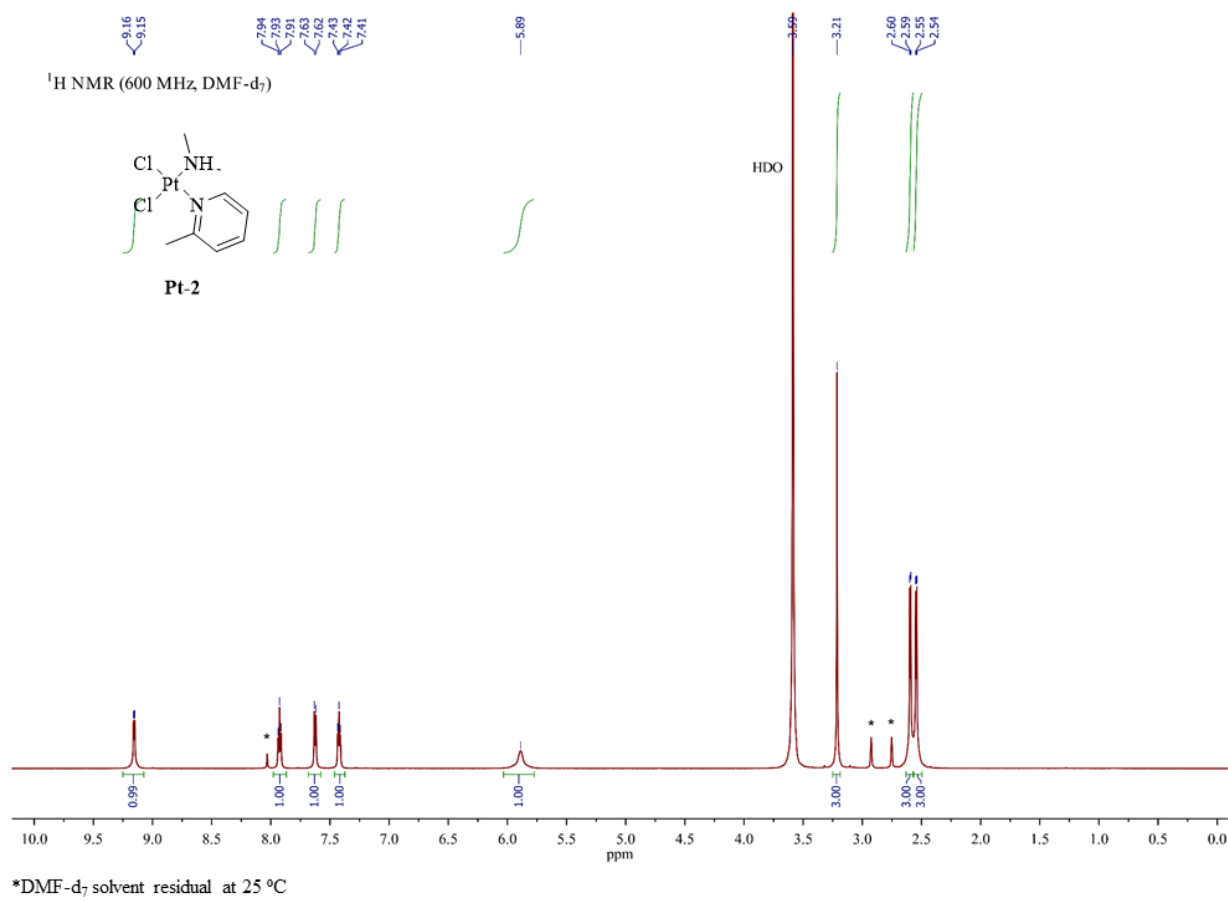
^{195}Pt NMR (129 MHz, DMF- d_7)



Pt-1

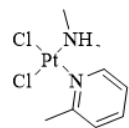


^{195}Pt NMR spectrum of **Pt-1** in DMF- d_7

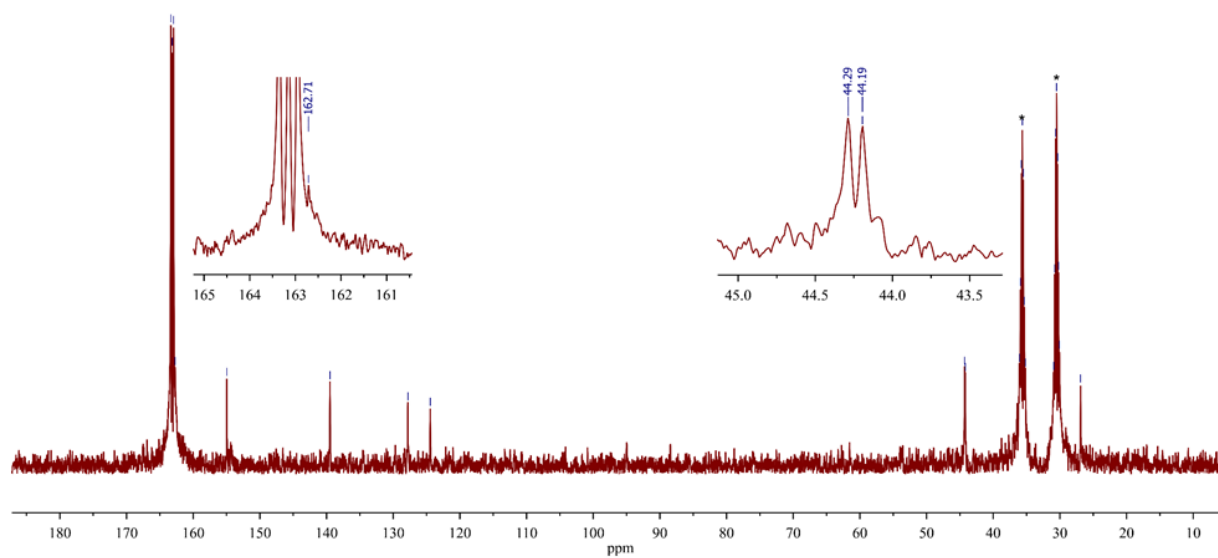


¹H NMR spectrum of **Pt-2** in DMF-d₇

^{13}C NMR (151 MHz, DMF-d_7)



Pt-2

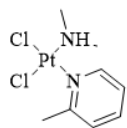


* DMF-d_7 solvent residual at 25 °C

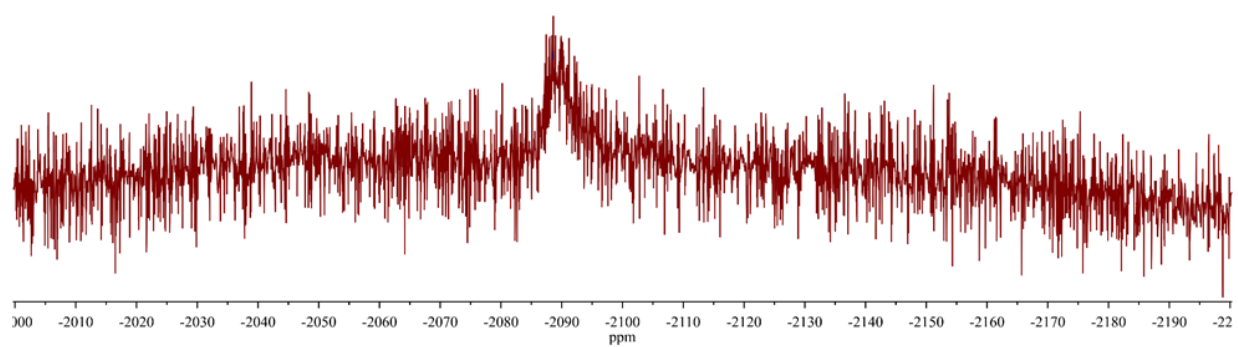
^{13}C NMR spectrum of **Pt-2** in DMF-d_7

^{195}Pt NMR (129 MHz, DMF- d_7)

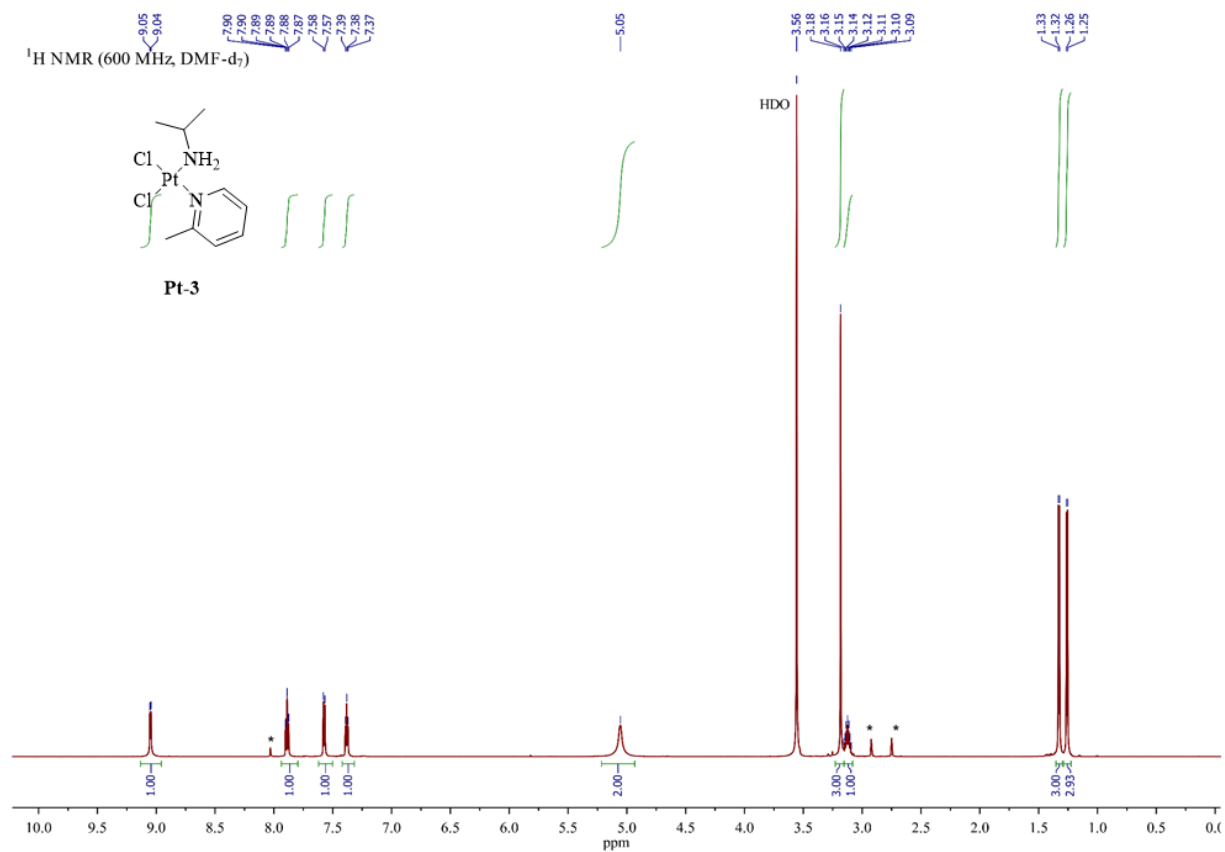
—2088.57



Pt-2

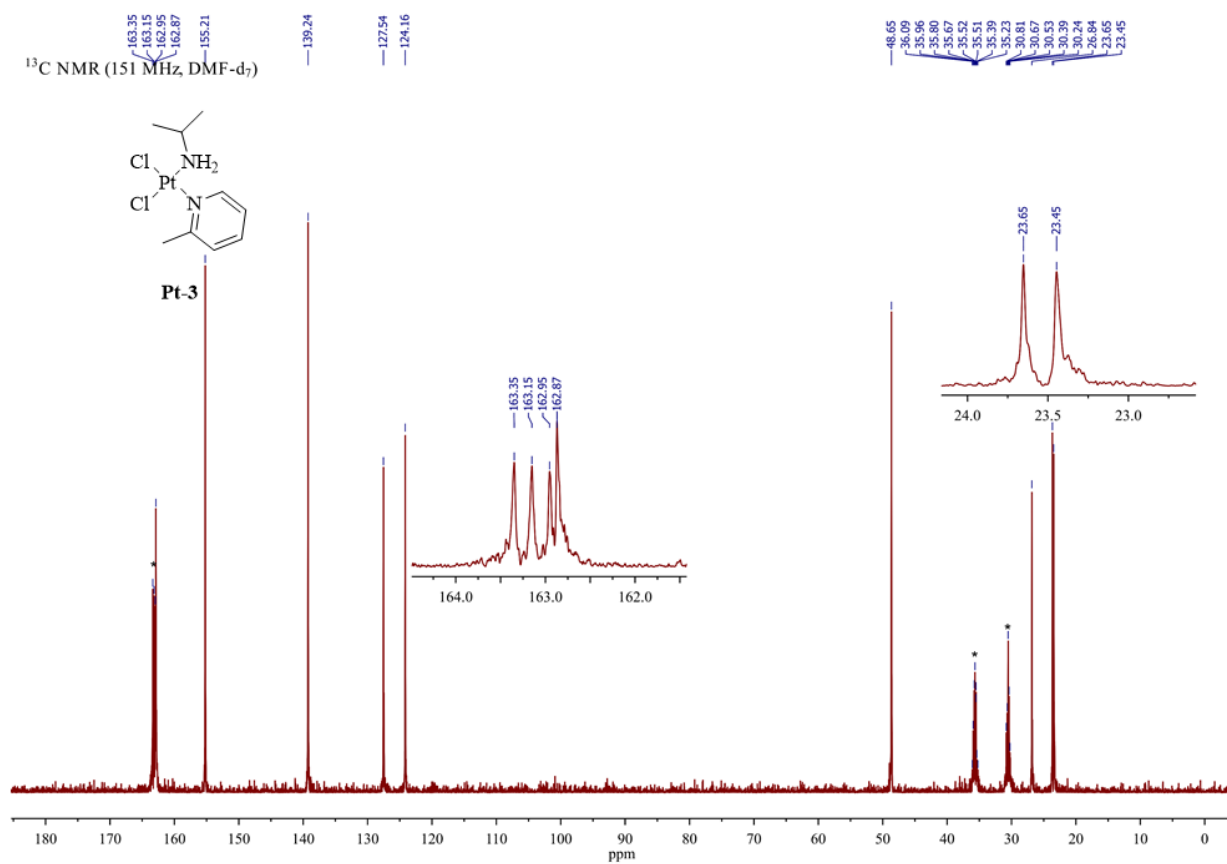


^{195}Pt NMR spectrum of **Pt-2** in DMF- d_7



*DMF-d₇ solvent residual at 25 °C

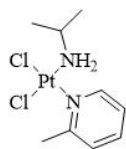
¹H NMR spectrum of **Pt-3** in DMF-d₇



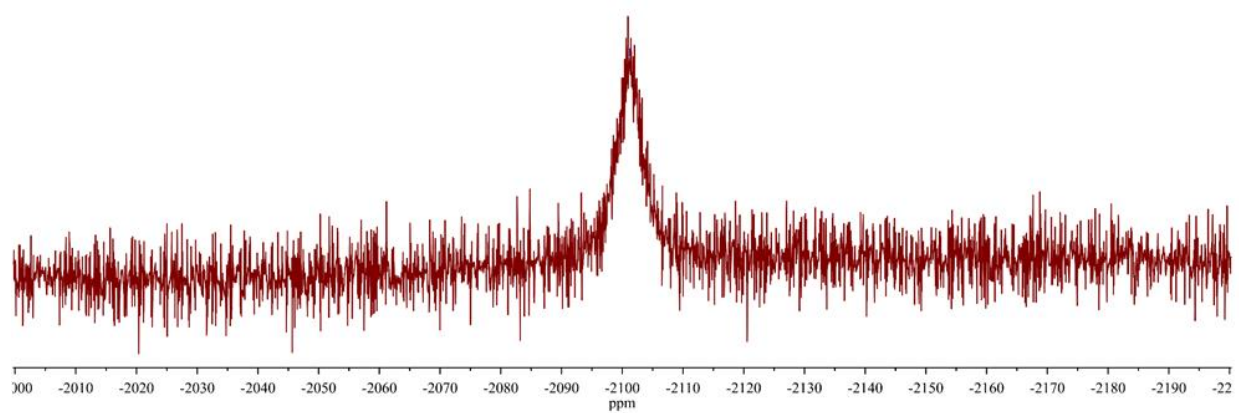
*DMF-d₇ solvent residual at 25 °C

¹³C NMR spectrum of **Pt-3** in DMF-d₇

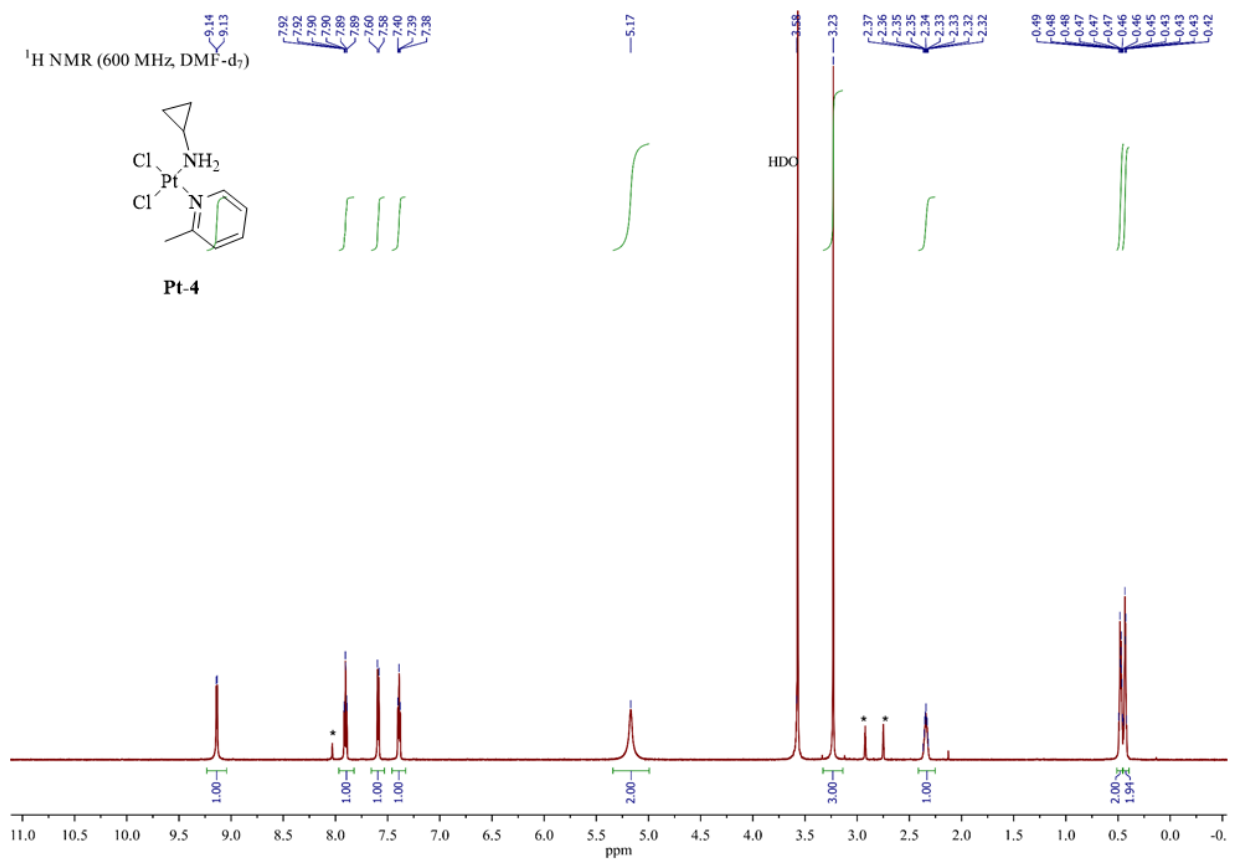
^{195}Pt NMR (129 MHz, DMF- d_7)



Pt-3

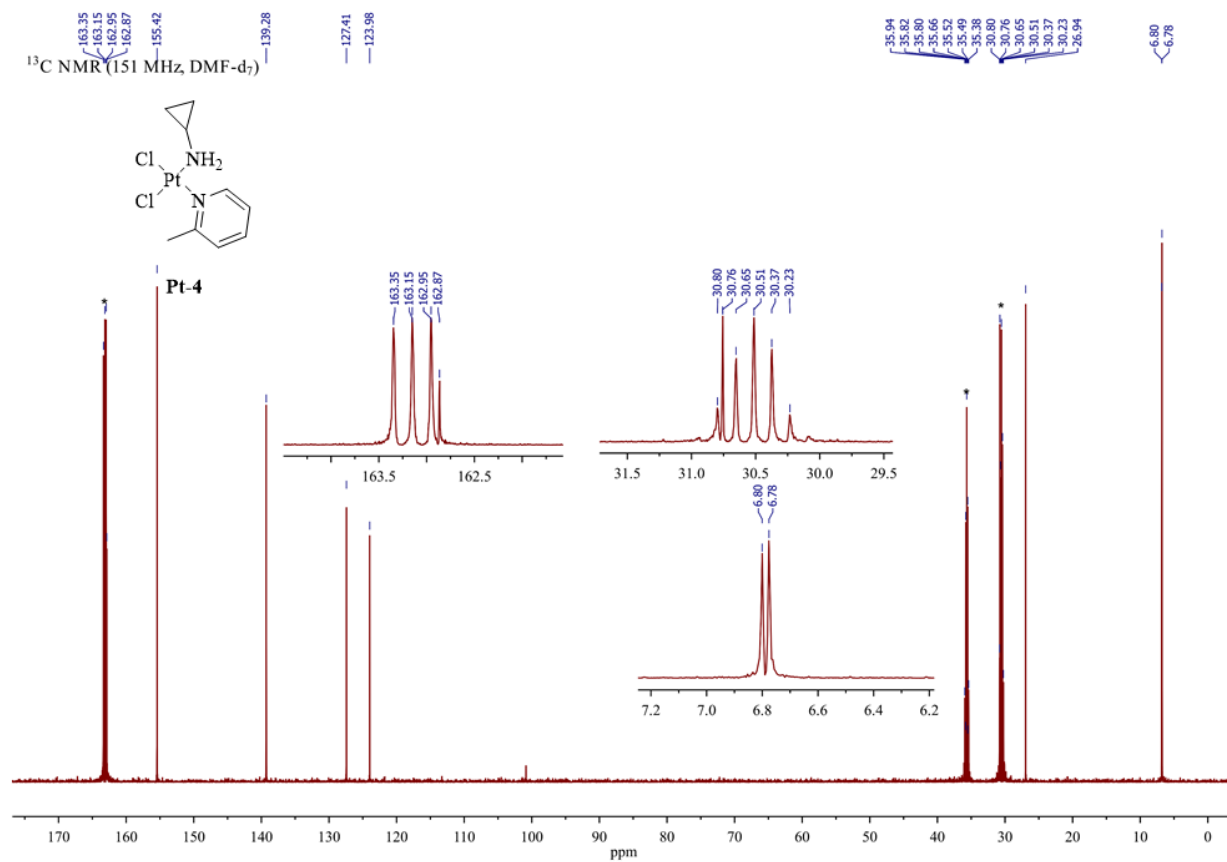


^{195}Pt NMR spectrum of **Pt-3** in DMF- d_7



*DMF-d₇ solvent residual at 25 °C

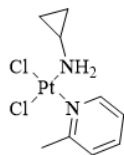
¹H NMR spectrum of **Pt-4** in DMF-d₇



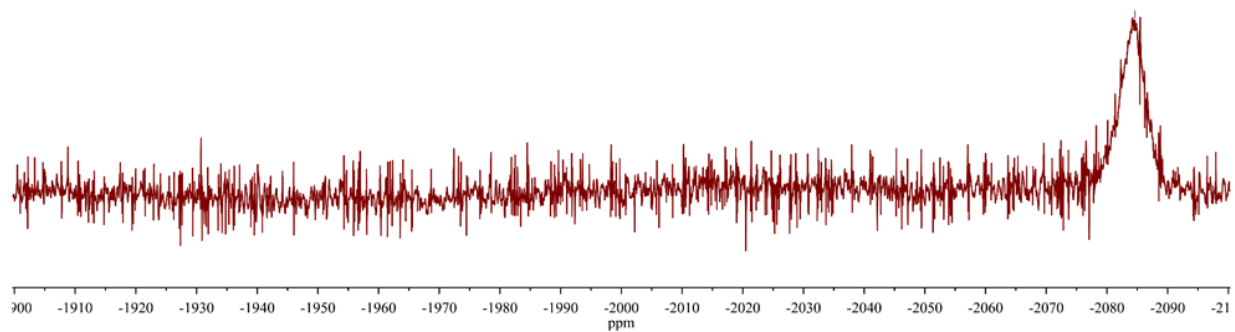
*DMF-d₇ solvent residual at 25 °C

¹³C NMR spectrum of **Pt-4** in DMF-d₇

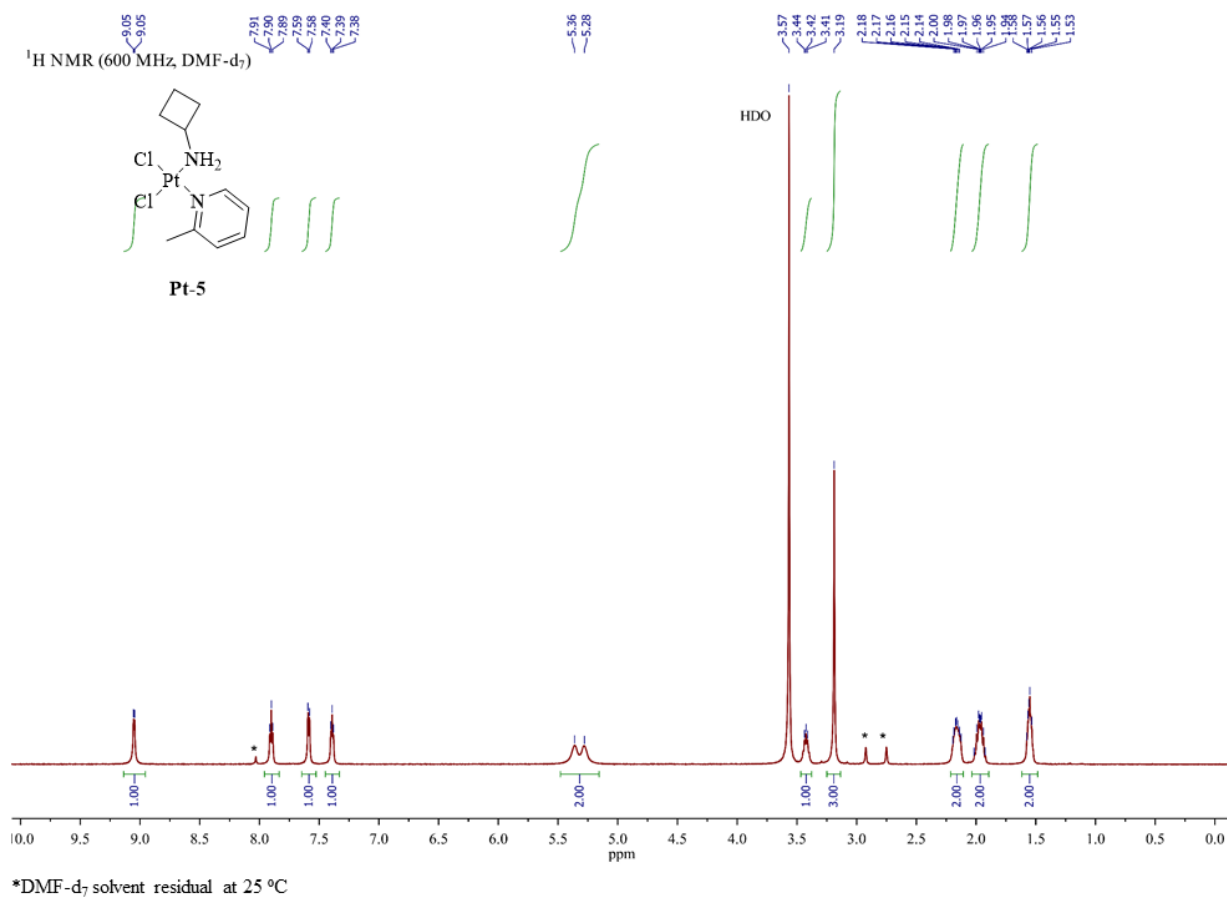
^{195}Pt NMR (129 MHz, DMF- d_7)



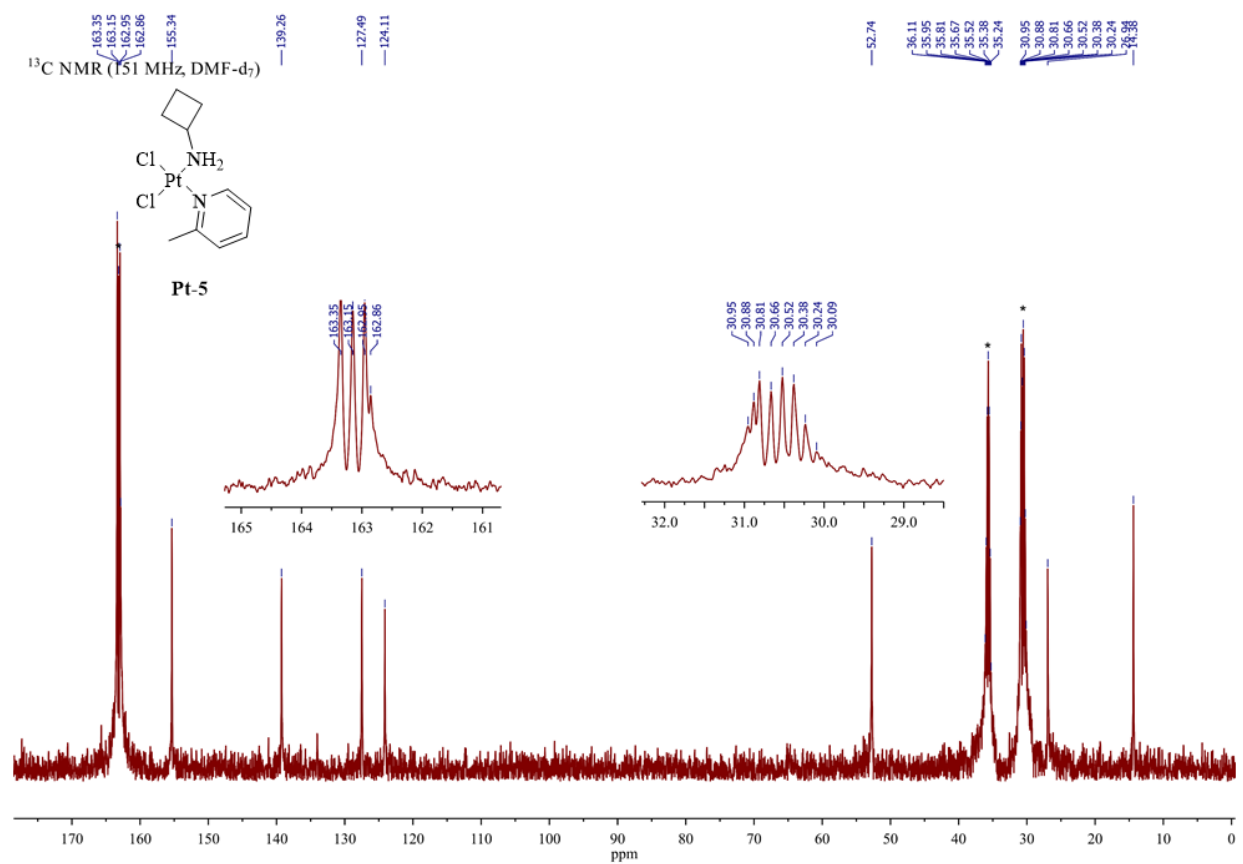
Pt-4



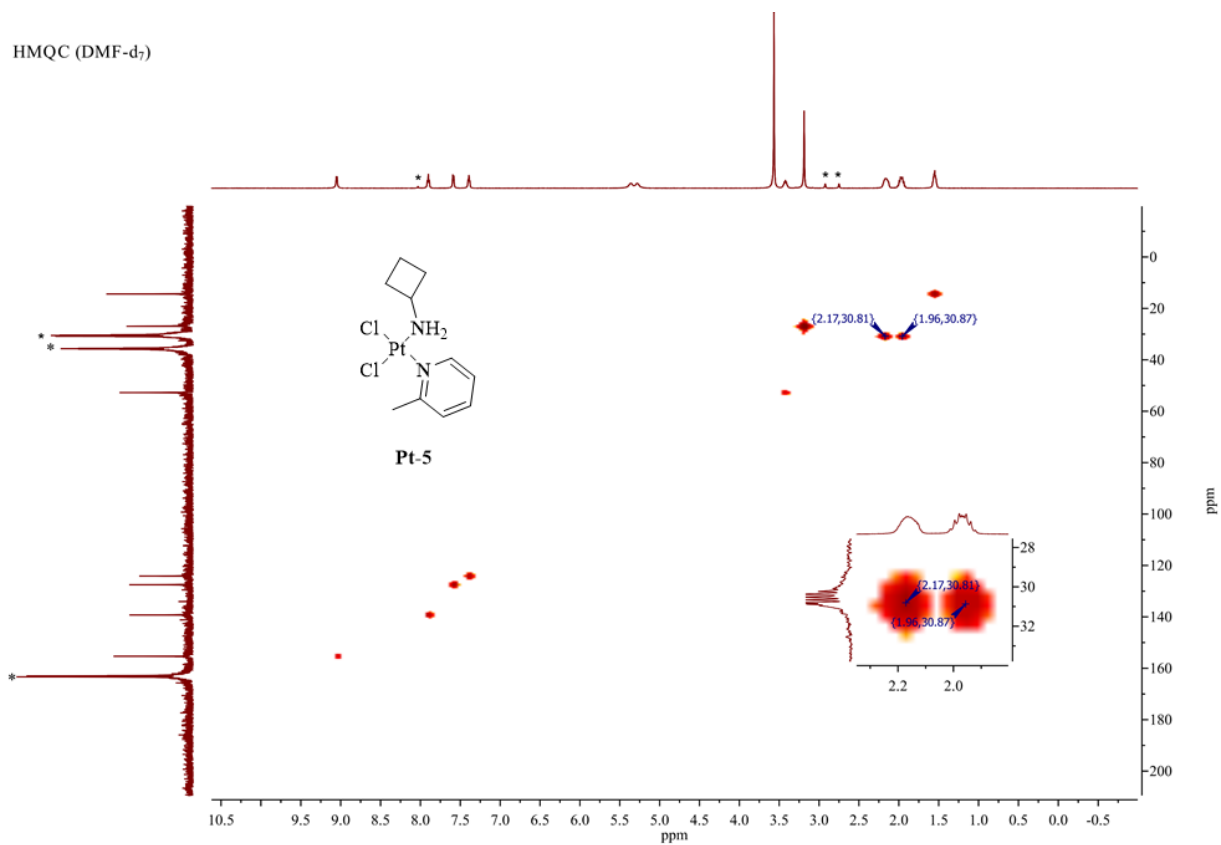
^{195}Pt NMR spectrum of **Pt-4** in DMF- d_7



¹H NMR spectrum of **Pt-5** in DMF-d₇



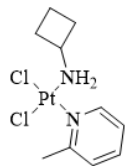
¹³C NMR spectrum of **Pt-5** in DMF-d₇



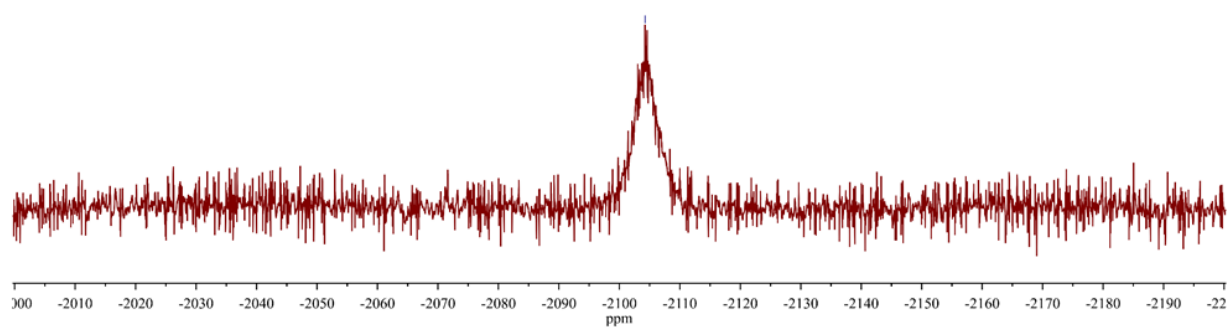
*DMF-d₇ solvent residual at 25 °C

HMQC NMR spectrum of **Pt-5** in DMF-d₇ (¹³C δ 30.81, 30.87 overlaps with solvent residual peak)

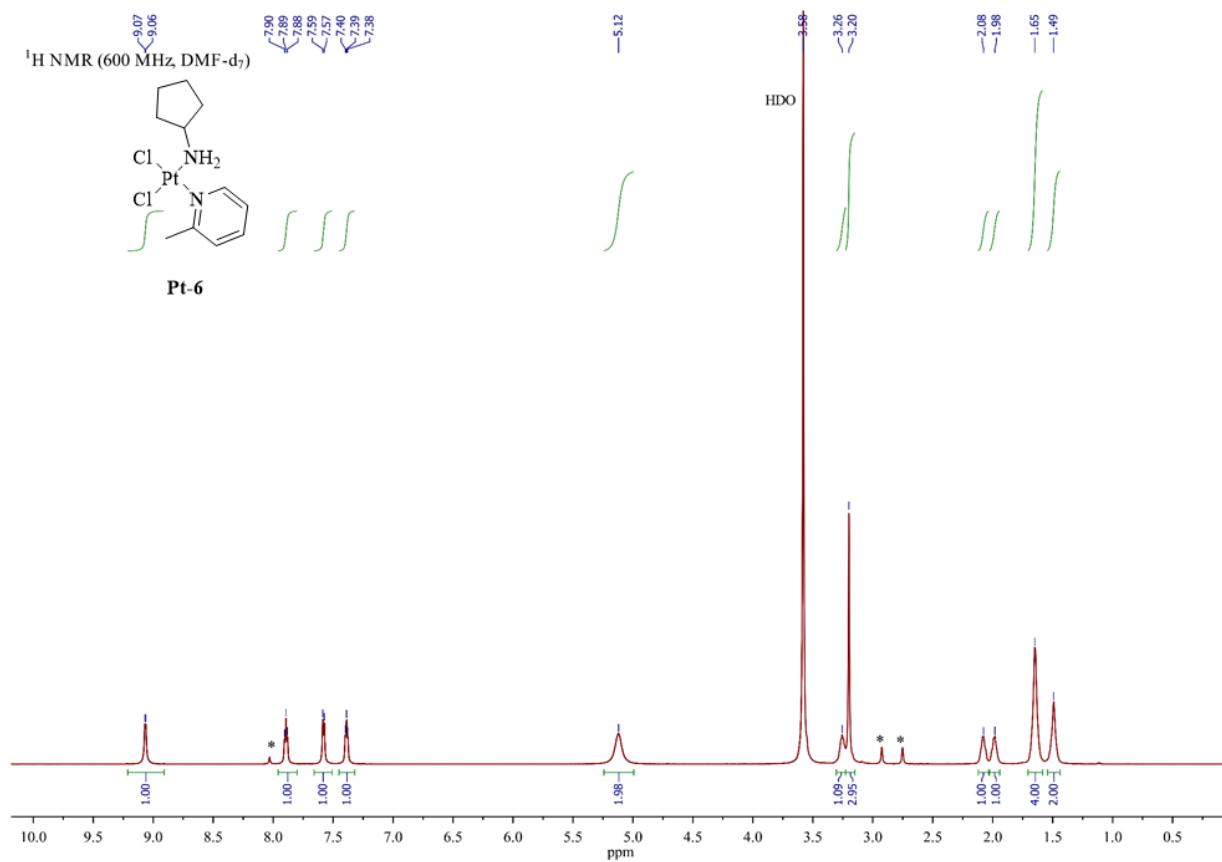
^{195}Pt NMR (129 MHz, DMF- d_7)



Pt-5

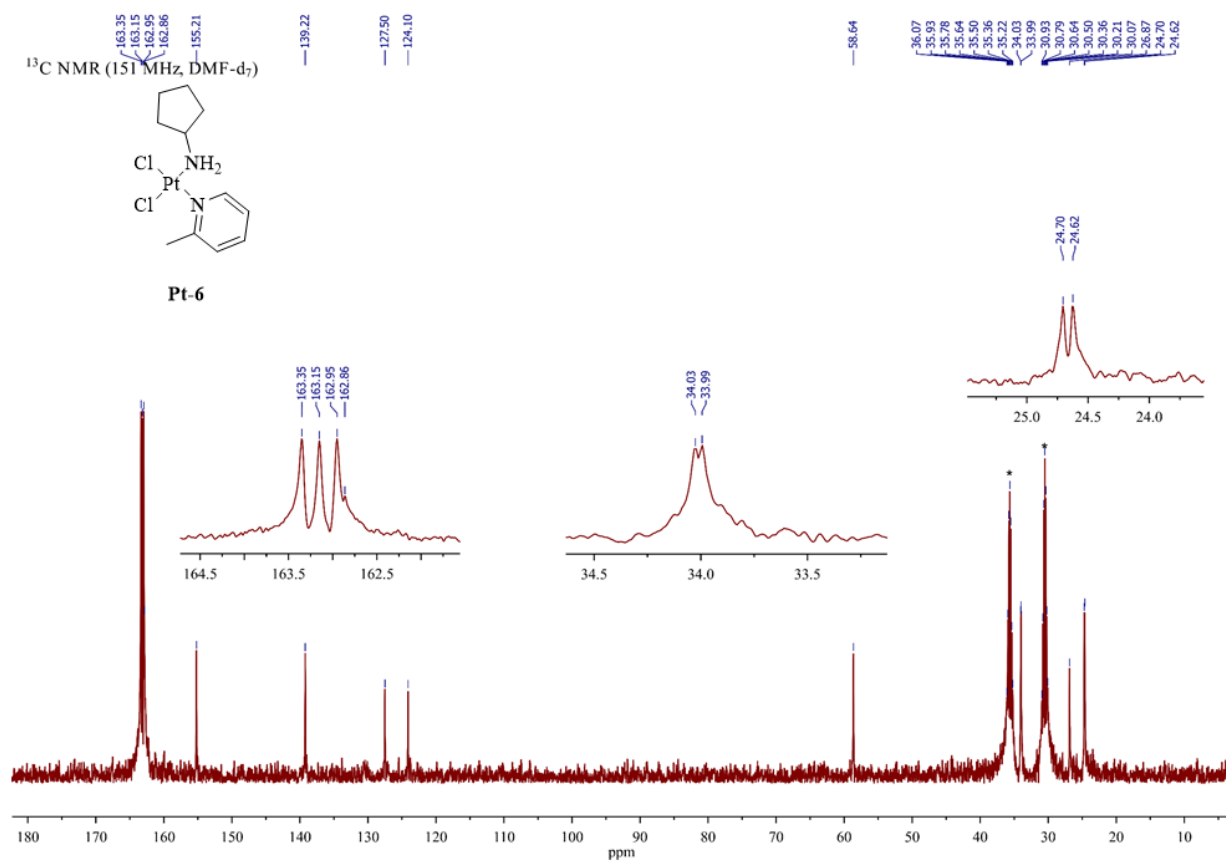


^{195}Pt NMR spectrum of **Pt-5** in DMF- d_7



*DMF-d₇ solvent residual at 25 °C

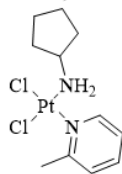
¹H NMR spectrum of **Pt-6** in DMF-d₇



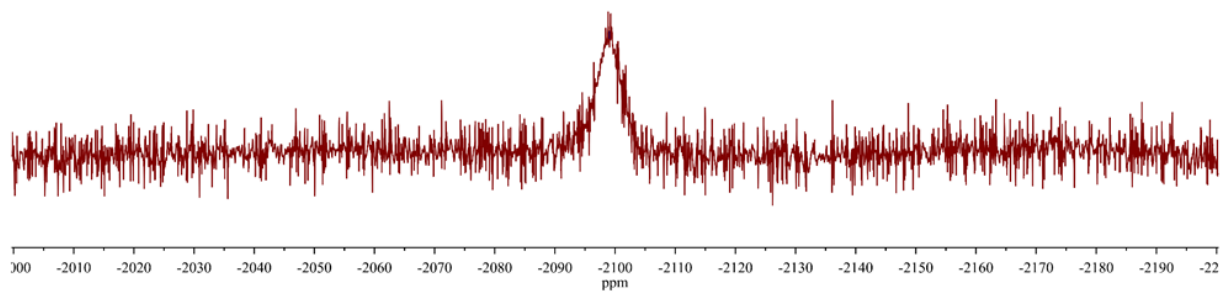
*DMF-d₇ solvent residual at 25 °C

¹³C NMR spectrum of **Pt-6** in DMF-d₇

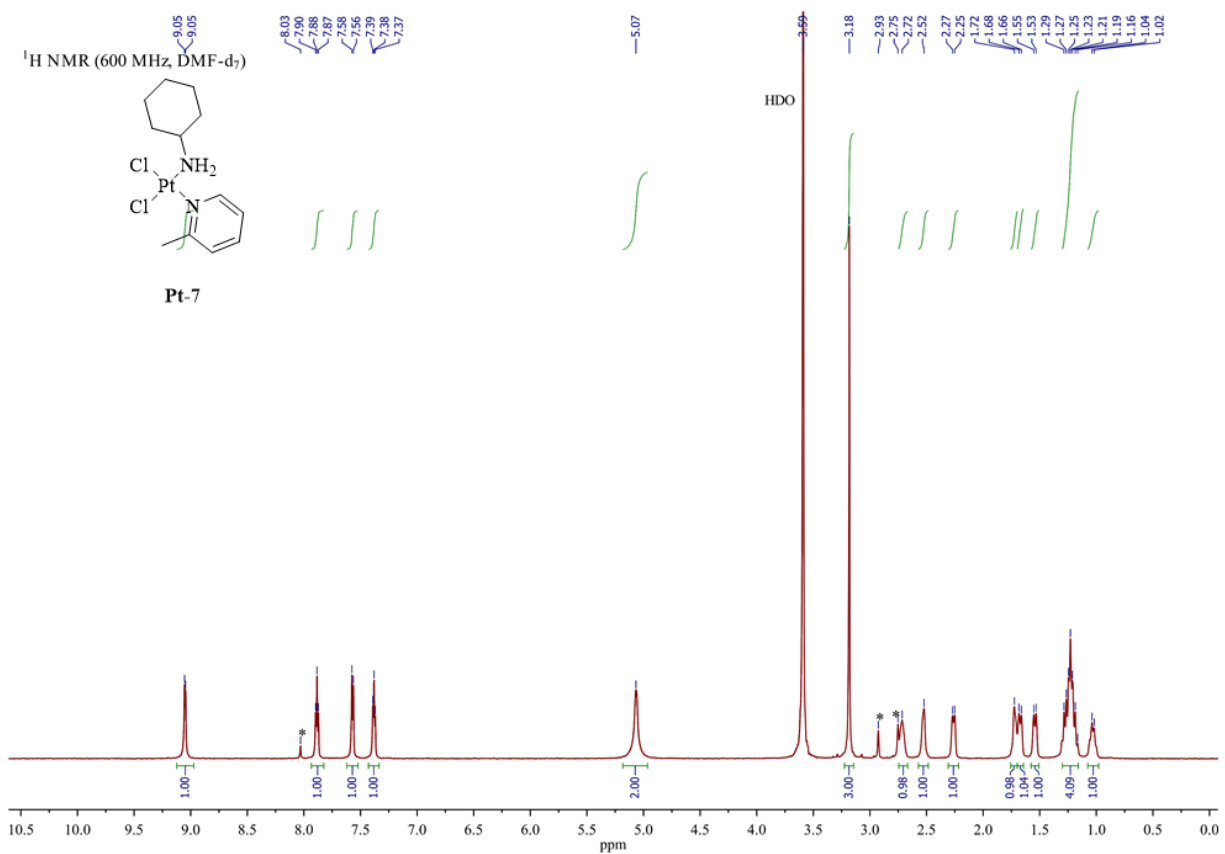
^{195}Pt NMR (129 MHz, DMF- d_7)



Pt-6

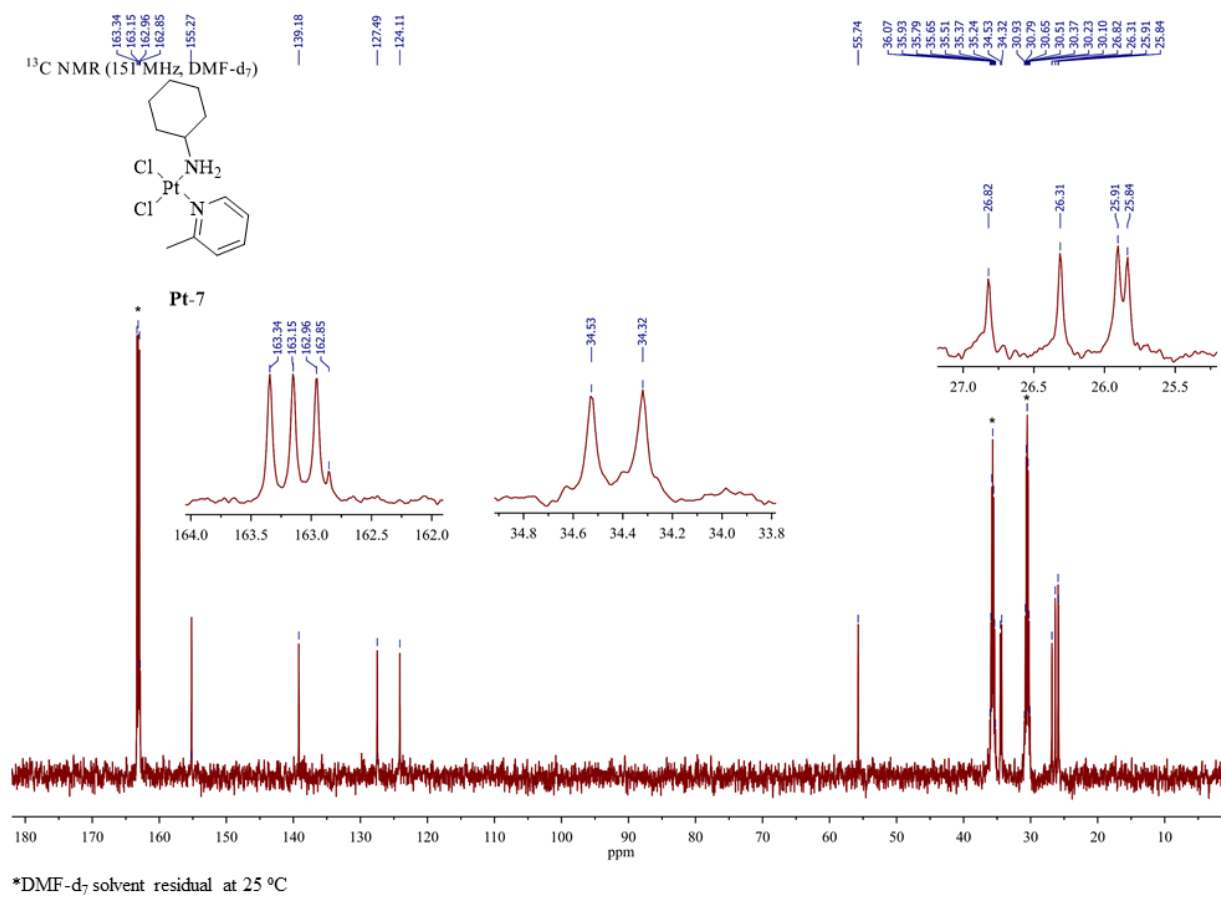


^{195}Pt NMR spectrum of **Pt-6** in DMF- d_7



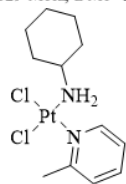
*DMF-d₇ solvent residual at 25 °C

¹H NMR spectrum of **Pt-7** in DMF-d₇

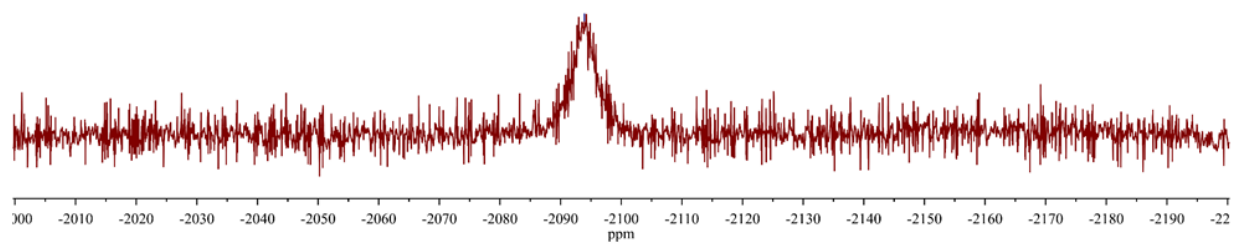


¹³C NMR spectrum of **Pt-7** in DMF-d₇

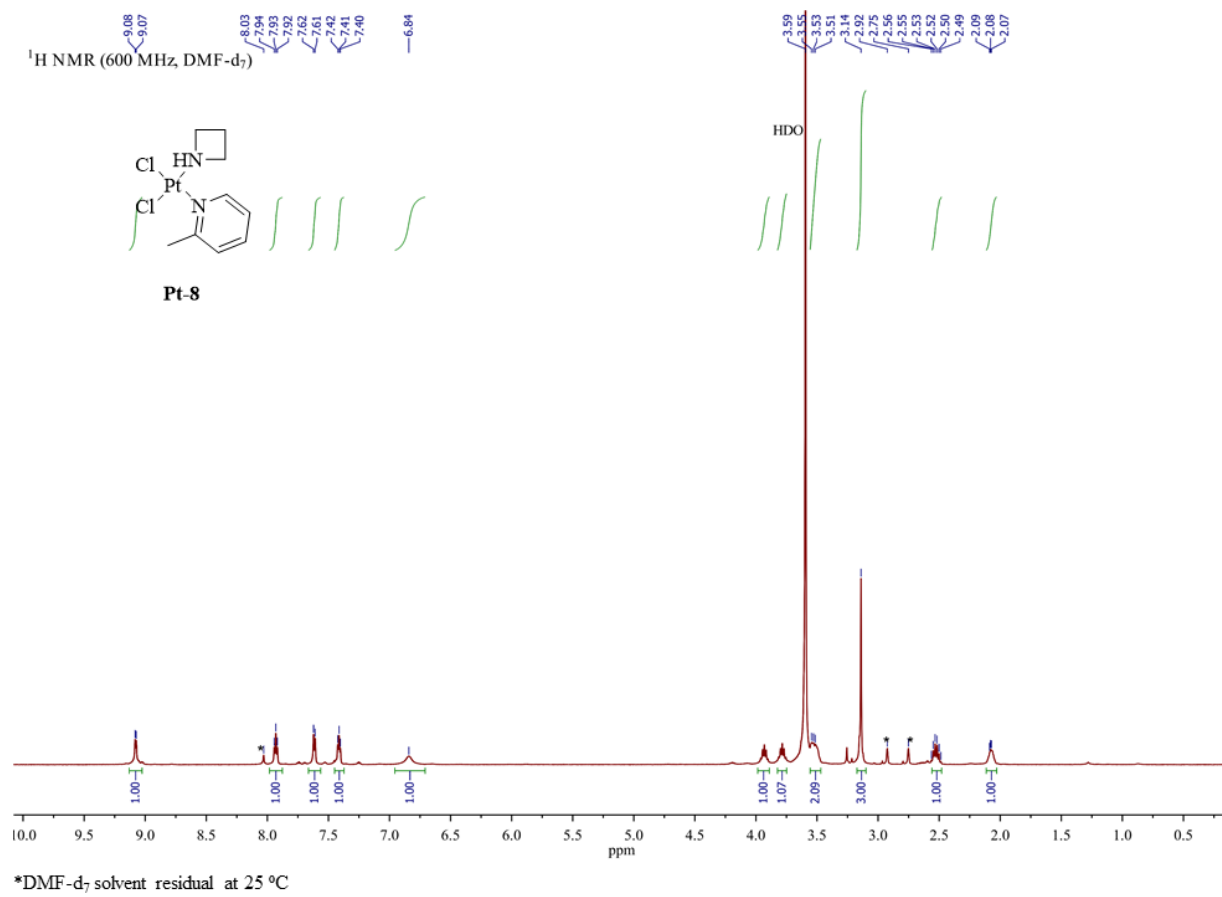
^{195}Pt NMR (129 MHz, DMF-d₇)



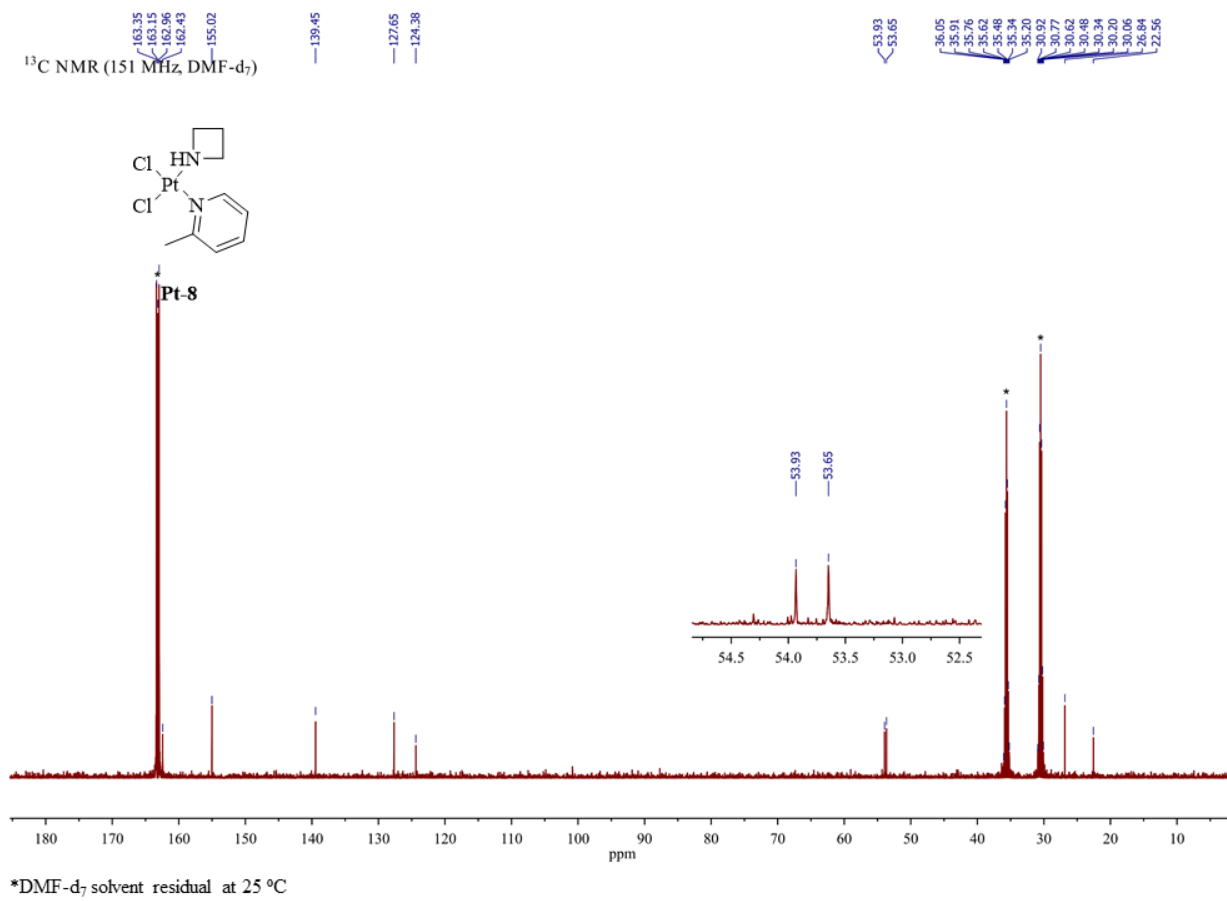
Pt-7



^{195}Pt NMR spectrum of **Pt-7** in DMF-d₇

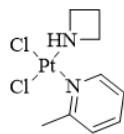


¹H NMR spectrum of **Pt-8** in DMF-d₇

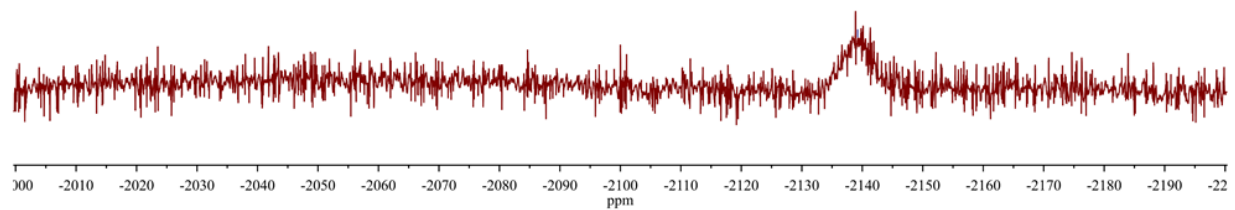


^{13}C NMR spectrum of **Pt-8** in DMF-d_7

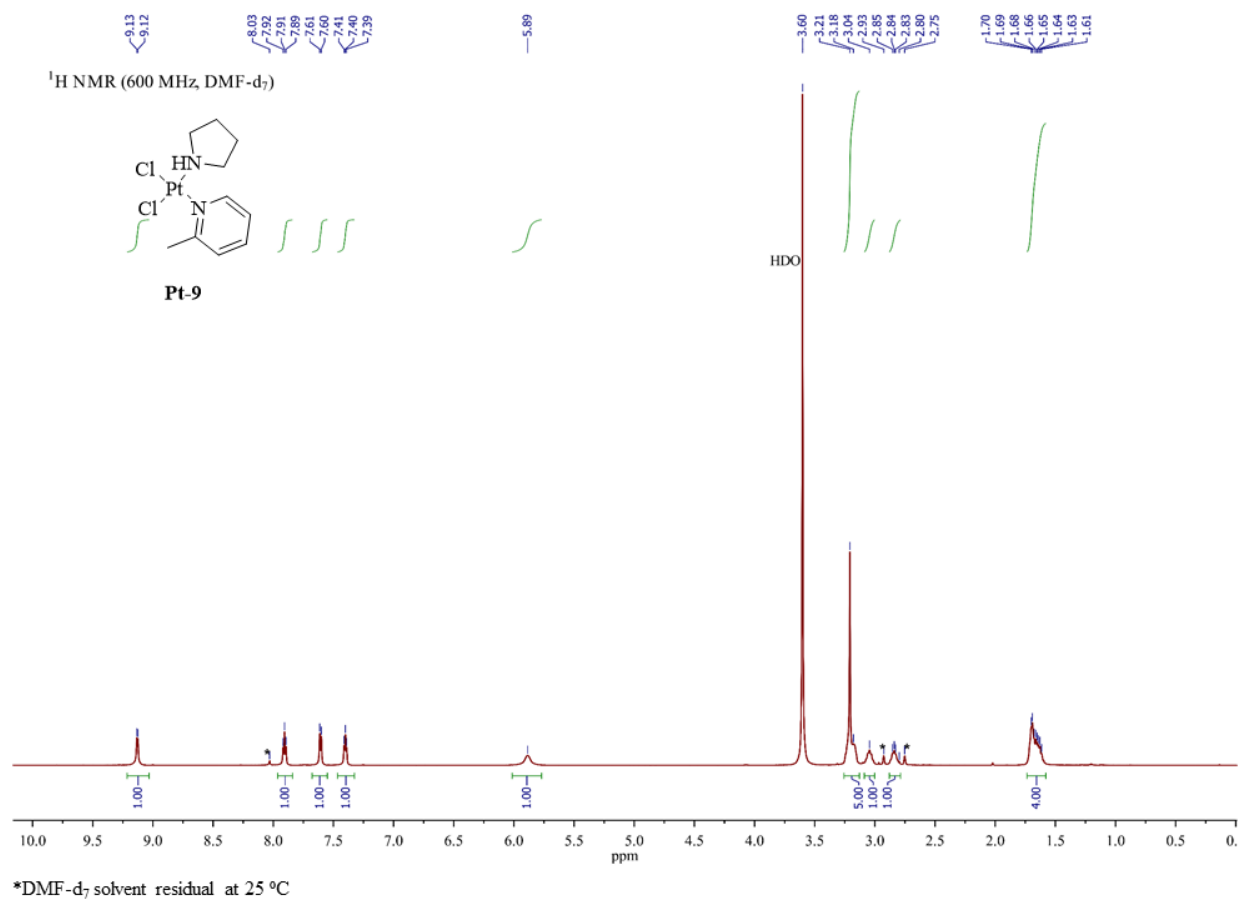
^{195}Pt NMR (129 MHz, DMF- d_7)



Pt-8

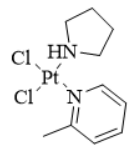


^{195}Pt NMR spectrum of **Pt-8** in DMF- d_7

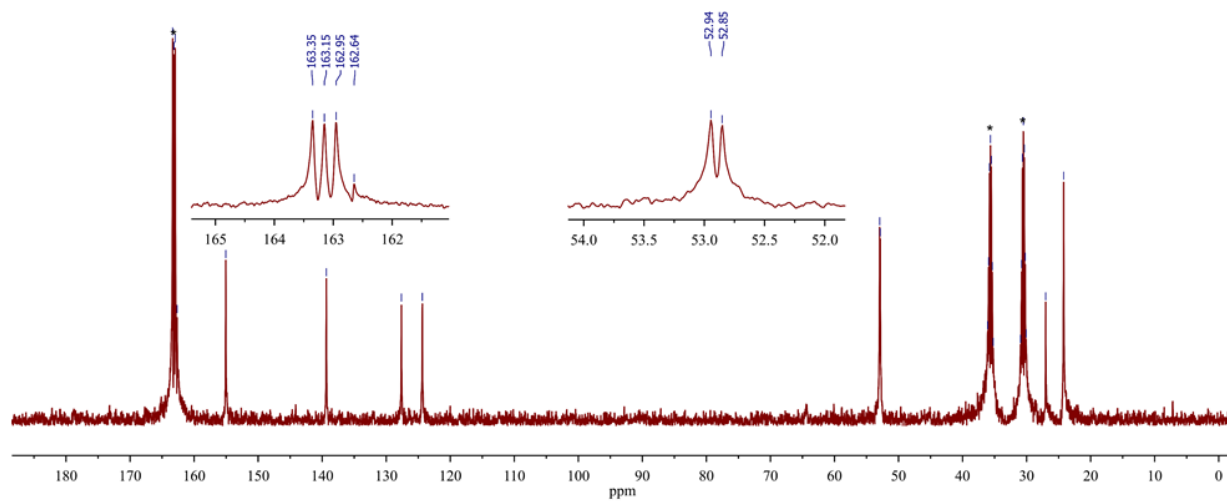


¹H NMR spectrum of **Pt-9** in DMF-d₇

^{13}C NMR (151 MHz, DMF-d_7)

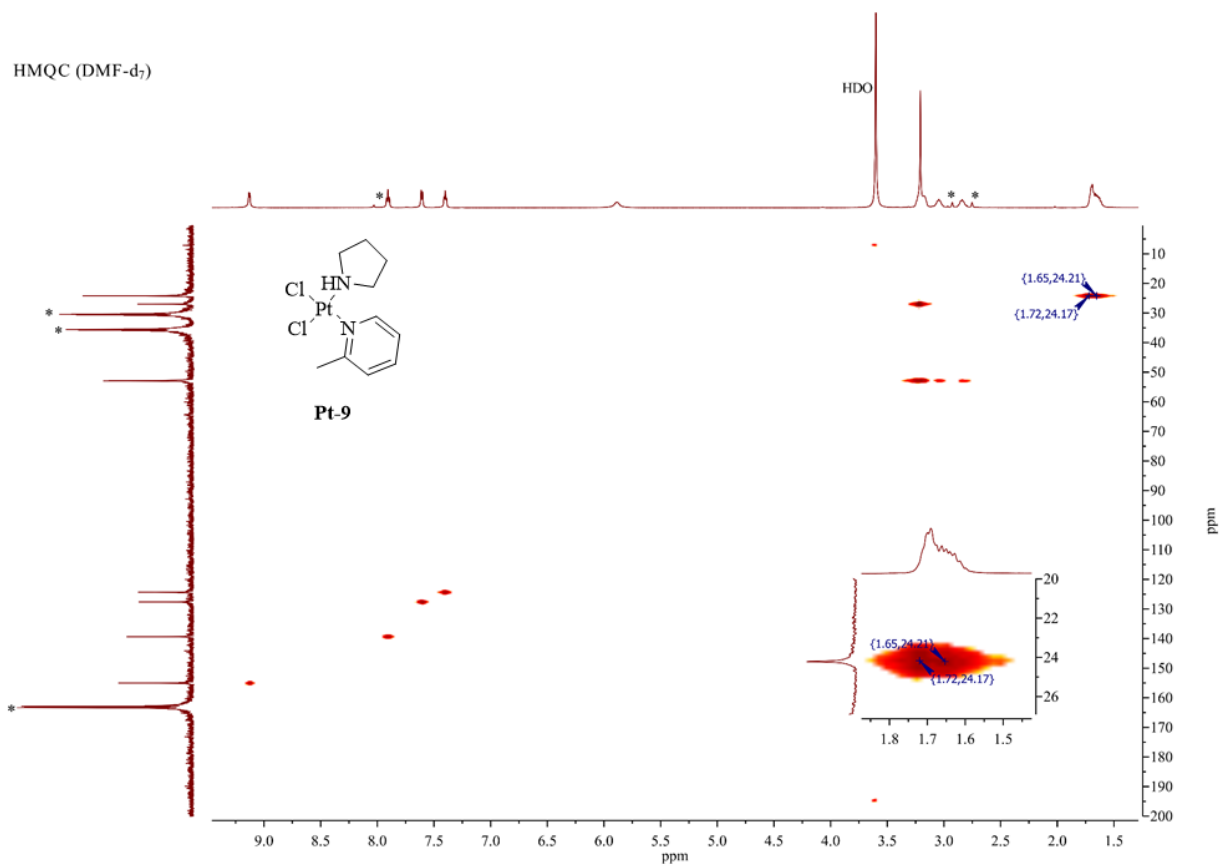


Pt-9



* DMF-d_7 solvent residual at 25 °C

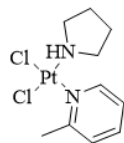
^{13}C NMR spectrum of **Pt-9** in DMF-d_7



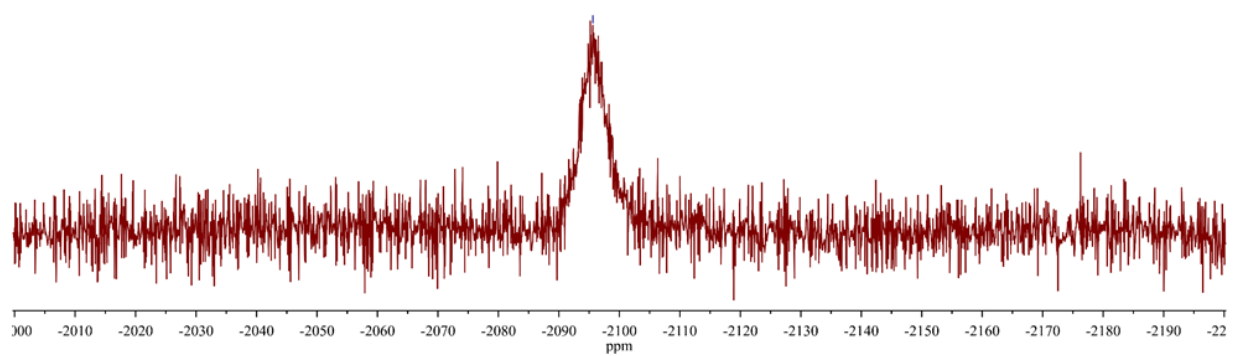
*DMF-d₇ solvent residual at 25 °C

HMQC NMR spectrum of **Pt-9** in DMF-d₇ (¹³C δ 24.21, 24.17 overlap)

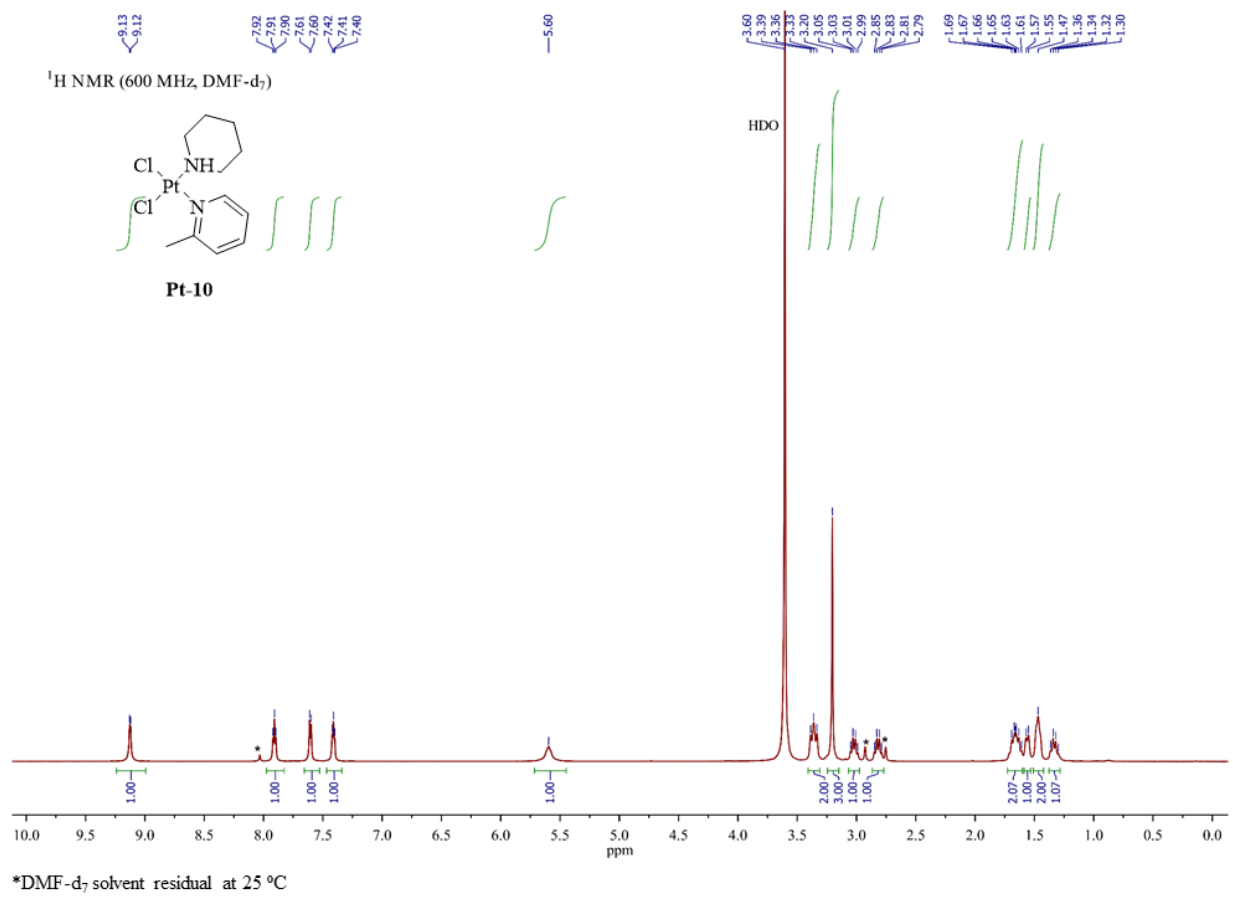
^{195}Pt NMR (129 MHz, DMF- d_7)



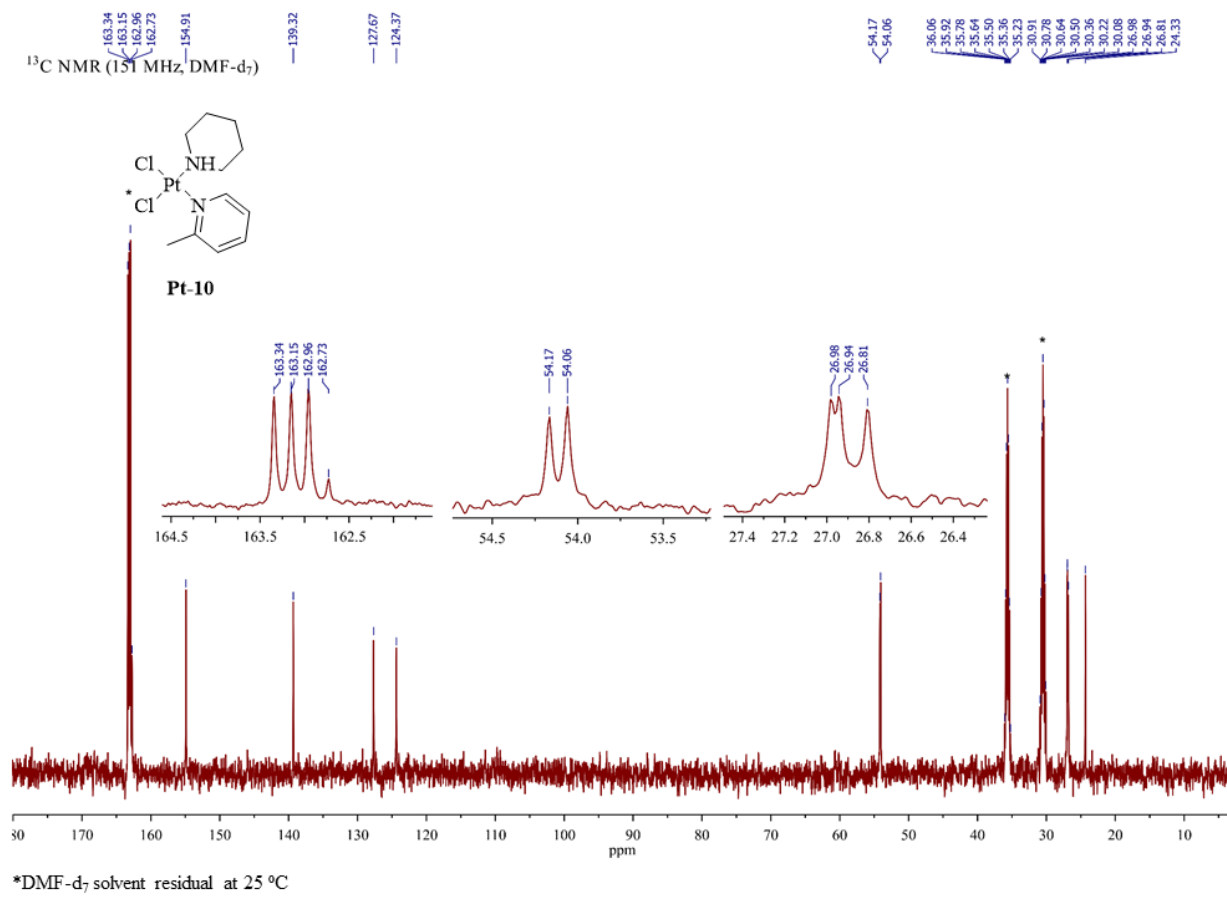
Pt-9



^{195}Pt NMR spectrum of **Pt-9** in DMF- d_7

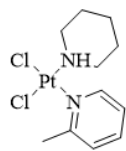


¹H NMR spectrum of **Pt-10** in DMF-d₇

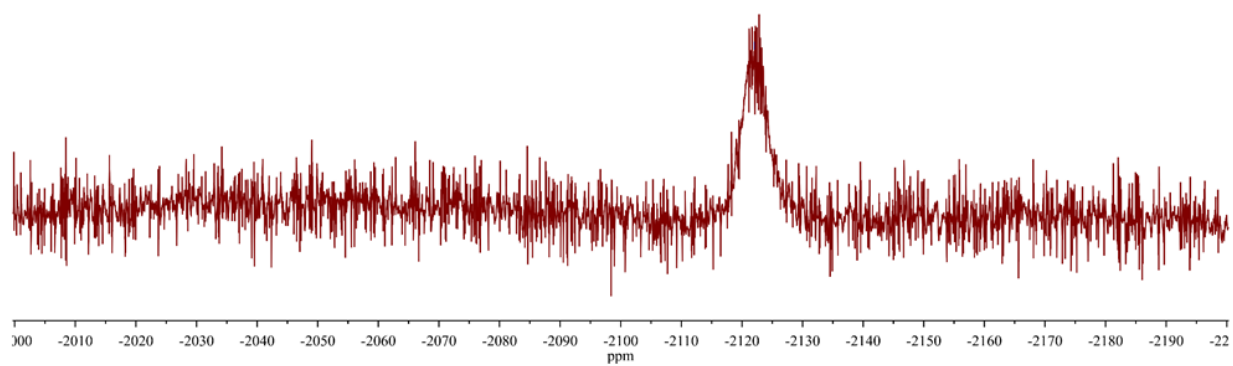


^{13}C NMR spectrum of **Pt-10** in DMF-d₇

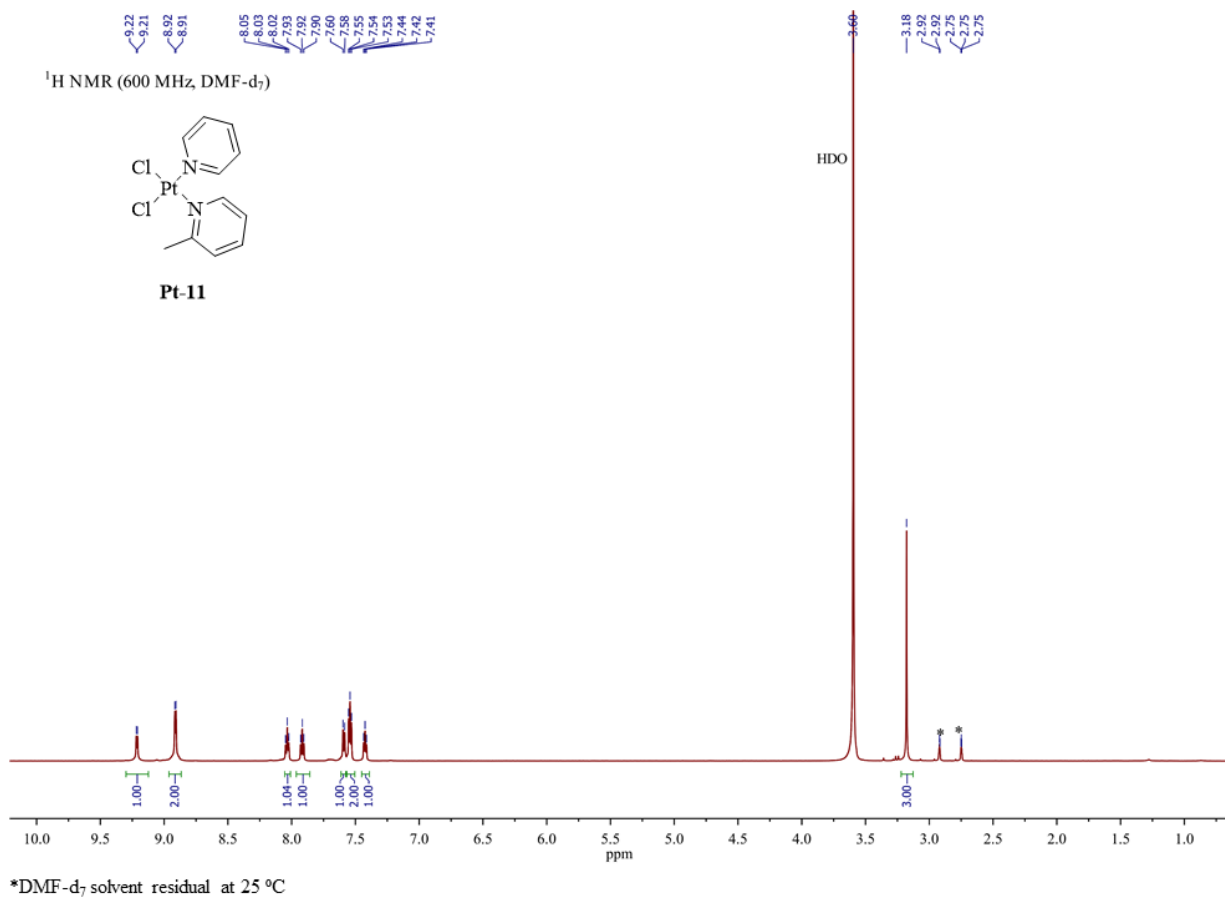
^{195}Pt NMR (129 MHz, DMF- d_7)



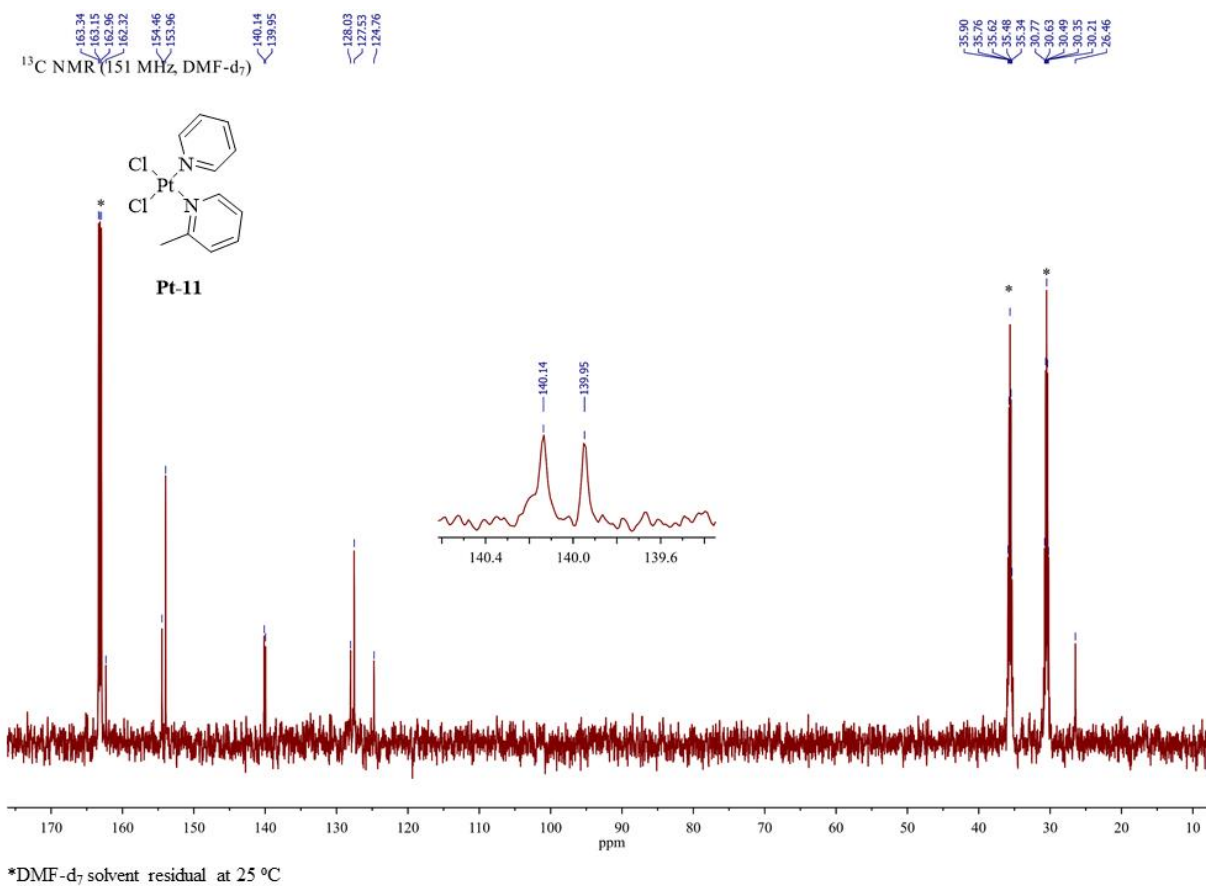
Pt-10



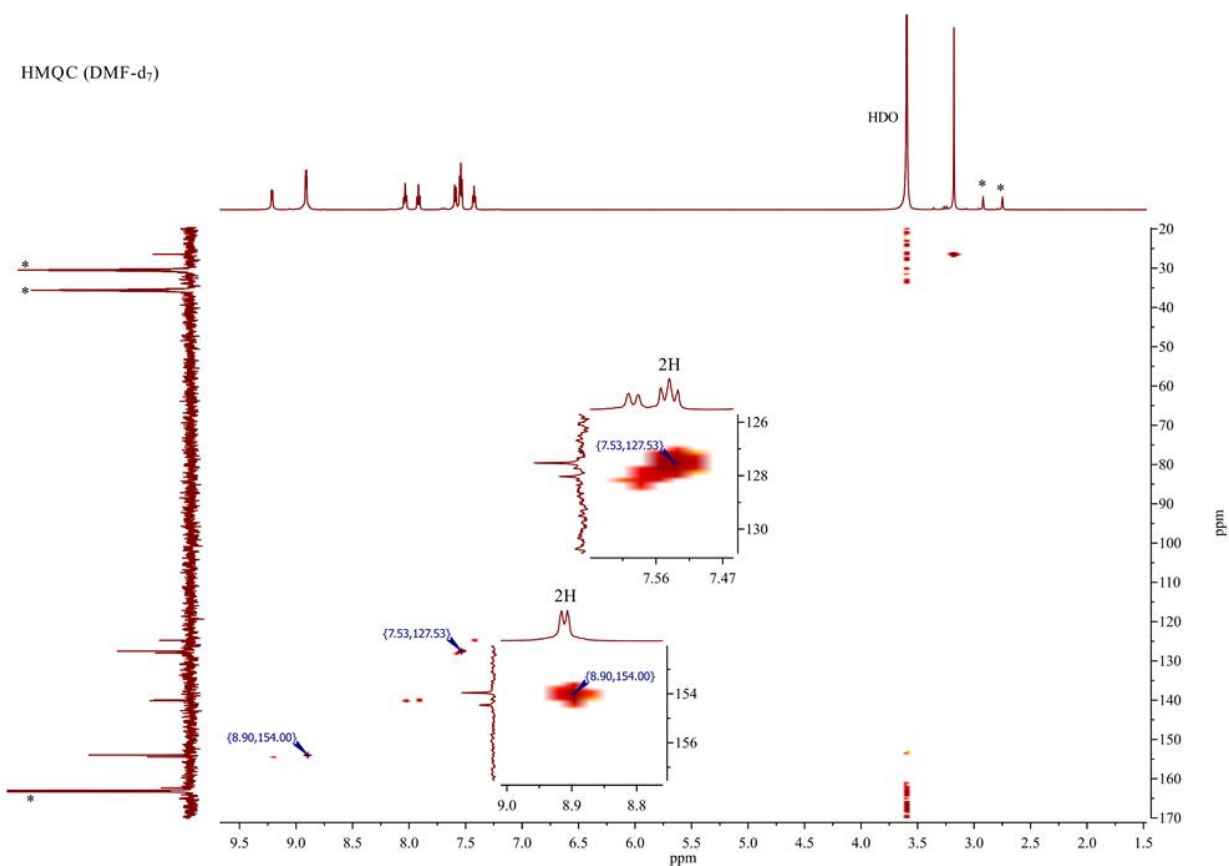
^{195}Pt NMR spectrum of **Pt-10** in DMF- d_7



¹H NMR spectrum of **Pt-11** in DMF-d₇



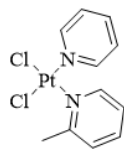
¹³C NMR spectrum of **Pt-11** in DMF-d₇



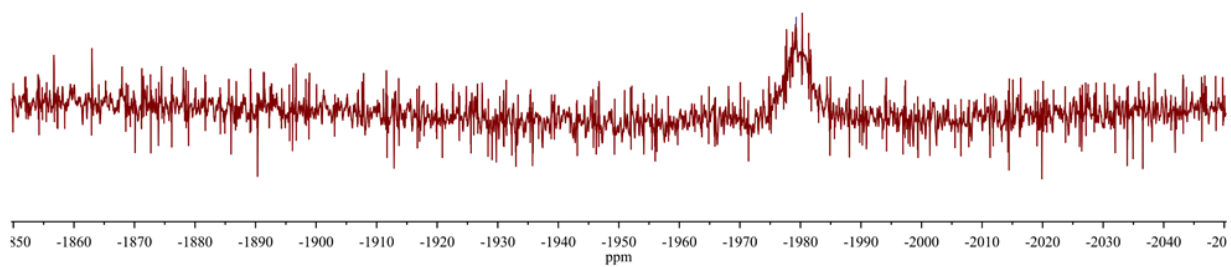
*DMF-d₇ solvent residual at 25 °C

HMQC NMR spectrum of **Pt-11** in DMF-d₇ (¹³C δ 154.00, 127.53 represents 2 aromatic ¹³C respectively)

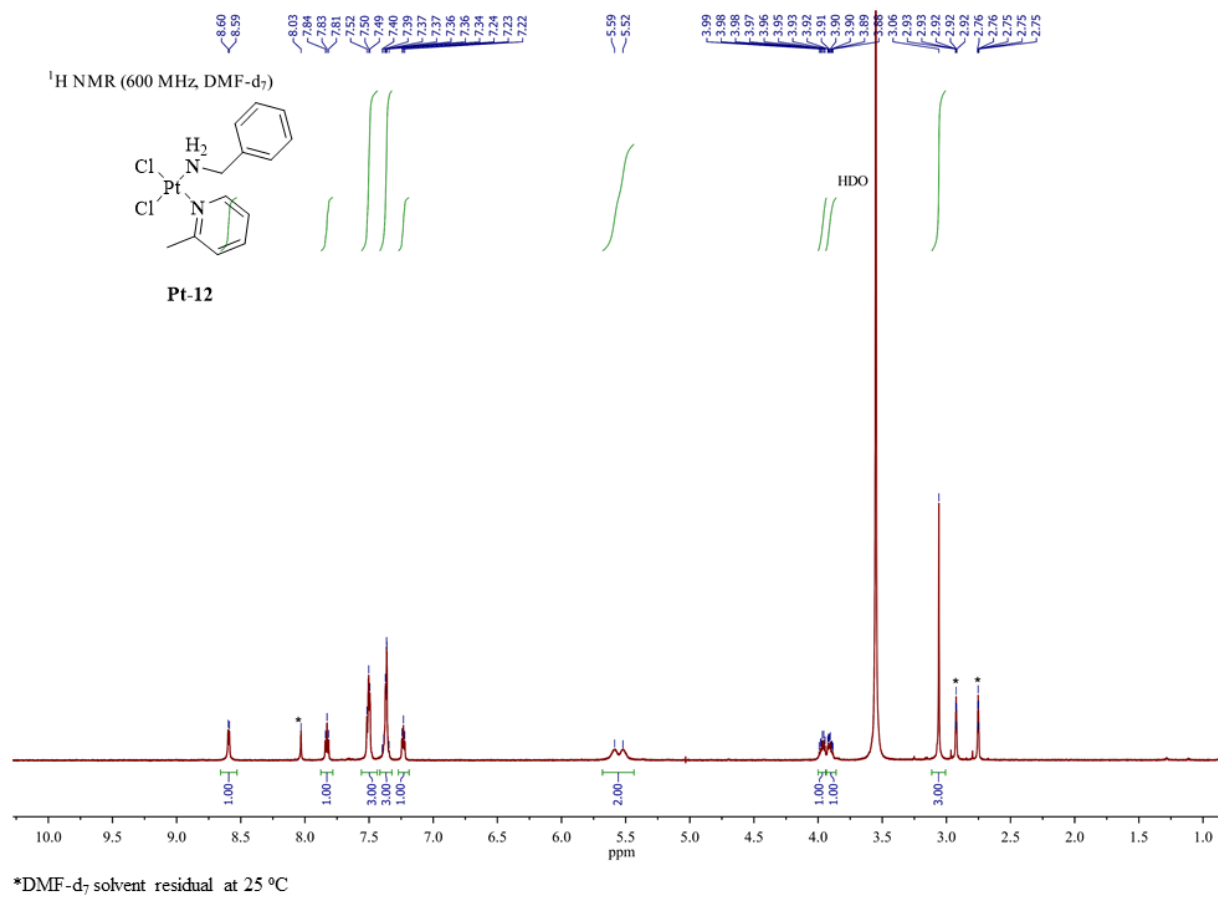
^{195}Pt NMR (129 MHz, DMF- d_7)



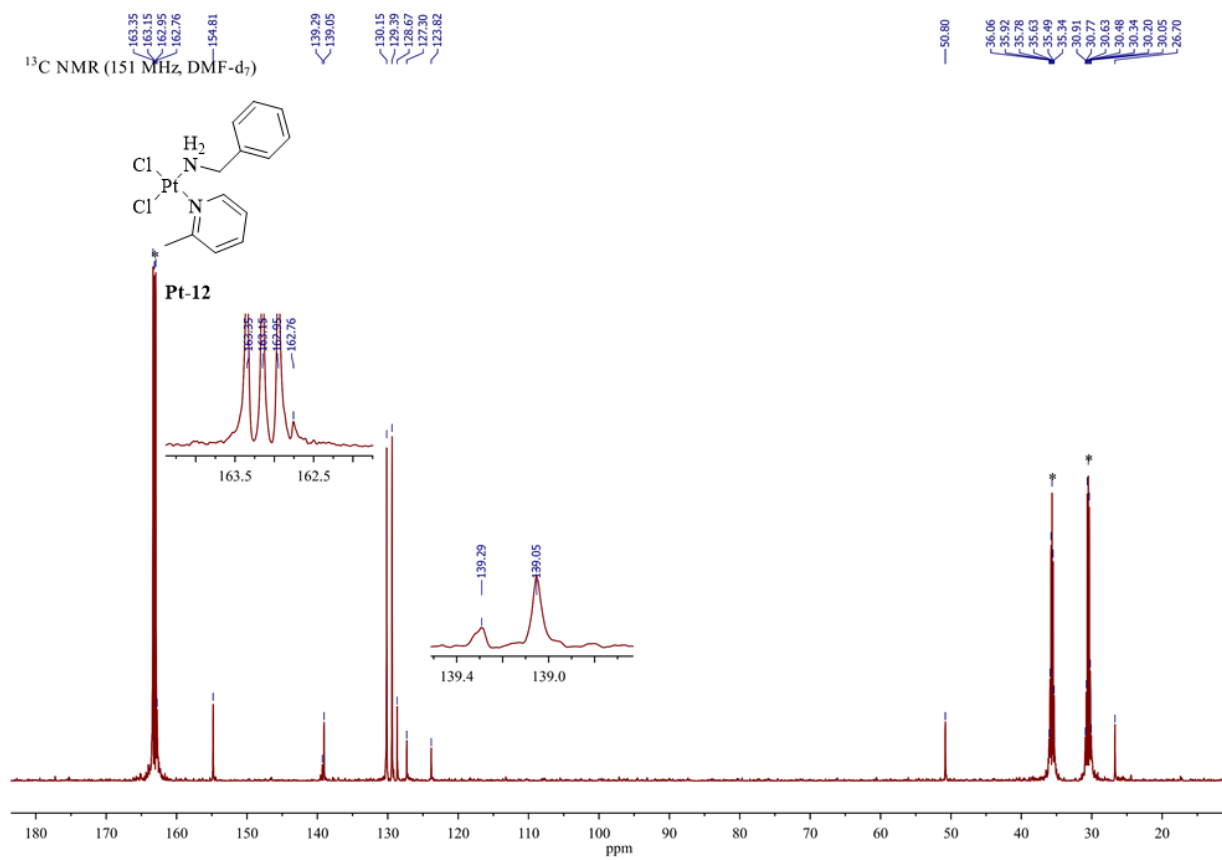
Pt-11



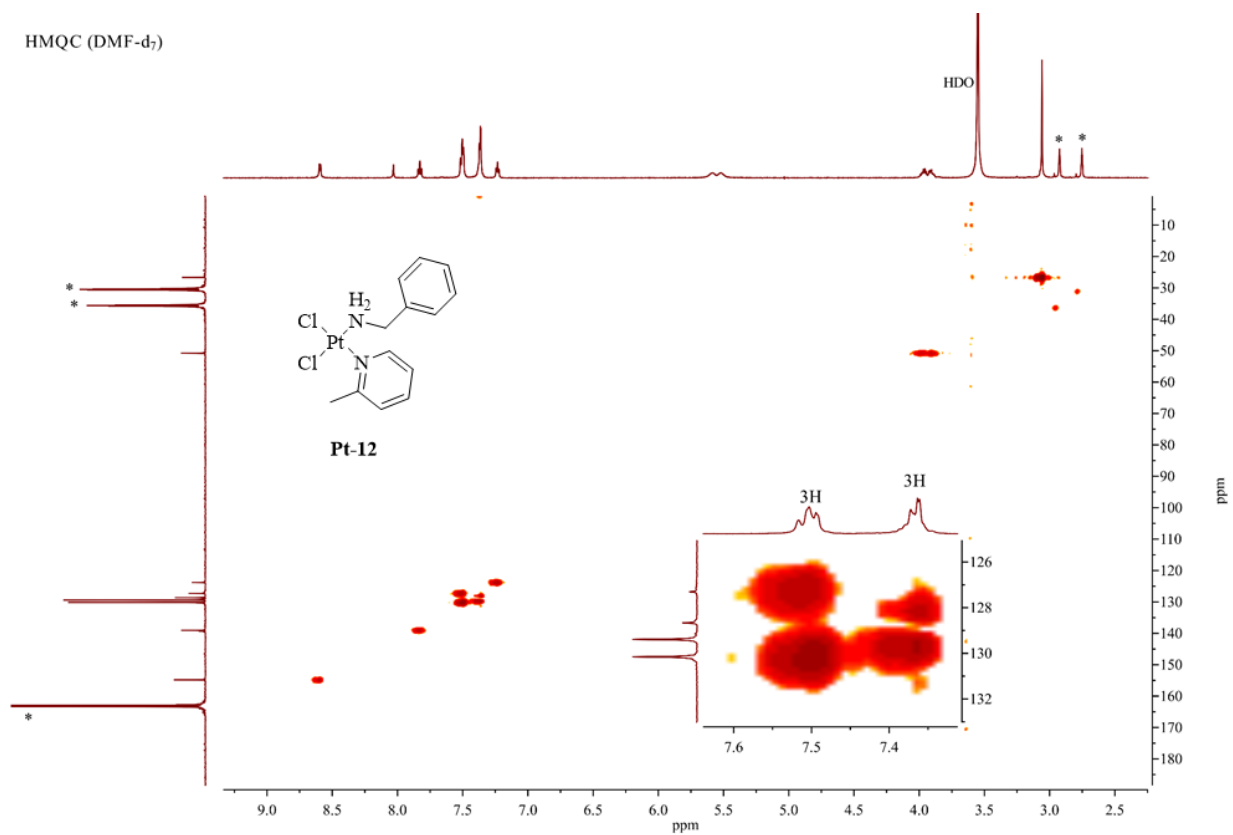
^{195}Pt NMR spectrum of **Pt-11** in DMF- d_7



¹H NMR spectrum of **Pt-12** in DMF-d₇



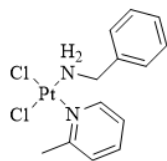
¹³C NMR spectrum of **Pt-12** in DMF-d₇



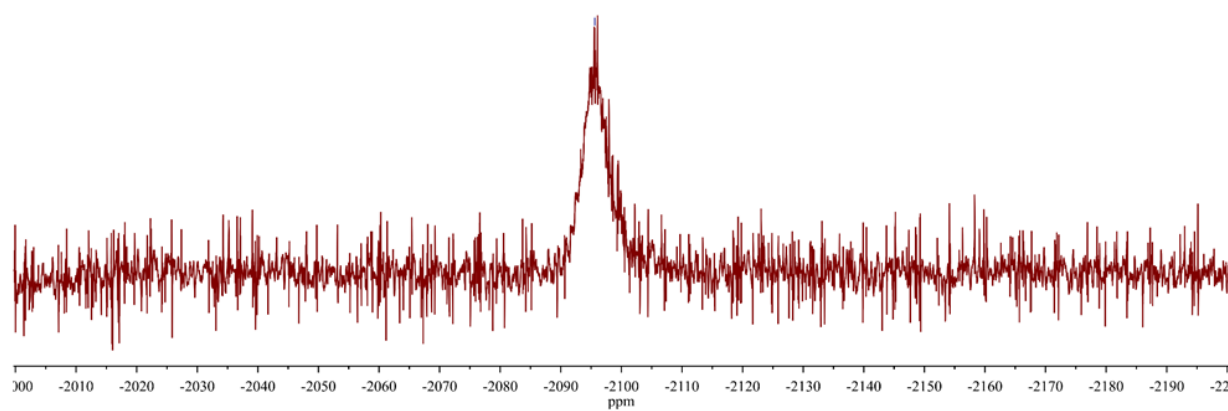
*DMF-d₇ solvent residual at 25 °C

HMQC NMR spectrum of **Pt-12** in DMF-d₇ (The ¹³C peak signals between 127.30 and 130.15 ppm represent 6 aromatic ¹³C)

^{195}Pt NMR (129 MHz, DMF- d_7)

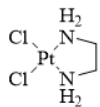


Pt-12

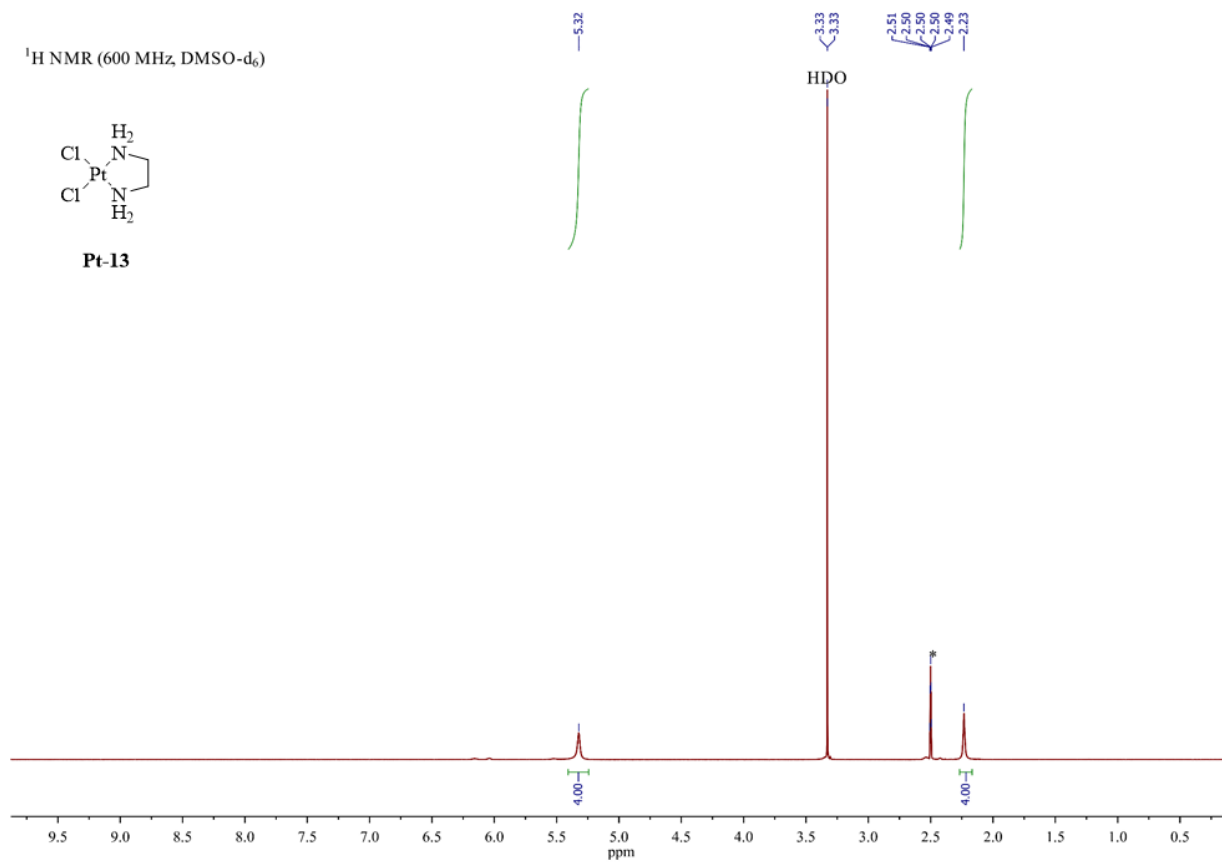


^{195}Pt NMR spectrum of **Pt-12** in DMF- d_7

¹H NMR (600 MHz, DMSO-d₆)

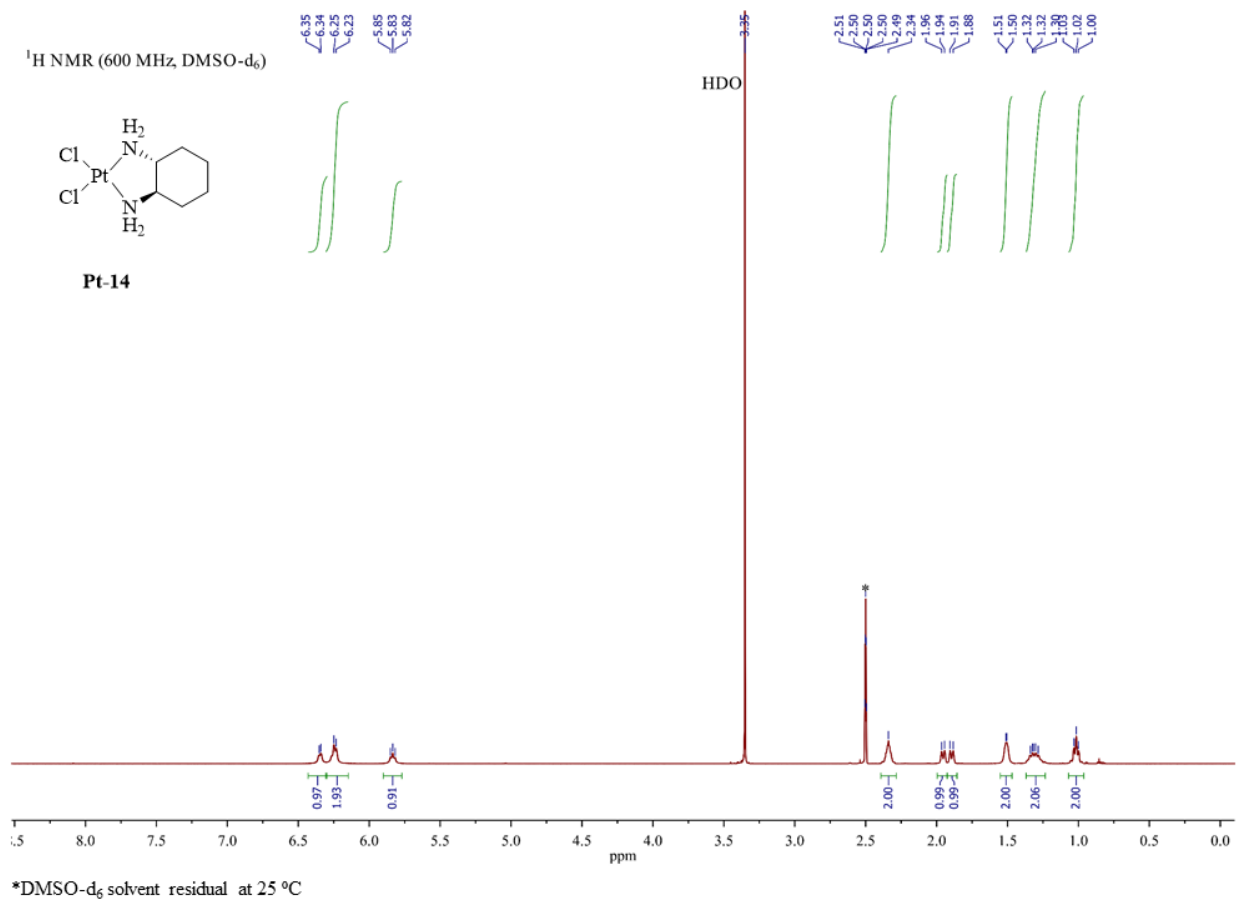


Pt-13

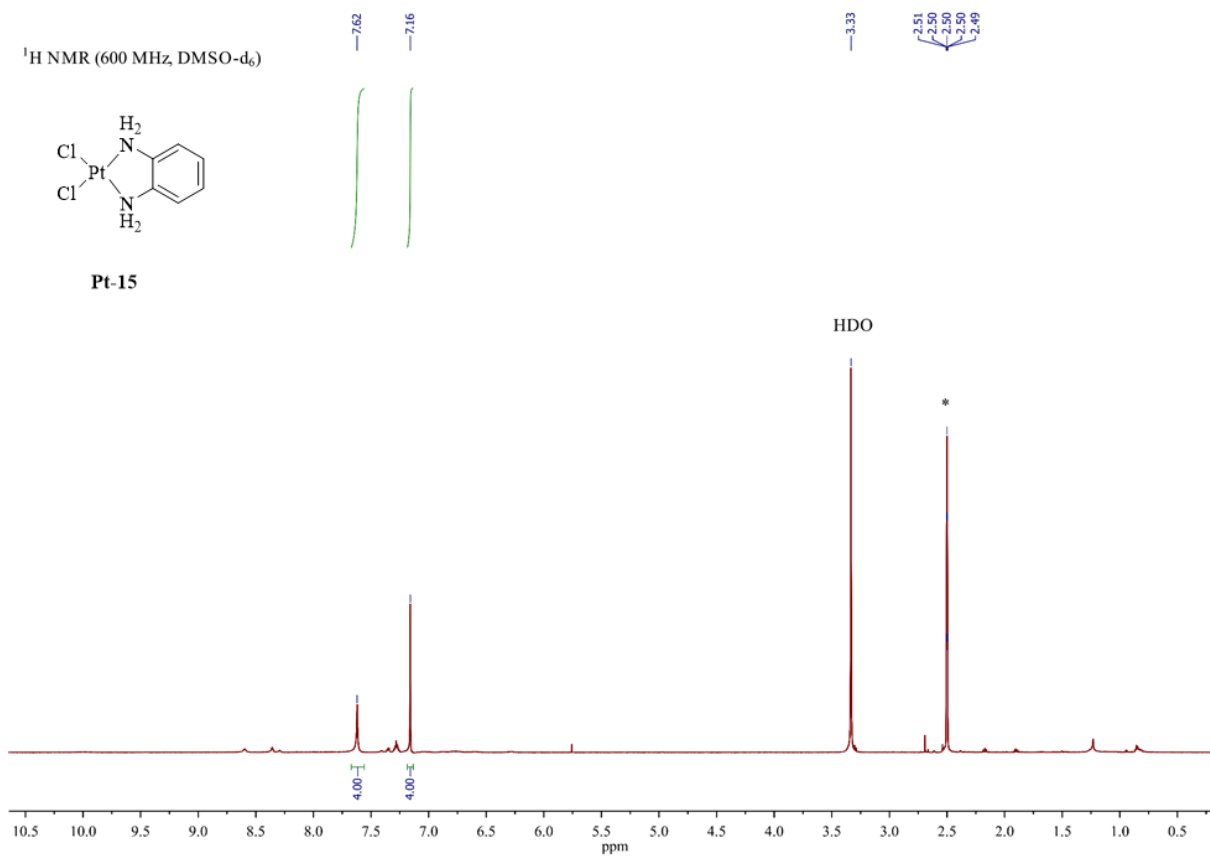


*DMSO-d₆ solvent residual at 25 °C

¹H NMR spectrum of **Pt-13** in DMSO-d₆

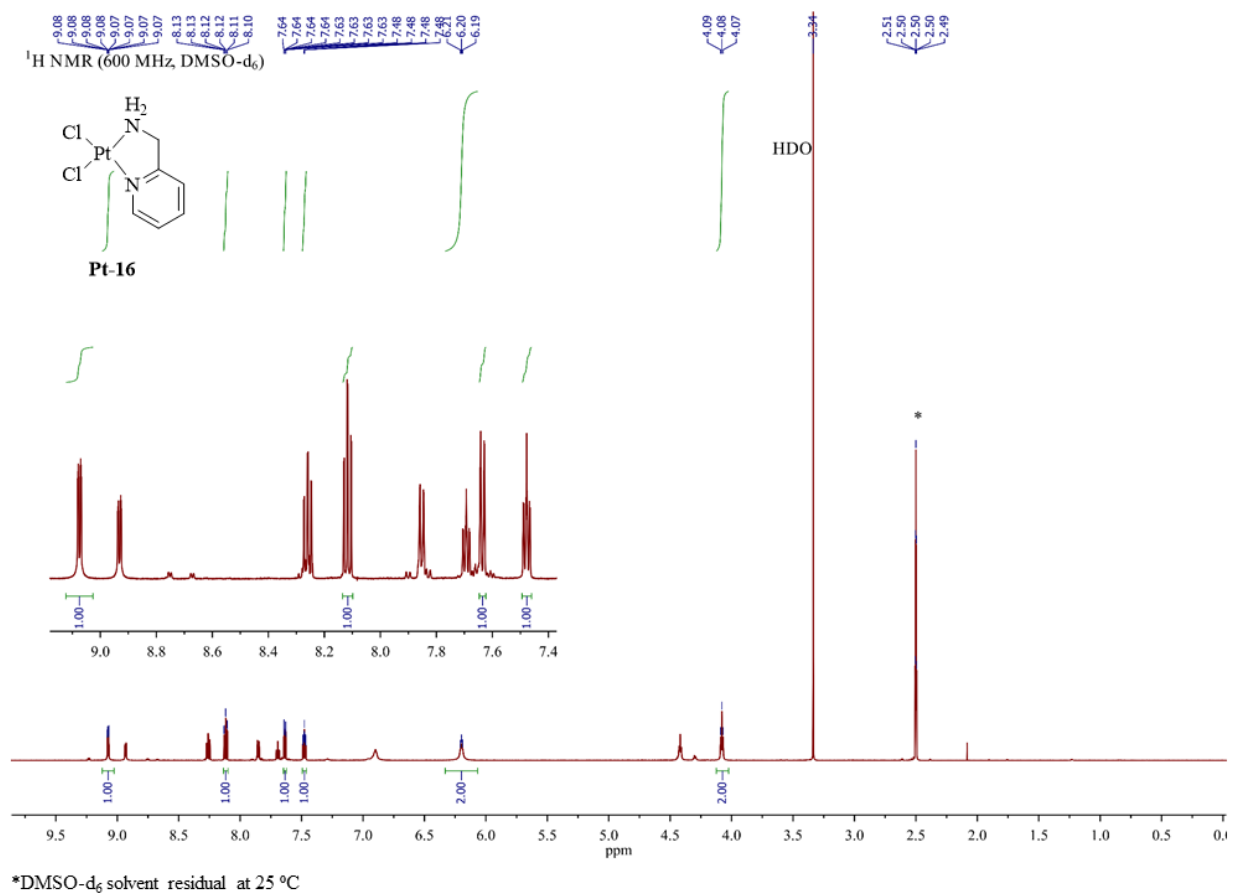


¹H NMR spectrum of **Pt-14** in DMSO-d₆

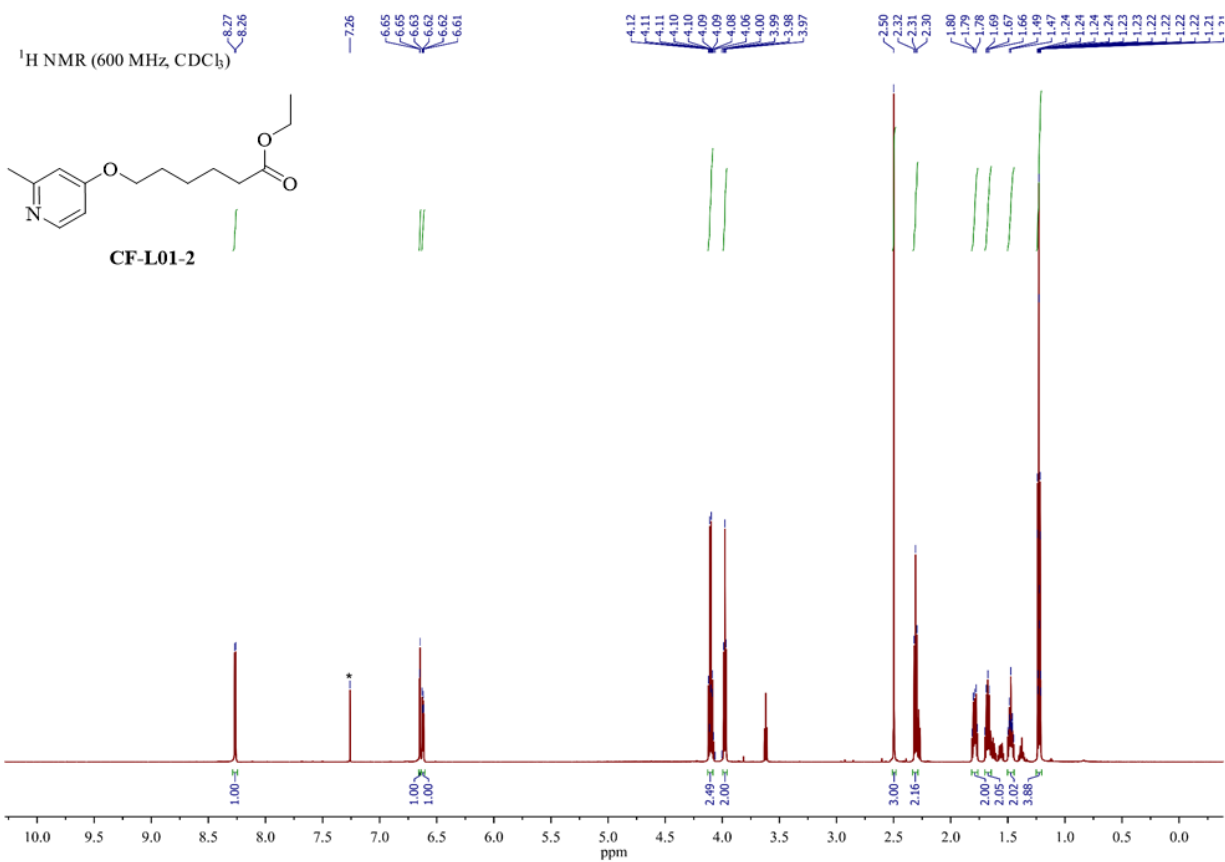


*DMSO-d₆ solvent residual at 25 °C

¹H NMR spectrum of **Pt-15** in DMSO-d₆

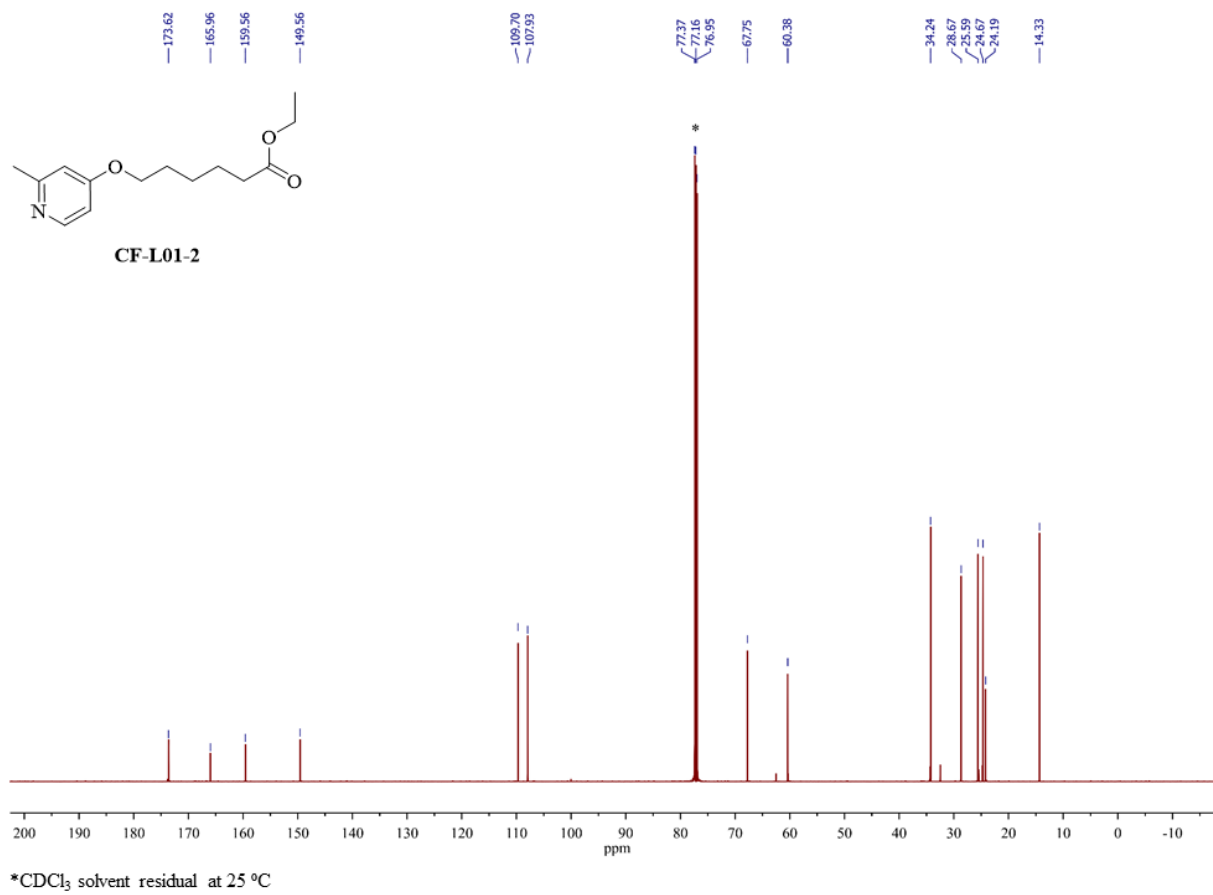


¹H NMR spectrum of **Pt-16** in DMSO-d₆

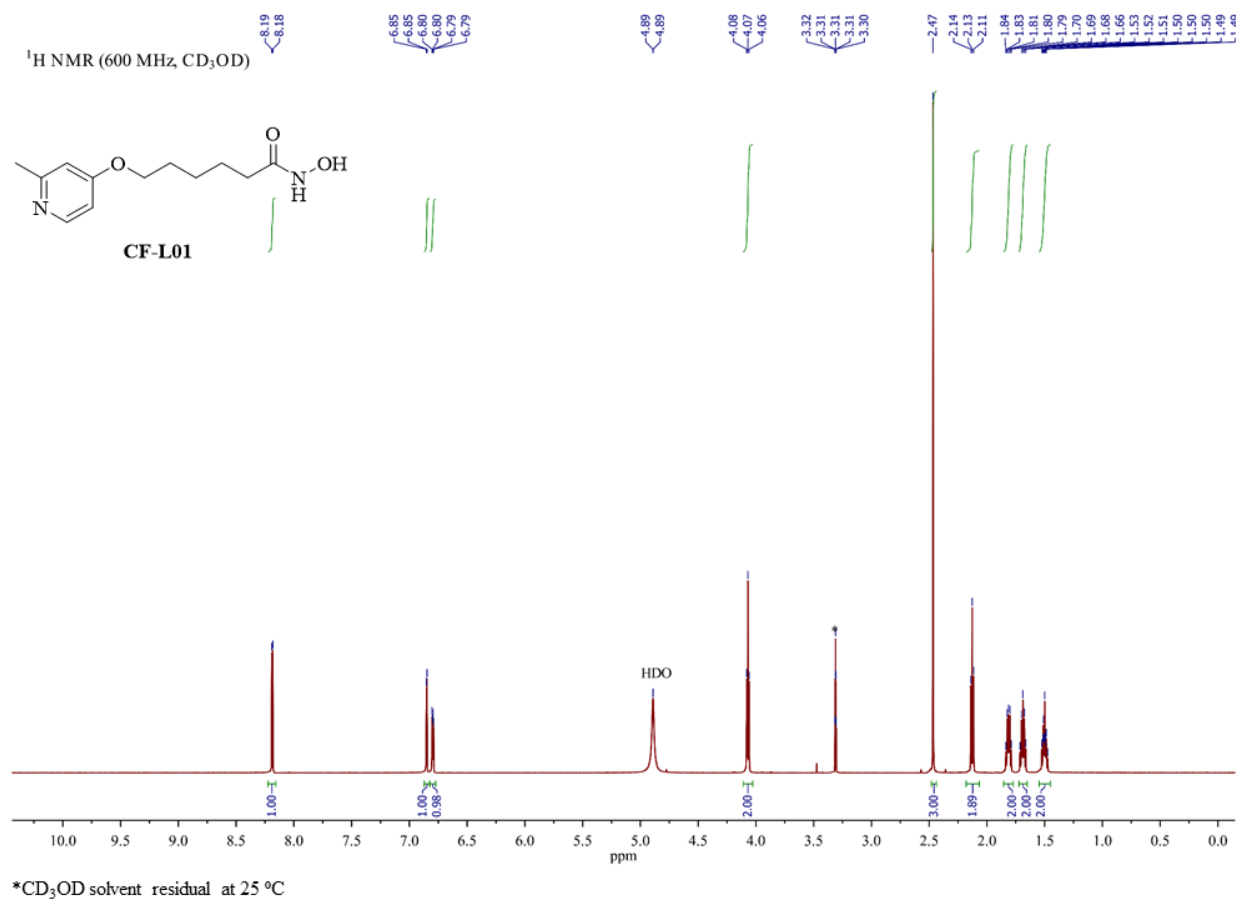


*CDCl₃ solvent residual at 25 °C

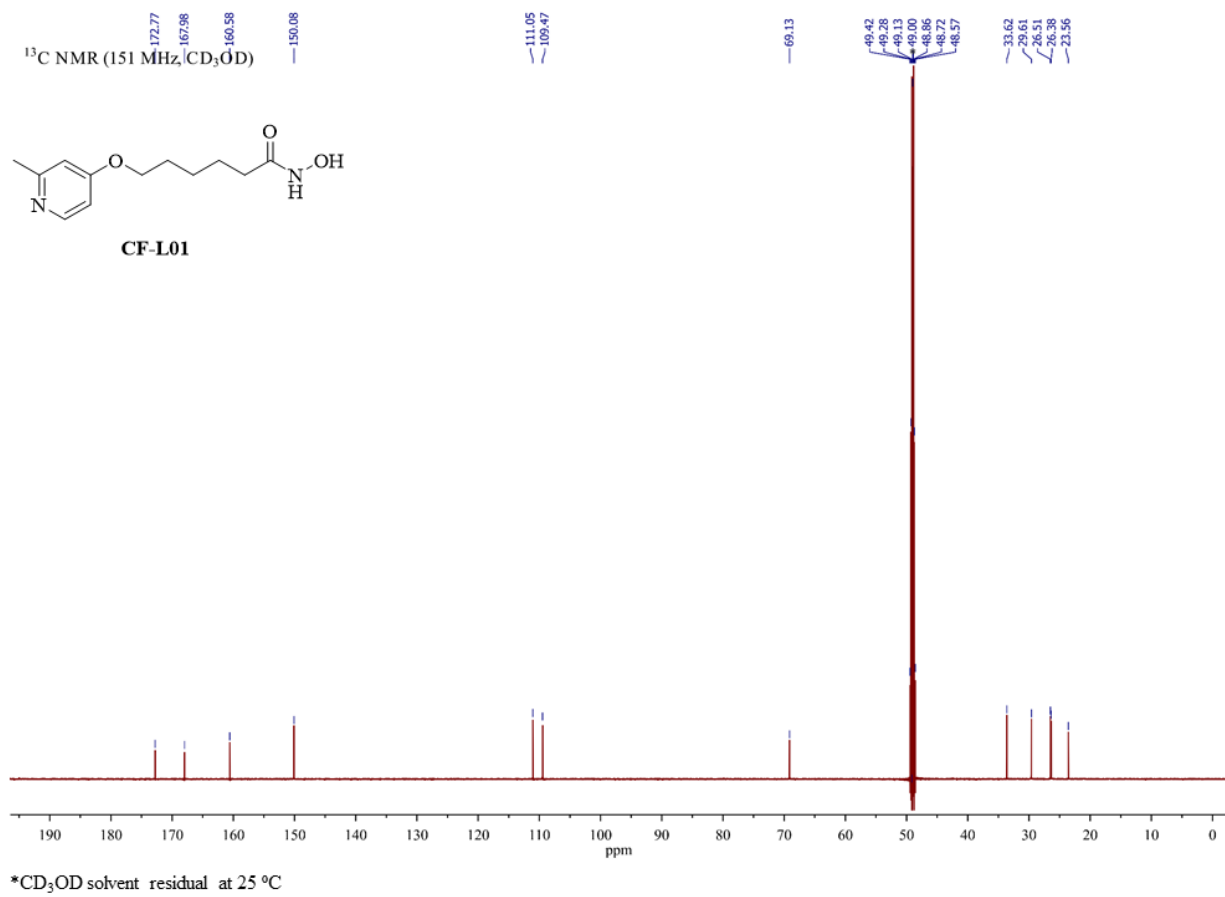
¹H NMR spectrum of **CF-L01-2** in CDCl₃



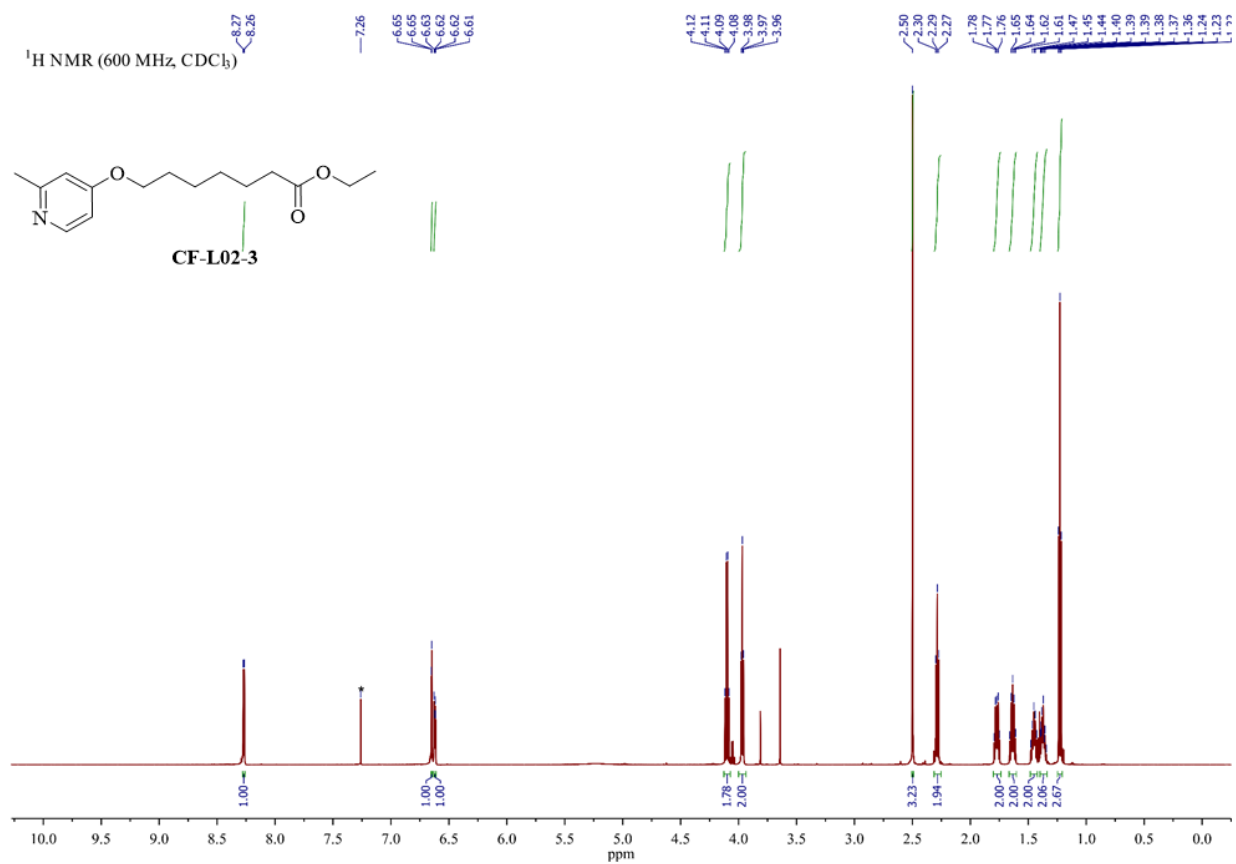
¹³C NMR spectrum of **CF-L01-2** in CDCl₃



¹H NMR spectrum of **CF-L01** in CD₃OD

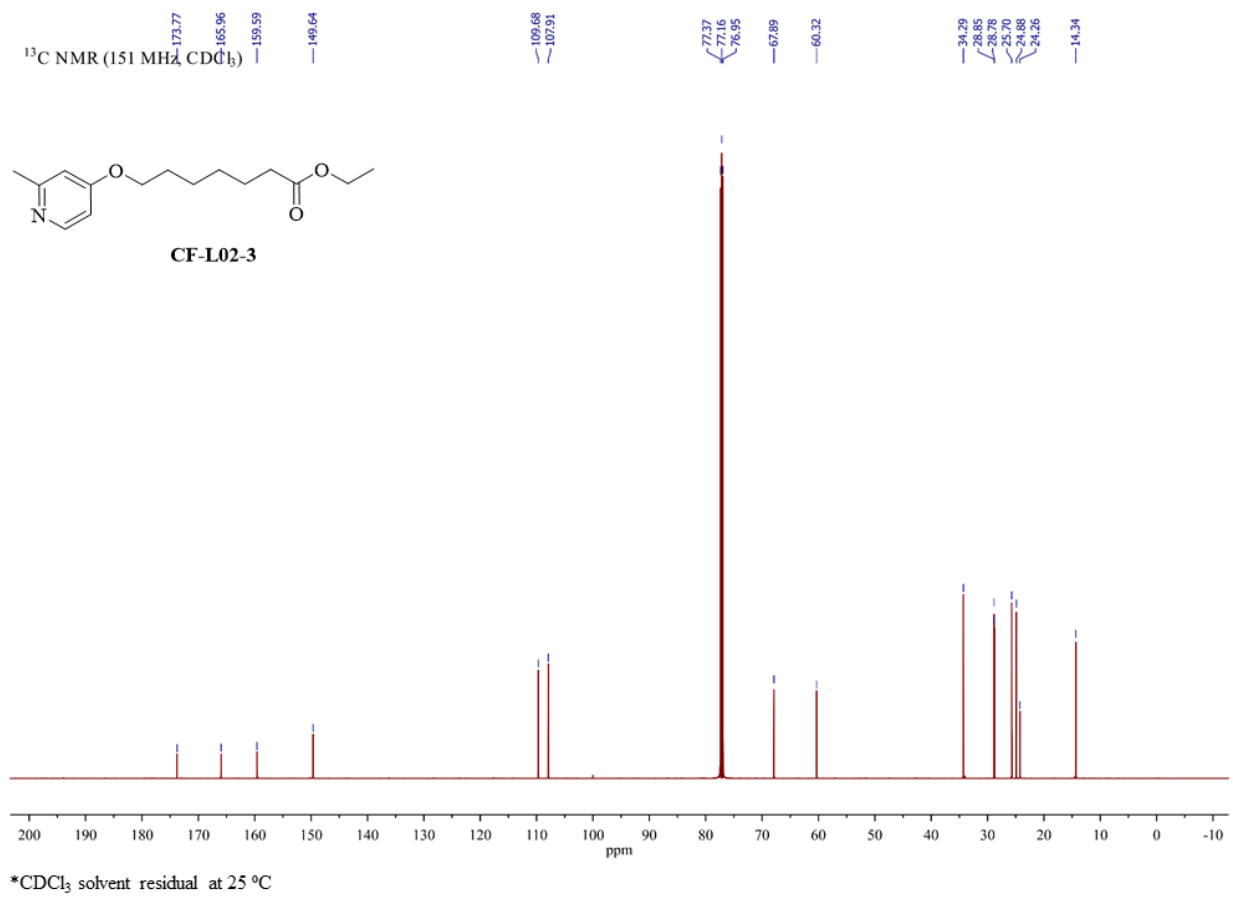


¹³C NMR spectrum of **CF-L01** in CD₃OD

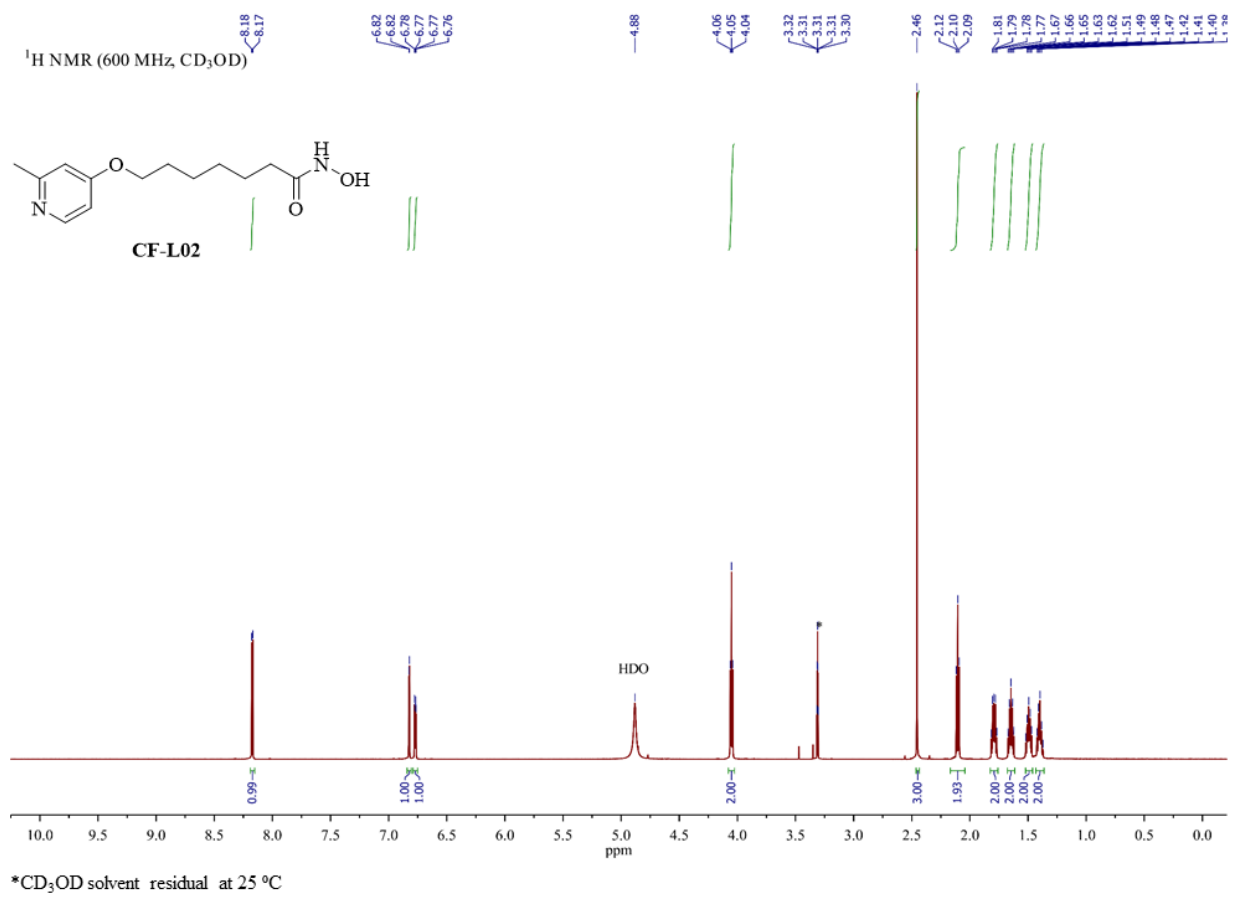


*CDCl₃ solvent residual at 25 °C

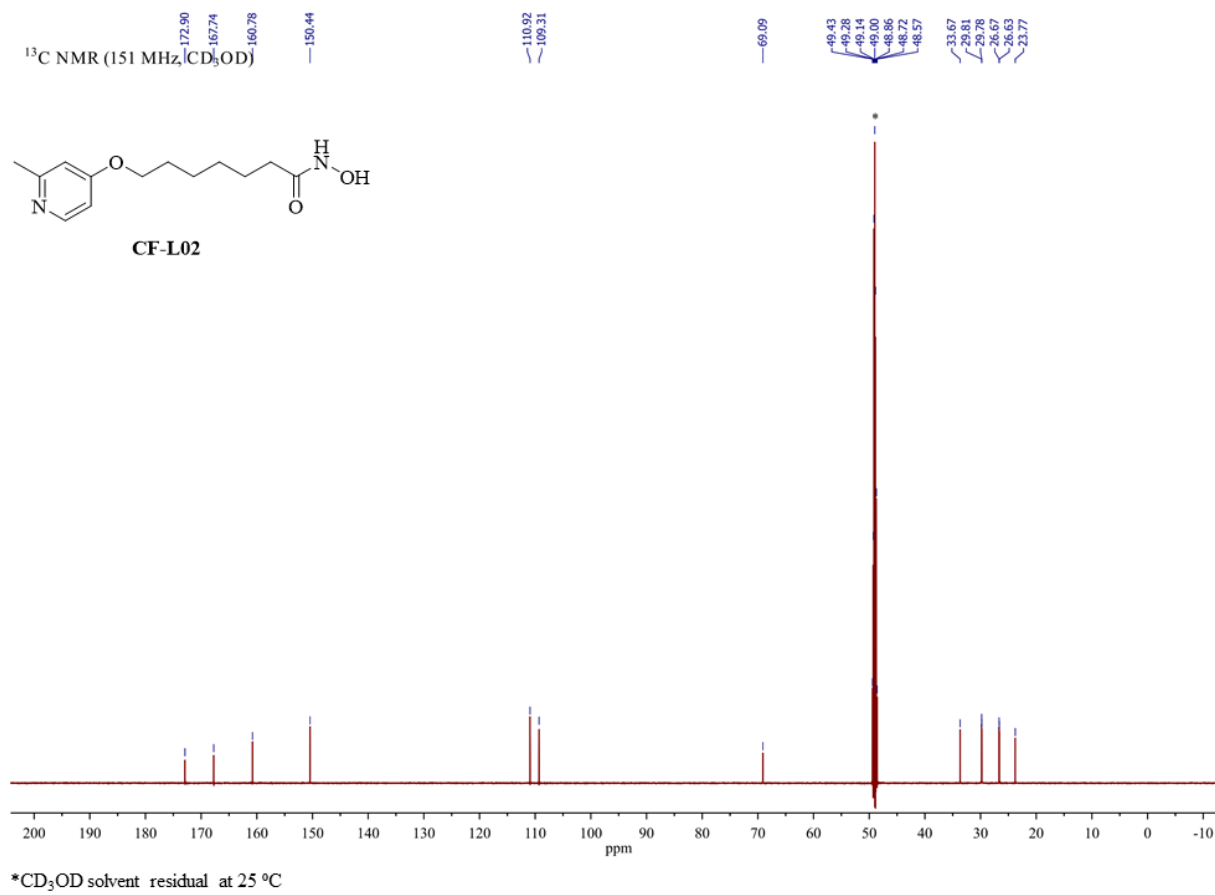
¹H NMR spectrum of CF-L02-3 in CDCl₃



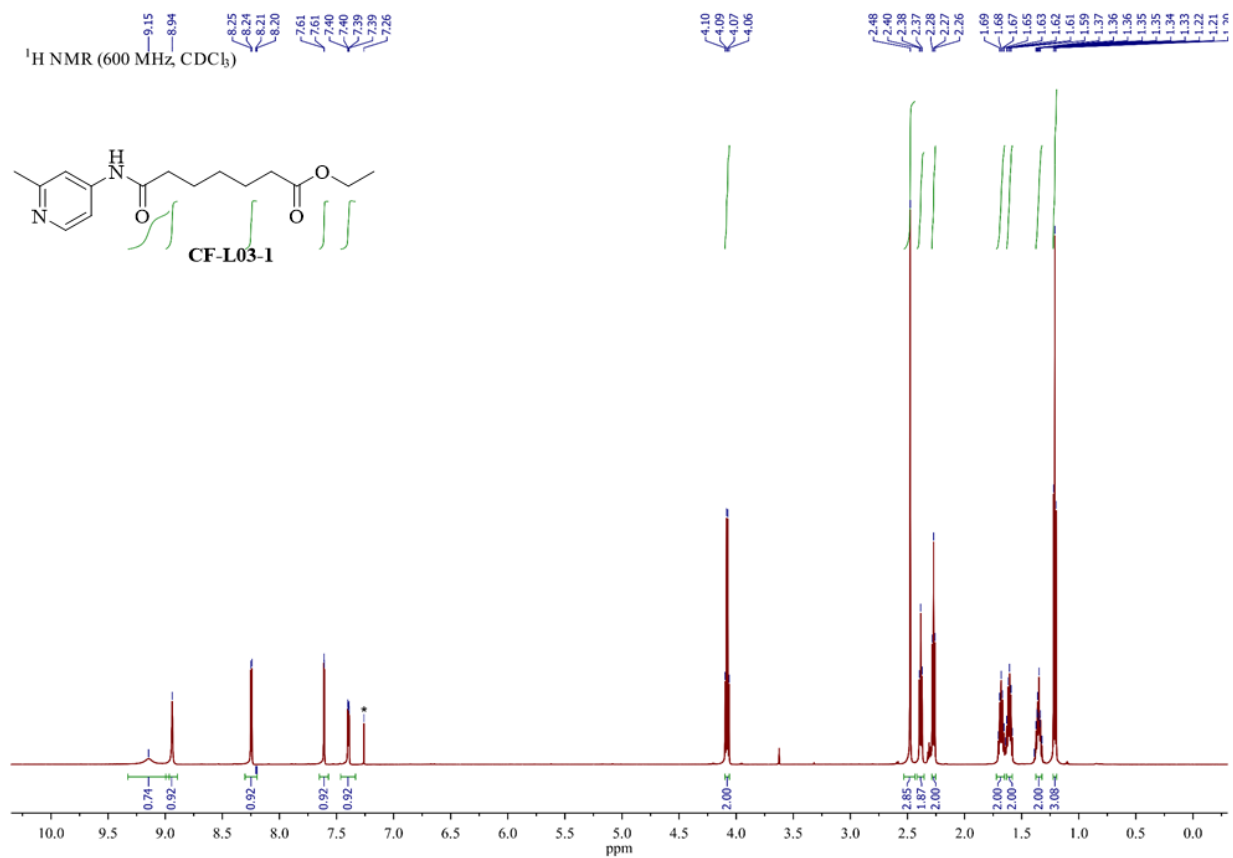
¹³C NMR spectrum of CF-L02-3 in CDCl₃



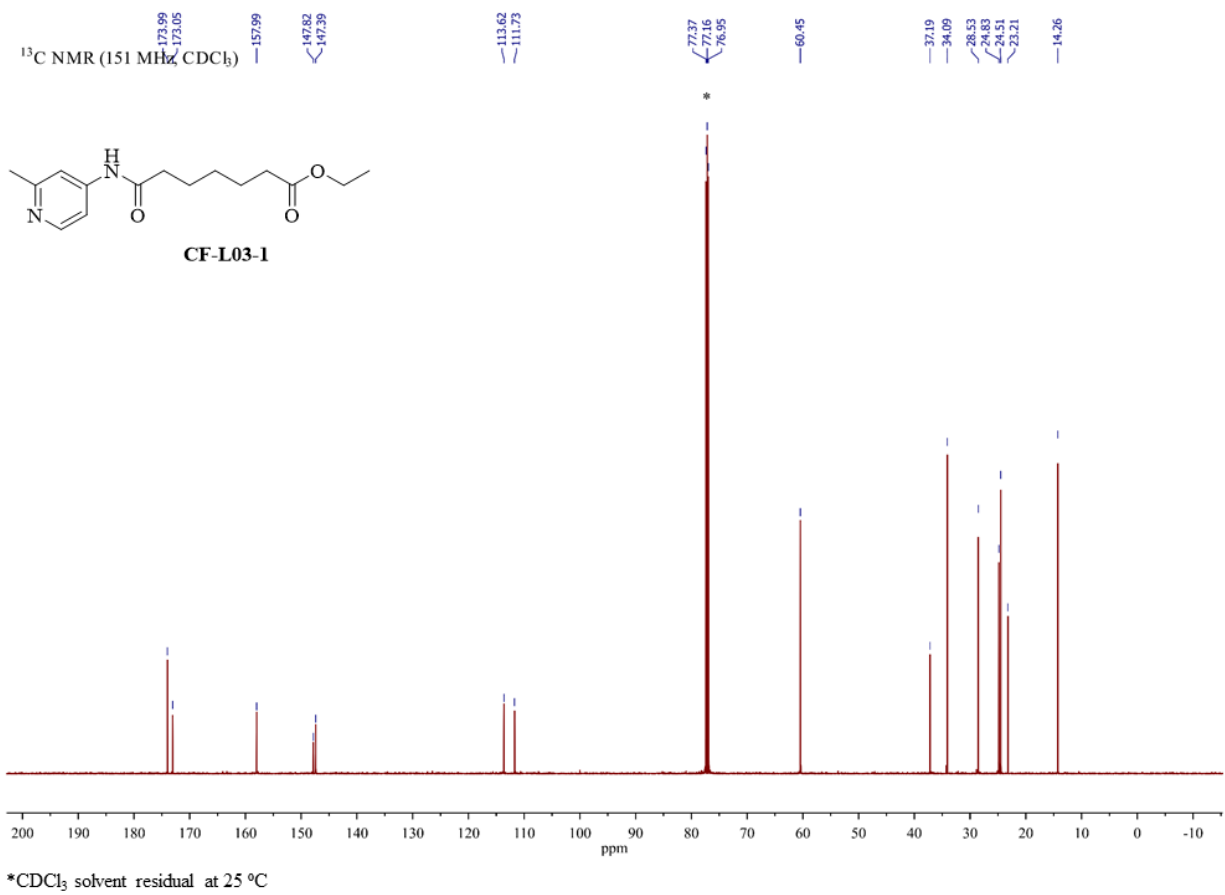
¹H NMR spectrum of **CF-L02** in CD₃OD



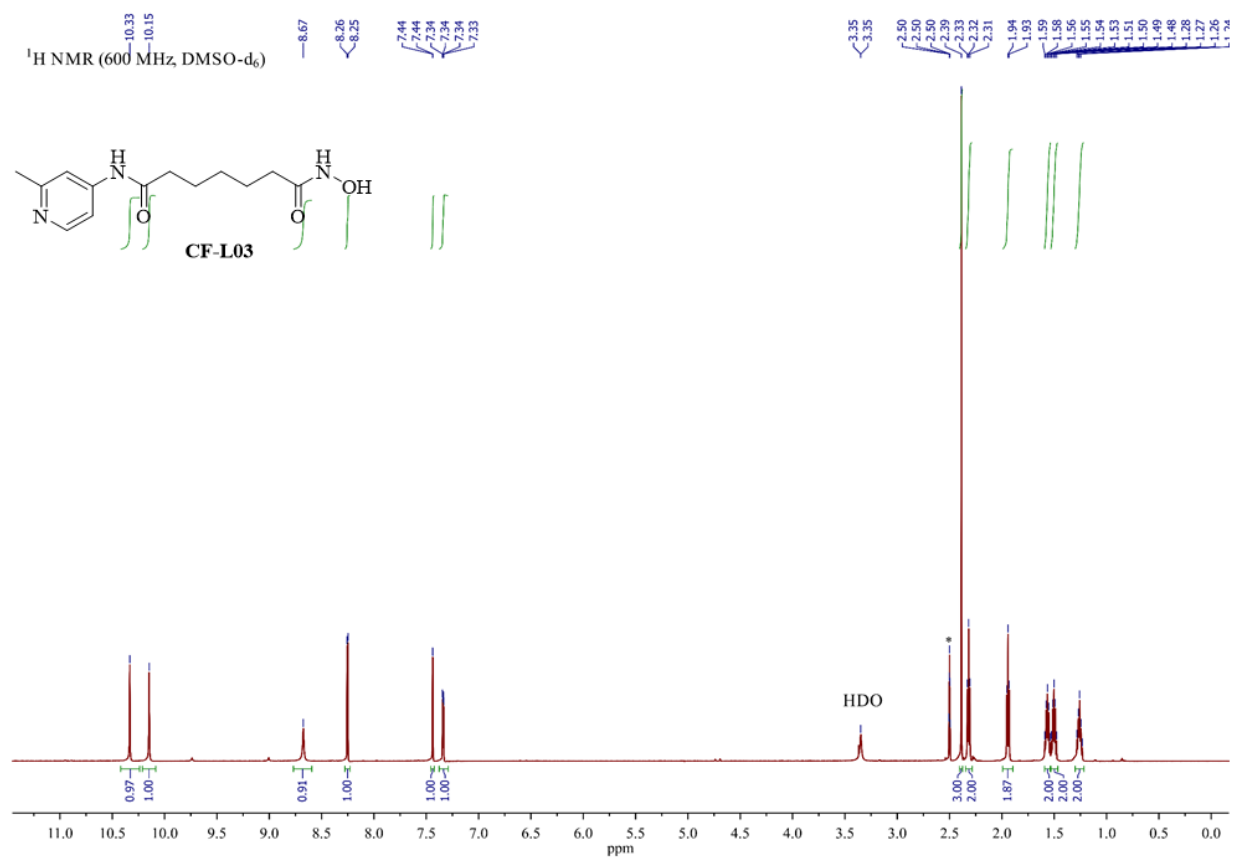
¹³C NMR spectrum of **CF-L02** in CD₃OD



¹H NMR spectrum of CF-L03-1 in CDCl₃

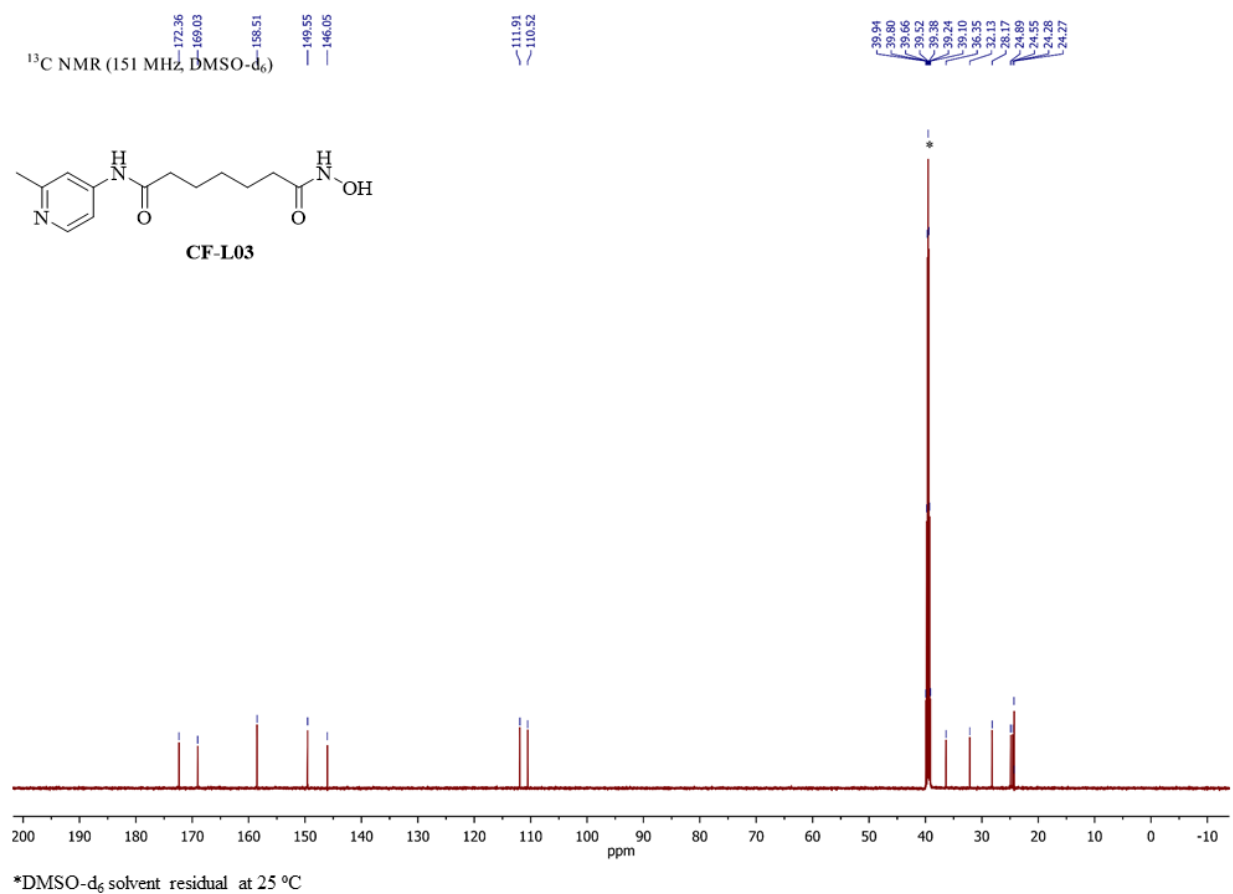


¹³C NMR spectrum of **CF-L03-1** in CDCl₃

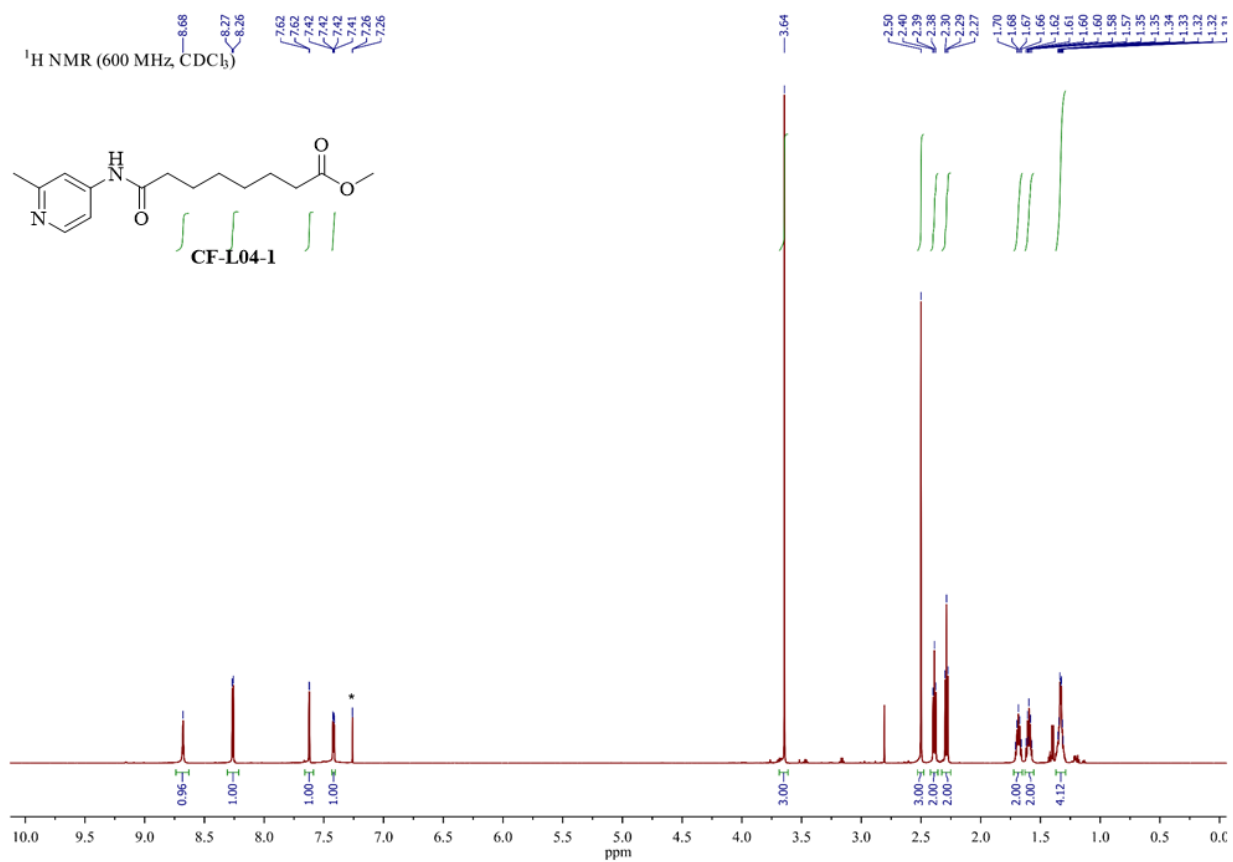


*DMSO-d₆ solvent residual at 25 °C

¹H NMR spectrum of CF-L03 in DMSO-d₆

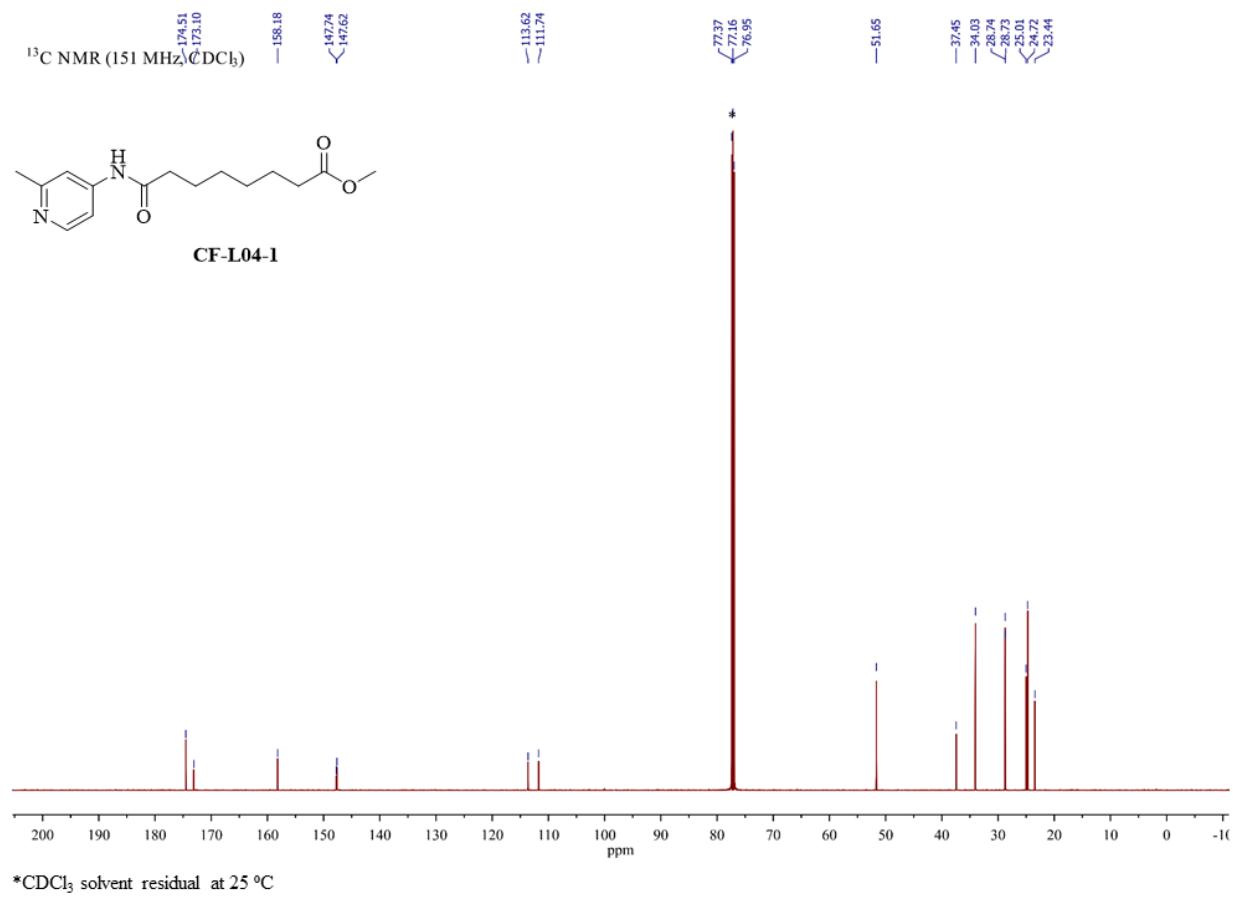


¹³C NMR spectrum of CF-L03 in DMSO-d₆

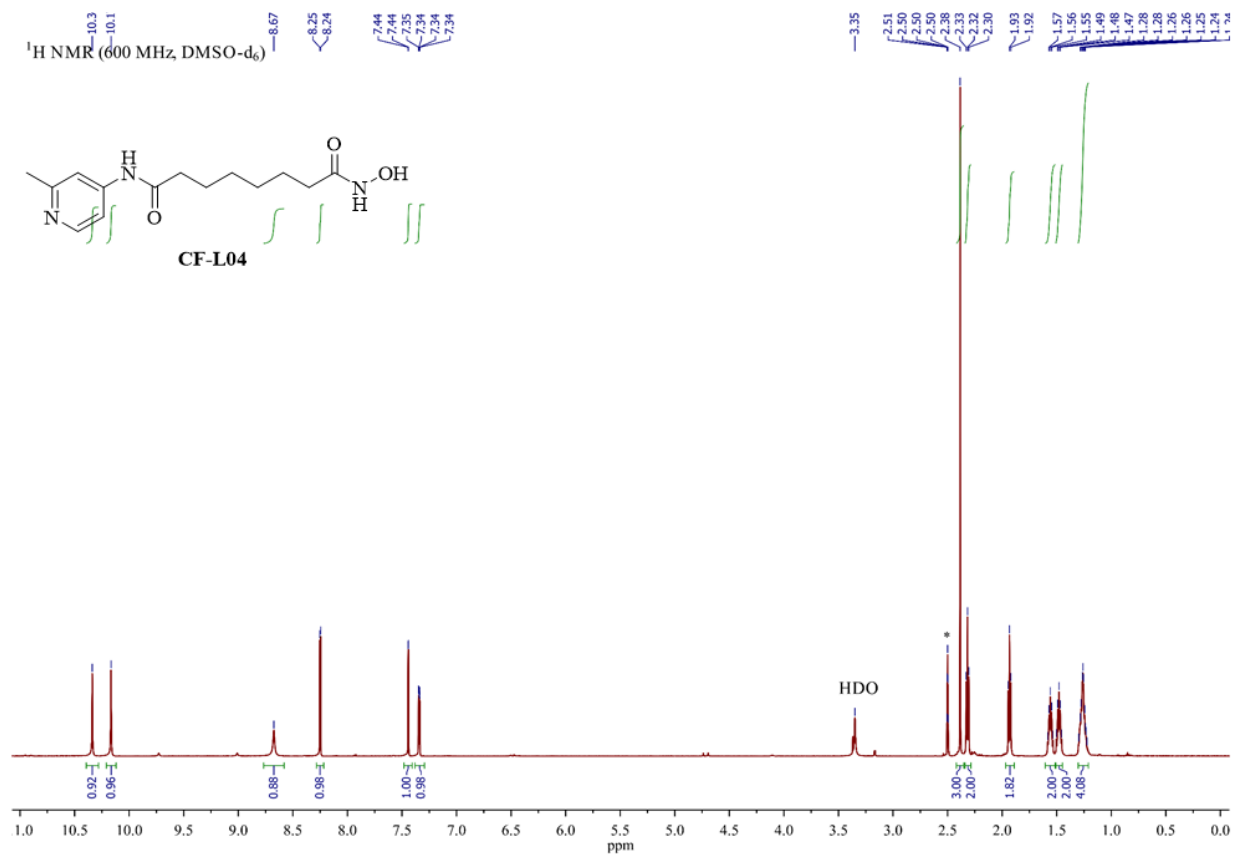


*CDCl₃ solvent residual at 25 °C

¹H NMR spectrum of CF-L04-1 in CDCl₃

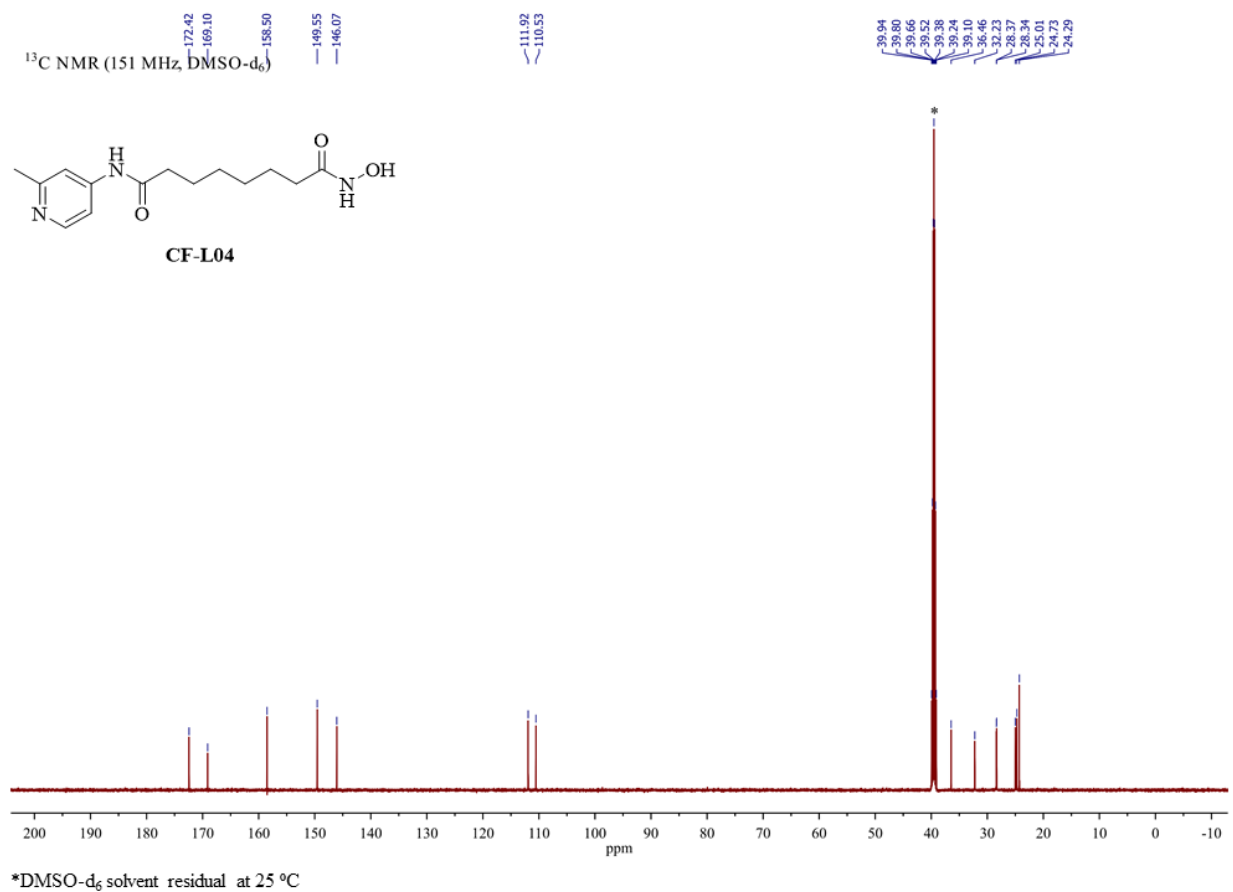


¹³C NMR spectrum of CF-L04-1 in CDCl₃

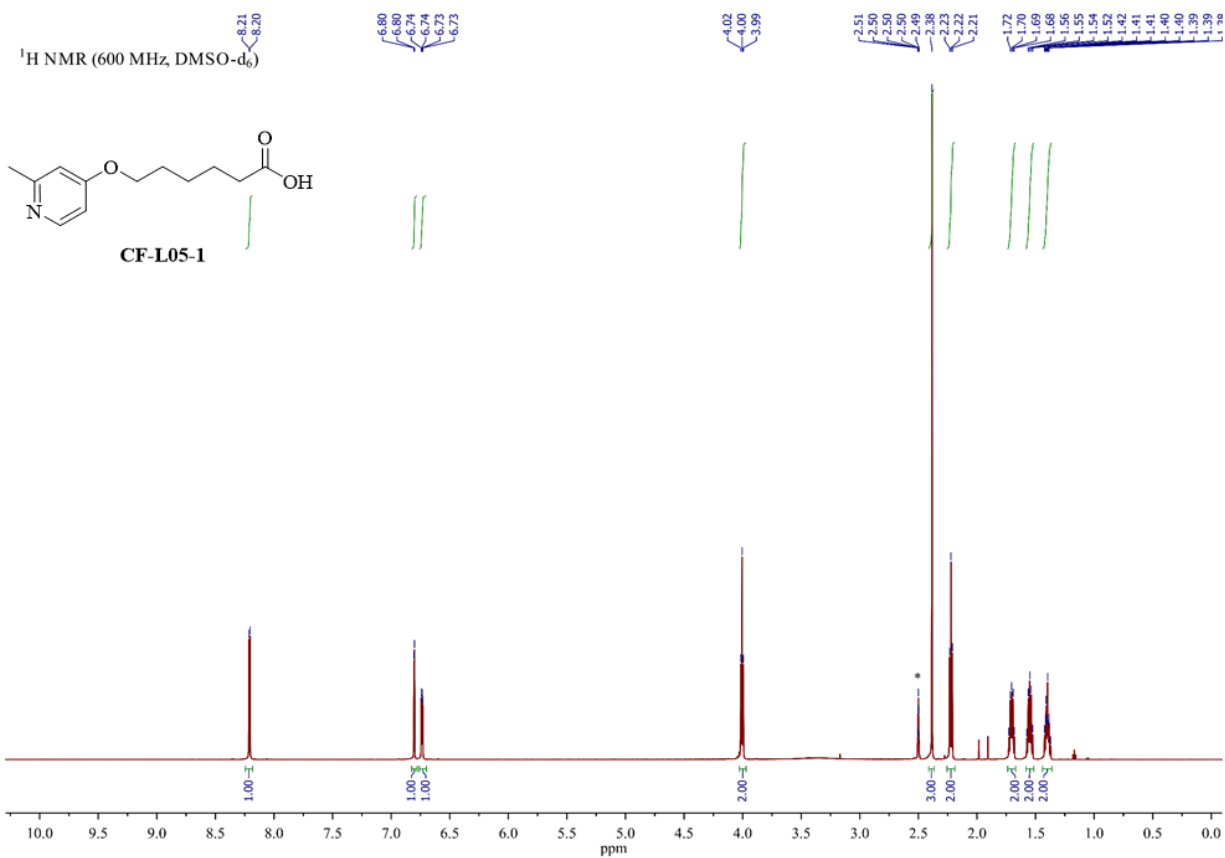


*DMSO-d₆ solvent residual at 25 °C

¹H NMR spectrum of **CF-L04** in DMSO-d₆

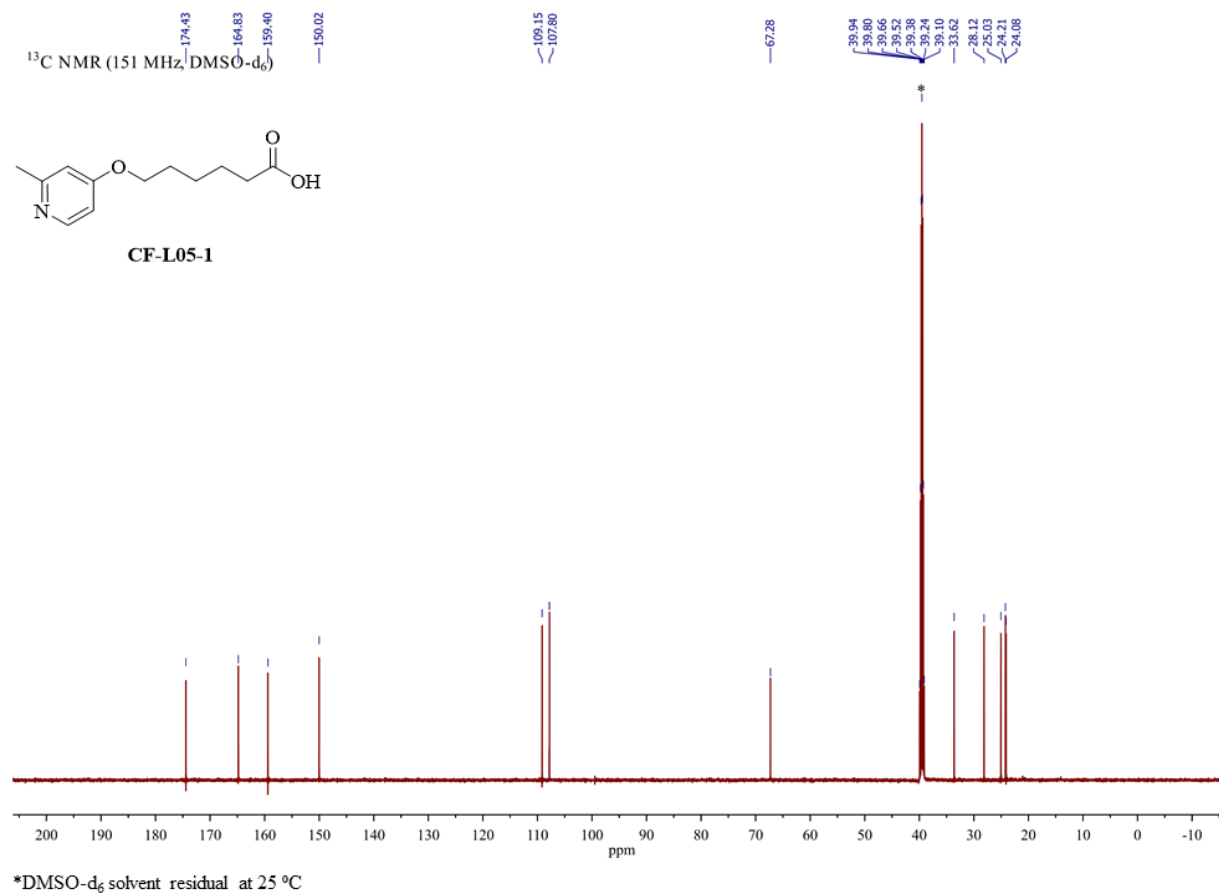


¹³C NMR spectrum of CF-L04 in DMSO-d₆

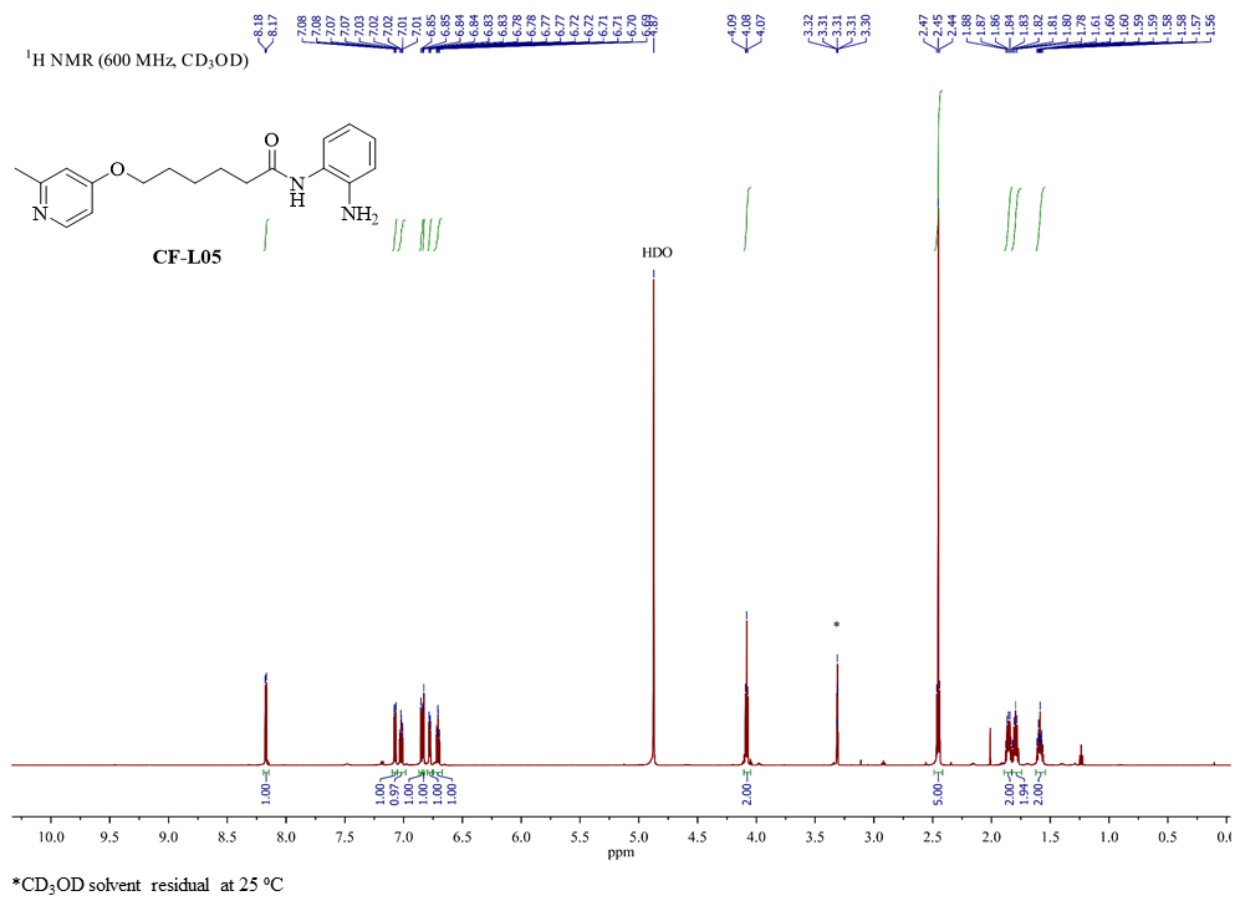


*DMSO-d₆ solvent residual at 25 °C

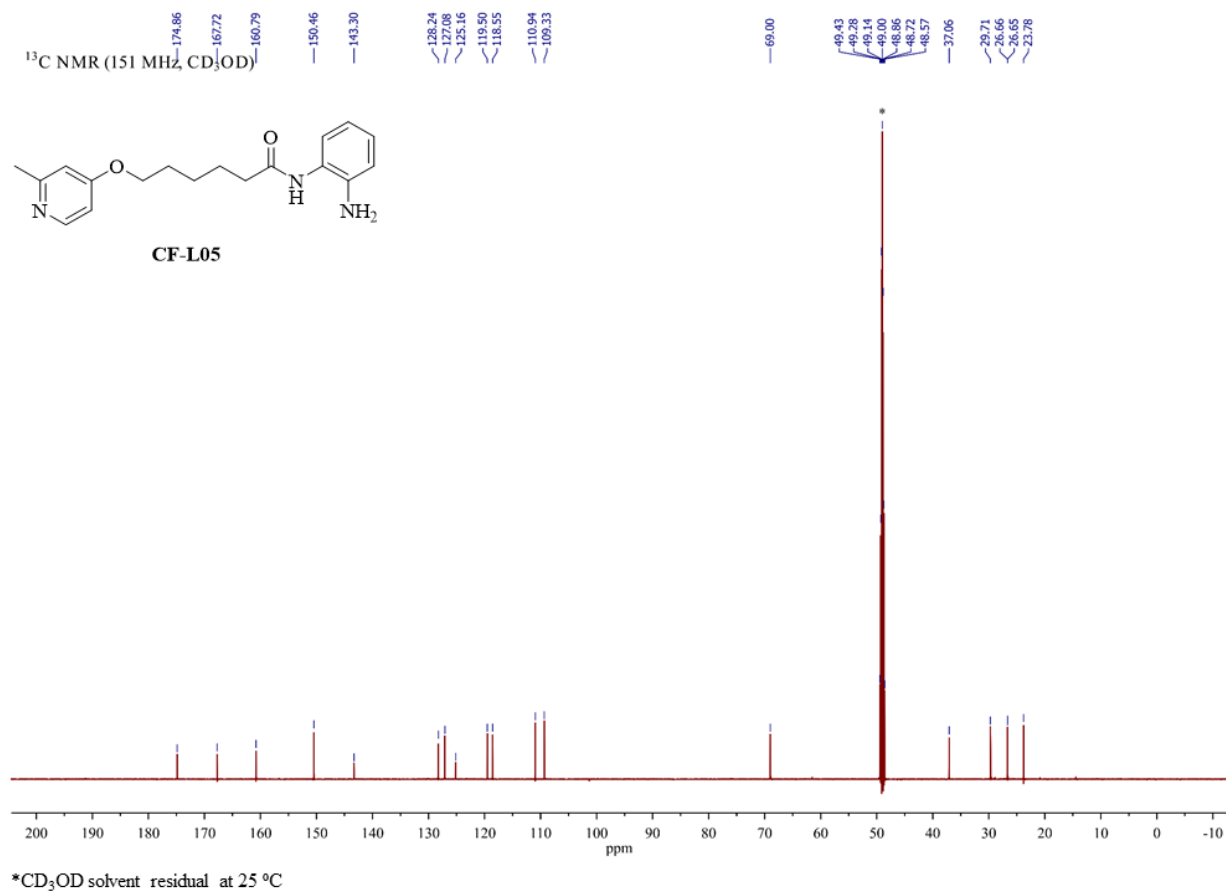
¹H NMR spectrum of **CF-L05-1** in DMSO-d₆



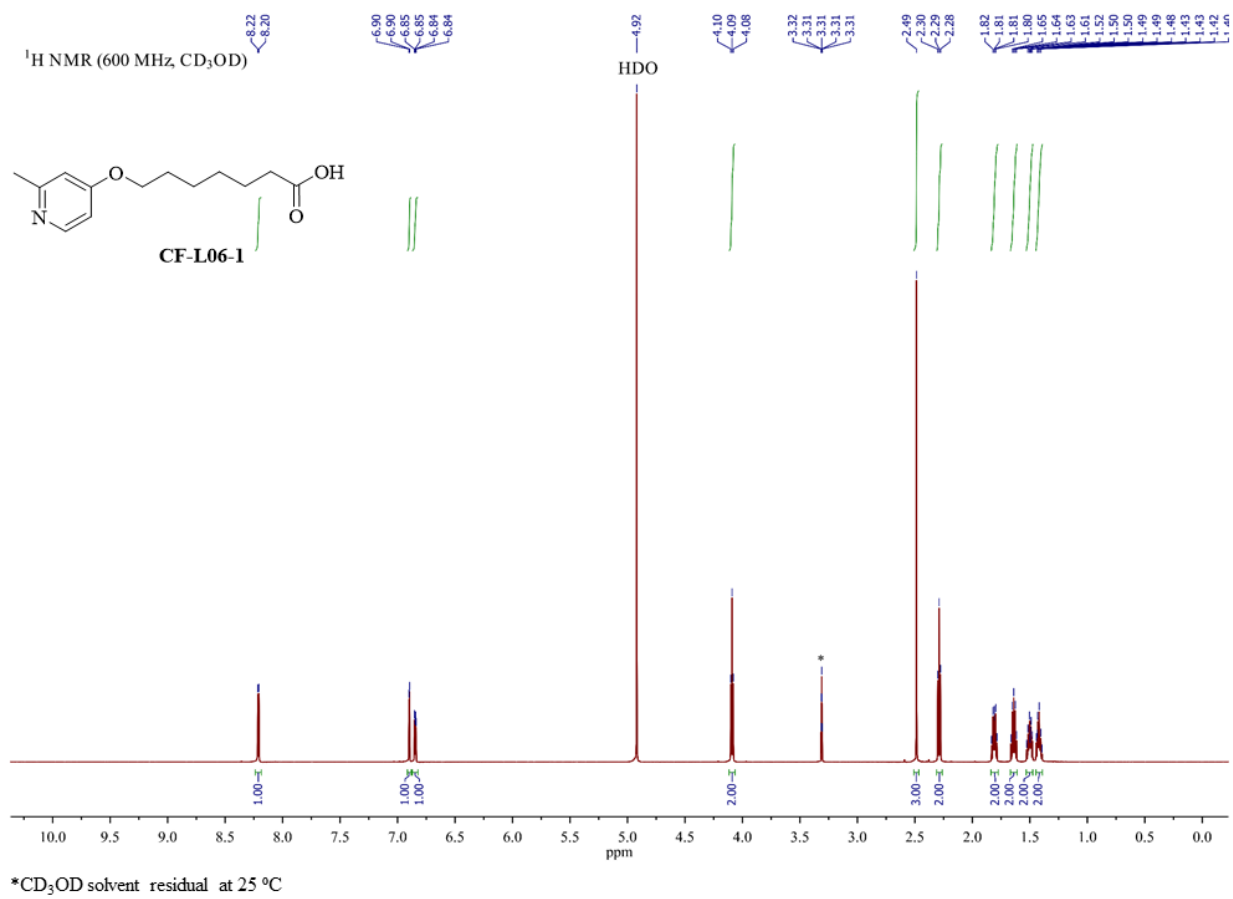
¹³C NMR spectrum of **CF-L05-1** in DMSO-d₆



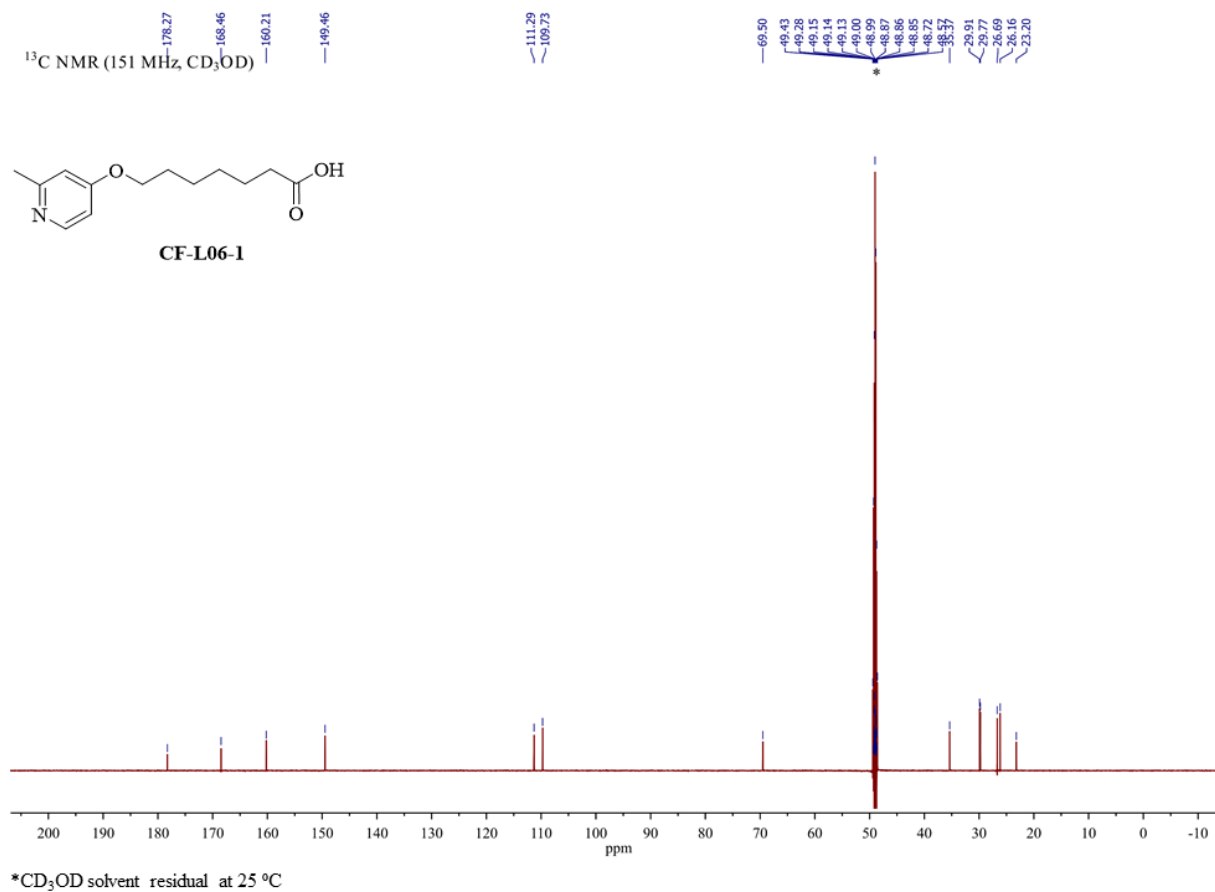
¹H NMR spectrum of CF-L05 in CD₃OD



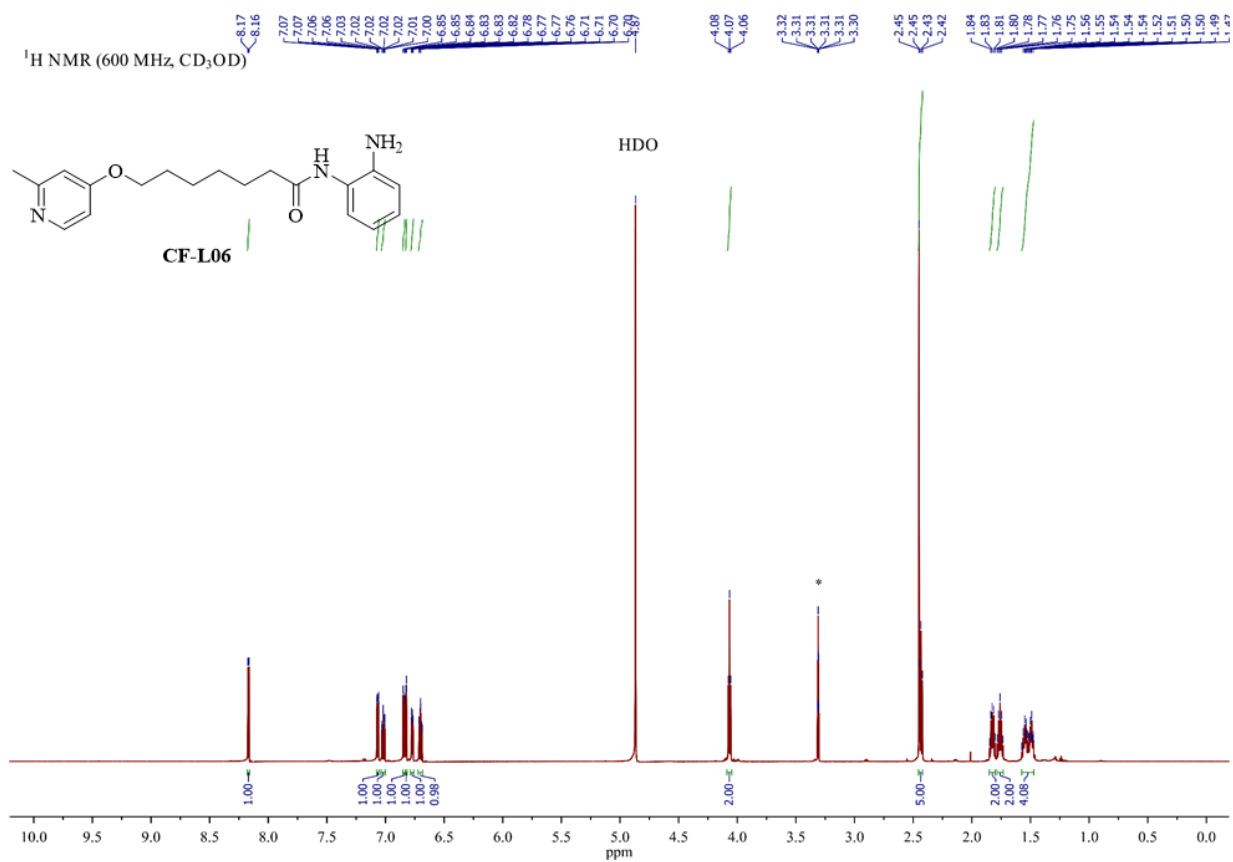
¹³C NMR spectrum of **CF-L05** in CD₃OD



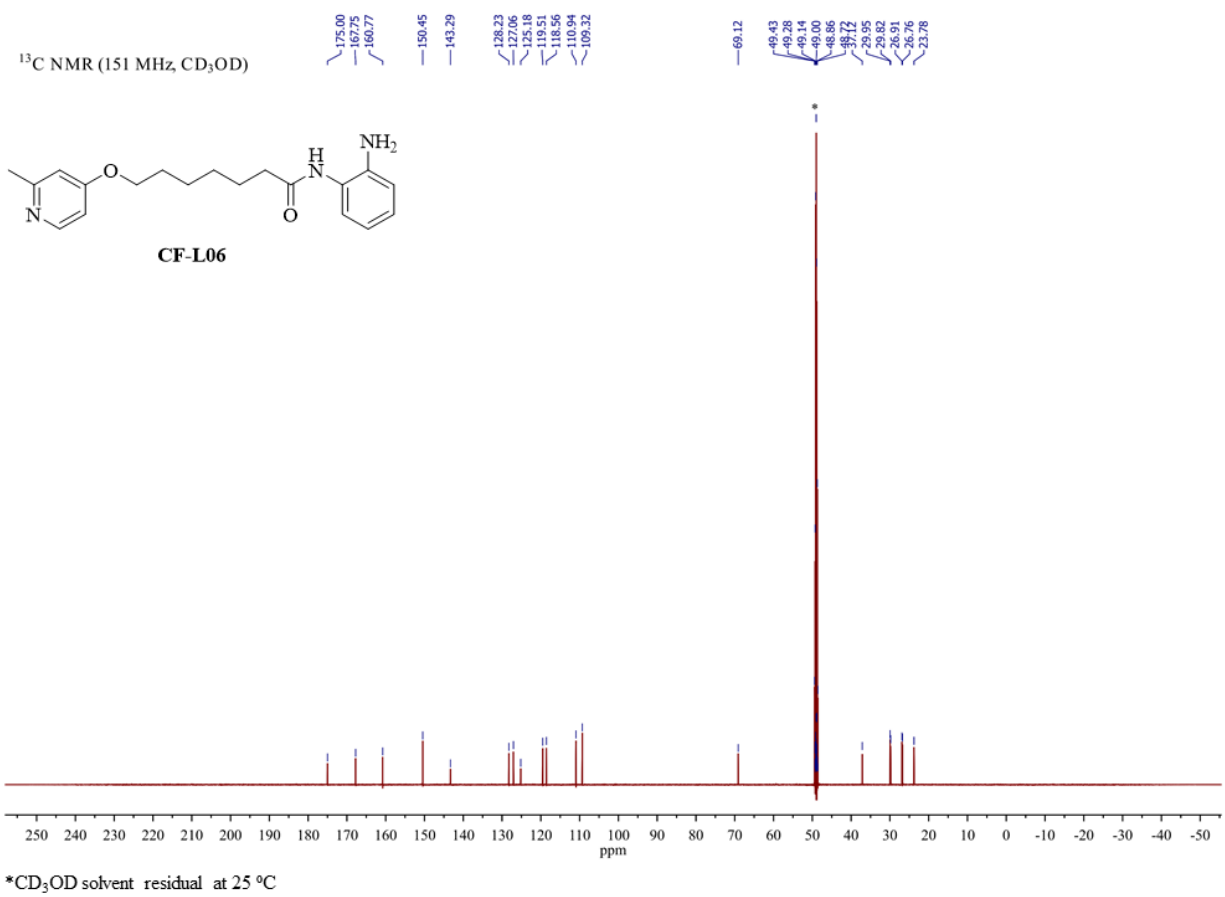
¹H NMR spectrum of CF-L06-1 in CD₃OD



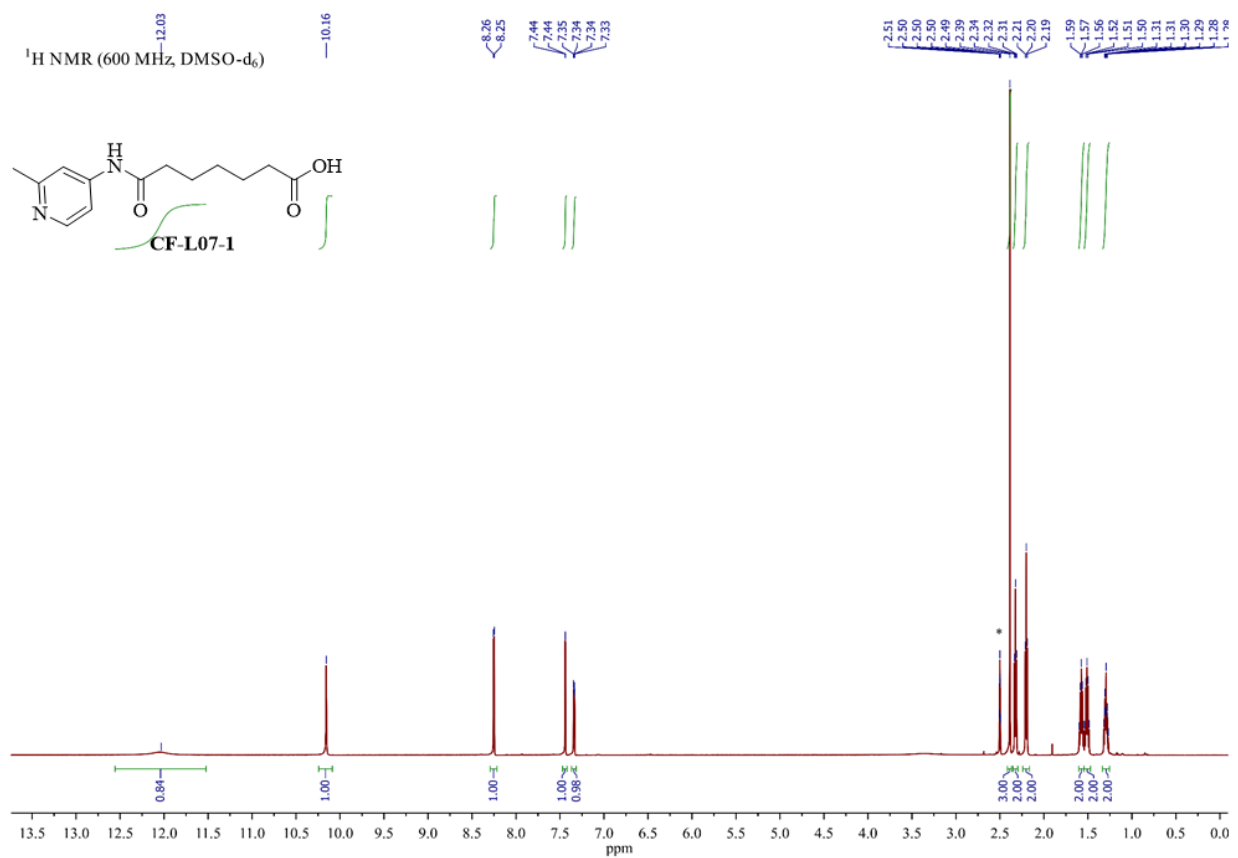
¹³C NMR spectrum of CF-L06-1 in CD₃OD



¹H NMR spectrum of **CF-L06** in CD₃OD

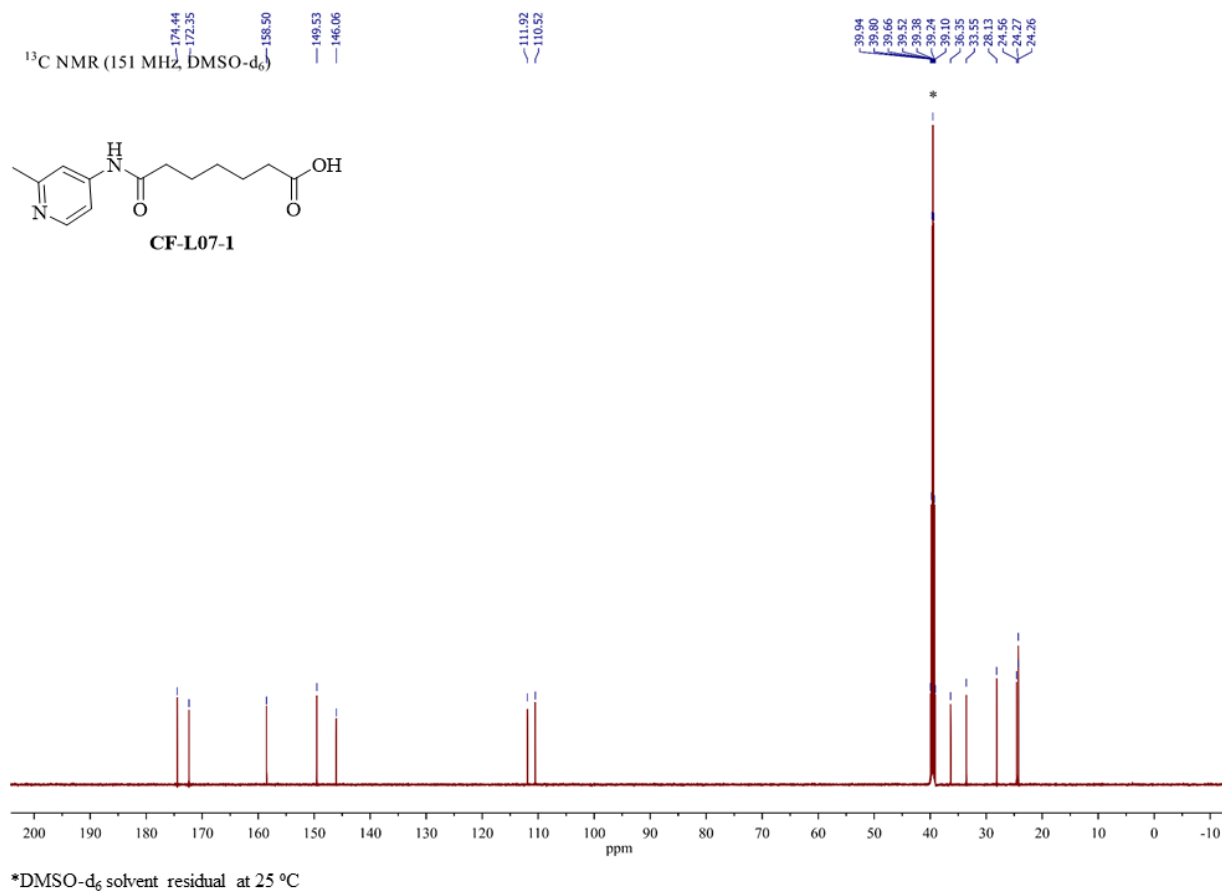


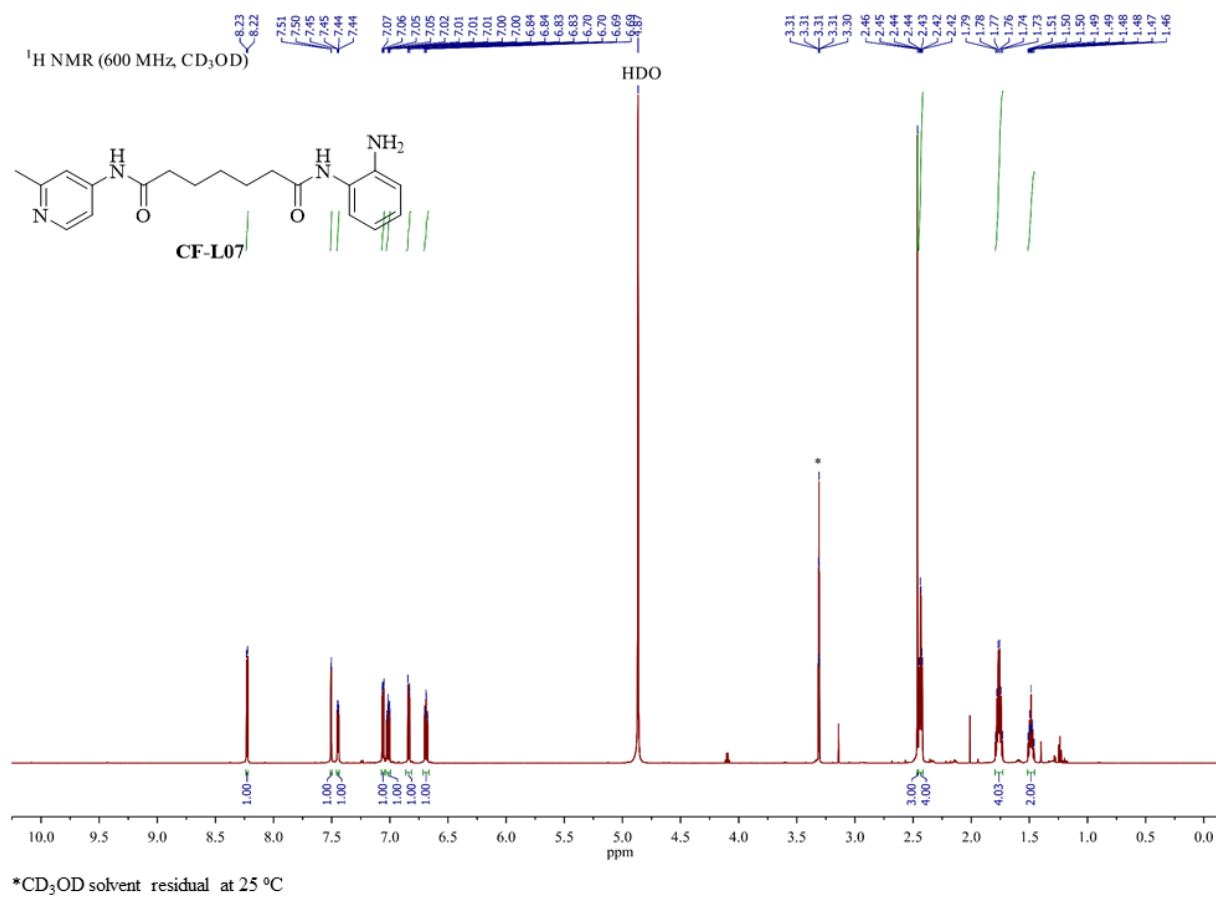
¹³C NMR spectrum of **CF-L06** in CD₃OD



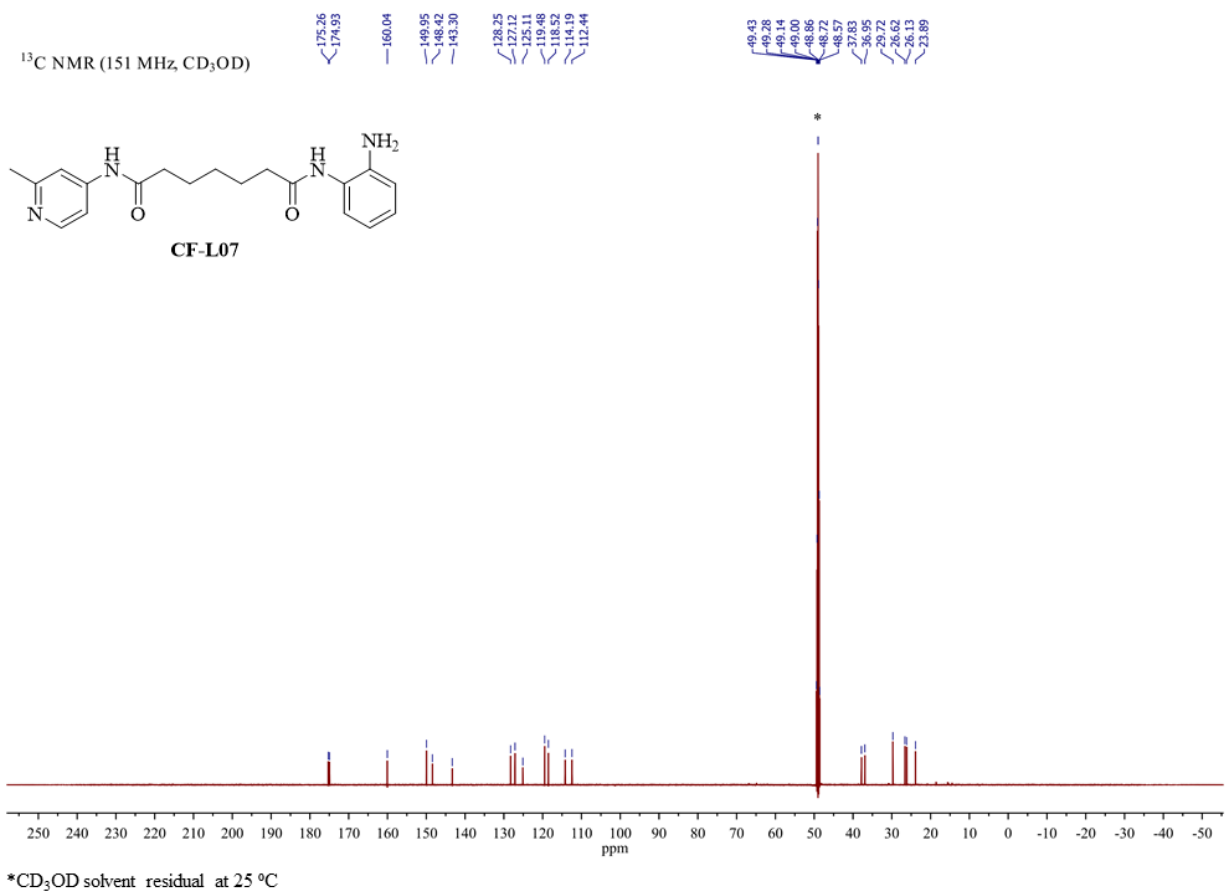
*DMSO-d₆ solvent residual at 25 °C

¹H NMR spectrum of CF-L07-1 in DMSO-d₆

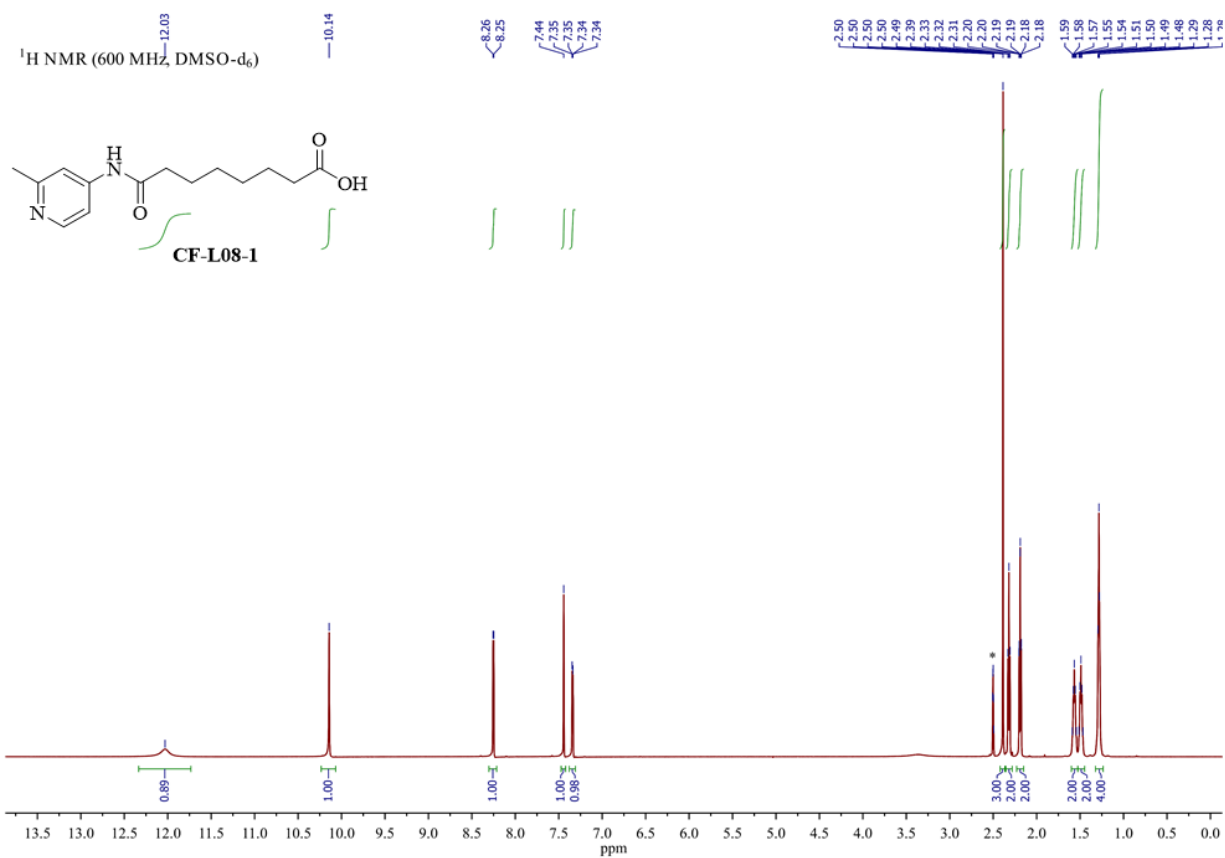




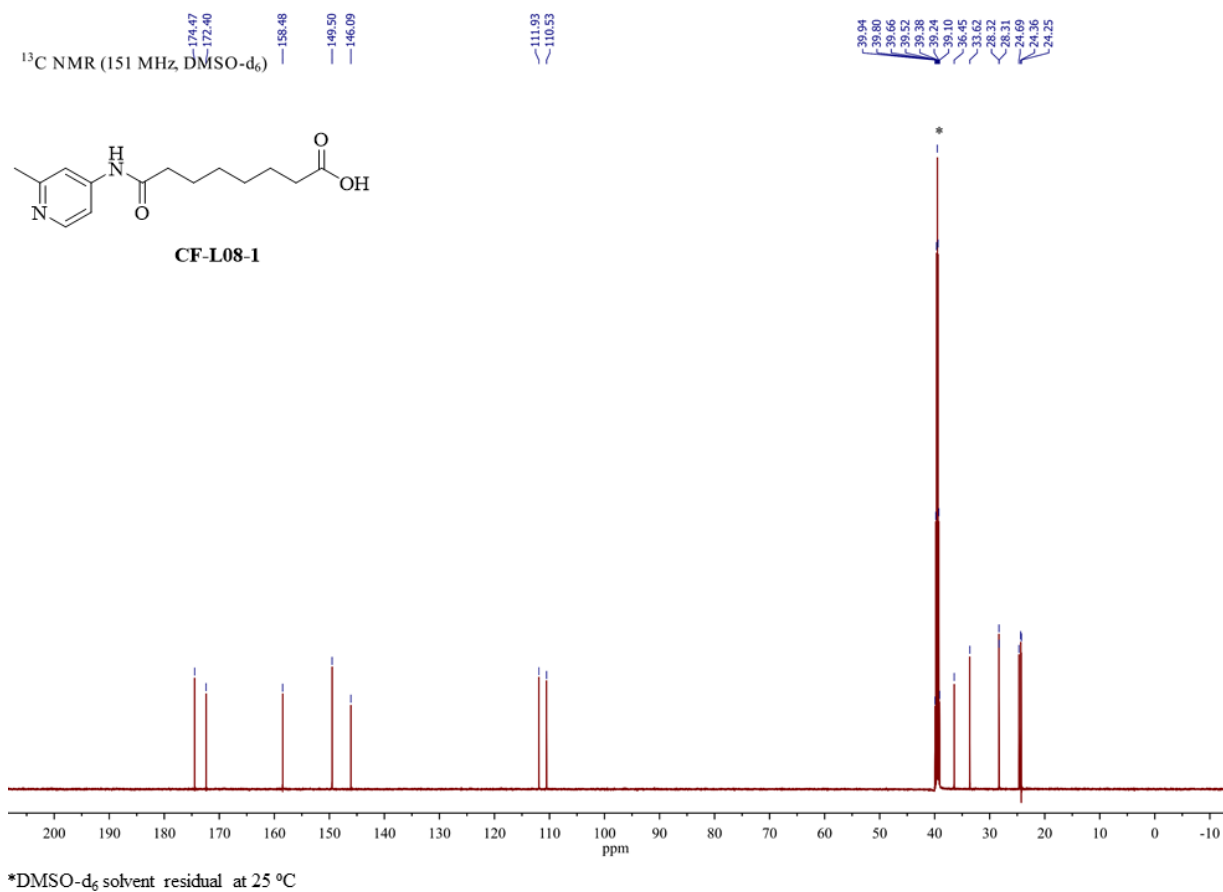
¹H NMR spectrum of CF-L07 in CD₃OD



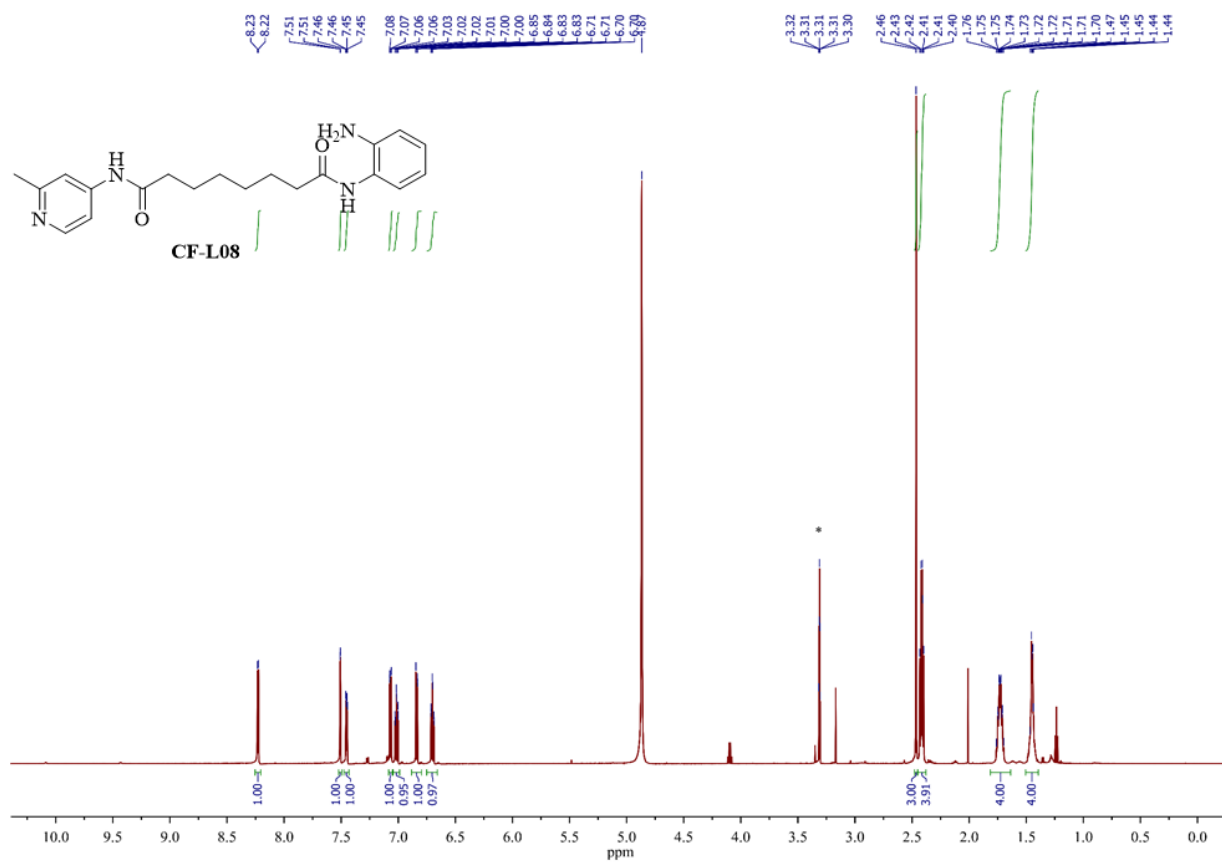
¹³C NMR spectrum of **CF-L07** in CD₃OD



¹H NMR spectrum of **CF-L08-1** in DMSO-d₆

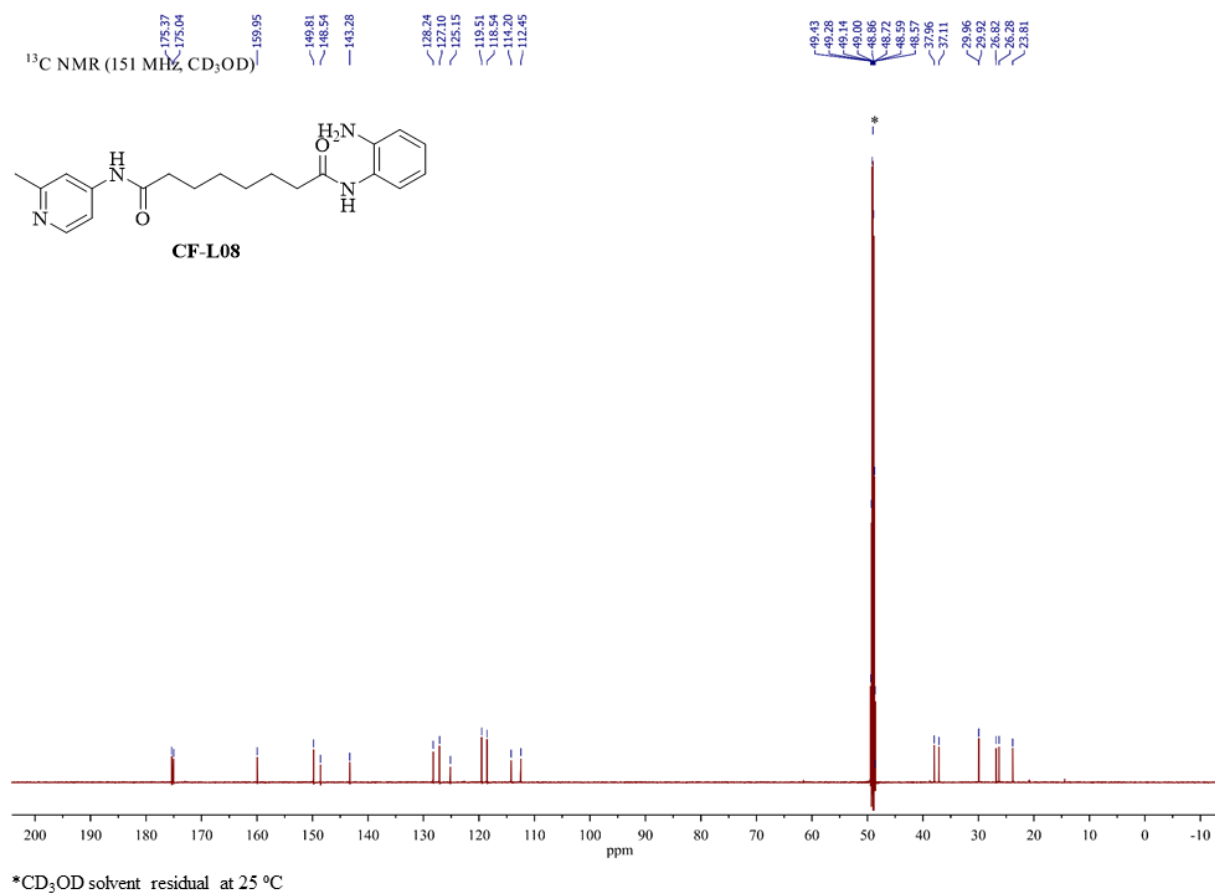


^{13}C NMR spectrum of **CF-L08-1** in DMSO-d_6

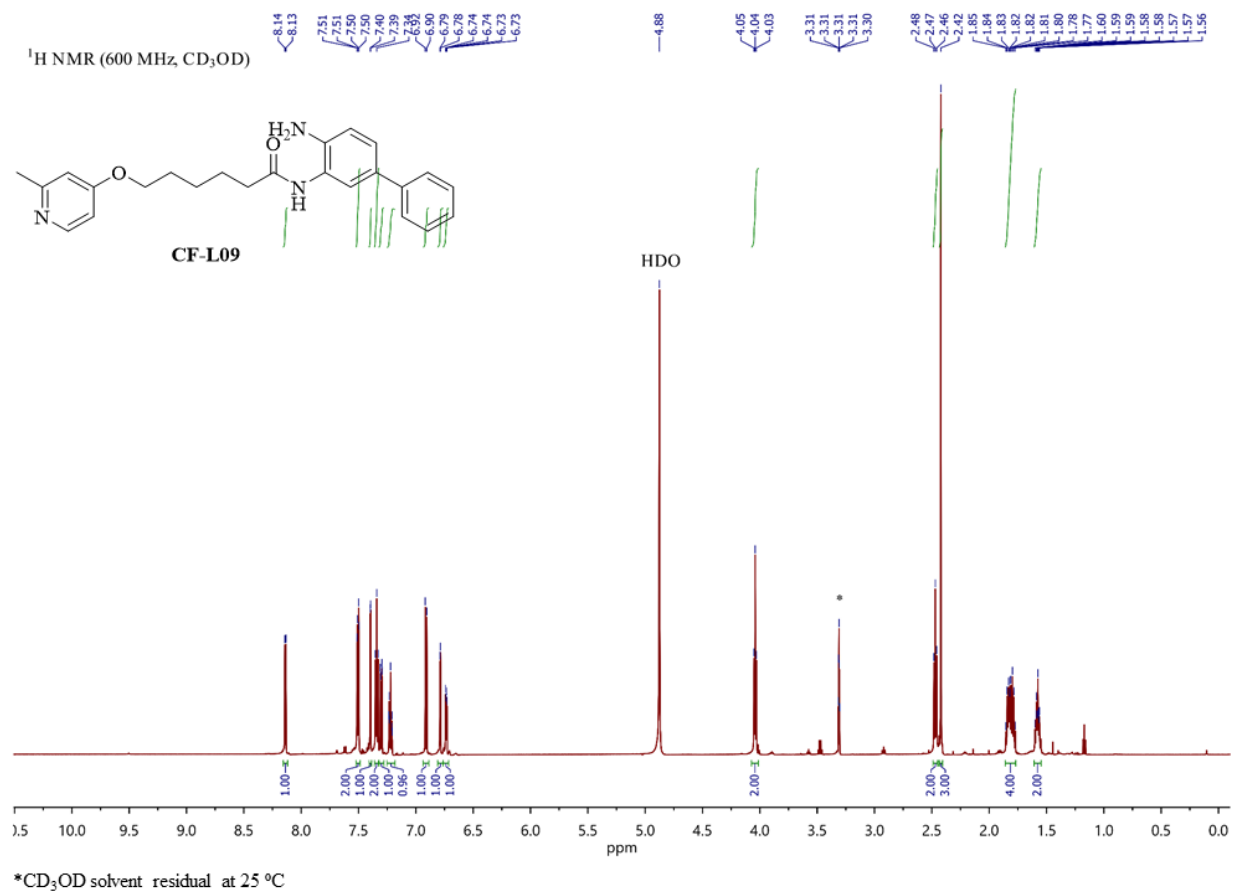


*CD₃OD solvent residual at 25 °C

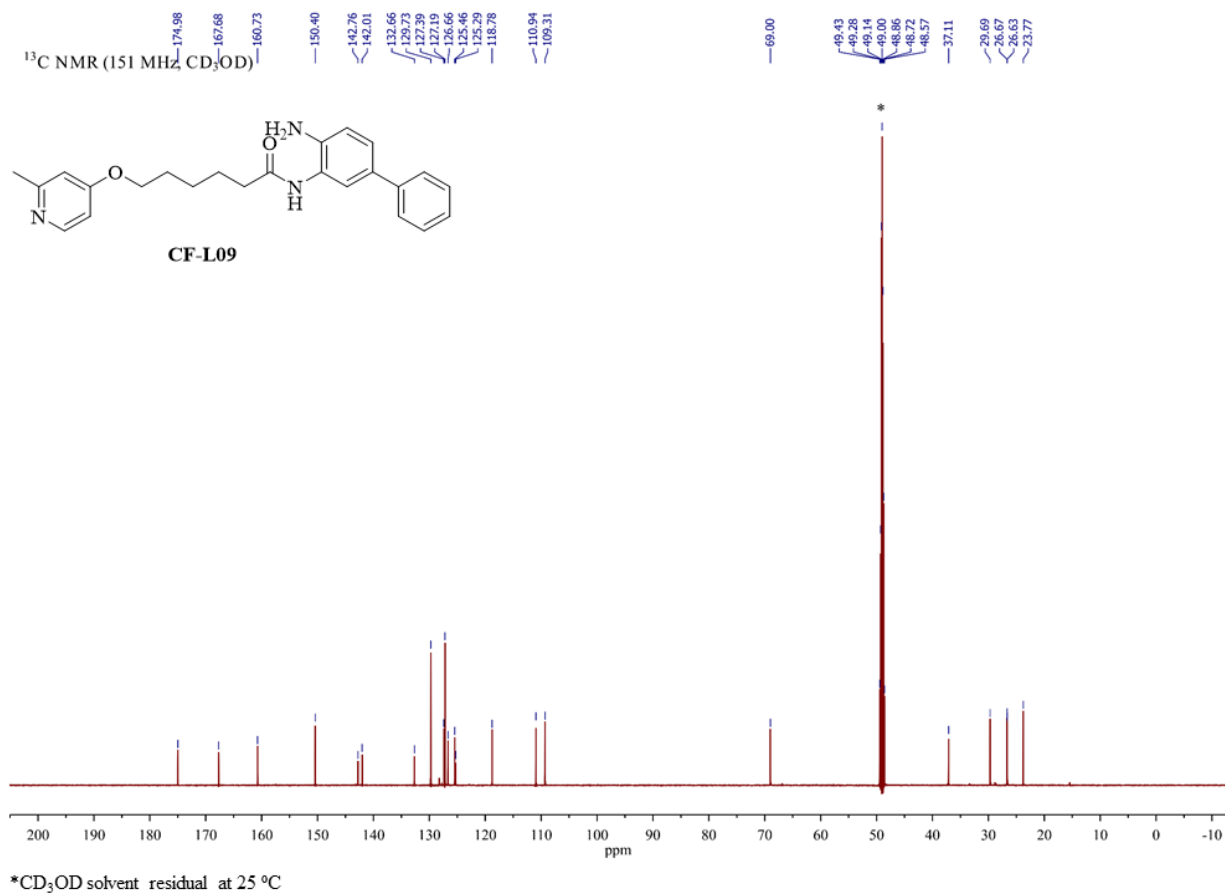
¹H NMR spectrum of **CF-L08** in CD₃OD



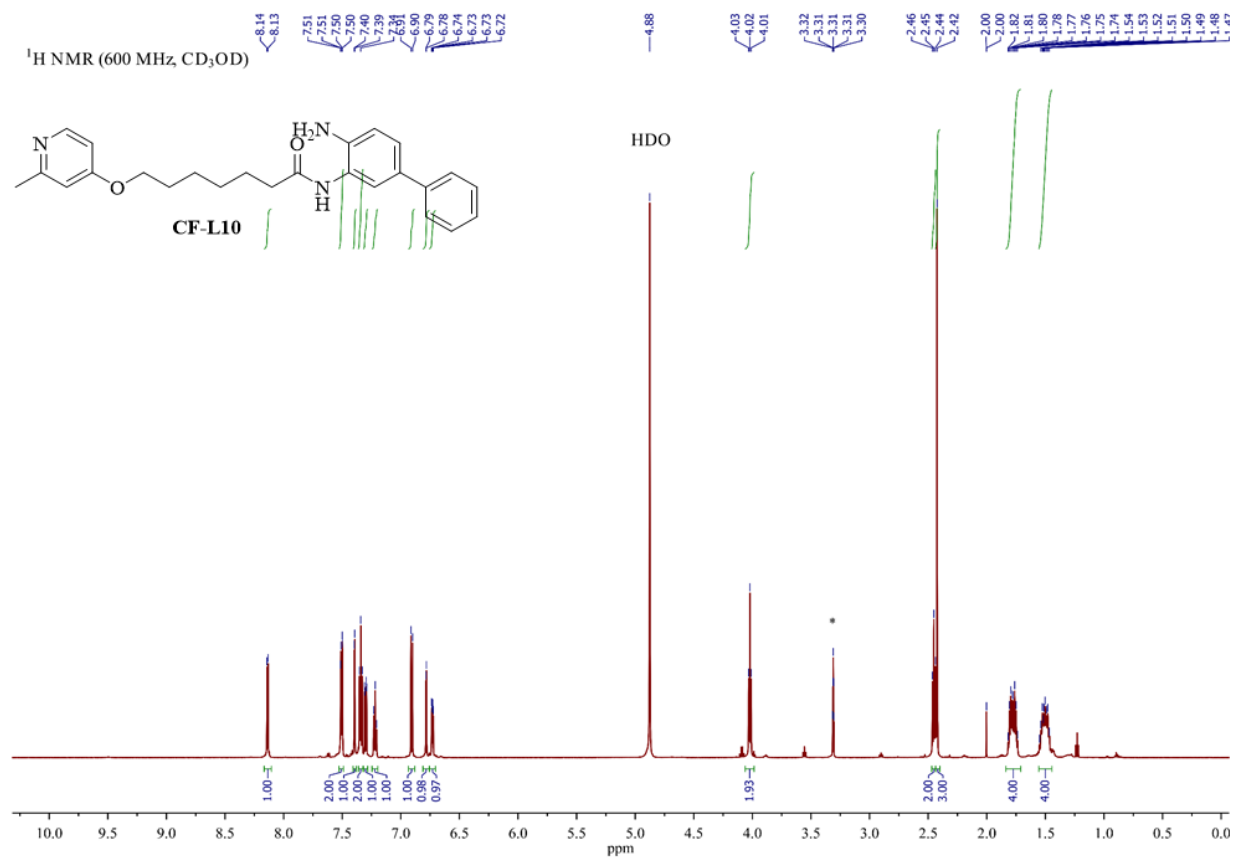
¹³C NMR spectrum of **CF-L08** in CD₃OD



¹H NMR spectrum of **CF-L09** in CD₃OD

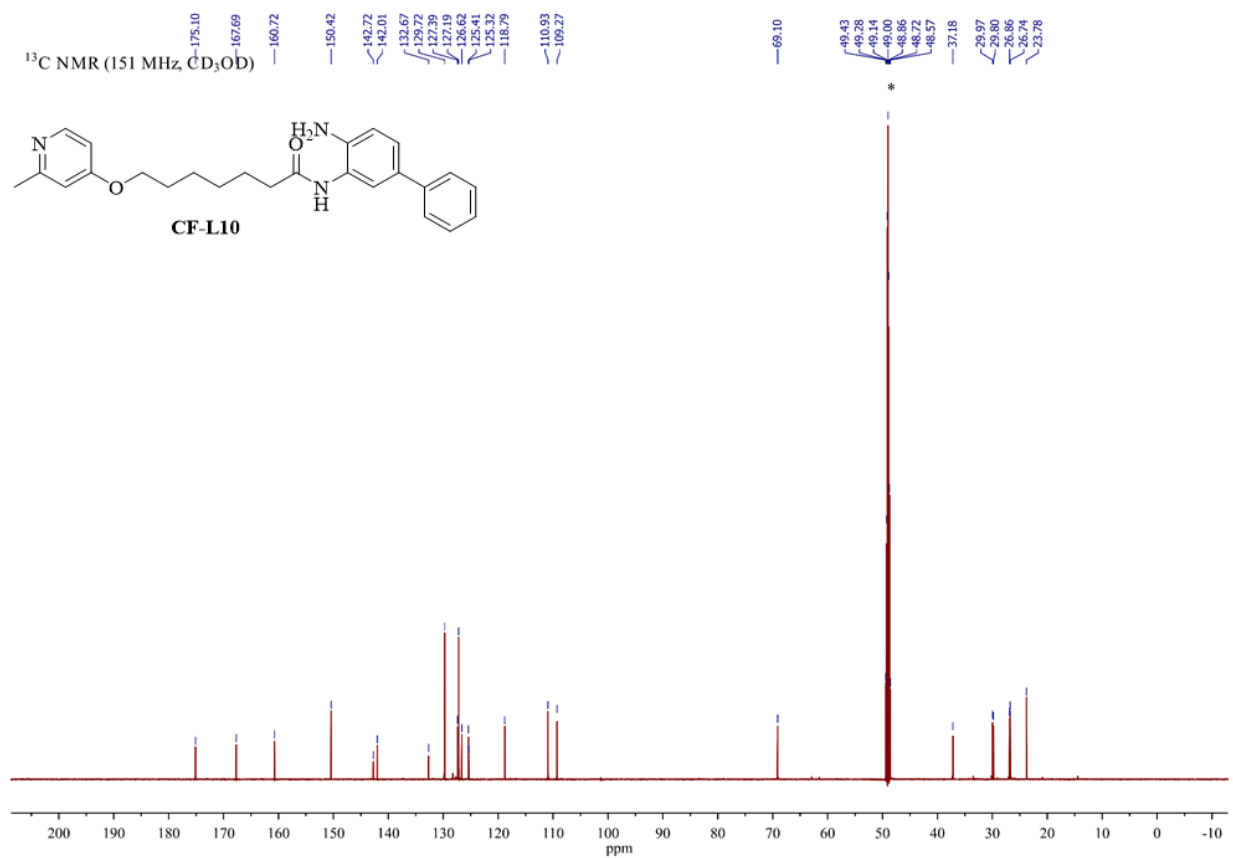


¹³C NMR spectrum of **CF-L09** in CD₃OD



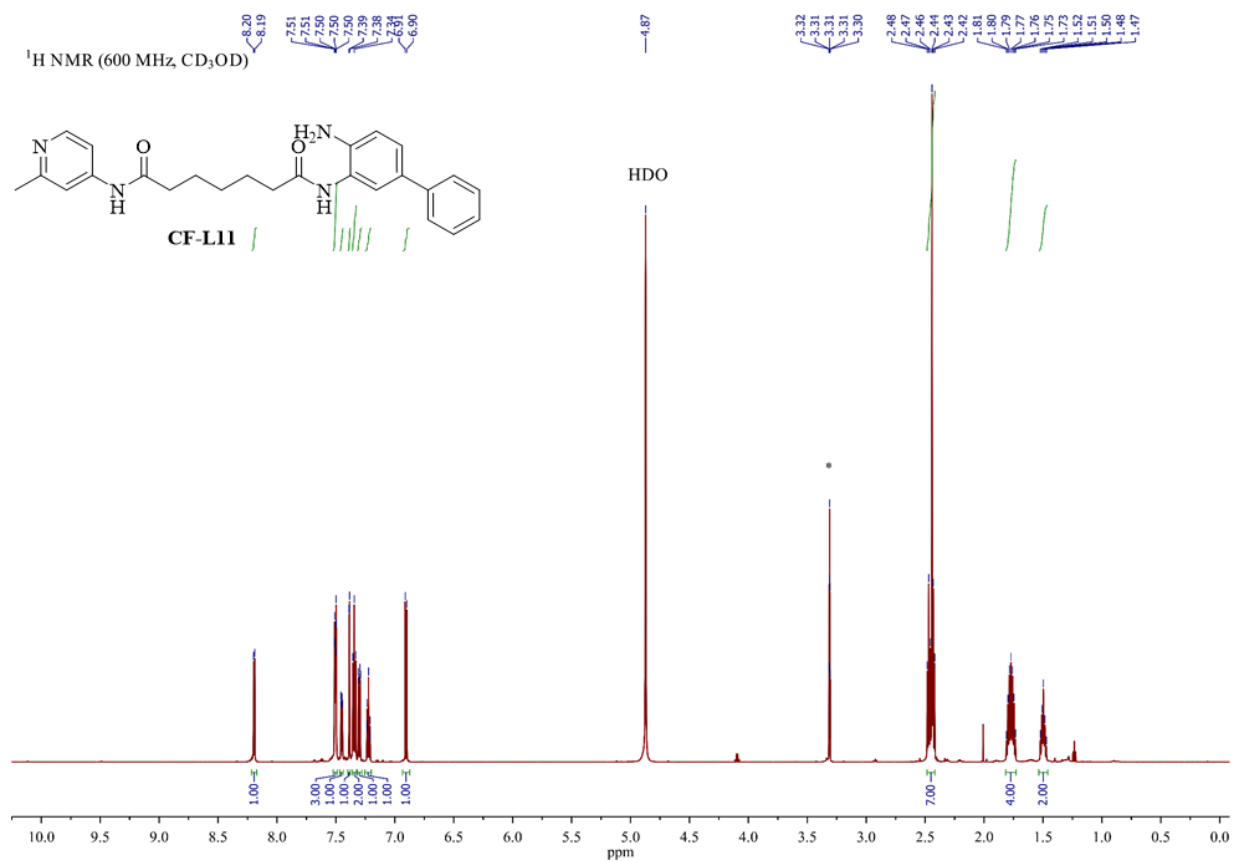
*CD₃OD solvent residual at 25 °C

¹H NMR spectrum of **CF-L10** in CD₃OD



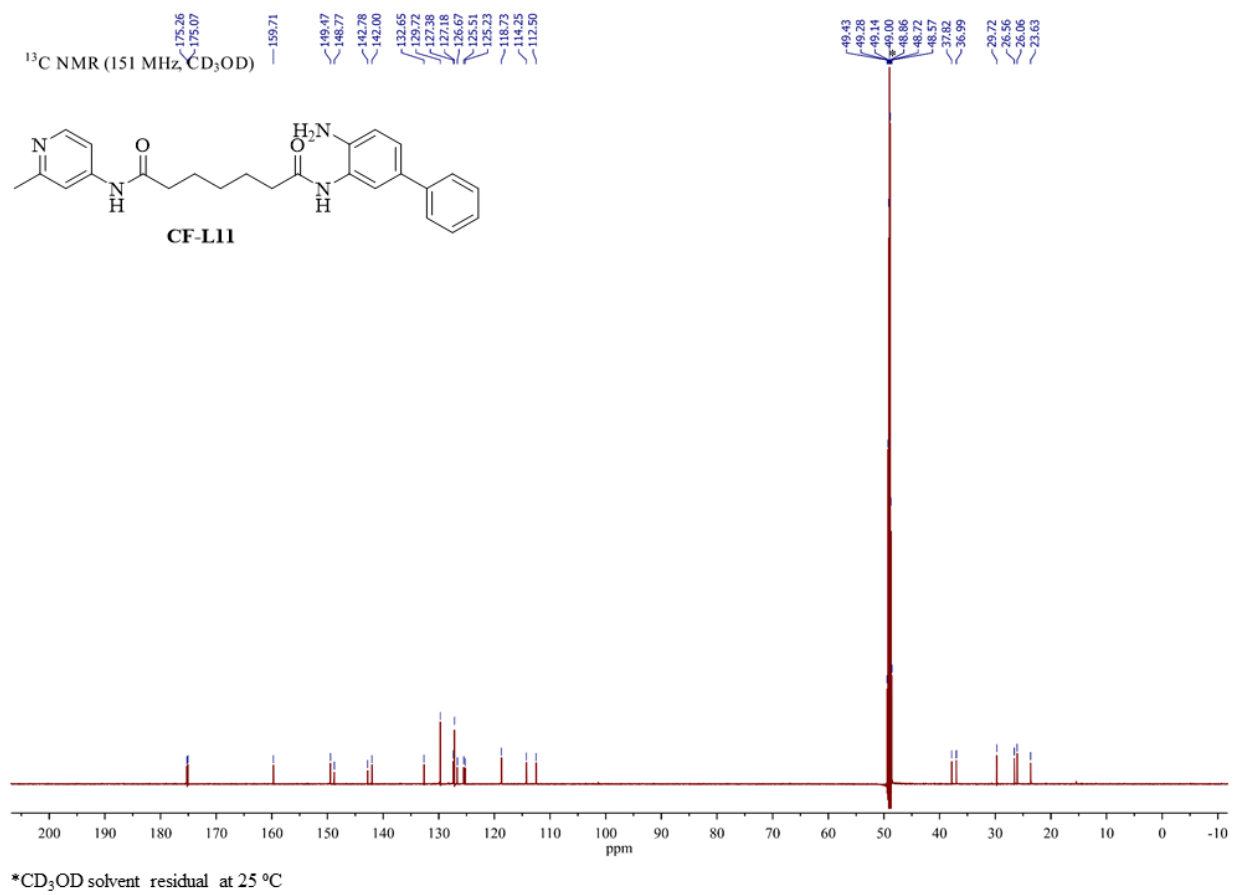
*CD₃OD solvent residual at 25 °C

¹³C NMR spectrum of **CF-L10** in CD₃OD

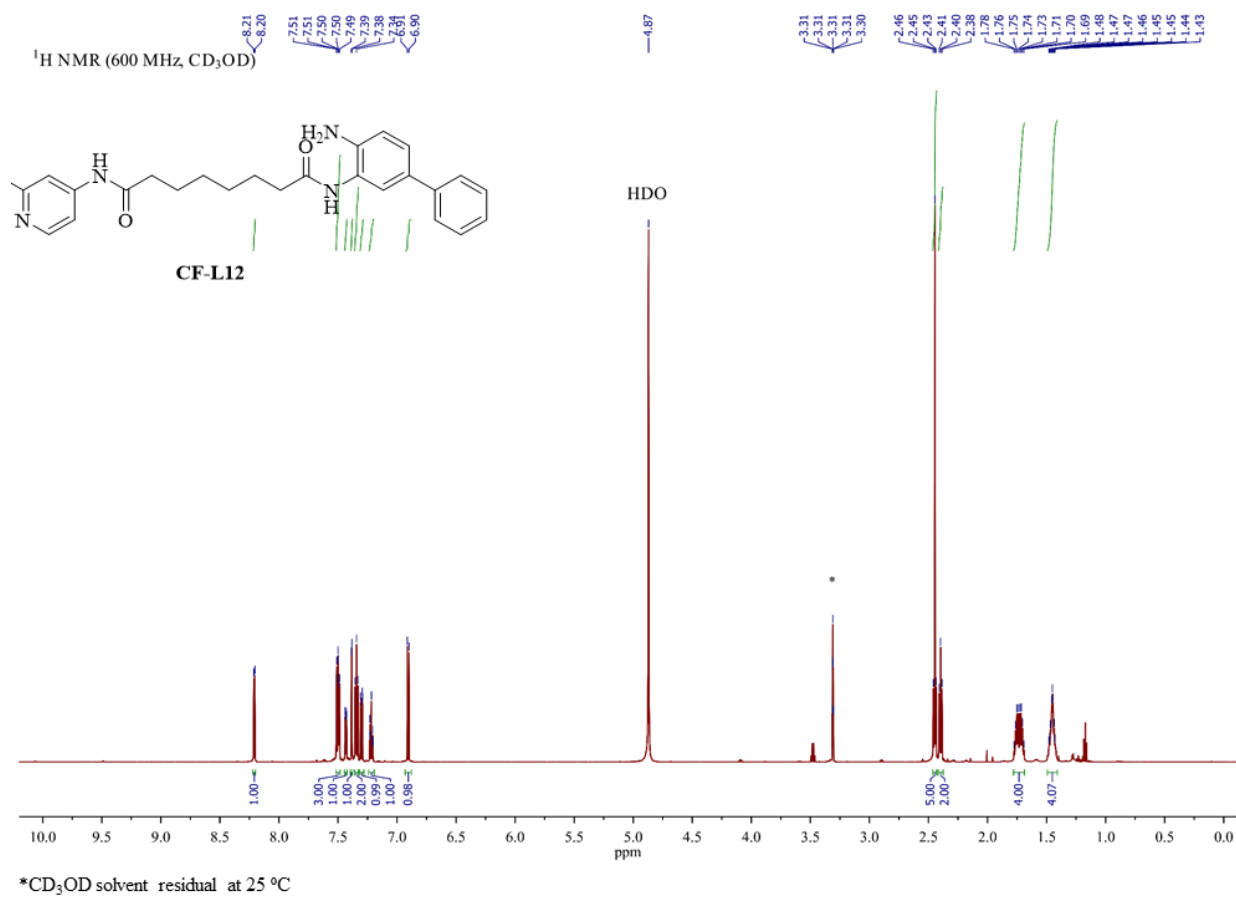


*CD₃OD solvent residual at 25 °C

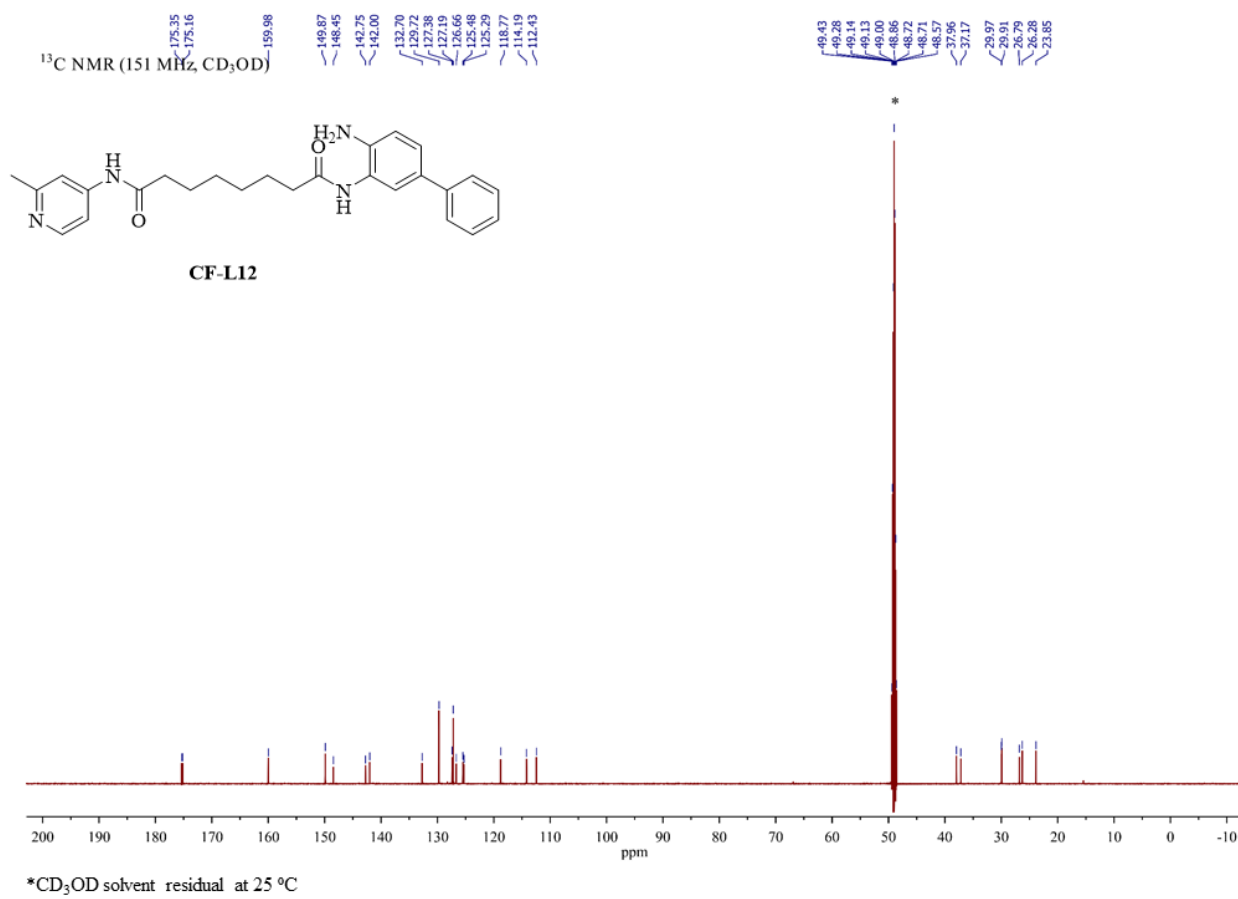
¹H NMR spectrum of **CF-L11** in CD₃OD



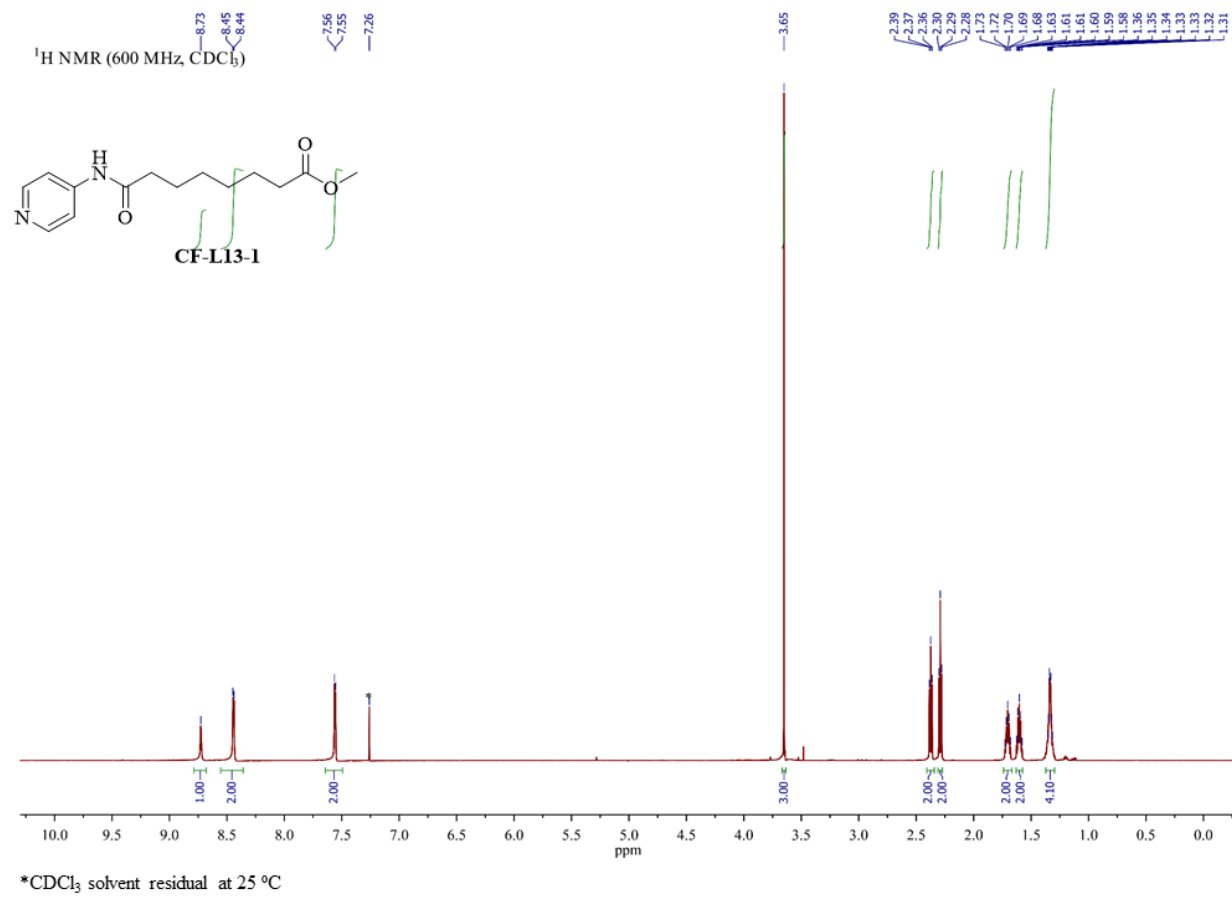
¹³C NMR spectrum of **CF-L11** in CD₃OD



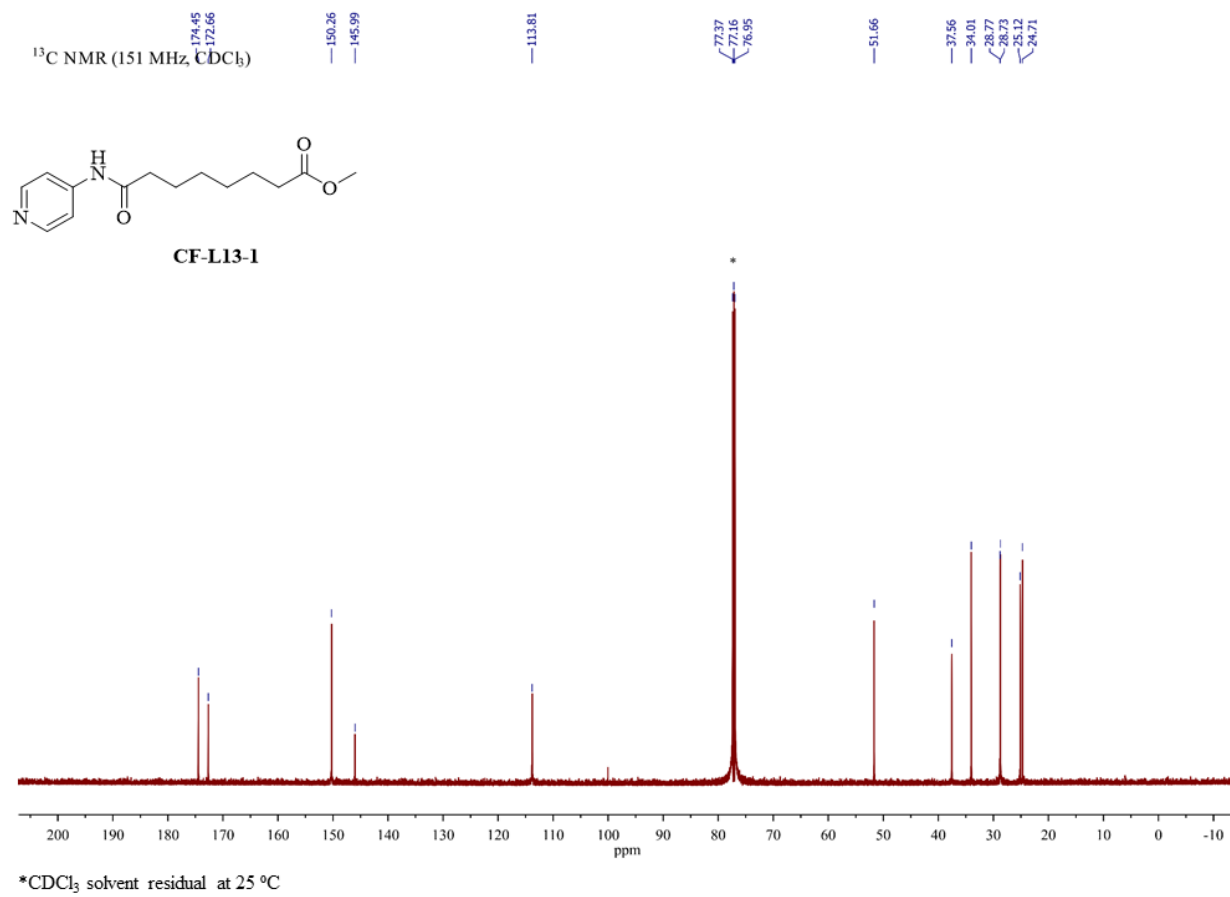
¹H NMR spectrum of **CF-L12** in CD₃OD



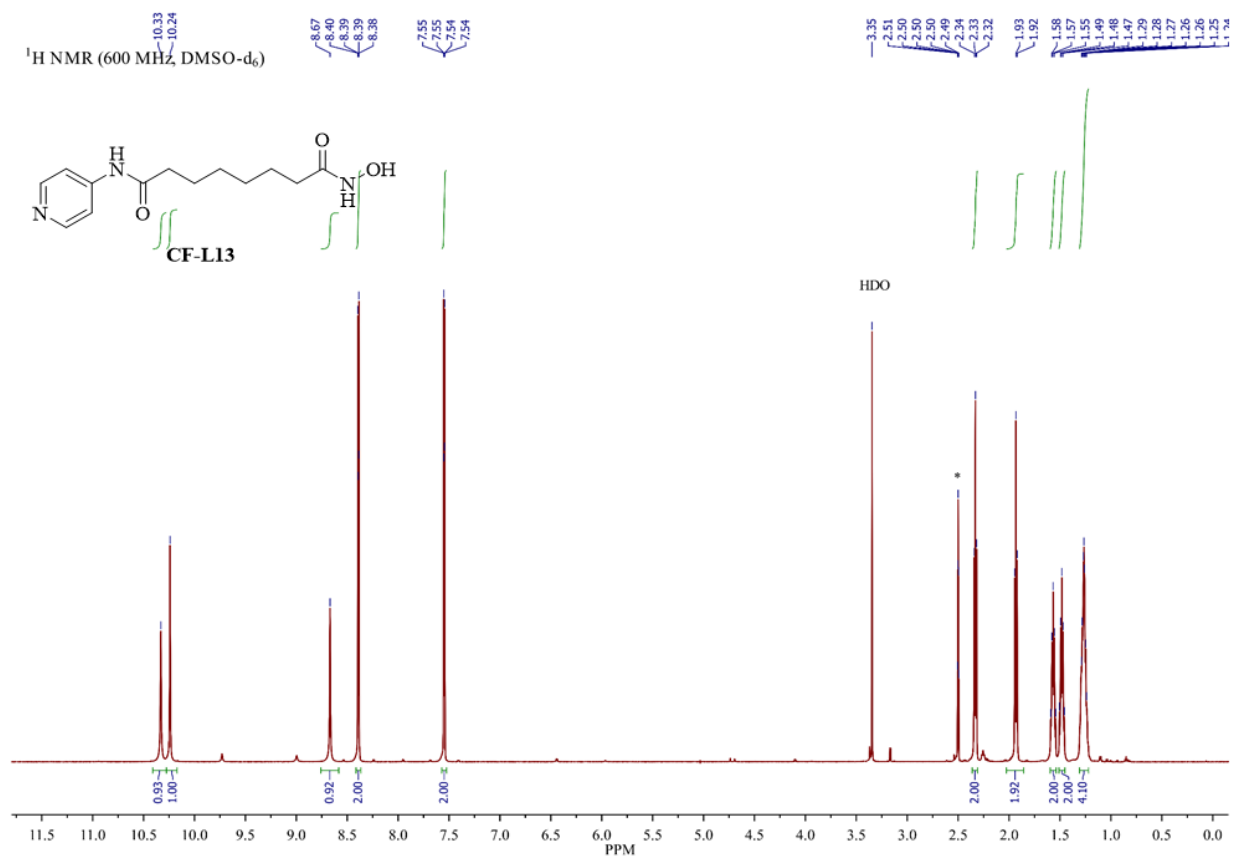
¹³C NMR spectrum of **CF-L12** in CD₃OD



¹H NMR spectrum of CF-L13-1 in CDCl₃

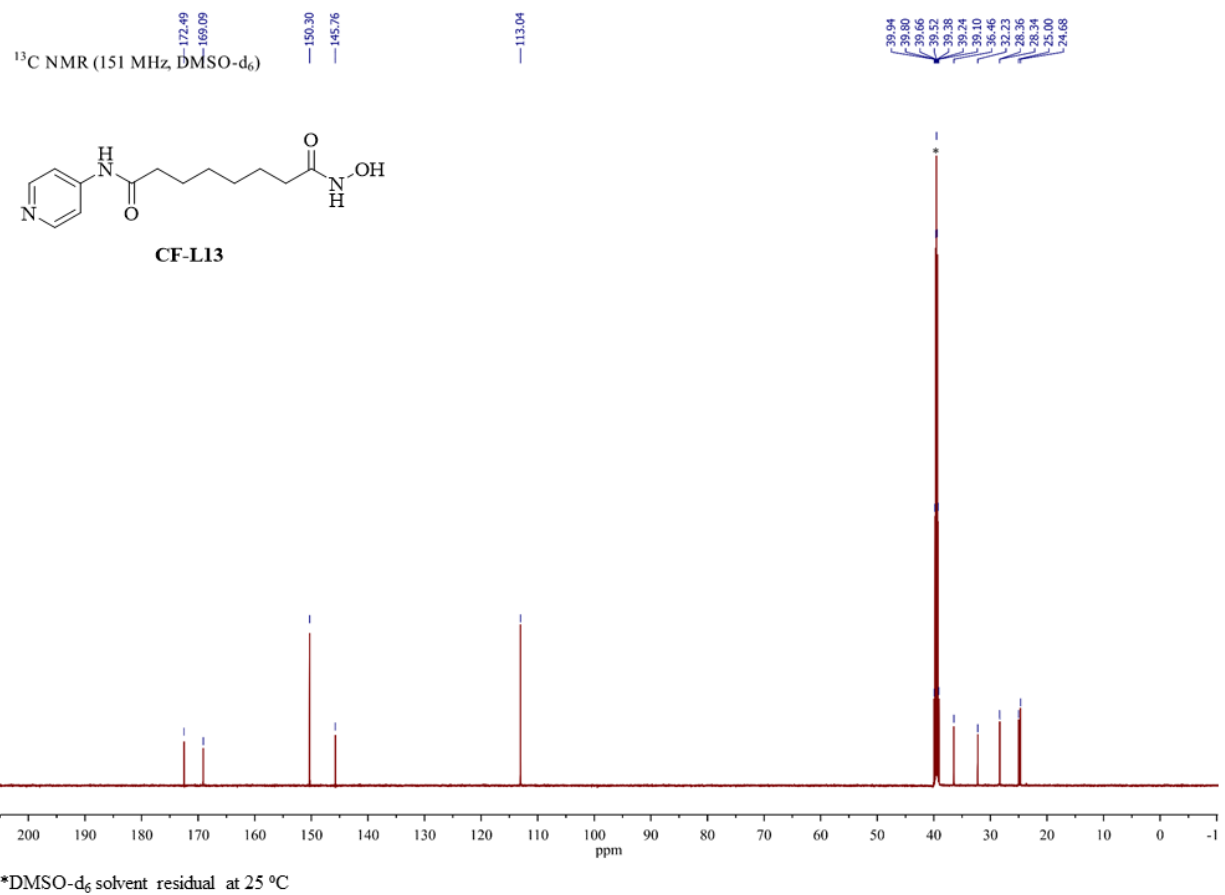


¹³C NMR spectrum of **CF-L13-1** in CDCl₃

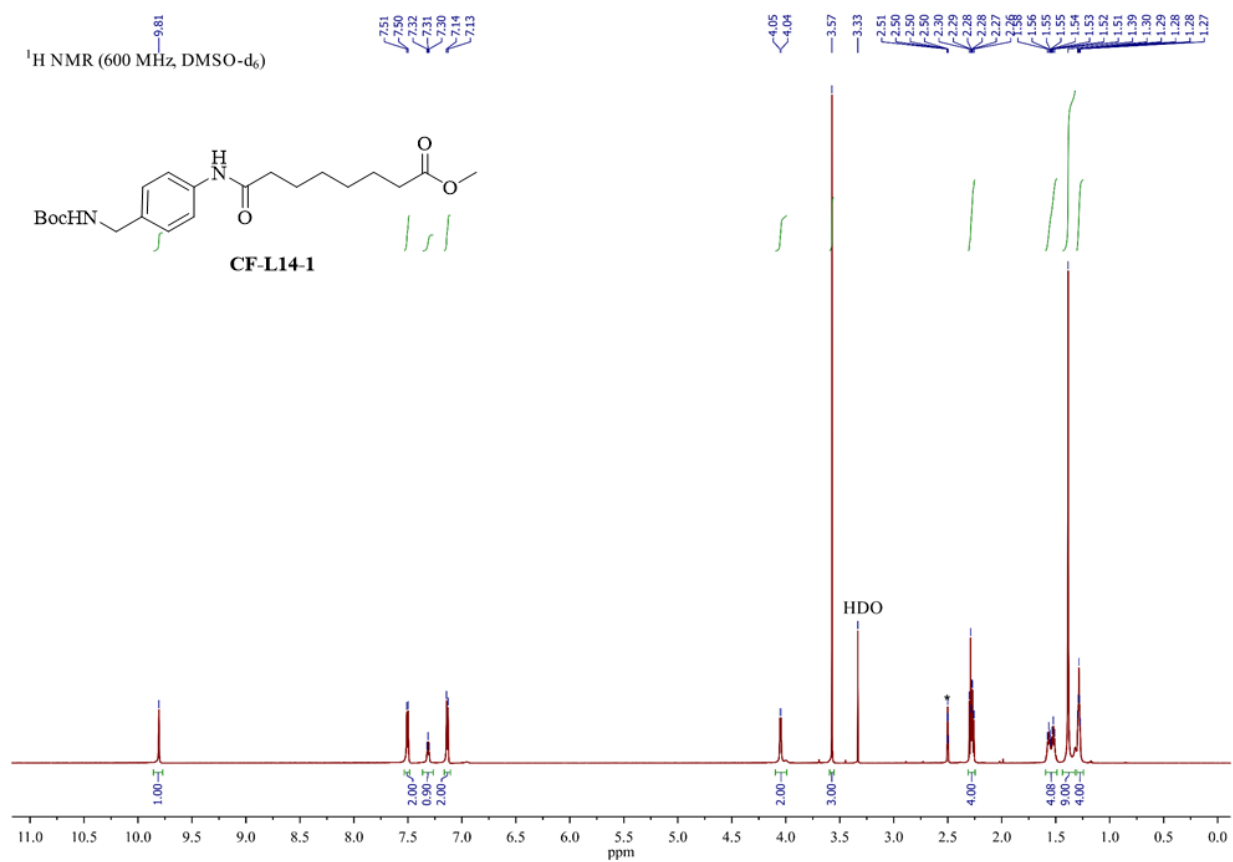


*DMSO-d₆ solvent residual at 25 °C

¹H NMR spectrum of CF-L13 in DMSO-d₆

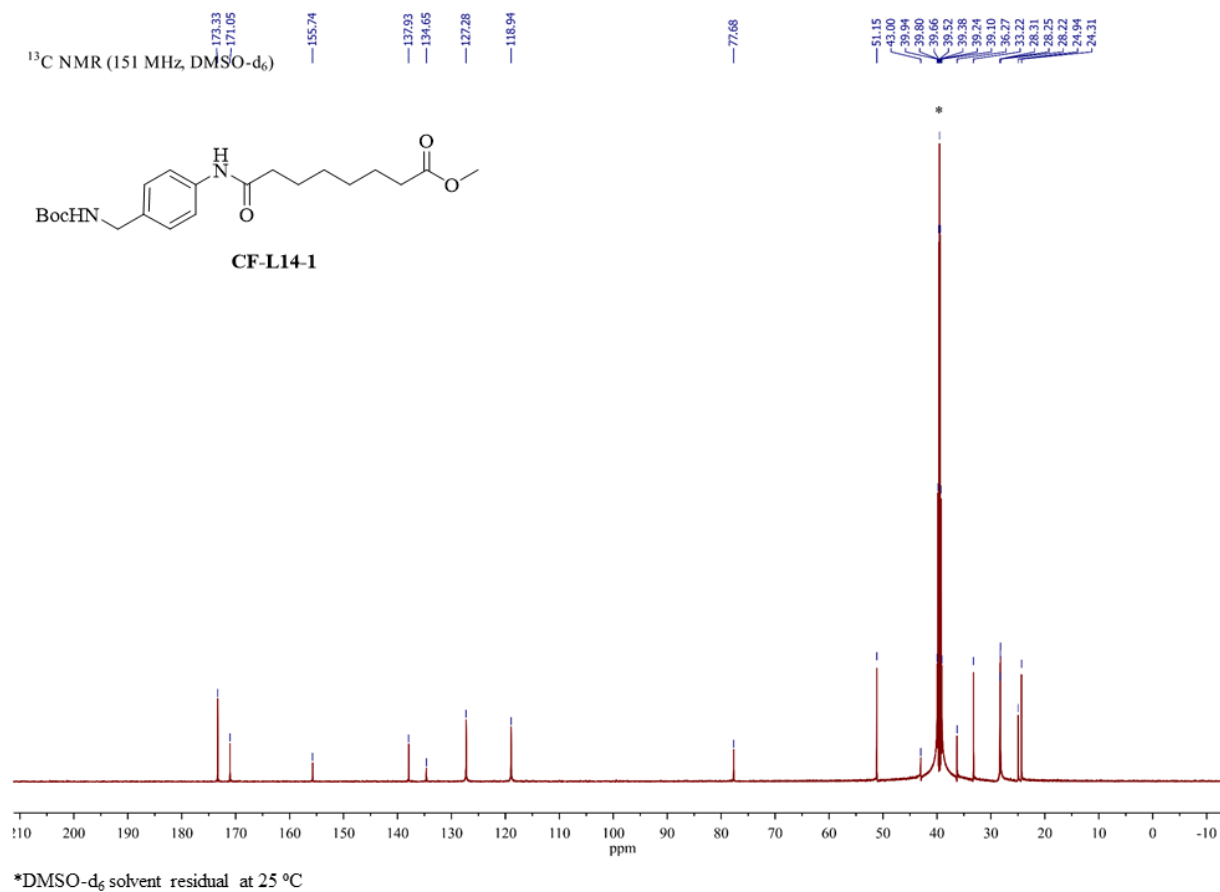


¹³C NMR spectrum of CF-L13 in DMSO-d₆

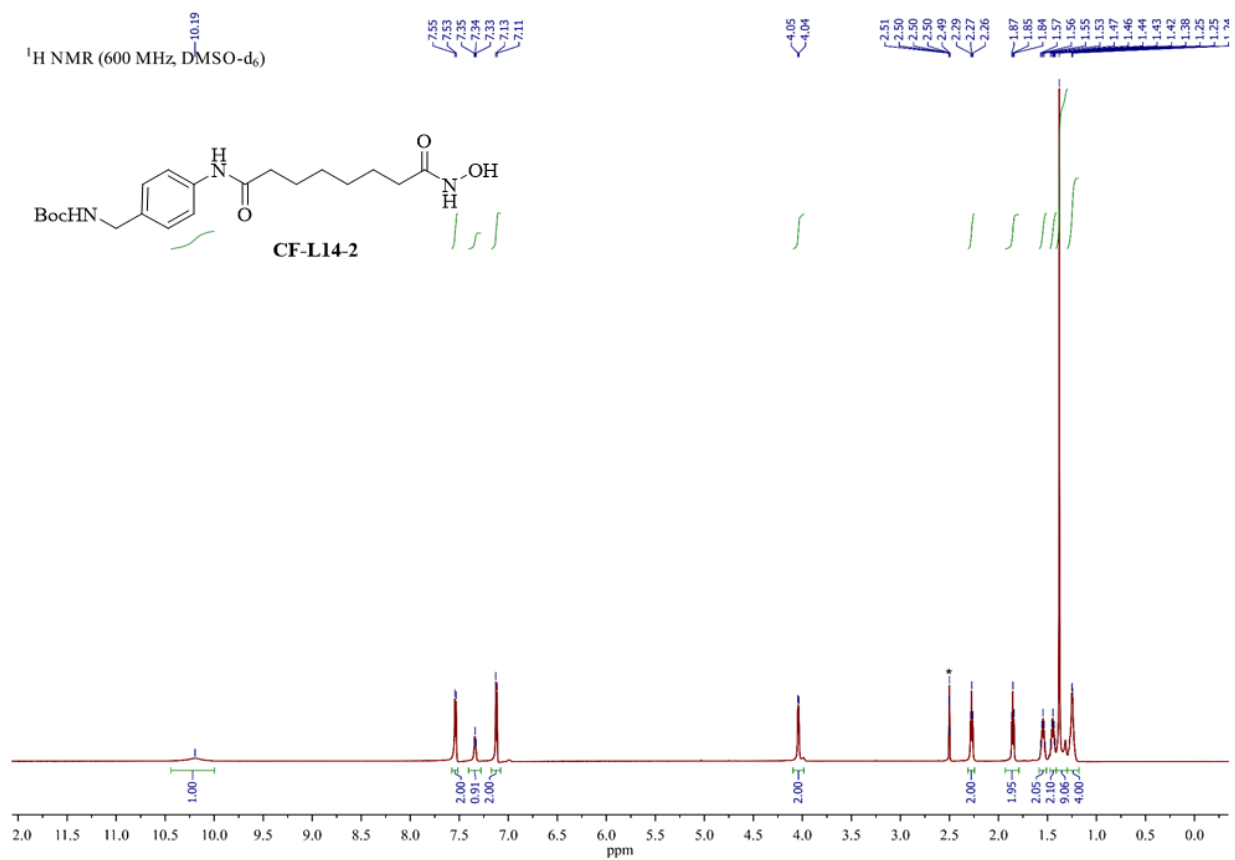


*DMSO-d₆ solvent residual at 25 °C

¹H NMR spectrum of CF-L14-1 in DMSO-d₆

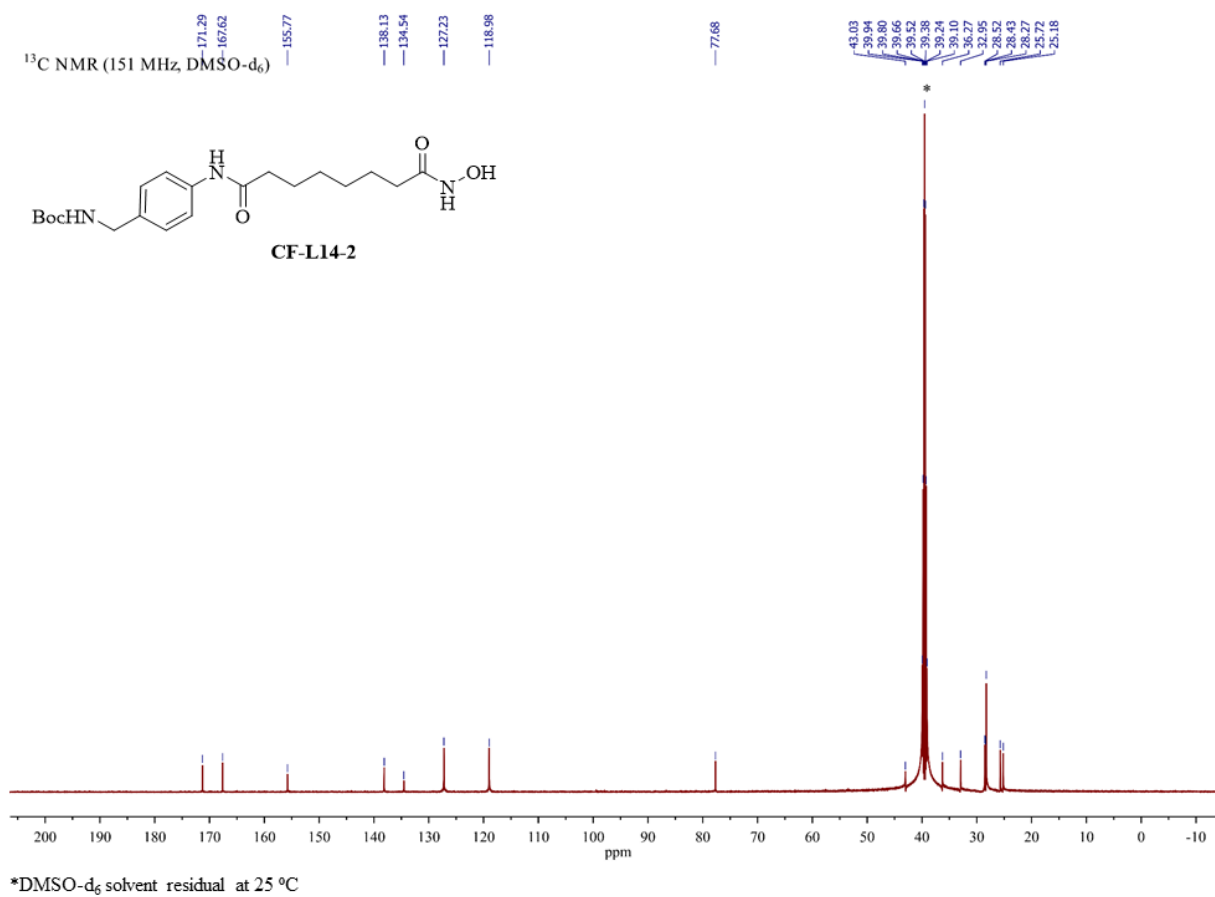


^{13}C NMR spectrum of **CF-L14-1** in DMSO-d_6

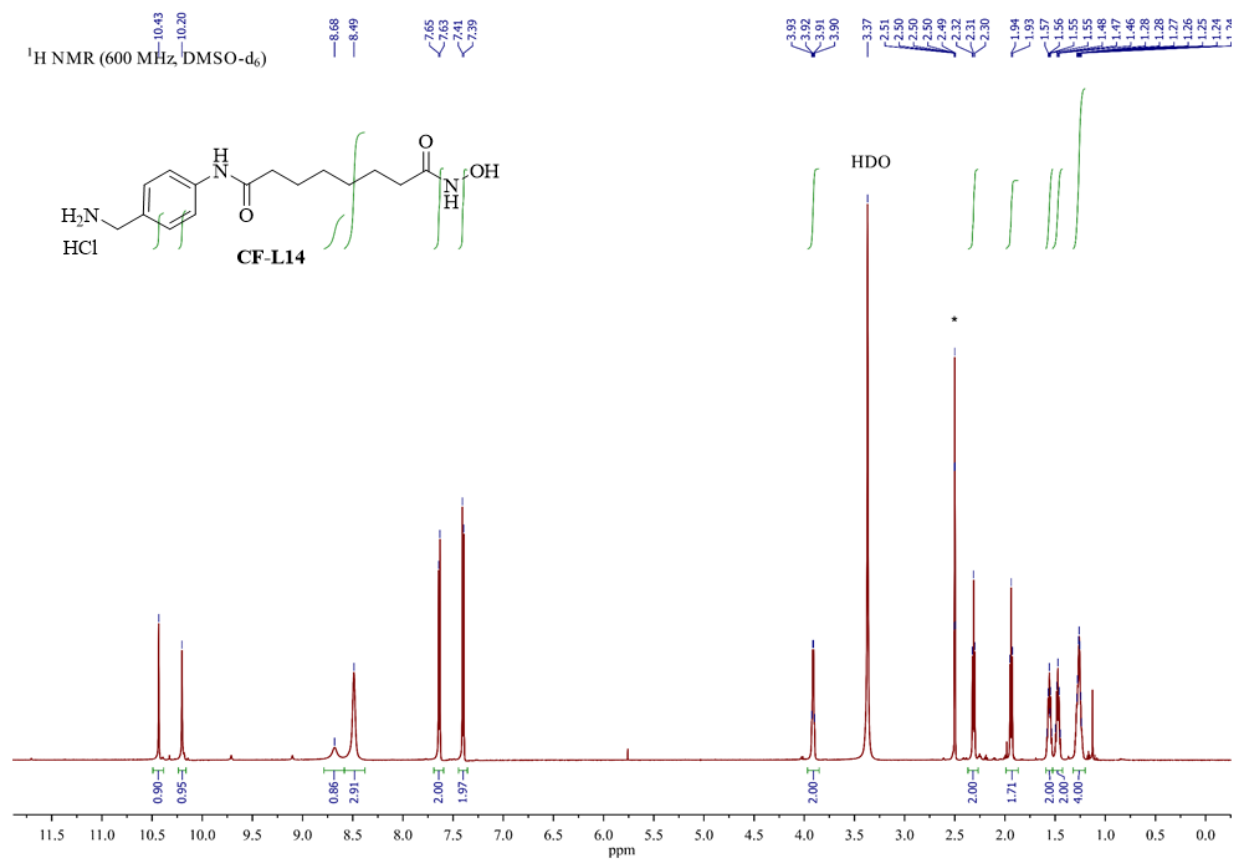


*DMSO-d₆ solvent residual at 25 °C

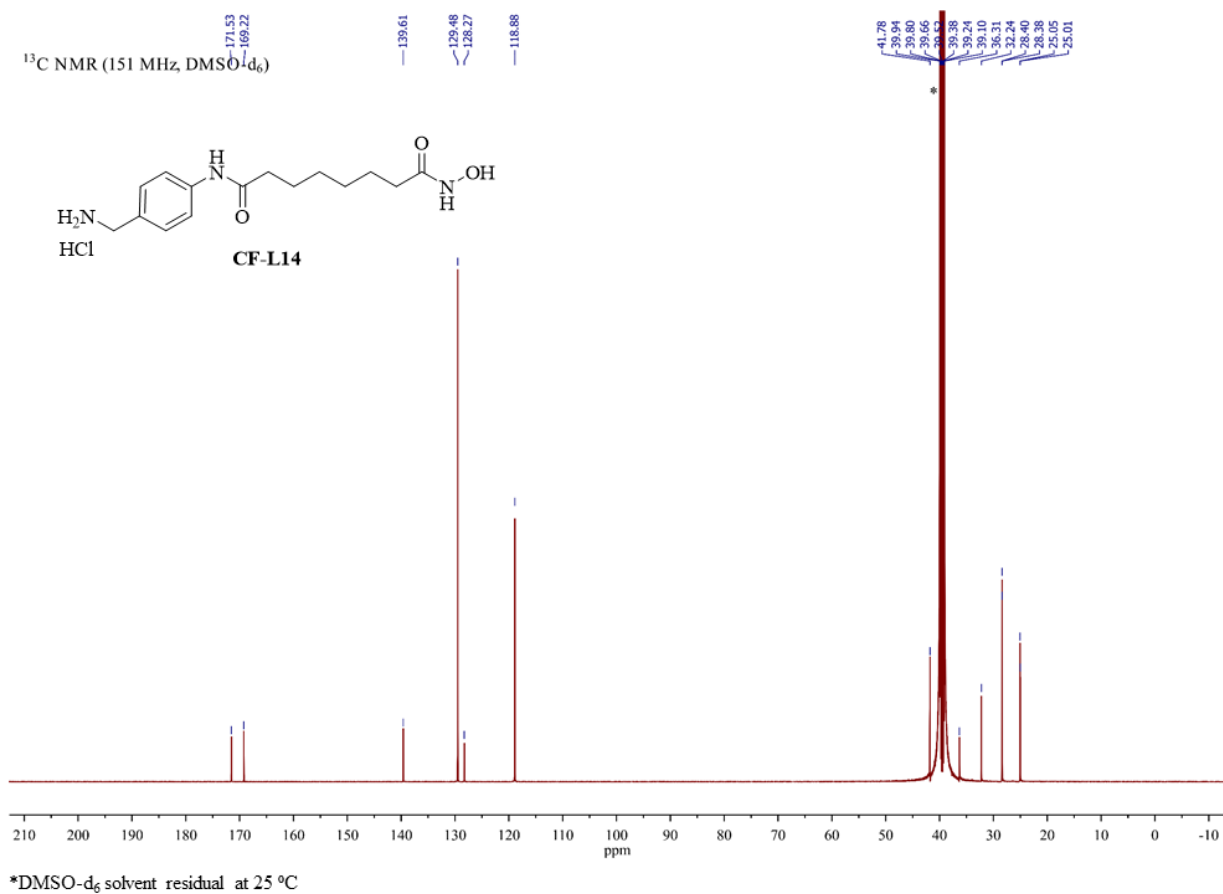
¹H NMR spectrum of CF-L14-2 in DMSO-d₆



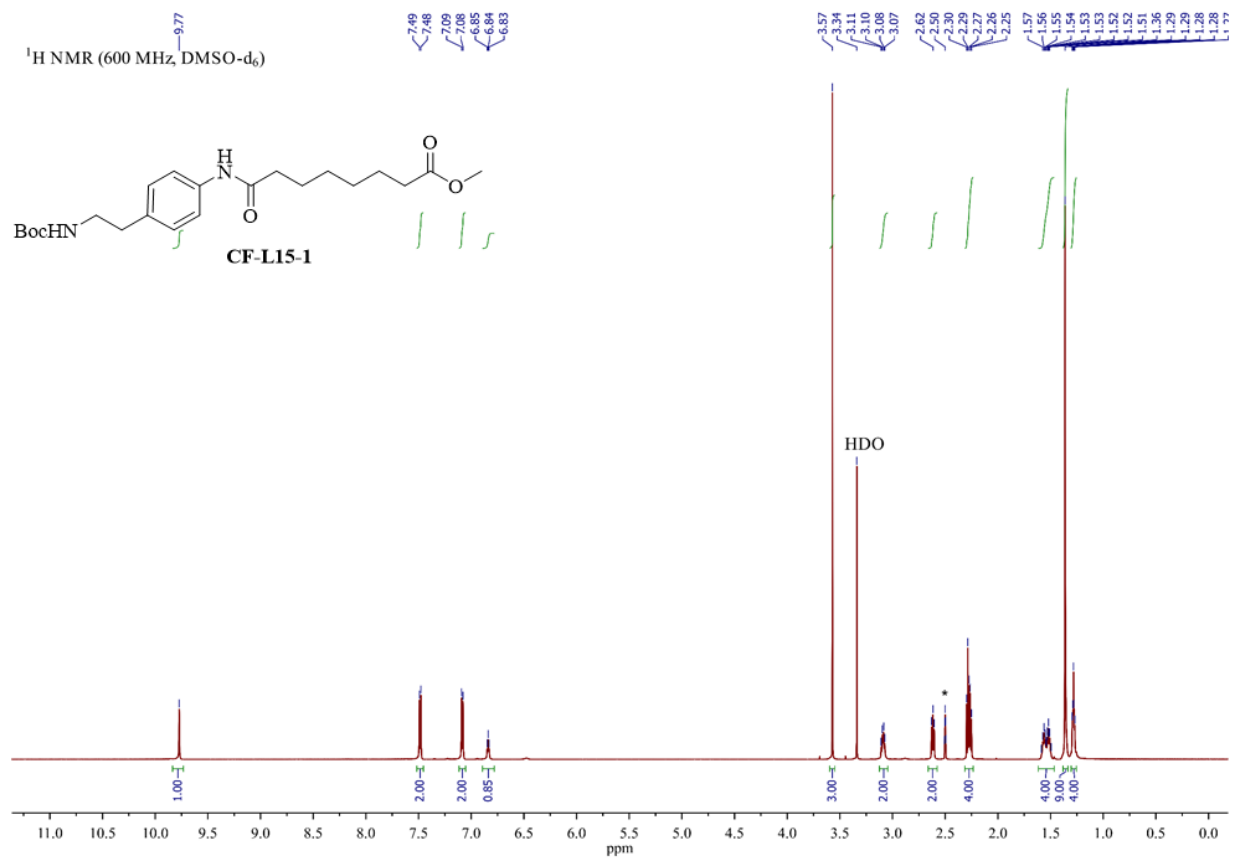
¹³C NMR spectrum of CF-L14-2 in DMSO-d₆



¹H NMR spectrum of CF-L14 in DMSO-d₆

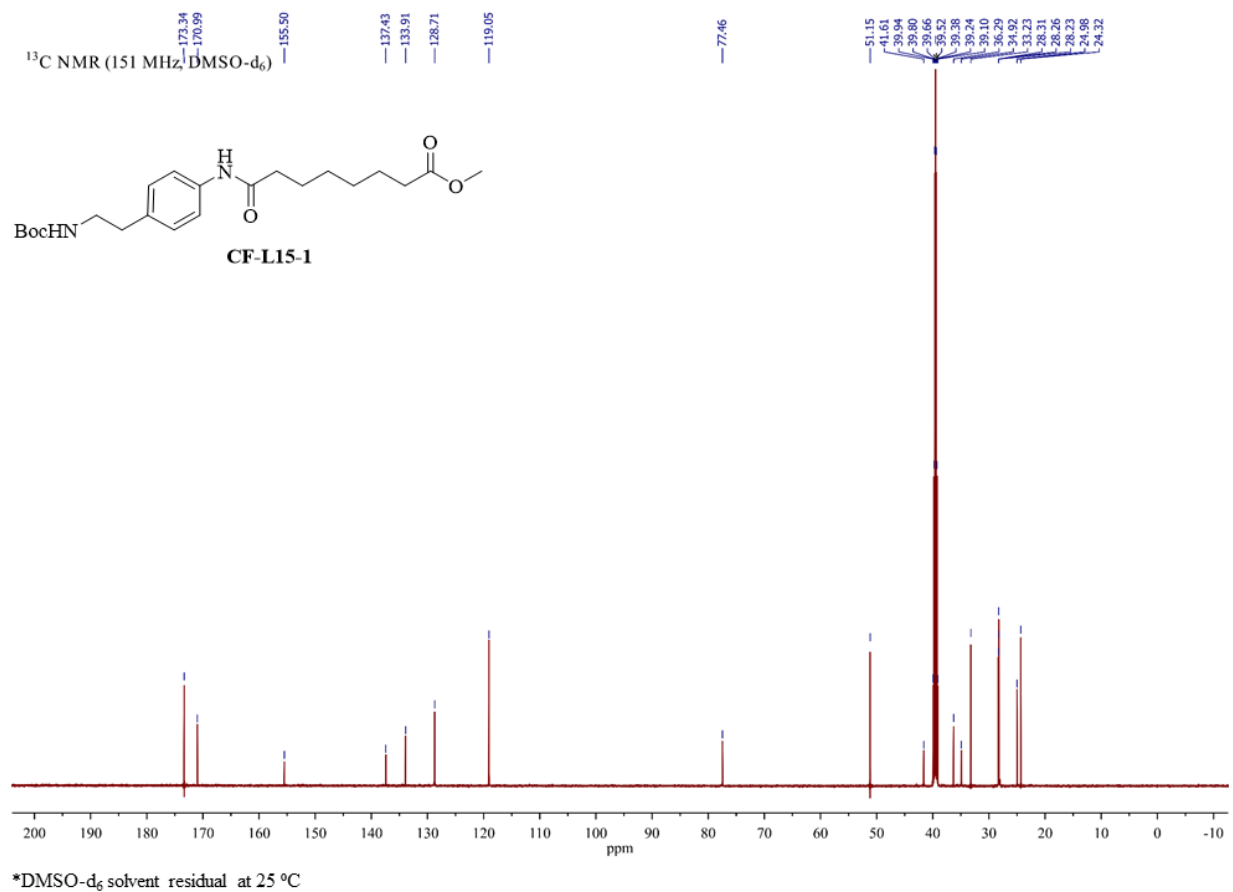


¹³C NMR spectrum of **CF-L14** in DMSO-d₆

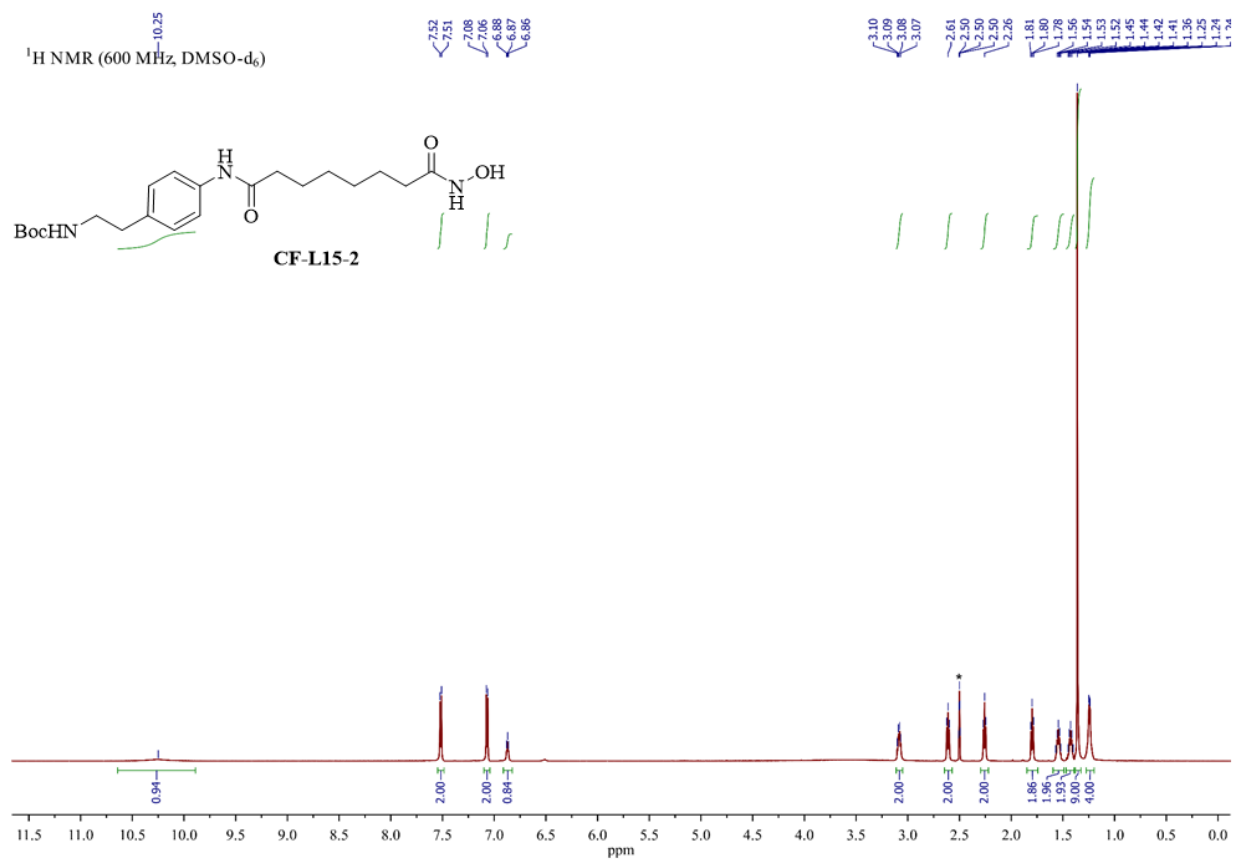


*DMSO-d₆ solvent residual at 25 °C

¹H NMR spectrum of CF-L15-1 in DMSO-d₆

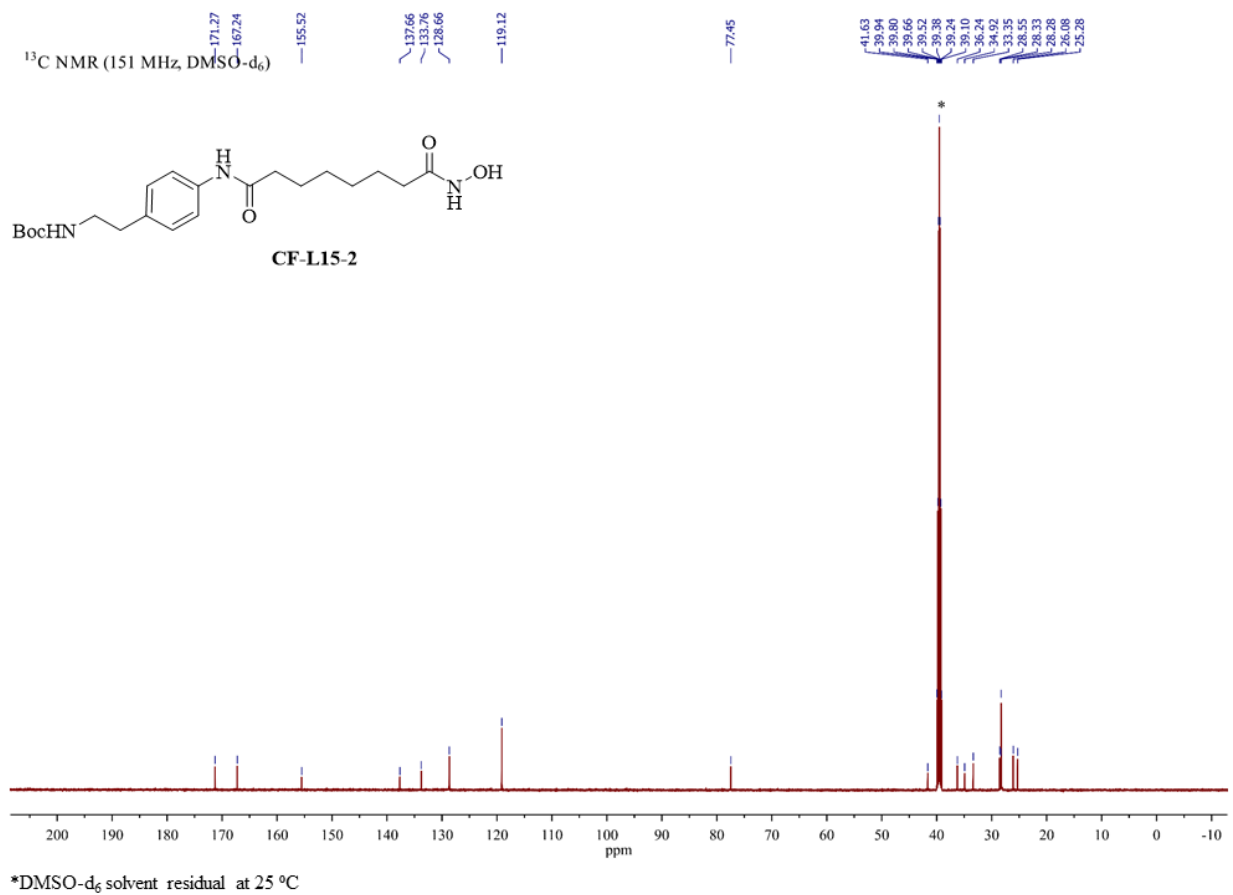


¹³C NMR spectrum of **CF-L15-1** in DMSO-d₆

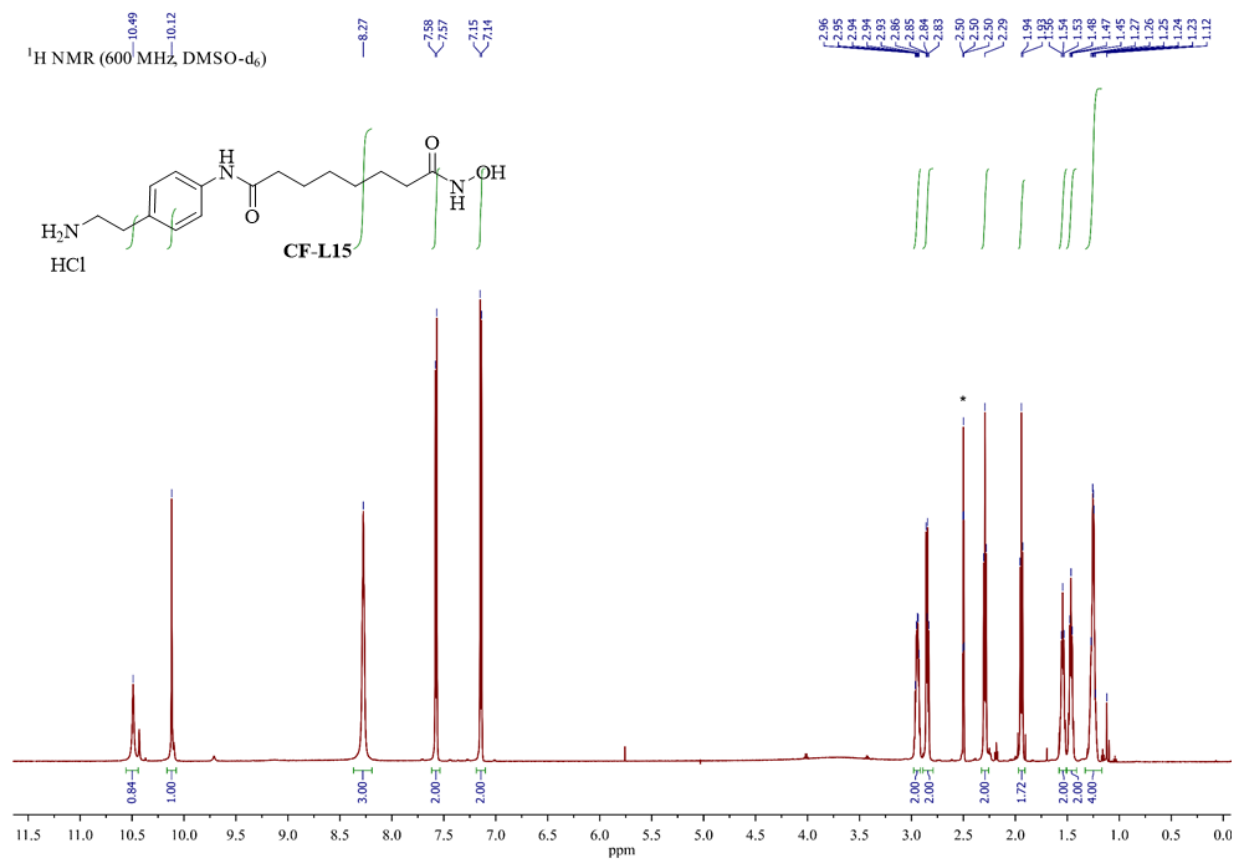


*DMSO-d₆ solvent residual at 25 °C

¹H NMR spectrum of CF-L15-2 in DMSO-d₆

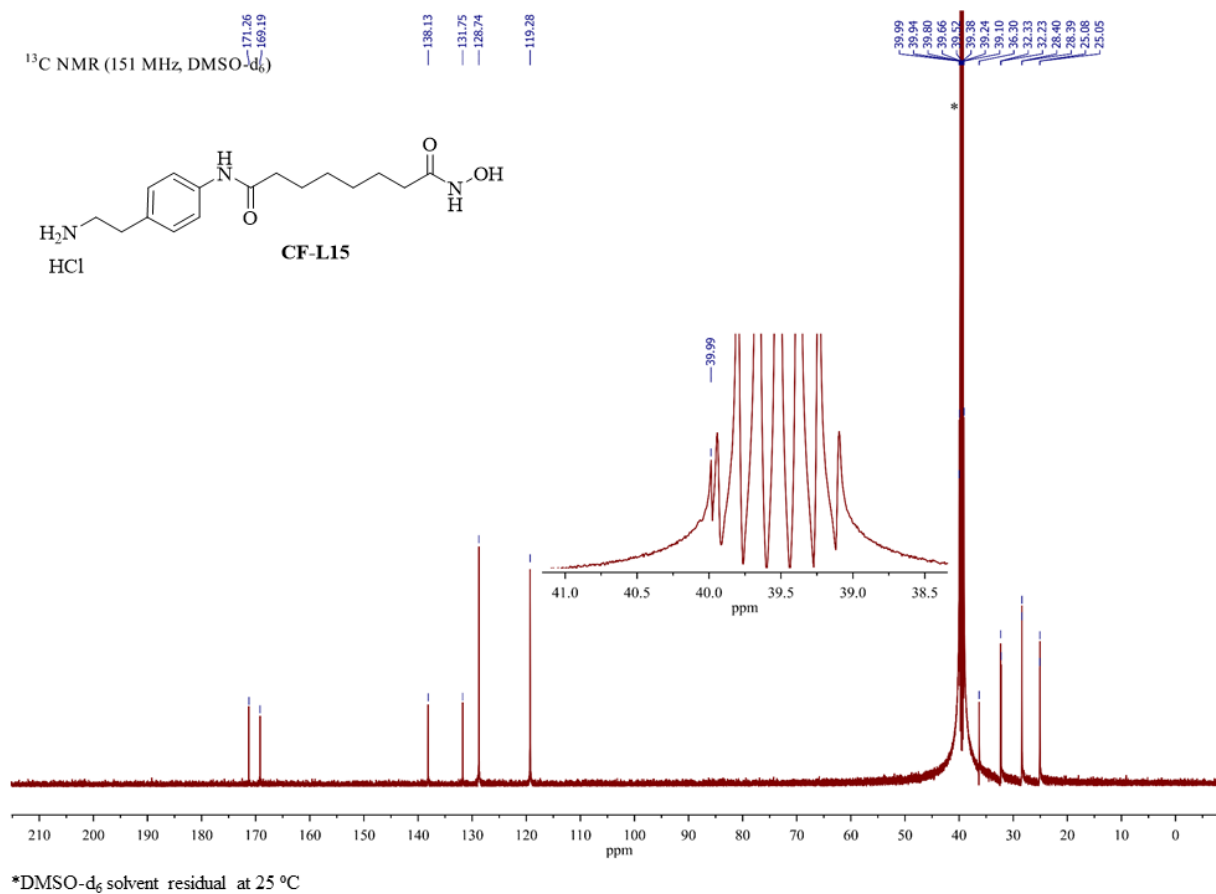


¹³C NMR spectrum of CF-L15-2 in DMSO-d₆

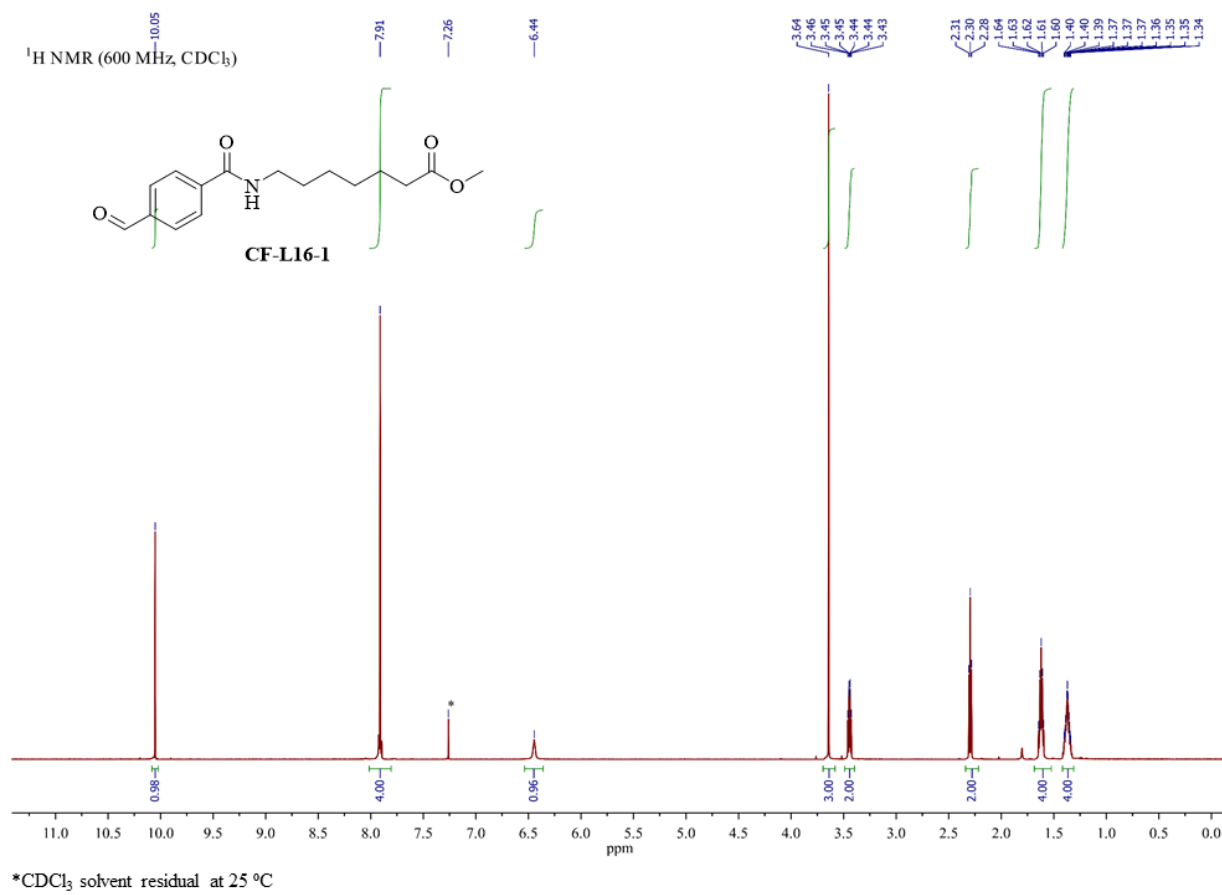


* DMSO-d_6 solvent residual at 25 °C

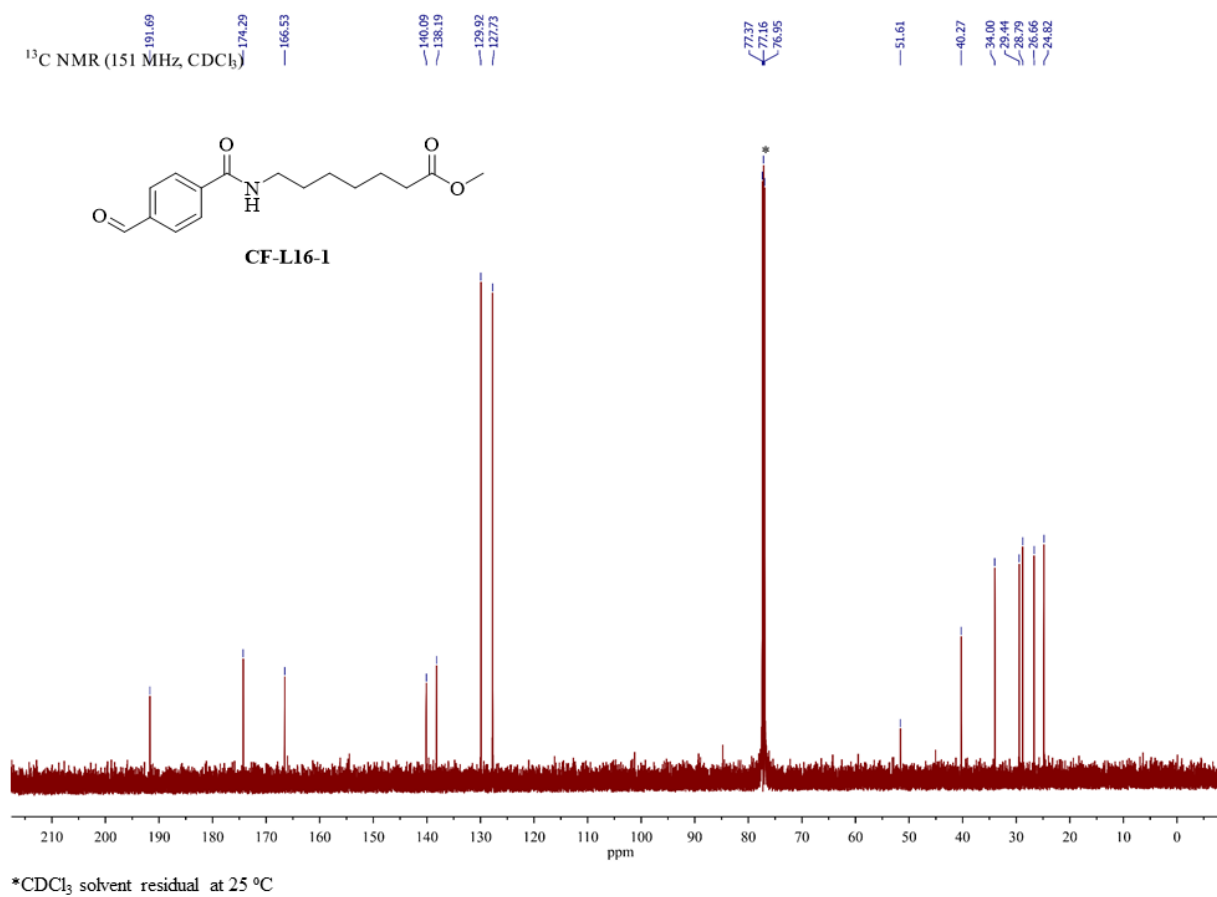
^1H NMR spectrum of CF-L15 in DMSO-d_6



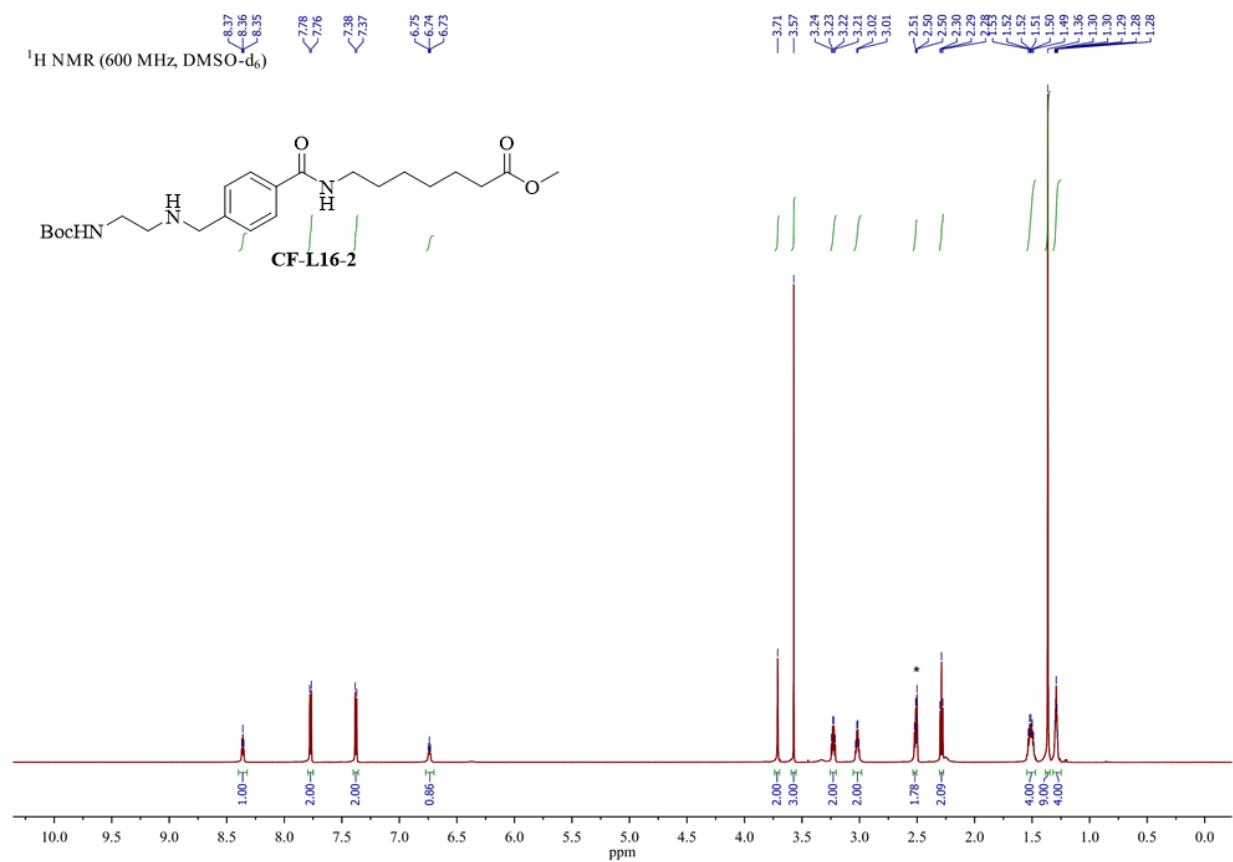
¹³C NMR spectrum of CF-L15 in DMSO-d₆



¹H NMR spectrum of CF-L16-1 in CDCl₃

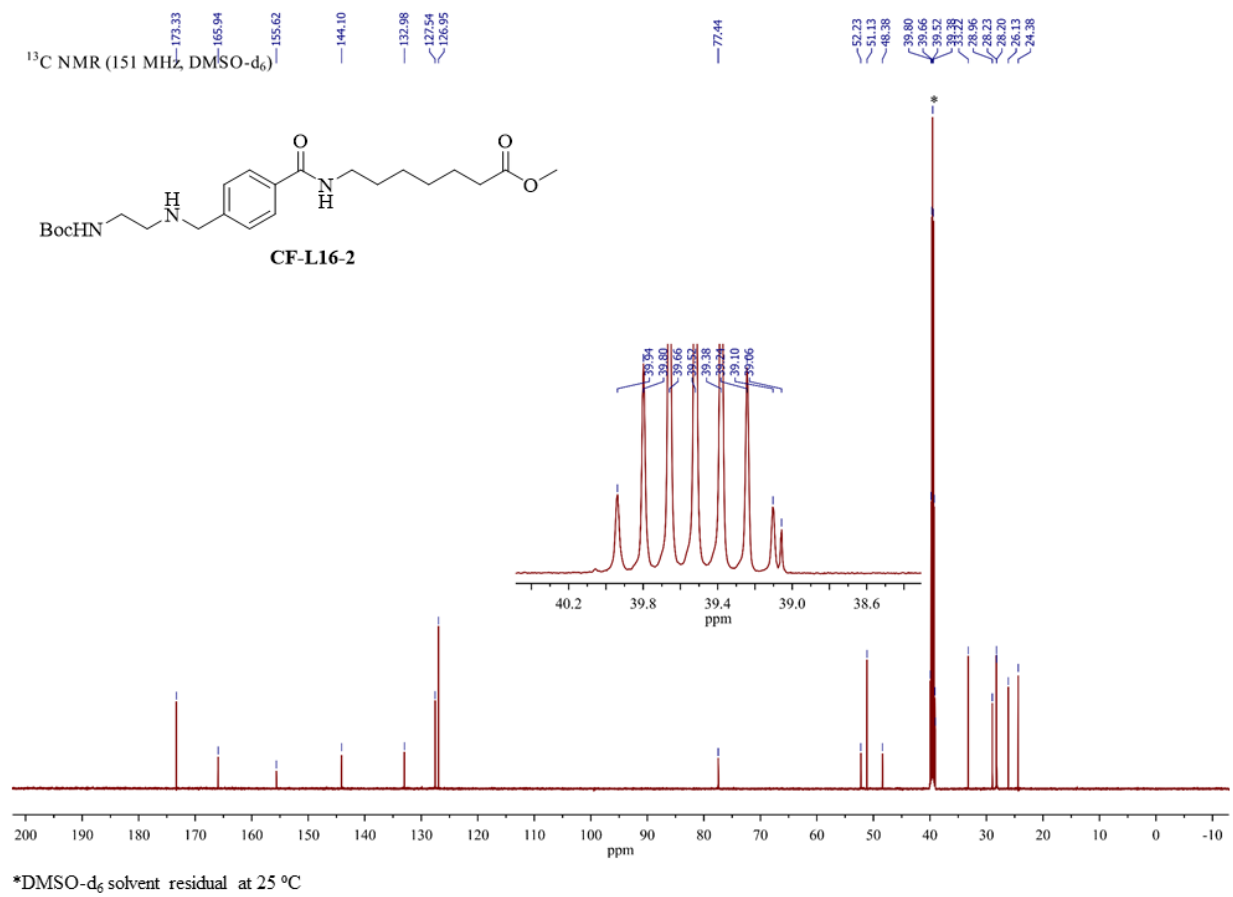


^{13}C NMR spectrum of **CF-L16-1** in CDCl_3

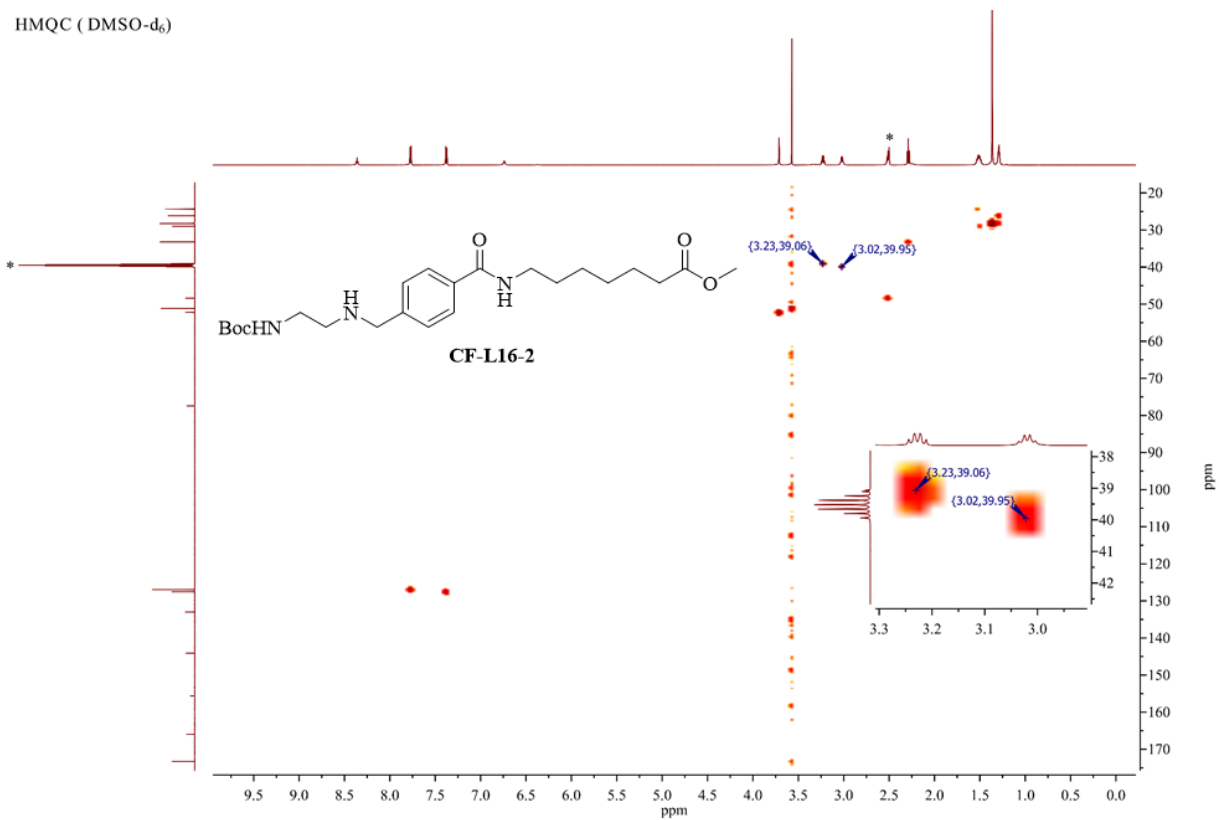


*DMSO-d₆ solvent residual at 25 °C

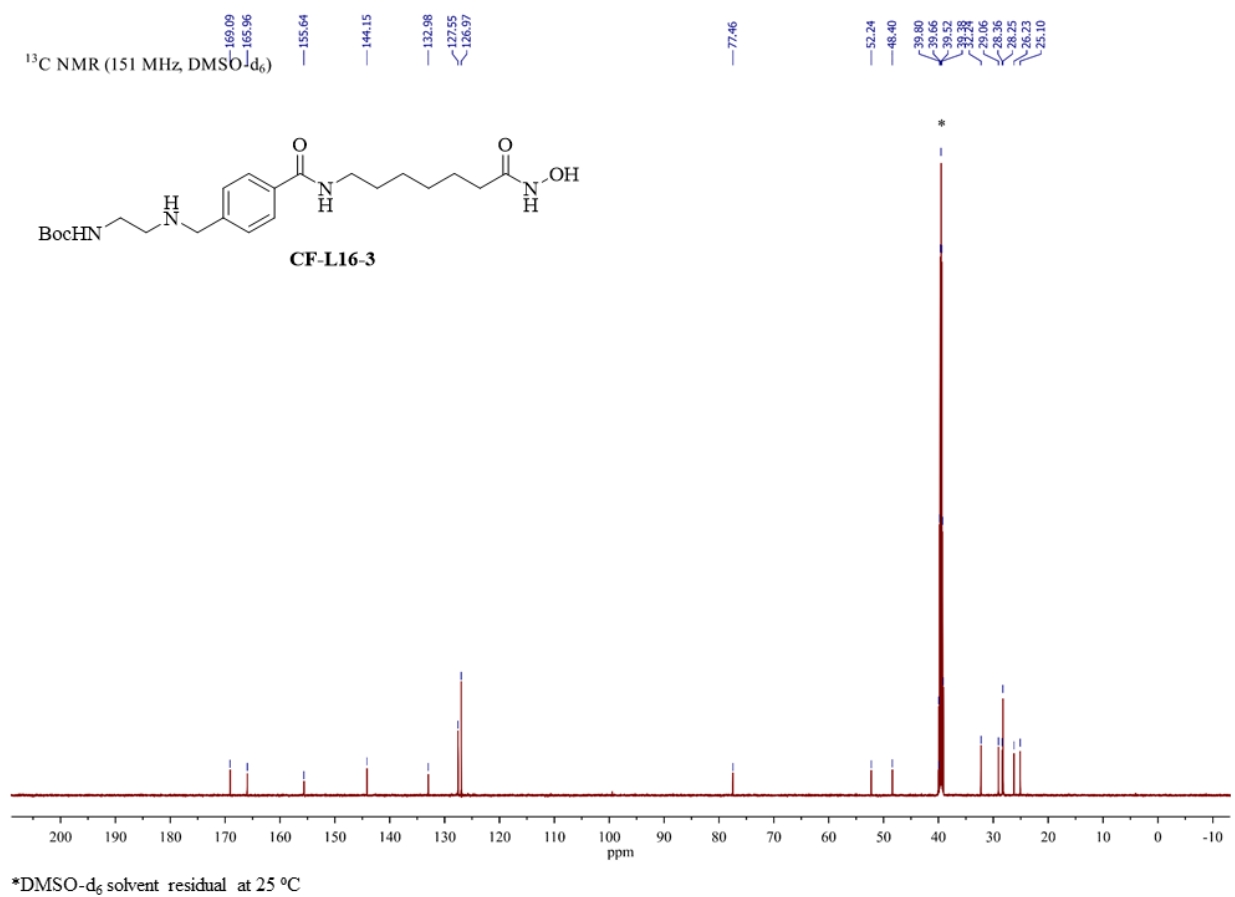
¹H NMR spectrum of CF-L16-2 in DMSO-d₆



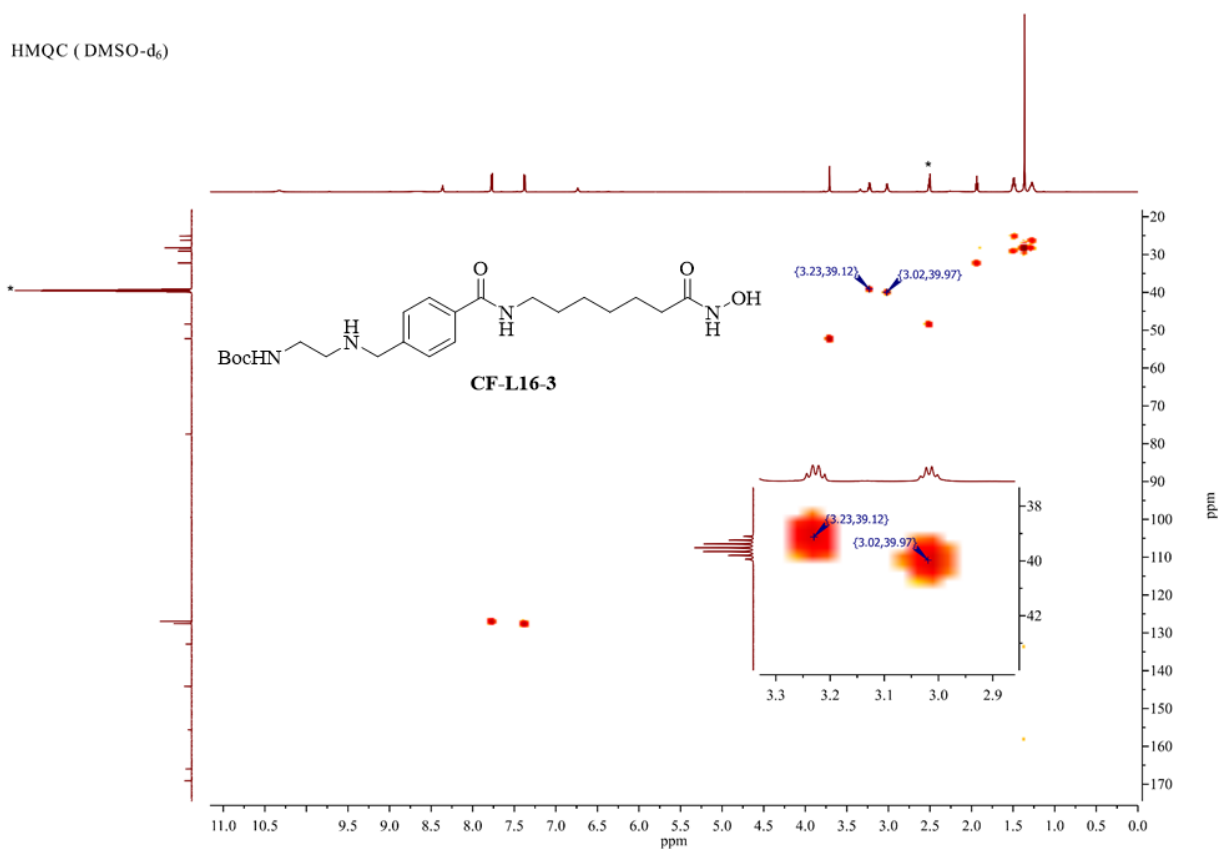
¹³C NMR spectrum of **CF-L16-2** in DMSO-d₆



HMQC NMR spectrum of **CF-L16-2** in DMSO-d₆ (^{13}C δ 39.95 overlaps with solvent residual peak)

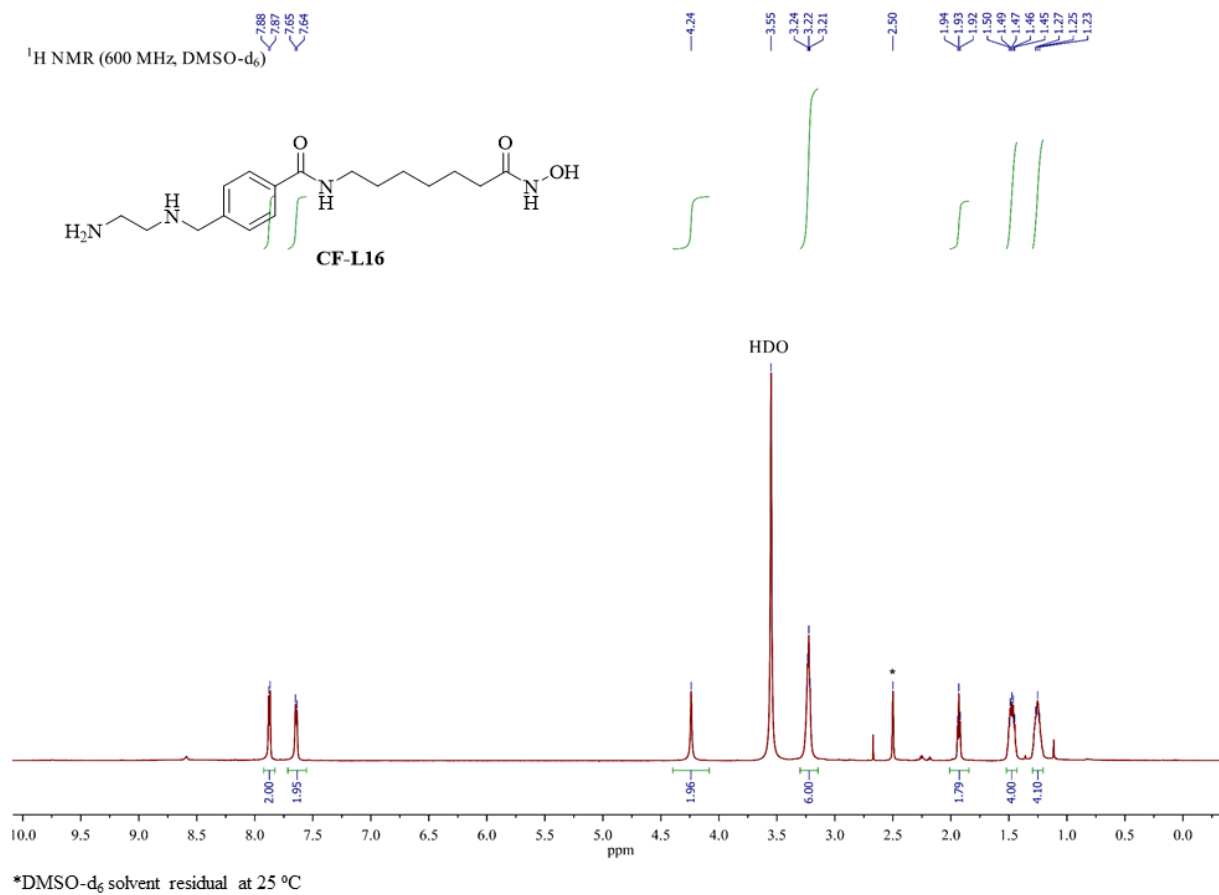


¹³C NMR spectrum of **CF-L16-3** in DMSO-d₆

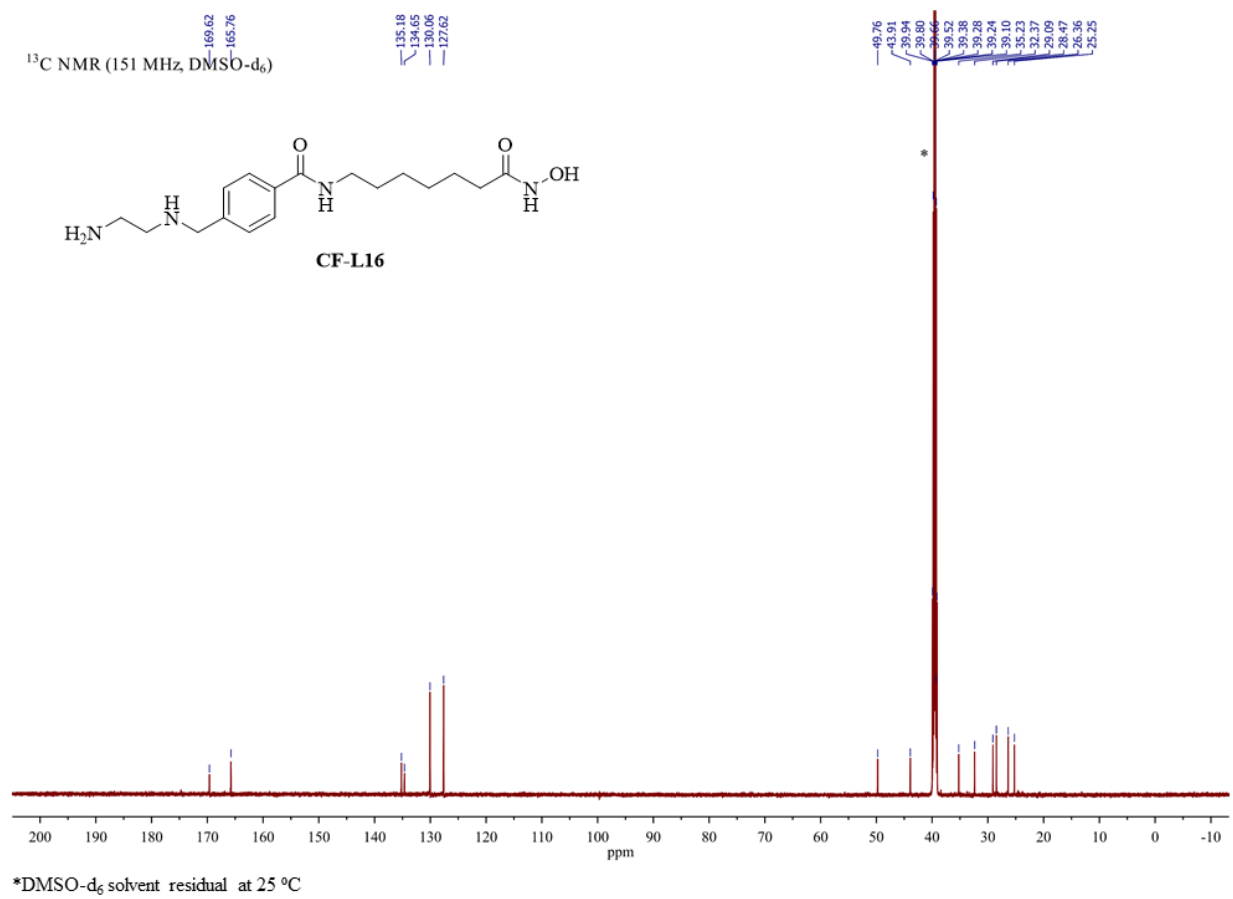


*DMSO-d₆ solvent residual at 25 °C

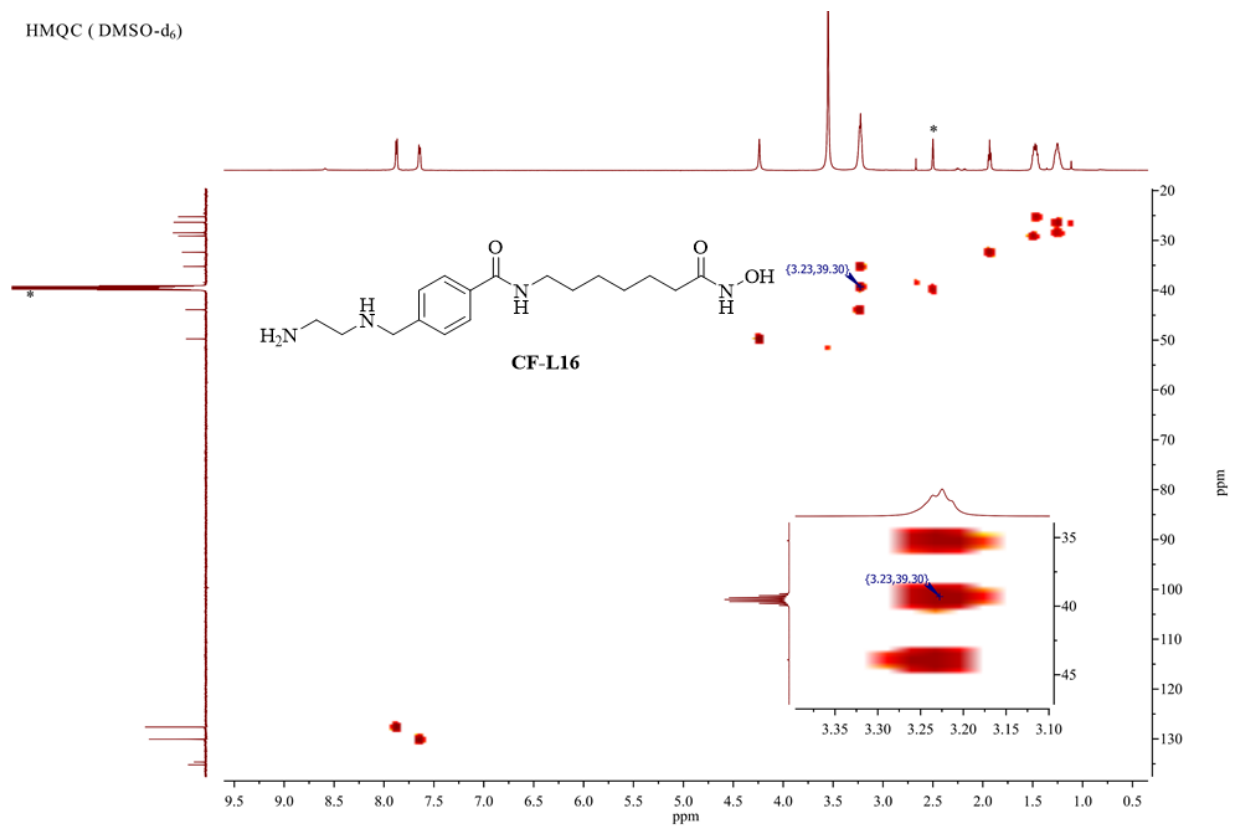
HMQC NMR spectrum of **CF-L16-3** in DMSO-d₆ (^{13}C δ 39.12, 39.97 overlaps with solvent residual peak)



¹H NMR spectrum of **CF-L16** in DMSO-d₆+ D₂O (2-3 drops)

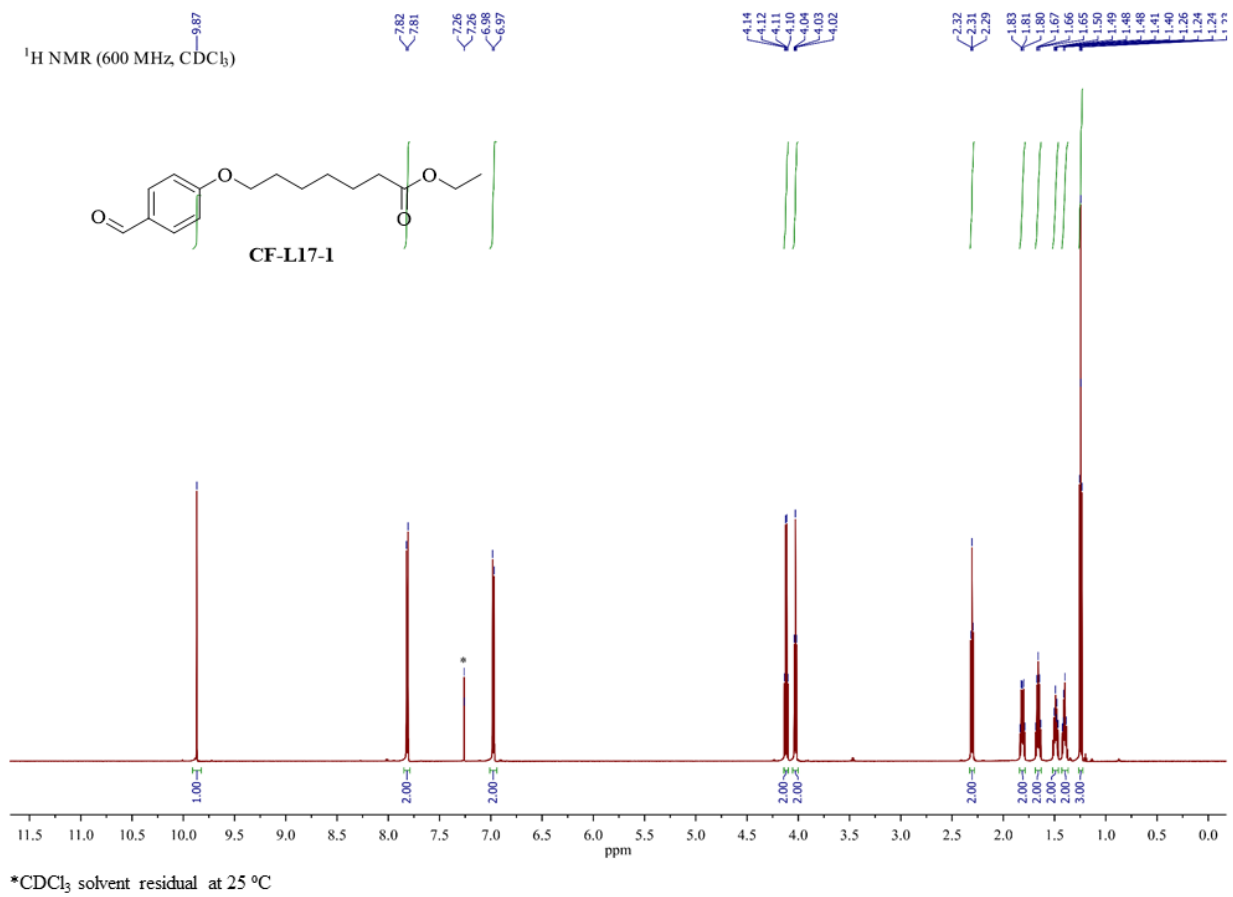


¹³C NMR spectrum of **CF-L16** in DMSO-d₆+ D₂O (2-3 drops)

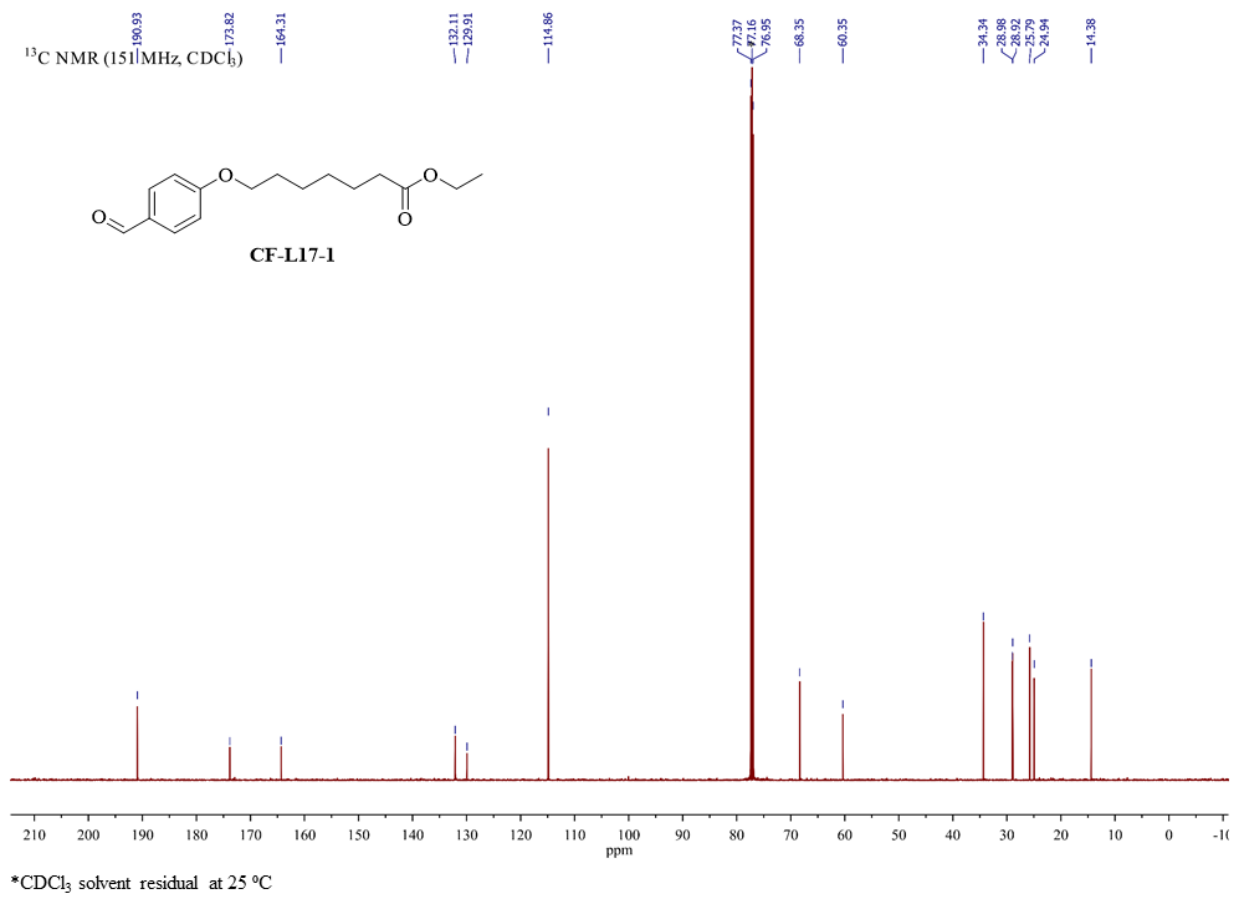


*DMSO-d₆ solvent residual at 25 °C

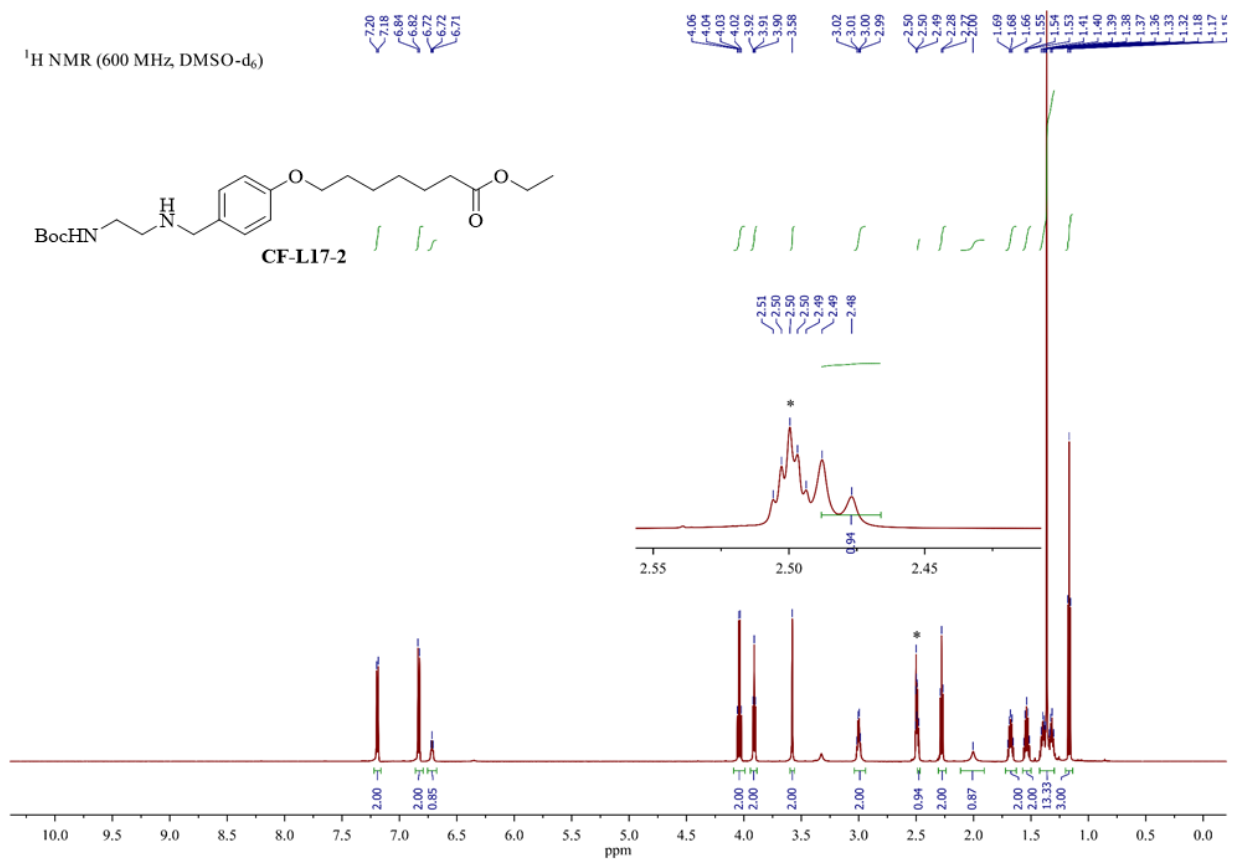
HMQC NMR spectrum of **CF-L16** in DMSO-d₆+ D₂O (¹³C δ 39.30 overlaps with solvent residual peak)



¹H NMR spectrum of CF-L17-1 in CDCl₃

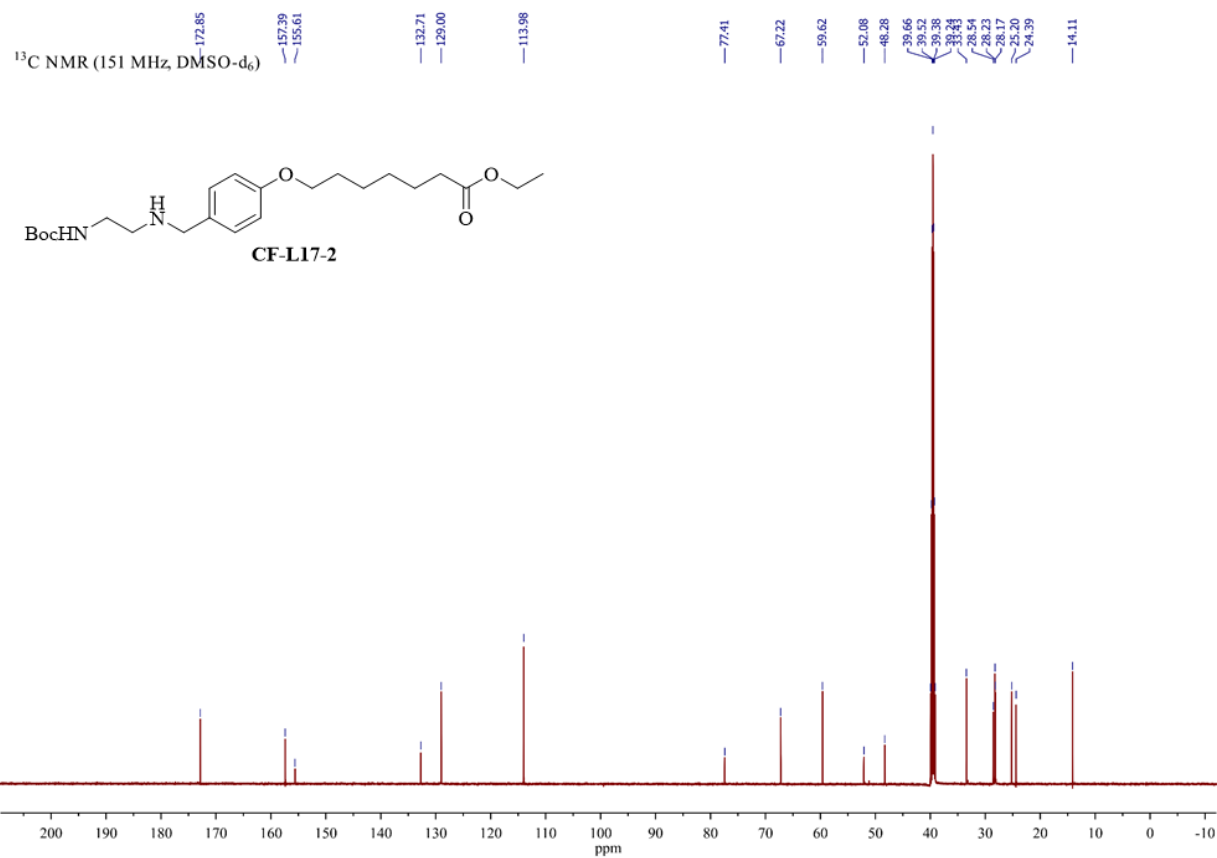


¹³C NMR spectrum of **CF-L17-1** in CDCl₃



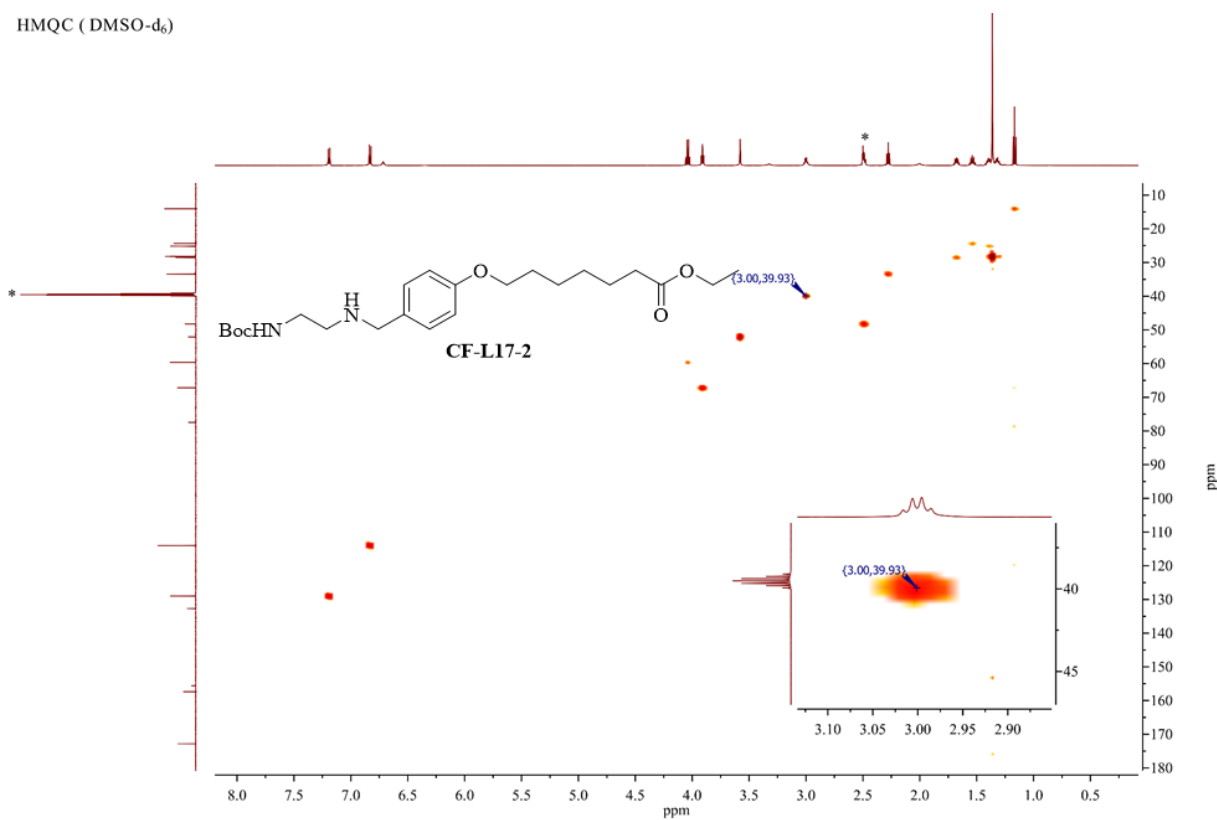
*DMSO-d₆ solvent residual at 25 °C

¹H NMR spectrum of **CF-L17-2** in DMSO-d₆

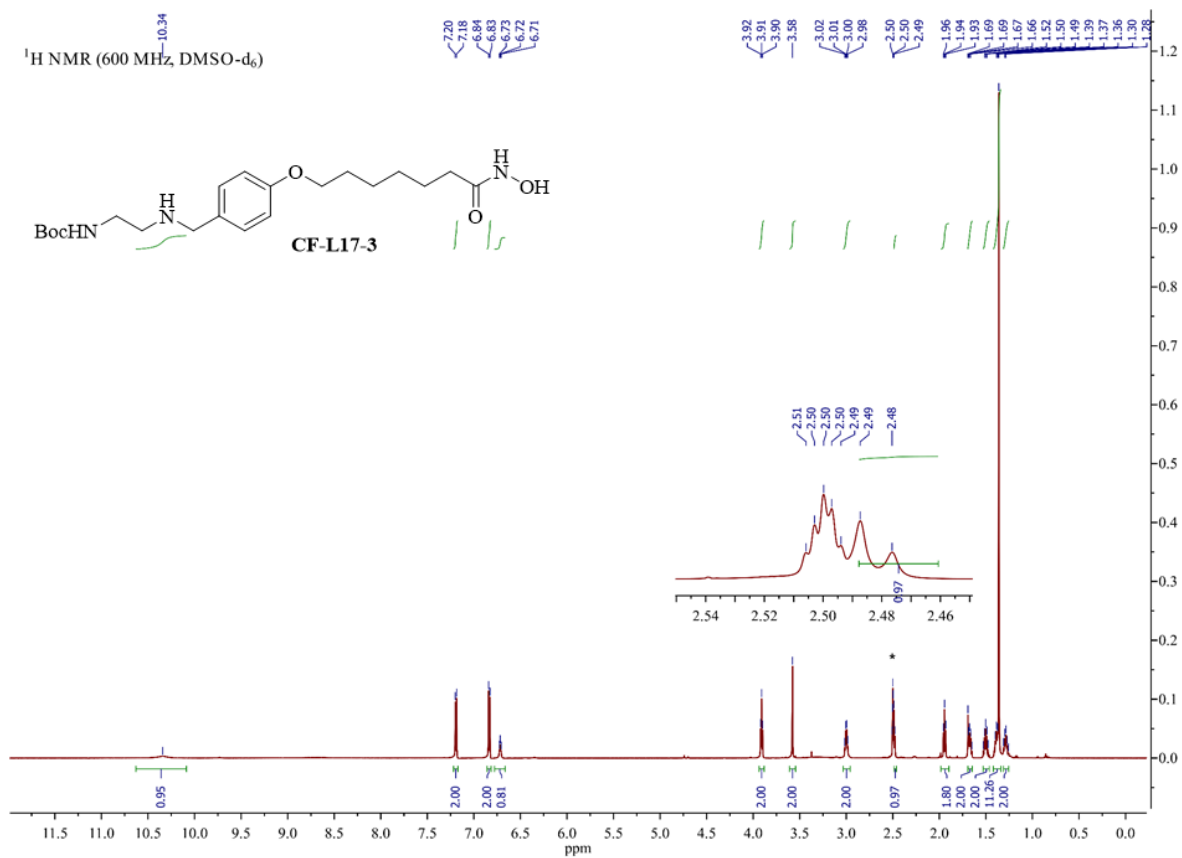


*DMSO-d₆ solvent residual at 25 °C

¹³C NMR spectrum of **CF-L17-2** in DMSO-d₆

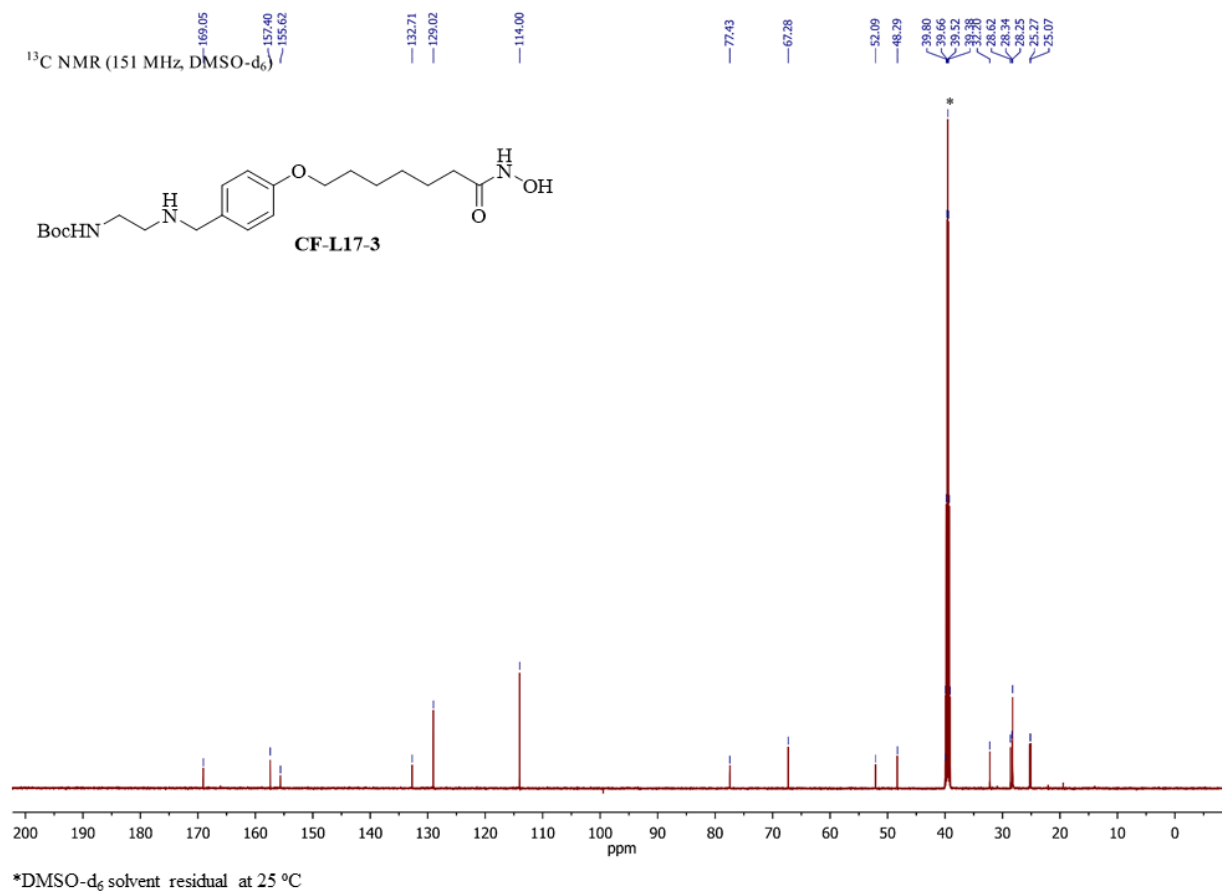
HMQC (DMSO-d₆)*DMSO-d₆ solvent residual at 25 °C

HMQC NMR spectrum of **CF-L17-2** in DMSO-d₆+ D₂O (¹³C δ 39.93 overlaps with solvent residual peak)

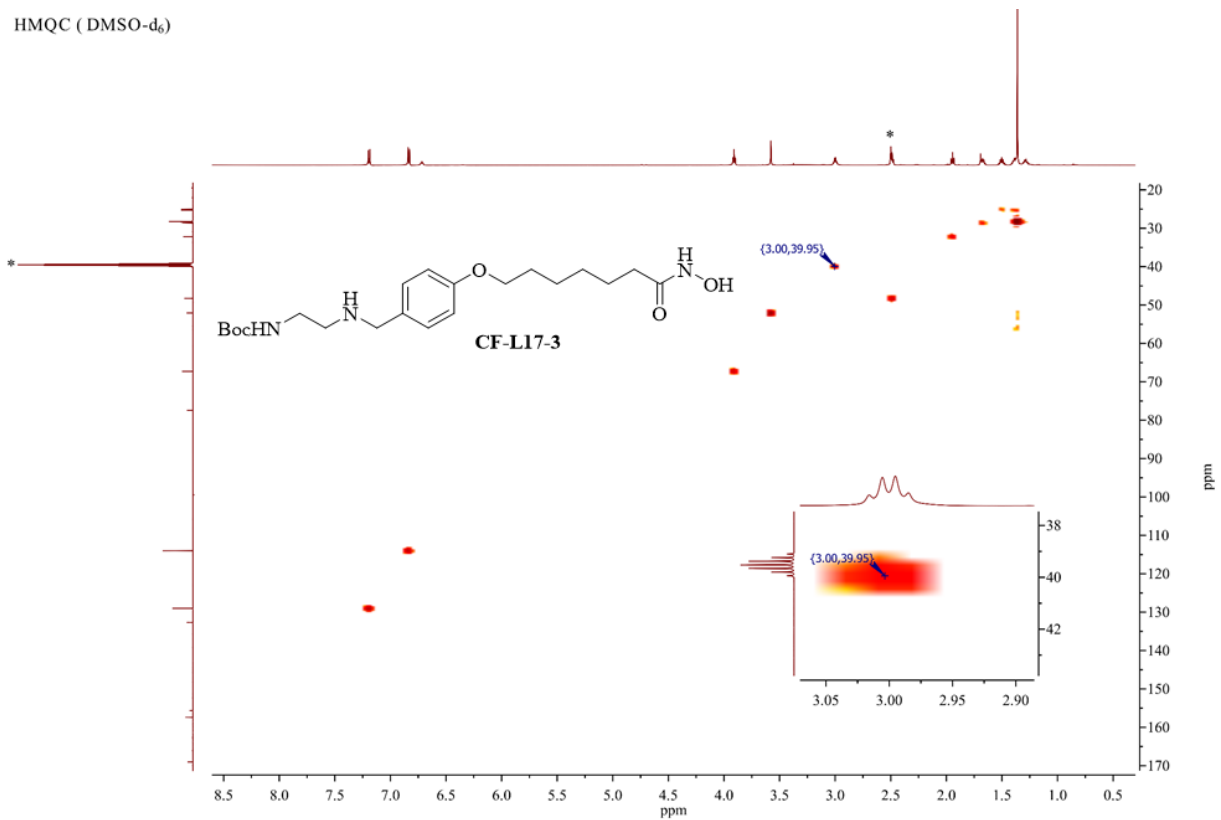


*DMSO-d₆ solvent residual at 25 °C

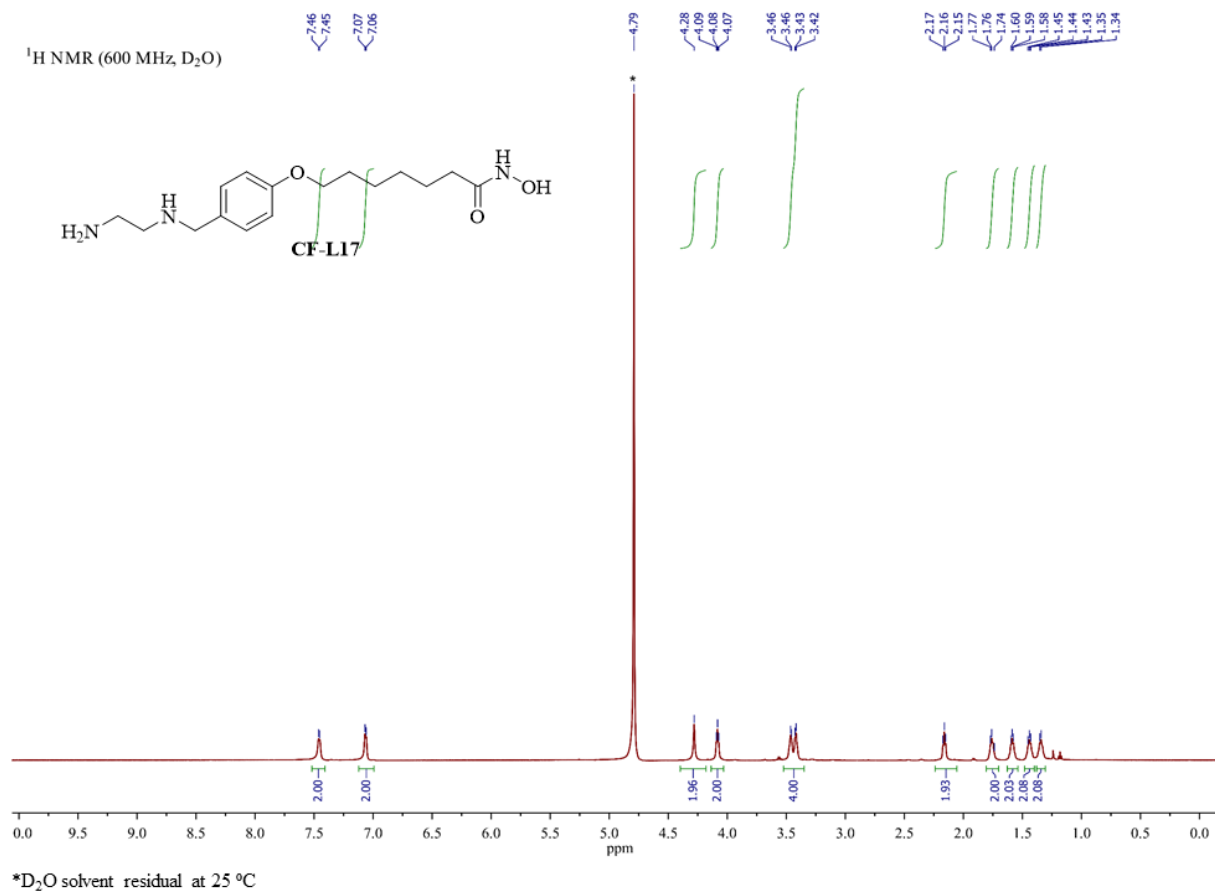
¹H NMR spectrum of CF-L17-3 in DMSO-d₆



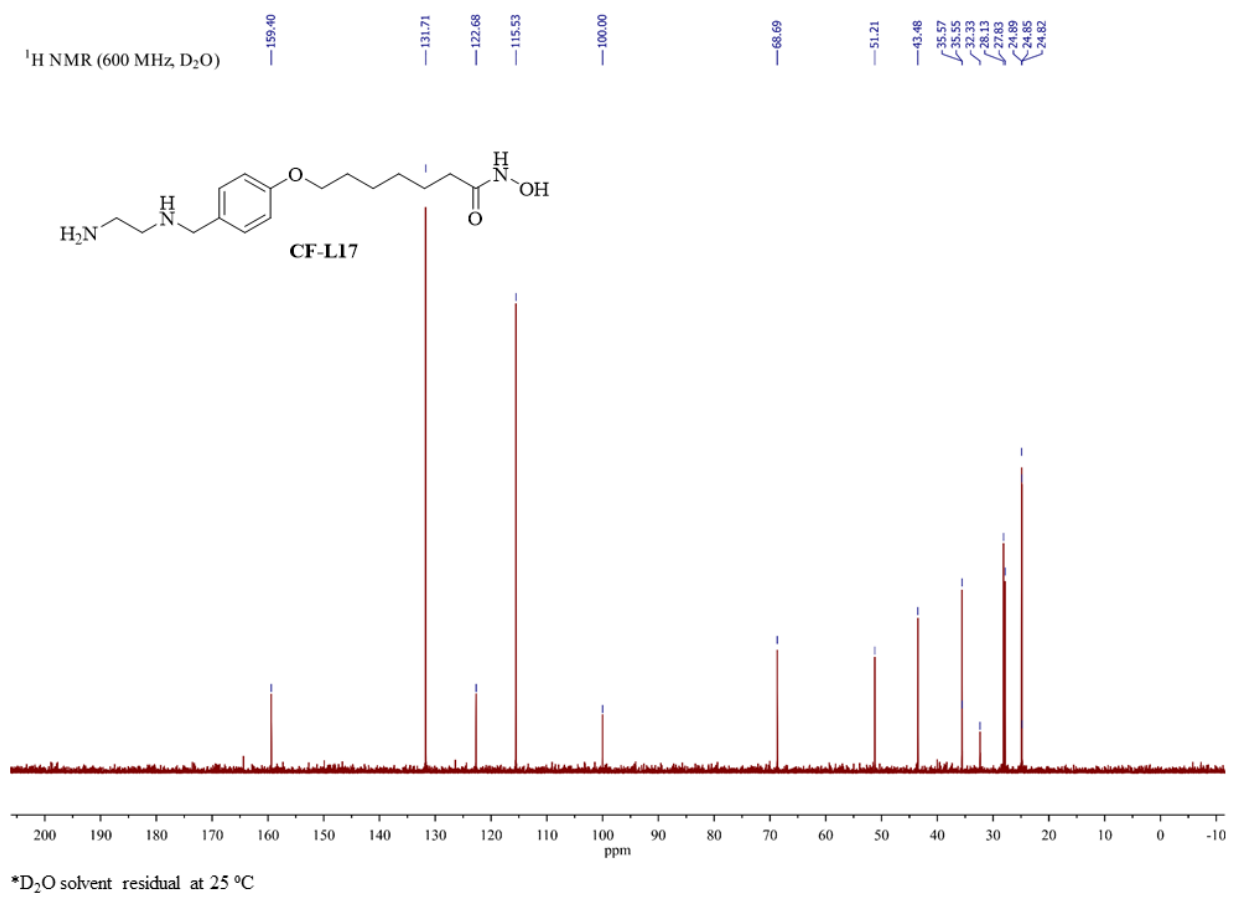
¹³C NMR spectrum of **CF-L17-3** in DMSO-d₆



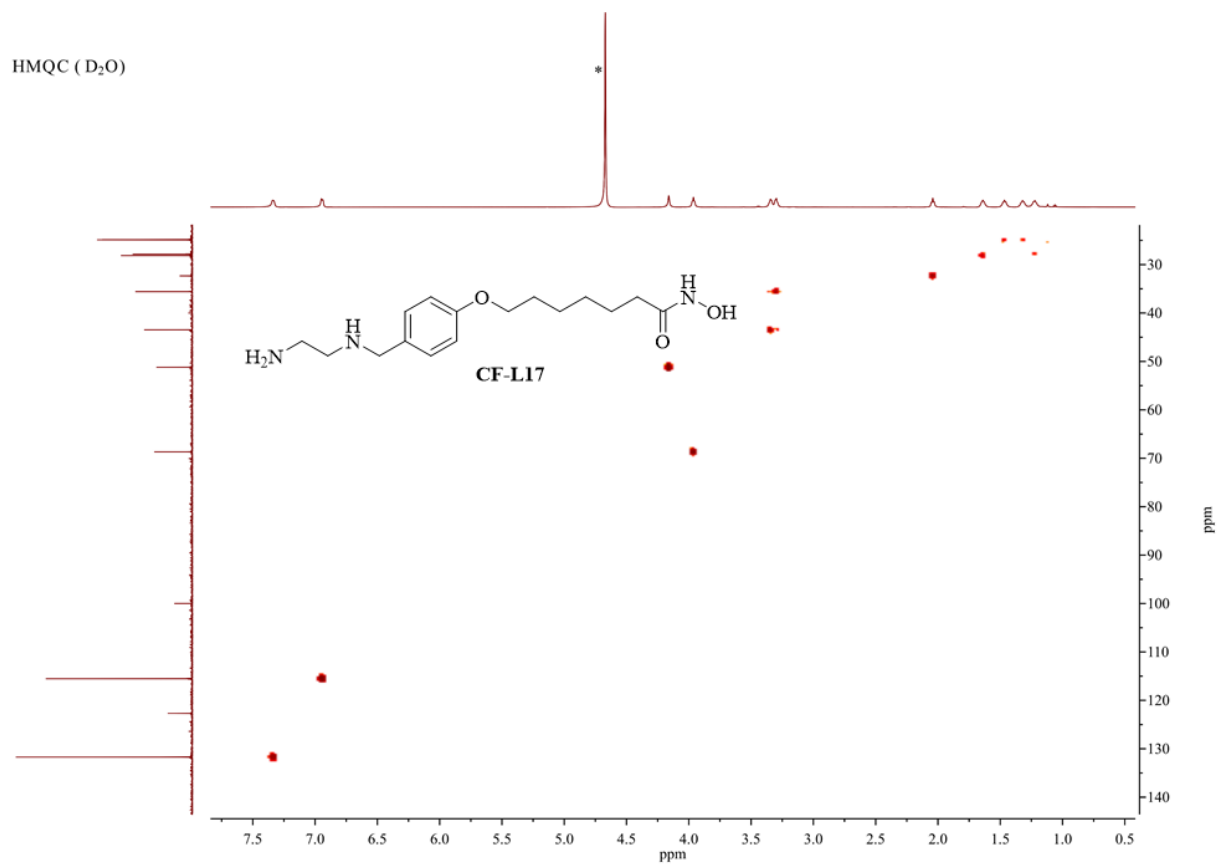
HMQC NMR spectrum of **CF-L17-3** in DMSO-d₆ (¹³C δ 39.95 overlaps with solvent residual peak)



¹H NMR spectrum of CF-L17 in D₂O

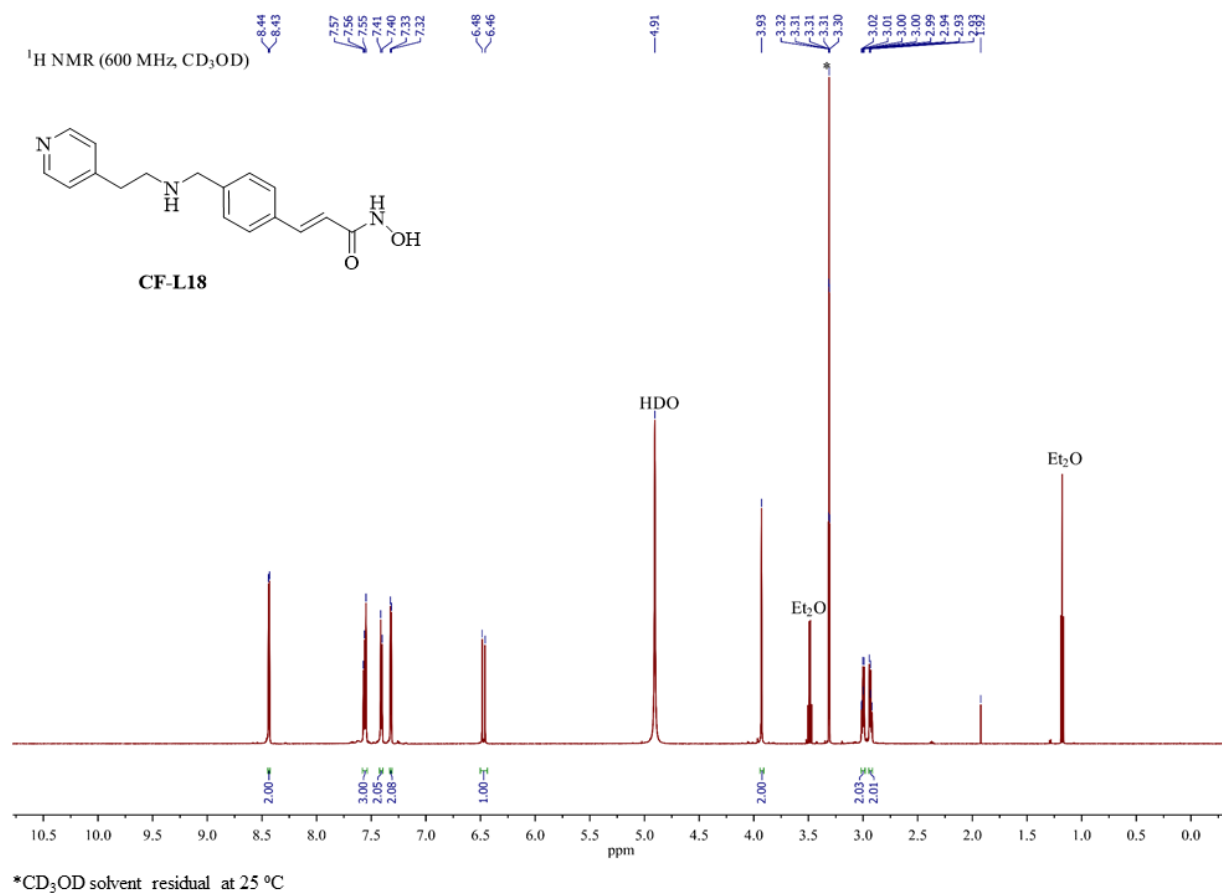


¹³C NMR spectrum of CF-L17 in D₂O

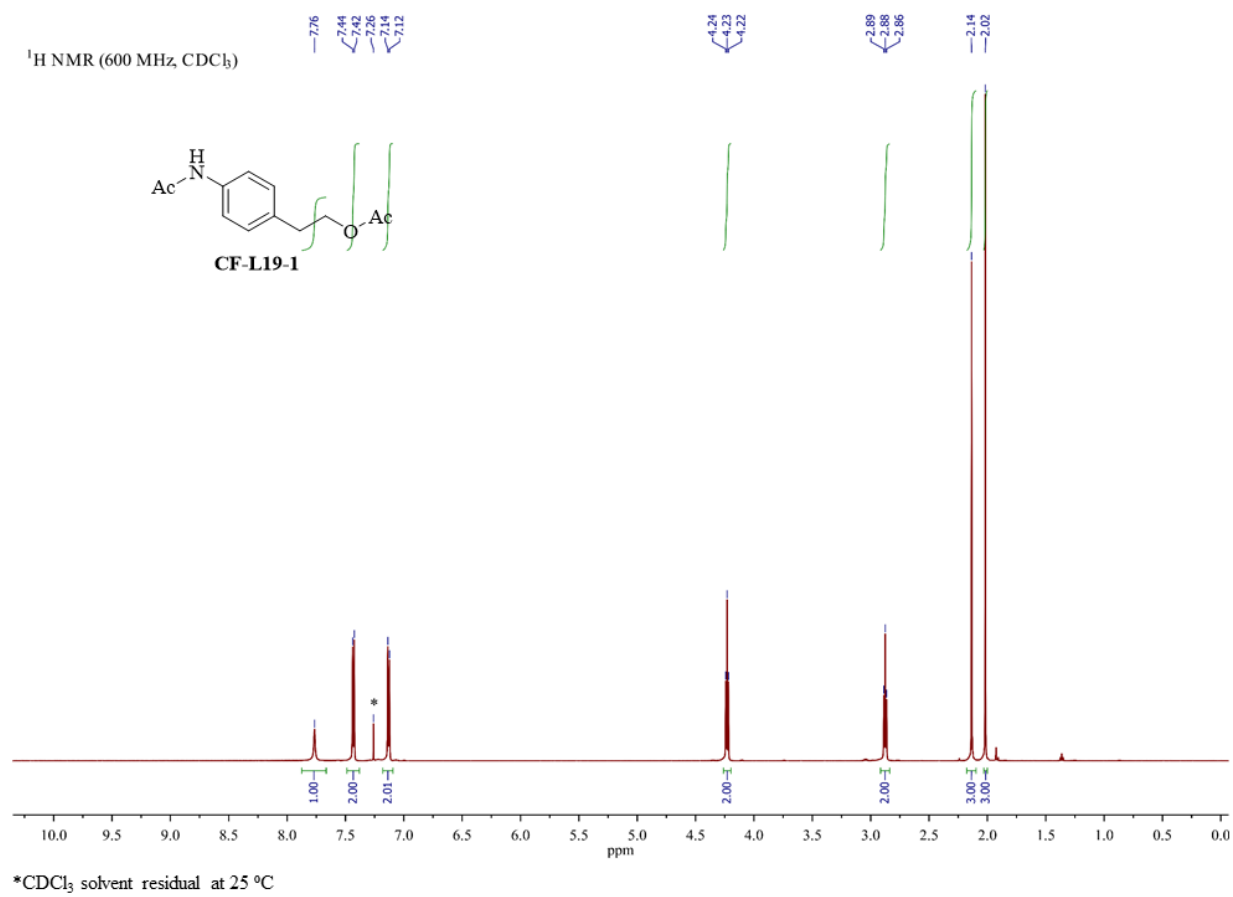


*D₂O solvent residual at 25 °C

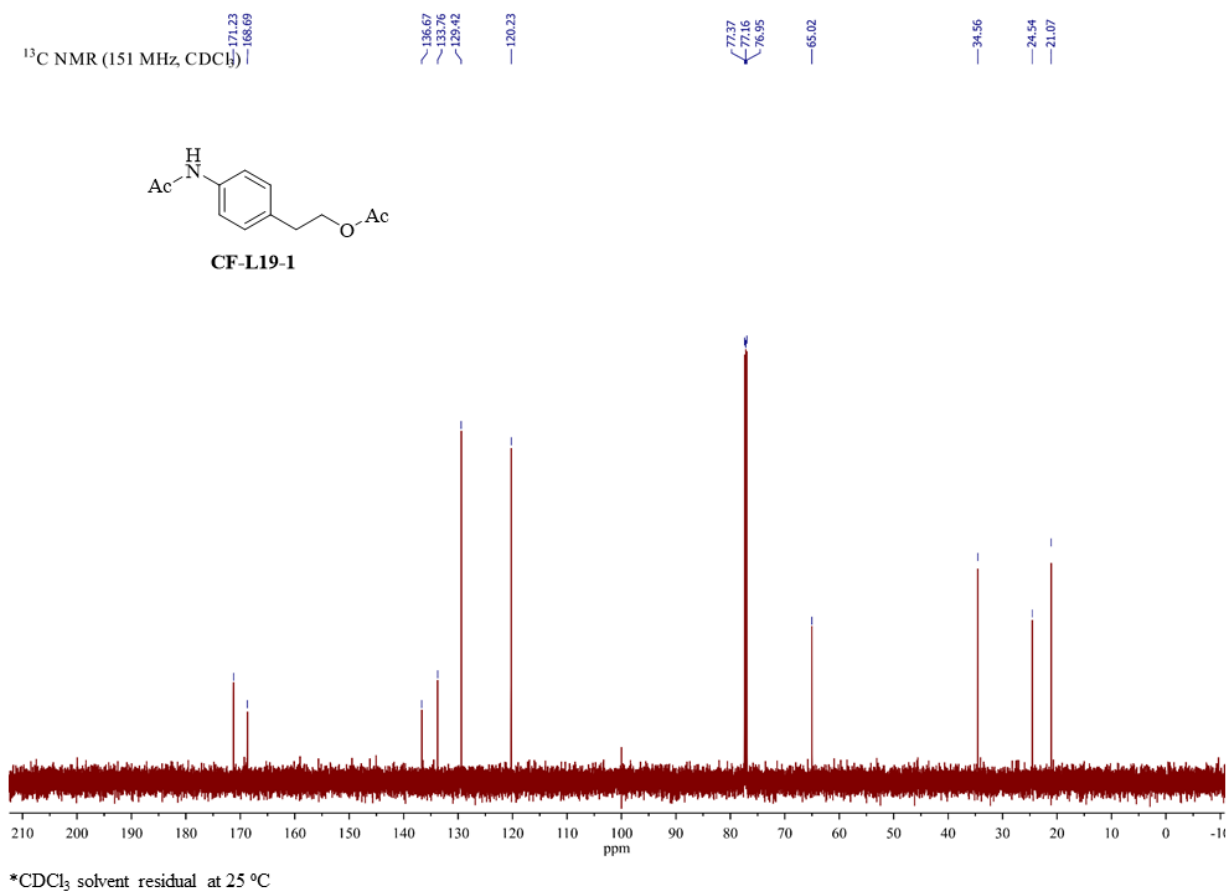
HMQC NMR spectrum of **CF-L17** in D₂O



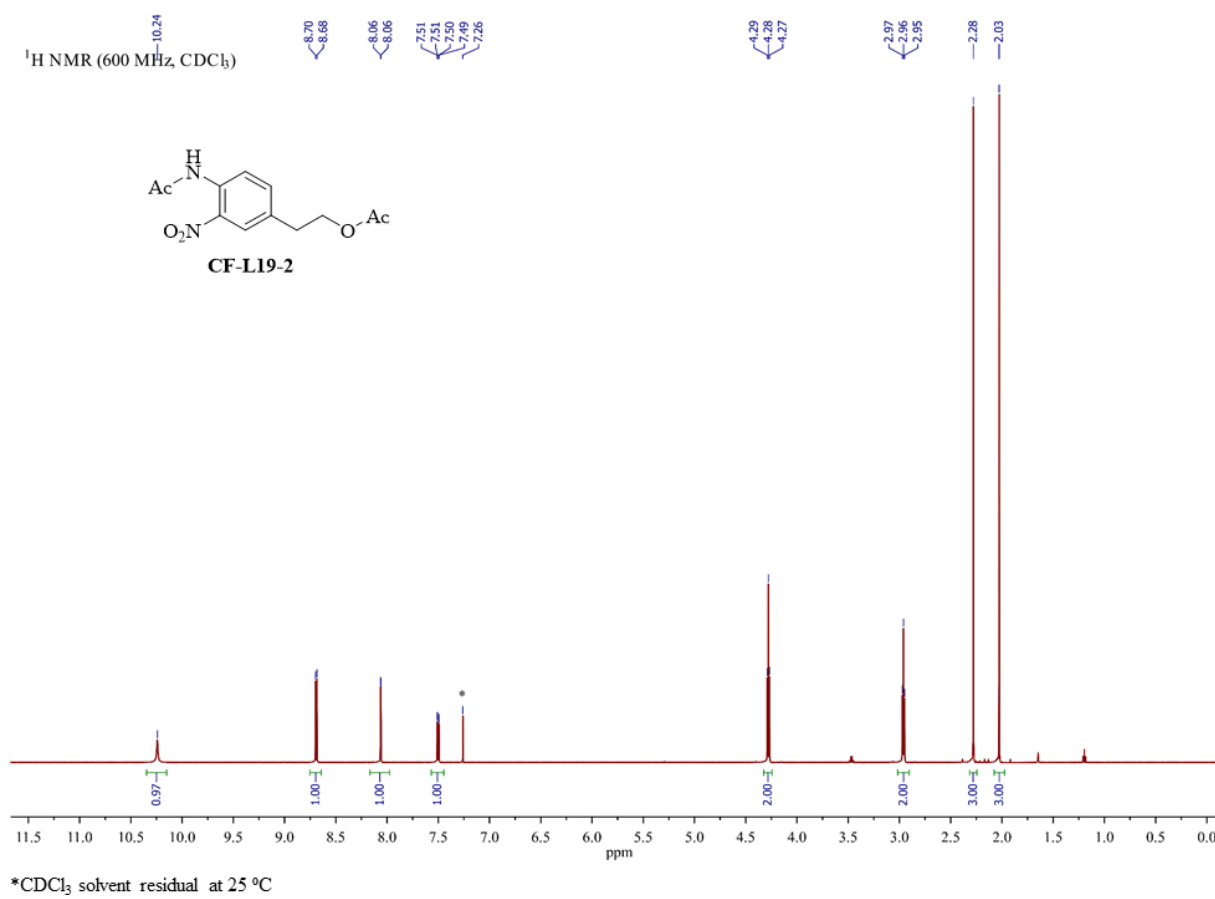
¹H NMR spectrum of **CF-L18** in CD₃OD



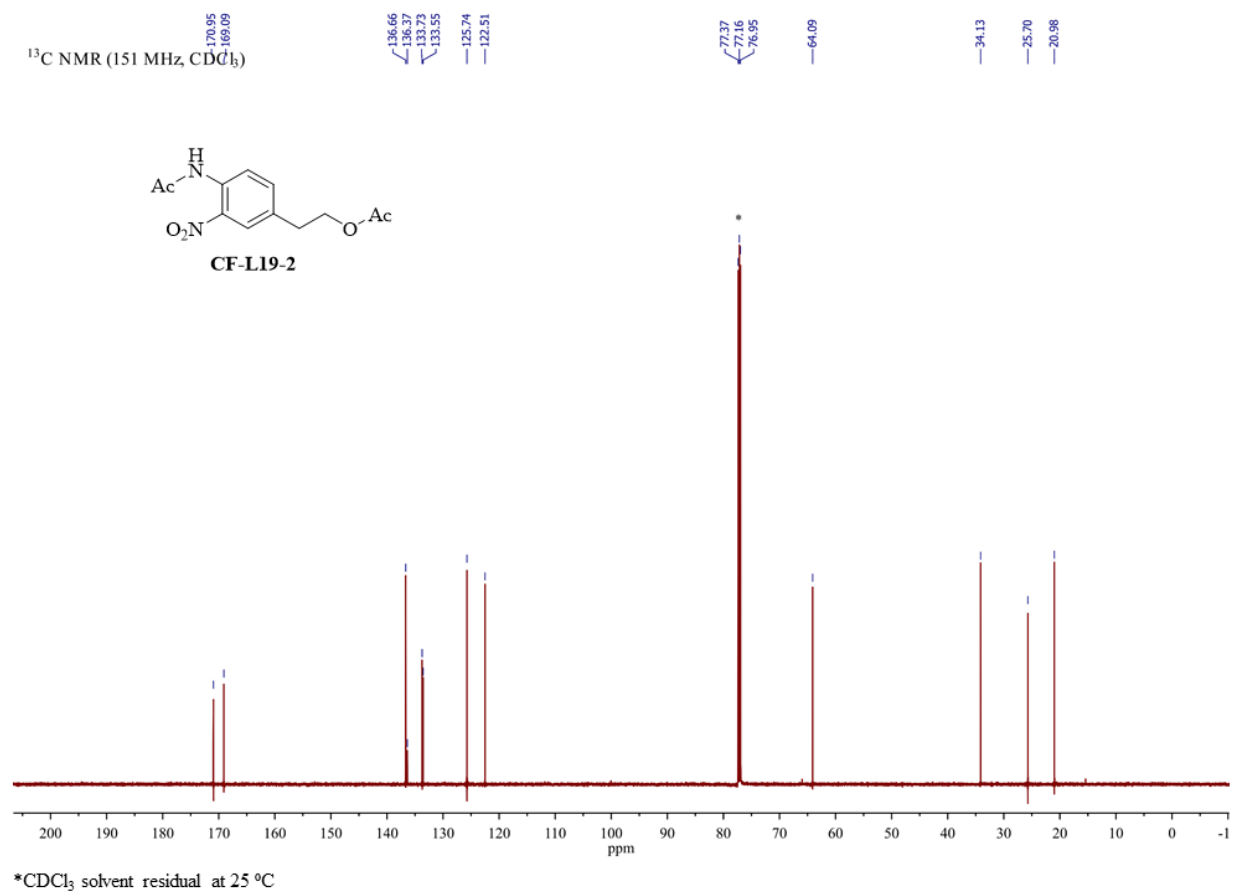
¹H NMR spectrum of CF-L19-1 in CDCl₃



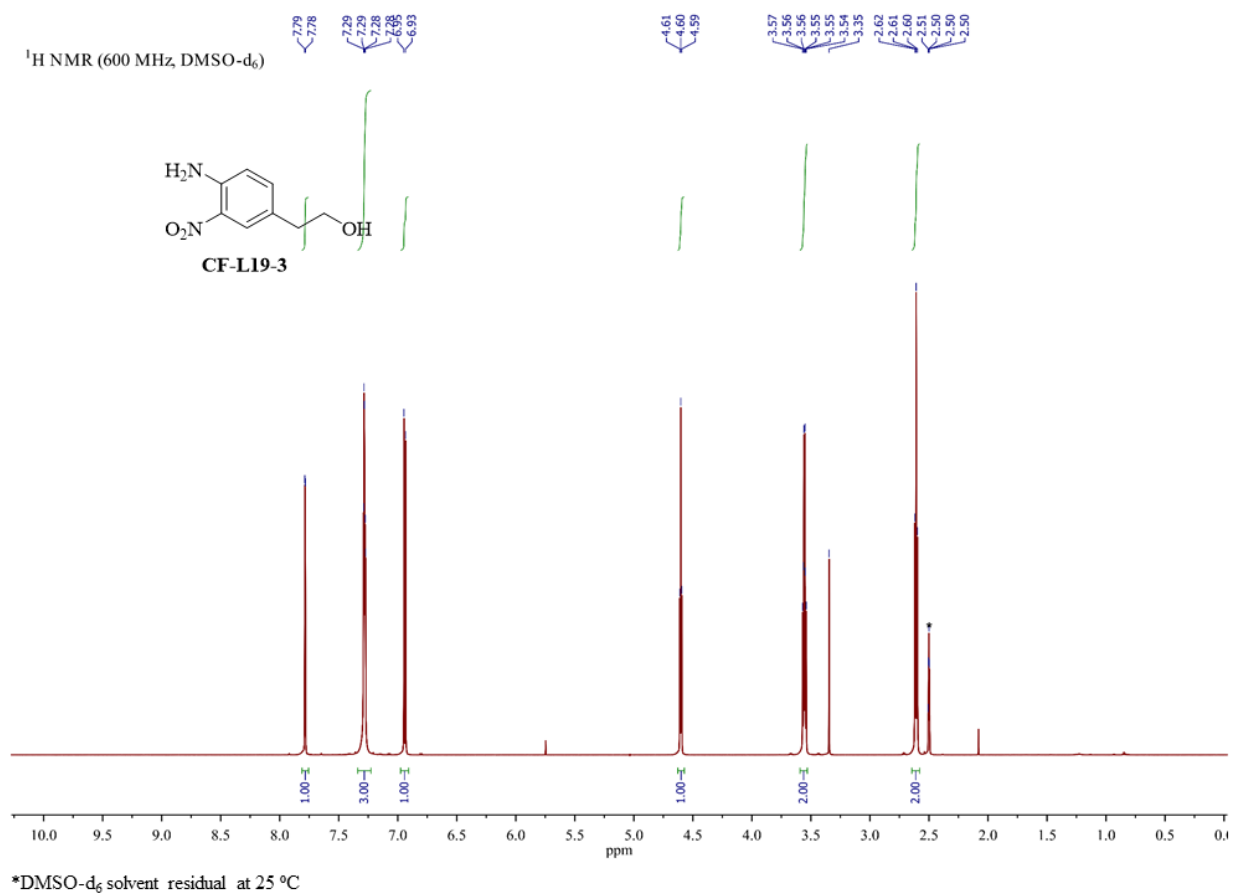
¹³C NMR spectrum of **CF-L19-1** in CDCl₃



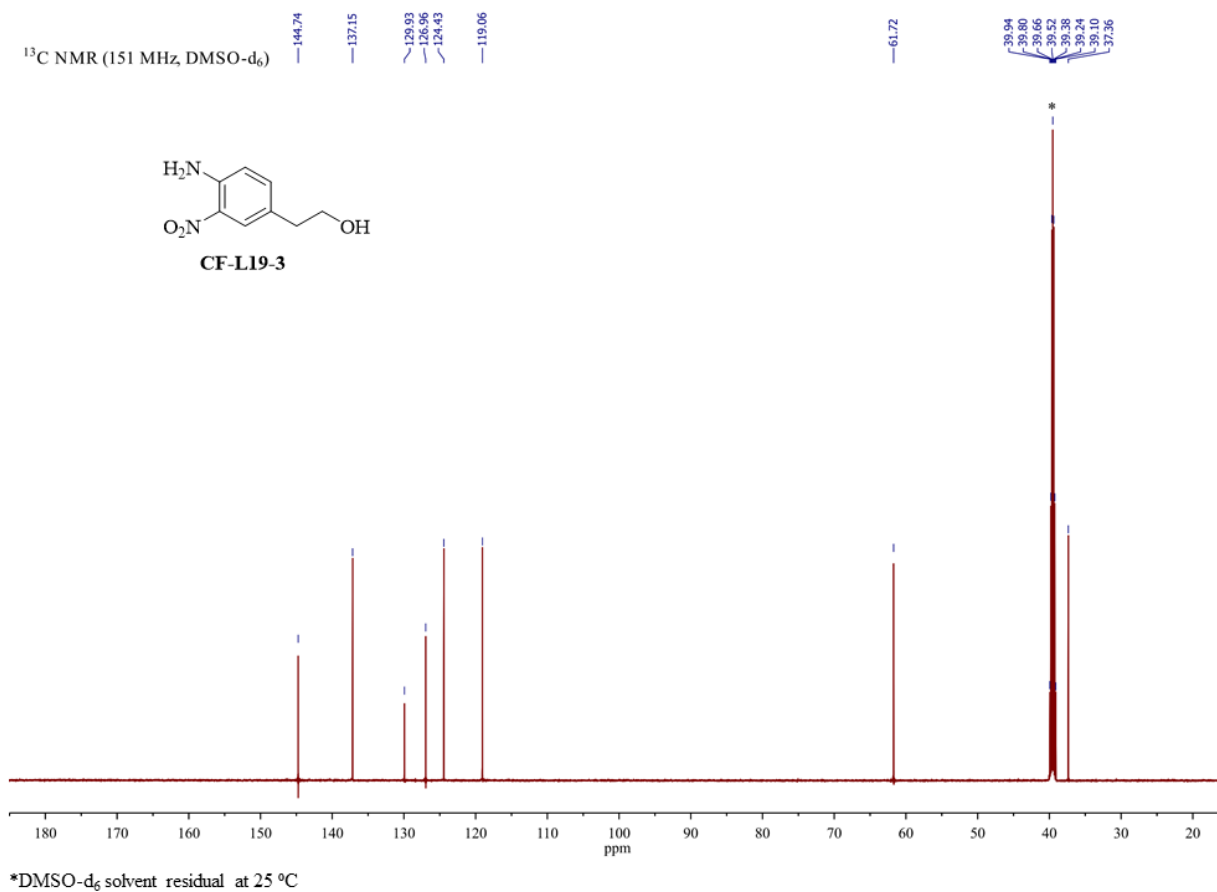
¹H NMR spectrum of **CF-L19-2** in CDCl₃



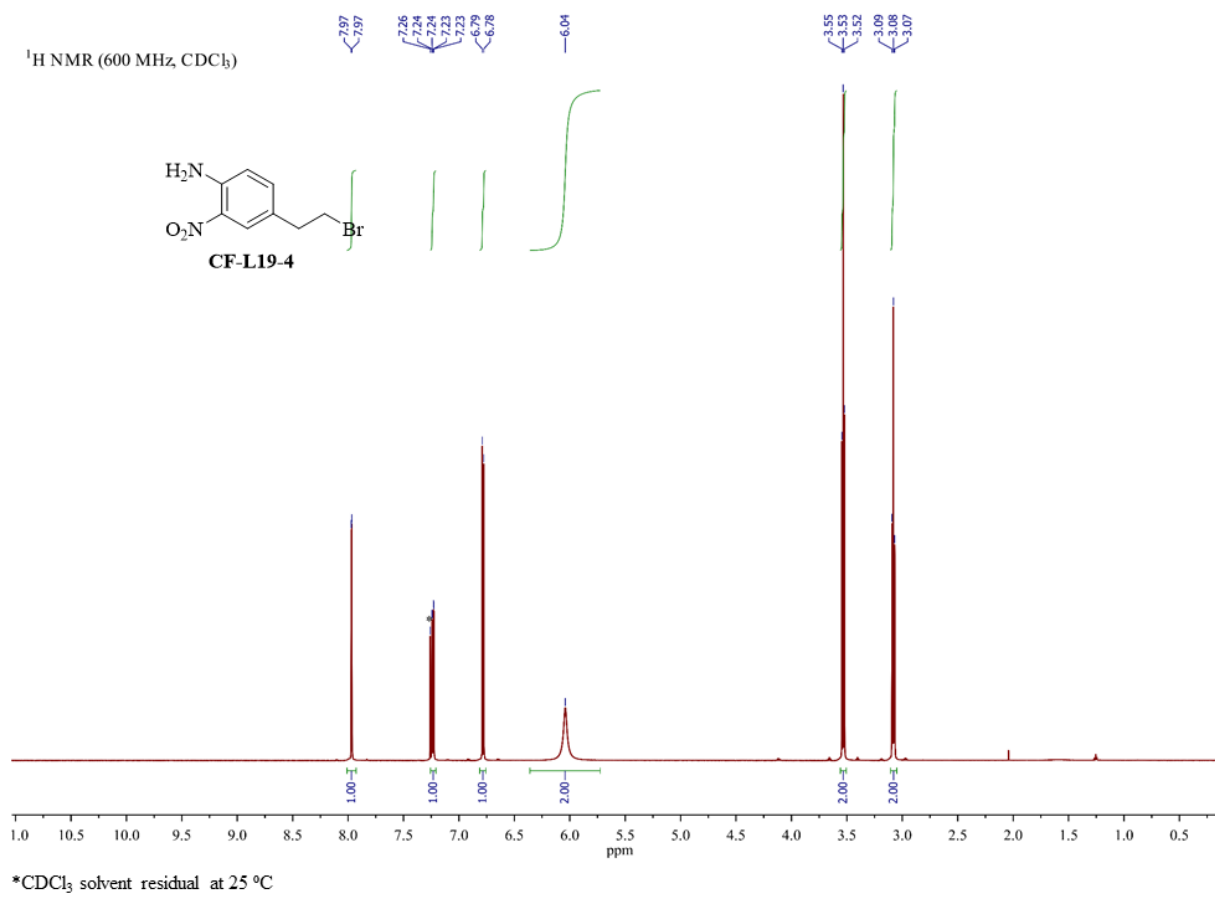
¹³C NMR spectrum of **CF-L19-2** in CDCl₃



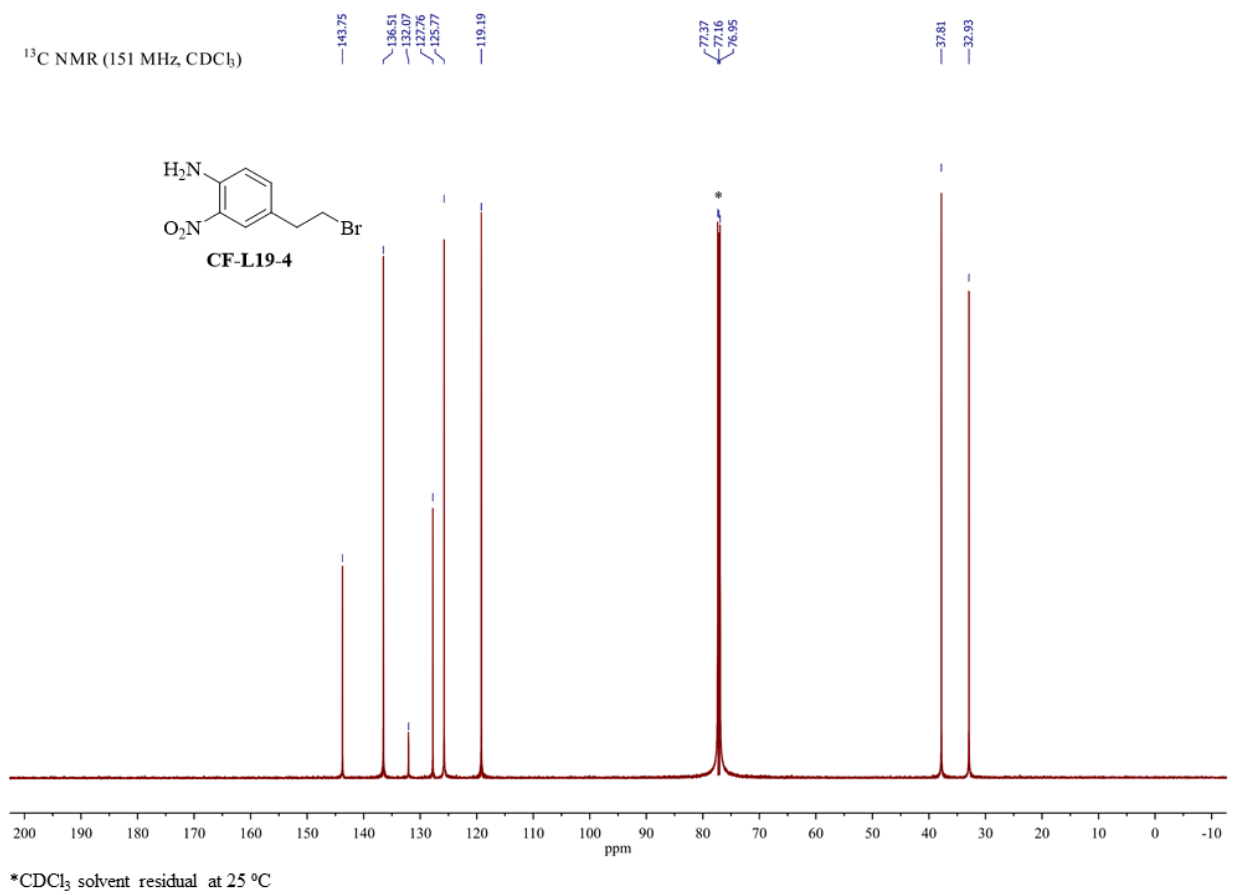
¹H NMR spectrum of CF-L19-3 in DMSO-d₆



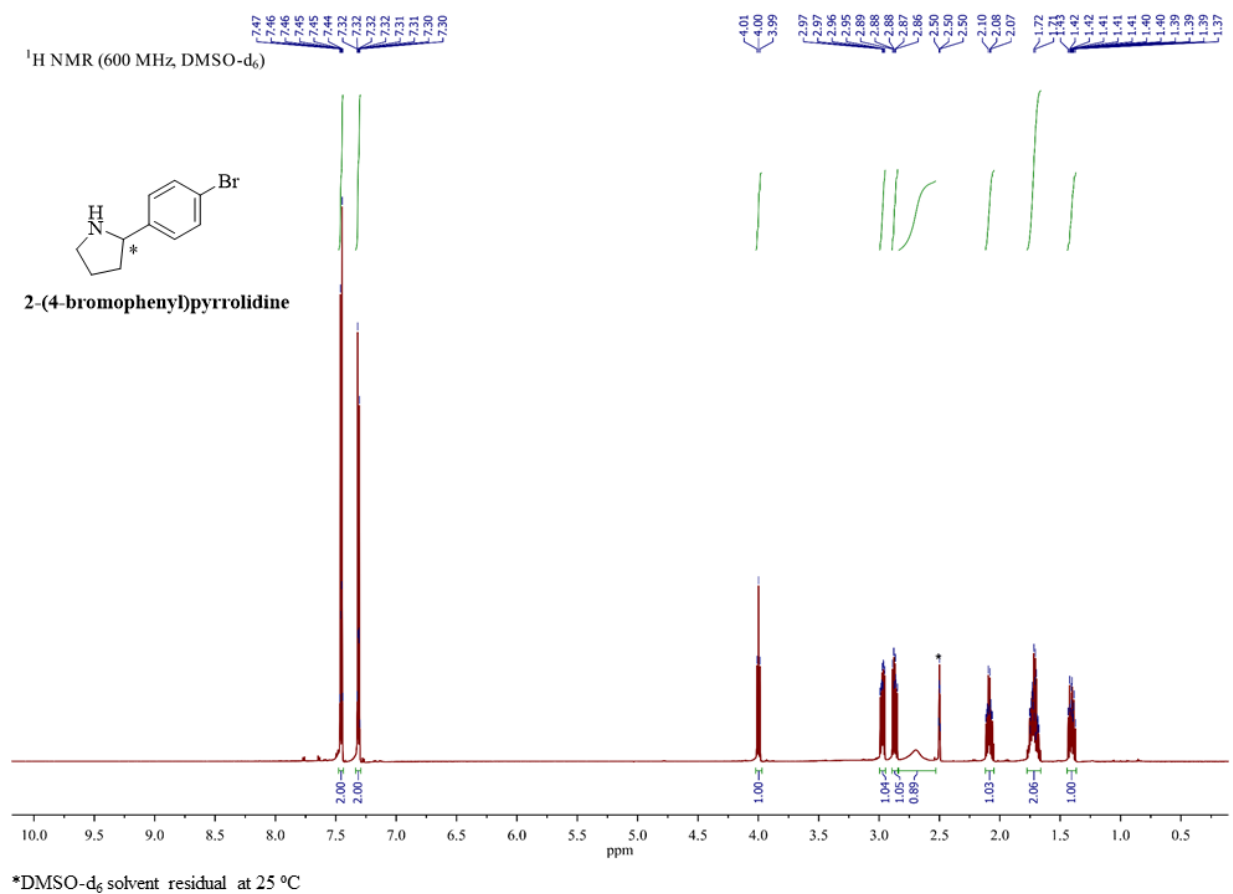
^{13}C NMR spectrum of **CF-L19-3** in DMSO- d_6



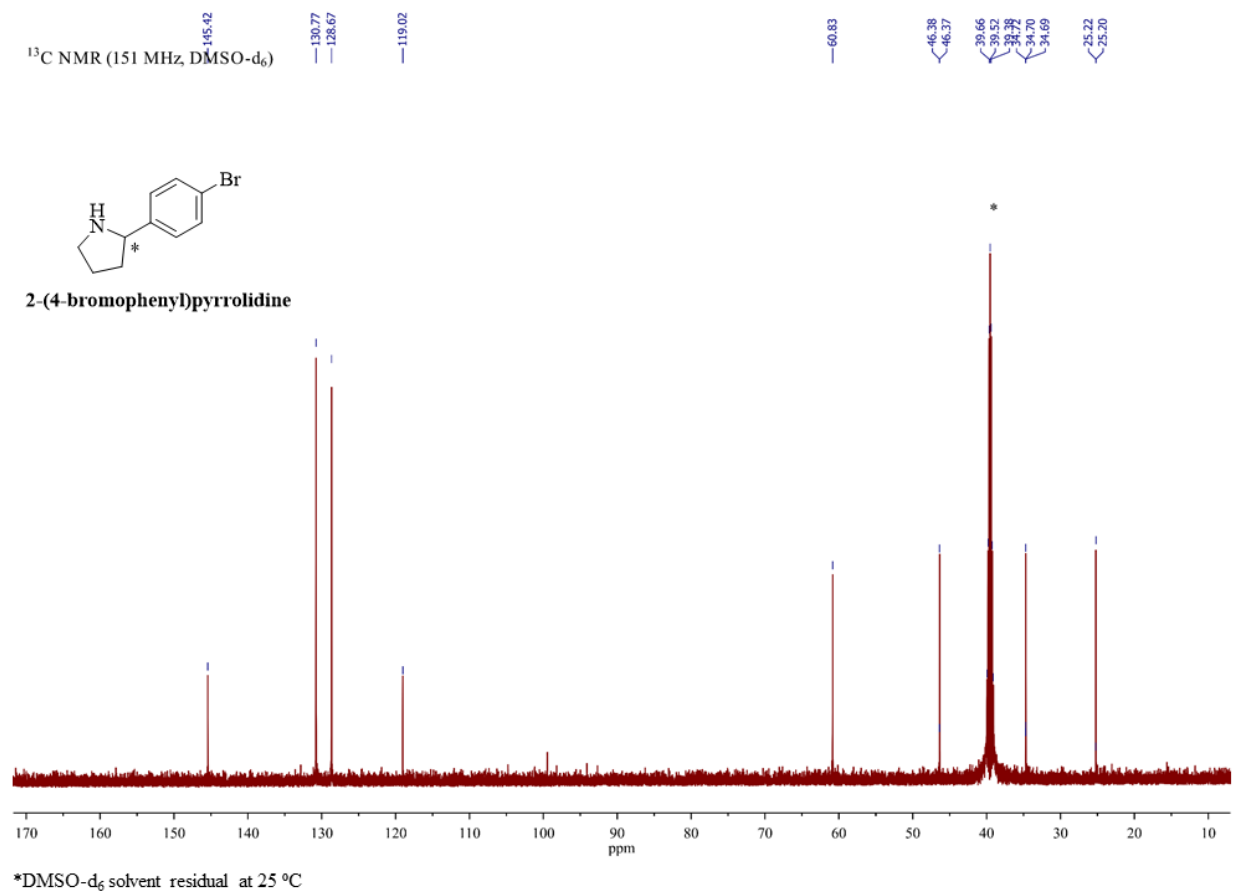
¹H NMR spectrum of **CF-L19-4** in CDCl₃



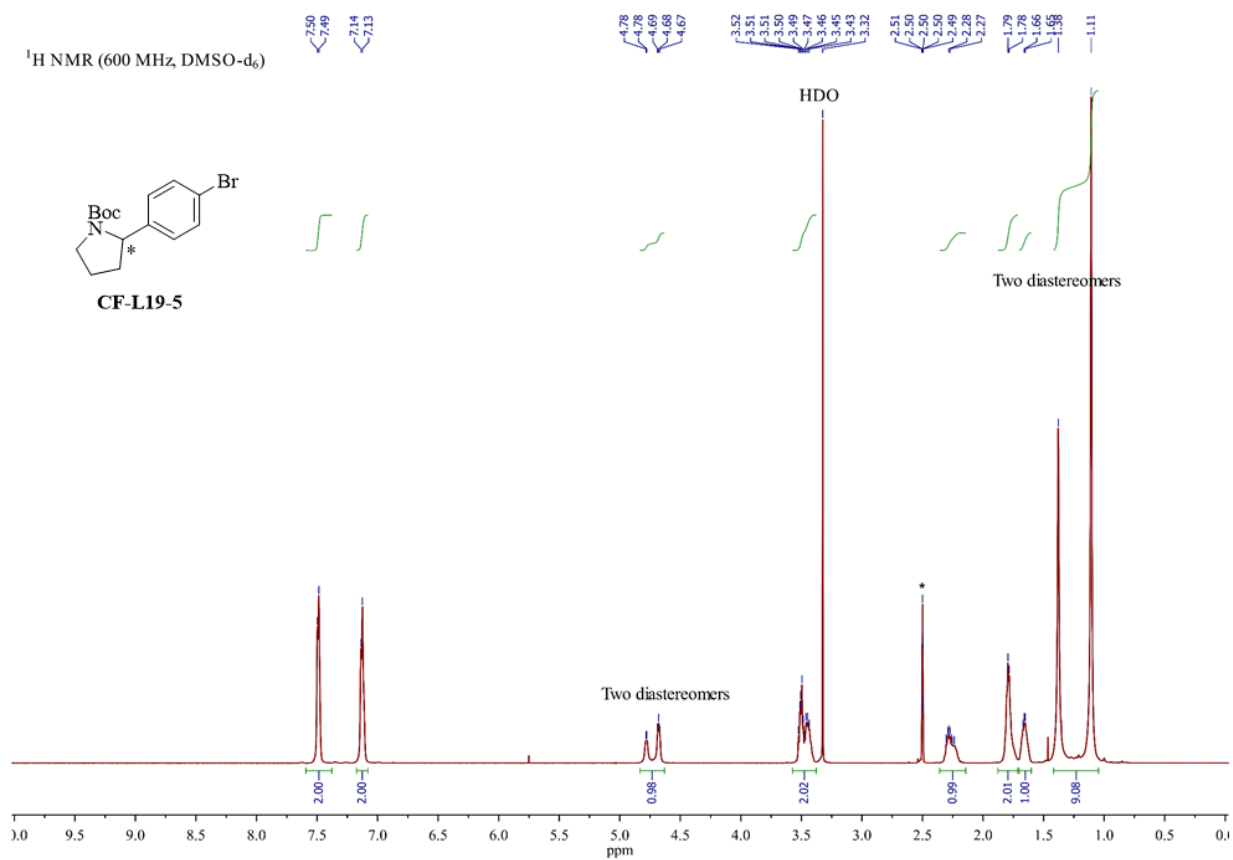
¹³C NMR spectrum of **CF-L19-4** in CDCl₃



¹H NMR spectrum of 2-(4-bromophenyl)pyrrolidine in DMSO-d₆ (couldn't differentiate enantiomers)

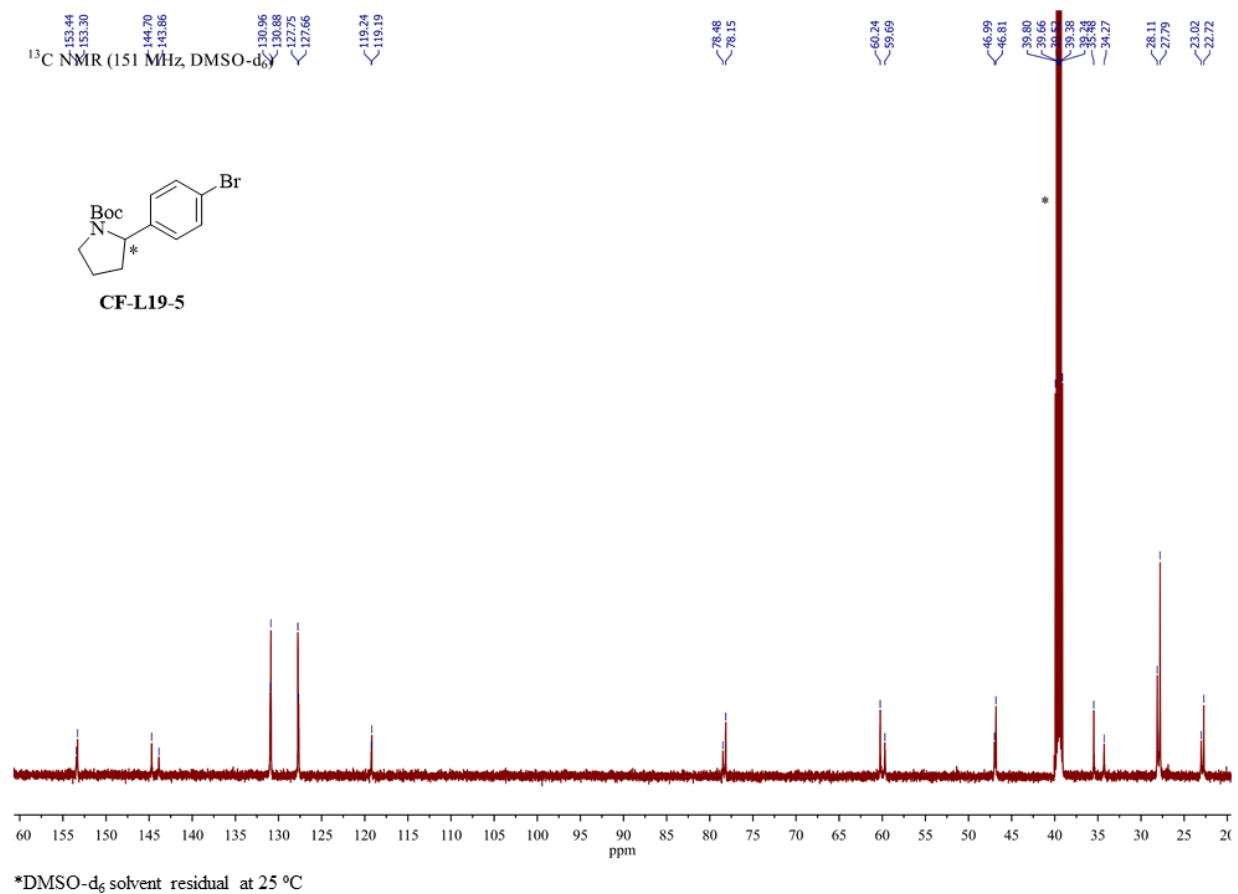


¹³C NMR spectrum of 2-(4-bromophenyl)pyrrolidine in DMSO-d₆ (couldn't differentiate enantiomers)

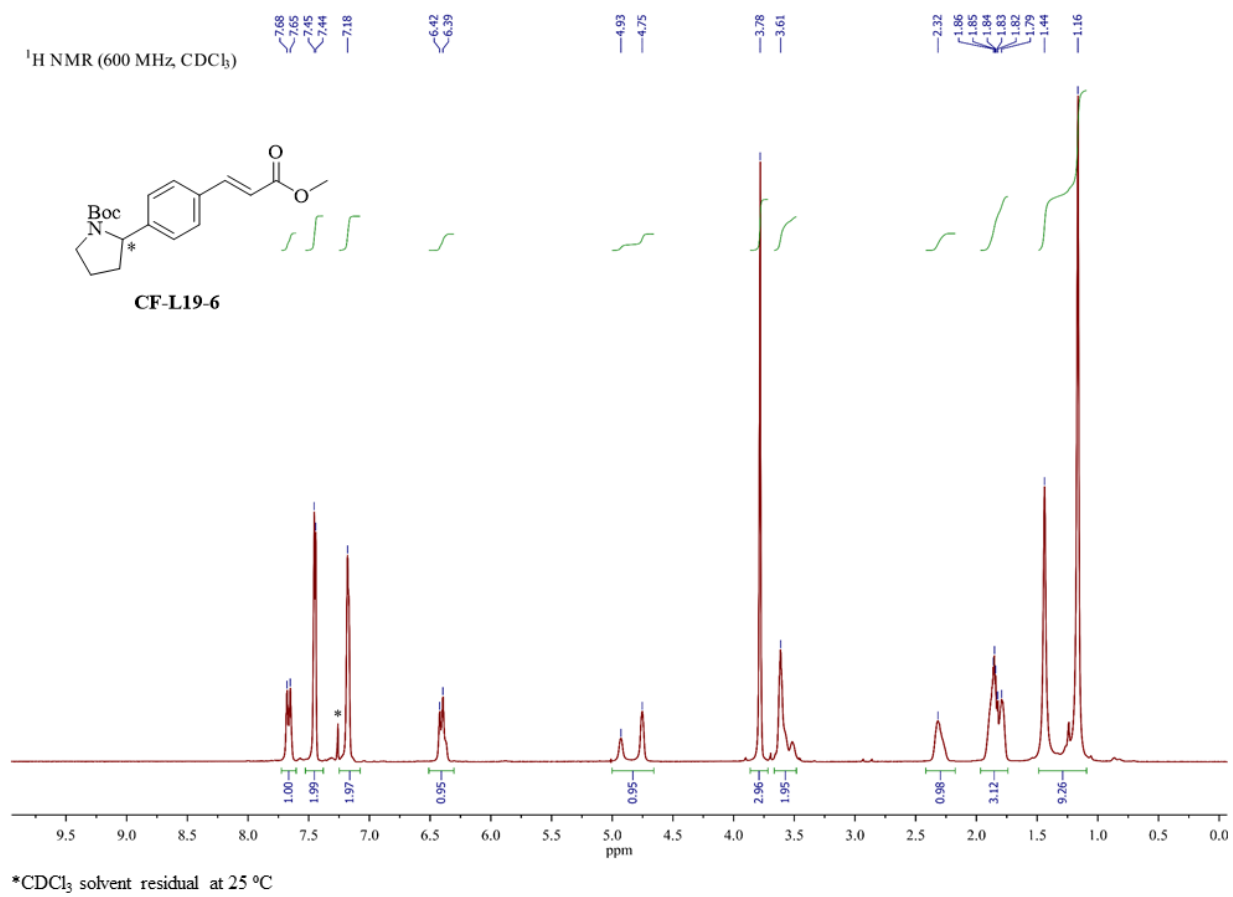


*DMSO-d₆ solvent residual at 25 °C

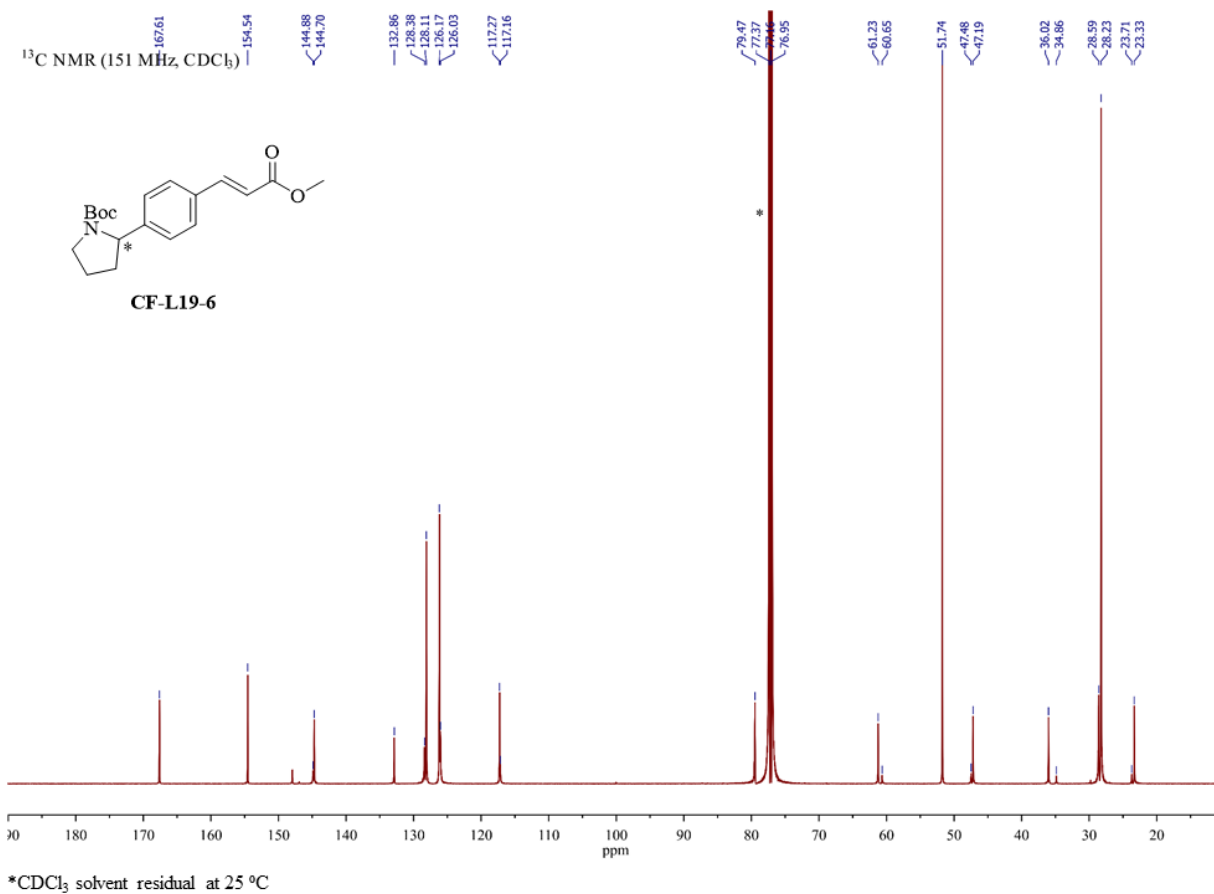
¹H NMR spectrum of **CF-L19-5** in DMSO-d₆ (two sets of signals indicate diastereomers)



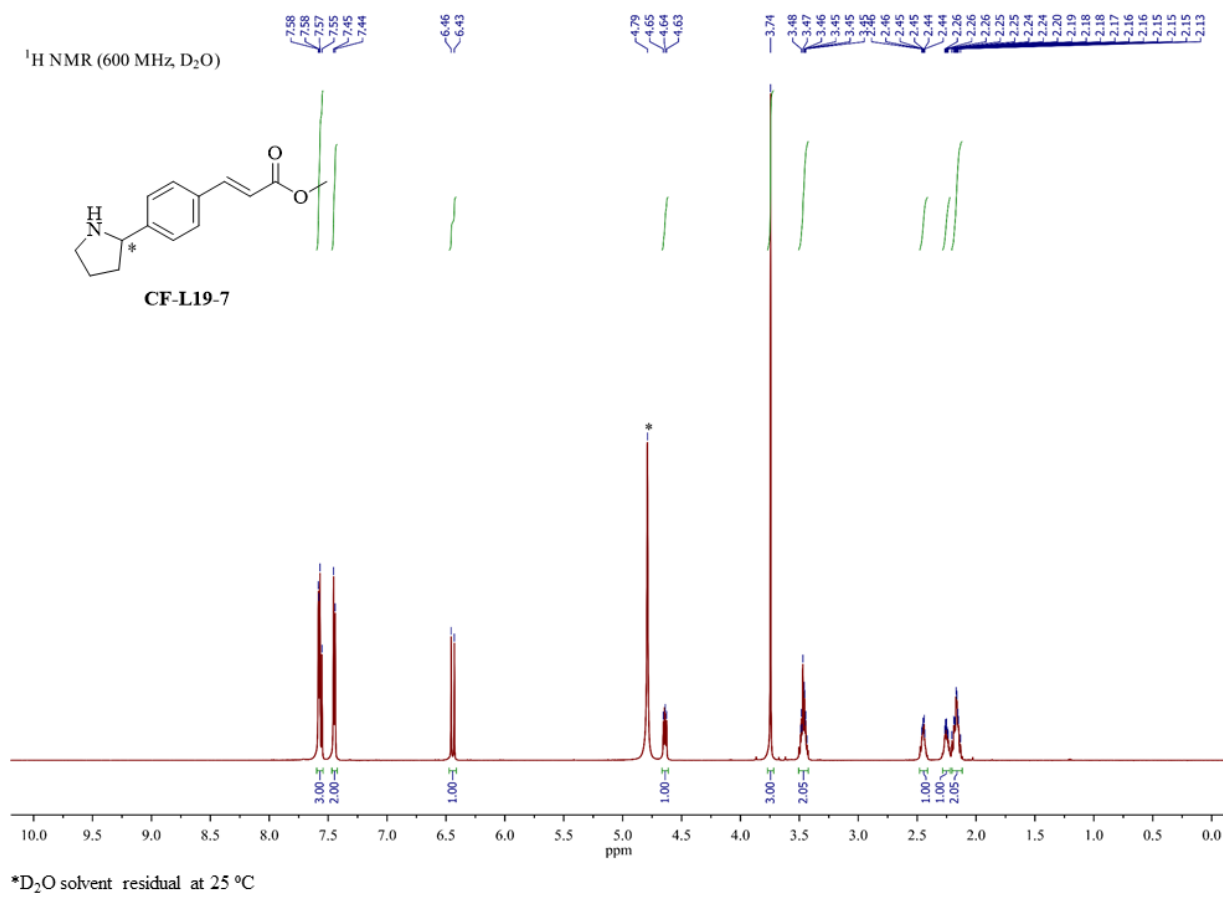
¹³C NMR spectrum of **CF-L19-5** in DMSO-d₆ (two sets of signals indicate diastereomers)



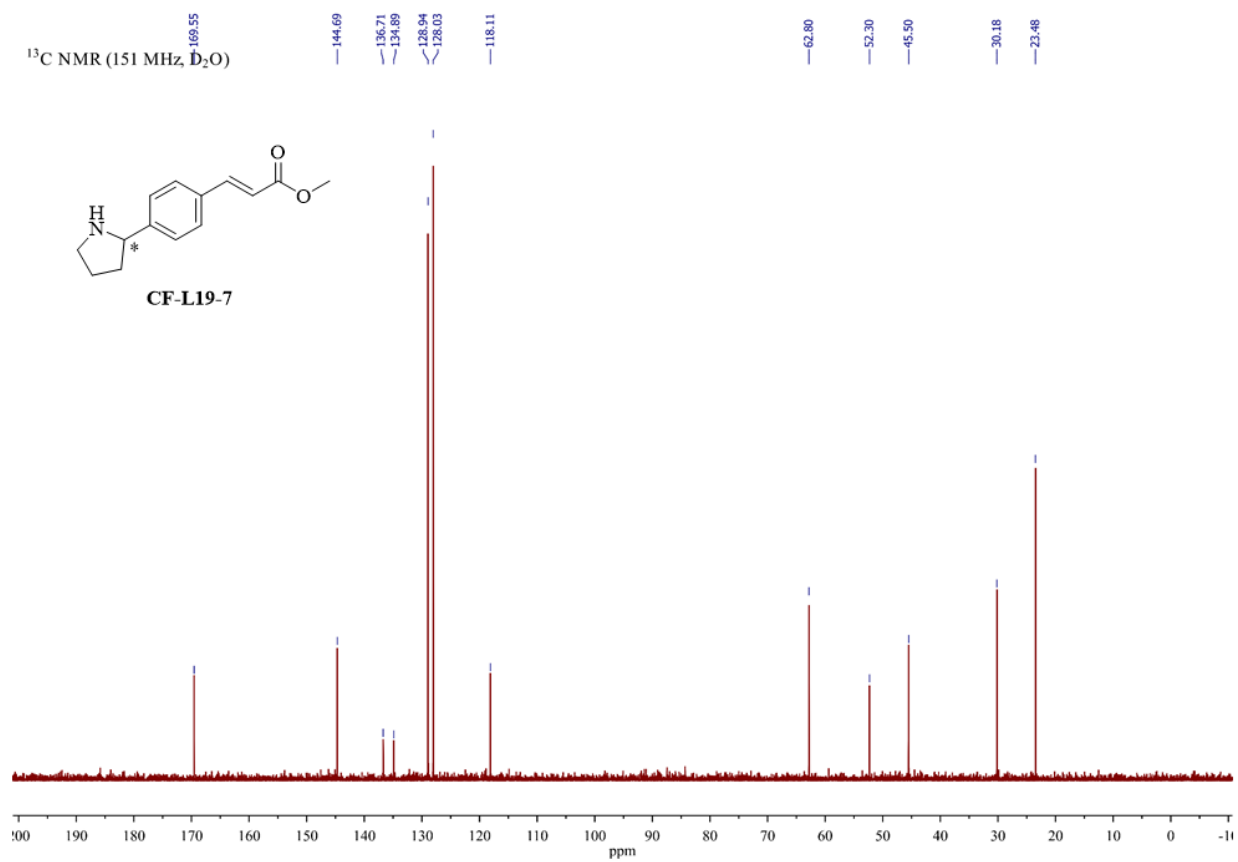
¹H NMR spectrum of **CF-L19-6** in CDCl₃ (two sets of signals indicate diastereomers)



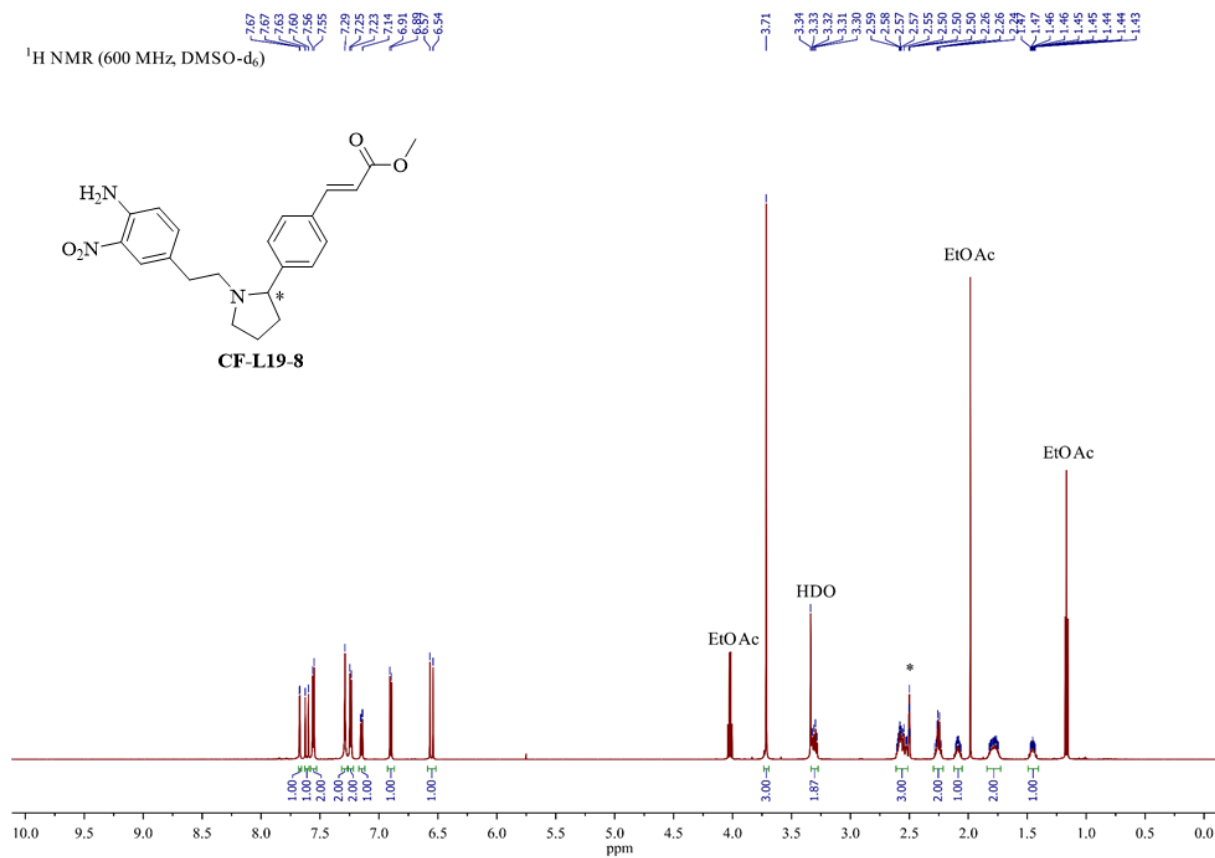
¹³C NMR spectrum of **CF-L19-6** in CDCl₃ (two sets of signals indicate diastereomers)



¹H NMR spectrum of **CF-L19-7** in D₂O

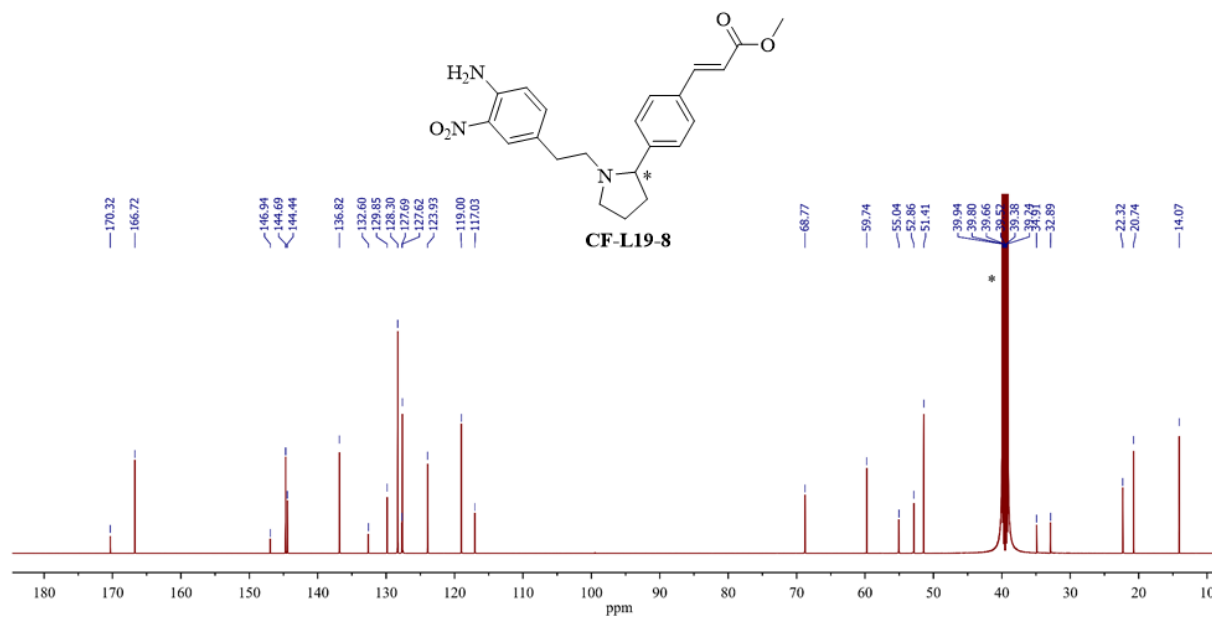
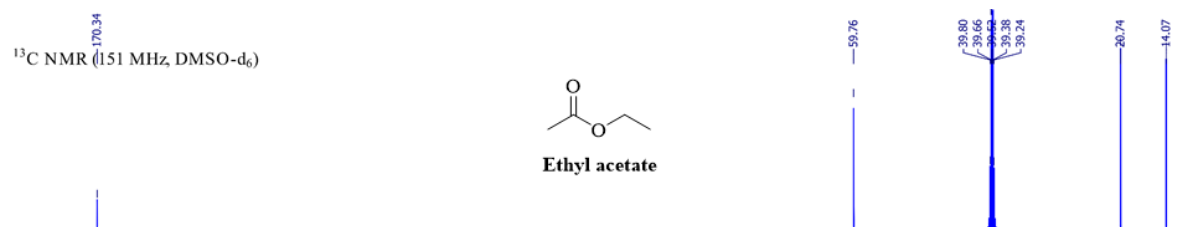


¹³C NMR spectrum of CF-L19-7 in D₂O



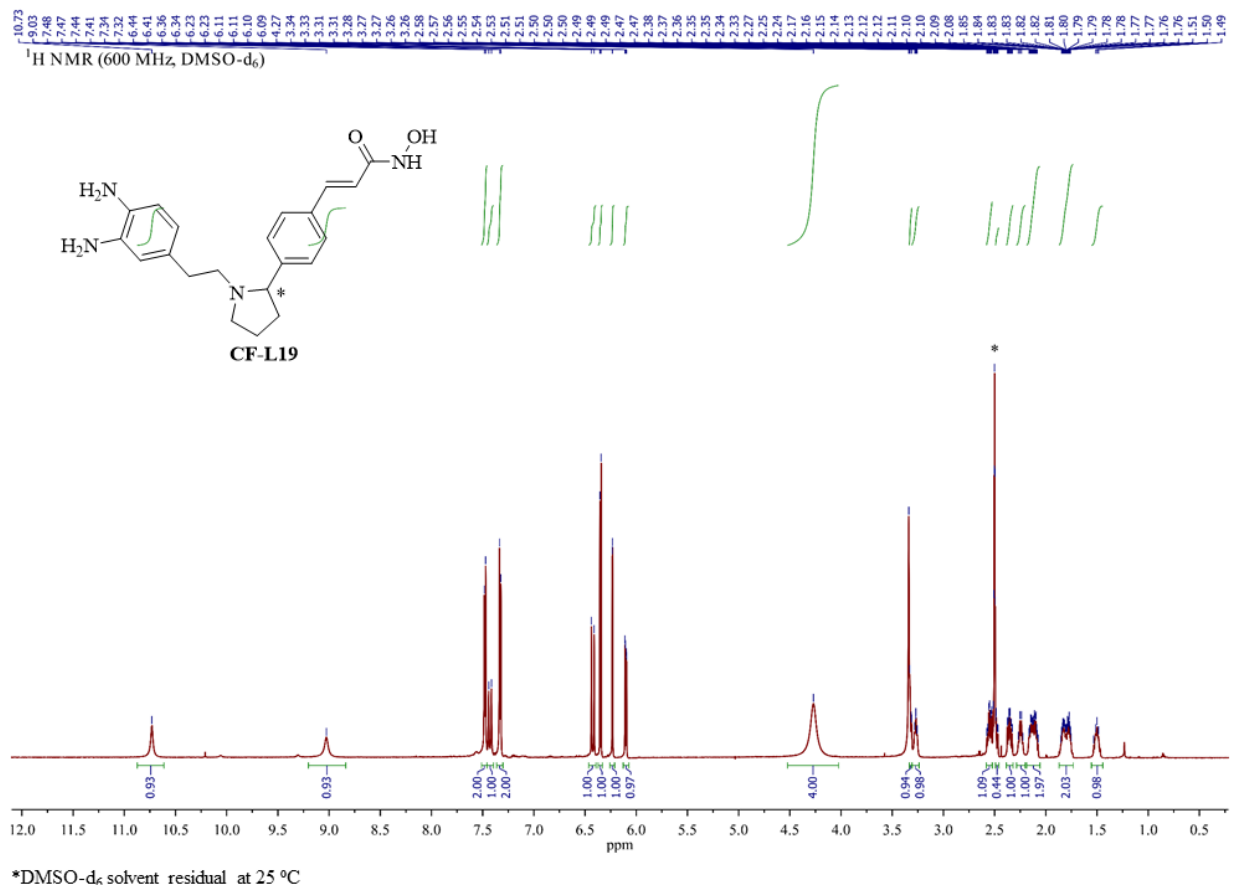
*DMSO-d₆ solvent residual at 25 °C

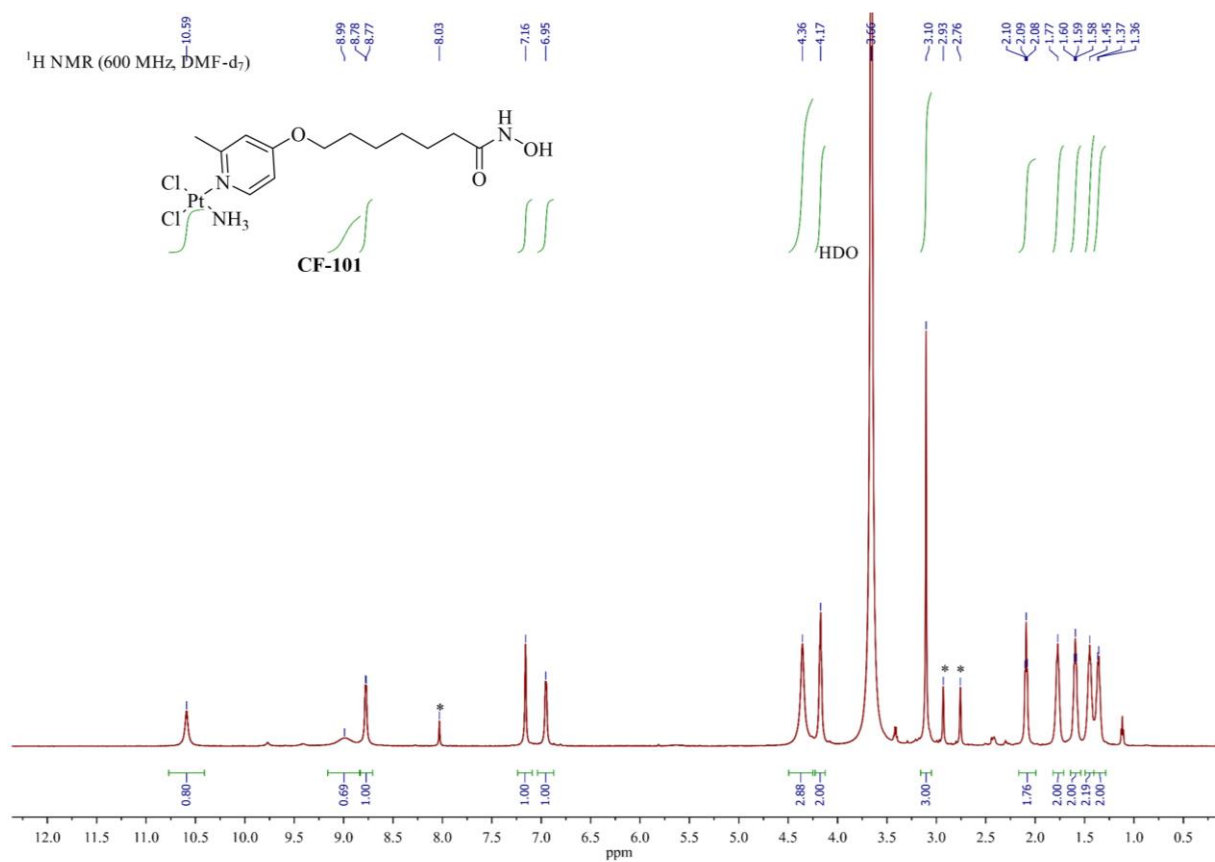
¹H NMR spectrum of **CF-L19-8** in DMSO-d₆



*DMSO- d_6 solvent residual at 25 °C

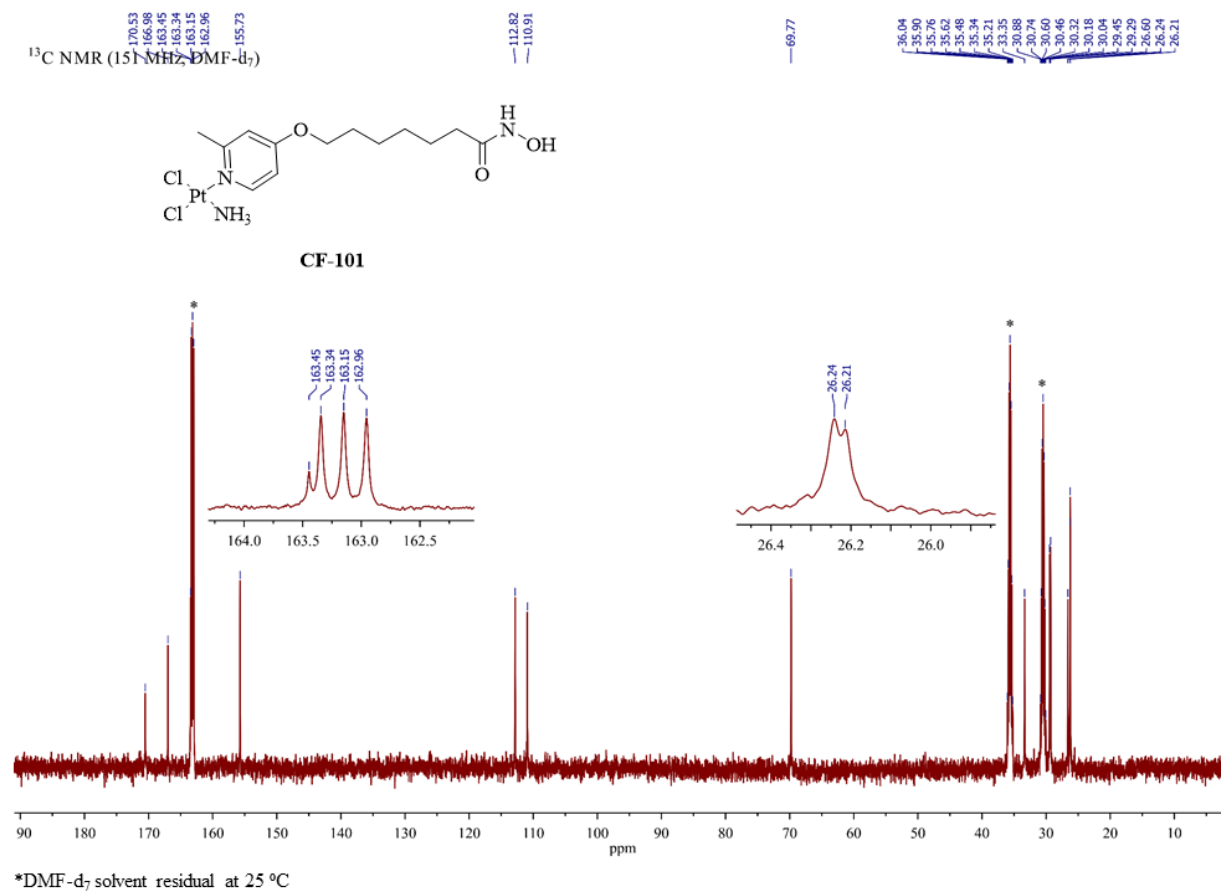
^{13}C NMR spectrum of **CF-L19-8** in DMSO- d_6 (EtOAc peaks also exist)





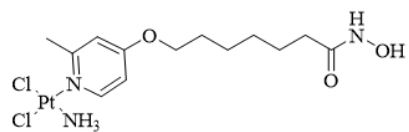
*DMF-d₇ solvent residual at 25 °C

¹H NMR spectrum of **CF-101** in DMF-d₇

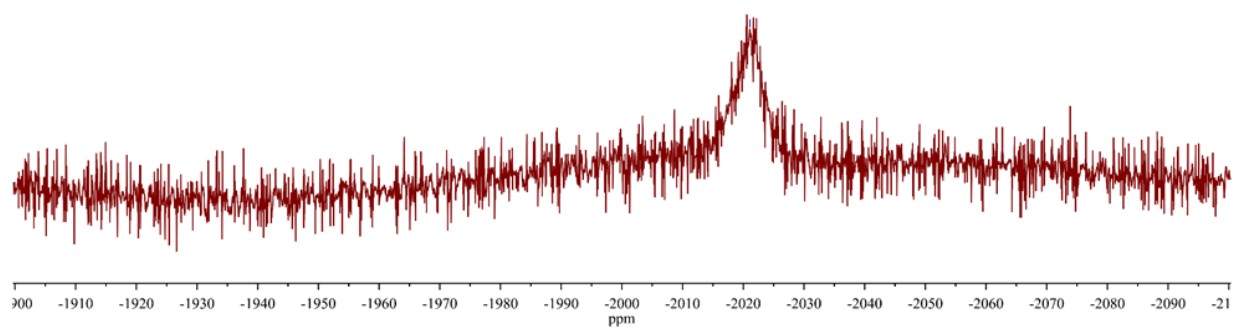


¹³C NMR spectrum of CF-101 in DMF-d₇

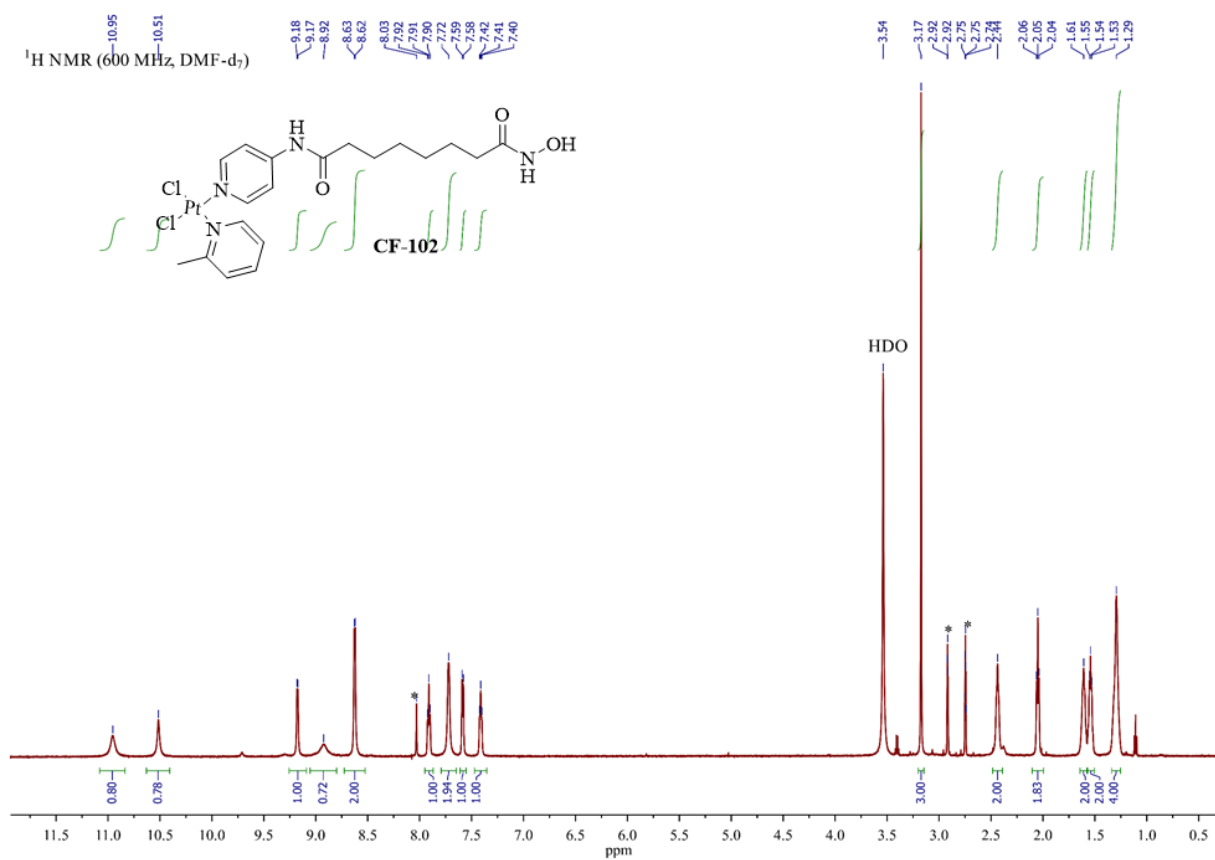
^{195}Pt NMR (129 MHz, DMF- d_7)



CF-101

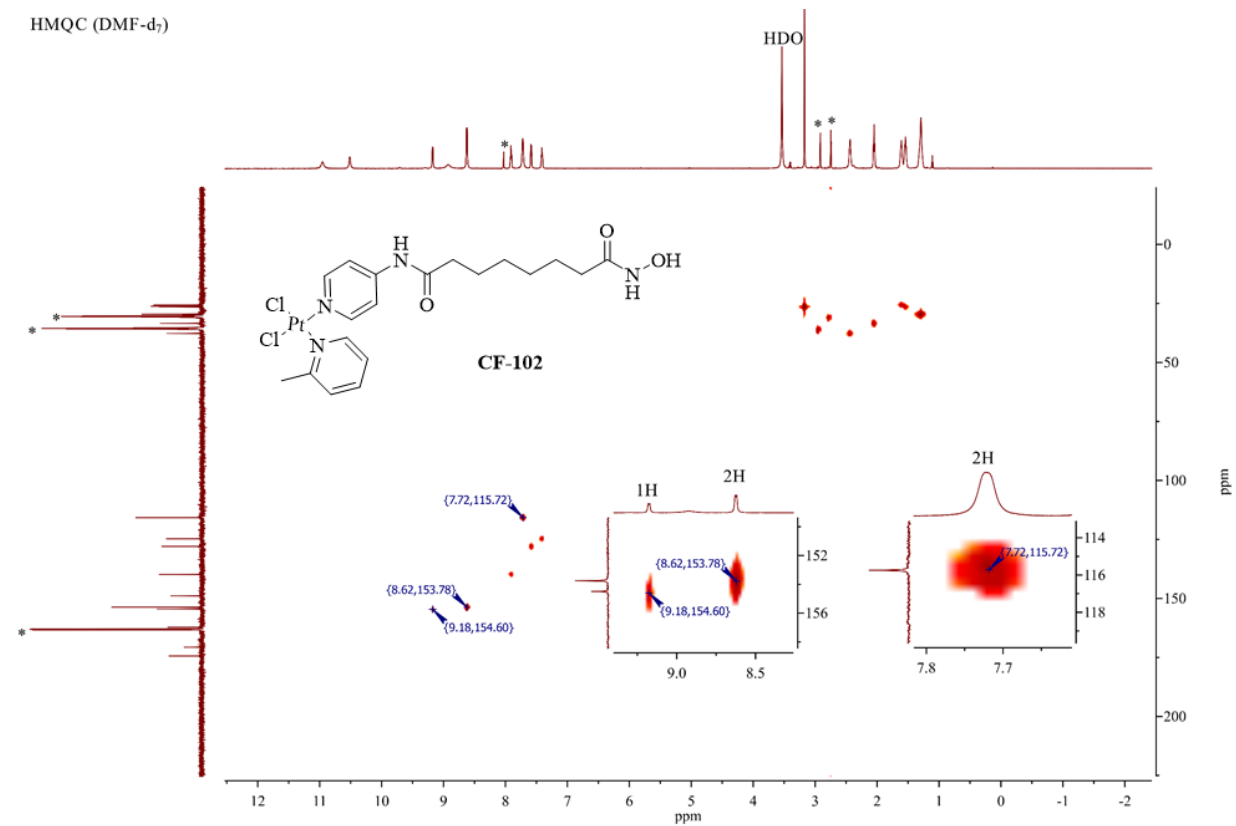


^{195}Pt NMR spectrum of **CF-101** in DMF- d_7



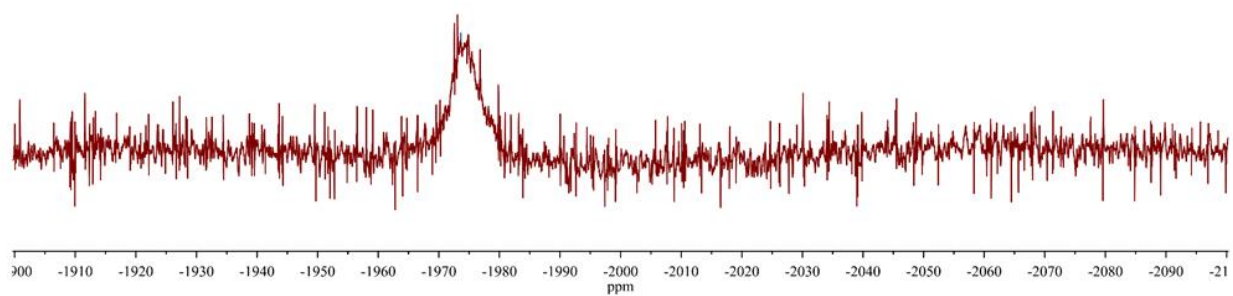
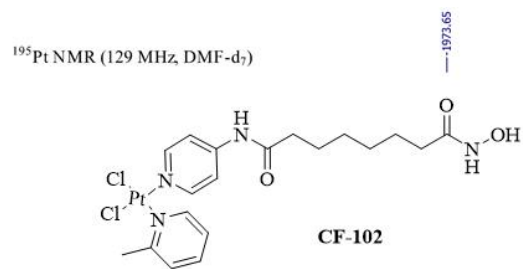
*DMF-d₇ solvent residual at 25 °C

¹H NMR spectrum of CF-102 in DMF-d₇

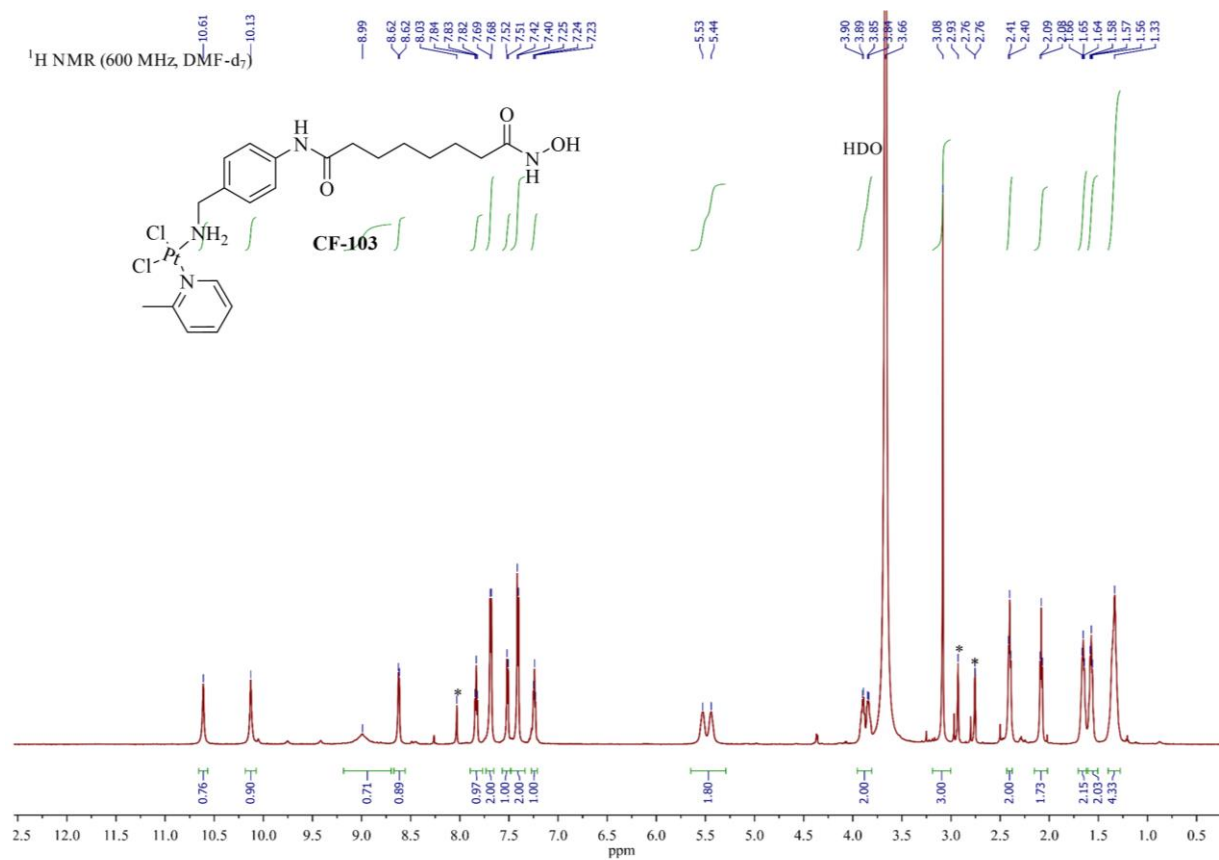


*DMF-d₇ solvent residual at 25 °C

HMQC NMR spectrum of **CF-102** in DMF-d₇ (^{13}C δ 153.78, 115.72 represents 2 aromatic ^{13}C respectively)

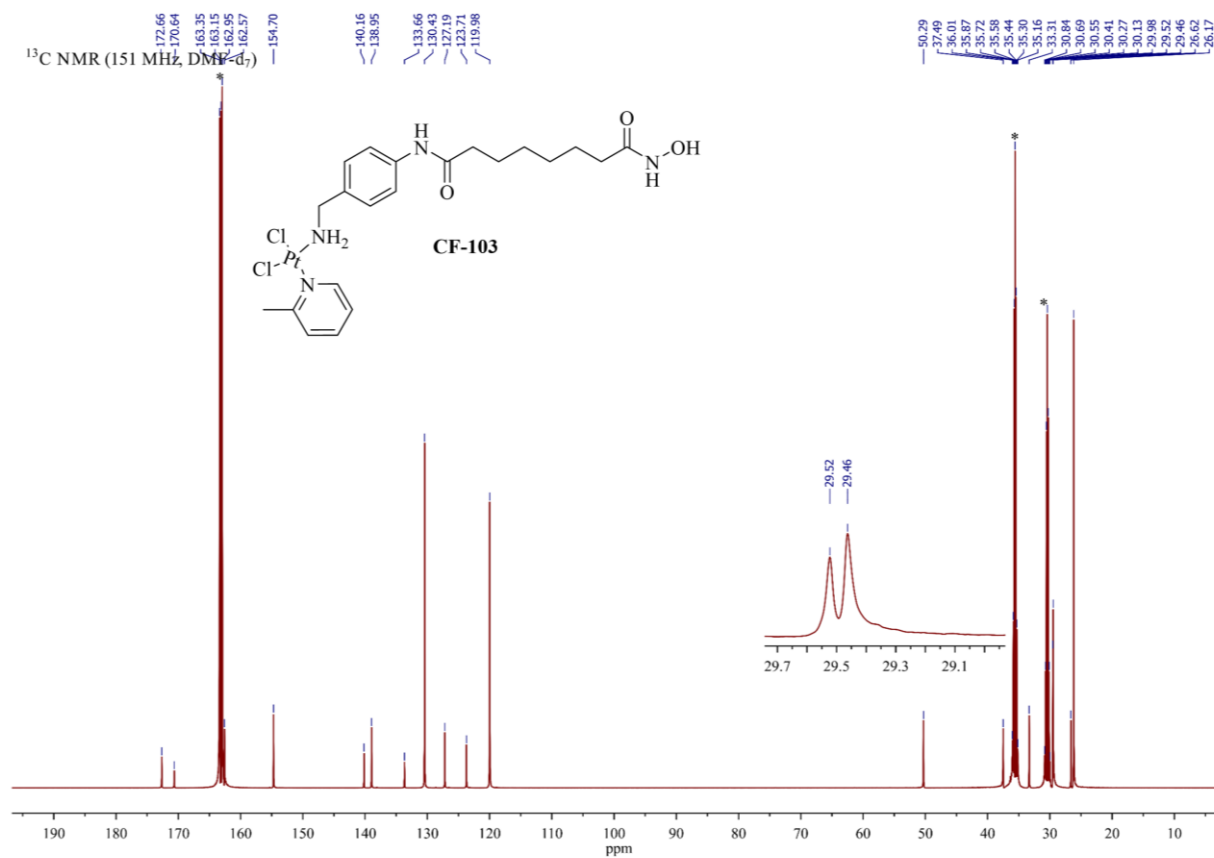


^{195}Pt NMR spectrum of **CF-102** in DMF- d_7



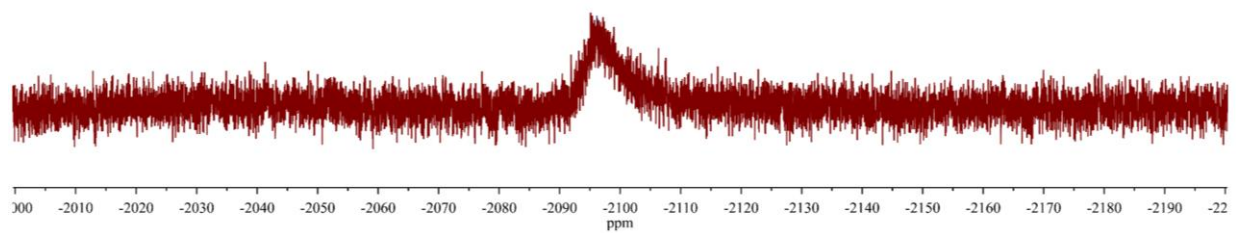
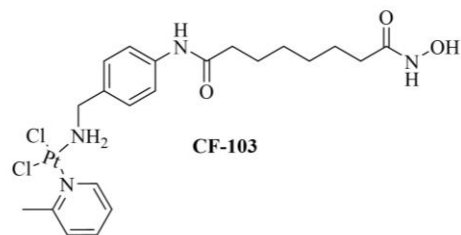
*DMF-d₇ solvent residual at 25 °C

¹H NMR spectrum of **CF-103** in DMF-d₇

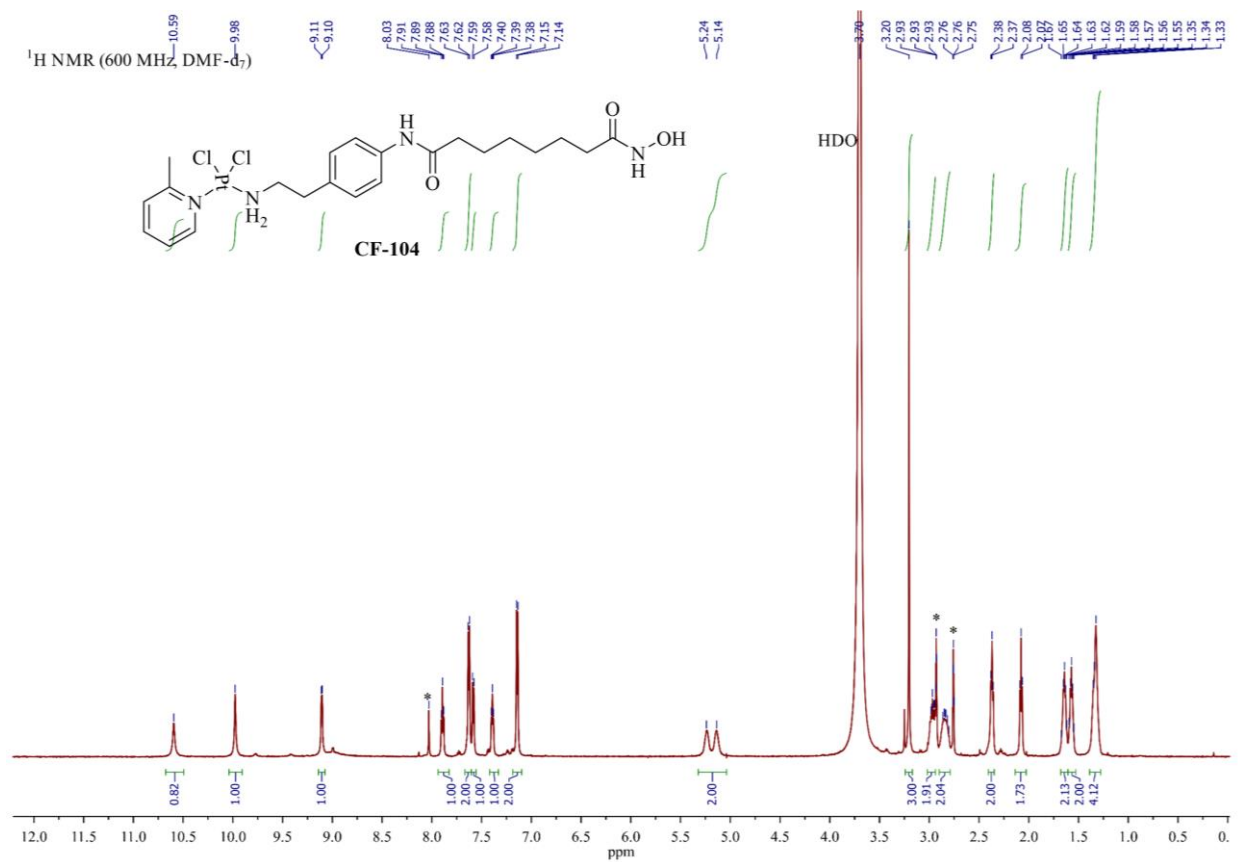


¹³C NMR spectrum of **CF-103** in DMF-d₇

^{195}Pt NMR (129 MHz, DMF- d_7)

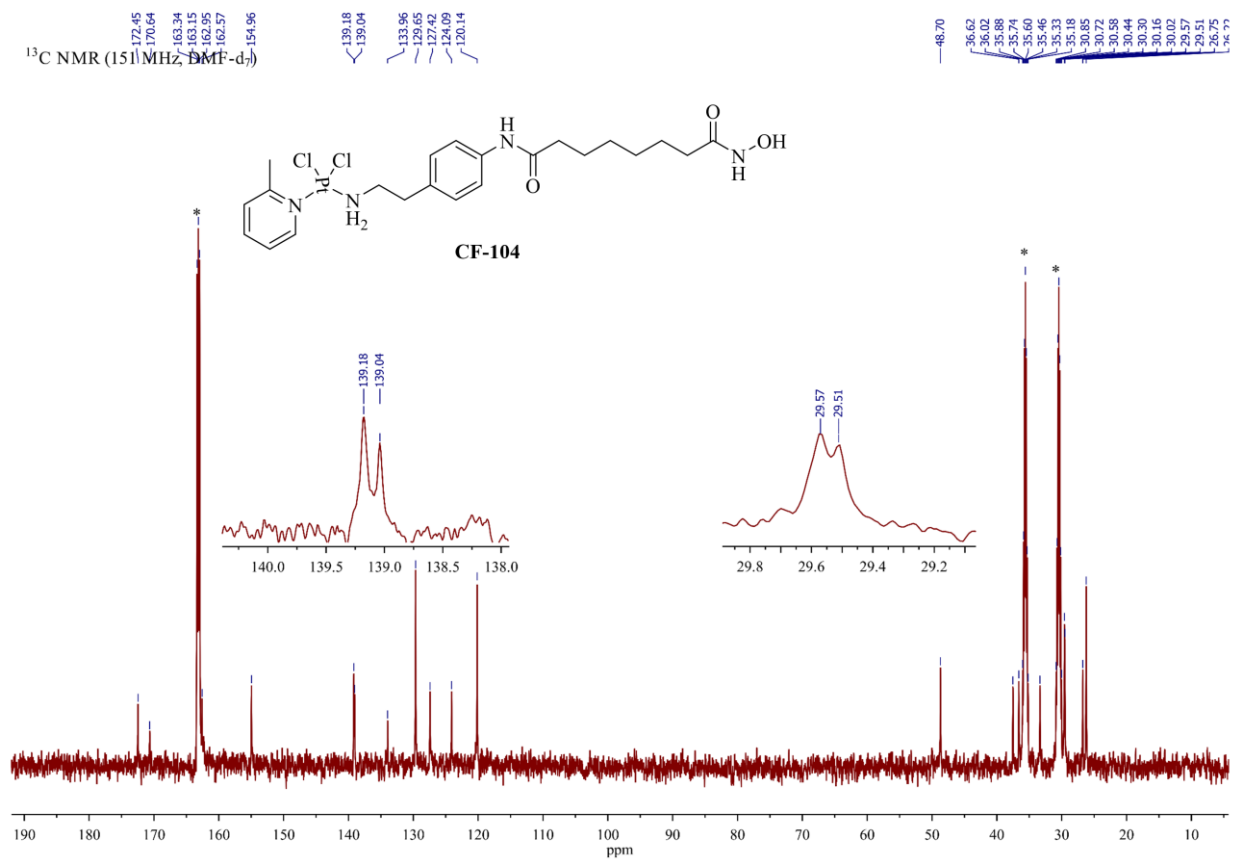


^{195}Pt NMR spectrum of **CF-103** in DMF- d_7

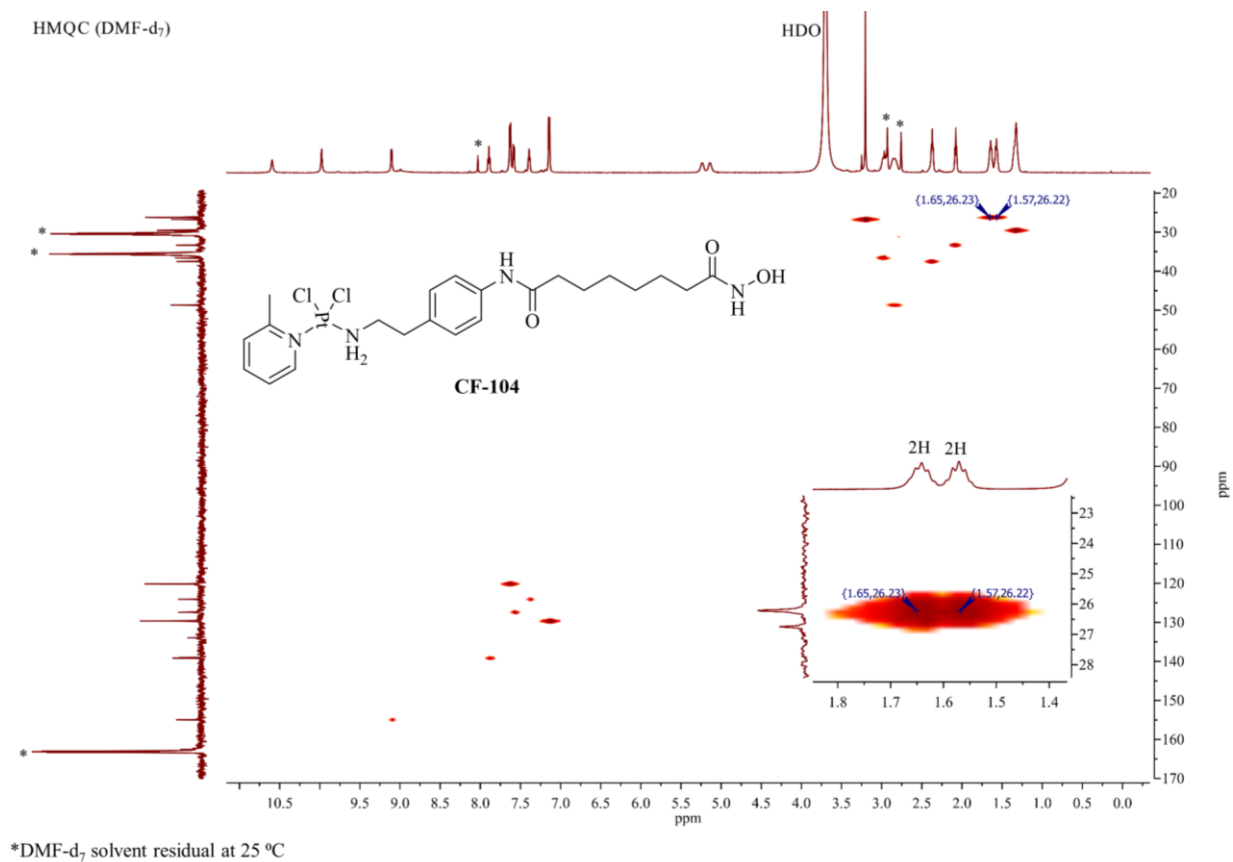


*DMF-d₇ solvent residual at 25 °C

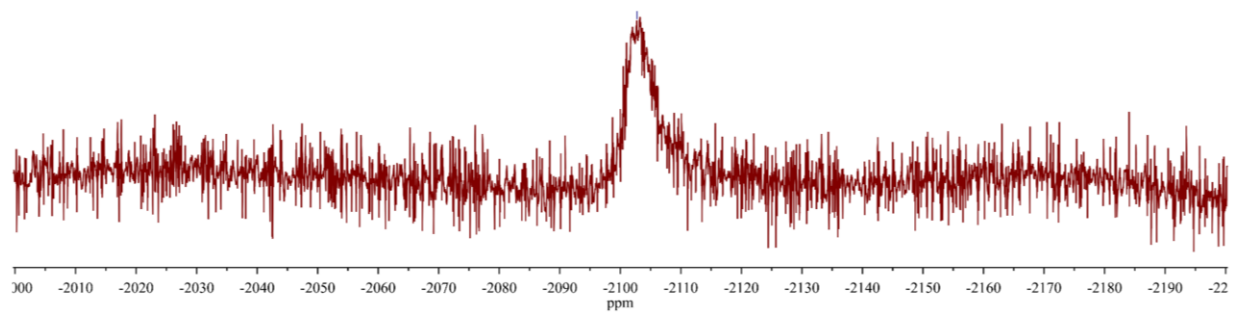
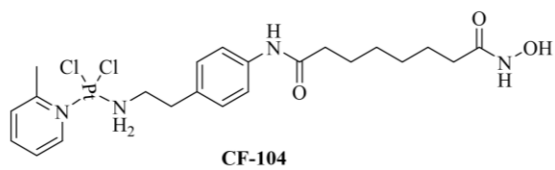
¹H NMR spectrum of CF-104 in DMF-d₇



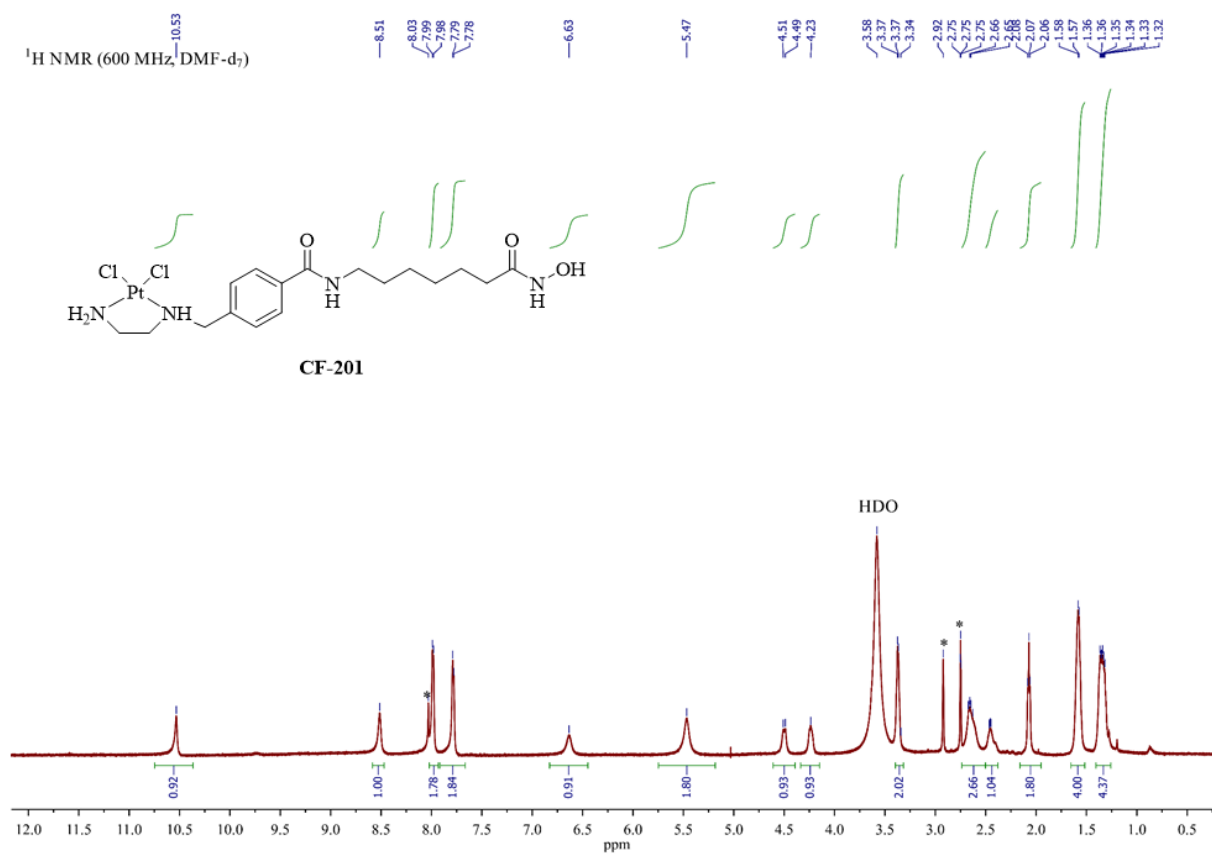
^{13}C NMR spectrum of **CF-104** in DMF-d_7

HMQC NMR spectrum of **CF-104** in DMF-d₇

^{195}Pt NMR (129 MHz, DMF- d_7)

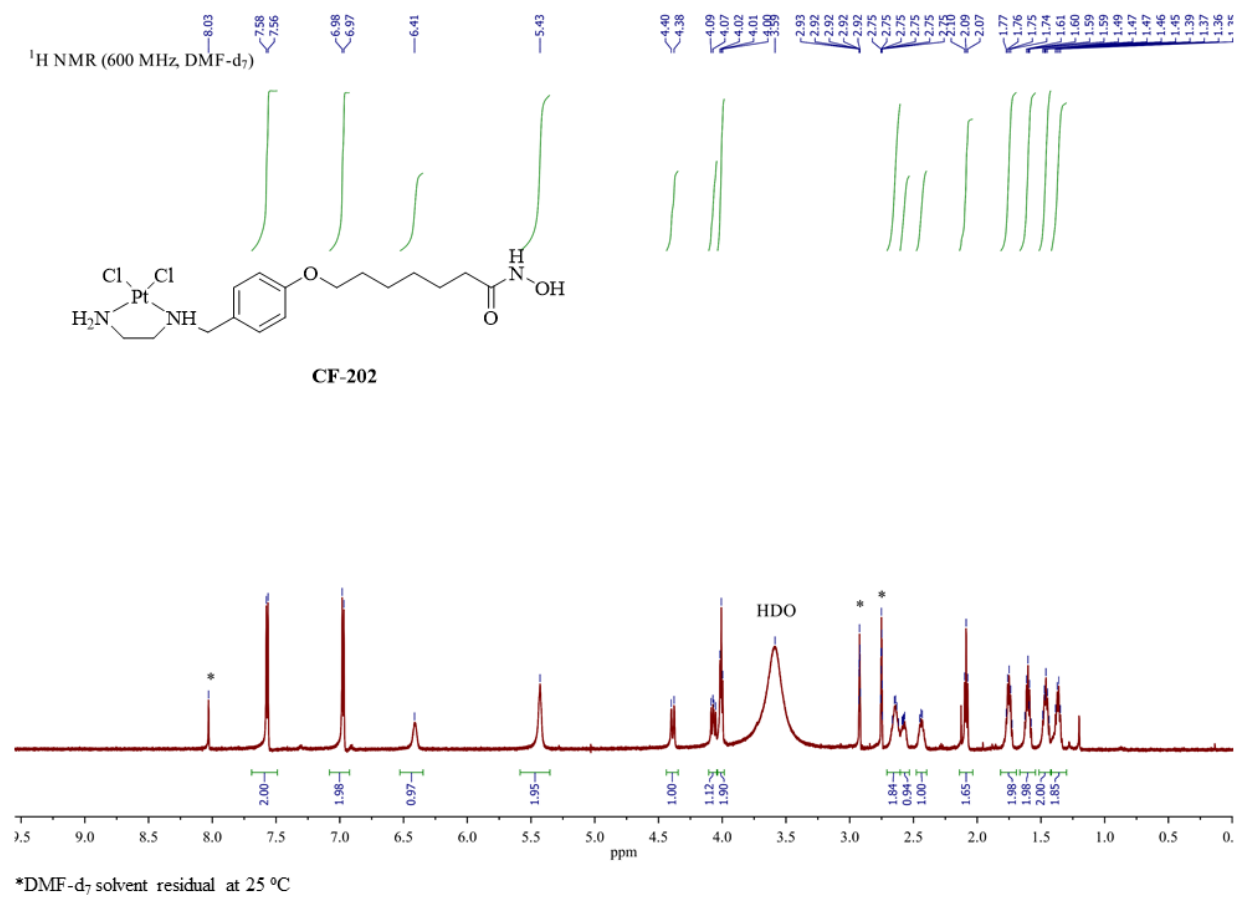


^{195}Pt NMR spectrum of **CF-104** in DMF- d_7



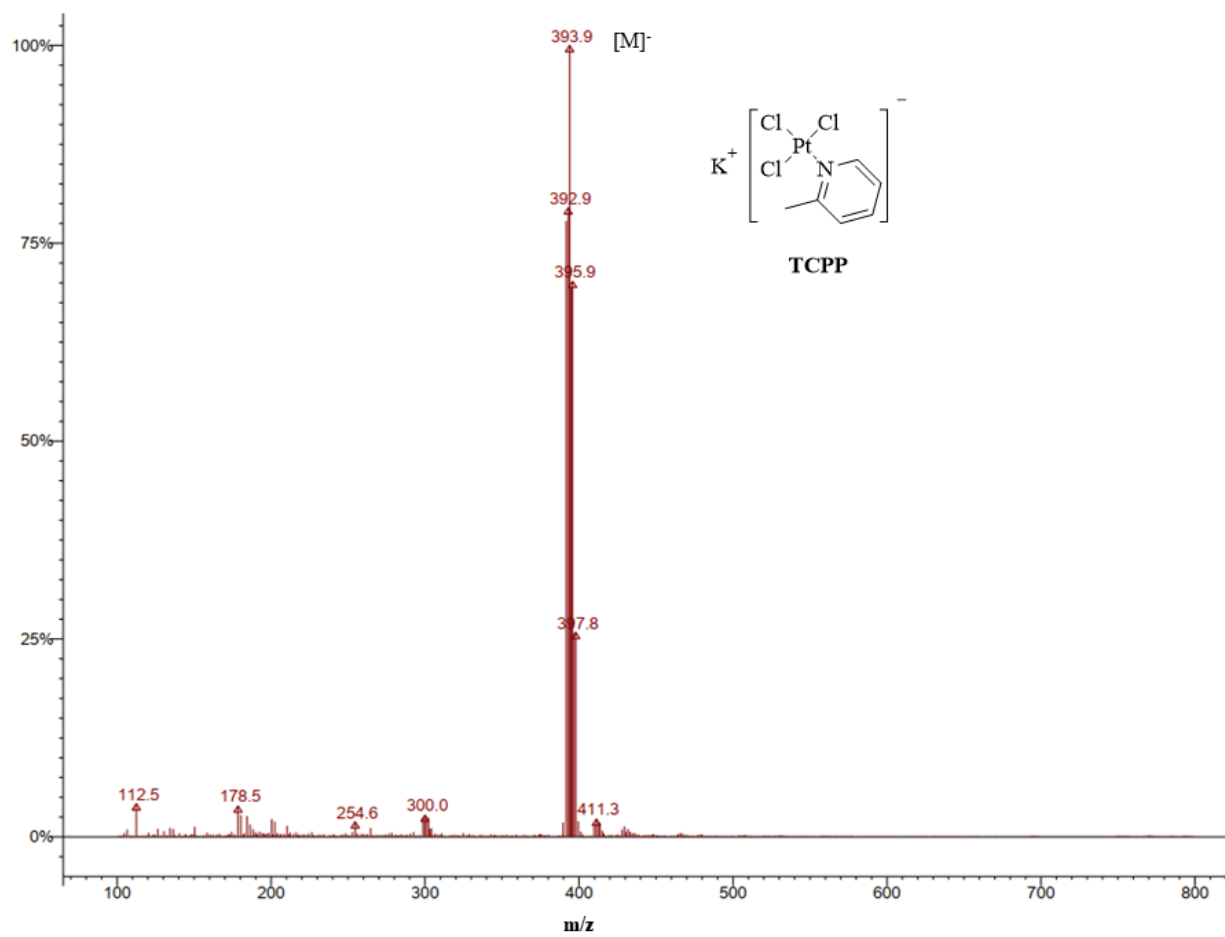
* DMF-d_7 solvent residual at 25 °C

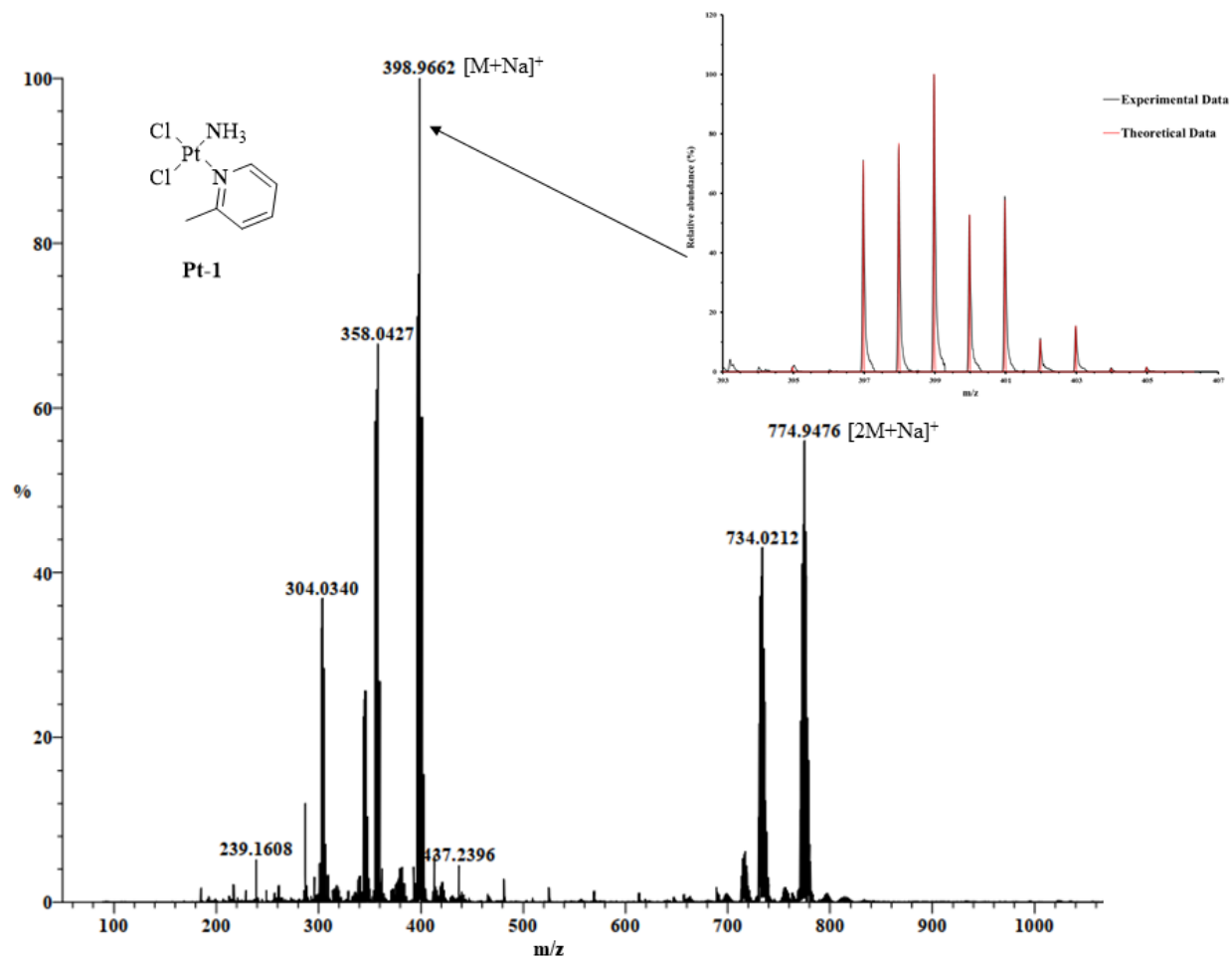
$^1\text{H NMR}$ spectrum of **CF-201** in DMF-d_7

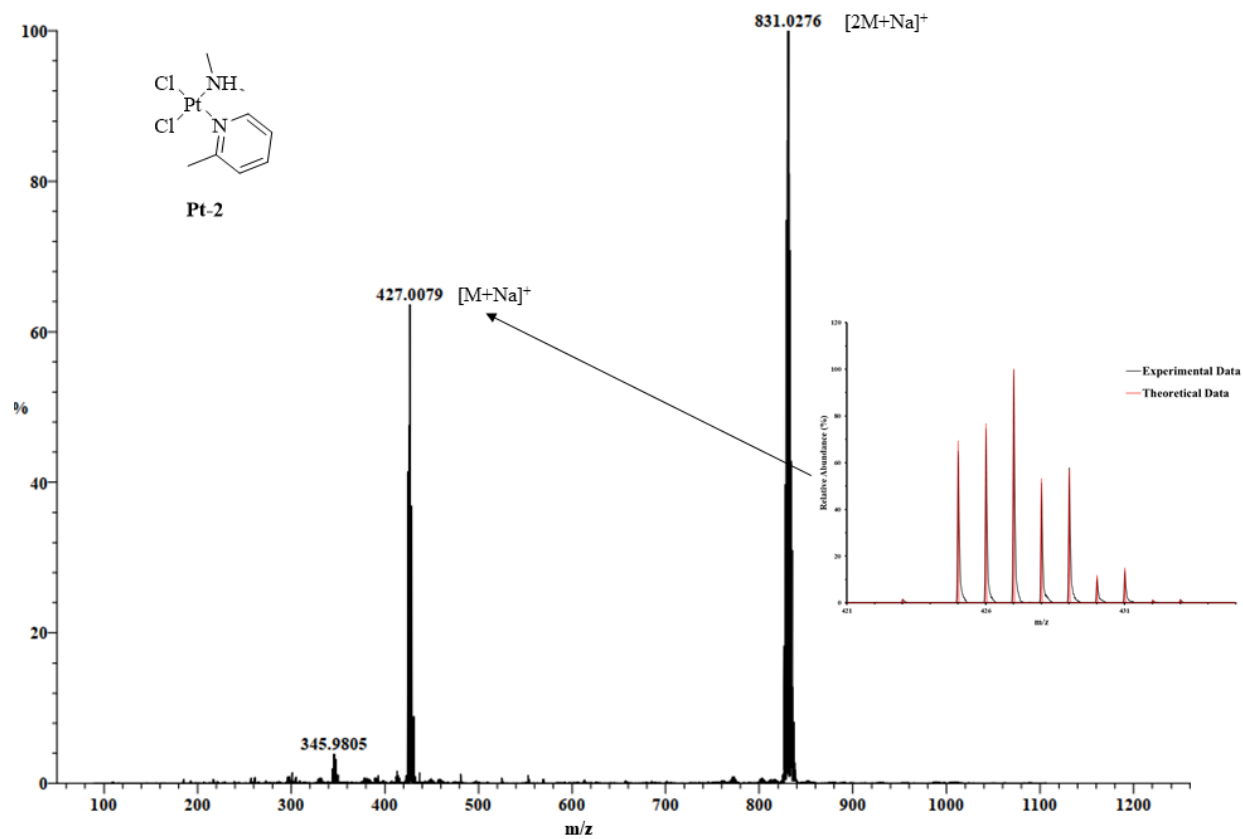


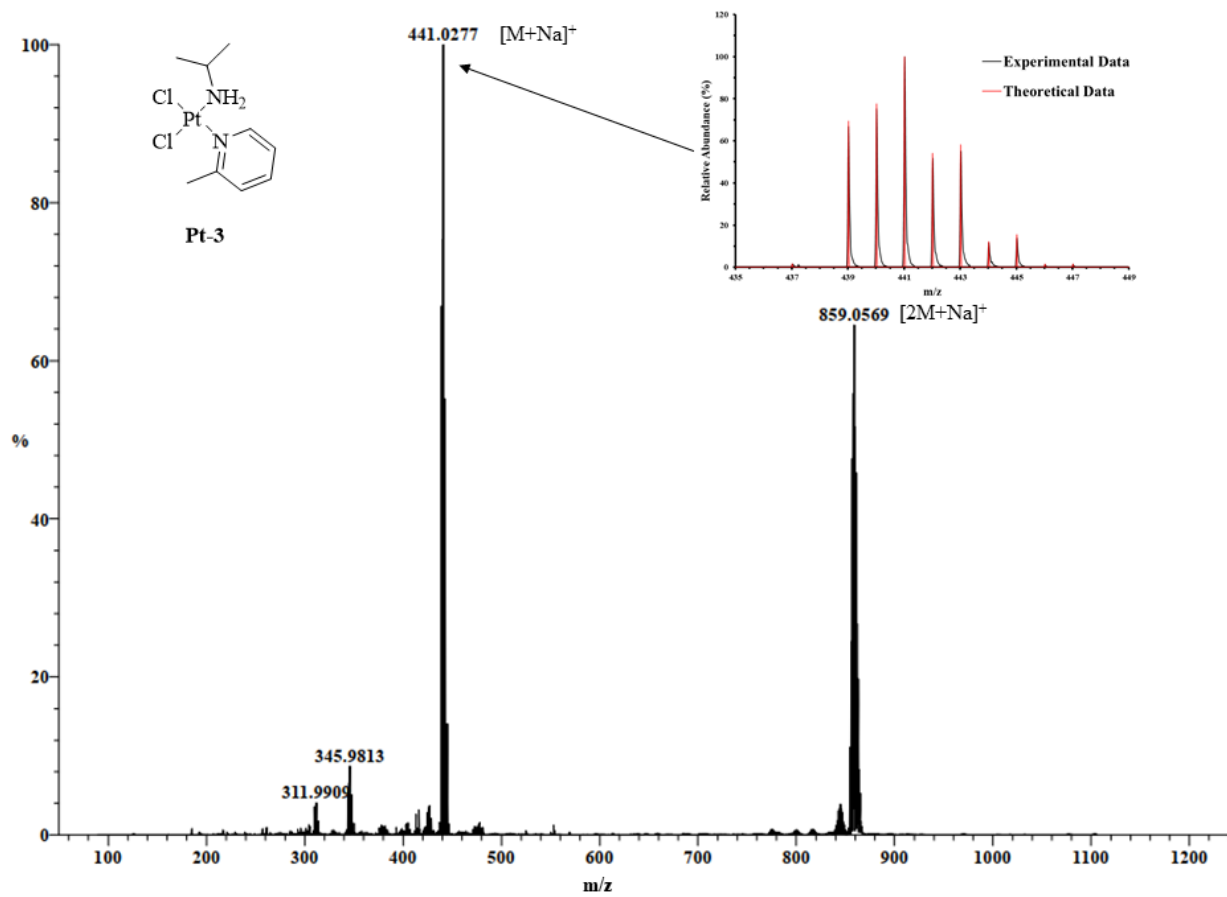
¹H NMR spectrum of CF-202 in DMF-d₇

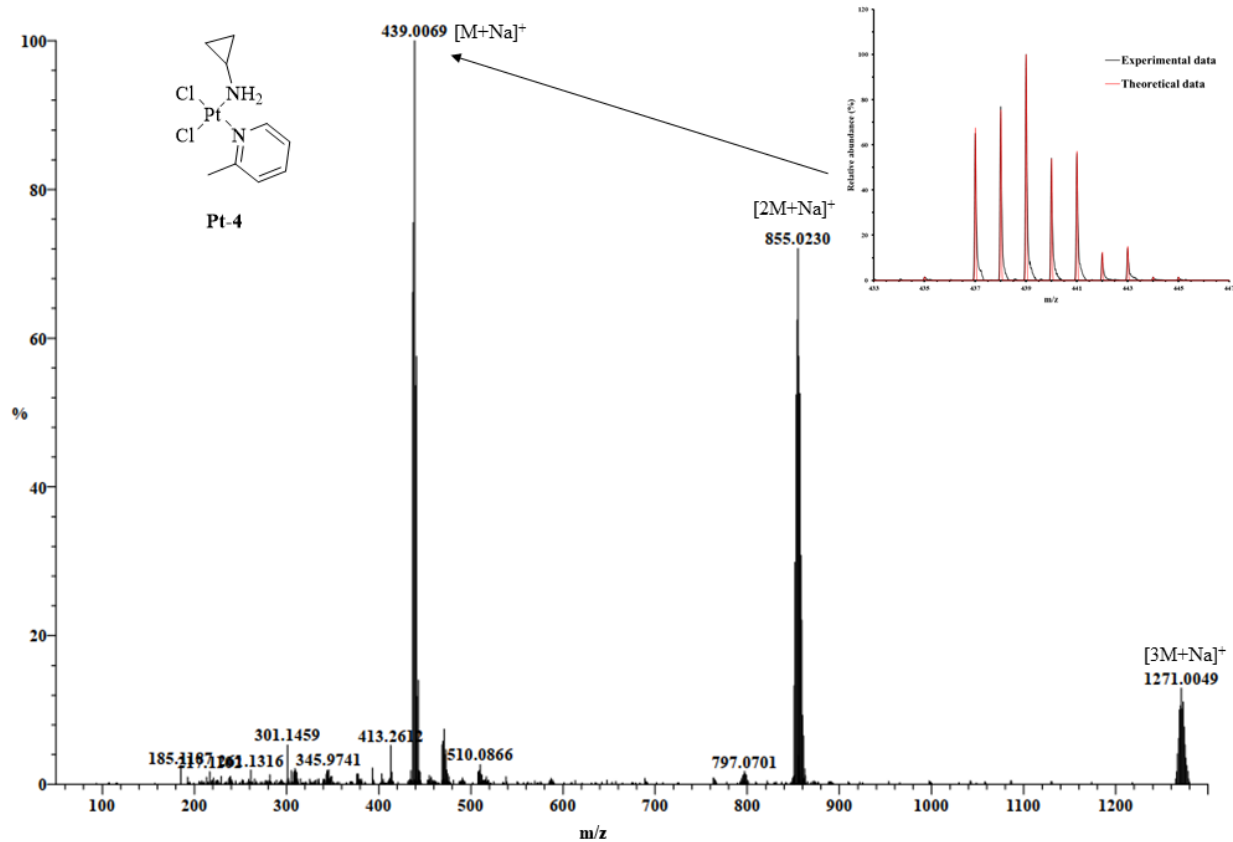
APPENDIX C: MASS SPECTRA DATA

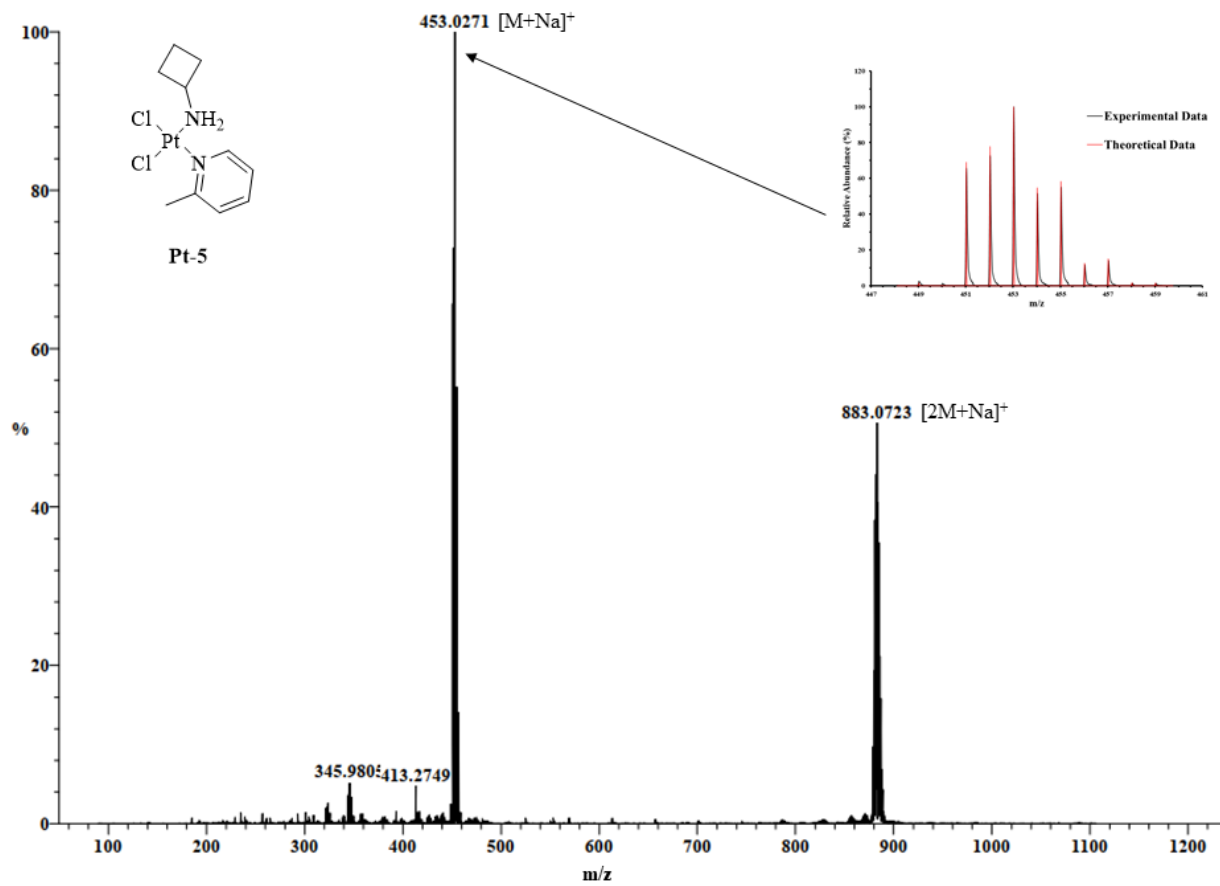
ESI-MS mass spectrum of **TCPP**

ESI-AccuTOF mass spectrum of **Pt-1**

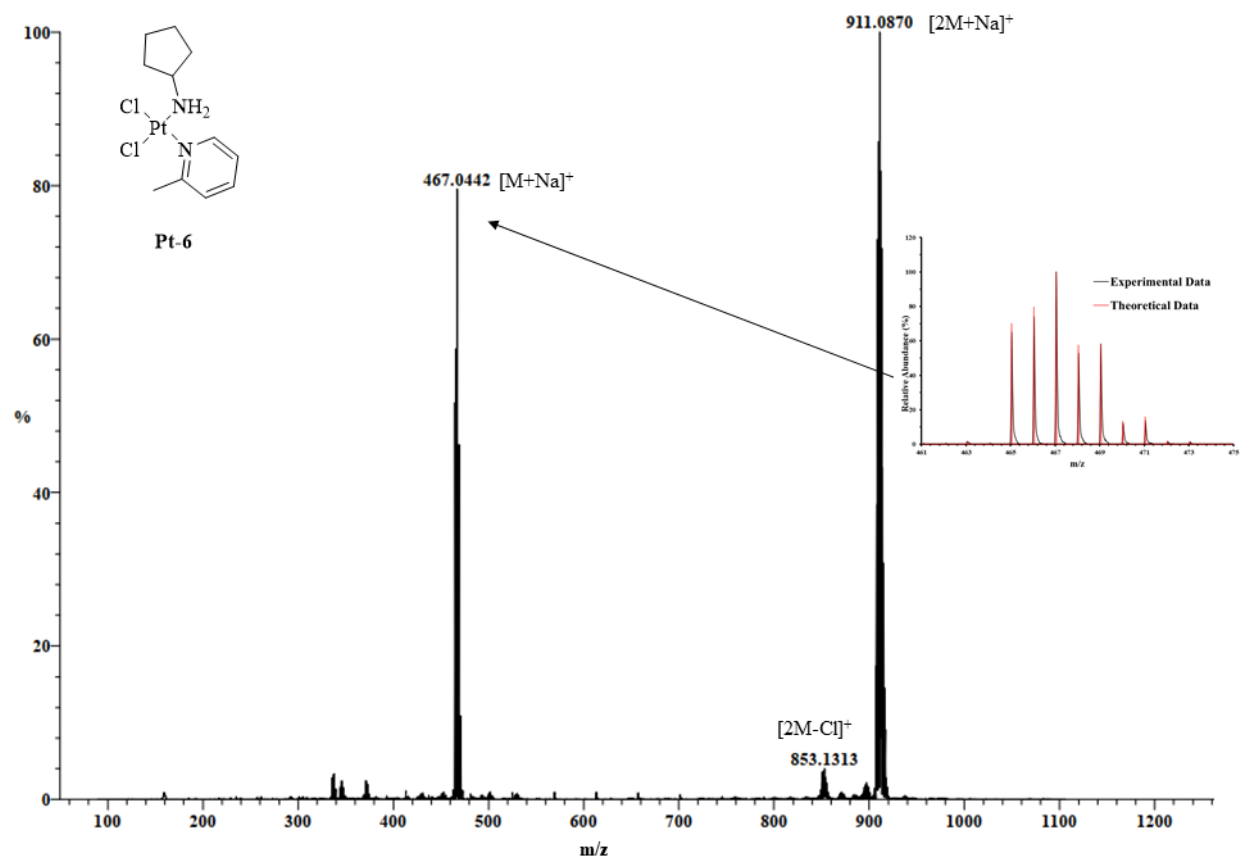
ESI-AccuTOF mass spectrum of **Pt-2**

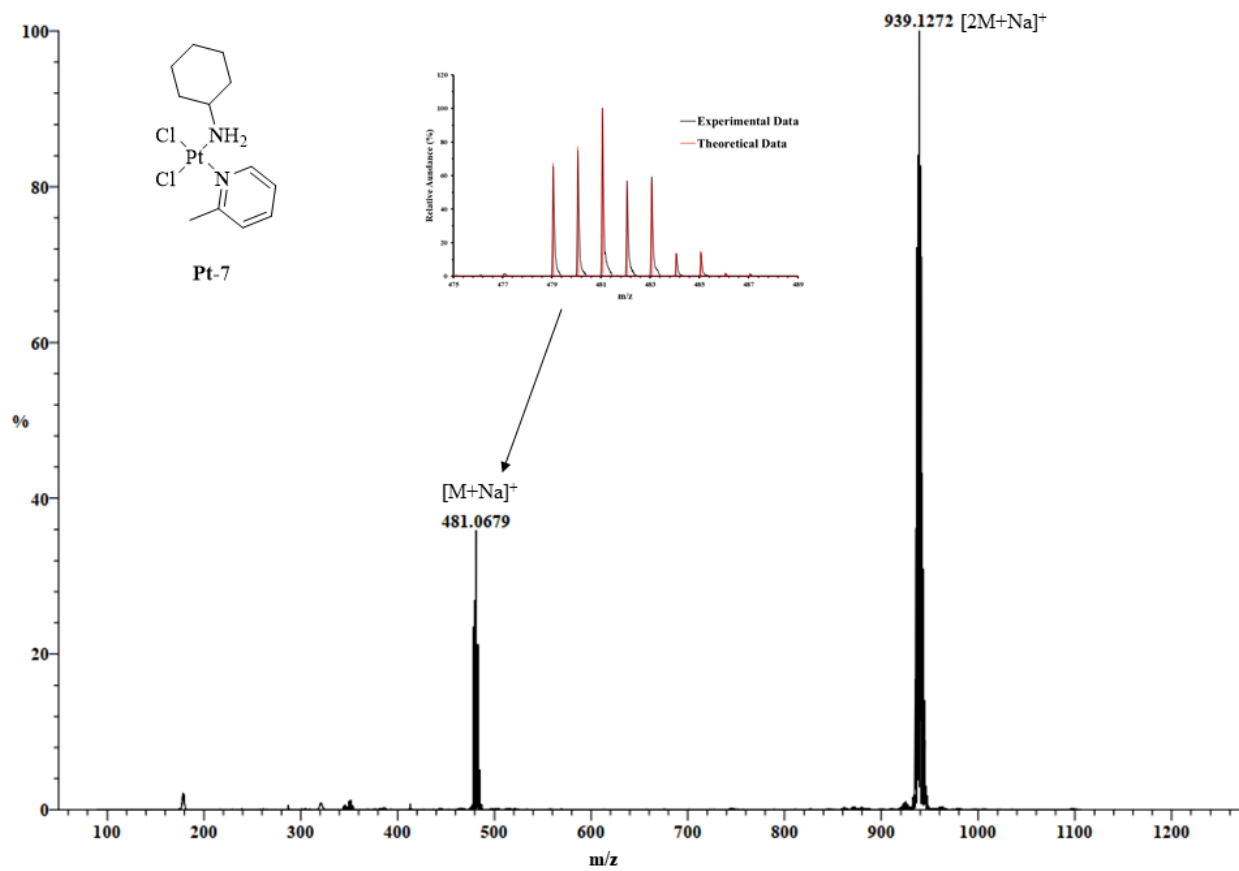
ESI-AccuTOF mass spectrum of **Pt-3**

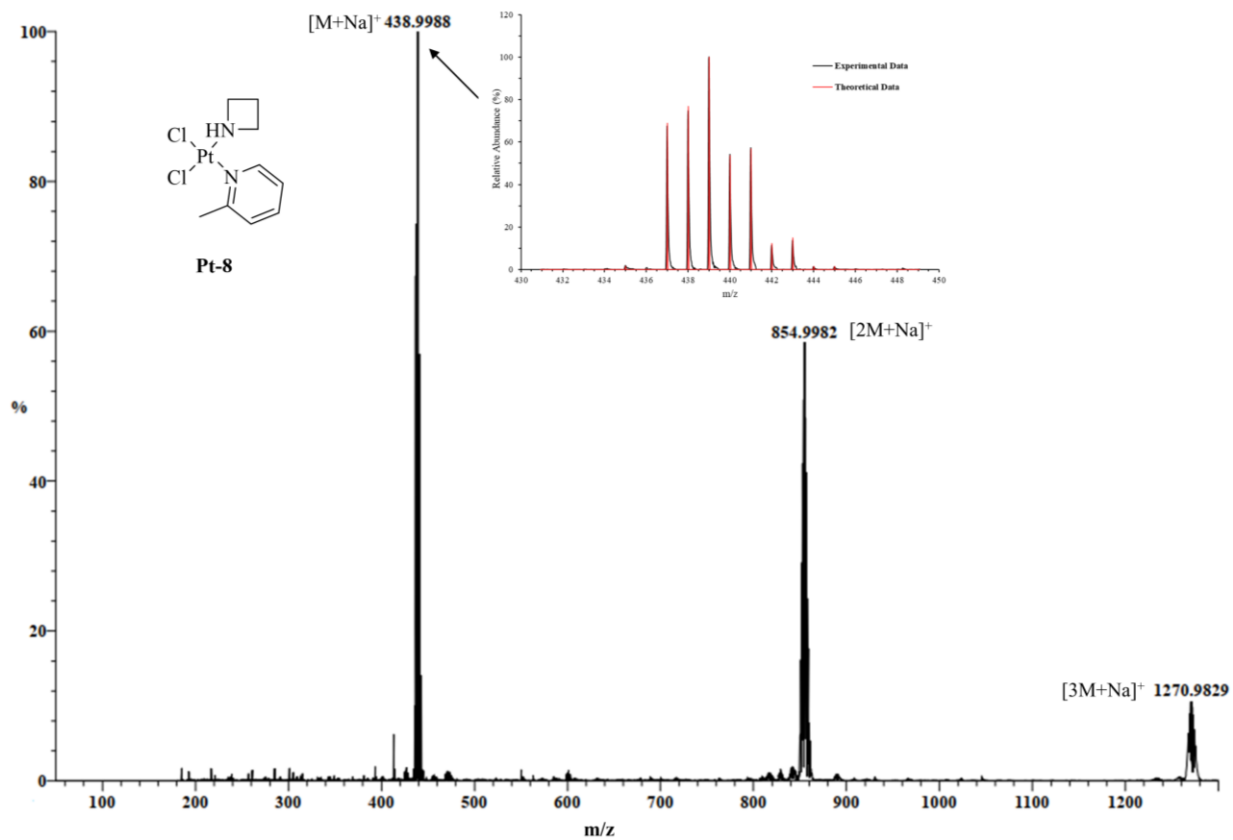
ESI-AccuTOF mass spectrum of **Pt-4**

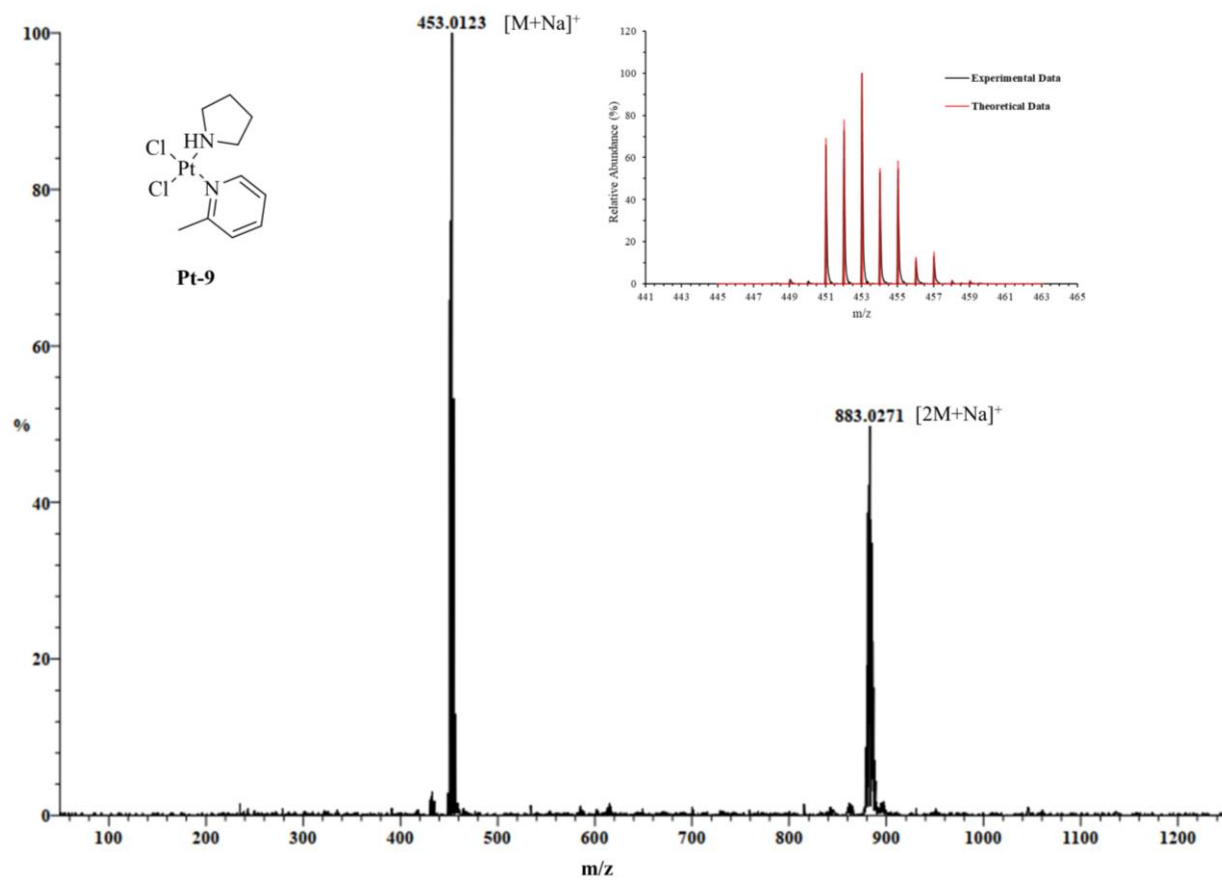


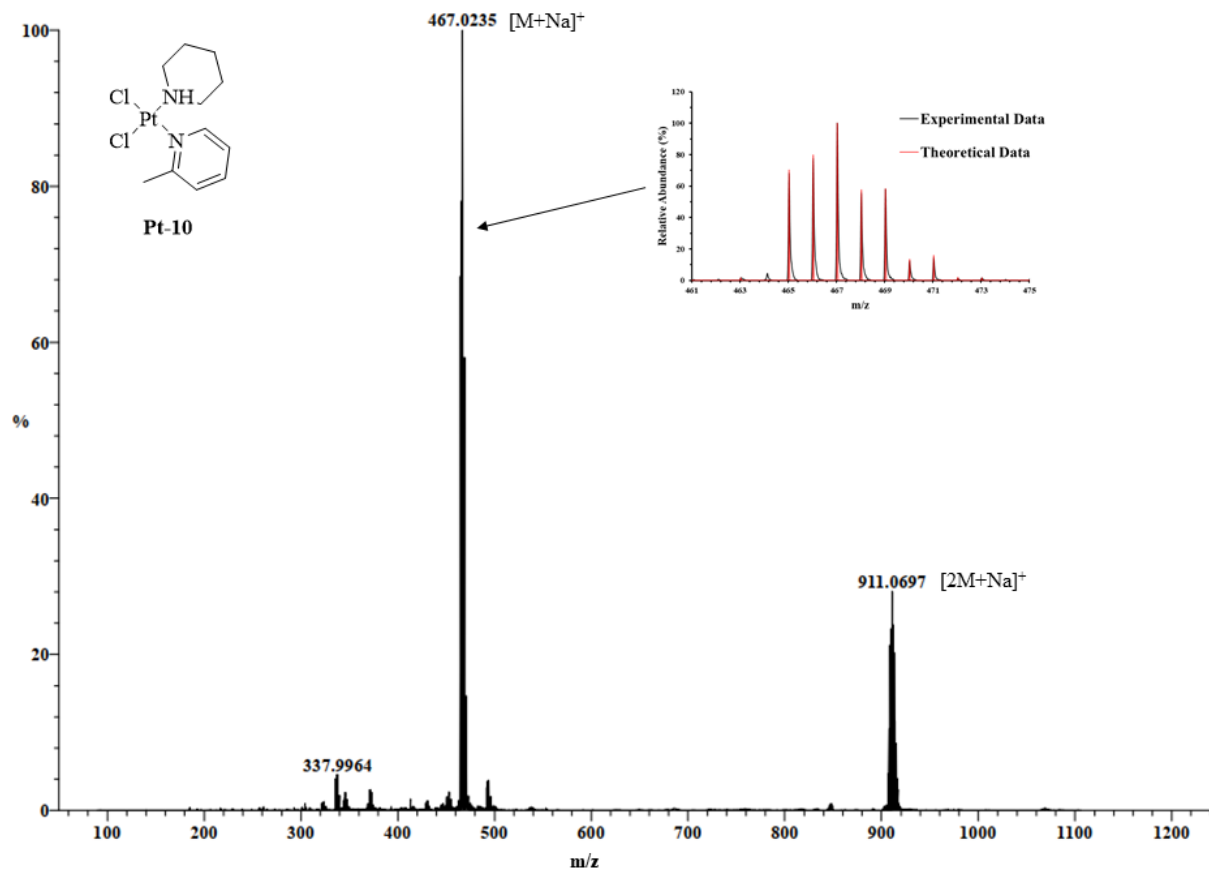
ESI-AccuTOF mass spectrum of Pt-5

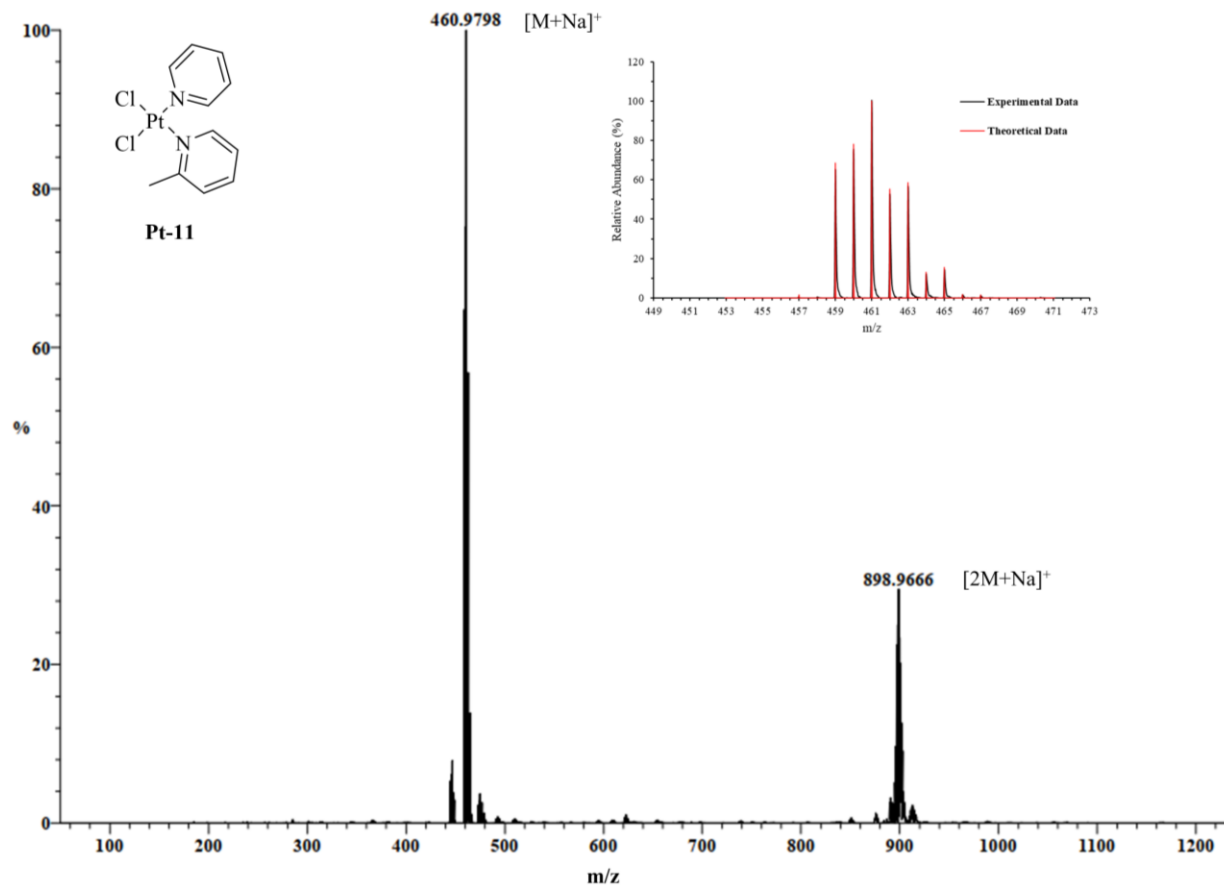
ESI-AccuTOF mass spectrum of **Pt-6**

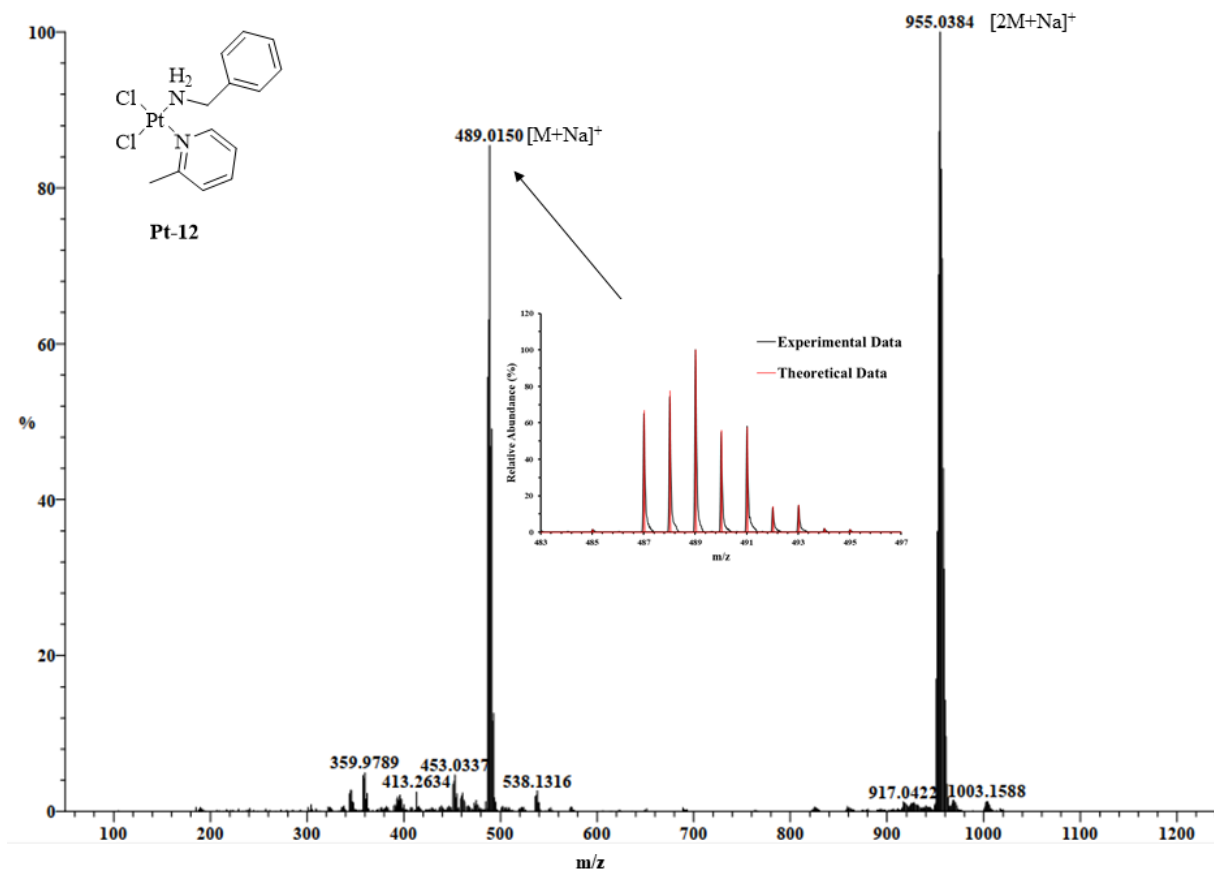
ESI-AccuTOF mass spectrum of **Pt-7**

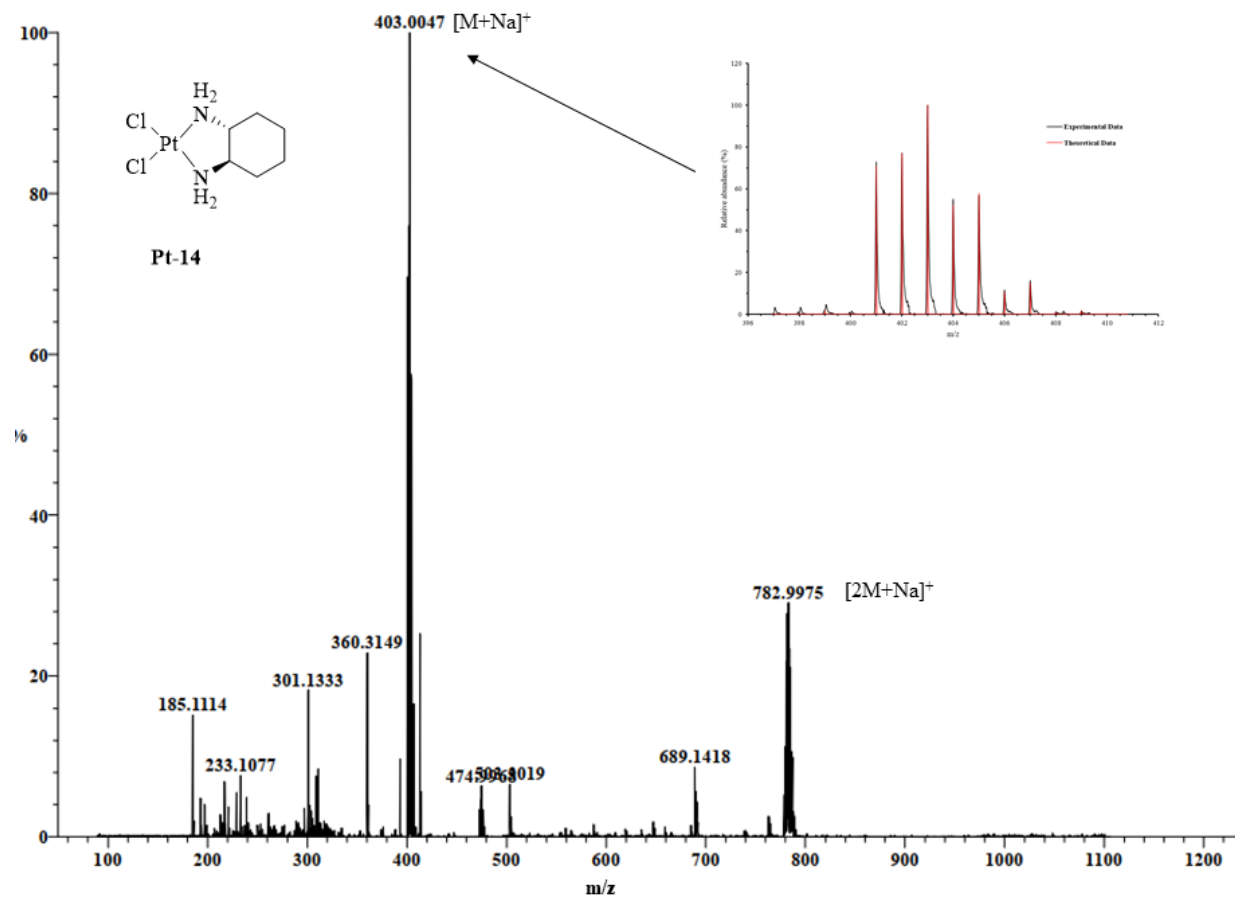
ESI-AccuTOF mass spectrum of **Pt-8**

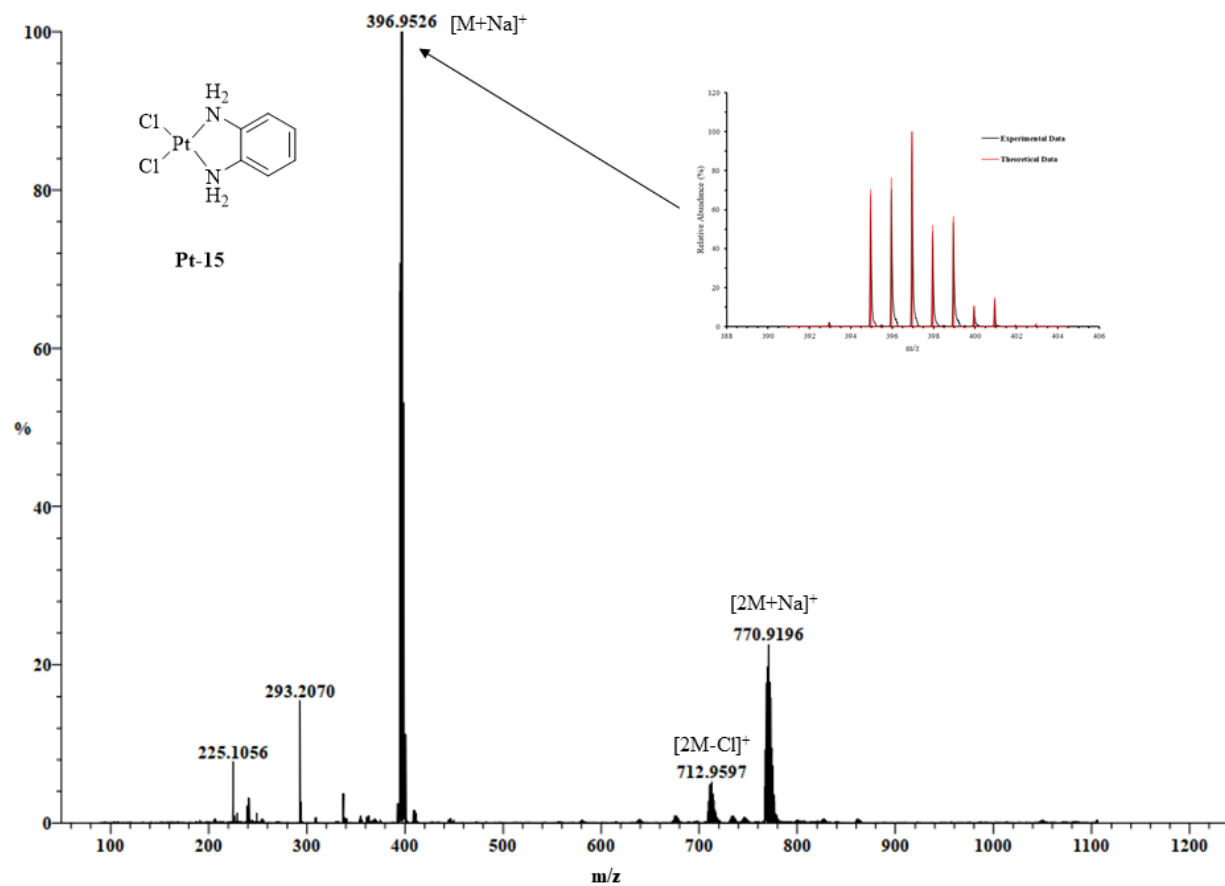
ESI-AccuTOF mass spectrum of **Pt-9**

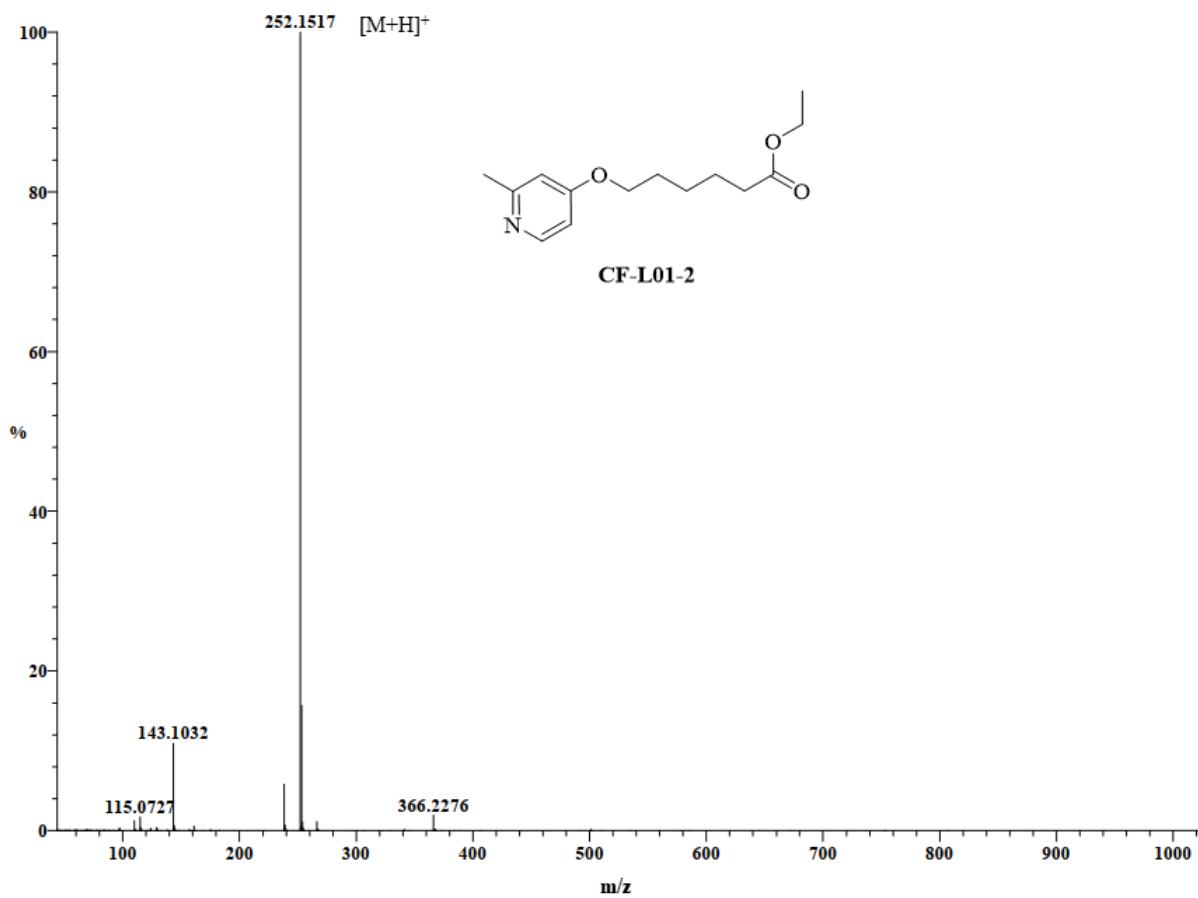
ESI-AccuTOF mass spectrum of **Pt-10**

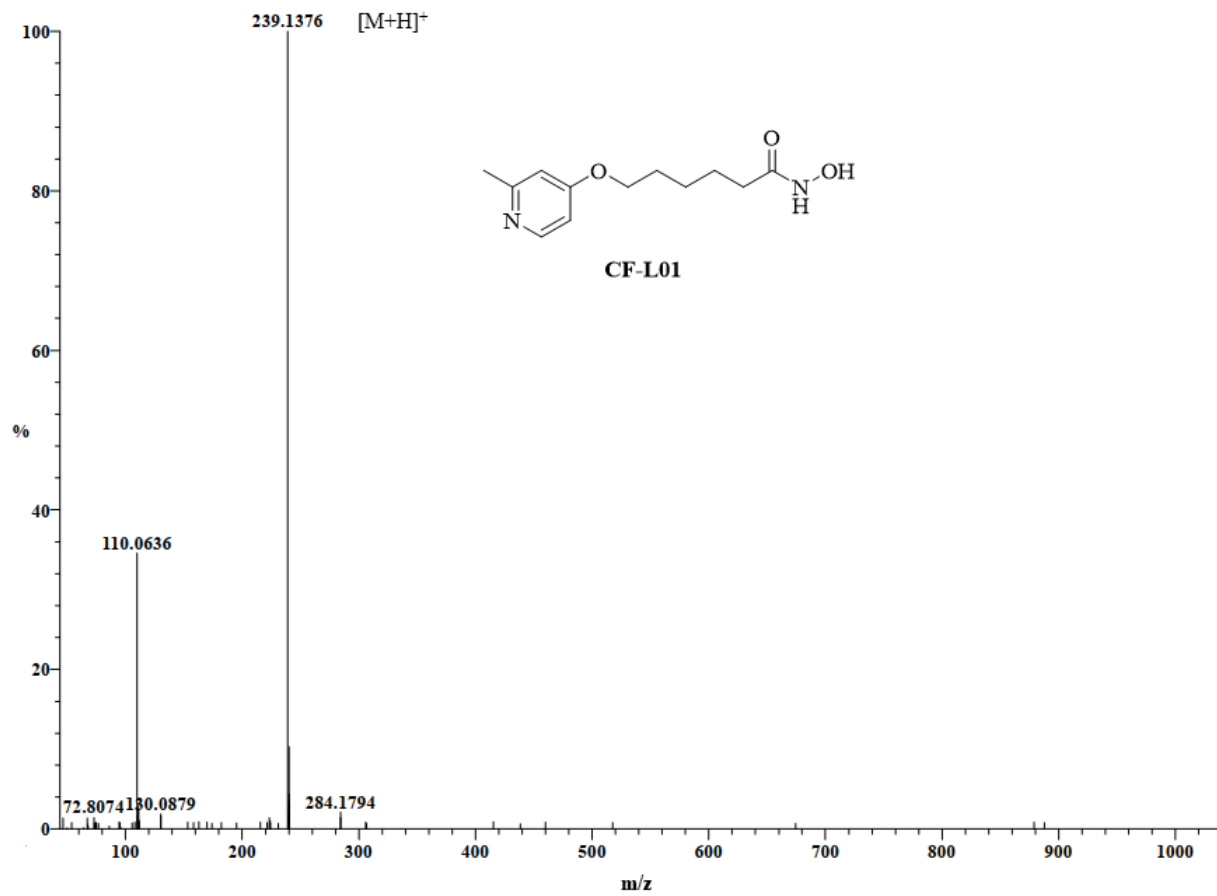
ESI-AccuTOF mass spectrum of **Pt-11**

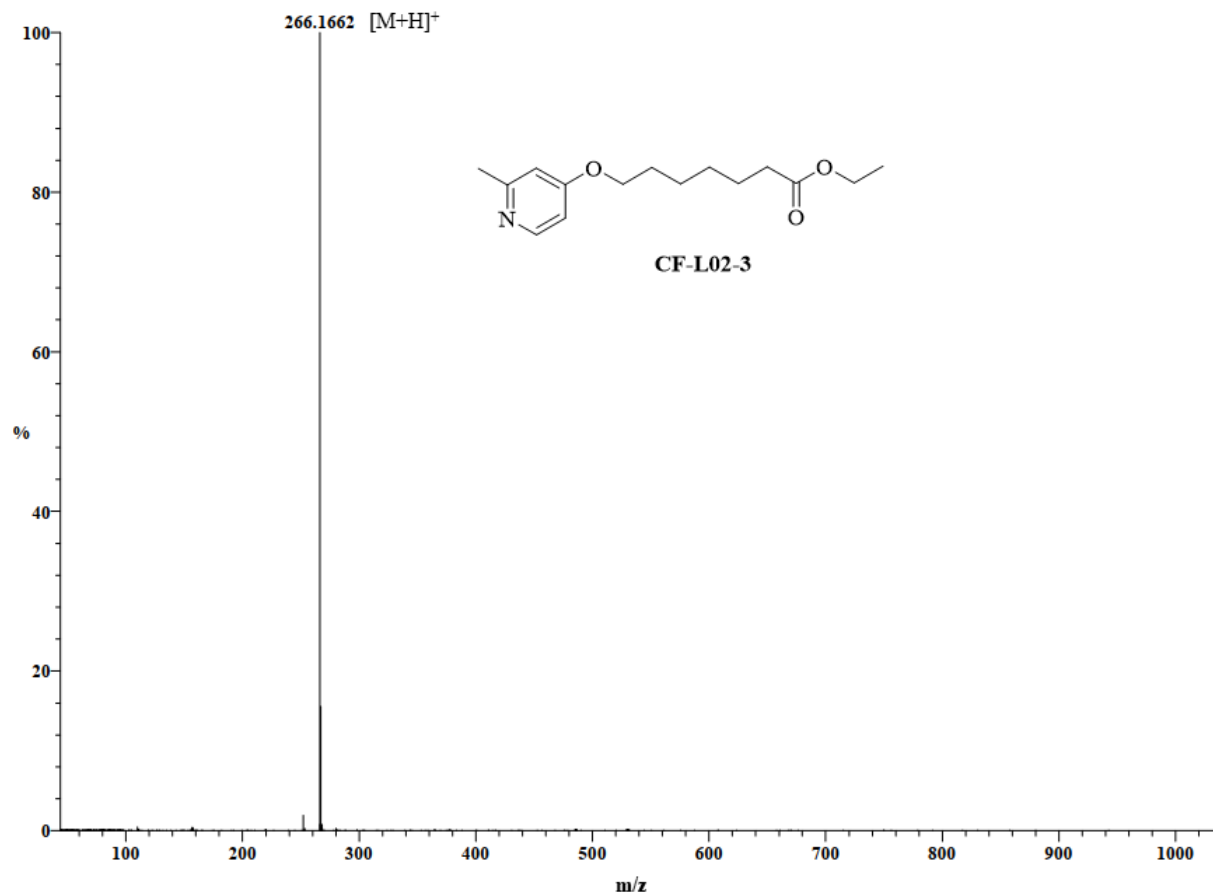
ESI-AccuTOF mass spectrum of **Pt-12**

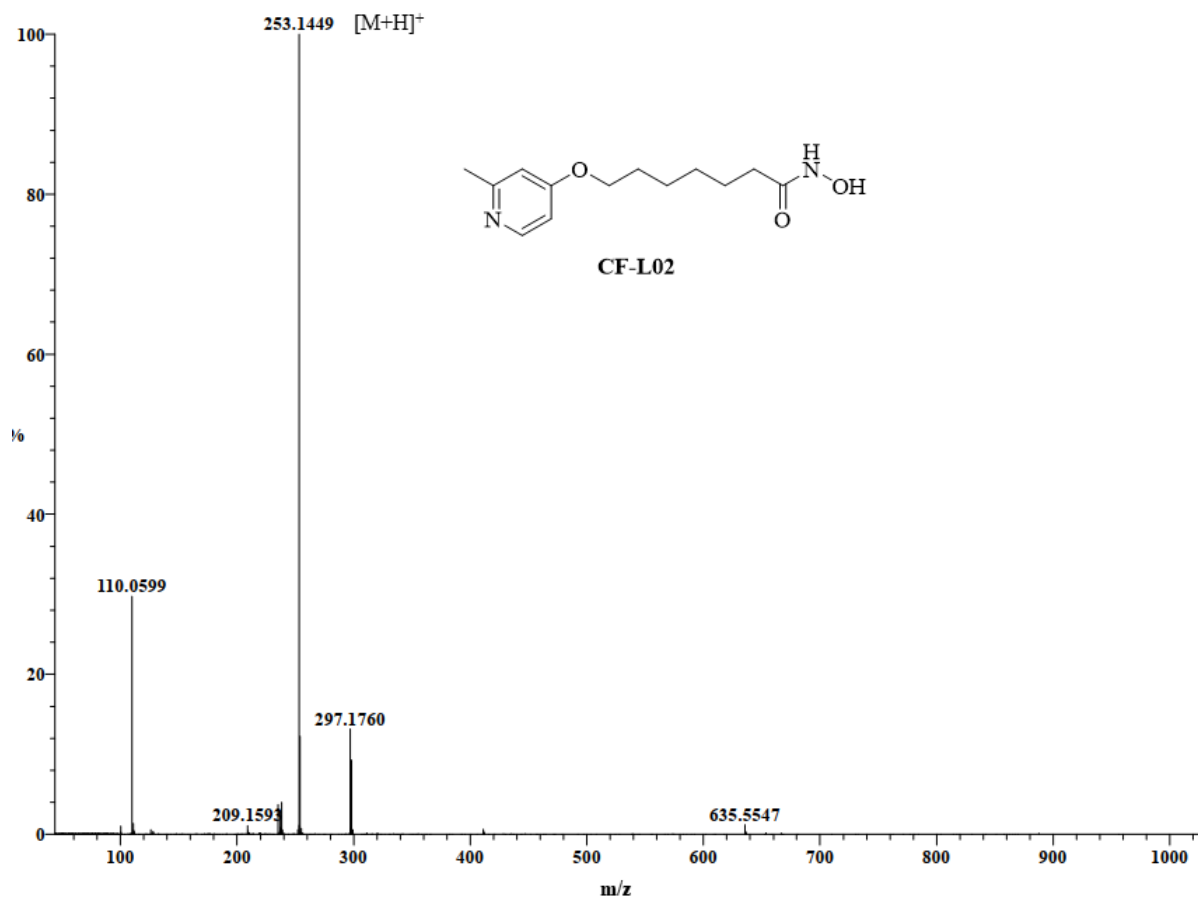
ESI-AccuTOF mass spectrum of **Pt-14**

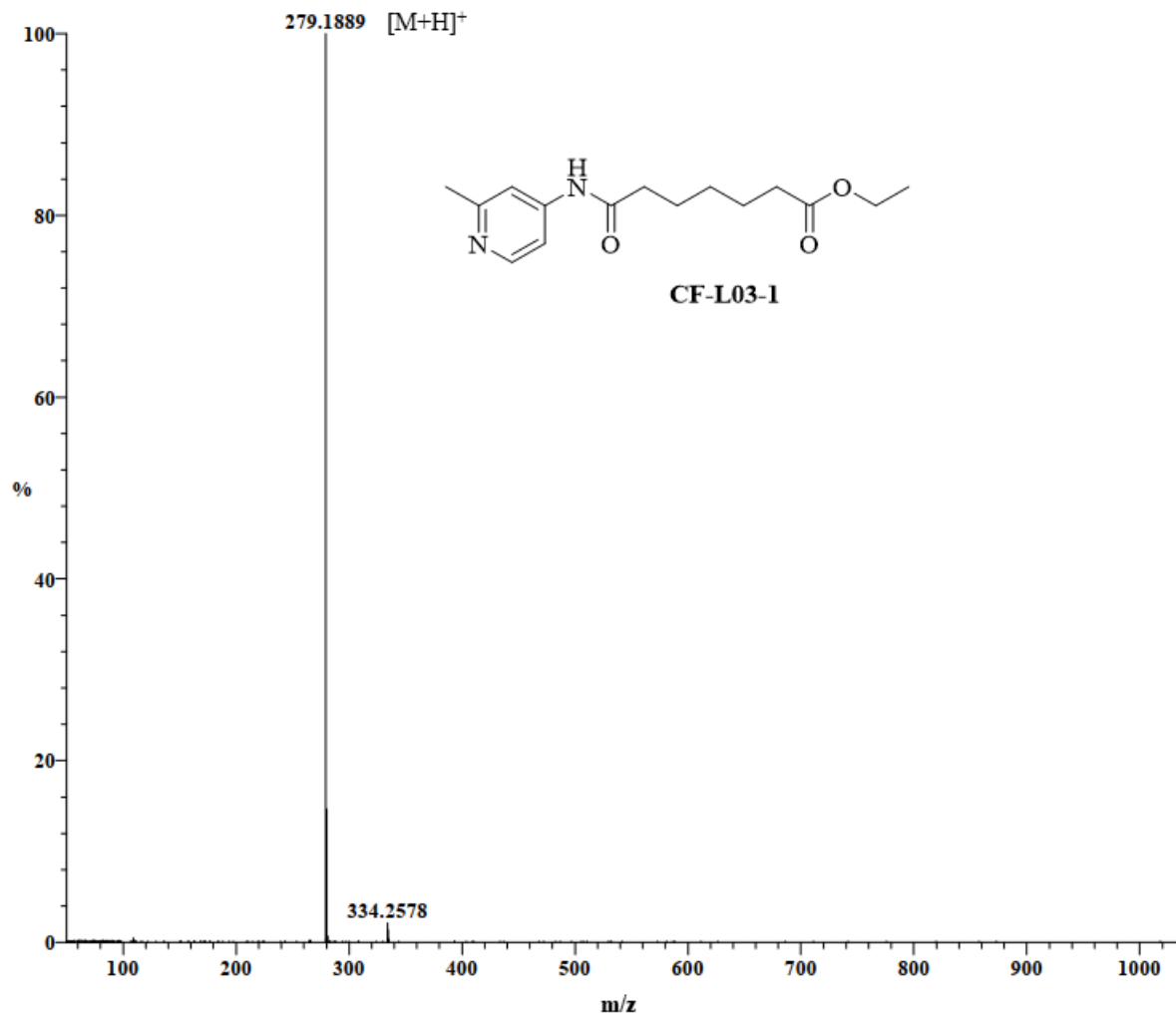
ESI-AccuTOF mass spectrum of **Pt-15**

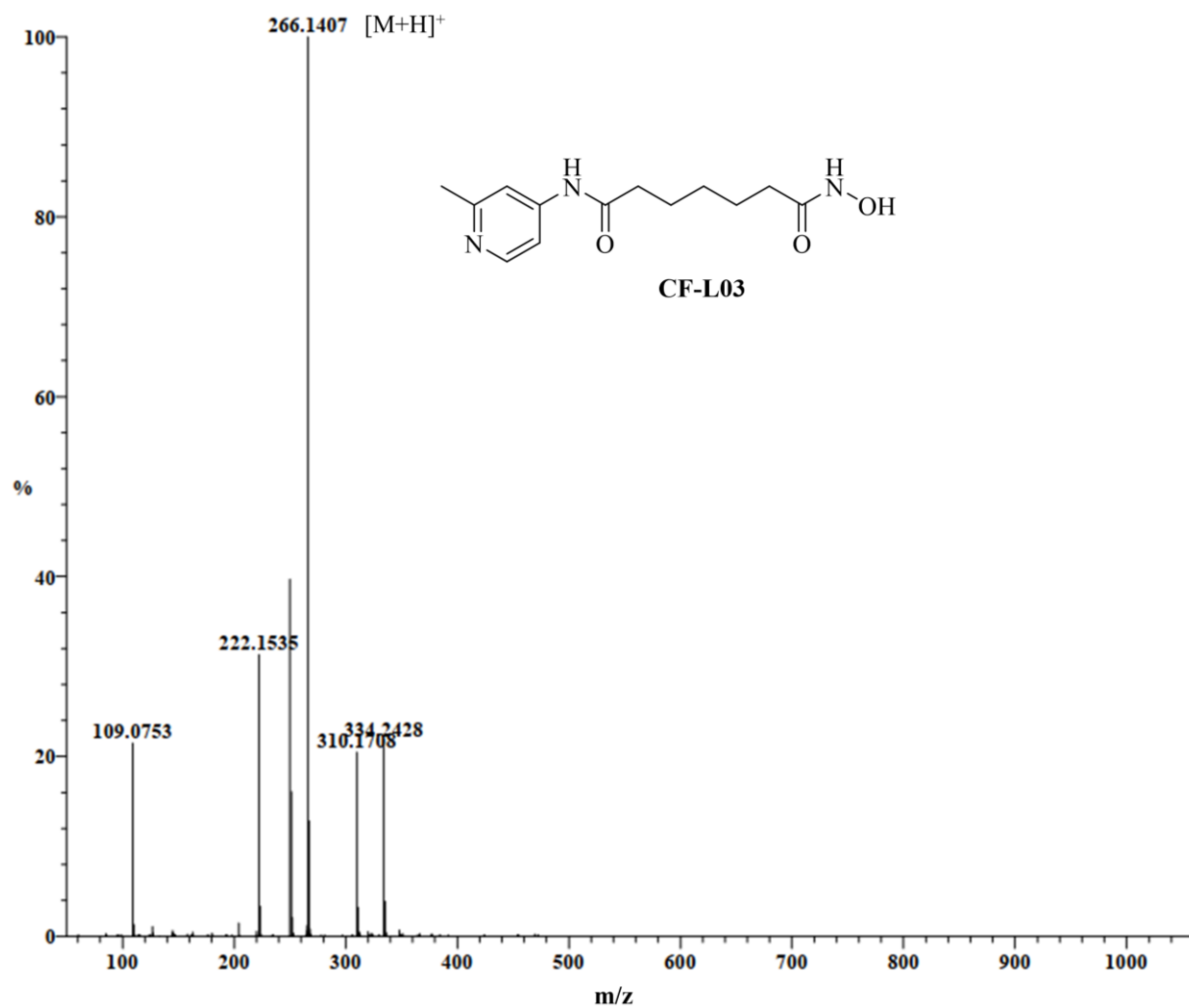
DART-AccuTOF mass spectrum of **CF-L01-2**

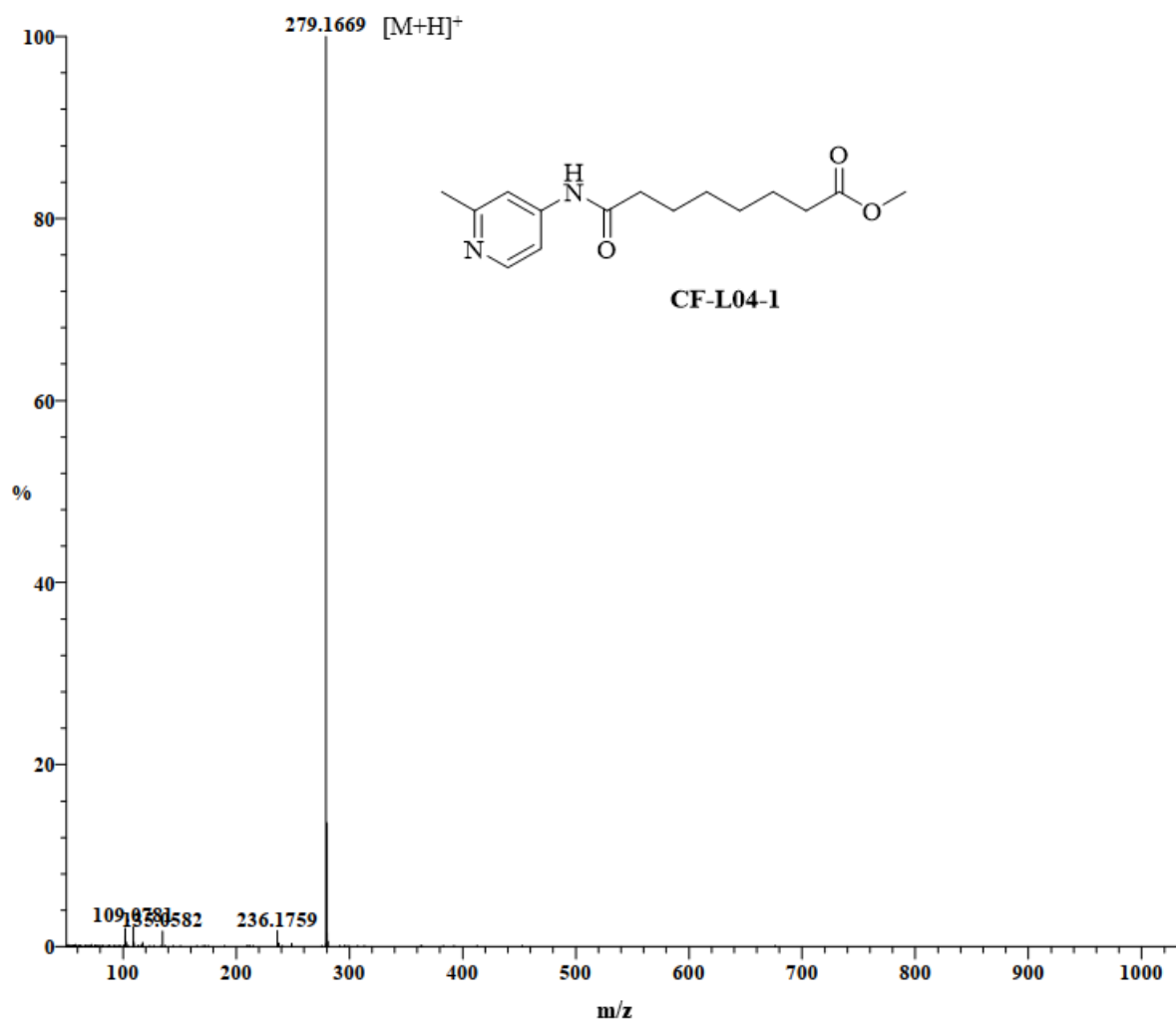
DART-AccuTOF mass spectrum of **CF-L01**

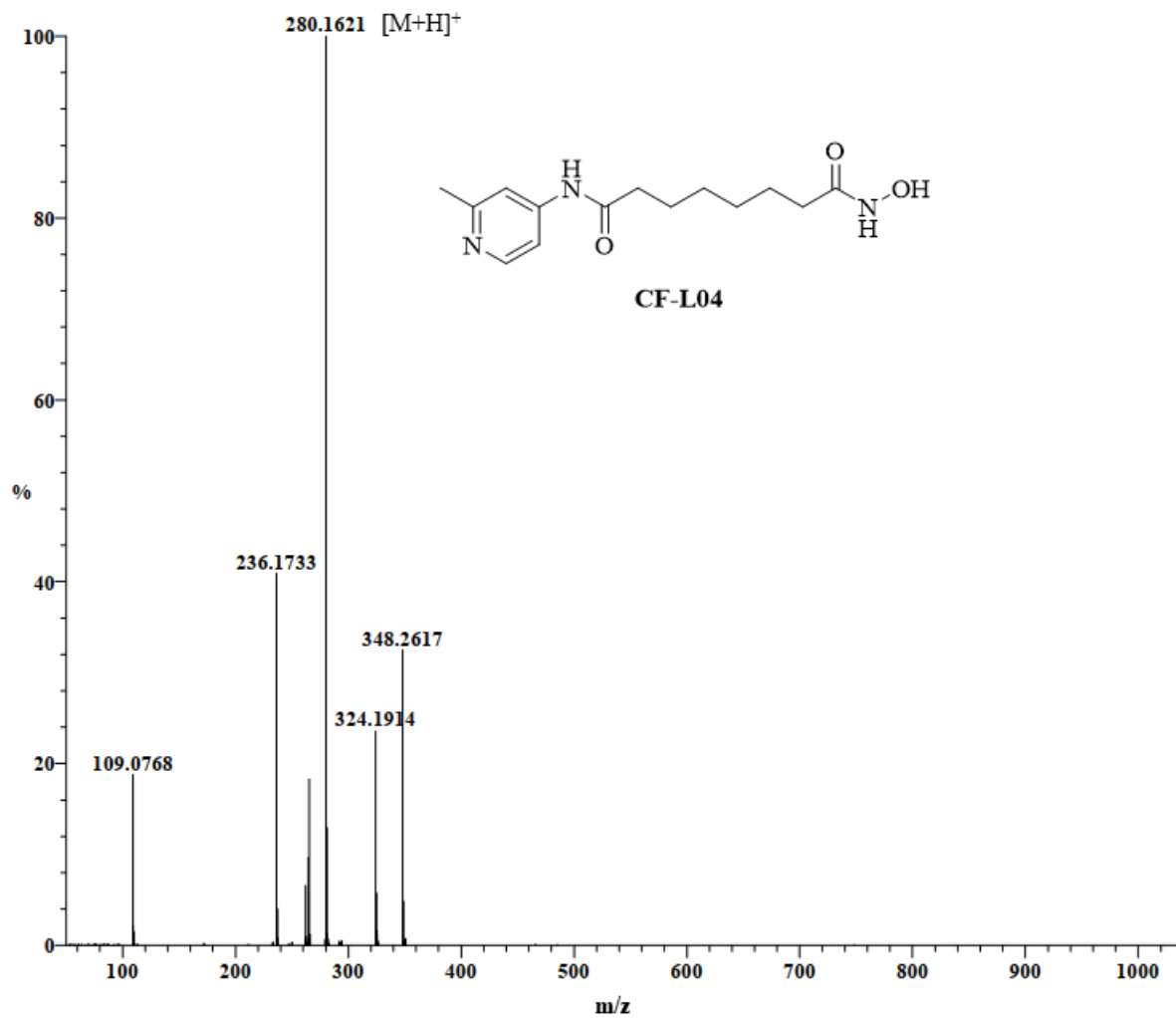
DART-AccuTOF mass spectrum of **CF-L02-3**

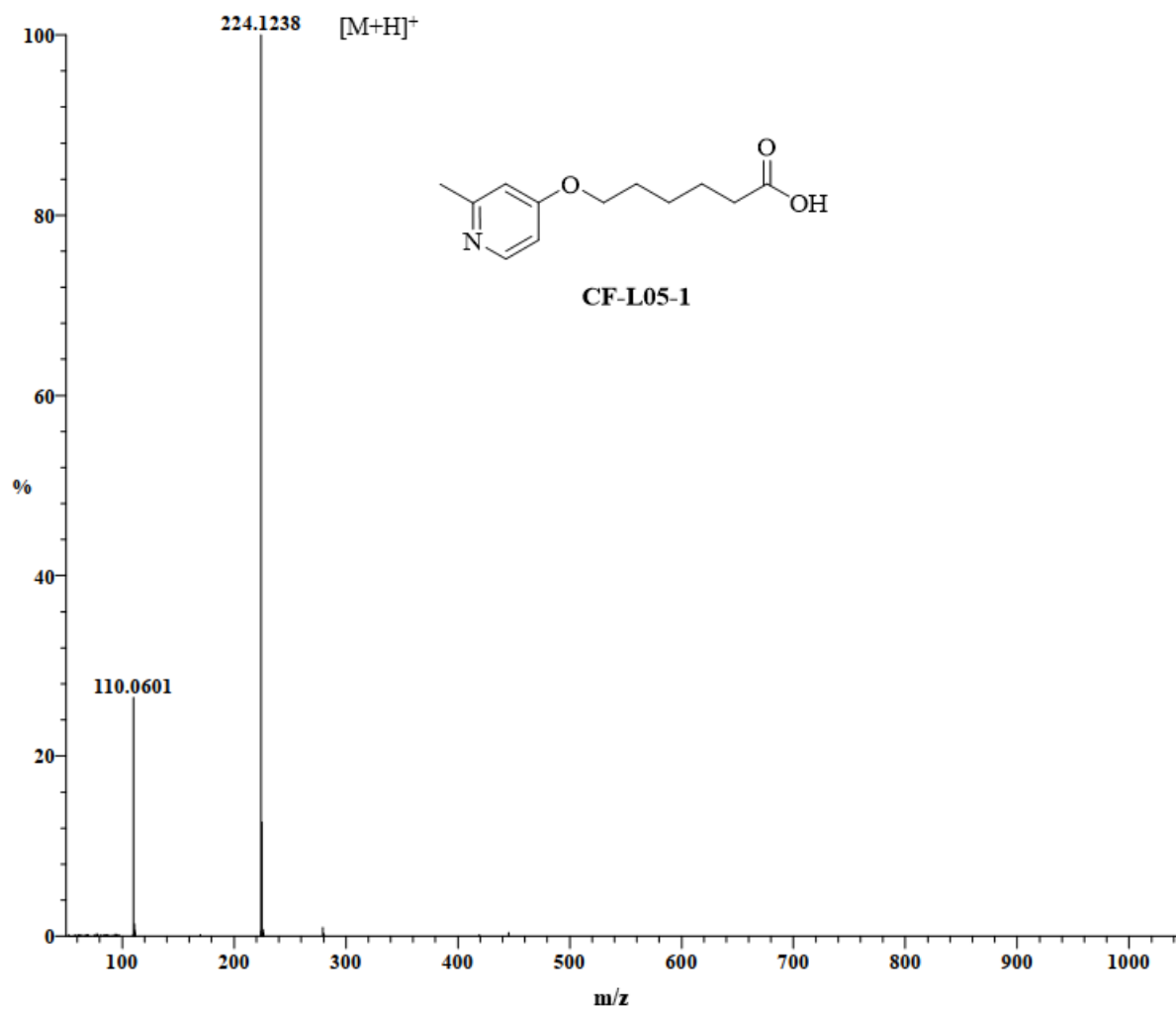
DART-AccuTOF mass spectrum of **CF-L02**

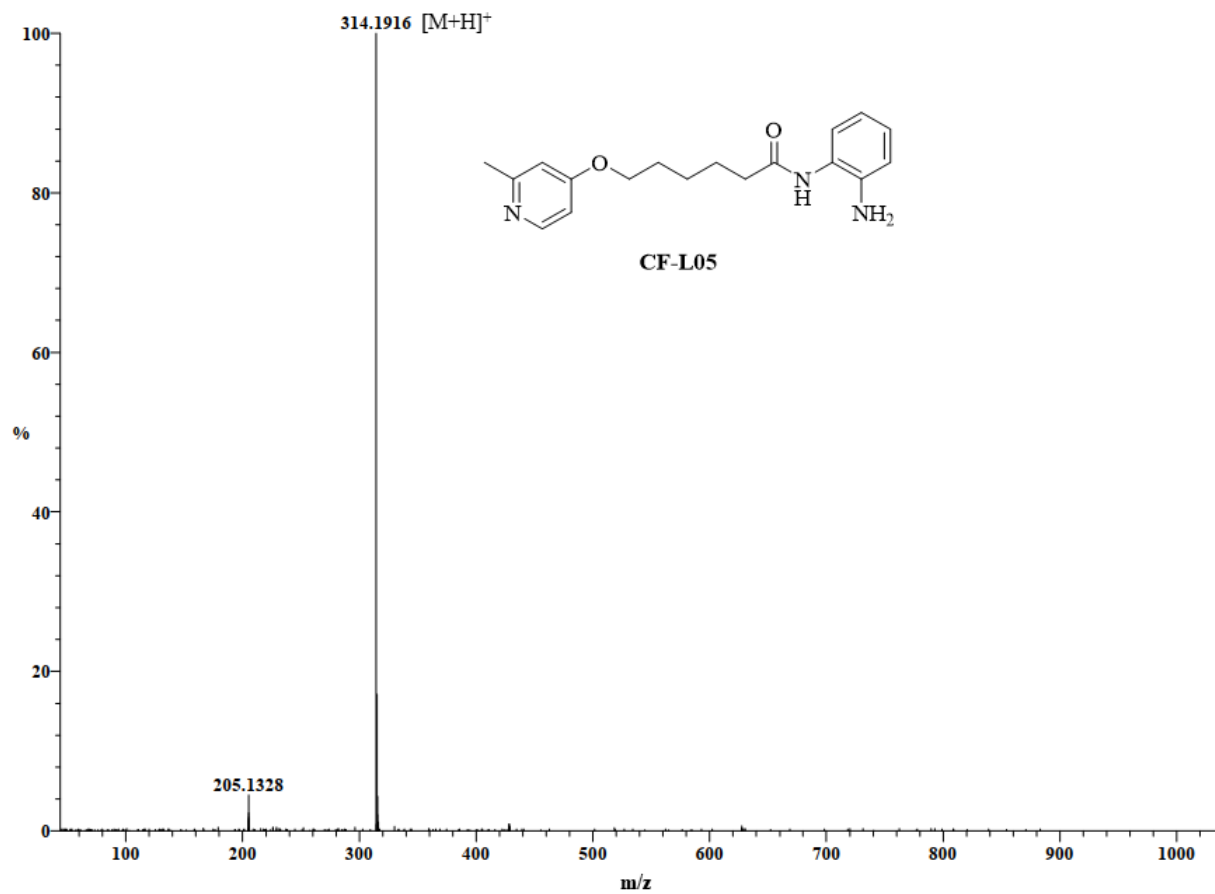
DART-AccuTOF mass spectrum of **CF-L03-1**

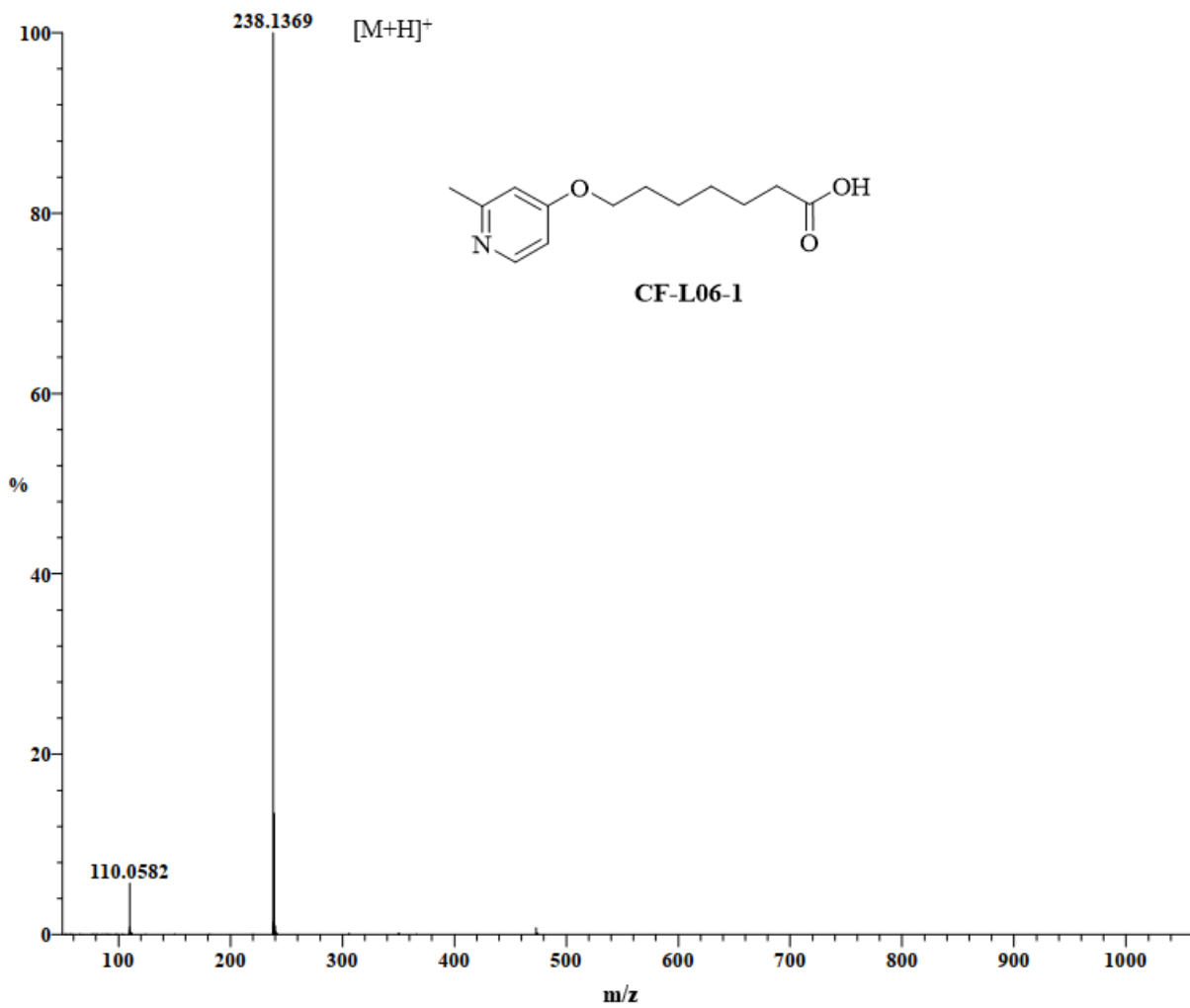
DART-AccuTOF mass spectrum of **CF-L03**

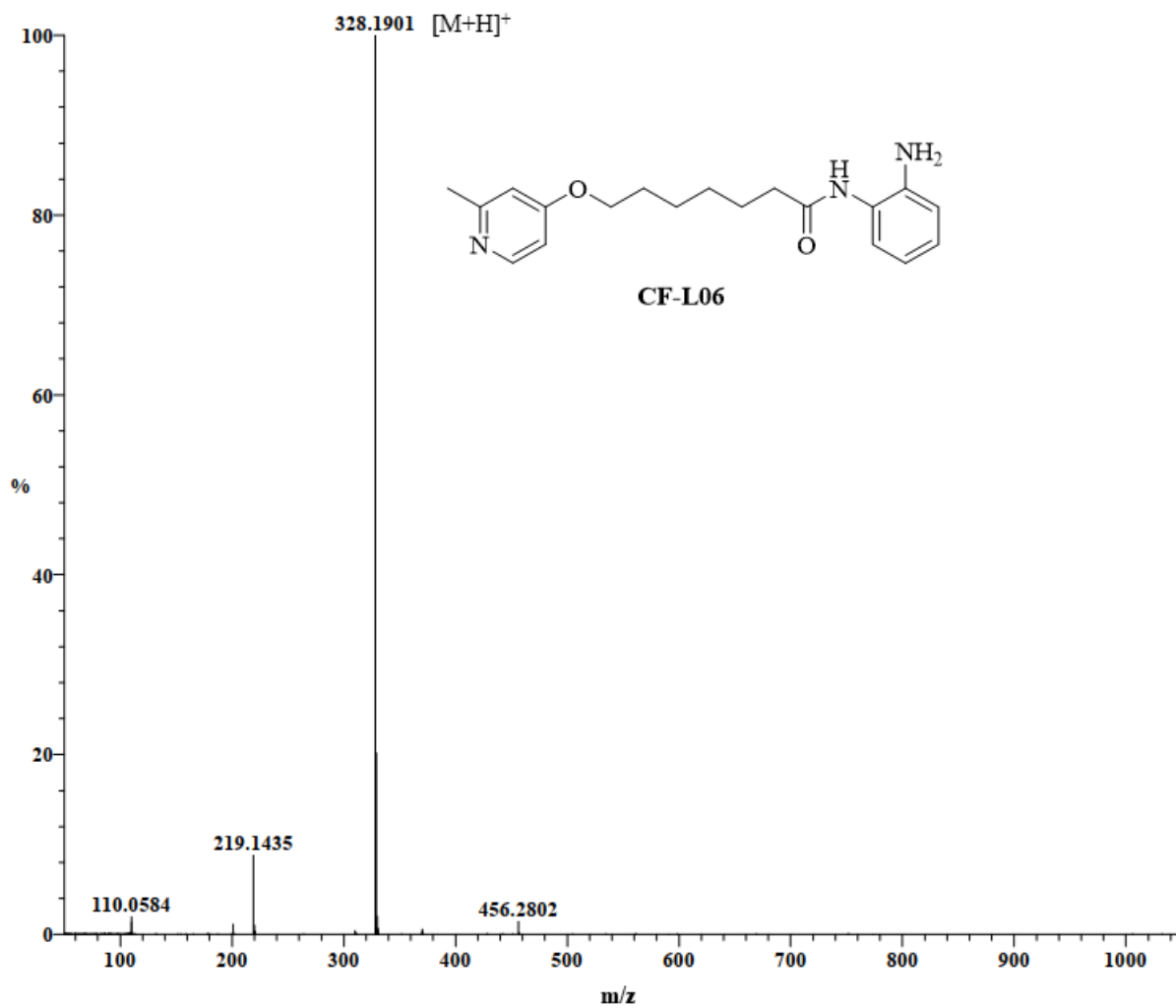
DART-AccuTOF mass spectrum of **CF-L04-1**

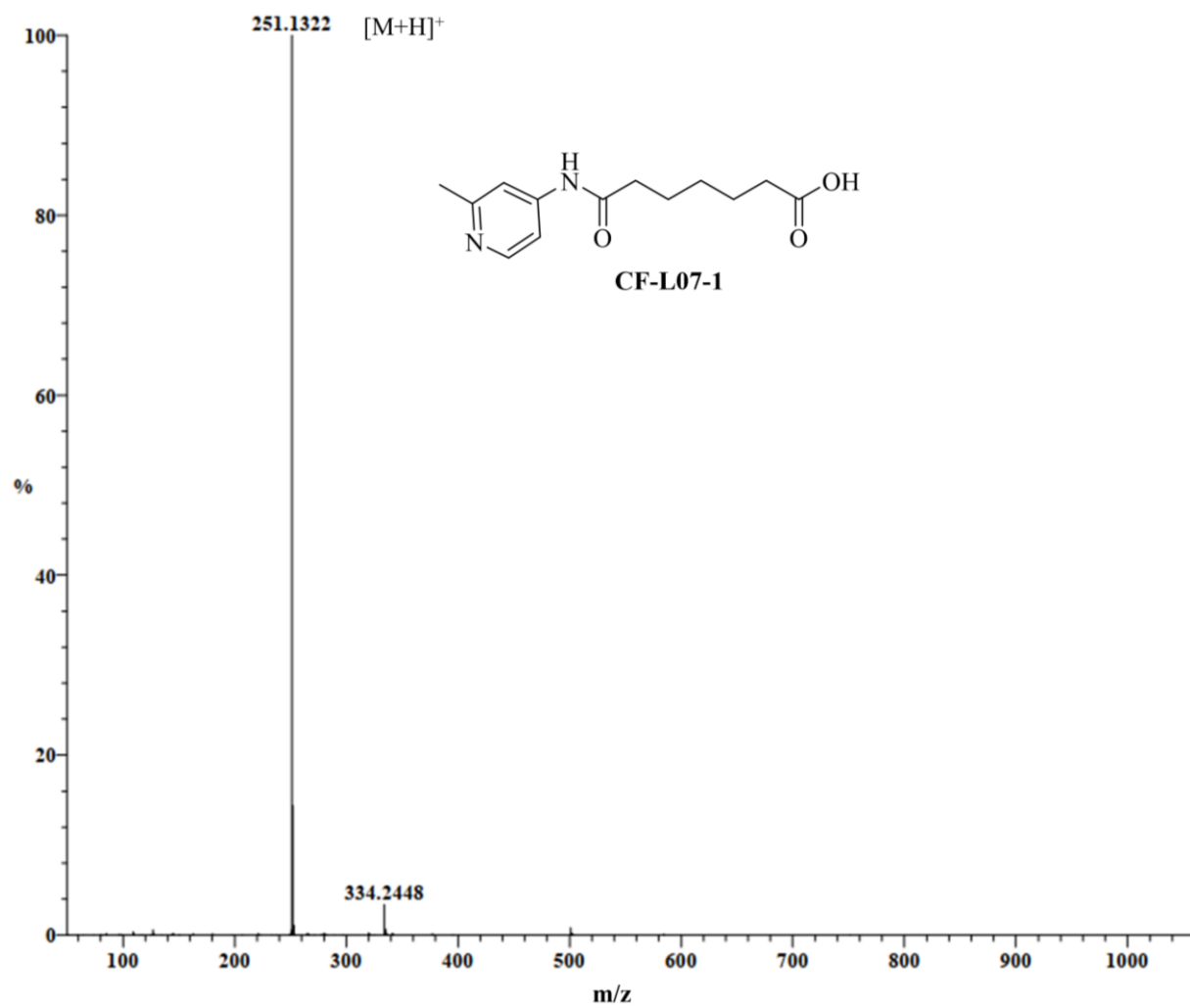
DART-AccuTOF mass spectrum of **CF-L04**

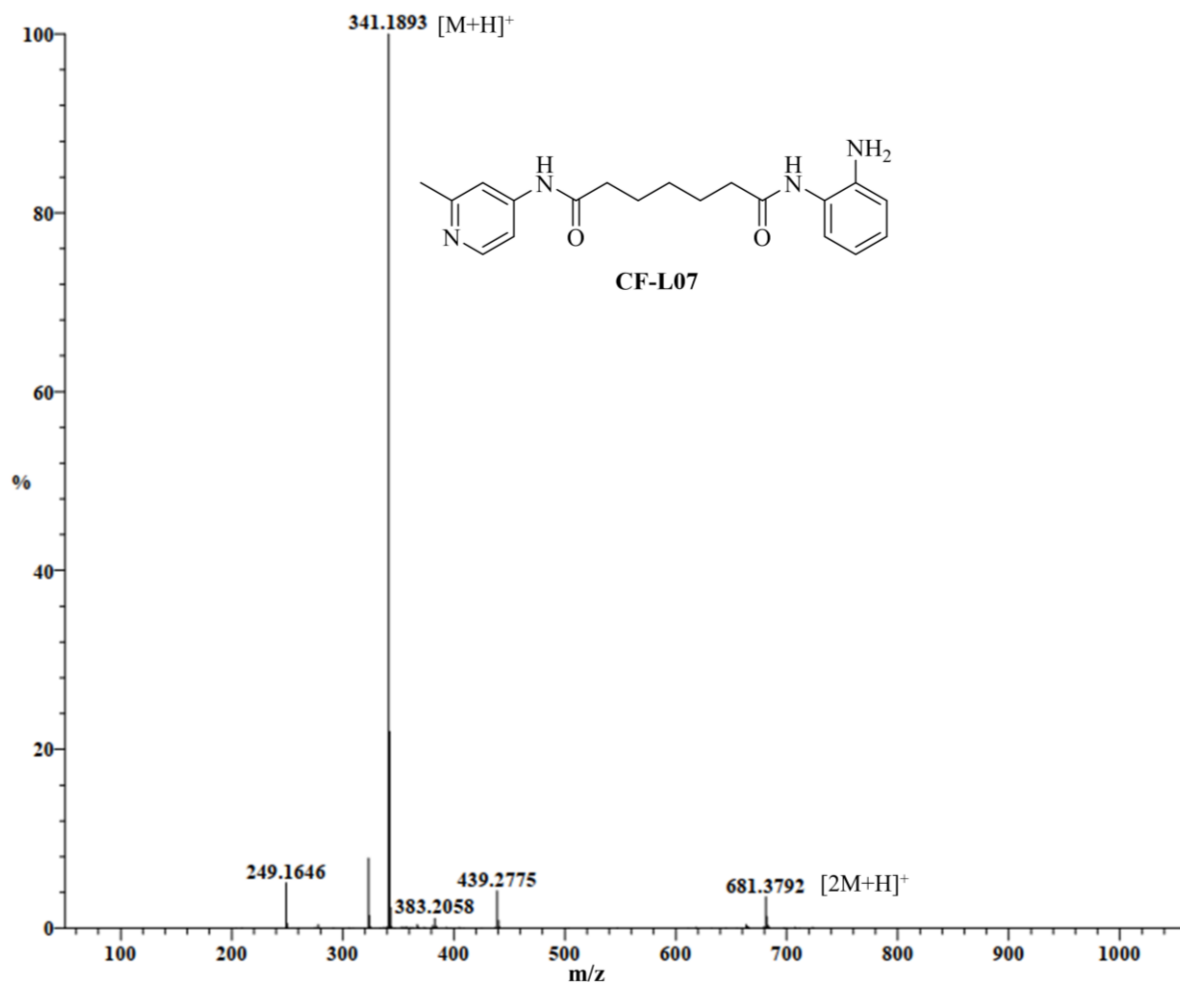
DART-AccuTOF mass spectrum of **CF-L05-1**

DART-AccuTOF mass spectrum of **CF-L05**

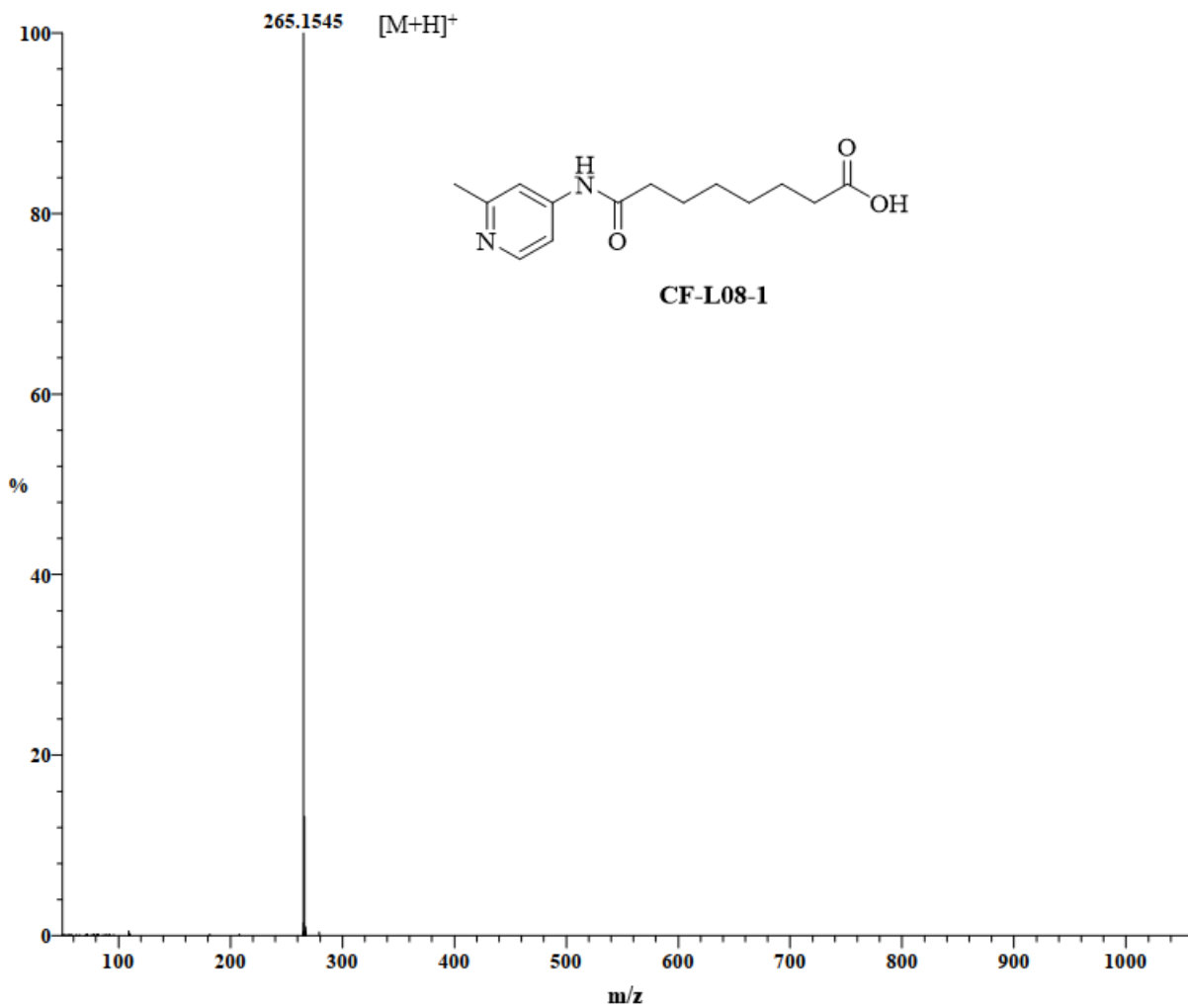
DART-AccuTOF mass spectrum of **CF-L06-1**

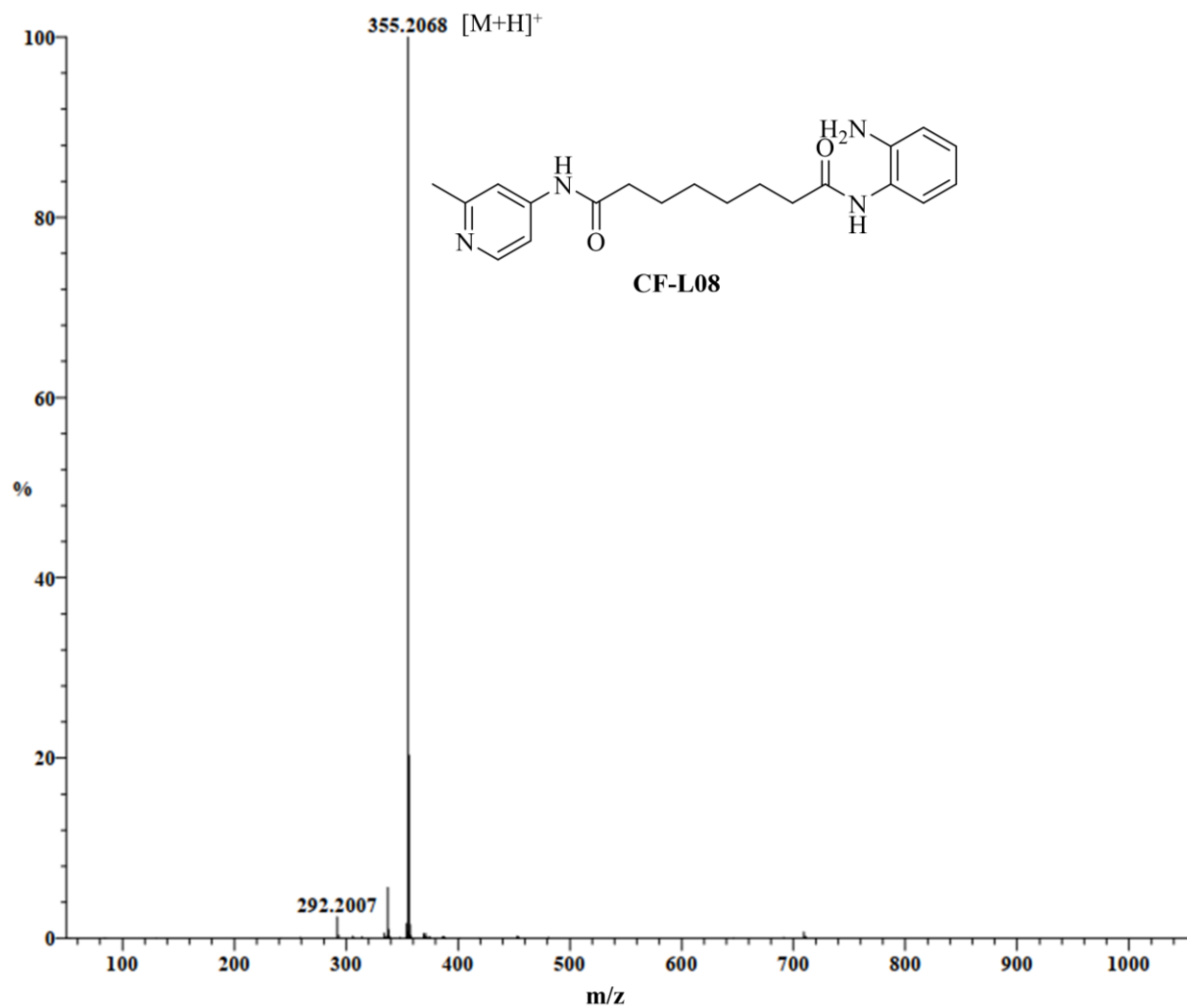
DART-AccuTOF mass spectrum of **CF-L06**

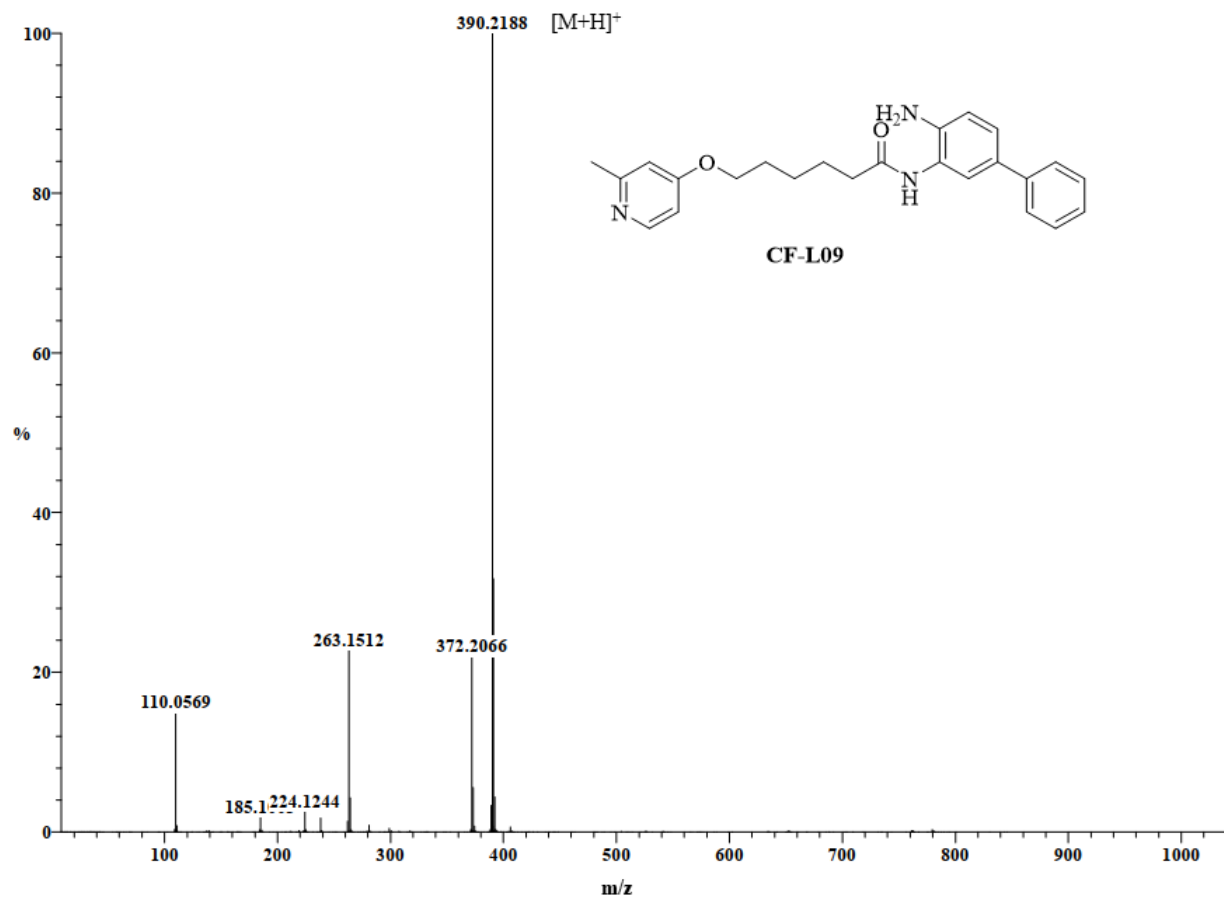
DART-AccuTOF mass spectrum of **CF-L07-1**

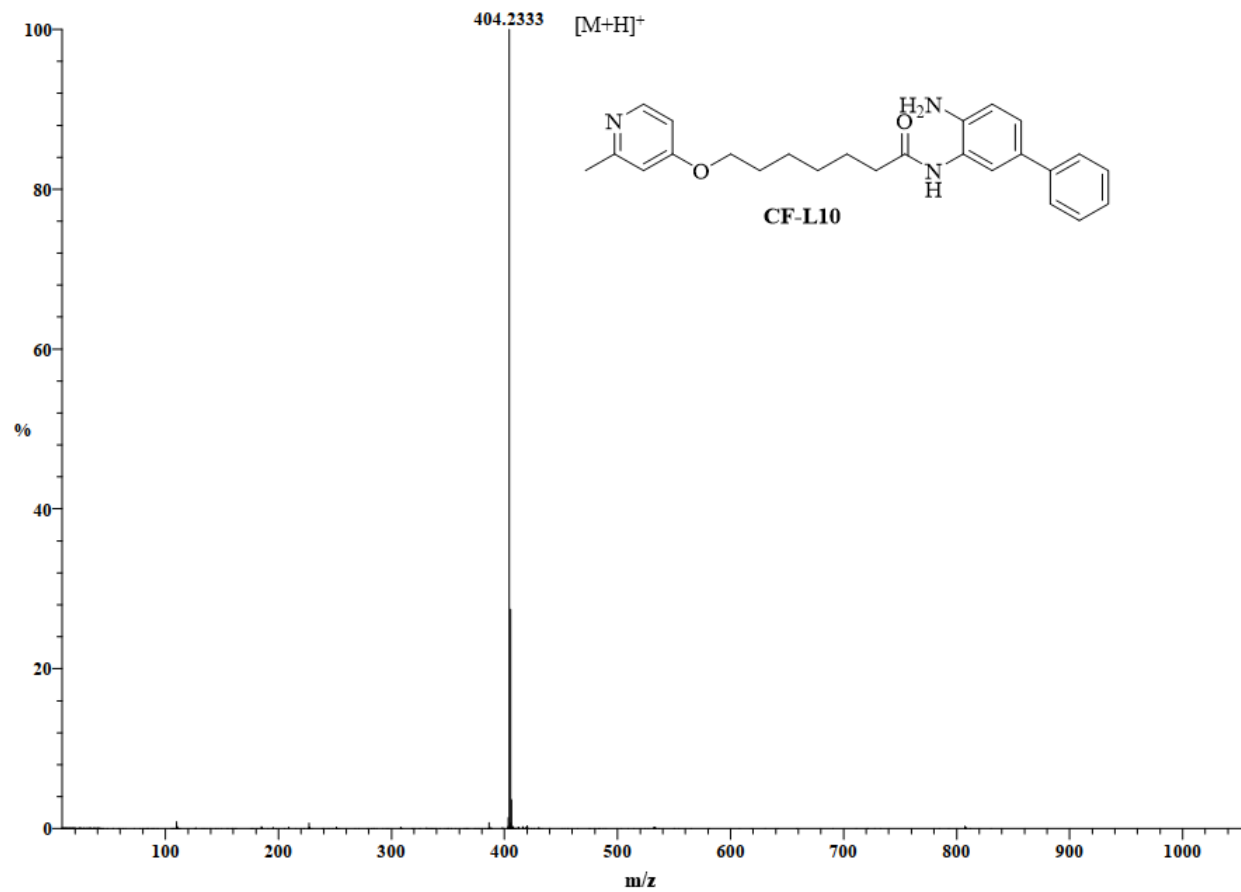


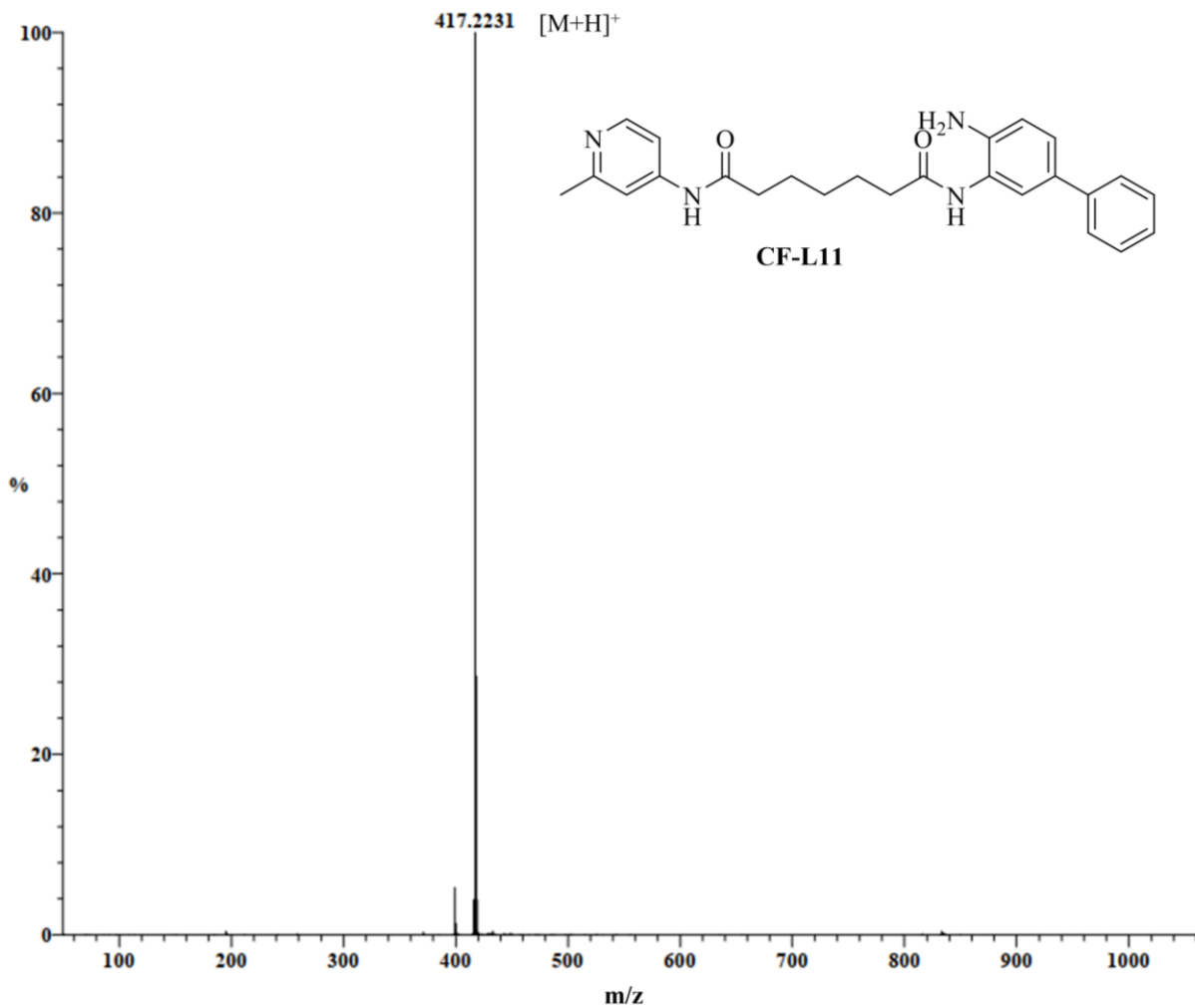
DART-AccuTOF mass spectrum of CF-L07

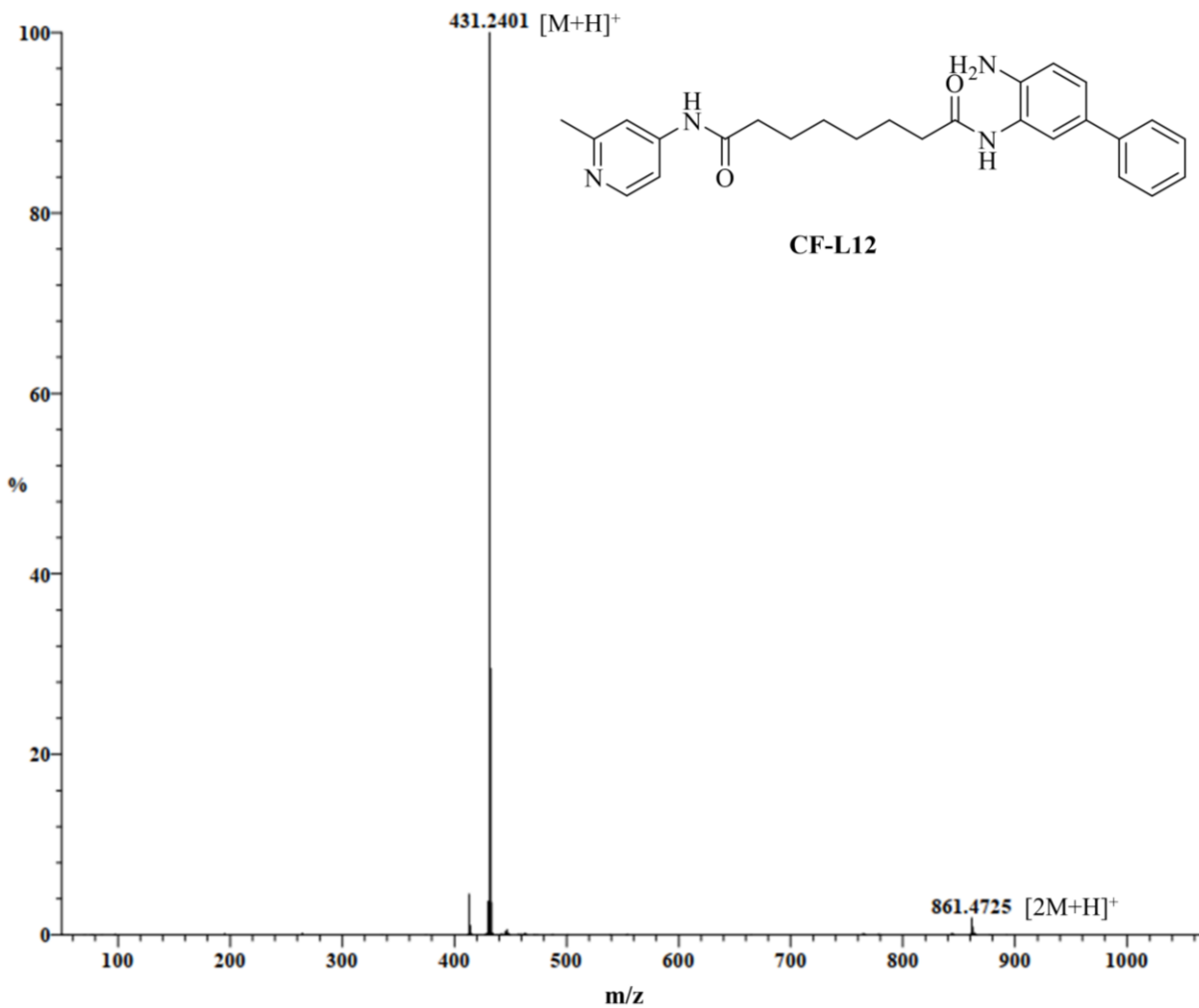
DART-AccuTOF mass spectrum of **CF-L08-1**

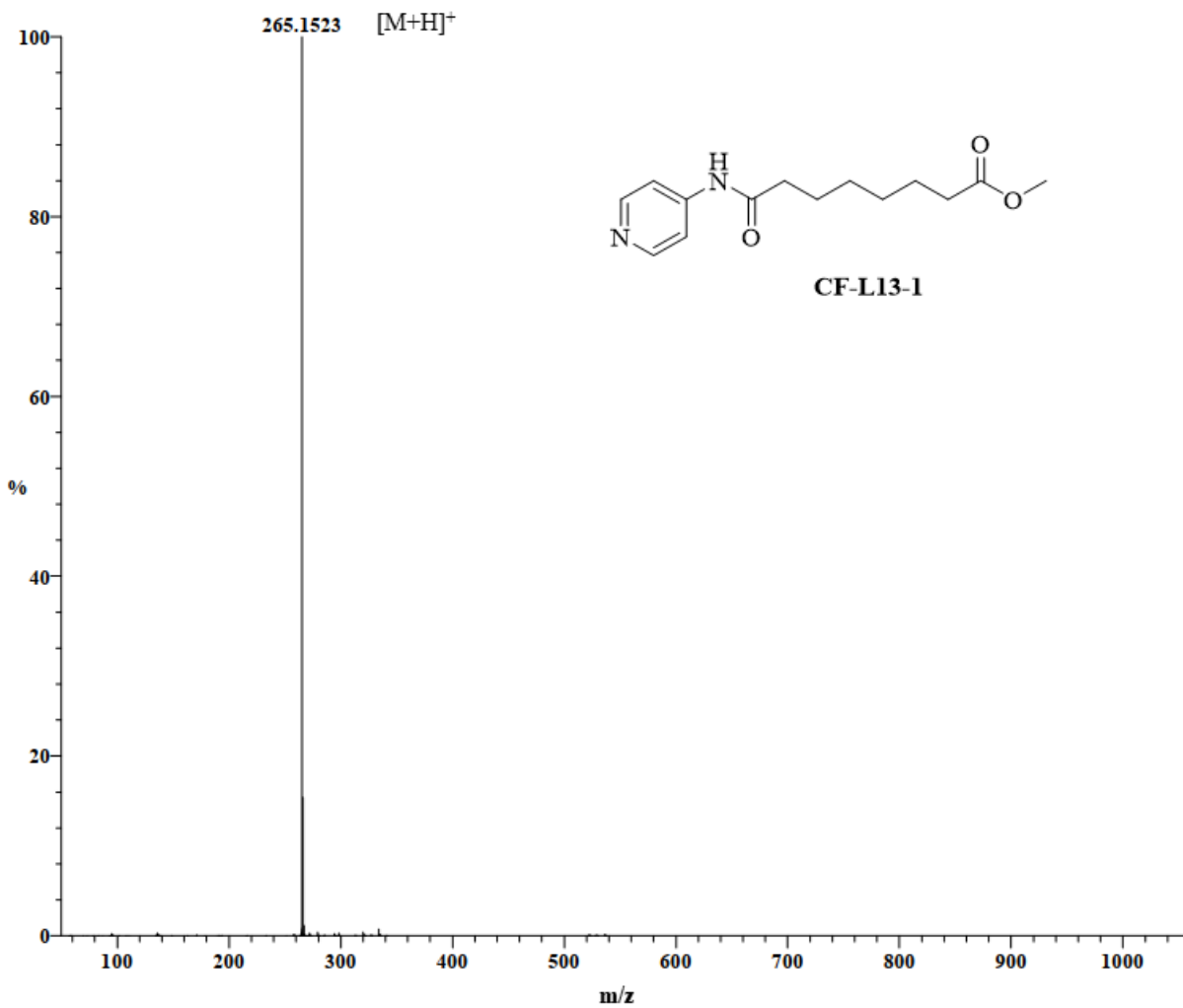
DART-AccuTOF mass spectrum of **CF-L08**

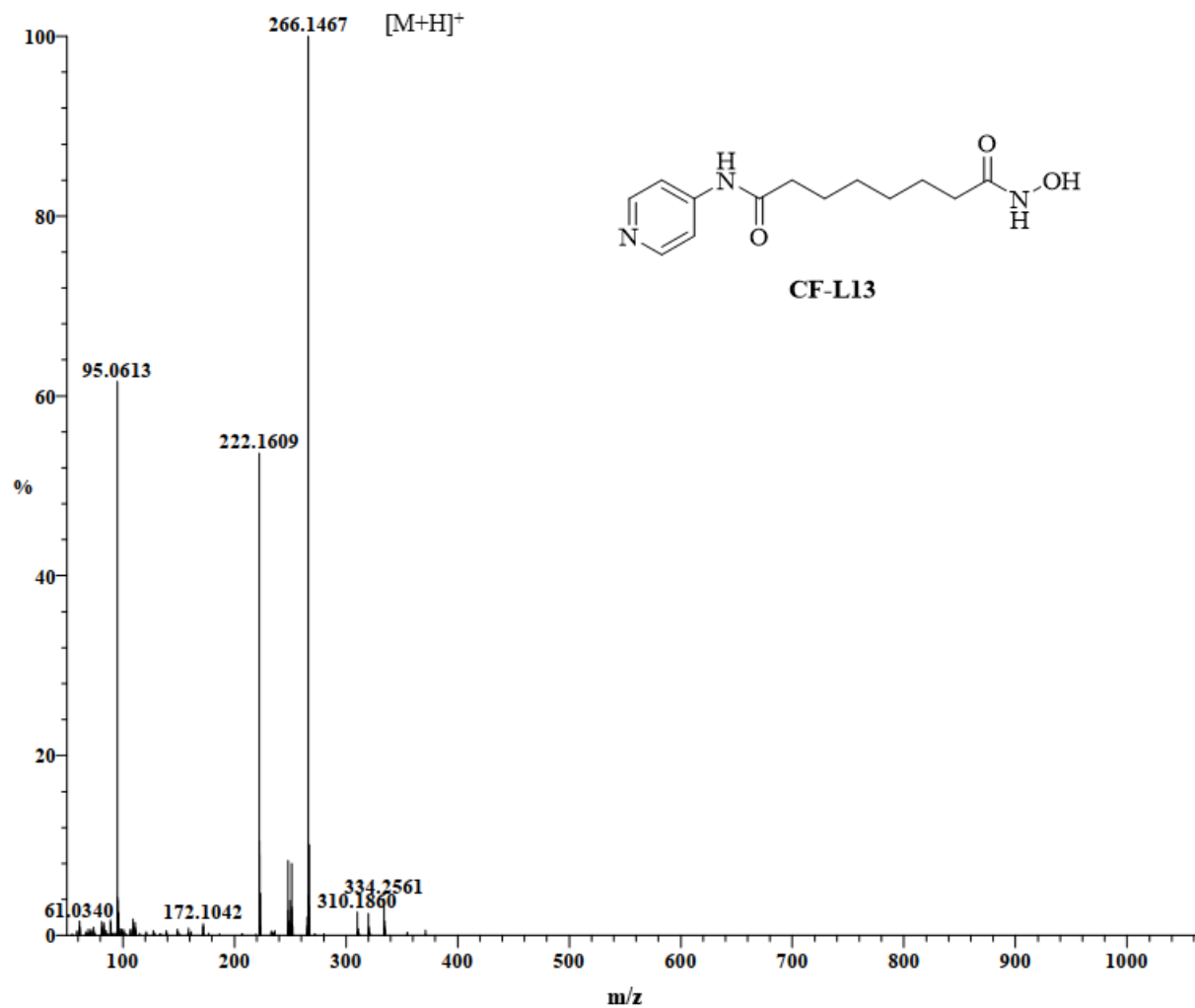
DART-AccuTOF mass spectrum of **CF-L09**

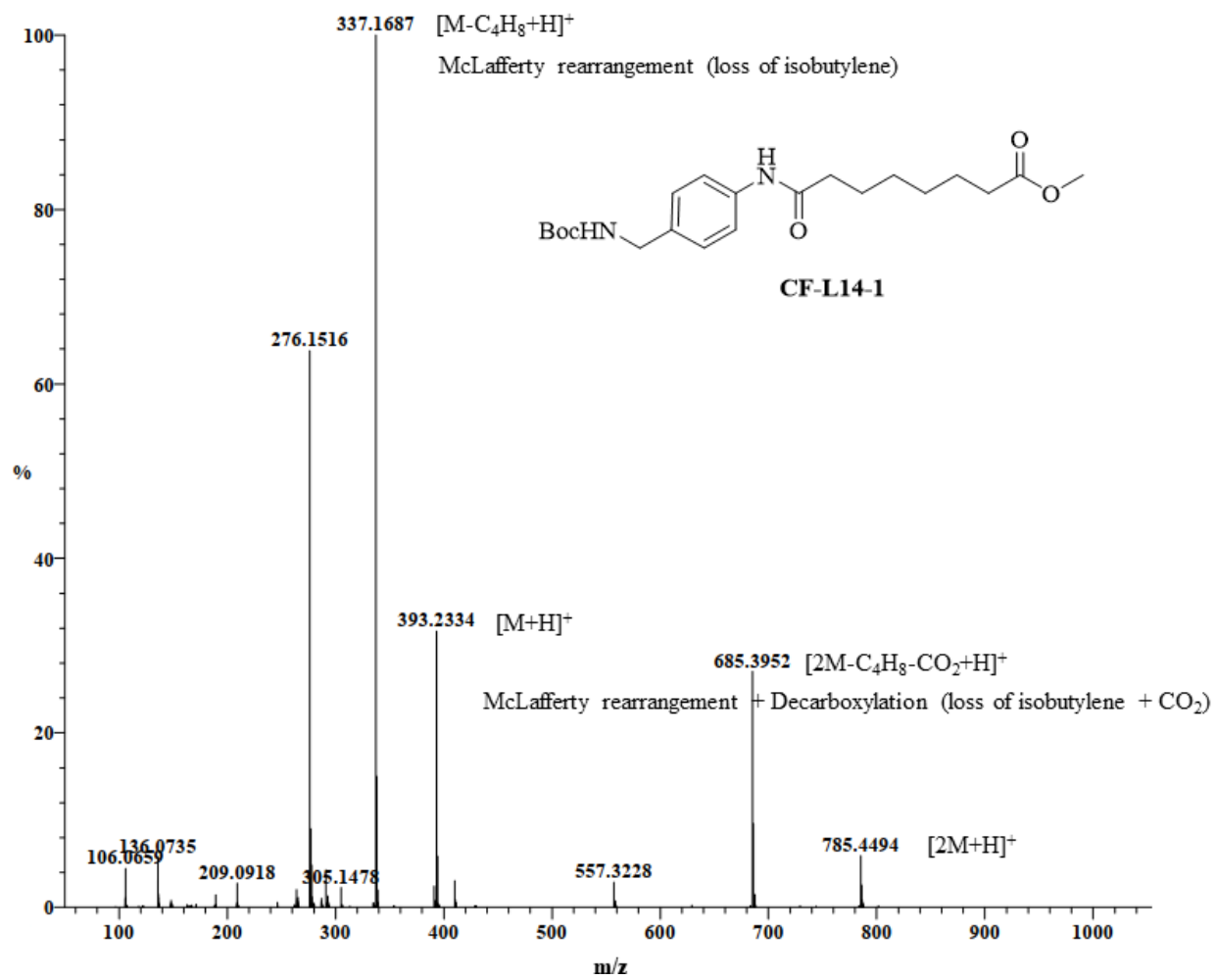
DART-AccuTOF mass spectrum of **CF-L10**

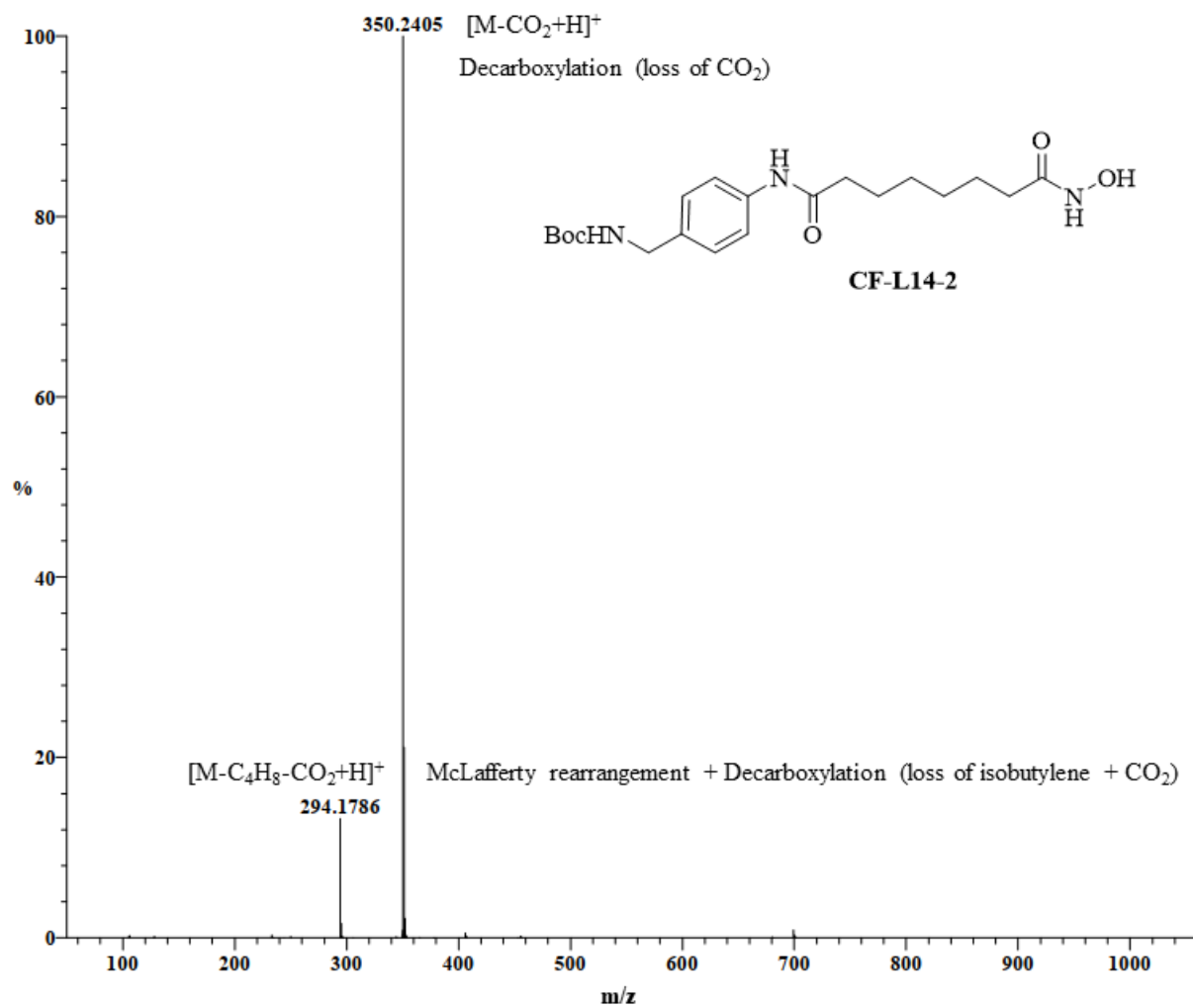
DART-AccuTOF mass spectrum of **CF-L11**

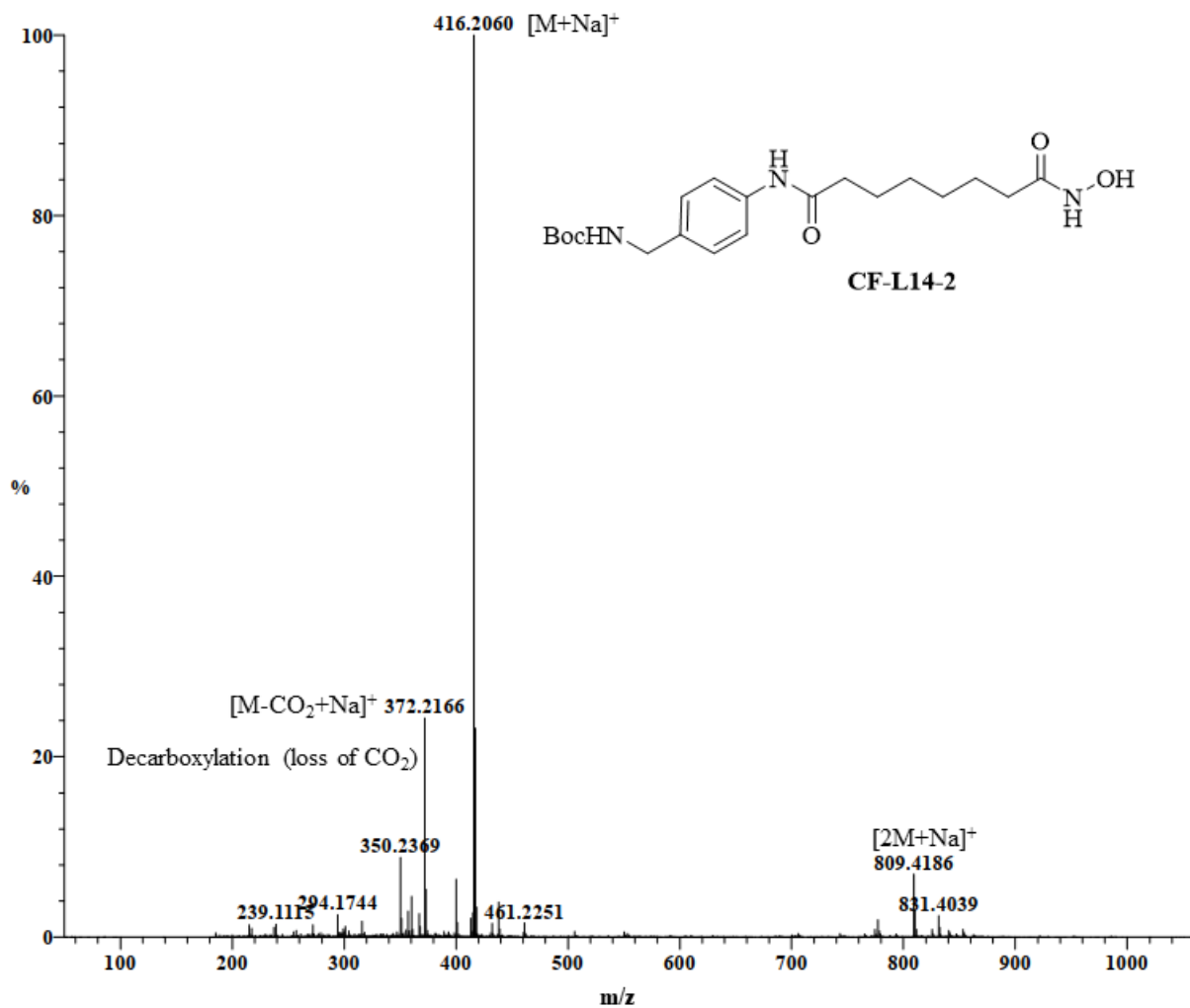
DART-AccuTOF mass spectrum of **CF-L12**

DART-AccuTOF mass spectrum of **CF-L13-1**

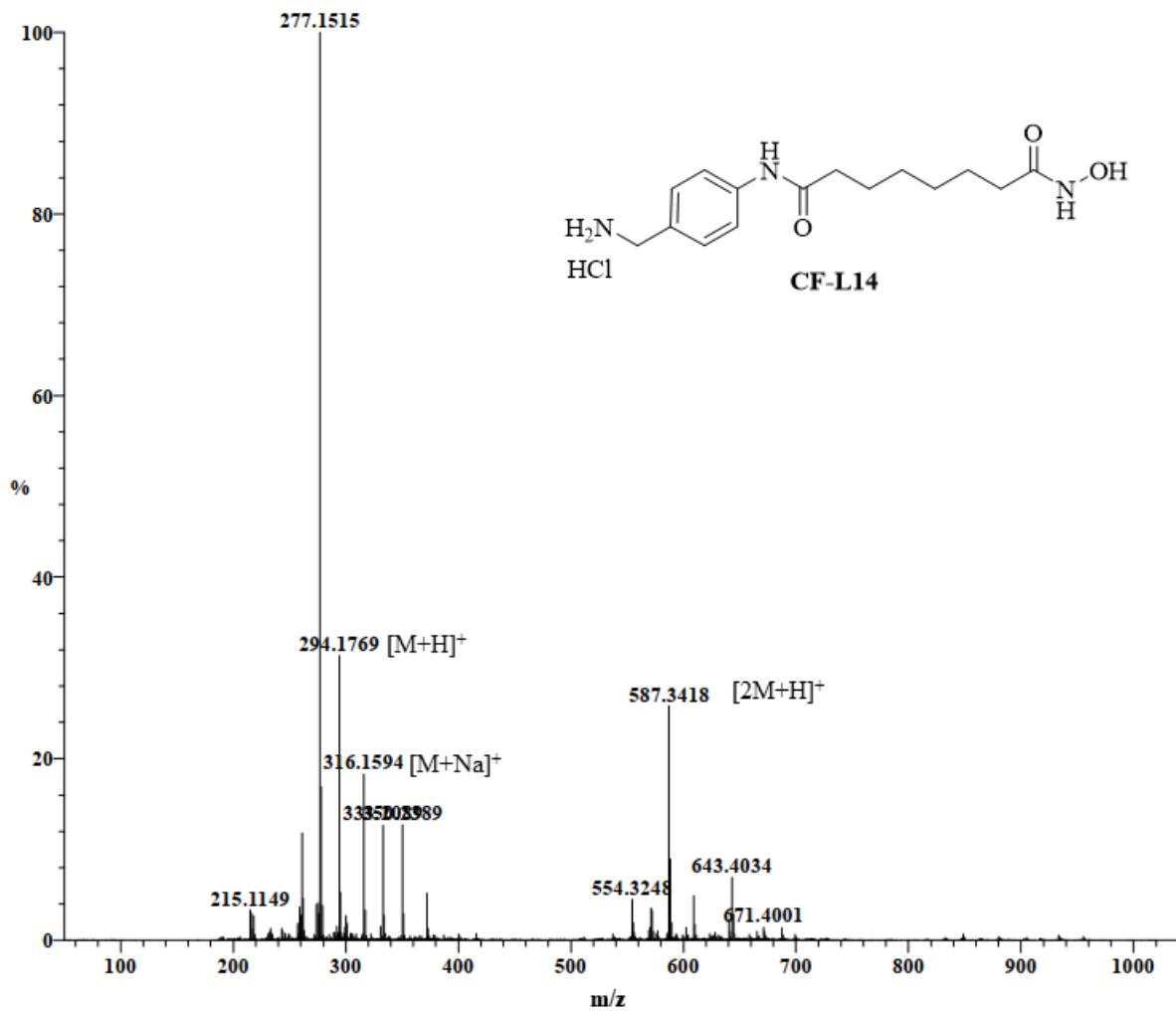
DART-AccuTOF mass spectrum of **CF-L13**

DART-AccuTOF mass spectrum of **CF-L14-1**

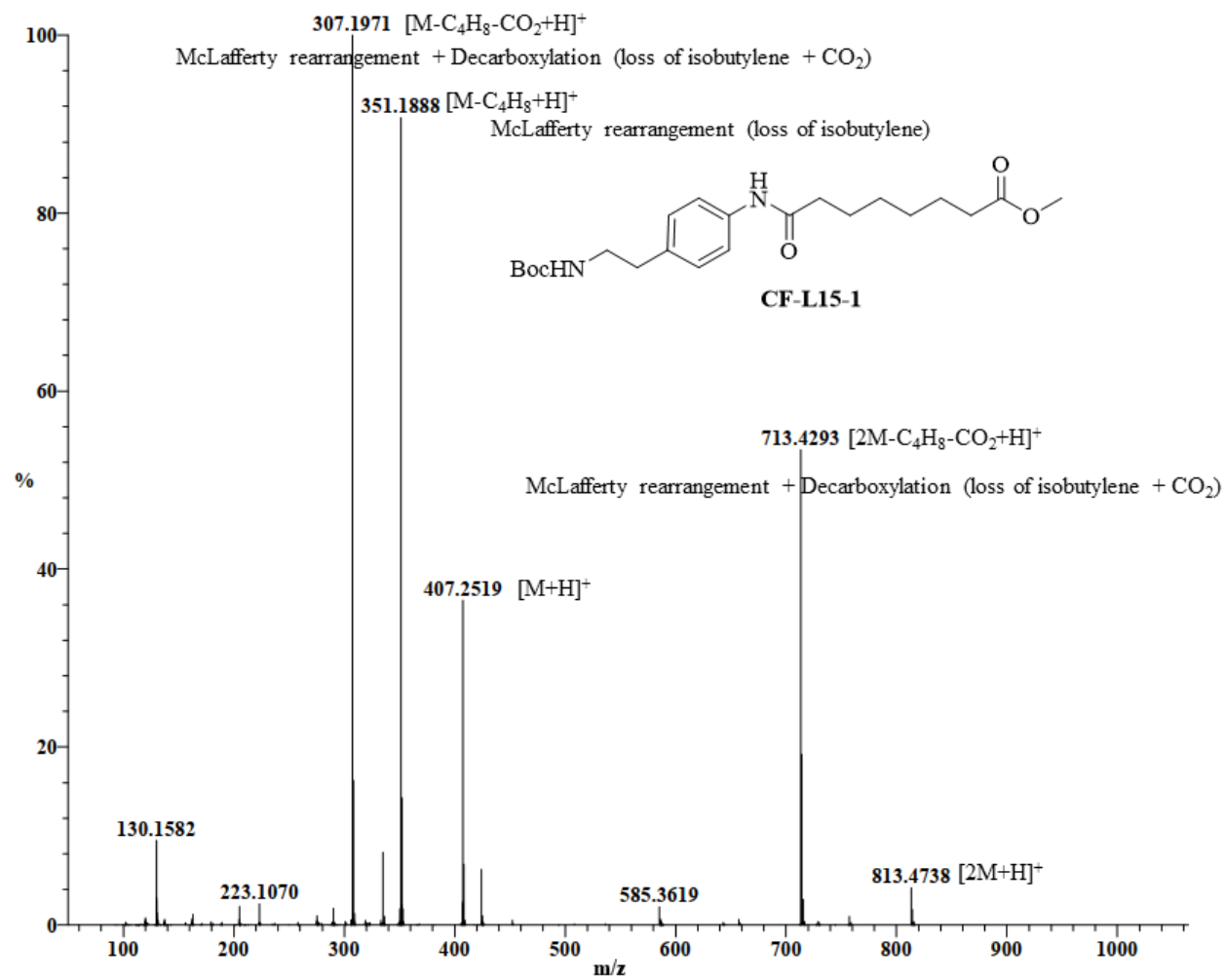
DART-AccuTOF mass spectrum of **CF-L14-2**

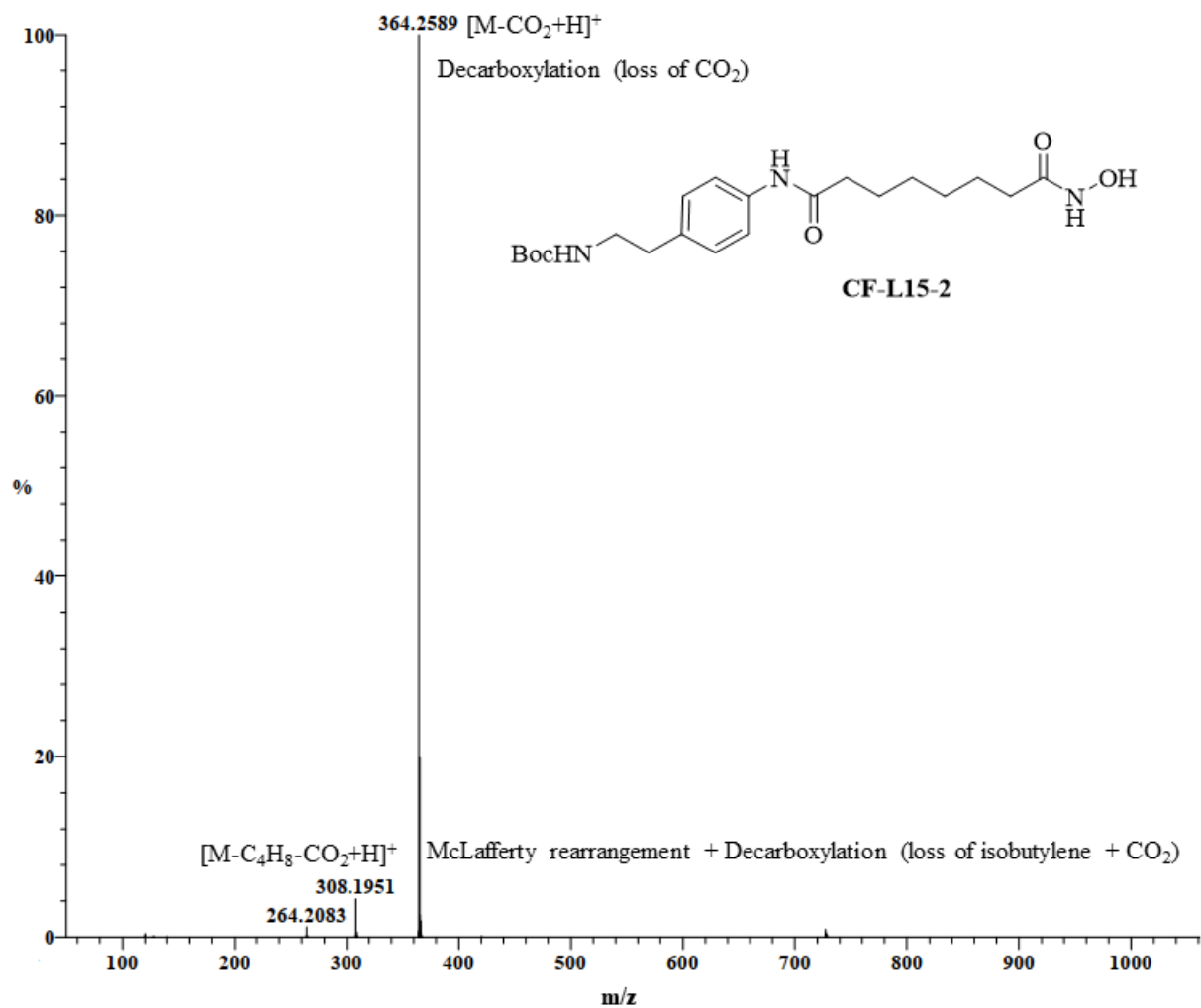


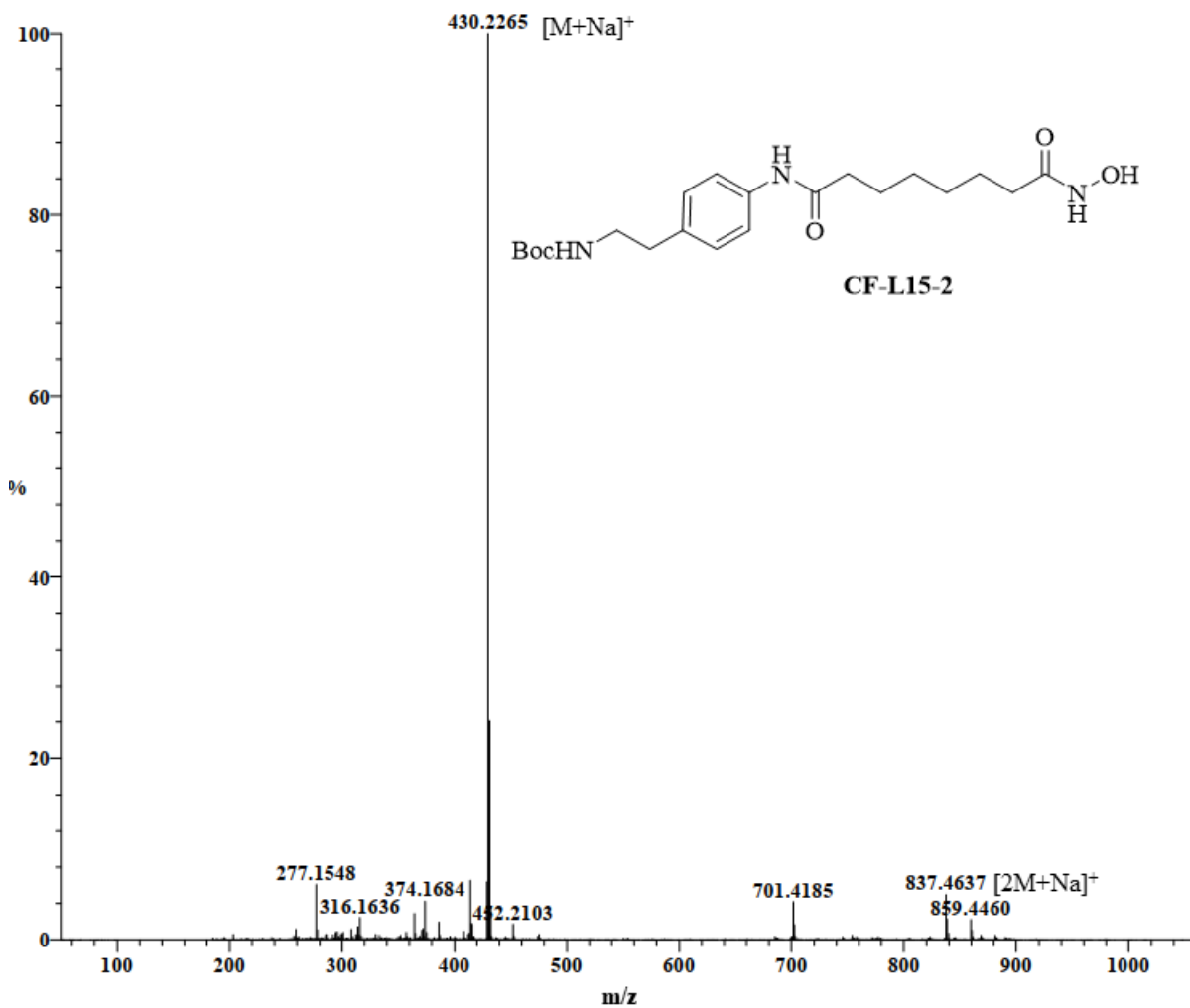
ESI-AccuTOF mass spectrum of CF-L14-2



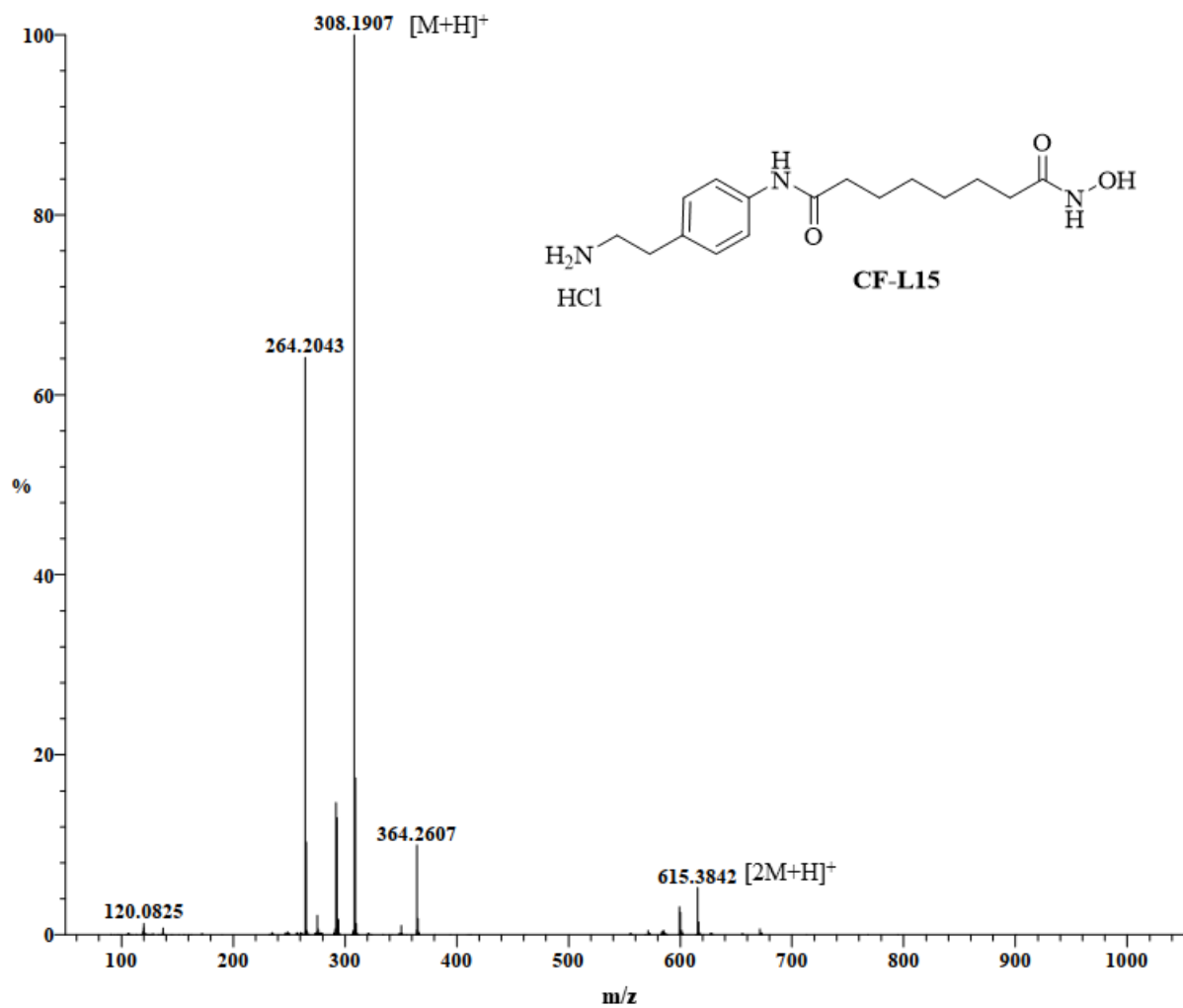
ESI-AccuTOF mass spectrum of CF-L14

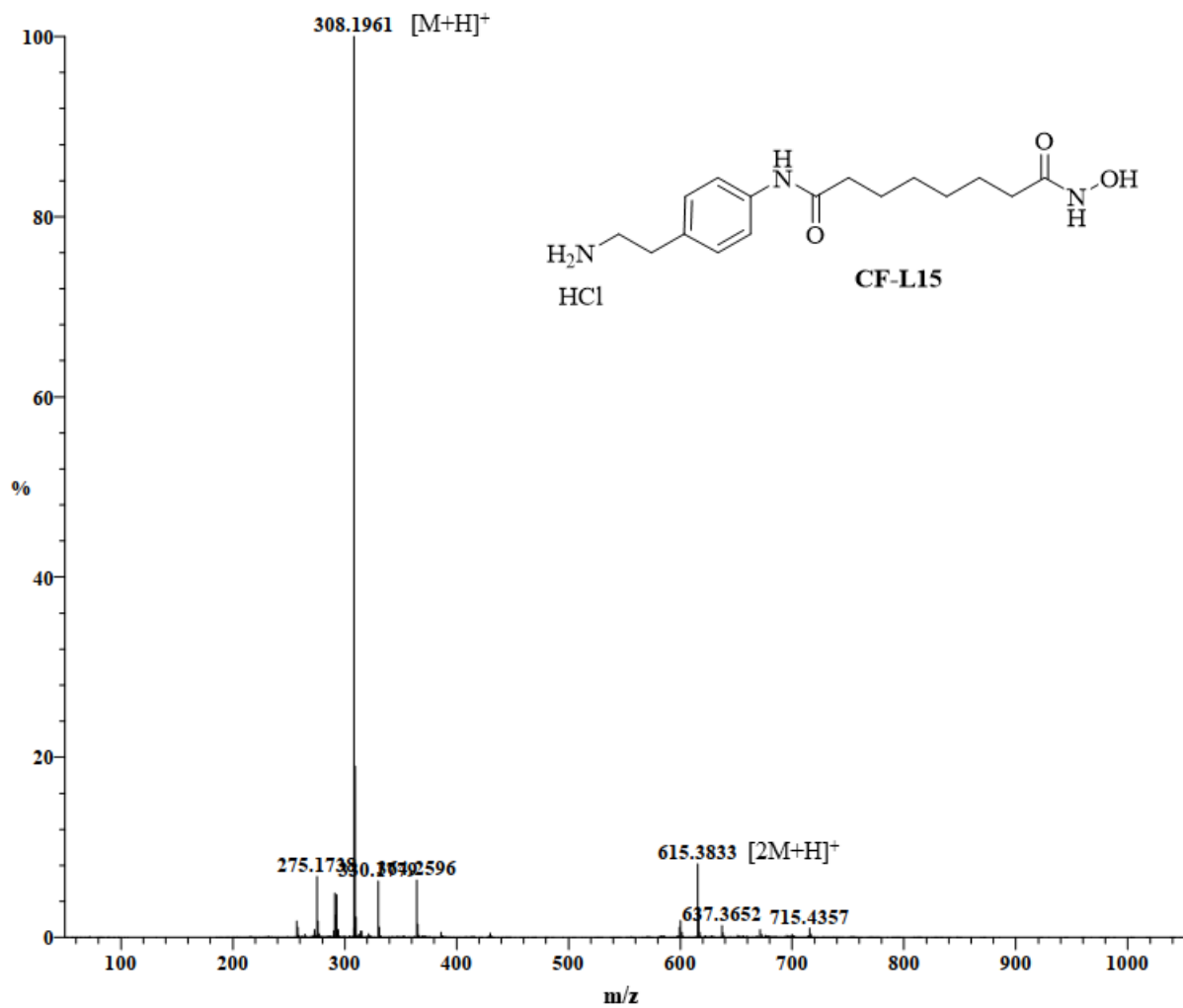
DART-AccuTOF mass spectrum of **CF-L15-1**

DART-AccuTOF mass spectrum of **CF-L15-2**

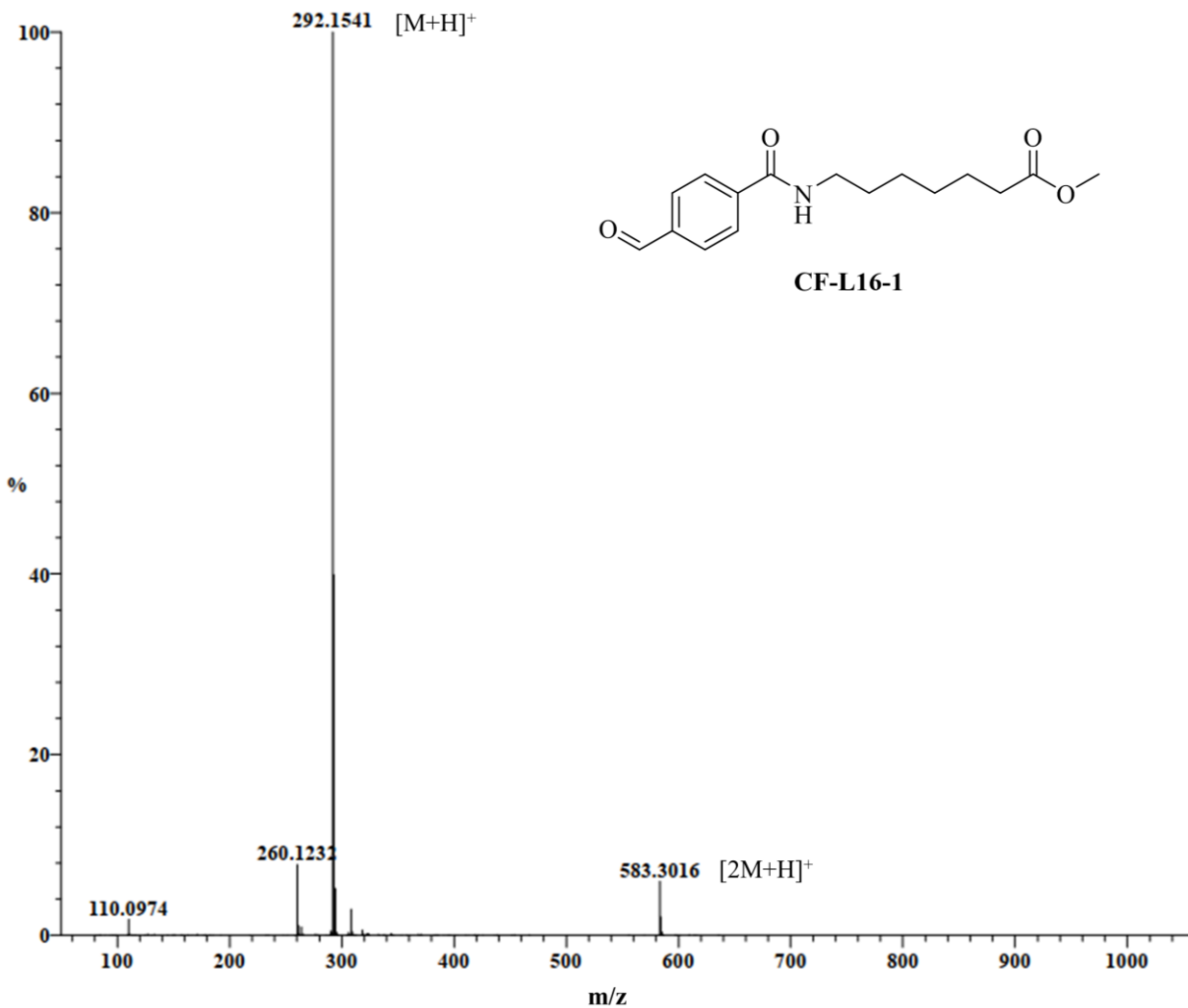


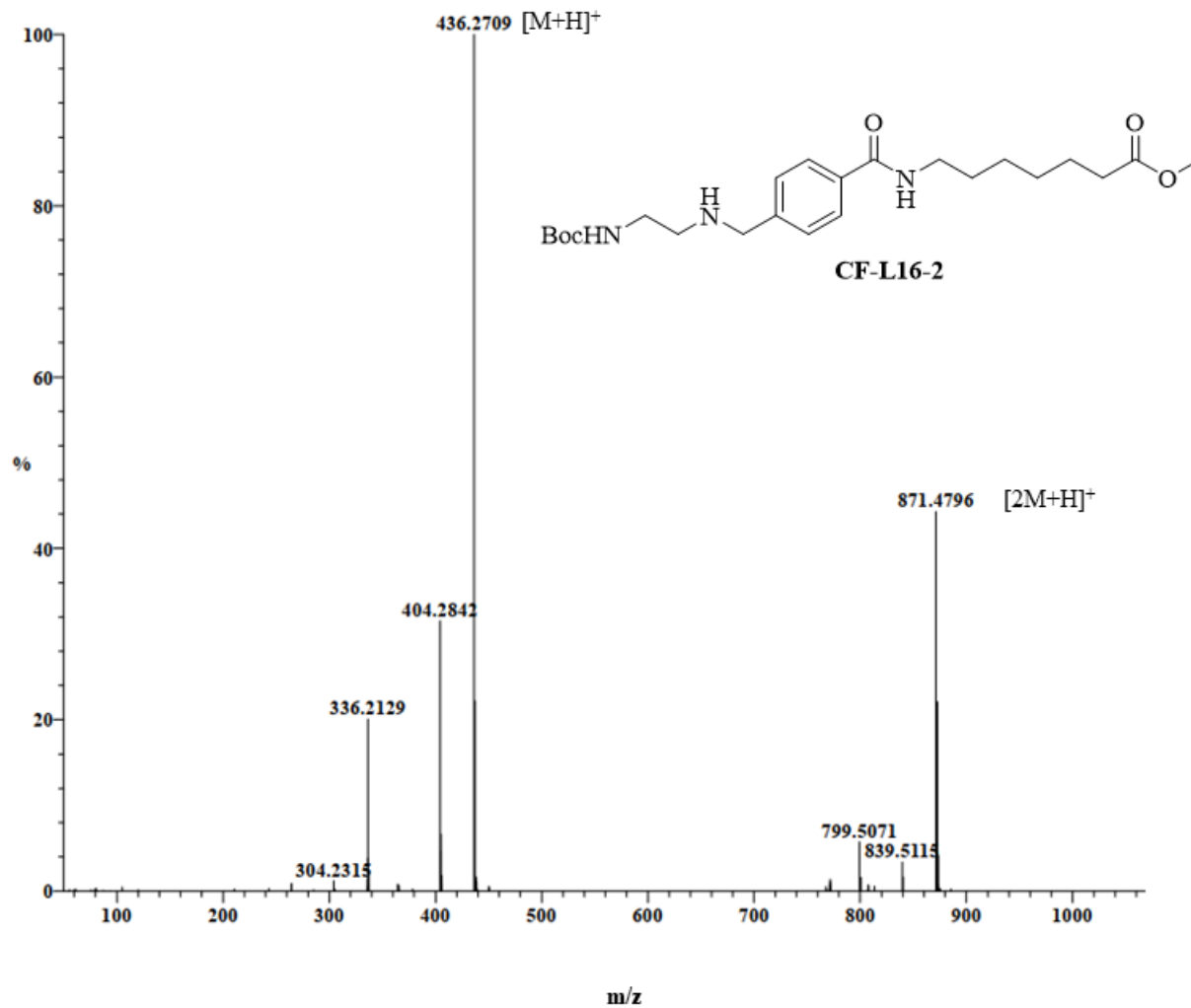
ESI-AccuTOF mass spectrum of CF-L15-2

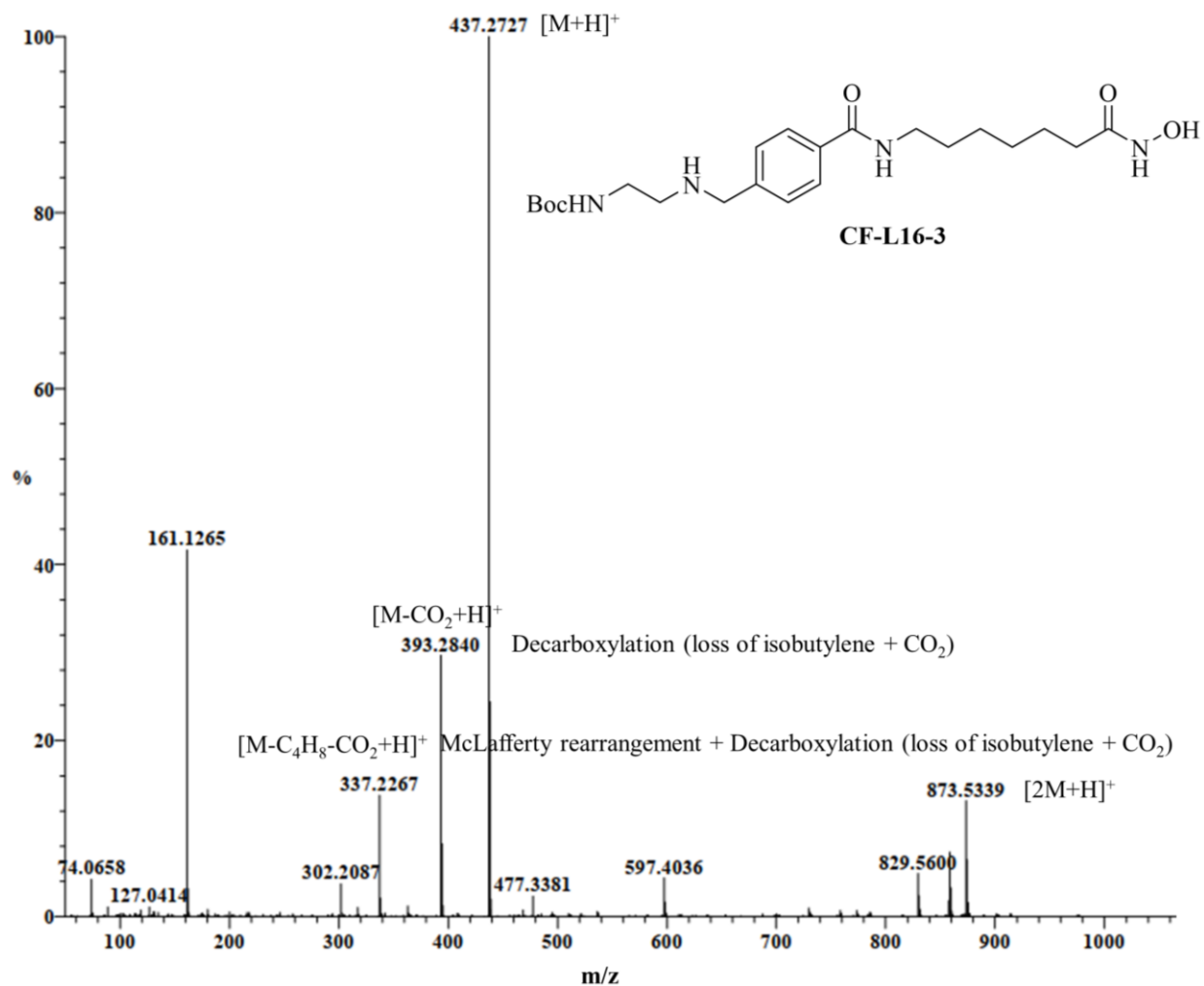
DART-AccuTOF mass spectrum of **CF-L15**

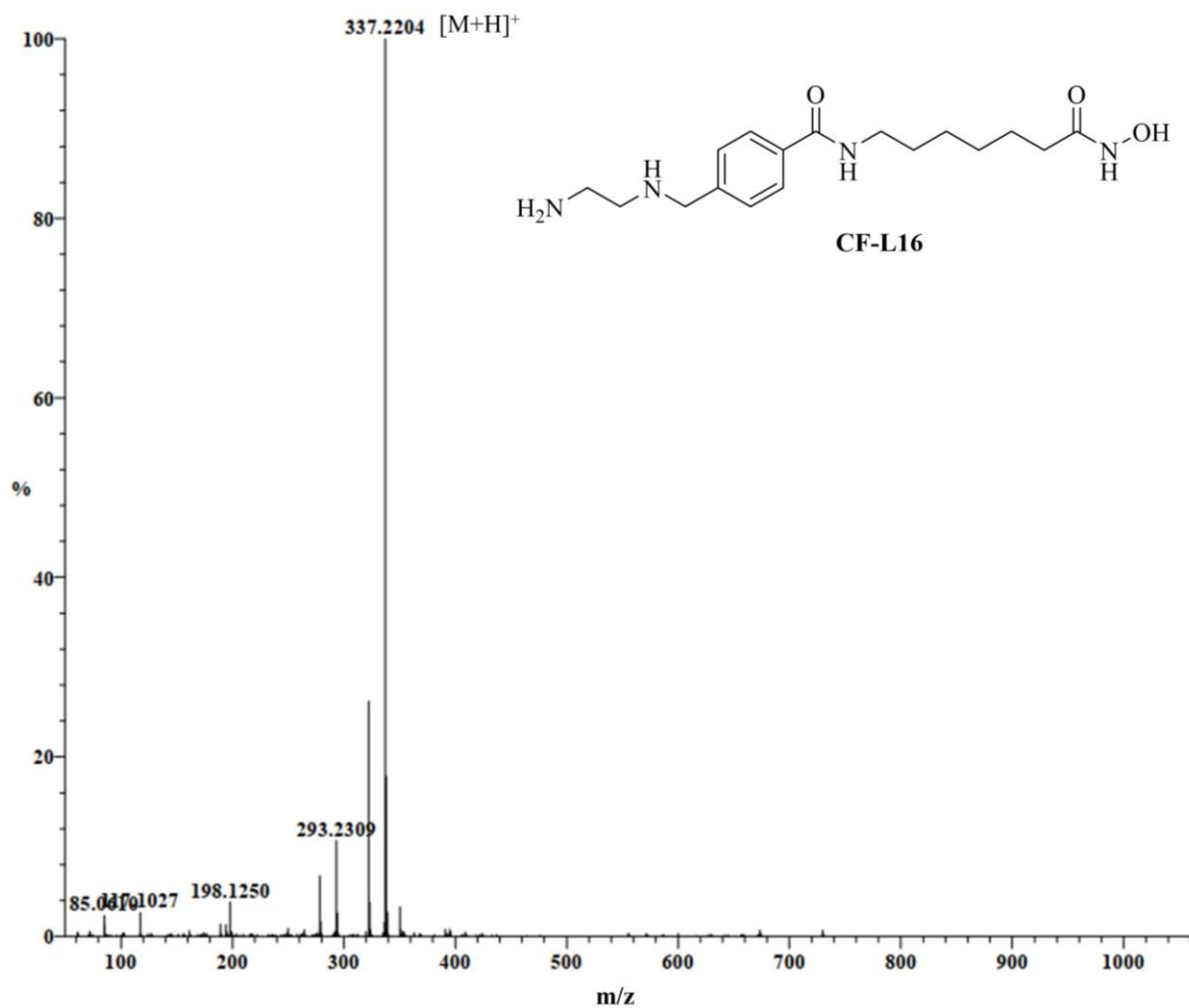


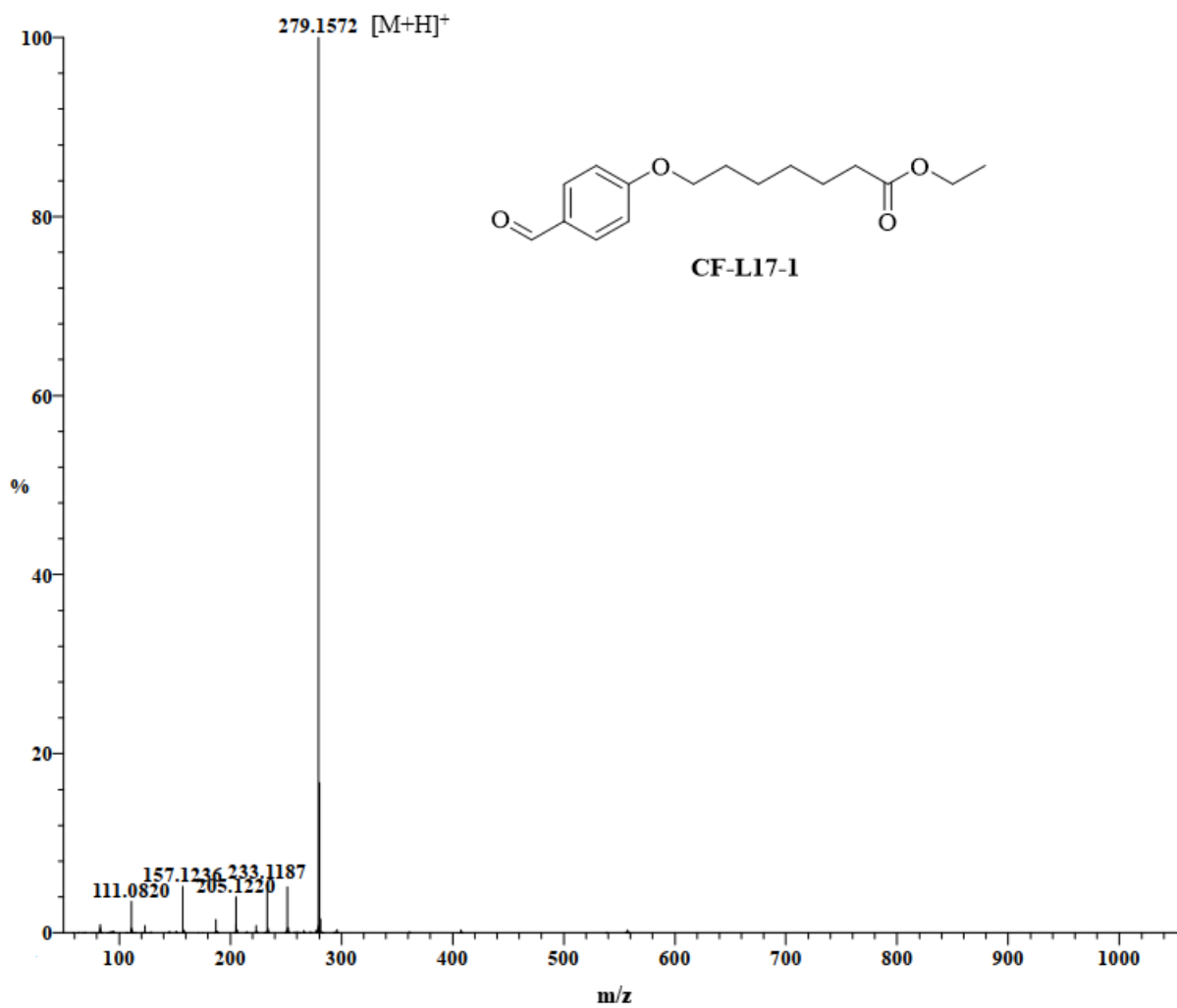
ESI-AccuTOF mass spectrum of CF-L15

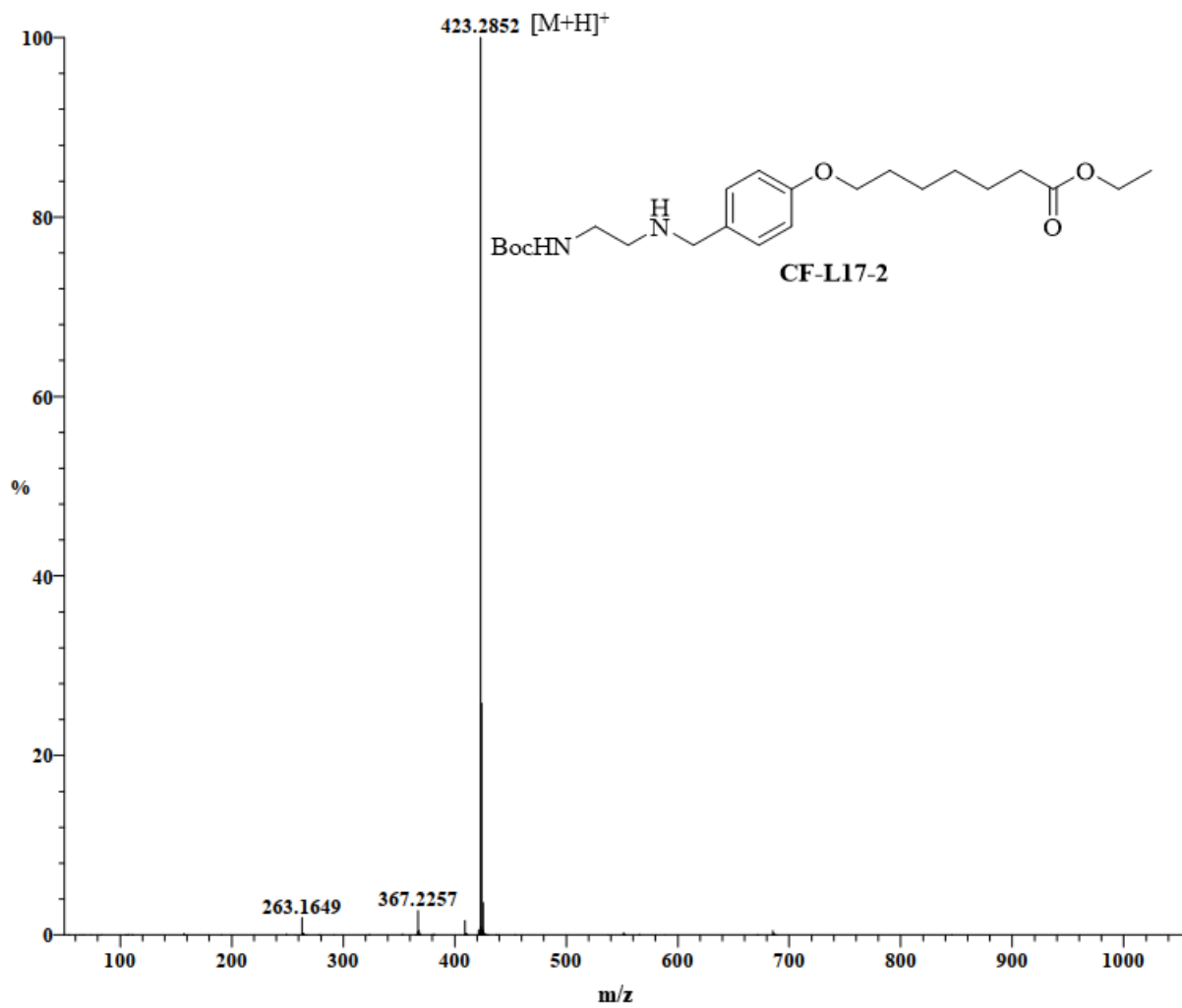
DART-AccuTOF mass spectrum of **CF-L16-1**

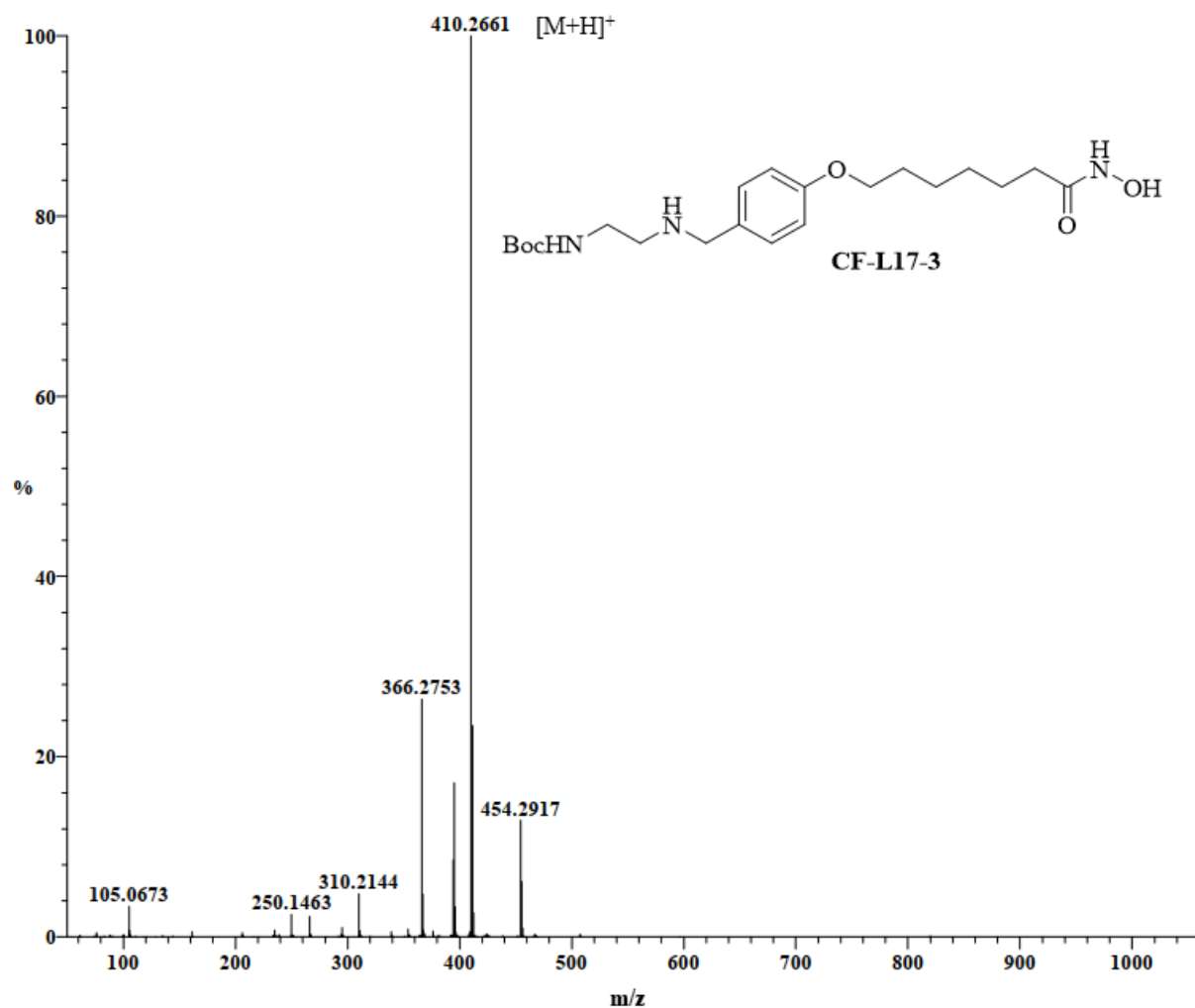
DART-AccuTOF mass spectrum of **CF-L16-2**

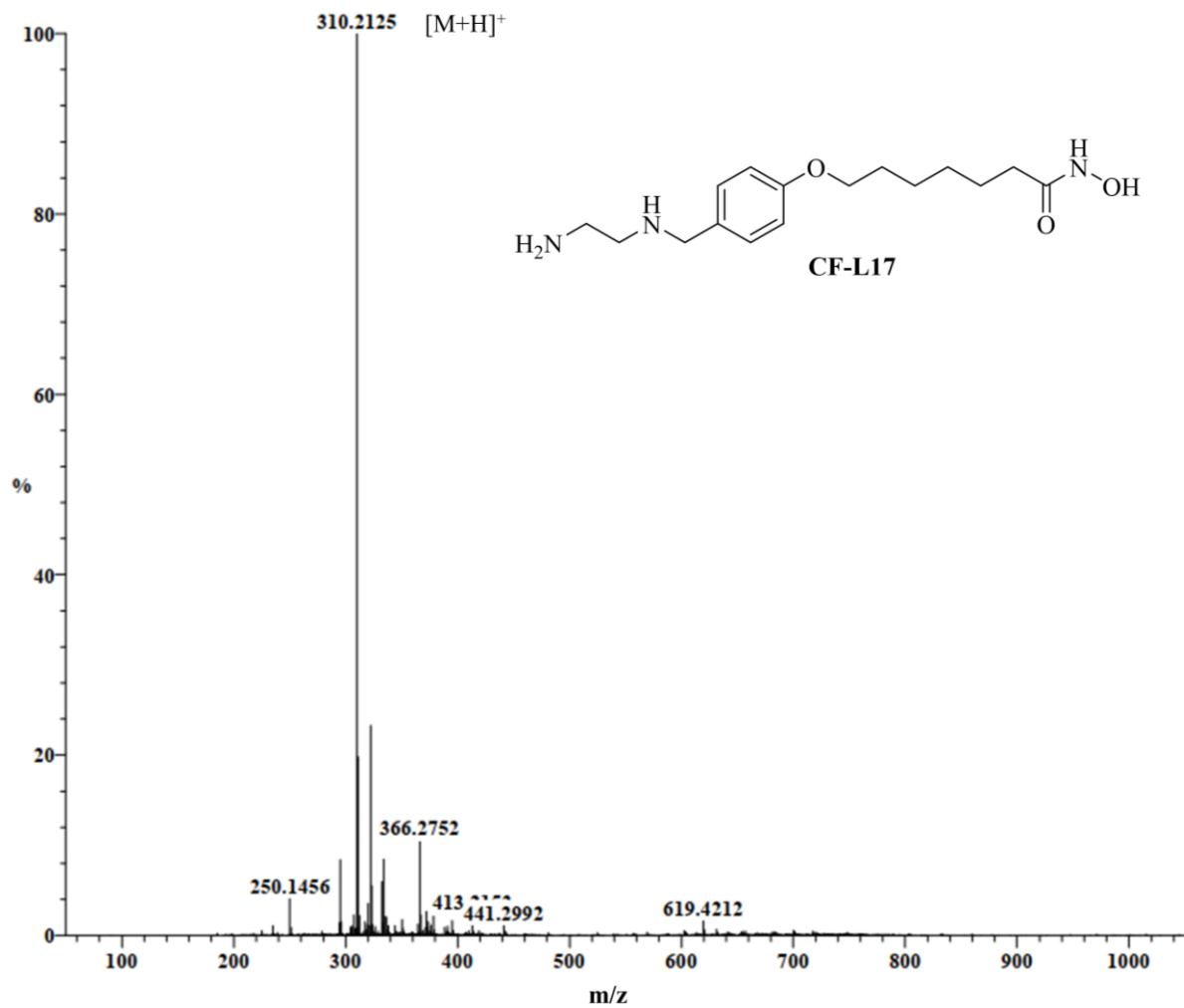
DART-AccuTOF mass spectrum of **CF-L16-3**

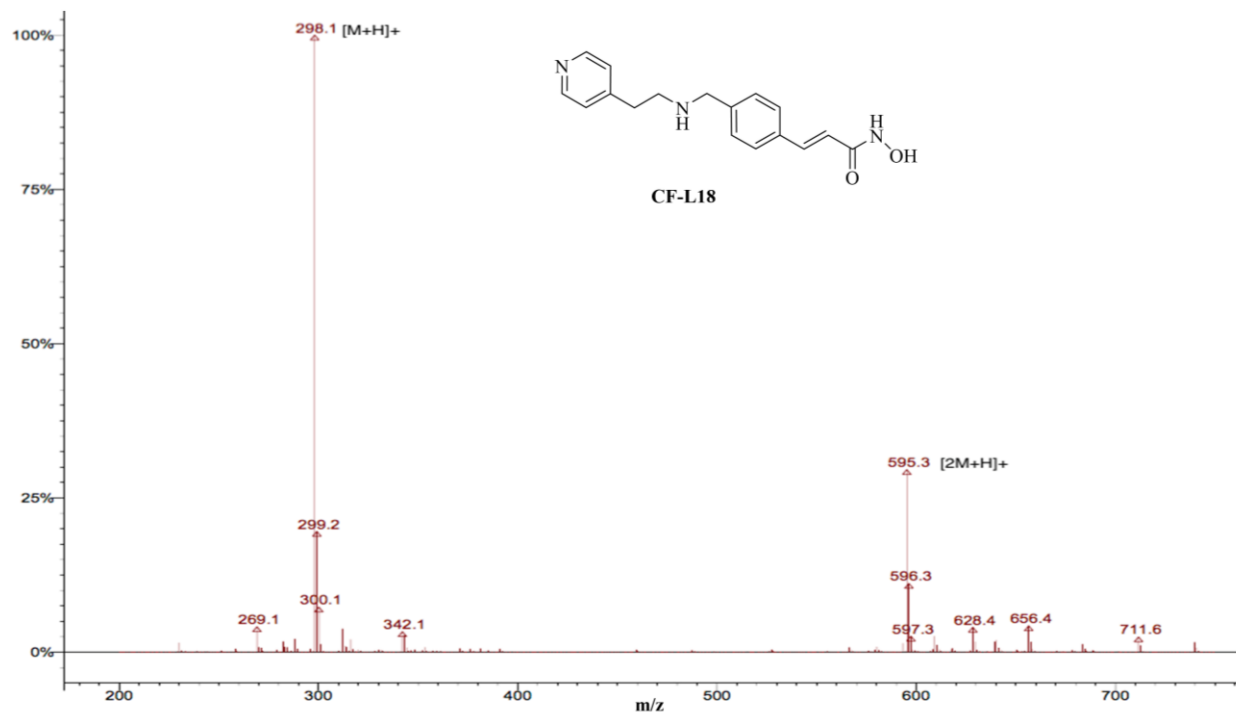
DART-AccuTOF mass spectrum of **CF-L16**

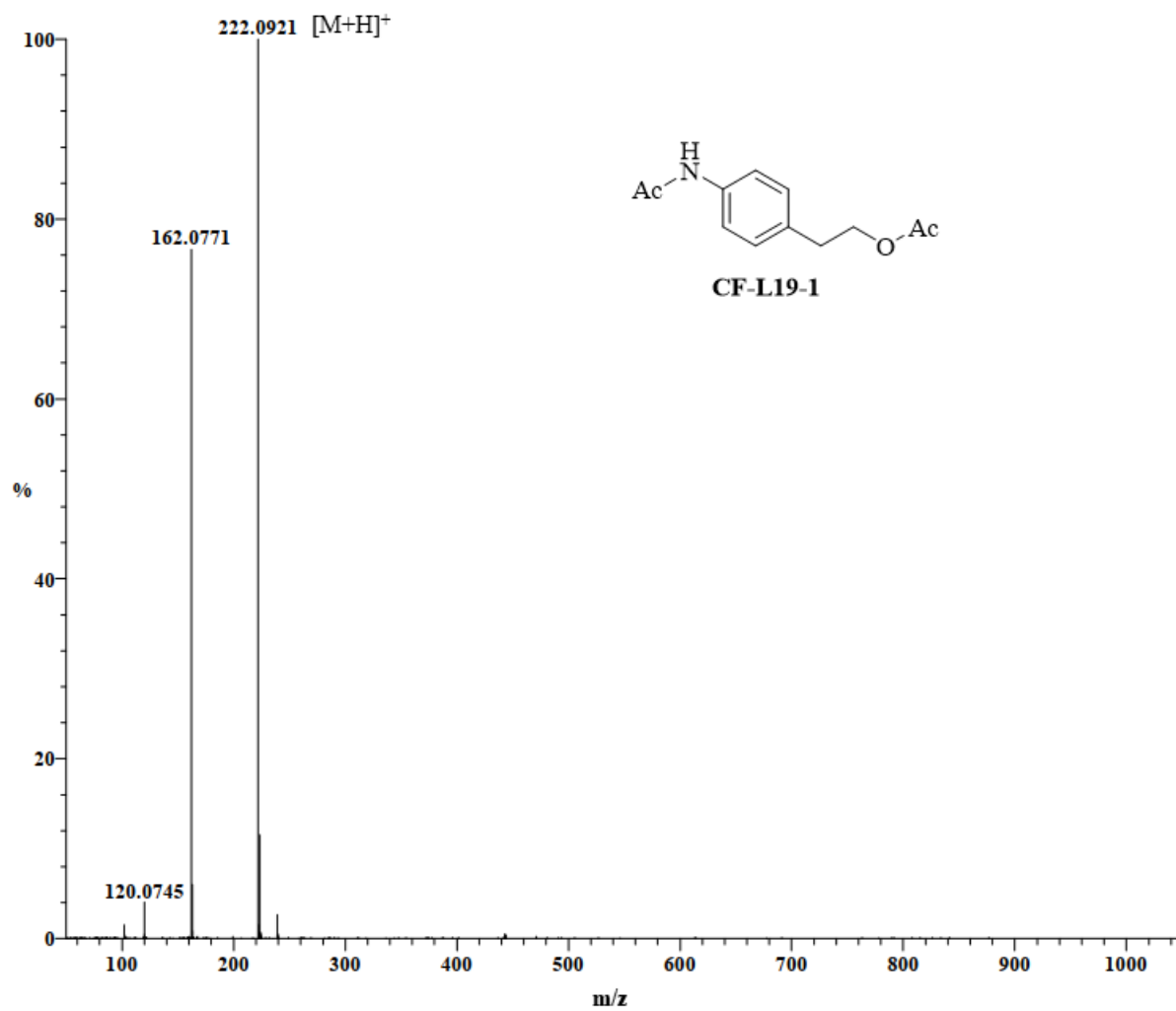
DART-AccuTOF mass spectrum of **CF-L17-1**

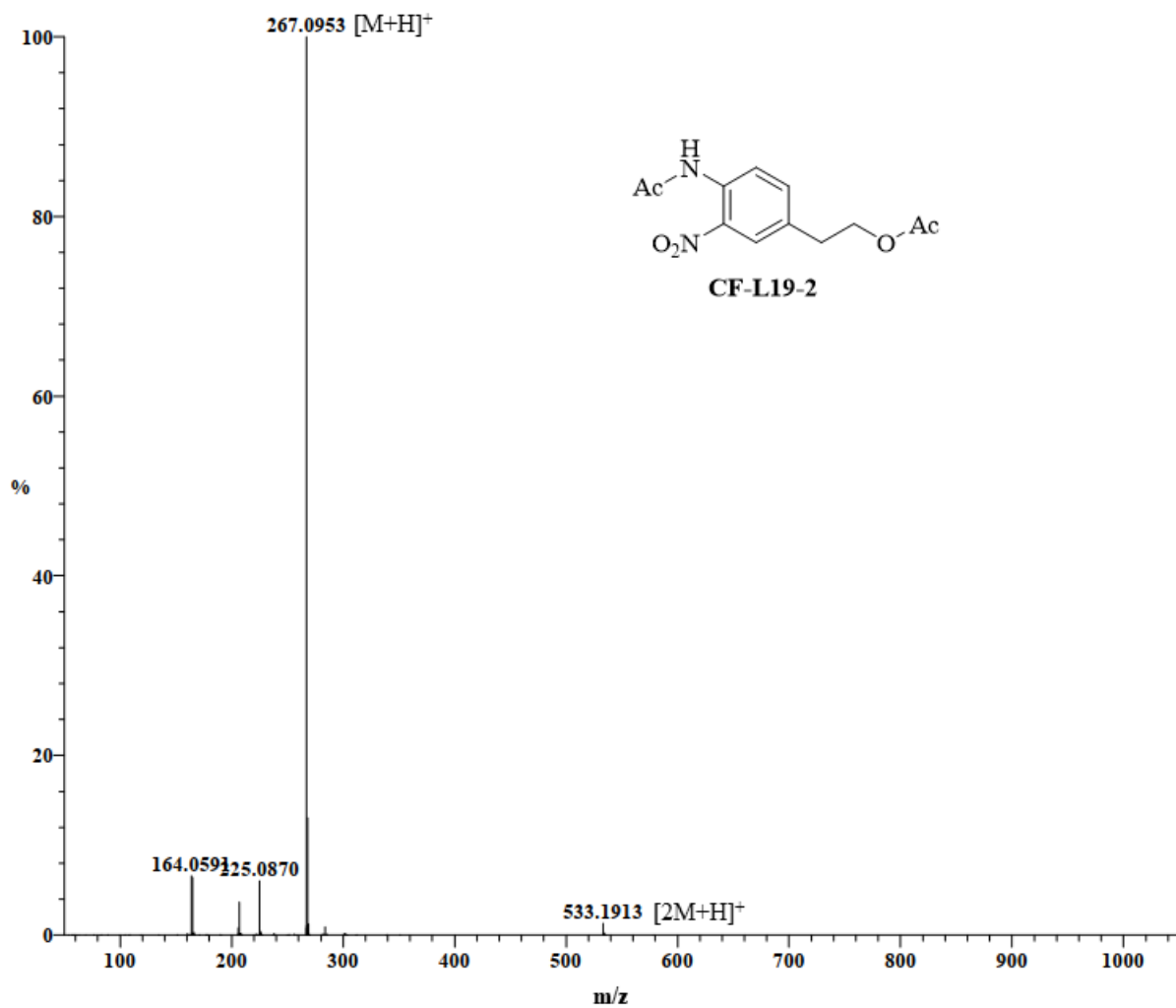
DART-AccuTOF mass spectrum of **CF-L17-2**

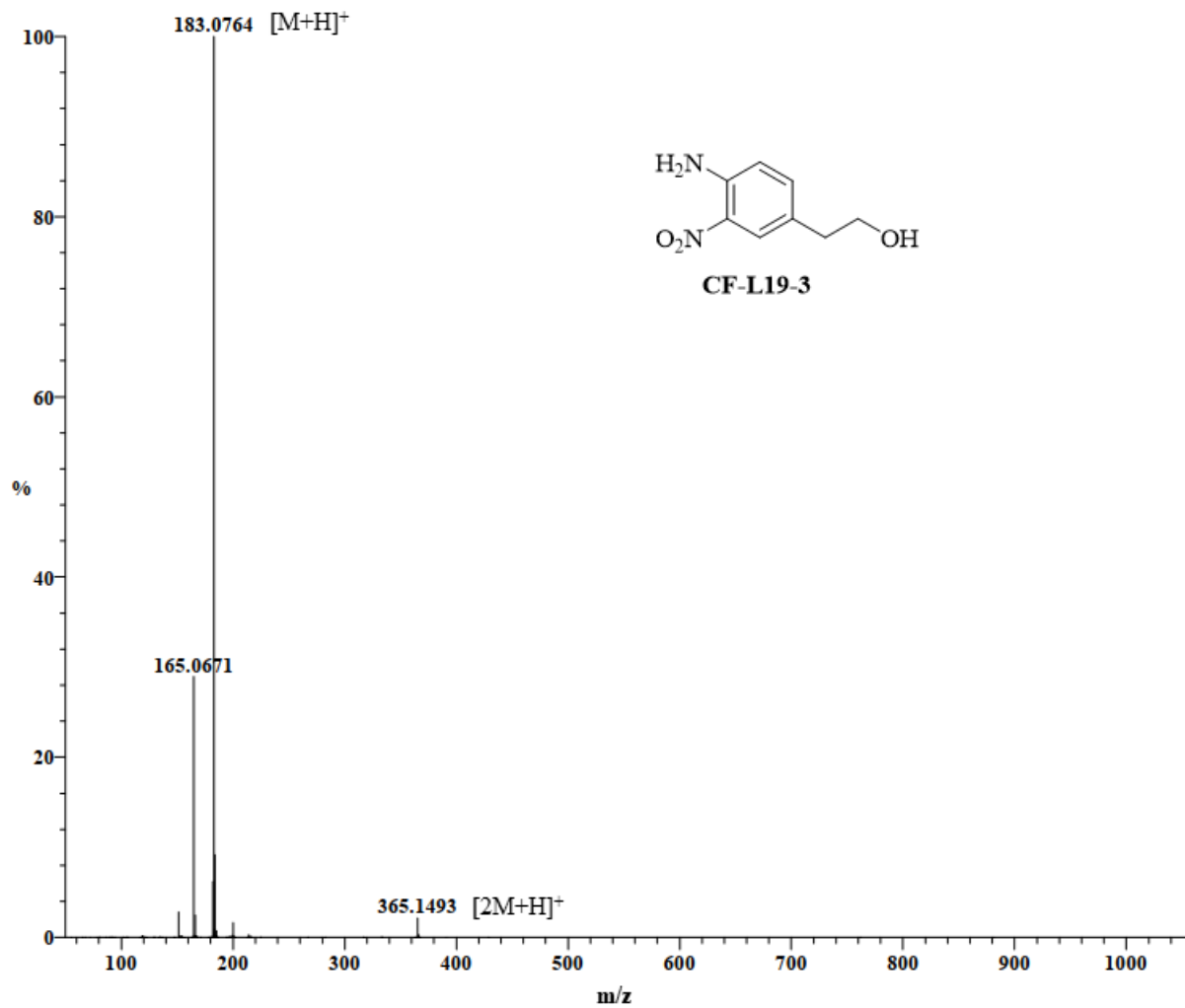
DART-AccuTOF mass spectrum of **CF-L17-3**

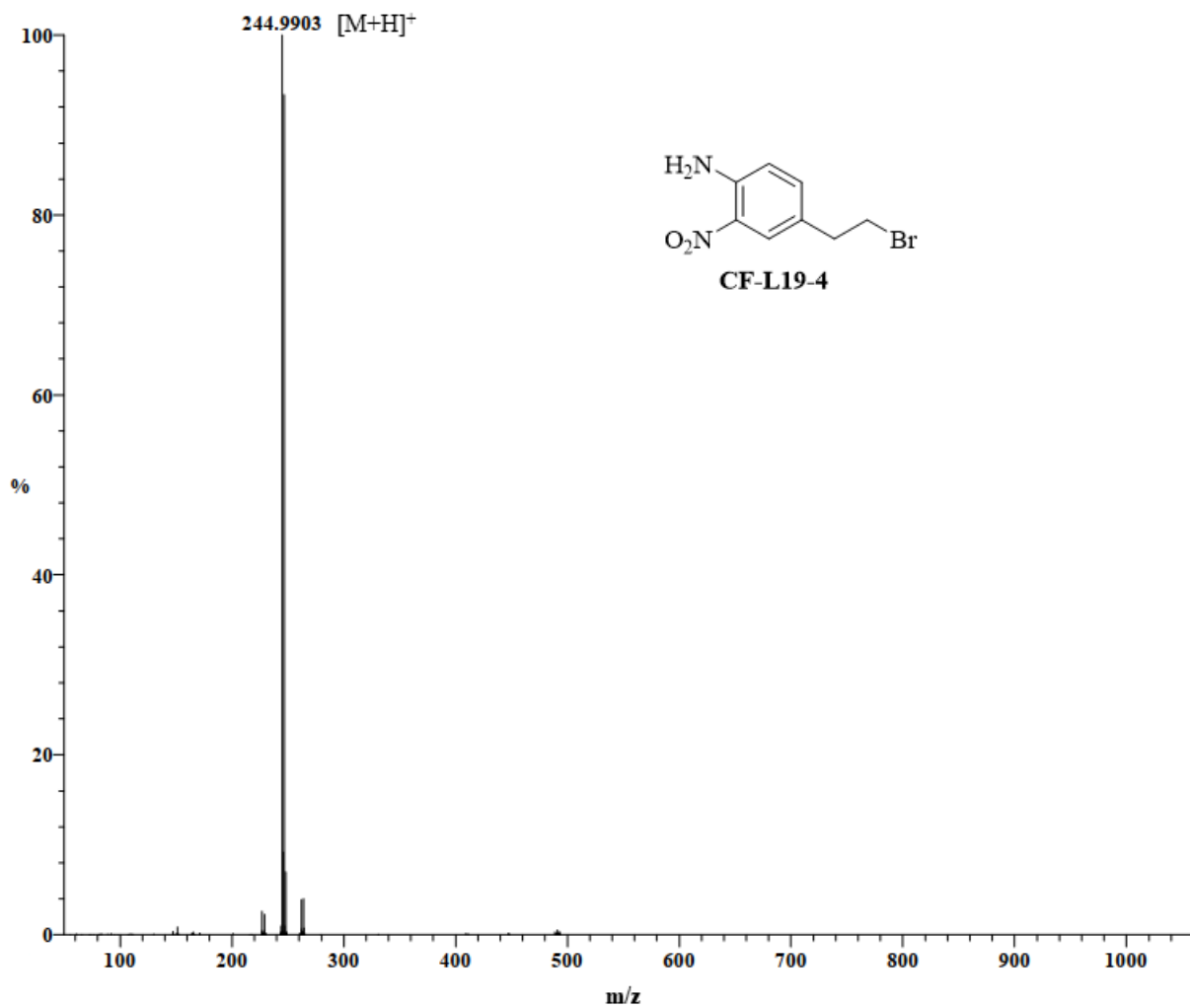
ESI-AccuTOF mass spectrum of **CF-L17**

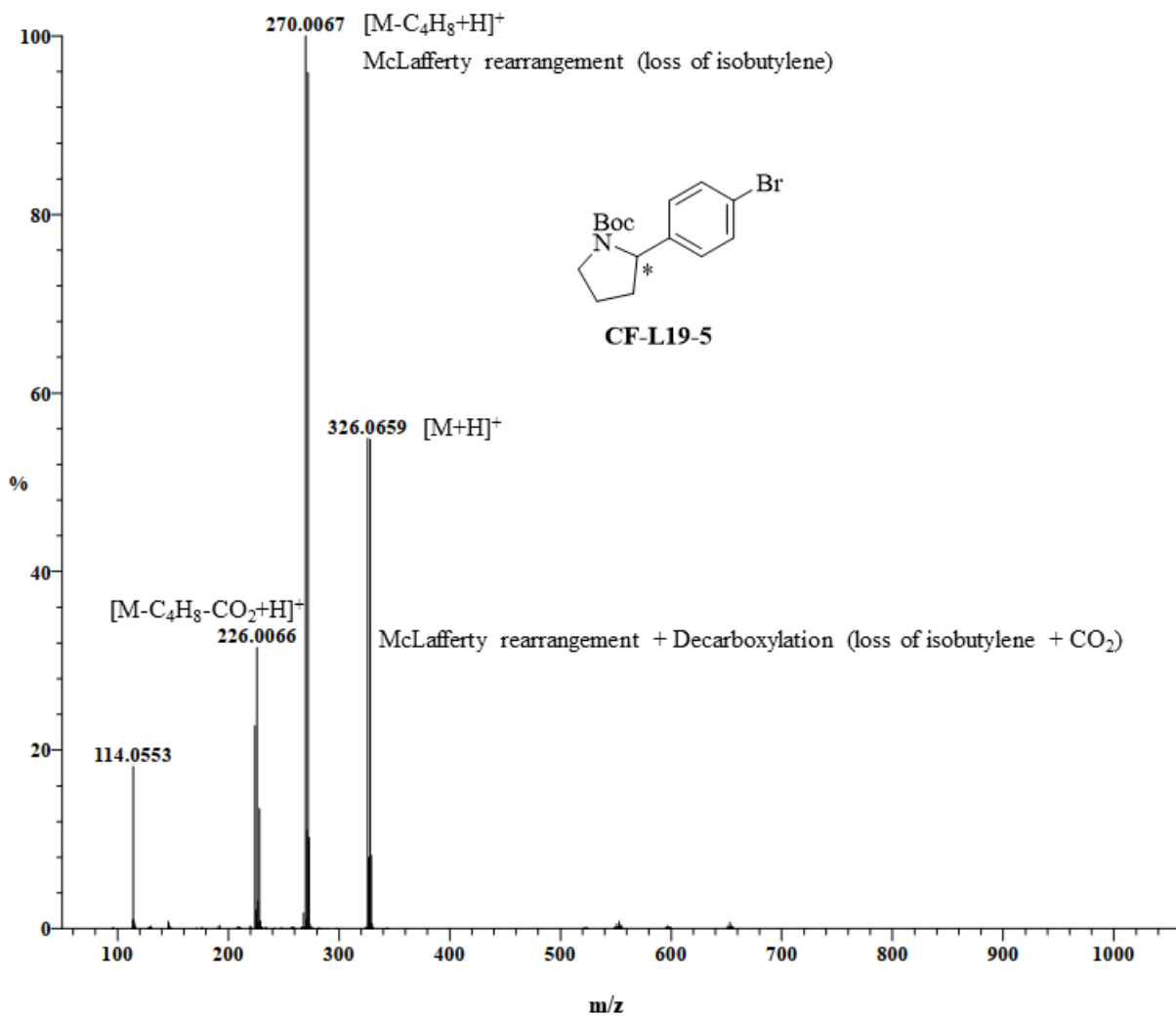
Varian 320 ESI mass spectrum of **CF-L18**

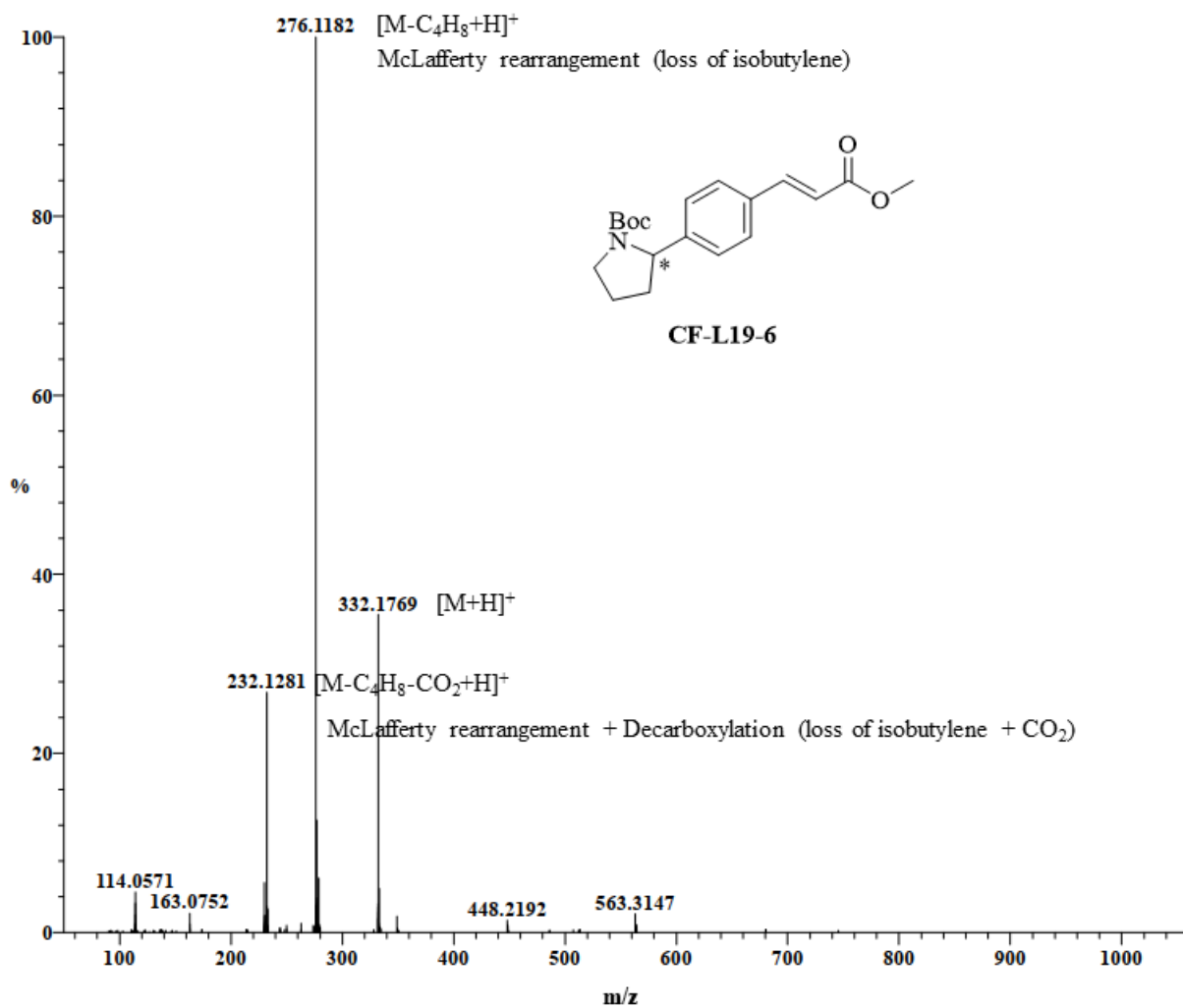
DART-AccuTOF mass spectrum of **CF-L19-1**

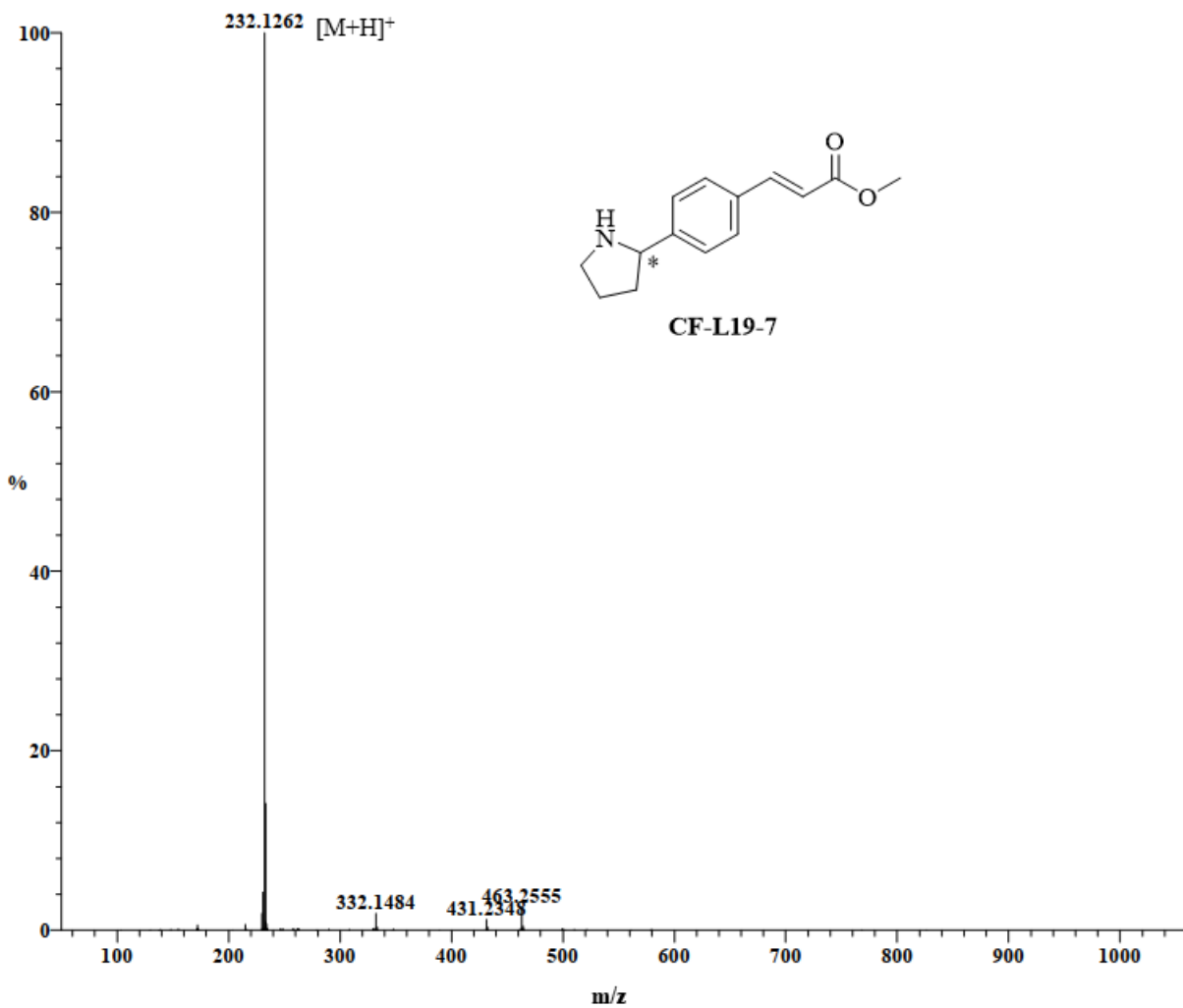
DART-AccuTOF mass spectrum of **CF-L19-2**

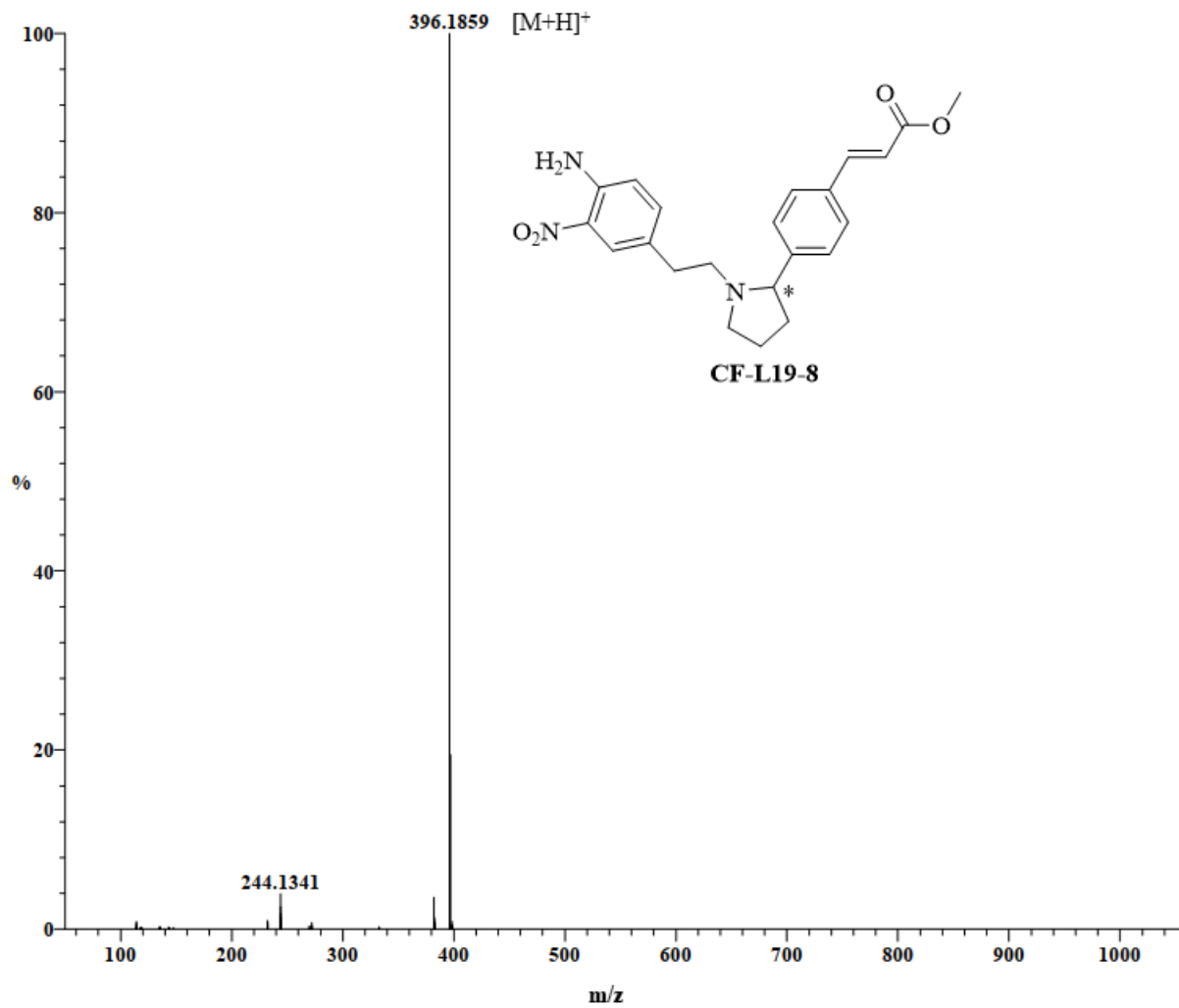
DART-AccuTOF mass spectrum of **CF-L19-3**

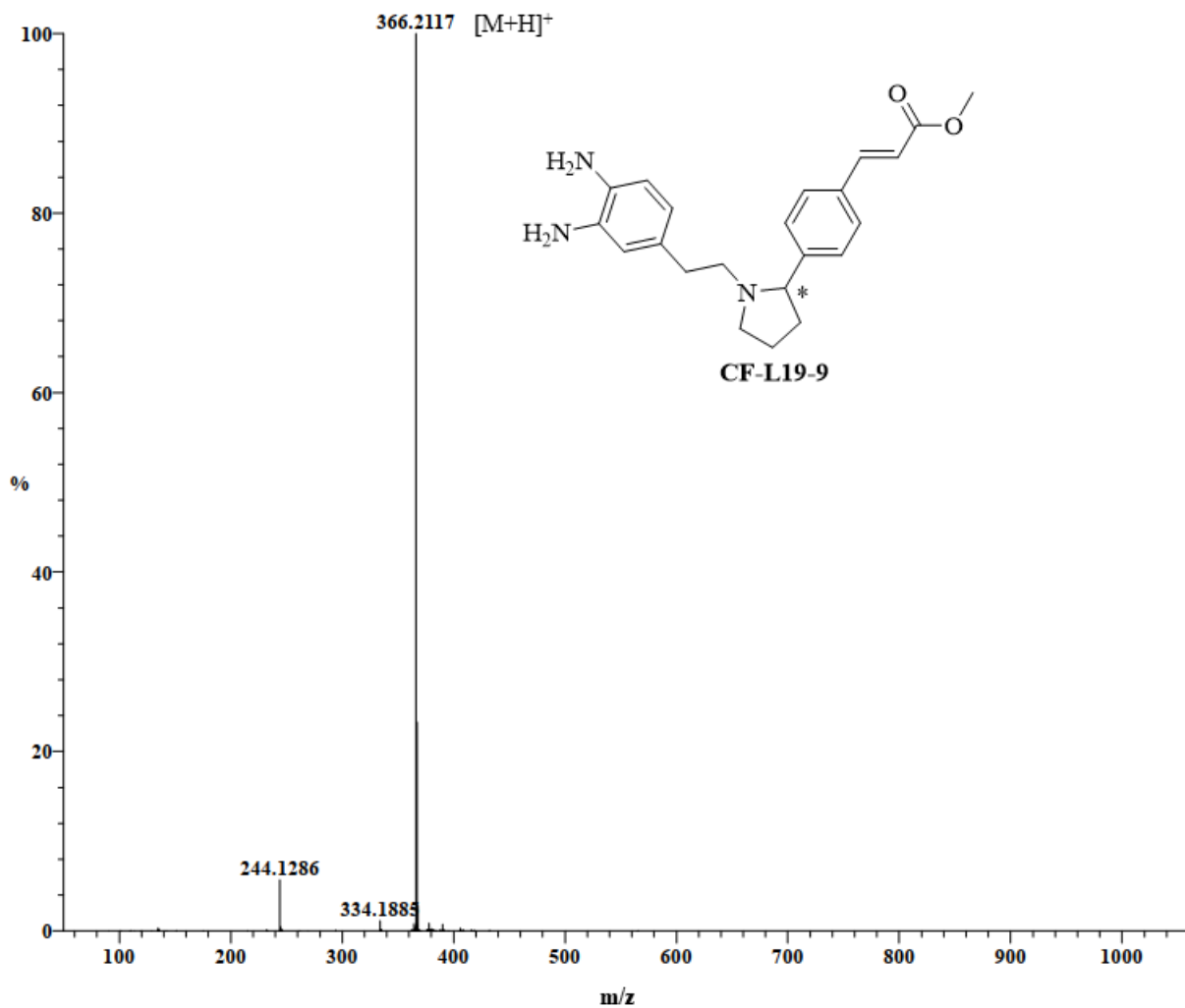
DART-AccuTOF mass spectrum of **CF-L19-4**

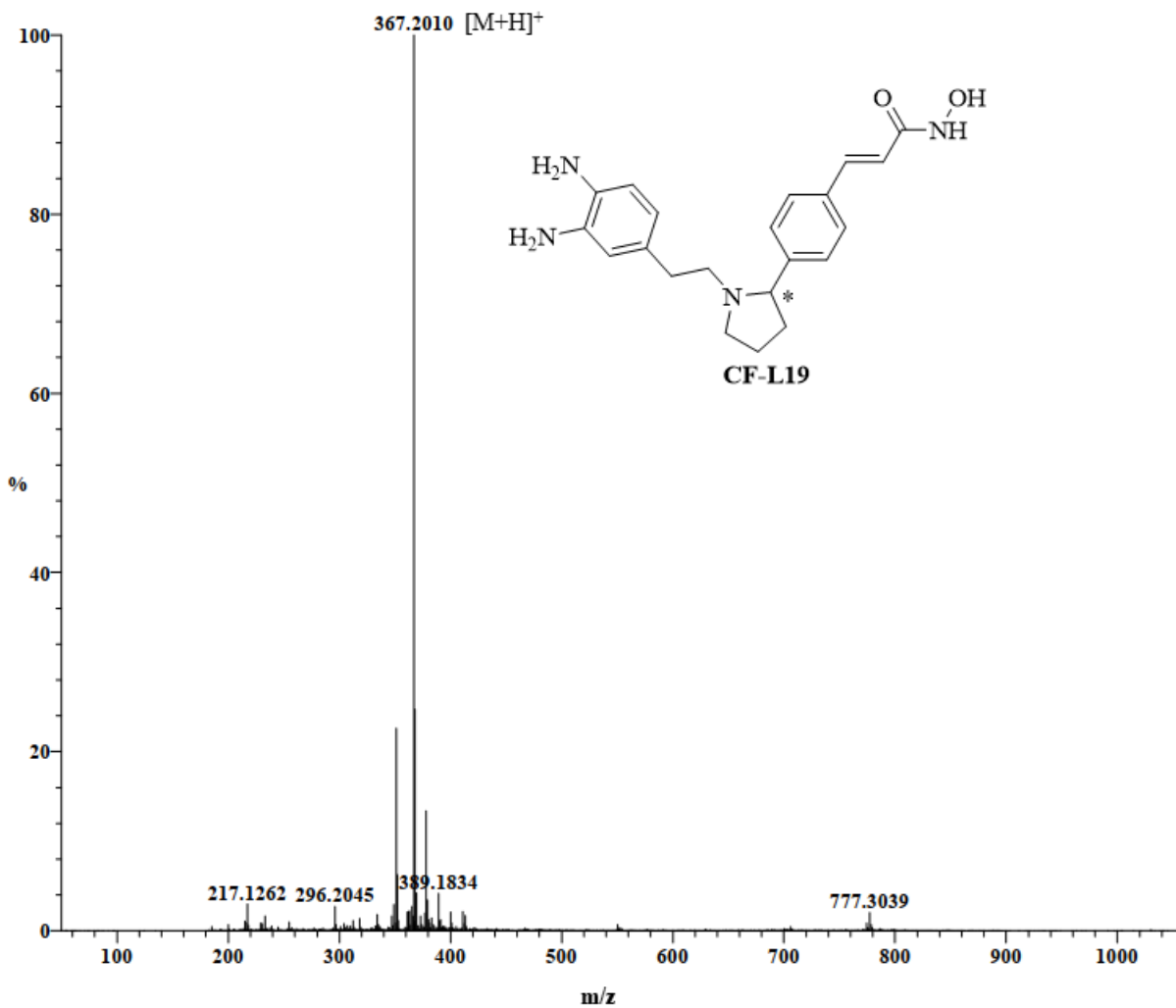
DART-AccuTOF mass spectrum of **CF-L19-5**

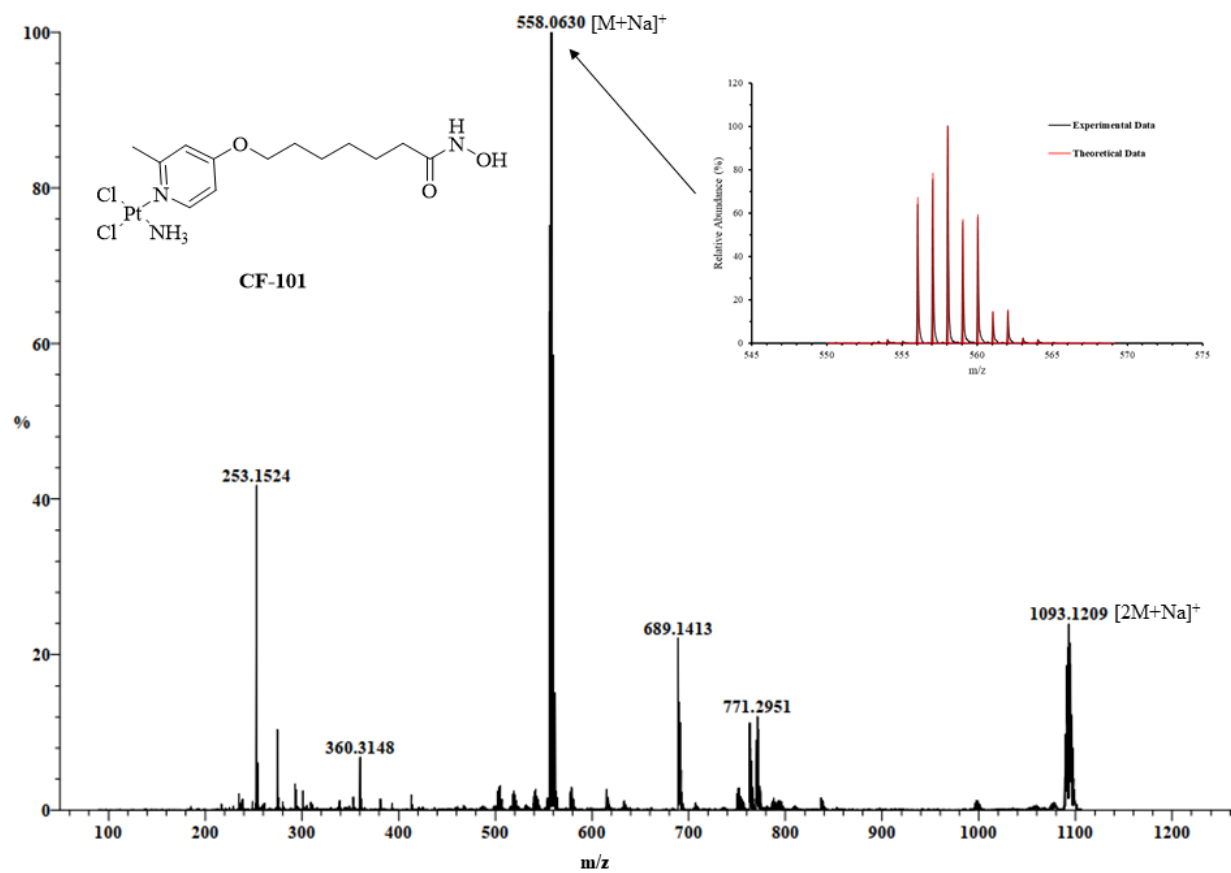
DART-AccuTOF mass spectrum of **CF-L19-6**

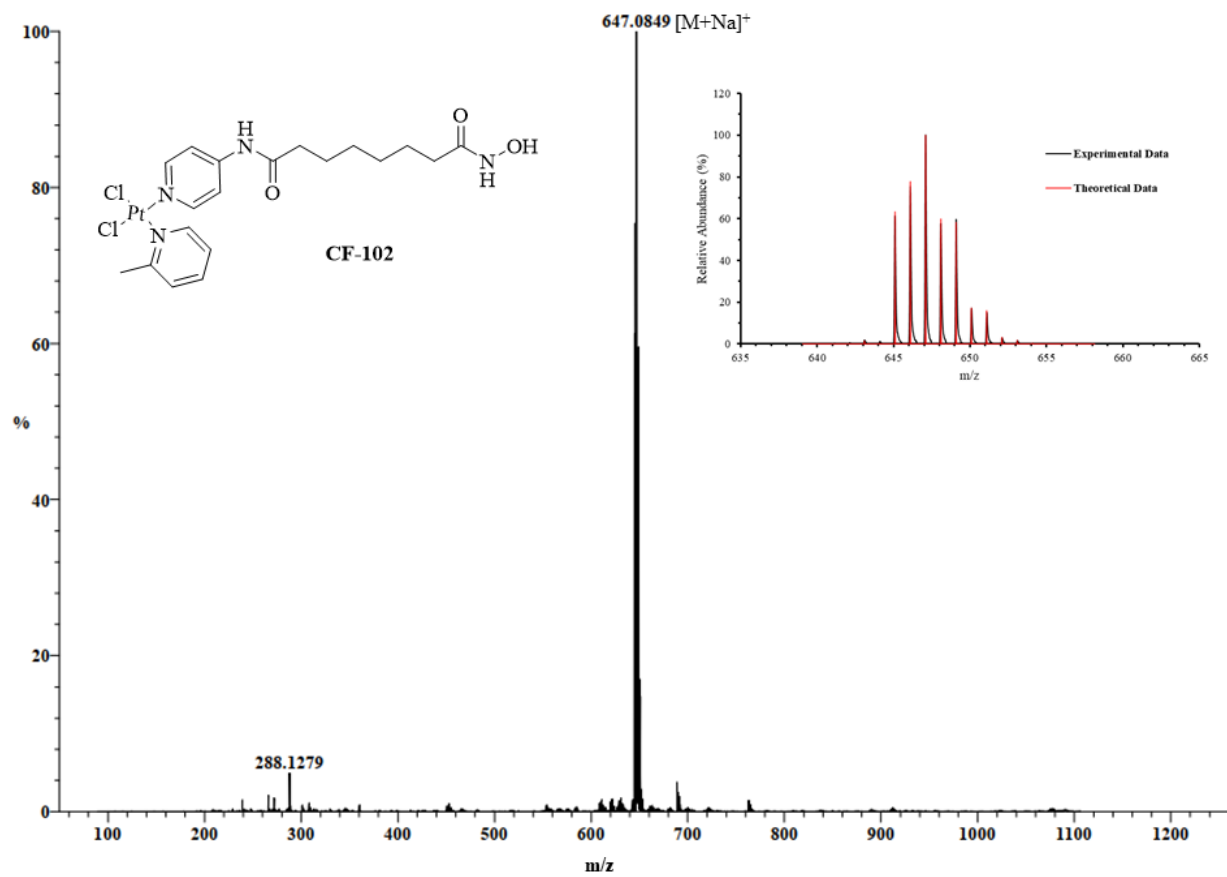
DART-AccuTOF mass spectrum of **CF-L19-7**

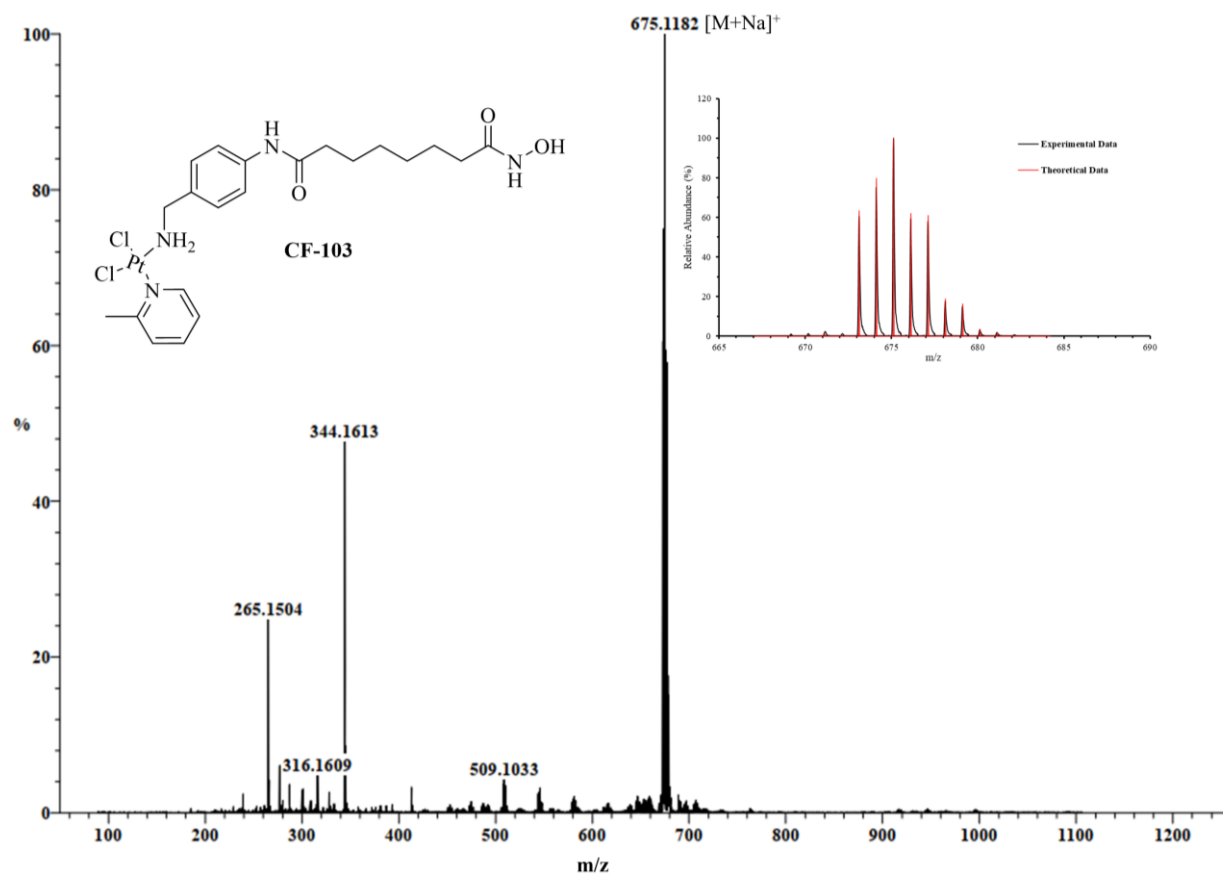
DART-AccuTOF mass spectrum of **CF-L19-8**

DART-AccuTOF mass spectrum of **CF-L19-9**

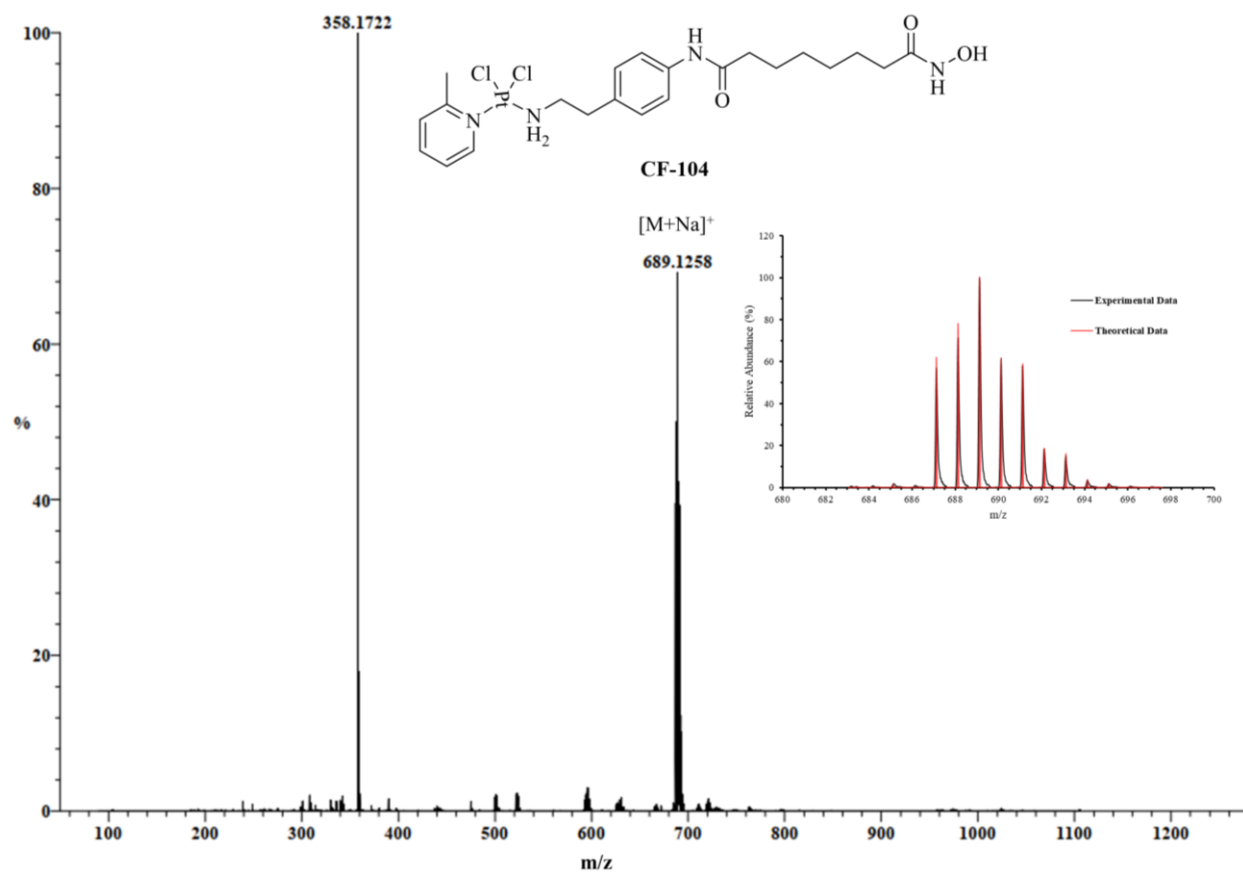
ESI-AccuTOF mass spectrum of **CF-L19**

ESI-AccuTOF mass spectrum of **CF-101**

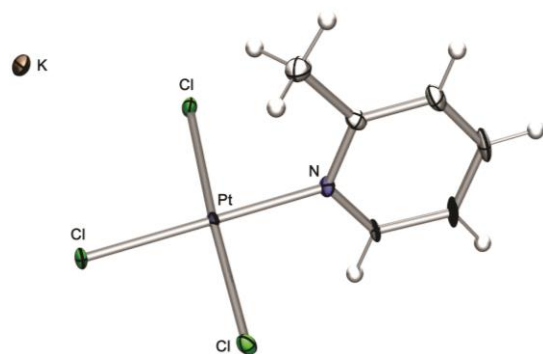
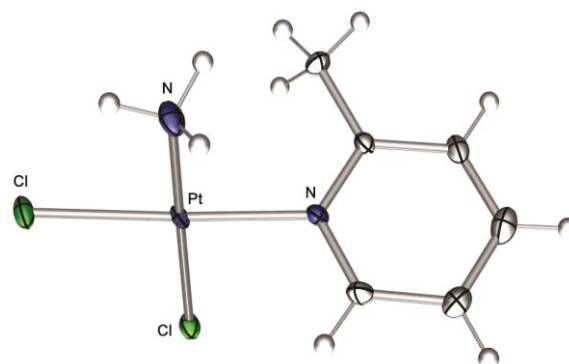
ESI-AccuTOF mass spectrum of **CF-102**



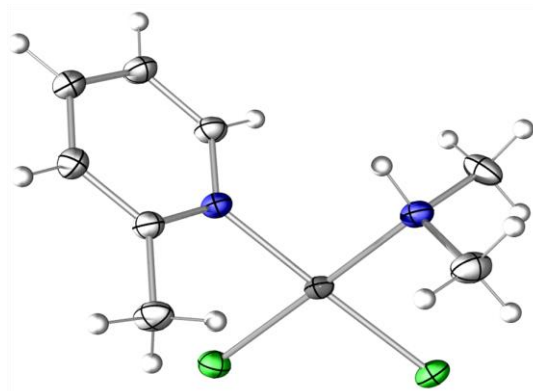
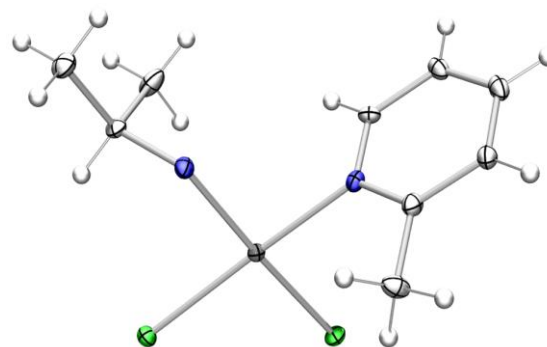
ESI-AccuTOF mass spectrum of CF-103

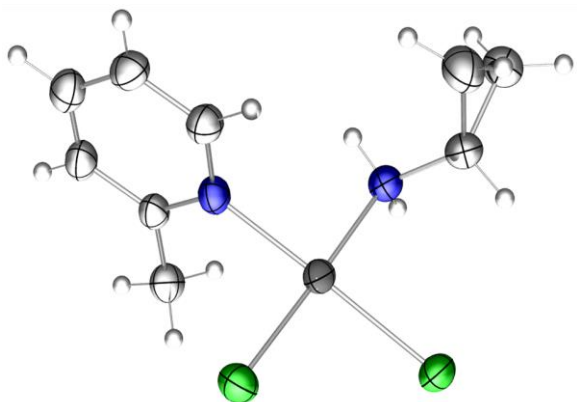
ESI-AccuTOF mass spectrum of **CF-104**

APPENDIX D: X-RAY DATA

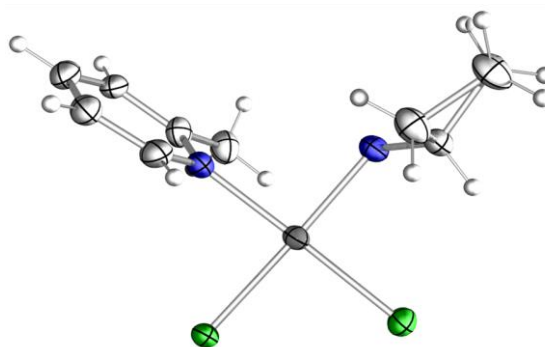
X-ray structure of **TCPP**

X-ray structure of Picoplatin

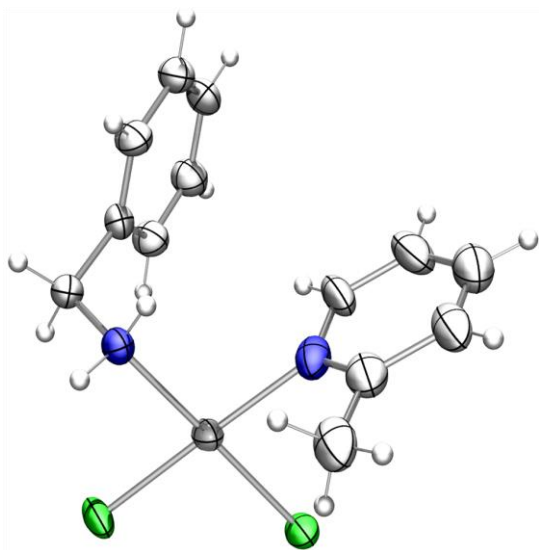
X-ray structure of **Pt-2**X-ray structure of **Pt-3**



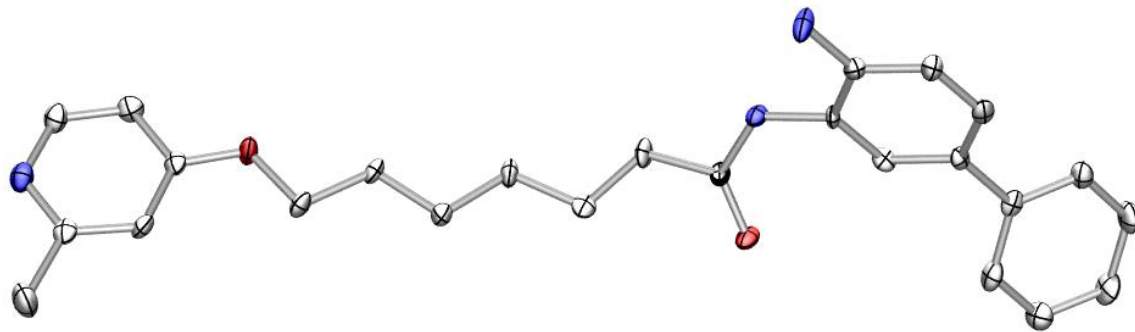
X-ray structure of **Pt-4**



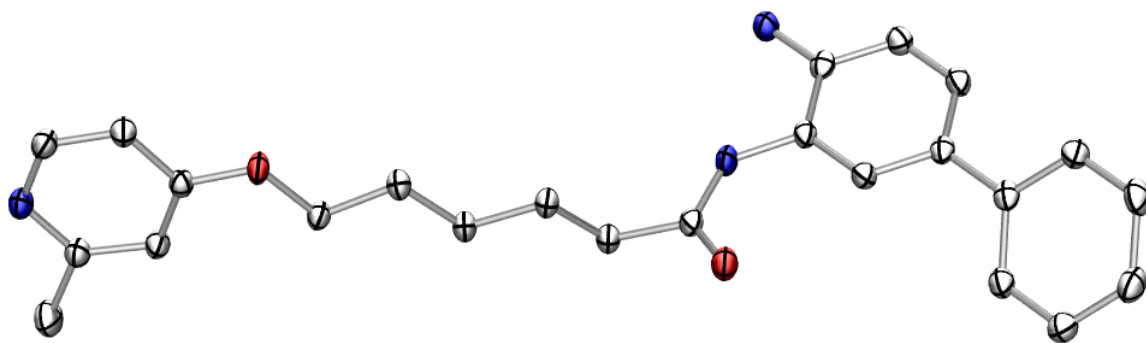
X-ray structure of **Pt-5**



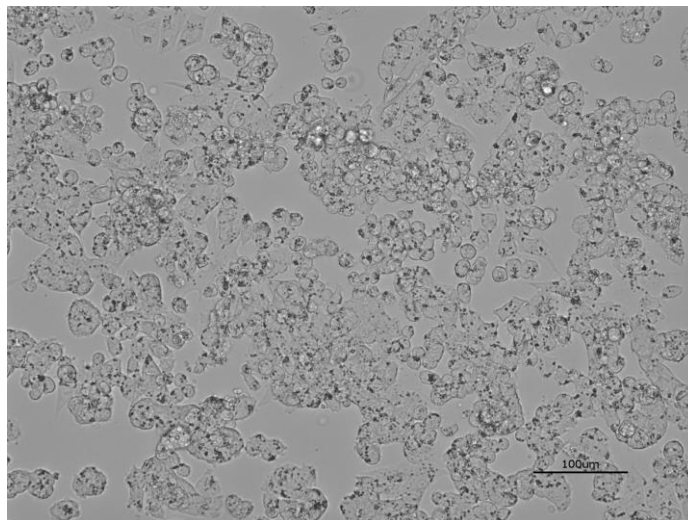
X-ray structure of **Pt-12**



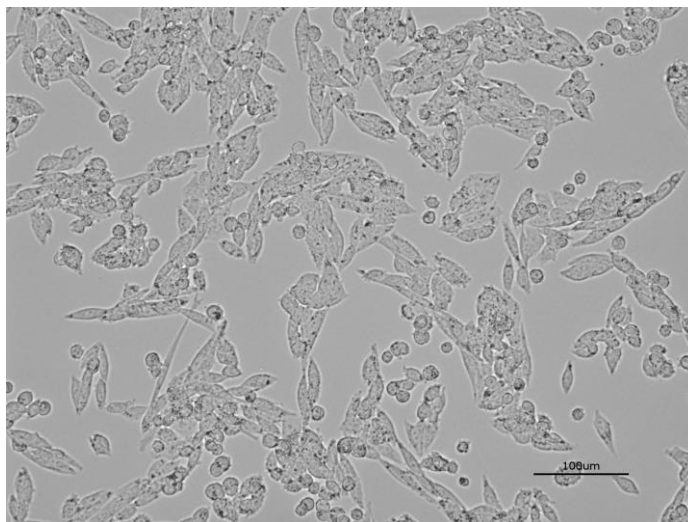
X-ray structure of **CF-L09**



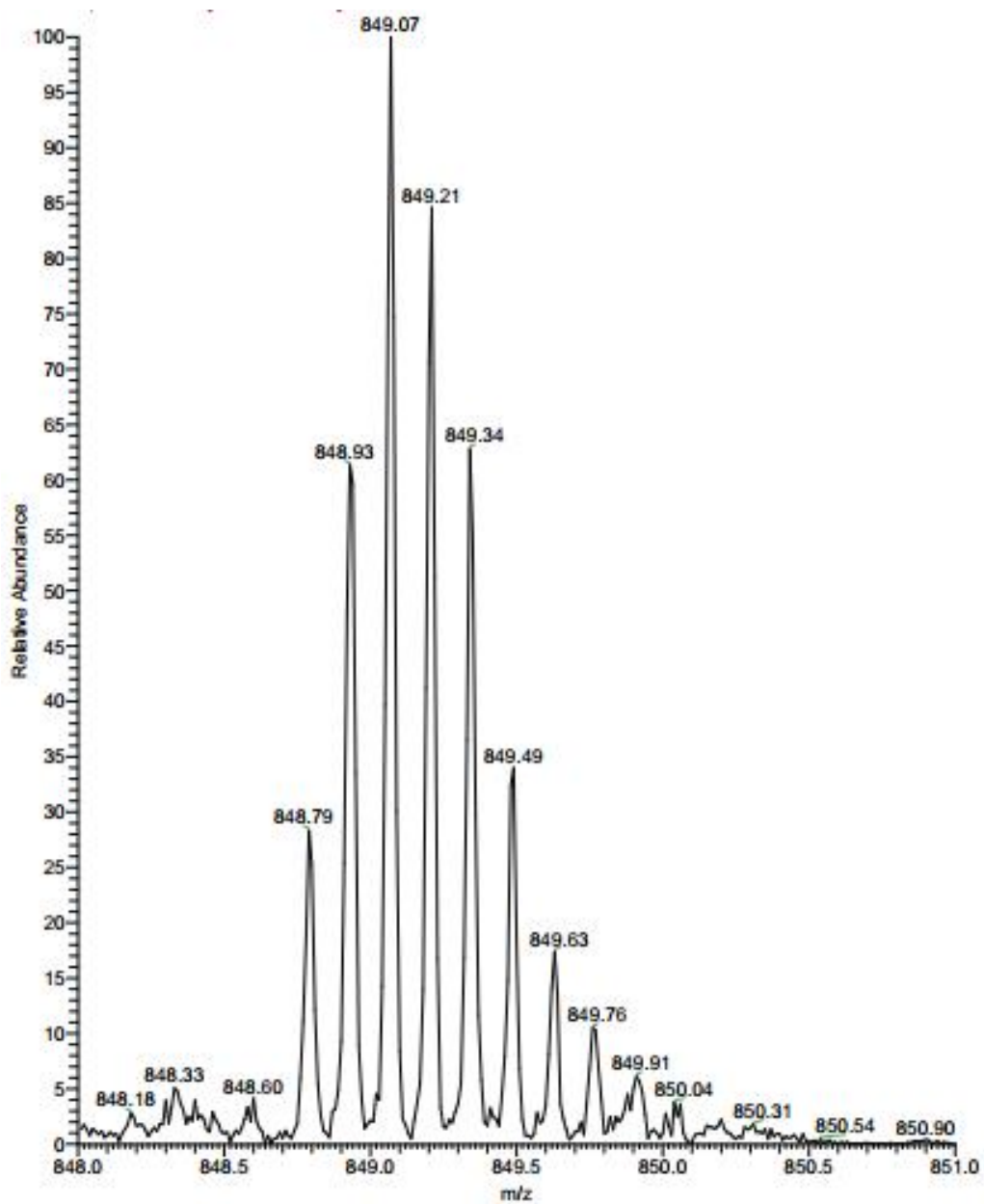
X-ray structure of **CF-L10**

APPENDIX E: BIOSTUDY DATA

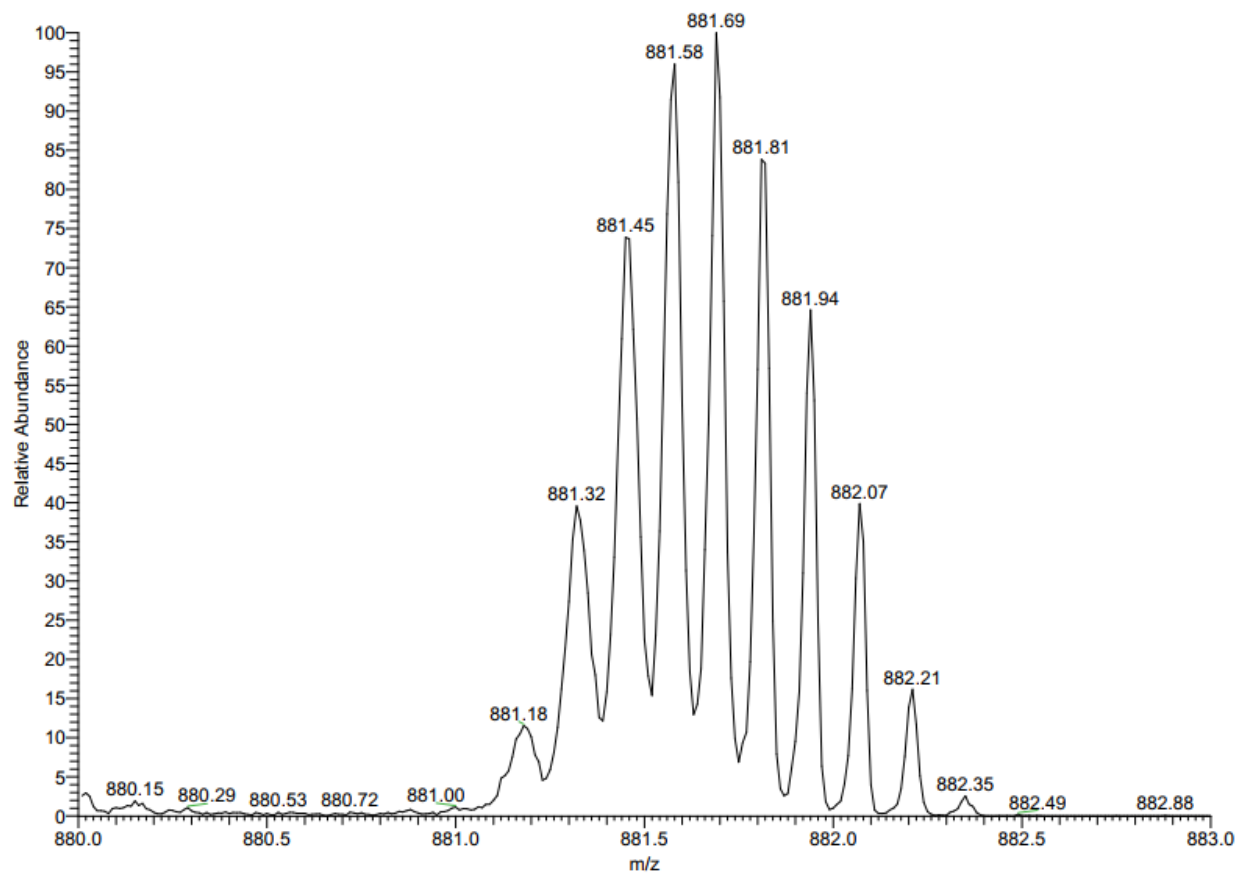
A2780 cells (20 ×) with round shape morphology



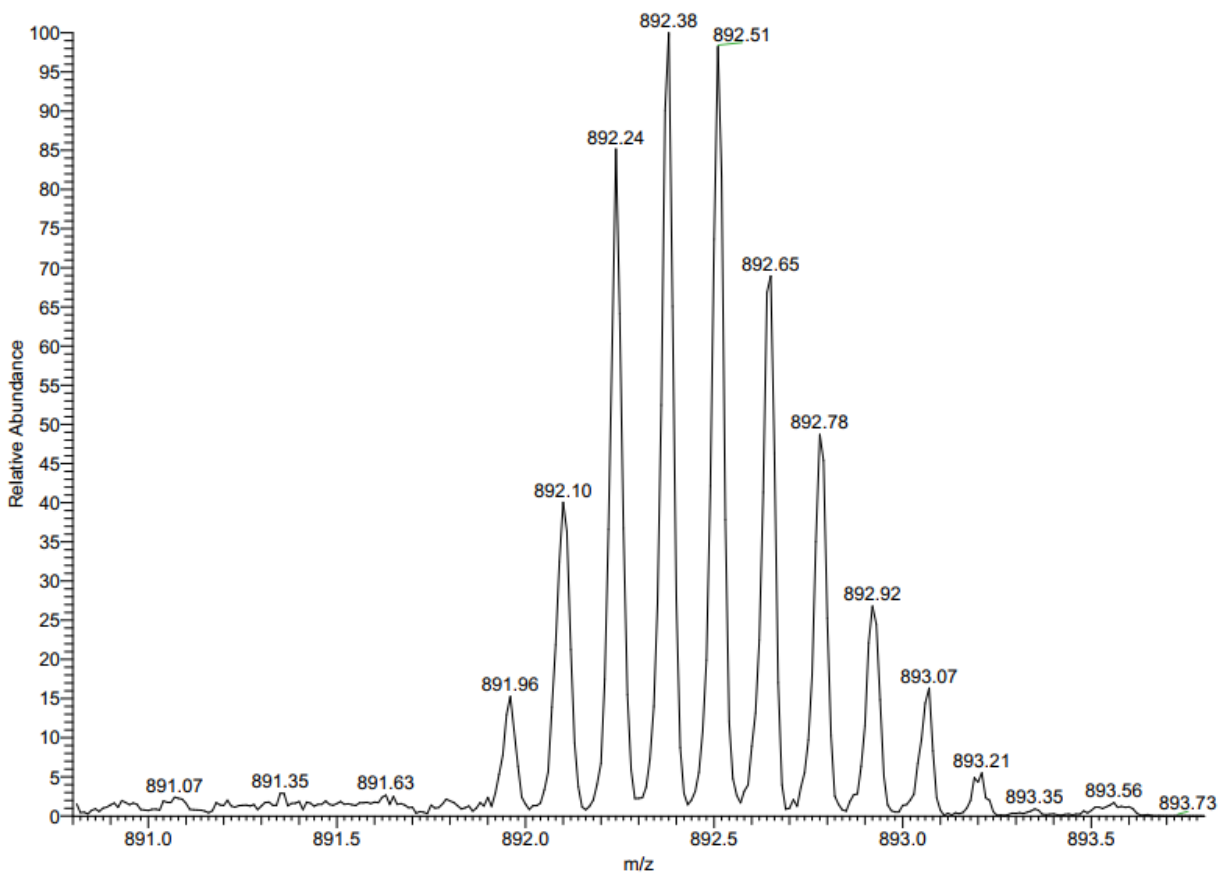
A2780cis cells (20 ×) with fibroblastic morphology



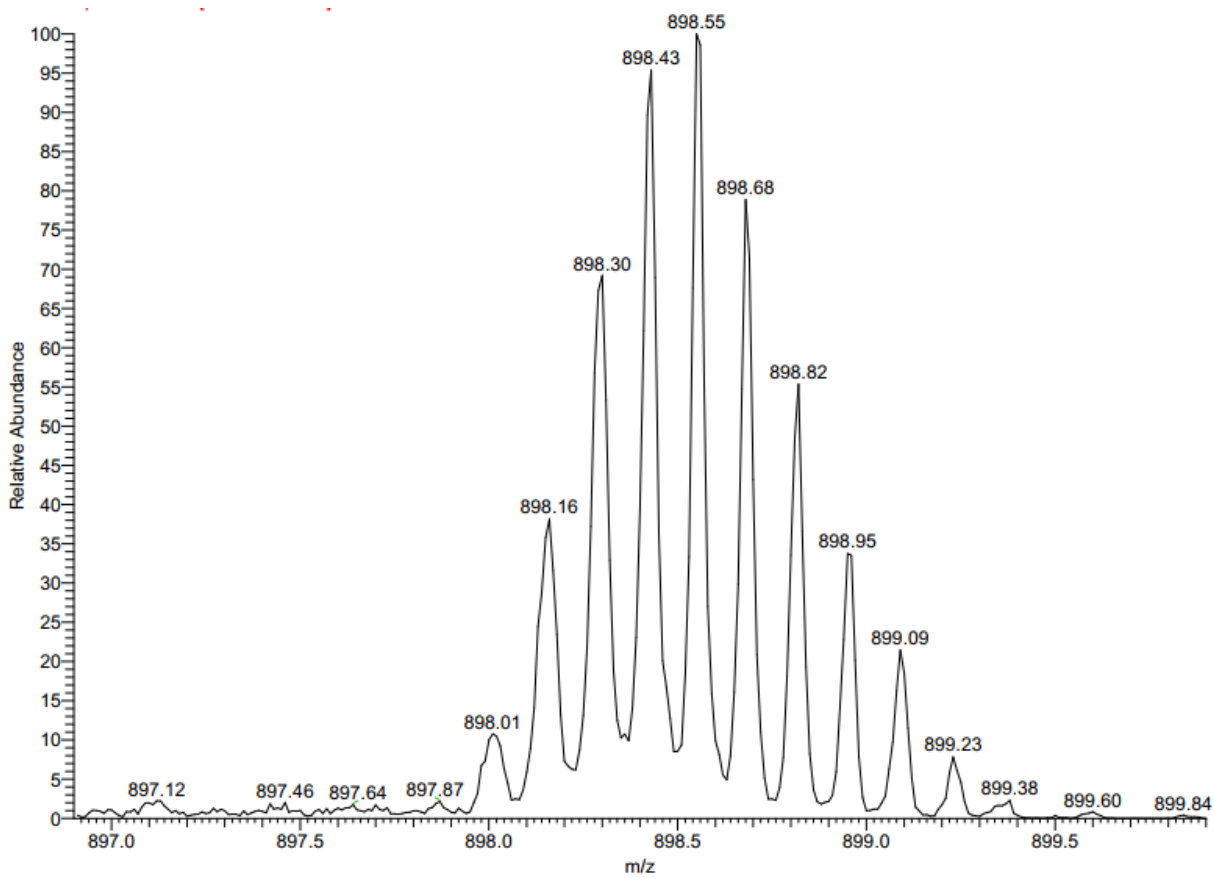
Thermal ESI-LTQ mass spectrum of pure DNA with 7 negative charges.



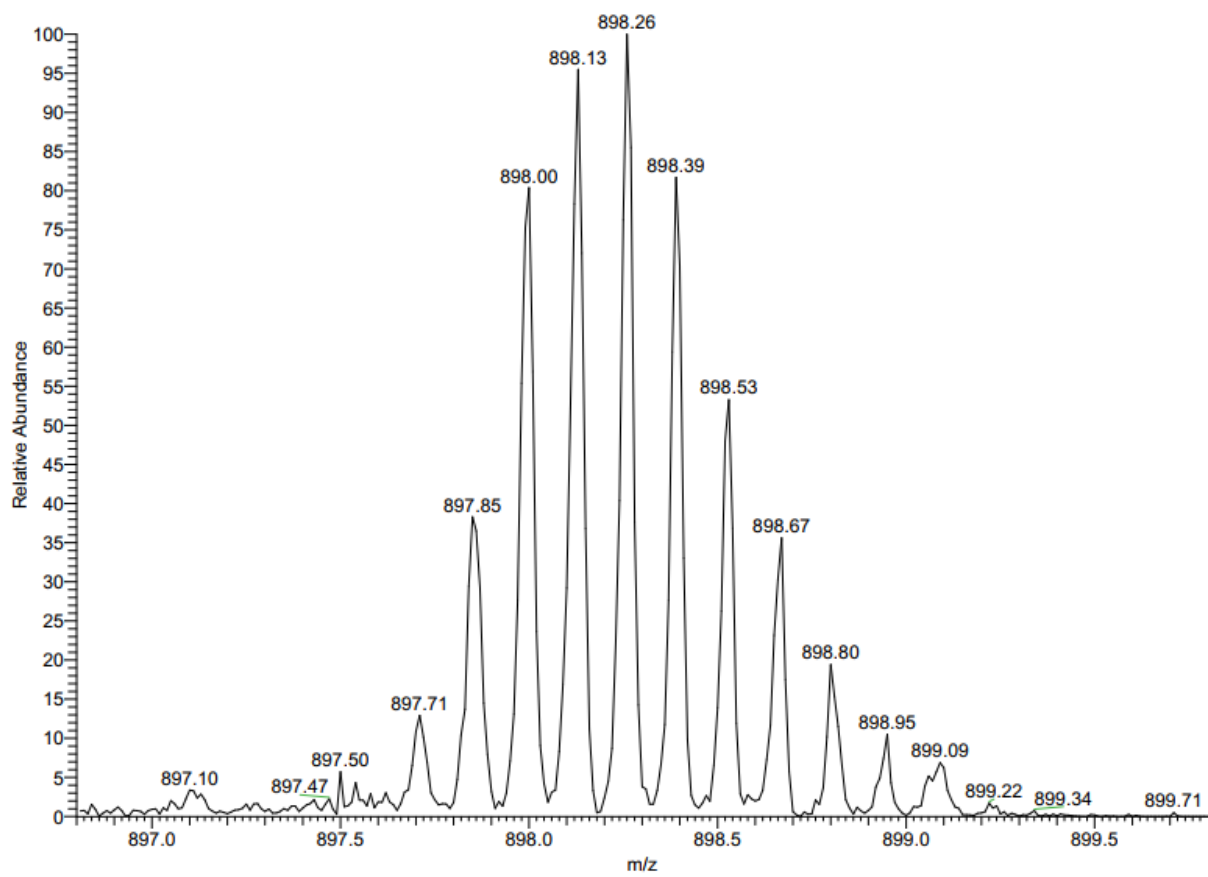
Thermal ESI-LTQ mass spectrum of DNA-cisplatin adduct with 7 negative charges.



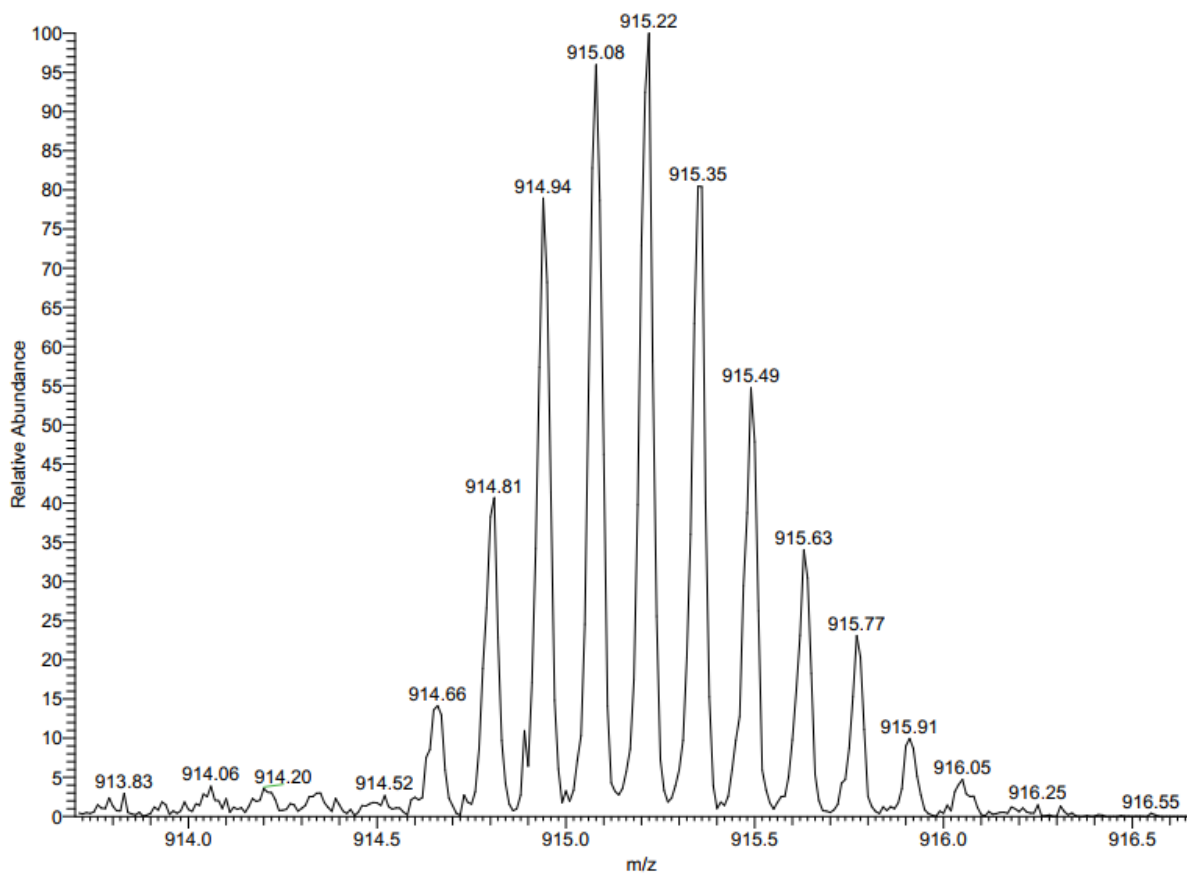
Thermal ESI-LTQ mass spectrum of **DNA-Pt-1** (picoplatin) adduct with 7 negative charges.



Thermal ESI-LTQ mass spectrum of **DNA-Pt-3** adduct with 7 negative charges.

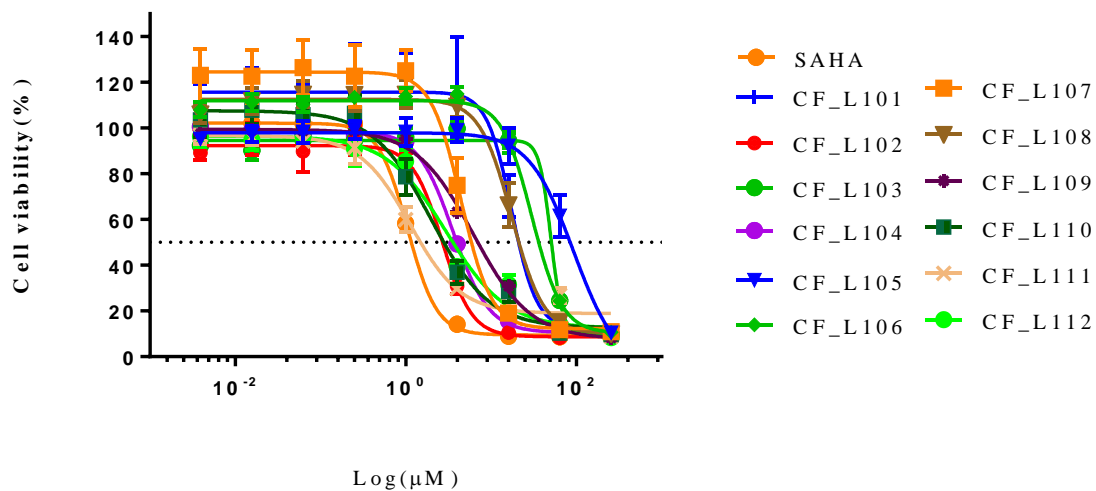


Thermal ESI-LTQ mass spectrum of **DNA-Pt-4** adduct with 7 negative charges.

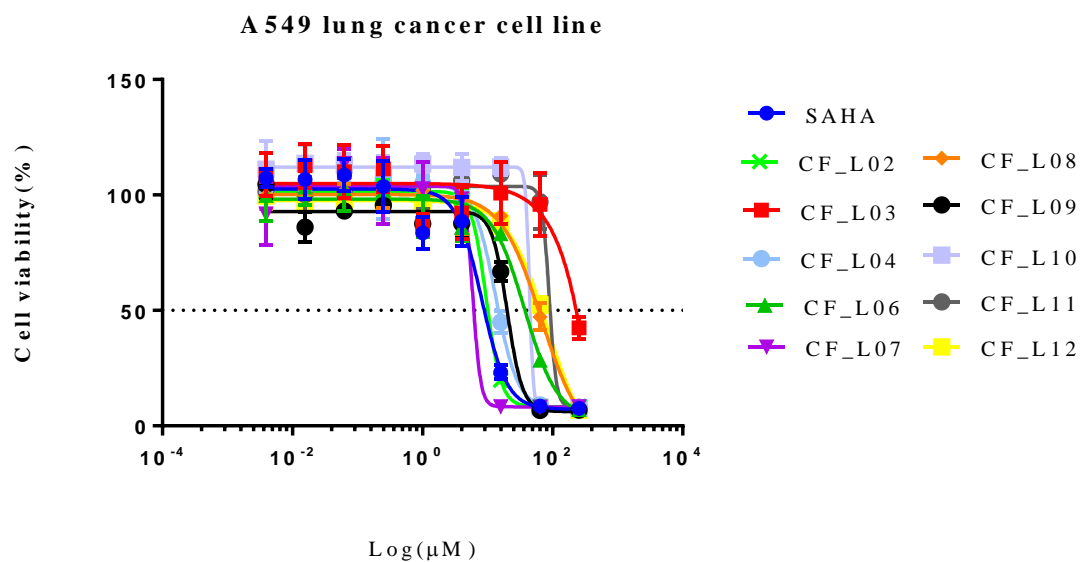


Thermal ESI-LTQ mass spectrum of **DNA-CF-101** adduct with 7 negative charges.

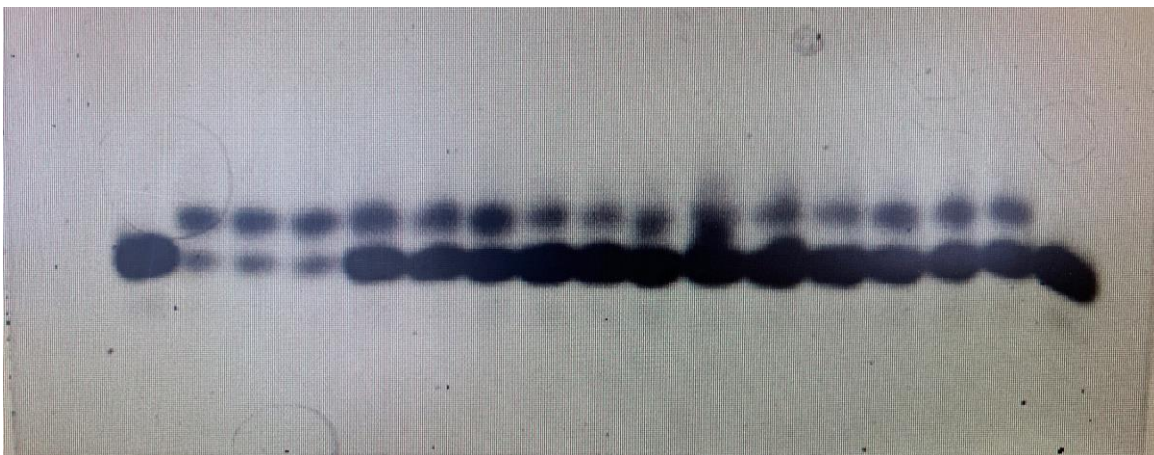
HCT-116 colon cancer cell line



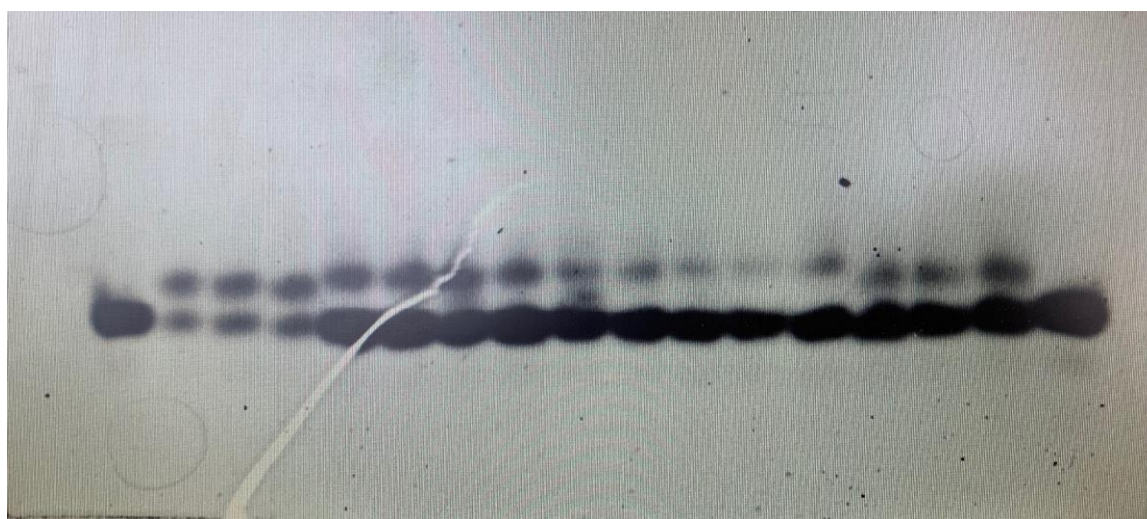
IC₅₀ curve of CF-L01 to CF-L12 in HCT-116



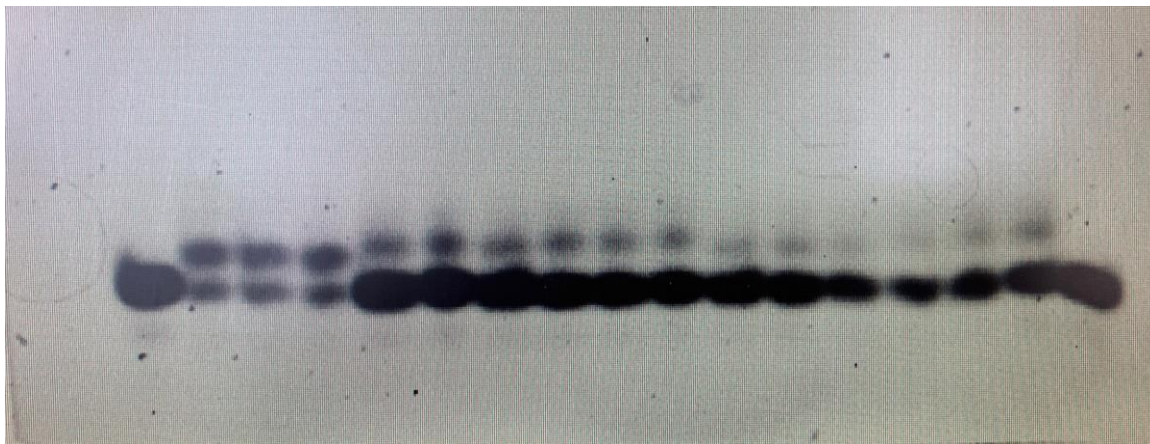
IC₅₀ curve of CF-L01 to CF-L12 in A549



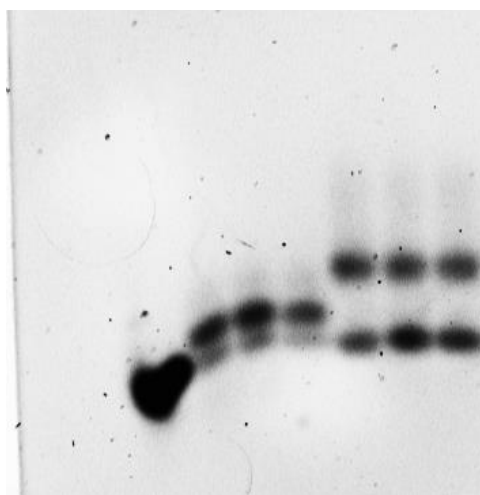
DNA gel electrophoresis of cisplatin, **Pt-1**, **Pt-2**, **Pt-3** and **Pt-4** (left to right) with three runs for each.



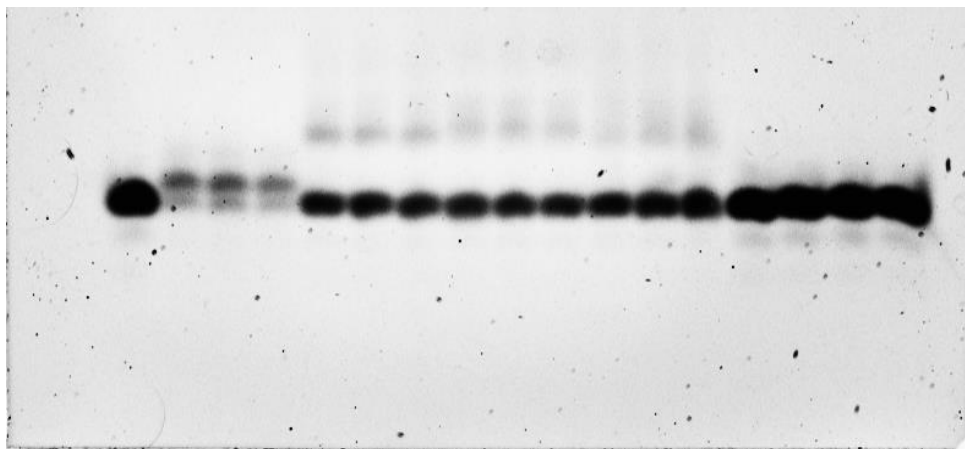
DNA gel electrophoresis of cisplatin, **Pt-5**, **Pt-6**, **Pt-7** and **Pt-8** (left to right) with three runs for each.



DNA gel electrophoresis of cisplatin, **Pt-9**, **Pt-10**, **Pt-11** and **Pt-12** (left to right) with three runs for each.



DNA gel electrophoresis of cisplatin and **CF-101** (left to right) with three runs for each.



DNA gel electrophoresis of cisplatin, **CF-102**, **CF-103**, **CF-104** and SAHA (left to right) with three runs for each.